CISM COURSES AND LECTURES

The series presents lecture notes, monographs, edited works and proceedings in the field of Mechanics, Engineering, Computer Science and Applied Mathematics.
Purpose of the series is to make known in the international scientific and technical community results obtained in some of the activities organized by CISM, the International Centre for Mechanical Sciences.

INTERNATIONAL CENTRE FOR MECHANICAL SCIENCES

COURSES AND LECTURES - No. 523

ASYMPTOTIC METHODS IN FLUID MECHANICS: SURVEY AND RECENT ADVANCES

EDITED BY

HERBERT STEINRÜCK
VIENNA UNIVERSITY OF TECHNOLOGY, AUSTRIA

SpringerWienNewYork

This volume contains 119 illustrations

All contributions have been typeset by the authors.

PREFACE

Rational asymptotic methods developed in the fifties and sixties of the last century have played an important role in theoretical physics, mechanics and in particular in fluid mechanics. Among the most powerful methods used in fluid mechanics are the method of matched asymptotic expansions and multiple scales methods. Matched asymptotic expansions are based on the idea of Prandtl's boundary-layer theory. In case of high Reynolds number flows the flow field can be approximated by an inviscid flow with the exception of a thin boundary-layer along the wall where the viscosity has to be taken into account. Both approximations have to match in an intermediate region. In some cases the inviscid flow and the viscous flow in a sub-layer have to be determined simultaneously. Thus one speaks of interacting boundary-layers. An introduction to triple deck problems and recent applications to internal flows, external sub- or supersonic flows, thermal flows and free surface flows will be presented.

Another fruitful application is the theory of separated laminar incompressible flows. Various examples of fluid flows involving separation will be considered, including self-induced separation of the boundary-layer in supersonic gas flows, and incompressible flow separation at the leading edge of an aerofoil. A characteristic feature of a multiple scales problem is that the solution exhibits almost periodic structures whose properties vary on a large scale. Recently, multiple scales methods have been applied to problems in meteorology. Thus well established ad hoc approximations have been verified by applying the method of multiple scales to the basic equations of fluid flow in the atmosphere. It will be demonstrated how a large collection of well-established models of theoretical meteorology can be recovered systematically, how new insight into scale interaction processes is gained, and how the asymptotic analyses provide hints for the construction of accurate and efficient numerical methods. The known limitations of the approach are also discussed.

Many problems in fluid mechanics involve asymptotic expansions in the form of power series. Such expansions necessarily fail to provide terms which are exponentially smaller than all terms in the series. Although small, these missing terms are often of physical importance. How to find such exponentially small terms, using as the

main tool matched asymptotic expansions in the complex plane and Borel summation will be discussed. The techniques will be developed in the context of model problems related to the theory of weakly nonlocal solitary waves which arise in the study of gravity-capillary waves and also for internal waves.

This volume comprises the lecture notes of a course with the title "Asymptotic Methods in Fluid Mechanics - Survey and Recent Advances" held at the Centre for Mechanical Sciences in Udine, September 21-25, 2009. Also included are contributed papers presented at a workshop embedded in the course.

The organizer of the course thanks all lectures and participants of the workshop for their valuable contributions and their cooperation. My personal thanks are to former rector of CISM Prof. Wilhelm Schneider who suggested this course and for his advice during the preparation. Thanks also to the staff of CISM for the perfect organization and the support in producing these lecture notes.

Herbert Steinrück

CONTENTS

Introduction to Matched Asymptotic Expansions

Herbert Steinrück[*]

[*] Vienna University of Technology, Institute of Fluid Mechanics and Heat Transfer, Vienna, Austria

Abstract The method of *matched asymptotic expansions* will be presented by applying it to three examples showing the wide applicability of the method.

1 Introduction

The governing equations describing a flow field are in general a set of nonlinear partial differential equations. Only in few situation exact solutions mostly in the form of similarity solutions exist. Thus asymptotic expansions with respect to an appropriate dimensionless parameter (e.g. Reynolds number, Mach number, thickness ratio, ...) which tends to a limiting value (zero or infinity) are sought. Let $\phi(x, \varepsilon)$ with $x \in D \subset R^3$ be a function of a variable x depending on a small, positive parameter ε with $0 < \varepsilon \ll 1$. We call

$$[\phi]^{(n)} = \delta_1(\varepsilon)\phi_1(x) + \delta_2(\varepsilon)\phi_2(x) + \cdots + \delta_n(\varepsilon)\phi_n(x) \qquad (1)$$

a n-term asymptotic series of ϕ with respect to $\varepsilon \ll 1$ if the gauge functions $\delta_k(\varepsilon)$ form an asymptotic series, i.e. $\delta_{k+1}(\varepsilon) = o(\delta_k(\varepsilon))$ for $k = 1, \cdots, n-1$ and $\phi(x, \varepsilon) - [\phi^{(n)}] = o(\delta_n(\varepsilon))$.

Note a function $f(\varepsilon)$ is called a small 'o' of the function $g(\varepsilon)$, $f(\varepsilon) = o(g(\varepsilon))$ if $\lim_{\varepsilon \to 0} f(\varepsilon)/g(\varepsilon) = 0$ holds, see Van Dyke (1975). The expansion (1) is called uniformly valid if there exist constants c_1,...,c_n independent of x with

$$\left| \frac{\phi(x, \varepsilon) - [\phi]^{(m)}}{\delta_{m+1}(\varepsilon)} \right| < c_m, \quad m = 1, ..., n. \qquad (2)$$

However, the solutions of many perturbation problems in fluid mechanics do not permit an approximation by an asymptotic series of type (1). Such problems are called singularly perturbed. Most of these problems are characterized by two different (length) scales. For example consider the attached high Reynolds number flow. A regular (outer) expansion fails near a

solid surface and a local variable has to be introduced to describe the local behavior near the wall and a local (inner) expansion of the flow field can be found. To get a uniformly valid approximation of the entire flow region both expansions have to match. Thus one speaks of matched asymptotic expansion.

Boundary layers have been first introduced by Prandtl (1904) by explaining the role of viscosity in large Reynolds number flows. As a mathematical tool the method of matched asymptotic expansions has been developed systematically in between the 50s and 70s of the last century, see Kaplun (1967), Lagerström and Van Dyke (1975), Fraenkel (1969)

Matched asymptotic expansions are used if a regular asymptotic expansion fails near located singularities. Then the problem has to be rescaled appropriately by using local variables before expanding its solution asymptotically. Both expansion have to agree in some overlap region, i.e. a region where both expansions hold. We will demonstrate the method by considering three typical examples showing the wide applicability of the method.

Inviscid potential flow around a thin profile.   The flow potential is expanded with respect to a small aspect ratio of the profile. At first glance one might think that a regular expansion will be sufficient. However, it turns out that the tentative regular expansion is not uniformly valid near the leading and the trailing edge. Thus local expansions turn out to be necessary to obtain a uniformly valid solution, cf. Van Dyke (1975).

Flow between two rotating discs: Ekman-layer.   A common reason for the necessity to introduce a local expansion is that the perturbation parameter multiplies the highest derivative of the unknown function in a differential equation. As a consequence the solution of the limiting differential equation cannot satisfy all required boundary conditions. By introducing a local variable the small coefficient of the highest derivative can be rescaled and the local expansion can satisfy all boundary conditions.

As a representative of that class of problems the flow between two rotating discs in the limit of a small Ekman number will be discussed, see Ungarish (1993).

Model equation: turbulent pipe flow.   Here the asymptotic behavior off an ordinary differential equation is analyzed modeling turbulent pipe flow in the limit of large Reynolds numbers. The limiting differential equation is of the same order as the perturbed one. However, the coefficient of the highest derivative vanishes only at the boundary where a boundary

condition has to be satisfied. Thus again a local expansion turns out to be necessary. The matching of the two expansions will be discussed and an short introduction to turbulence asymptotics will be given.

2 Flow around a thin elliptical airfoil $\varepsilon \ll 1$
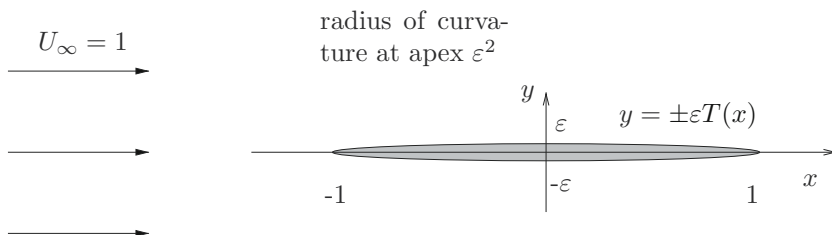
Figure 1. Elliptical thin airfoil

As a first example we consider the two-dimensional inviscid irrotational flow past a thin airfoil. For simplicity we consider a symmetric profile in a uniform free stream parallel to its center line. We place the x-axis of a coordinate system at the centerline of the airfoil such that leading and trailing edge are at $x = \mp 1$ in dimensionless coordinates, respectively. The contour of the profile is given by $y = \pm \varepsilon T(x)$, where ε is the thickness of the airfoil assumed to be small, see figure 1.

The dimensionless flow field can be described by a flow potential $\phi = \phi(x, y)$ where the dimensionless velocity components in x and y direction are given by $u = \phi_x$ and $v = \phi_y$. Thus ϕ is the solution of the potential equation

$$\phi_{xx} + \phi_{yy} = 0 \tag{3}$$

subject to the kinematic boundary condition at the surface of the airfoil

$$\phi_y(x, \pm \varepsilon T(x)) = \pm \varepsilon T'(x) \phi_x(x, \pm \varepsilon T(x)), \quad -1 < x < 1 \tag{4}$$

and the incident flow condition

$$\phi \to x, \quad \text{for} \quad x^2 + y^2 \to \infty. \tag{5}$$

2.1 Asymptotic expansion of the flow potential (regular expansion)

In order to find an asymptotic expansion of the flow potential with respect to a small thickness parameter $\varepsilon \ll 1$ a regular expansion in terms of

powers of ε is employed. In the limiting case $\varepsilon = 0$ the undisturbed parallel flow ($\phi = x$) is obtained. Thus we try to determine a regular expansion in powers of the perturbation parameter ε

$$\phi = x + \varepsilon\phi_1 + \varepsilon^2\phi_2 + \dots, \tag{6}$$

where ϕ_i are the solutions of the potential equation. In order to satisfy the kinematic boundary condition derivatives of the flow potential have to be evaluated at $y = \pm\varepsilon T(x)$. However, the evaluation at $y = \varepsilon T(x)$ is approximated by a Taylor expansion of the corresponding quantity around $(x, 0+)$, i.e.

$$\phi_x(x, \varepsilon T(x)) \sim 1 + \varepsilon\phi_{1,x}(x, 0+) +$$
$$+ \varepsilon^2 \left(\phi_{1,xy}(x, 0+)T(x) + \phi_{2,x}(x, 0+)\right) + \dots \tag{7}$$

Thus the expansion of the kinematic boundary conditions yields conditions for the perturbation potentials ϕ_k

$$\phi_{k,y}(x, \pm 0) = \begin{cases} \pm T'(x), & k = 1, \\ \pm(T(x)\phi_{1,x}(x, 0\pm))_x, & k = 2, \\ \pm(T(\phi_{2,x} + \frac{1}{2}TT''))_x, & k = 3, \end{cases} \quad -1 < x < 1 \tag{8}$$

The incident flow condition requires that flow field vanishes for large $x^2 + y^2 \to \infty$.

$$\phi_i(x, y) \to 0, \quad x, y \to \infty. \tag{9}$$

Note the flow potential of a source at the origin of strength q is $\phi^{(q)} = \frac{q}{2\pi} \ln \sqrt{x^2 + y^2}$. The perturbation potentials ϕ_k can be obtained by placing distributed sources along the centerline of the airfoil on the interval $(-1, 1)$ and one can verify that the corresponding velocity fields can be represented by:

$$u_k(x, y) = \phi_{k,x}(x, y) = \frac{1}{\pi} \int_{-1}^{1} \frac{x - \xi}{(x - \xi)^2 + y^2} \phi_{k,y}(\xi, 0) \, d\xi, \tag{10a}$$

$$v_k(x, y) = \phi_{k,y}(x, y) = \frac{1}{\pi} \int_{-1}^{1} \frac{y}{(x - \xi)^2 + y^2} \phi_{k,y}(\xi, 0) \, d\xi, \tag{10b}$$

cf. Van Dyke (1975). Using the perturbation potentials ϕ_i the surface velocity u_s has the expansion

$$u_s(x) = \sqrt{\phi_x^2(x, \pm\varepsilon T(x)) + \phi_y^2(x, \pm\varepsilon T(x))} \sim$$

$$+ \varepsilon\phi_1(x, 0) + \varepsilon^2 \left[\phi_{2x}(x, 0) + T(x)T''(x) + \frac{1}{2}T'^2(x)\right] + \cdots \quad . \tag{11}$$
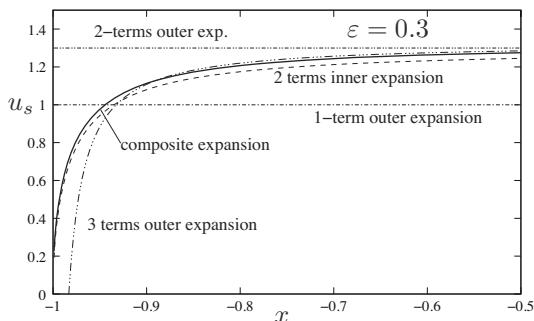
Figure 2. Asymptotic expansion of surface velocity

To be more specific we consider an elliptical airfoil with the shape function $T(x) = \sqrt{1 - x^2}$. Using the notation of complex variables $z = x + iy$ the perturbation potentials ϕ_1, ϕ_2 are

$$\phi_1 = \phi_2 = \Re\left(z - \sqrt{z^2 - 1}\right),\tag{12}$$

where $\Re z$ denotes the real part of a complex number z. In order to make the square root unique the complex plane is sliced along the interval (-1,1). We have $\phi_{1,x}(x, \pm 0) = \phi_{2,x}(x, \pm 0) = \pm 1$. Thus the expansion of the surface velocity

$$u_s(x) \sim 1 + \varepsilon - \frac{\varepsilon^2}{2}\frac{x^2}{1 - x^2} + \cdots\tag{13}$$

turns out to be not uniformly valid. If x is close to the leading or trailing edge, say $|x + 1| \ll \varepsilon^2$ the second order correction term will become larger than the first, (see figure 2).

It is interesting to note that the flow potential of a source or sink flow at the leading or trailing edge can be added to the perturbation potential ϕ_1. In particular the flow potential

$$\phi_1 = \Re\left(z - \sqrt{z^2 - 1} - \frac{C}{2\pi}\ln\frac{z + 1}{z - 1}\right)\tag{14}$$

satisfies all required conditions for an arbitrary constant C.

2.2 Local expansion at leading/trailing edge

Since the expansion presented previously fails near the leading edge we introduce local coordinates to describe the flow field there. A natural length

scale near the leading edge is the radius of curvature of the profile, which in case of the elliptical airfoil is ε^2. Thus we define the local coordinates

$$X = \frac{1+x}{\varepsilon^2}, \quad Y = \frac{y}{\varepsilon^2}, \tag{15}$$

and the local flow potential by $\Phi(X, Y)$ by

$$\phi(x, y) = \phi(-1, 0) + \varepsilon^2 \Phi(X, Y). \tag{16}$$

The local potential satisfies again the Laplace equation. The contour of the airfoil written in local coordinates is given by

$$Y = \pm \sqrt{2X + \varepsilon^2 X^2} \sim \sqrt{2X} \left(1 + \frac{\varepsilon^2}{4} X + ... \right). \tag{17}$$

Thus the kinematic boundary condition in local coordinates reads

$$\Phi_Y \left(X, \sqrt{2X - \varepsilon^2 X^2} \right) - \frac{1 - \varepsilon^2 X}{\sqrt{2X - \varepsilon^2 X^2}} \Phi_X \left(X, \sqrt{2X - \varepsilon^2 X^2} \right) = 0. \tag{18}$$

We expand the local solution with respect to ε asymptotically

$$\Phi(X, Y) = \Phi_0 + \varepsilon \Phi_1 + \varepsilon^2 \Phi_2 + ... \tag{19}$$

and obtain for the first two terms the kinematic boundary condition

$$\Phi_{i,Y} \left(X, \sqrt{2X} \right) - \frac{1}{\sqrt{2X}} \Phi_{i,X} \left(X, \sqrt{2X} \right) = 0, \quad i = 0, 1. \tag{20}$$

This can be interpreted as the kinematic boundary condition for the inviscid flow around a parabola. Due to symmetry the stagnation point is in the apex of the parabola. The flow potential can be determined by conformal mapping, cf. Betz (1964). It is given by

$$\Phi_i = U_{loc,i} \Re \left(Z - 1 + \sqrt{1 - 2Z} \right), \quad i = 0, 1, \tag{21}$$

where the velocities of the free stream $U_{loc,i}$ with $i = 1, 2$ are unknown. They have to be determined by matching with the outer (global) expansion. The expansion of the local surface velocity is given by

$$U_s \sim (U_{loc,0} + \varepsilon U_{loc,1}) \sqrt{\frac{2X}{1 + 2X}}. \tag{22}$$
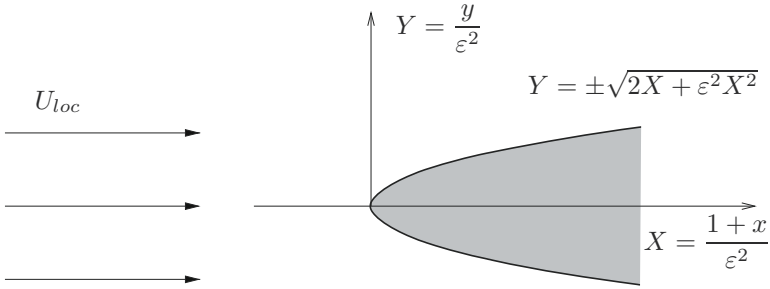
Figure 3. Airfoil in local coordinates

2.3 Matching procedure

We have now determined asymptotic expansions on two different length scales: the outer (global) length scale and a local expansion around the leading edge of the profile, where the radius of curvature is the reference length scale. Both expansions are not uniformly valid in the entire flow domain. The basic hypothesis is that there exists (asymptotically) an overlap where both expansions are valid. Thus we take the outer (global) expansion and rewrite it in the inner (local) variable. For the matching procedure we use the velocity field instead of the flow potential.

We introduce an intermediate variable $\xi(\varepsilon)$ such that

$$z(\varepsilon) = -1 + \varepsilon^2 \xi(\varepsilon) \to -1, \quad Z(\varepsilon) = \xi(\varepsilon) \to \infty \quad \text{as} \quad \varepsilon \to 0, \qquad (23)$$

and insert it into the global and local expansion, respectively.

The outer expansion of the velocity field in the overlap region is:

$$\phi' \sim 1 - \varepsilon \frac{z}{\sqrt{z^2 - 1}} + \frac{C}{2\pi} \left(\frac{1}{1+z} - \frac{1}{z-1} \right) \cdots \sim \qquad (24)$$

$$1 + \varepsilon \left(1 - \frac{-1 + \varepsilon^2 \xi}{\sqrt{-2\varepsilon^2 \xi + \varepsilon^4 \xi^4}} + \frac{C}{\varepsilon^2 \xi} \right) \sim 1 + \varepsilon + \frac{1}{\sqrt{-2\xi}} + \frac{C}{\varepsilon \xi}. \qquad (25)$$

The local expansion of the velocity field in the overlap region is given by

$$\Phi' \sim (U_{loc,0} + \varepsilon U_{loc,1}) \left(1 + \frac{1}{\sqrt{1 - 2Z}} \right)$$

$$\sim U_{loc,0} \left(1 + \frac{1}{\sqrt{-2\xi}} \right) + \varepsilon U_{loc,1}. \qquad (26)$$

Thus both expansions agree in the overlap region if

$$U_{loc,0} = U_{loc,1} = 0, \quad \text{and} \quad C = 0 \tag{27}$$

holds.

Van Dyke (1975) has formalized the matching procedure in the matching principle. Fraenkel (1969) discussed criteria on the inner and outer expansion for the validity of the matching principle. For example when the gauge functions in the outer and inner expansion are powers of the expansion parameter, which is defined as the ratio of the scales of the inner and outer variable, the matching principle holds. Problems may arise when the gauge functions are a combination of powers and logarithmic terms of the perturbation parameter.

Matching principle: n-terms of the outer expansion rewritten in the inner variable and expanded into m terms must agree with m terms of the inner expansion rewritten in the outer variable and expanded into n terms.

$$\left[\left[\phi \right]_{out}^{(n)} \right]_{in}^{(m)} = \left[\left[\phi \right]_{in}^{(m)} \right]_{out}^{(n)}. \tag{28}$$

We demonstrate the Matching Principle at the surface velocity of a thin airfoil. We start with the 3 term outer expansion and rewrite it in the local (inner) variables

$$[u_s]_{out}^{(3)} = 1 + \varepsilon - \frac{\varepsilon^2}{2} \frac{x^2}{1 - x^2} = 1 + \varepsilon - \frac{1}{X} \frac{(-1 + \varepsilon^2 X)^2}{2 - \varepsilon^2 X}. \tag{29}$$

Expanding the above expression into two terms yields

$$\left[[u_s]_{out}^{(2)} \right]_{in}^{(3)} = 1 - \frac{1}{4X} + \varepsilon. \tag{30}$$

On the other hand two terms of the inner expansion rewritten in the outer variables gives

$$\left[[u_s]_{in}^{(2)} \right]_{out}^{(2)} = \left[(1 + \varepsilon) \sqrt{\frac{2X}{1 + 2X}} \right]_{out}^{(2)} = 1 + \varepsilon - \frac{\varepsilon^2}{4(1 + x)}. \tag{31}$$

Thus both expressions agree.

2.4   Composite approximation

In order to get a uniformly valid approximation one has to combine the inner and outer expansion. This can be done by adding both expansions. Doing so the overlap region is represented twice. Thus the common part of both expansion has to be subtracted.

$$u_s \sim [u_s]_{in}^{(2)} + [u_s]_{out}^{(3)} - \left[\left[\phi\right]_{out}^{(3)}\right]_{in}^{(3)} = \tag{32}$$

$$= (1+\varepsilon)\sqrt{\frac{2X}{1+2X}} - \frac{\epsilon^2}{2}\frac{x^2}{1-x^2} + \frac{1}{4X}.$$

In figure 2 the outer, the inner expansion and the composite approximation of the surface velocity are shown for $\varepsilon = 0.3$.

3   Flow between rotating discs - Ekman layers

In many applications local expansions have to be introduced since the solution of the limiting problem cannot satisfy all boundary conditions. Often this is due the fact that the small perturbation parameters multiplies the highest derivative of the unknown function in the governing differential equation. As a representative example we study here the incompressible flow between two infinite parallel discs, which rotate coaxially but at different speeds in the limit of a small Ekman number.
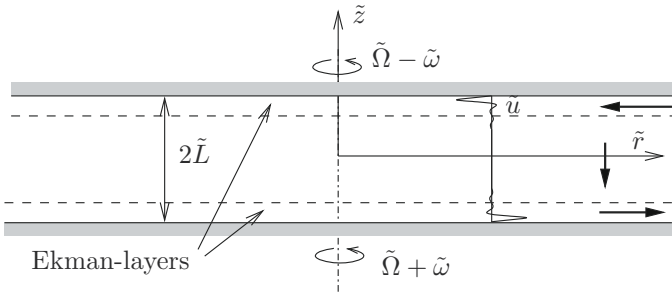
Figure 4. Flow between two coaxially rotating discs

The distance between the two discs is $2\tilde{L}$. Here and in the following we denote dimensional quantities with a tilde. The upper disc rotates with speed $\tilde{\Omega} - \tilde{\omega}$ and the lower with $\tilde{\Omega} + \tilde{\omega}$. We choose a cylindrical coordinate system with the axis of rotation as the z-axis and its origin in the mid-

dle between the two plates. The fluid between the discs is assumed to be incompressible and its kinematic viscosity $\tilde{\nu}$ to be constant.

Thus two independent dimensionless group can be formed: The Ekman number $Ek = \tilde{\nu}/\tilde{\Omega}\tilde{L}^2$ and the Rossby number $Ro = \tilde{\omega}/\tilde{\Omega}$. If the Rossby number is zero both discs rotate at the same angular speed. In that case the fluid between the two discs would do the same. Thus the Rossby number is a measure of the deviation of the solid body rotation of the fluid. Here we will assume that the Rossby number is small.

The Ekman number can be interpreted as the reciprocal value of a Reynolds number based on the reference velocity $\tilde{\Omega}\tilde{L}$. Here we are interested in the limit of small Ekman numbers.

The governing Navier-Stokes equation written in cylindrical coordinates can be found in Schlichting (2000). We use the dimensionless vertical coordinate $Z = \frac{\tilde{z}}{\tilde{L}}$ and introduce the similarity ansatz

$$\tilde{u} = \tilde{r}\tilde{\omega}U(Z), \qquad \tilde{v} = \tilde{r}\tilde{\Omega} + \tilde{r}\tilde{\omega}V(Z), \qquad \tilde{w} = \tilde{L}\tilde{\omega}W(Z), \tag{33a}$$

$$\tilde{p} = \frac{1}{2}\tilde{\rho}\tilde{\Omega}^2\tilde{r}^2 + \frac{1}{2}\tilde{\rho}\tilde{\Omega}\tilde{\omega}\tilde{r}^2 A + \tilde{\rho}\tilde{\Omega}\tilde{\omega}\tilde{L}^2 B(Z). \tag{33b}$$

Thus the Navier-Stokes equation reduce to a set of nonlinear ordinary differential equations for the secondary flow induced by the difference of the angular velocities.

$$Ro\,(U^2 - V^2 + WU_Z) = 2V - A + Ek\,U_{ZZ}, \tag{34a}$$

$$Ro\,(2UV + WV_Z) = -\,2U + Ek\,V_{ZZ}, \tag{34b}$$

$$Ro\,WW_Z = -B_Z + Ek\,W_{ZZ}, \tag{34c}$$

$$2U + W_Z = 0. \tag{34d}$$

At the two discs the no slip boundary conditions have to be satisfied.

$$U(\pm 1) = 0, \quad V(\pm 1) = \mp 1, \quad W(\pm 1) = 0. \tag{35}$$

These are a set of ordinary differential equations for the velocity profiles U, V, W, the pressure profile B and the constant A. At first glance one might think that the six no-slip boundary conditions are not enough. But we have to consider equation (34a), (34b) as second order equations for U and V, respectively. The continuity equation (34d) can be considered as first order equation for the vertical velocity profile W and equation (34c) can be considered as an algebraic equation for the vertical pressure gradient B_Z. Thus in total six boundary conditions are needed to determine U, V, W, B_Z and A .

Assuming a small difference in the speeds of rotation of the two discs (small Rossby number Ro) we can neglect the nonlinear terms and obtain a linear set of ordinary differential equations with constant coefficients.

$$Ek\,U_{ZZ} = A - 2V, \quad Ek\,V_{ZZ} = 2U, \quad W_Z - 2U, \quad B_Z = Ek\,W_{ZZ}. \quad (36)$$

We remark that for positive Ro-numbers the solution can be expanded into a regular power series with respect to powers of Ro.

3.1 Small Ekman numbers

Of course the set of ordinary differential equations (36) can be solved analytically. Here we want to demonstrate how to find an asymptotic solution in the limit $Ek \to 0$.

3.2 Core region

We expand the constant $A = A_0 + Ek^\alpha A_1 + ...$ and the solution (U, V, W) in the core region into powers of the Ekman number Ek

$$
\begin{pmatrix} U(Z; Ek) \\ V(Z; Ek) \\ W(Z; Ek) \end{pmatrix} = \begin{pmatrix} \bar{U}_0(Z) \\ \bar{V}_0(Z) \\ \bar{W}_0(Z) \end{pmatrix} + Ek^\alpha \begin{pmatrix} \bar{U}_1(Z) \\ \bar{V}_1(Z) \\ \bar{W}_1(Z) \end{pmatrix} + ... \quad (37)
$$

and insert it into (36). Comparing like powers we obtain

$$\bar{U}_i = 0, \quad \bar{V}_i = \frac{A_i}{2}, \quad \bar{W}_i = W_i, \quad i = 0, 1. \quad (38)$$

However, the constants A_0, A_1, W_0 and W_1 remain undetermined yet. Unfortunately (38) cannot satisfy all boundary conditions for V and W.

3.3 Boundary layers

Thus we expect that the solution will vary rapidly near the boundary in order to satisfy the boundary conditions. In order to capture this rapid variation we introduce local variables near the boundaries at $Z = \pm 1$.

$$\eta = \frac{1 - Z}{Ek^\beta}, \quad \zeta = \frac{1 + Z}{Ek^\beta} \quad (39)$$

The independent variable will be stretched with the factor Ek^β. The exponent β will be determined appropriately later.

Setting $U(Z) = \hat{U}(\eta)$ and similarly V and W and inserting into (36) we obtain the differential equations describing the local behavior of the flow near the lower disc.

$$Ek^{1-2\beta}\hat{U}'' = A_0 - 2\hat{V}, \quad Ek^{1-2\beta}\hat{V}'' = 2\hat{U}, \quad Ek^{-\beta}\hat{W}' = \mp 2\hat{U}. \quad (40)$$

We remark that for the local behavior near the upper disc we obtain a similar differential equation. Only the sign in front of $\hat{W}'$ has to be changed. Inspecting the local differential equation and setting $Ek = 0$ we see immediately that a nontrivial differential equation is obtained if $\beta = 1/2$. Thus we expand

$$\begin{pmatrix} U \\ V \\ W \end{pmatrix} \sim \begin{pmatrix} \hat{U}_0(\zeta) \\ \hat{V}_0(\zeta) \\ \hat{W}_0(\zeta) \end{pmatrix} + \sqrt{Ek} \begin{pmatrix} \hat{U}_1(\zeta) \\ \hat{V}_1(\zeta) \\ \hat{W}_1(\zeta) \end{pmatrix} + \cdots \quad . \tag{41}$$

From the boundary condition at the lower disc ($Z = -1$) we obtain the boundary condition for the local expansion

$$\hat{U}_0(0) = \hat{U}_1(0), \quad \hat{V}_0(0) = 1, \quad \hat{V}_1(0) = 0, \quad \hat{W}_0(0) = \hat{W}_1(0). \tag{42}$$

Inserting the expansion (41) into (40) and after some elementary manipulations we obtain a fourth-order differential equation for $\hat{V}_0$

$$\hat{V}_0^{(iv)} + 4\hat{V}_0 = 2A_0, \quad \hat{V}_0(0) = 1, \quad \hat{V}_0''(0) = 0, \tag{43}$$

with the solution

$$\hat{V}_0(\xi) = \frac{A_0}{2} + \left(1 - \frac{A_0}{2}\right) e^{-\xi} \cos\xi + c_1 \sinh\xi \cos\xi + c_2 \cosh\xi \sin\xi. \tag{44}$$

For the radial velocity component we obtain from $\hat{U}_0 = -\frac{1}{2}\hat{V}_0''$

$$\hat{U}_0(\xi) = \left(1 - \frac{A_0}{2}\right) e^{-\xi} \sin\xi - 2c_1 \cosh\xi \sin\xi + 2c_2 \sinh\xi \cos\xi \tag{45}$$

and for the vertical component $\hat{W}_0 = 0$ and

$$\hat{W}_1(\xi) = \left(1 - \frac{A_0}{2}\right) [1 - e^{-\xi}(\sin\xi + \cos\xi)] - \tag{46}$$

$$\frac{c_1 - c_2}{2} \sinh\xi \sin\xi - \frac{c_1 + c_2}{2}(\cosh\xi \cos\xi - 1)$$

follows.

3.4 Matching

Applying the matching principle yields that all quantities in the overlap region between the core layer and the boundary layer have to be constant. Thus we conclude that $c_1 = c_2 = 0$. Furthermore we obtain

$$\bar{U}_0 = 0, \quad \bar{W}_0 = -1 + \frac{A_0}{2}. \tag{47}$$
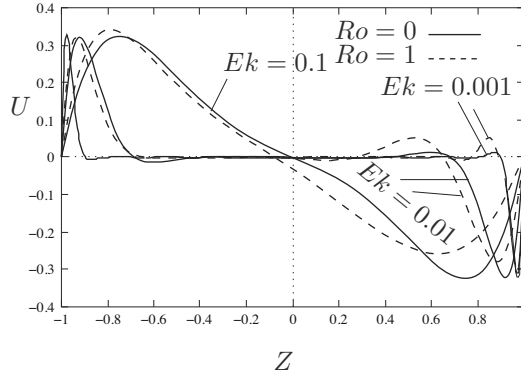
a) radial velocity component
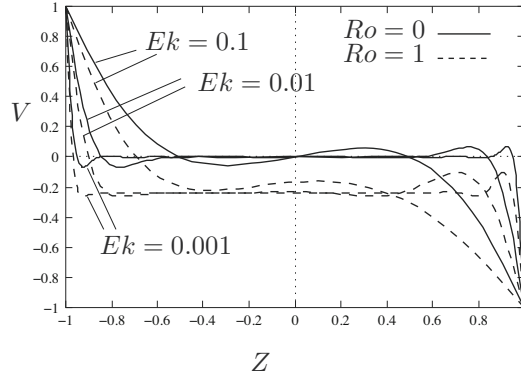
b) azimuthal velocity component
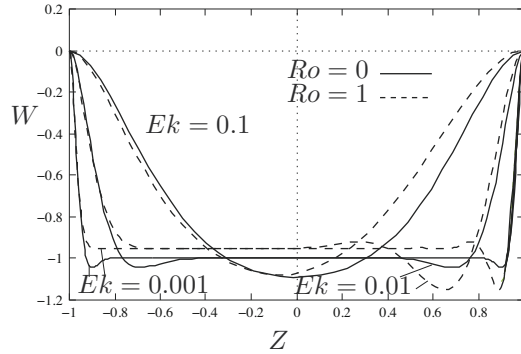
c) vertical velocity component

Figure 5. Velocity profiles between two rotating discs (solution of differential eq. (33)) for $Ek = 0.1, 0.01, 0.001$ and $Ro = 0, 1$.

The analysis of the boundary layer at $Z = 1$ follows the same lines as indicated above. Only the sign in front of the first derivatives and in the boundary condition for the azimuthal velocity V has to be changed.

After matching with the upper layer with the core region we obtain

$$\bar{U}_0 = 0, \quad \bar{W}_0 = -1 - \frac{A_0}{2}. \tag{48}$$

Thus we conclude that $A_0 = 0$ and we have determined all leading order terms of the asymptotic expansion of the velocity profile.

Combining the expansion of the core region with that of the Ekman-layers we obtain the uniformly valid approximation.

$$U \sim e^{-\xi} \sin \xi - e^{-\eta} \sin \eta, \quad V \sim e^{-\xi} \cos \xi - e^{-\eta} \cos \eta, \tag{49a}$$

$$W \sim \sqrt{Ek} \left[-1 + e^{-\xi}(\sin \xi + \cos \xi) + e^{-\eta}(\sin \eta + \cos \eta) \right]. \tag{49b}$$

In figure 5 numerical solutions of the similarity equations (33) are shown for different Ekman- and Rossby numbers. As expected, the velocity profiles exhibit Ekman-layers near the rotating walls.

4   Model equation for fully developed turbulent channel flow

As the third example of matched asymptotic expansions we will study the fully developed turbulent channel flow in the limit of large Reynolds numbers. We expect that the reader is familiar with the basic terminology in turbulent flows, namely the Reynolds decomposition of the flow and pressure field into mean flow, mean pressure and fluctuating velocities and pressure, respectively.

Assuming a fully developed flow, i.e. all averaged flow quantities do not depend on the coordinate $\tilde{x}$ in flow direction the mean velocity $\tilde{u}$ and the shear stress $\tilde{\tau}$ are function of the lateral coordinate $\tilde{y}$ only.

The momentum balance yields an equilibrium between the pressure gradient $d\tilde{p}/d\tilde{x}$ and the $\tilde{y}$-derivative of the shear stress $\tilde{\tau}$

$$0 = -\frac{d\tilde{p}}{d\tilde{x}} + \frac{d\tilde{\tau}}{d\tilde{y}}. \tag{50}$$

The averaged shear stress $\tilde{\tau}$ is the sum of the Reynolds shear stress $\tilde{\tau}_t = -\tilde{\rho}\overline{(\tilde{u}'\tilde{v}')}$ and the viscous stress

$$\tilde{\tau} = \tilde{\tau}_t + \tilde{\mu}\frac{d\tilde{u}}{d\tilde{y}}. \tag{51}$$

At the channel wall $\tilde{y} = 0$ the no slip boundary condition $\tilde{u} = 0$ holds and at the centerline $\tilde{y} = \tilde{d}$ due to symmetry the shear stress $\tilde{\tau}$ vanishes. Here we consider the center line velocity $\tilde{u}_c$ as a given quantity and want to determine the velocity profile $\tilde{u} = \tilde{u}(\tilde{y})$ and the pressure gradient, respectively. A more physical boundary condition is that the mean velocity (or volume flux) is prescribed, but for the sake of simplicity of the analysis we prescribe here the center line velocity.

In order to close the problem, a relation between the mean flow $\tilde{u}$ or its derivatives and the turbulent shear stress is missing. There is a vast literature and several approaches how such a closure can be accomplished. We assume here a simple turbulence model for wall bounded shear flows, namely the mixing length model

$$\tilde{\tau}_t = \tilde{\rho}\tilde{l}^2 \left| \frac{d\tilde{u}}{d\tilde{y}} \right| \frac{d\tilde{u}}{d\tilde{y}}. \tag{52}$$

In case of a channel flow an expression for the mixing length $\tilde{l} = \tilde{l}(\tilde{y}) = \tilde{d}l(y)$ as a function of the dimensionless distance $y = \tilde{y}/\tilde{l}$ from the wall can be found in Schlichting (2000)

$$l(y) = c_0 - \left(2c_0 - \frac{\kappa}{2} \right)(1 - y)^2 - \left(\frac{\kappa}{2} - c_0 \right)(1 - y)^4. \tag{53}$$

Note that the mixing length $\tilde{l}$ vanishes at the wall $\tilde{y} = 0$ and that $l(y) \sim \kappa y + l_2 y^2/2 + O(y^3)$ for $y \ll 1$ holds.

We introduce dimensionless variables by referring the velocity to the center line velocity $\tilde{u}_c$, the shear stress to the double stagnation pressure $\tilde{\rho}\tilde{u}_c^2$, the unknown pressure gradient to $\tilde{\rho}\tilde{u}_c^2/\tilde{d}$.

We define

$$\gamma^2 = -\frac{\tilde{d}}{\tilde{\rho}\tilde{u}_c^2} \frac{d\tilde{p}}{d\tilde{x}} = \frac{\tilde{\tau}_w}{\tilde{\rho}\tilde{u}_c^2} = \frac{\tilde{u}_\tau^2}{\tilde{u}_c^2}, \quad \varepsilon = \frac{1}{Re} = \frac{\tilde{\mu}}{\tilde{\rho}\tilde{u}_c\tilde{d}}, \tag{54}$$

where we have made use of the force balance $-d\tilde{p}/d\tilde{x} = \tilde{\tau}_w/\tilde{d}$ for a fully developed flow and the definition of the wall shear stress velocity $\tilde{u}_\tau = \sqrt{\tilde{\tau}_w/\tilde{\rho}}$ with $\tilde{\tau}_w$ denoting the wall shear stress. The dimensionless equations reduce to the stress balance

$$0 = \gamma^2 + \frac{d\tau}{dy}, \tag{55}$$

and stress relation

$$\tau = \varepsilon \frac{du}{dy} + l(y)^2 \left(\frac{du}{dy} \right)^2, \tag{56}$$

subject to the boundary conditions

$$u(0) = 0, \quad u(1) = 1, \quad \tau(1) = 0. \tag{57}$$

Integration of the momentum balance yields

$$\tau(y) = \gamma^2(1 - y). \tag{58}$$

and it remains to solve the first order ordinary differential equation (56) for the velocity profile u and the dimensionless wall shear stress (or negative pressure gradient) γ^2.

4.1 Defect Layer

We expand the solution with respect to small values of ε (large Reynolds numbers). However, we also have to determine γ whose order of magnitude as a function of ε is not obvious. We anticipate that $\gamma = o(1)$ as $\varepsilon \to 0$. From the stress relation we deduce that $\mathrm{d}u/\mathrm{d}y = O(\gamma)$. Thus we expand u

$$u(y, \varepsilon) \sim u_0^{(D)}(y) + \gamma(\varepsilon)u_1^{(D)}(y) + \varepsilon u_2^{(D)}(y). \tag{59}$$

Inserting into the stress relation we obtain that $u_0^{(D)}$ is a constant. However, we have two contradicting boundary conditions to determine $u_0^{(D)}$. For the next order term $u_1^{(D)}$ we obtain from the stress relation

$$1 - y = l(y)^2 \left(\frac{\mathrm{d}u_1^{(D)}}{\mathrm{d}y} \right)^2. \tag{60}$$

Integration yields

$$u_1^{(D)}(y) = \frac{1}{\kappa} \ln y + F^{(D)}(y) + u_1^{(D)}(1), \tag{61}$$

where

$$F^{(D)}(y) = \int_1^y \left(\frac{\sqrt{1 - y'}}{l(y')} - \frac{1}{\kappa y'} \right) \mathrm{d}y' \tag{62}$$

is a smooth bounded function of y on the interval $(0, 1)$.

Now it is obvious to see that $u_1^{(D)}$ is smooth at the centerline $y = 1$ and thus $u_0^{(D)} = 1$ and $u_1^{(D)}(1) = 0$. The velocity profile deviates only by a small velocity defect of order γ from its maximum value at the center line. Therefore this layer is called defect layer. Near the wall $y = 0$ the velocity component $u_1^{(D)}(y)$ is singular. Its asymptotic behavior is given by

$$u_1^{(D)}(y) \sim \frac{1}{\kappa} \ln y + C_D - \frac{\kappa + l_2}{2\kappa^2} y, \quad \text{with} \quad C_D = F^{(D)}(0) \quad \text{as} \quad y \to 0. \tag{63}$$

For the term of order ε we obtain the equation

$$0 = \frac{du_1^{(D)}}{dy} + 2l^2(y)\frac{du_1^{(D)}}{dy}\frac{du_2^{(D)}}{dy}. \tag{64}$$

Integration yields

$$u_2^{(D)} = -\int_1^y \frac{dy}{2l^2(y)} \sim \frac{1}{2\kappa^2 y} + \frac{l_2}{2\kappa^3}\ln y + C_{D,2} + \cdots \tag{65}$$

with $l_2 = l''(0)$.

4.2 Viscous wall layer

At the wall $y = 0$ the no slip boundary condition cannot be satisfied by the defect expansion (59). Thus we introduce a local variable η

$$u = \gamma u_1^{(v)}(\eta) + \gamma\sigma u_2^{(v)}(\eta) + \cdots, \quad \eta = \frac{y}{\sigma(\varepsilon)} \tag{66}$$

with a stretching $\sigma(\varepsilon)$ which will be determined appropriately. Inserting yields

$$1 = \frac{du_1^{(v)}}{d\eta} + \kappa^2\eta^2\left(\frac{du_1^{(v)}}{d\eta}\right)^2, \quad u_1^{(v)}(0) = 0, \tag{67}$$

$$-\eta - 2l_2\kappa\eta^3\left(\frac{du_1^{(v)}}{d\eta}\right)^2 = \frac{du_2^{(v)}}{d\eta} + 2\kappa^2\eta^2\frac{du_1^{(v)}}{d\eta}\frac{du_2^{(v)}}{d\eta}, \quad u_2^{(v)}(0) = 0, \tag{68}$$

with $\sigma(\varepsilon)\gamma(\varepsilon) = \varepsilon$. Integration of (67) yields

$$u_1^{(v)}(\eta) = \frac{1}{\kappa}\ln\eta + \frac{1}{\kappa}\ln\left(2\kappa + \sqrt{4\kappa^2 + 1/\eta^2}\right). \tag{69}$$

In order to match the viscous layer to the defect layer we consider the asymptotic behavior of $u_1^{(v)}(\eta)$ and $u_2^{(v)}(\eta)$ for $\eta \to \infty$.

$$\frac{du_1^{(v)}}{d\eta} \sim \frac{1}{\kappa\eta} - \frac{1}{2\kappa^2\eta^2} + \frac{1}{8\kappa^3\eta^3} + \cdots, \tag{70a}$$

$$u_1^{(v)}(\eta) = \frac{1}{\kappa}\ln\eta + C_V + \frac{1}{2\kappa^2\eta} - \frac{1}{16\kappa^2\eta^2} + \cdots,$$

$$\text{with} \quad C_V = \frac{1}{\kappa}(\ln 4\kappa - 1) \tag{70b}$$

$$\frac{\mathrm{d}u_2^{(v)}}{\mathrm{d}\eta} = -\frac{-\eta - \kappa l''\eta^3 (\frac{\mathrm{d}u_1^{(v)}}{\mathrm{d}\eta})^2}{1 + 2\kappa^2\eta^2 \frac{\mathrm{d}u_1^{(v)}}{\mathrm{d}\eta}} \sim -\frac{1}{2\kappa} - \frac{l_2}{2\kappa^2} + \frac{l_2}{2\kappa^3\eta} - \frac{3l_2}{8\kappa^4\eta^2} \qquad (70c)$$

$$u_2^{(v)}(\eta) \sim -\left(\frac{1}{2\kappa} + \frac{l_2}{2\kappa^2}\right)\eta + C_{V,2} + \frac{l_2}{2\kappa^3}\ln\eta + \frac{3l_2}{16\kappa^4\eta}, \qquad (70d)$$

where $C_{V,2}$ is an appropriate constant.

4.3 Matching

Finally it remains to match the velocity profile of the viscous layer with that of the defect layer. Applying the matching principle we have to care when counting the number of terms in the asymptotic expansions. In Fraenkel (1969) it had been shown that the Van Dykes matching principle is still valid when the asymptotic expansion contain besides powers of the perturbation parameter products of powers of ε and and powers of $\ln\varepsilon$. Than all logarithmic term multiplied by the same power of ε have to be considered as one term.

In the present example it will turn out that $\gamma(\varepsilon) \sim O(1/\ln(1/\varepsilon))$. Thus the two term expansion of the defect layer is $1 + \gamma U_1^{(D)} + \varepsilon u_2^{(D)}$. Expanding it in the viscous layer variable into two terms and using $\gamma\sigma = \varepsilon$ we obtain

$$\left[[u]_D^{(2)}\right]_V^{(2)} = \left[1 + \gamma u_1^{(D)} + \varepsilon u_2^{(D)}\right]_V^{(2)} =$$

$$= 1 + \gamma\left(\frac{1}{\kappa}\ln\sigma + \frac{1}{\kappa}\ln\eta + C_D + \frac{1}{2\kappa^2}\frac{1}{\eta}\right) + \qquad (71)$$

$$+\varepsilon\left(C_{D,2} - \frac{\kappa + l_2}{2\kappa^2}\eta + \frac{l_2}{2\kappa^3}\ln\eta + \frac{l_2}{2\kappa^3}\ln\sigma\right).$$

Taking two terms of the inner (viscous)-layer expansion $\gamma u_1^{(v)} + \gamma\sigma u_2^{(v)}$, rewriting it in the outer variables and expanding it into two term yields

$$\left[[u]_V^{(2)}\right]_D^{(2)} = \left[\gamma u_1^{(v)} + \gamma\sigma u_2^{(v)}\right]_D^{(2)} =$$

$$= \gamma\left(\frac{1}{\kappa}\ln y + C_V - \frac{1}{\kappa}\ln\sigma - \frac{\kappa + l_2}{2\kappa^2}y\right) + \qquad (72)$$

$$+\gamma\sigma\left(C_{V,2} + \frac{l_2}{2\kappa^3}\ln y - \frac{\sigma}{2\kappa^3}\ln\sigma + \frac{1}{2\kappa^2 y}\right).$$

Both expressions agree if the matching condition

$$\frac{1}{\gamma} = -\frac{1}{\kappa} \ln \sigma + C_V - C_D - \sigma \left(\frac{l_2}{2\kappa^3} \ln \sigma + C_{D,2} - C_{V,2} \right) \qquad (73)$$

is satisfied. Taking only the first order terms of both expansions the well known friction law

$$\frac{1}{\gamma} = \frac{1}{\kappa} \ln \frac{\gamma}{\varepsilon} + C_V - C_D \qquad (74)$$

is obtained. It can be interpreted as a relation between the dimensionless wall shear stress γ^2 and the Reynolds number ε^{-1}.
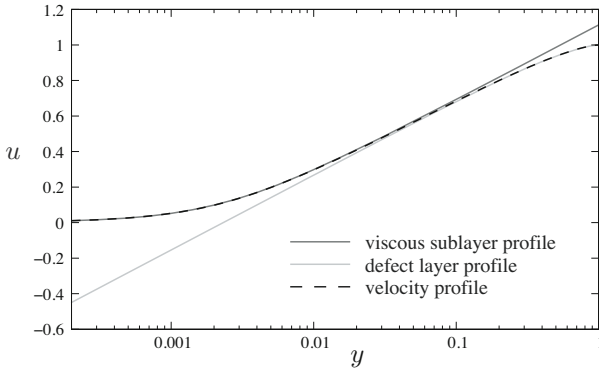
Figure 6. solution of model problem and viscous and defect layer approximation for $\varepsilon = 10^{-4}$

In figure 6 velocity profile as the solution of the force balance with the mixing length model (53) for $\varepsilon = 10^{-4}$, the approximation in the viscous sub-layer and the defect layer is shown in a logarithmic plot. It can be clearly seen that in the overlap region (here from 0.02 to 0.2) viscous and defect expansion agree. In the overlap region both expansions can be represented by a logarithmic velocity profile.

4.4   Turbulence asymptotics

Here we have considered a very simple turbulent shear flow and have made used of a simple turbulence model to reveal the asymptotic structure of flows near the wall. However, the weak point of this approach is the assumption of a turbulence model.

The traditional approach for the limit of large Reynolds numbers is that one considers the shear rate in the overlap region of the viscous and the

defect layer. From dimensional analysis one obtains

$$\frac{\tilde{y}}{\tilde{u}_\tau}\frac{\mathrm{d}\tilde{u}}{\mathrm{d}\tilde{y}} = \Phi(y, y_+), \quad \text{with} \quad y_+ = \frac{\tilde{y}\tilde{u}_\tau}{\tilde{\nu}}, \quad y = \frac{\tilde{y}}{\tilde{d}}. \tag{75}$$

Note that $y_+/y = \tilde{u}_\tau \tilde{d}/\tilde{\nu} = Re_\tau$. To get the behavior of Φ in the overlap region we have to consider the double limit $y_+ \to \infty, y \to 0$. Following von Karman (1930) we assume that this limit exists and its value is the reciprocal value of the von Karman constant,

$$\lim_{y_+ \to \infty, y \to 0} \Phi(y, y_+) = \Phi(\infty, 0) = \frac{1}{\kappa}. \tag{76}$$

Integration of (76) yields the logarithmic velocity profile in the overlap region. We emphasize that the existence of the limit (76) from a theoretical point of view is a nontrivial assumption (similarity of the first kind, see Barenblatt (1996). However, the logarithmic law, if interpreted correctly, is in excellent agreement with measured velocity profiles. Thus it can be considered as an empirical fact. On the other hand there are authors , e. g. Barenblatt (1996), who question the logarithmic law. Barenblatt (1996) considers that the limit (76) does not exist, but that the function Φ is a sophisticated power function of the Reynolds number (similarity of the second kind). Instead of the logarithmic velocity profile these authors obtain a power-law with an Reynolds-number dependent exponent. Although according to Barenblatt (1996) the power law seems to reproduce some data even better than the log-law it is a dead end from the asymptotic point of view since it does not comply with the requirements of a rational asymptotic expansion.

In modern papers concerning turbulence asymptotics the order of arguments is reversed, see Walker (1998), Kluwick and Scheichl (2009). Usually the dimensionless wall shear stress velocity $\gamma = u_\tau/U_{ref}$ is considered as a small perturbation parameter and the existence of a viscous sub-layer together with the log-law in the overlap region is postulated.

5   Conclusions

We have given an introduction to the method of matched asymptotic expansion by analyzing three different problems of fluid mechanics. Characteristic to all examples is the appearance of different length scales and that a uniformly valid asymptotic approximation can be constructed employing the matching principle.

Bibliography

G. I. Barenblatt. *Scaling, self-similarity and intermediate asymptotics.* Cambridge Univ. Press, 1996.

A. Betz. *Konforme Abbildungen.* Springer, 2nd edition, 1964.

L. E. Fraenkel. On the method of matched asymptotic expansions, part i: A matching principle. *Proc. Camb. Phil. Soc.*, 65:209–231, 1969.

S. Kaplun. In P.A. Lagerstrom, L. N. Howard, and C. S. Liu, editors, *Fluid Mechanics and Singular Perturbation.* Academic Press, 1967.

A. Kluwick and B. Scheichl. High-Reynolds-Number Asymptotics of Turbulent Boundary Layers: From Fully Attached to Marginally Separated Flows. In A. Hegarty, N. Kopteva, E. O'Riordan, and M. Stynes, editors, *BAIL 2008 - Boundary and Interior Layers*, volume 69 of *Lecture Notes in Computational Science and Engineering*, pages 3–22, 2009.

L. Prandtl. Über Flüssigkeitsbewegung bei sehr kleiner Reibung. In *Verhandl. d. III. Intern. Mathem. Kongresses, Heidelberg*, pages 484–491, 1904.

K. Schlichting, H. Gersten. *Boundary-layer theory.* Springer, 8th edition, 2000.

M. Ungarish. *Hydromechanics of Suspensions.* Springer, 1993.

M. Van Dyke. *Perturbation Methods in Fluid Mechanics.* The Parabolic Press, Stanford, annotated edition edition, 1975.

Th. von Karman. Mechanische Ähnlichkeit und Turbulenz. *Ges. Wiss. Göttingen, Math.-Phys. Kl.*, pages 58–76, 1930.

J. D. A. Walker. Turbulent boundary layers ii: Further developments. In A. Kluwick, editor, *Recent Advances in Boundary Layer Theory*, volume 390 of *CISM Courses and Lectures*, pages 145–230. Springer, 1998.

Asymptotic Methods For PDE Problems In Fluid Mechanics and Related Systems With Strong Localized Perturbations In Two-Dimensional Domains

Michael J. Ward[*‡] and Mary-Catherine Kropinski[†‡]

[*] Department of Mathematics University of British Columbia, Vancouver, B.C., Canada

[†] Department of Mathematics, Simon Fraser University, Burnaby, B.C., Canada

1 Introduction

The method of matched asymptotic expansions is a powerful systematic analytical method for asymptotically calculating solutions to singularly perturbed PDE problems. It has been successfully used in a wide variety of applications (cf. Kevorkian and Cole (1993), Lagerstrom (1988), Dyke (1975)). However, there are certain special classes of problems where this method has some apparent limitations.

In particular, for singular perturbation PDE problems leading to infinite logarithmic series in powers of $\nu = -1/\log\varepsilon$, where ε is a small positive parameter, it is well-known that this method may be of only limited practical use in approximating the exact solution accurately. This difficulty stems from the fact that $\nu \to 0$ very slowly as ε decreases. Therefore, unless many coefficients in the infinite logarithmic series can be obtained analytically, the resulting low order truncation of this series will typically not be very accurate unless ε is very small. Singular perturbation problems involving infinite logarithmic expansions arise in many areas of application in two-dimensional spatial domains including, low Reynolds number fluid flow past bodies of cylindrical cross-section, low Peclet number convection-diffusion problems with localized obstacles, and the calculation of the mean first passage time for Brownian motion in the presence of small traps, etc.

In this article we survey consider various singularly perturbed PDE problems in two-dimensional spatial domains where hybrid asymptotic-numerical methods have been formulated and implemented to effectively 'sum' infinite logarithmic expansions. Some of the problems considered herein directly relate to fluid mechanics, whereas other problems arise in different scientific

contexts. One primary goal of this chapter is to highlight how a common analytical framework can be used to treat a diverse class of problems having strong localized perturbations in two-dimensional domains.

2 Infinite Logarithmic Expansions: Simple Pipe Flow

We first consider the simple model problem of Titcombe and Ward (1999) to illustrate some main ideas for treating PDE problems with infinite logarithmic expansions. We consider steady, incompressible, laminar flow in a straight pipe containing a thin core. Both the pipe and the core have a constant cross-section of arbitrary shape, and thus the problem is two-dimensional. With these assumptions, the pipe flow is unidirectional and the velocity component w in the axial direction satisfies (cf. Ward-Smith (1980))

$$\triangle w = -\beta\,, \quad \mathbf{x} \in \Omega \backslash \Omega_\varepsilon\,, \tag{1a}$$

$$w = 0\,, \quad \mathbf{x} \in \partial\Omega\,, \tag{1b}$$

$$w = 0\,, \quad \mathbf{x} \in \partial\Omega_\varepsilon\,. \tag{1c}$$

Here $\Omega \in \mathbb{R}^2$ is the dimensionless pipe cross-section and Ω_ε is the cross-section of the thin core. We assume that Ω_ε has radius $\mathcal{O}(\varepsilon)$ and that $\Omega_\varepsilon \to \mathbf{x}_0$ uniformly as $\varepsilon \to 0$, where $\mathbf{x}_0 \in \Omega$. We denote the scaled subdomain that results from an $\mathcal{O}(\varepsilon^{-1})$ magnification of the length scale of Ω_ε by $\Omega_1 \equiv \varepsilon^{-1}\Omega_\varepsilon$. In (1a), β is defined in terms of the dynamic viscosity μ of the fluid and the constant pressure gradient dp/dz along the channel by $\beta \equiv -\mu^{-1}dp/dz$. In terms of w, the mean flow velocity $\bar{w}$ is defined by

$$\bar{w} \equiv \frac{1}{A_\Omega} \int_{\Omega \backslash \Omega_\varepsilon} w \, d\mathbf{x}\,. \tag{2}$$

Here A_Ω is the cross-sectional area of the pipe-core geometry. For laminar flow in pipes of non-circular cross-section, with or without cores, the friction coefficient f is expressed in terms of $\bar{w}$ by $f \equiv -L(dp/dz)/(2\rho\bar{w}^2)$ (cf. Ward-Smith (1980)). As a remark, the Reynolds number is defined by $\mathrm{Re} \equiv \bar{w}L\rho/\mu$, where ρ is the density of the fluid. Laminar flow occurs for Reynolds numbers in the approximate range $0 < \mathrm{Re} < 2000$. In the definition of Re, L is a characteristic diameter defined by $L = 4A_\Omega/P_\Omega$, where P_Ω is the wetted perimeter of the pipe and the core.

The asymptotic solution to (1) is constructed in two different regions: an outer region defined at an $\mathcal{O}(1)$ distance from the perturbing core, and an inner region defined in an $\mathcal{O}(\varepsilon)$ neighborhood of the thin core Ω_ε. The

analysis below will show how to calculate the sum of all the logarithmic terms for w in in the limit $\varepsilon \to 0$ of small core radius.

In the outer region we expand the solution to (1) as

$$w(\mathbf{x}; \varepsilon) = W_0(\mathbf{x}; \nu) + \sigma(\varepsilon)W_1(\mathbf{x}; \nu) + \cdots . \tag{3}$$

Here $\nu = \mathcal{O}(1/\log \varepsilon)$ is a gauge function to be chosen, and we assume that $\sigma \ll \nu^k$ for any $k > 0$ as $\varepsilon \to 0$. Thus, W_0 contains all of the logarithmic terms in the expansion. Substituting (3) into (1a) and (1b), and letting $\Omega_\varepsilon \to \mathbf{x}_0$ as $\varepsilon \to 0$, we get that W_0 satisfies

$$\triangle W_0 = -\beta , \quad \mathbf{x} \in \Omega \backslash \{\mathbf{x}_0\} , \tag{4a}$$

$$W_0 = 0 , \quad \mathbf{x} \in \partial\Omega , \tag{4b}$$

$$W_0 \quad \text{is singular as} \quad \mathbf{x} \to \mathbf{x}_0 . \tag{4c}$$

The matching of the outer and inner expansions will determine a singularity behavior for W_0 as $\mathbf{x} \to \mathbf{x}_0$.

In the inner region near Ω_ε we introduce the inner variables

$$\mathbf{y} = \varepsilon^{-1}(\mathbf{x} - \mathbf{x}_0) , \qquad v(\mathbf{y}; \varepsilon) = W(\mathbf{x}_0 + \varepsilon\mathbf{y}; \varepsilon) . \tag{5}$$

If we naively assume that $v = \mathcal{O}(1)$ in the inner region, we obtain the leading-order problem for v that $\triangle_{\mathbf{y}} v = 0$ outside Ω_1, with $v = 0$ on $\partial\Omega_1$ and $v \to W_0(\mathbf{x}_0)$ as $|\mathbf{y}| \to \infty$, where $\triangle_{\mathbf{y}}$ denotes the Laplacian in the $\mathbf{y}$ variable. This far-field condition as $|\mathbf{y}| \to \infty$ is obtained by matching v to the outer solution. However, in two-dimensions there is no solution to this problem since the Green's function for the Laplacian grows logarithmically at infinity. To overcome this difficulty, we require that $v = \mathcal{O}(\nu)$ in the inner region and we allow v to be logarithmically unbounded as $|\mathbf{y}| \to \infty$. Therefore, we expand v as

$$v(\mathbf{y}; \varepsilon) = V_0(\mathbf{y}; \nu) + \mu_0(\varepsilon)V_1(\mathbf{y}) + \cdots , \tag{6a}$$

where we write V_0 in the form

$$V_0(\mathbf{y}; \nu) = \nu\gamma v_c(\mathbf{y}) . \tag{6b}$$

Here $\gamma = \gamma(\nu)$ is a constant to be determined with $\gamma = \mathcal{O}(1)$ as $\nu \to 0$, and we assume that $\mu_0 \ll \nu^k$ for any $k > 0$ as $\varepsilon \to 0$. Substituting (5) and (6) into (1a) and (1c), and allowing $v_c(\mathbf{y})$ to grow logarithmically at infinity, we obtain that $v_c(\mathbf{y})$ satisfies

$$\triangle_{\mathbf{y}} v_c = 0 , \quad \mathbf{y} \notin \Omega_1 ; \qquad v_c = 0 , \quad \mathbf{y} \in \partial\Omega_1 , \tag{7a}$$

$$v_c \sim \log|\mathbf{y}| , \quad \text{as} \quad |\mathbf{y}| \to \infty . \tag{7b}$$

The unique solution to (7) has the following far-field asymptotic behavior:

$$v_c(\mathbf{y}) \sim \log|\mathbf{y}| - \log d + \frac{\mathbf{p} \cdot \mathbf{y}}{|\mathbf{y}|^2} + \cdots, \quad \text{as} \quad |\mathbf{y}| \to \infty. \qquad (7c)$$

The constant $d > 0$, called the logarithmic capacitance of Ω_1, depends on the shape of Ω_1 but not on its orientation. The vector $\mathbf{p}$ is called the dipole vector. Numerical values for d for different shapes of Ω_1 are given in Ransford (1995), and some of these are reproduced in Table 1. A boundary integral method to compute d for arbitrarily-shaped domains Ω_1 is described and implemented in Dijkstra and Hochstenbach (2008).

Table 1. The logarithmic capacitance, or shape-dependent parameter, d, for some cross-sectional shapes of $\Omega_1 = \varepsilon^{-1}\Omega_\varepsilon$.

Shape of $\Omega_1 \equiv \varepsilon^{-1}\Omega_\varepsilon$	Logarithmic Capacitance d
circle, radius a	$d = a$
ellipse, semi-axes a, b	$d = \frac{a+b}{2}$
equilateral triangle, side h	$d = \frac{\sqrt{3}\,\Gamma\left(\frac{1}{3}\right)^3 h}{8\pi^2} \approx 0.422h$
isosceles right triangle, short side h	$d = \frac{3^{3/4}\Gamma\left(\frac{1}{4}\right)^2 h}{2^{7/2}\pi^{3/2}} \approx 0.476h$
square, side h	$d = \frac{\Gamma\left(\frac{1}{4}\right)^2 h}{4\pi^{3/2}} \approx 0.5902h$

The leading-order matching condition between the inner and outer solutions will determine the constant γ in (6b). Upon writing (7c) in outer variables and substituting into (6b), we get the far-field behavior

$$v(\mathbf{y};\varepsilon) \sim \gamma\nu\left[\log|\mathbf{x} - \mathbf{x}_0| - \log(\varepsilon d)\right] + \cdots, \quad \text{as} \quad |\mathbf{y}| \to \infty. \qquad (8)$$

Choosing

$$\nu(\varepsilon) = -1/\log(\varepsilon d), \qquad (9)$$

and matching (8) to the outer expansion (3) for W, we obtain the singularity condition for W_0,

$$W_0 = \gamma + \gamma\nu\log|\mathbf{x} - \mathbf{x}_0| + o(1), \quad \text{as} \quad \mathbf{x} \to \mathbf{x}_0. \qquad (10)$$

The singularity behavior in (10) specifies both the regular and singular part of a Coulomb singularity. As such, it provides one constraint for the determination of γ. More specifically, the solution to (4) together with (10) must determine γ, since for a singularity condition of the form $W_0 \sim$

$S \log |\mathbf{x} - \mathbf{x}_0| + R$ for an elliptic equation, the constant R is not arbitrary but is determined as a function of S, $\mathbf{x}_0$, and Ω.

The solution for W_0 is decomposed as

$$W_0(\mathbf{x}; \nu) = W_{0H}(\mathbf{x}) - 2\pi\gamma\nu G_d(\mathbf{x}; \mathbf{x}_0) \,. \tag{11}$$

Here $W_{0H}(\mathbf{x})$ is the smooth function satisfying the unperturbed problem

$$\triangle W_{0H} = -\beta \,, \quad \mathbf{x} \in \Omega \,; \qquad W_{0H} = 0 \,, \quad \mathbf{x} \in \partial\Omega \,. \tag{12}$$

In (11), $G_d(\mathbf{x}; \mathbf{x}_0)$ is the Dirichlet Green's function satisfying

$$\triangle G_d = -\delta(\mathbf{x} - \mathbf{x}_0) \,, \quad \mathbf{x} \in \Omega \,; \qquad G_d = 0 \,, \quad \mathbf{x} \in \partial\Omega \,, \tag{13a}$$

$$G_d(\mathbf{x}; \mathbf{x}_0) = -\frac{1}{2\pi} \log |\mathbf{x} - \mathbf{x}_0| + R_d(\mathbf{x}_0; \mathbf{x}_0) + o(1) \,, \quad \text{as} \quad \mathbf{x} \to \mathbf{x}_0 \,. \tag{13b}$$

Here $R_{d00} \equiv R_d(\mathbf{x}_0; \mathbf{x}_0)$ is the regular part of the Dirichlet Green's function $G_d(\mathbf{x}; \mathbf{x}_0)$ at $\mathbf{x} = \mathbf{x}_0$. This regular part is also known as either the self-interaction term or the Robin constant (cf. Bandle and Flucher (1996)).

Upon substituting (13b) into (11) and letting $\mathbf{x} \to \mathbf{x}_0$, we compare the resulting expression with (10) to obtain that γ is given by

$$\gamma = \frac{W_{0H}(\mathbf{x}_0)}{1 + 2\pi\nu R_{d00}} \,. \tag{14}$$

Therefore, for this problem, γ is determined as the sum of a geometric series in ν. The range of validity of (14) is limited to values of ε for which $2\pi\nu |R_{d00}| < 1$. This yields,

$$0 < \varepsilon < \varepsilon_c \,, \qquad \varepsilon_c \equiv \frac{1}{d} \exp\left[2\pi R_{d00}\right] \,. \tag{15}$$

We summarize our result as follows:
Principal Result 1: For $\varepsilon \ll 1$, the outer expansion for (1) is

$$w \sim W_0(\mathbf{x}; \nu) = W_{0H}(\mathbf{x}) - \frac{2\pi\nu W_{0H}(\mathbf{x}_0)}{1 + 2\pi\nu R_{d00}} G_d(\mathbf{x}; \mathbf{x}_0) \,, \quad \text{for} \quad |\mathbf{x} - \mathbf{x}_0| = \mathcal{O}(1) \,, \tag{16a}$$

and the inner expansion with $\mathbf{y} = \varepsilon^{-1}(\mathbf{x} - \mathbf{x}_0)$ _is_

$$w \sim V_0(\mathbf{y}; \nu) = \frac{\nu W_{0H}(\mathbf{x}_0)}{1 + 2\pi\nu R_{d00}} v_c(\mathbf{y}) \,, \quad \text{for} \quad |\mathbf{x} - \mathbf{x}_0| = \mathcal{O}(\varepsilon) \,. \tag{16b}$$

Here $\nu = -1/\log(\varepsilon d)$, _d is defined in (7c), $v_c(\mathbf{y})$ satisfies (7), and W_{0H} satisfies the unperturbed problem (12). Also $G_d(\mathbf{x}; \mathbf{x}_0)$ and $R_{d00} \equiv R_d(\mathbf{x}_0; \mathbf{x}_0)$ are the Dirichlet Green's function and its regular part satisfying (13)._

This formulation is referred to as a hybrid asymptotic-numerical method since it uses the asymptotic analysis as a means of reducing the original problem (1) with a hole to the simpler asymptotically related problem (4) with singularity behavior (10). This related problem does not have a boundary layer structure and so is easy to solve numerically. The numerics required for the hybrid problem involve the computation of the unperturbed solution W_{0H} and the Dirichlet Green's function $G_d(\mathbf{x}; \mathbf{x}_0)$. In terms of G_d we then identify its regular part $R_d(\mathbf{x}_0; \mathbf{x}_0)$ at the singular point. From the solution to the canonical inner problem (7) we then compute the logarithmic capacitance, d. The result (16a) then shows that the asymptotic solution only depends on the product of εd and not on ε itself. This feature allows for an asymptotic equivalence between holes of different cross-sectional shape, based on an effective 'radius' of the cylinder. This equivalence is known as Kaplun's equivalence principle (cf. Kaplun (1957), Kropinski et al. (1995)).

An advantage of the hybrid method over the traditional method of matched asymptotic expansions is that the hybrid formulation is able to sum the infinite logarithmic series and thereby provide an accurate approximate solution. From another viewpoint, the hybrid problem is much easier to solve numerically than the full singularly perturbed problem (1). For the hybrid method a change of the shape of Ω_1 requires us to only re-calculate the constant d. This simplification does not occur in a full numerical approach.

We now outline how Principal Result 1 can be obtained by a direct summation of a conventional infinite-order logarithmic expansion for the outer solution given in the form

$$W \sim W_{0H}(\mathbf{x}) + \sum_{j=1}^{\infty} \nu^j W_{0j}(\mathbf{x}) + \mu_0(\varepsilon) W_1 + \cdots, \qquad (17)$$

with $\mu_0(\varepsilon) \ll \nu^k$ for any $k > 0$. By formulating a similar series for the inner solution, we will derive a recursive set of problems for the W_{0j} for $j \geq 0$ from the asymptotic matching of the inner and outer solutions. We will then sum this series to re-derive the result in Principal Result 1.

In the outer region we expand the solution to (1) as in (17). In (17), $\nu = \mathcal{O}(1/\log \varepsilon)$ is a gauge function to be chosen, while the smooth function W_{0H} satisfies the unperturbed problem (12) in the unperturbed domain. By substituting (17) into (1a) and (1b), and letting $\Omega_\varepsilon \to \mathbf{x}_0$ as $\varepsilon \to 0$, we

get that W_{0j} for $j \geq 1$ satisfies

$$\triangle W_{0j} = 0, \quad \mathbf{x} \in \Omega\backslash\{\mathbf{x}_0\}, \tag{18a}$$

$$W_{0j} = 0, \quad \mathbf{x} \in \partial\Omega, \tag{18b}$$

$$W_{0j} \quad \text{is singular as} \quad \mathbf{x} \to \mathbf{x}_0. \tag{18c}$$

The matching of the outer and inner expansions will determine a singularity behavior for W_{0j} as $\mathbf{x} \to \mathbf{x}_0$ for each $j \geq 1$.

In the inner region near Ω_ε we introduce the inner variables

$$\mathbf{y} = \varepsilon^{-1}(\mathbf{x} - \mathbf{x}_0), \qquad v(\mathbf{y}; \varepsilon) = W(\mathbf{x}_0 + \varepsilon\mathbf{y}; \varepsilon). \tag{19}$$

We then pose the explicit infinite-order logarithmic inner expansion

$$v(\mathbf{y}; \varepsilon) = \sum_{j=0}^{\infty} \gamma_j \nu^{j+1} v_c(\mathbf{y}). \tag{20}$$

Here γ_j are ε-independent coefficients to be determined. Substituting (20) and (1a) and (1c), and allowing $v_c(\mathbf{y})$ to grow logarithmically at infinity, we obtain that $v_c(\mathbf{y})$ satisfies (7) with far-field behavior (7c).

Upon using the far-field behavior (7c) in (20), and writing the resulting expression in terms of the outer variable $\mathbf{x} - \mathbf{x}_0 = \varepsilon\mathbf{y}$, we obtain that

$$v \sim \gamma_0 + \sum_{j=1}^{\infty} \nu^j \left[\gamma_{j-1} \log|\mathbf{x} - \mathbf{x}_0| + \gamma_j\right]. \tag{21}$$

The matching condition between the infinite-order outer expansion (17) as $\mathbf{x} \to \mathbf{x}_0$ and the far-field behavior (21) of the inner expansion is that

$$W_{0H}(\mathbf{x}_0) + \sum_{j=1}^{\infty} \nu^j W_{0j}(\mathbf{x}) \sim \gamma_0 + \sum_{j=1}^{\infty} \nu^j \left[\gamma_{j-1} \log|\mathbf{x} - \mathbf{x}_0| + \gamma_j\right]. \tag{22}$$

The leading-order match yields that

$$\gamma_0 = W_{0H}(\mathbf{x}_0). \tag{23}$$

The higher-order matching condition, from (22), shows that the solution W_{0j} to (18) must have the singularity behavior

$$W_{0j} \sim \gamma_{j-1} \log|\mathbf{x} - \mathbf{x}_0| + \gamma_j, \quad \text{as} \quad \mathbf{x} \to \mathbf{x}_0. \tag{24}$$

The unknown coefficients γ_j for $j \geq 1$, starting with $\gamma_0 = W_{0H}(\mathbf{x}_0)$, are determined recursively from the infinite sequence of problems (18) and (24)

for $j \geq 1$. The explicit solution to (18) with $W_{0j} \sim \gamma_{j-1} \log |\mathbf{x} - \mathbf{x}_0|$ as $\mathbf{x} \to \mathbf{x}_0$ is given explicitly in terms of $G_d(\mathbf{x}; \mathbf{x}_0)$ of (13) as

$$W_{0j}(\mathbf{x}) = -2\pi\gamma_{j-1} G_d(\mathbf{x}; \mathbf{x}_0). \tag{25}$$

Next, we expand (25) as $\mathbf{x} \to \mathbf{x}_0$ and compare it with the required singularity structure (24). This yields

$$-2\pi\gamma_{j-1} \left[-\frac{1}{2\pi} \log |\mathbf{x} - \mathbf{x}_0| + R_{d00} \right] \sim \gamma_{j-1} \log |\mathbf{x} - \mathbf{x}_0| + \gamma_j, \tag{26}$$

where $R_{d00} \equiv R_d(\mathbf{x}_0; \mathbf{x}_0)$. By comparing the non-singular parts of (26), we obtain a recursion relation for the γ_j, valid for $j \geq 1$, given by

$$\gamma_j = (-2\pi R_{d00}) \gamma_{j-1}, \qquad \gamma_0 = W_{0H}(\mathbf{x}_0), \tag{27}$$

which has the explicit solution

$$\gamma_j = [-2\pi R_{d00}]^j W_{0H}(\mathbf{x}_0), \quad j \geq 0. \tag{28}$$

Finally, to obtain the outer solution we substitute (25) and (28) into (17) to obtain

$$w - W_{0H}(\mathbf{x}) \sim \sum_{j=1}^{\infty} \nu^j (-2\pi\gamma_{j-1}) G_d(\mathbf{x}; \mathbf{x}_0) = -2\pi\nu G_d(\mathbf{x}; \mathbf{x}_0) \sum_{j=0}^{\infty} \nu^j \gamma_j$$

$$\sim -2\pi\nu W_{0H}(\mathbf{x}_0) G_d(\mathbf{x}; \mathbf{x}_0) \sum_{j=0}^{\infty} [-2\pi\nu R_{d00}]^j$$

$$\sim -\frac{2\pi\nu W_{0H}(\mathbf{x}_0)}{1 + 2\pi\nu R_{d00}} G_d(\mathbf{x}_0; \mathbf{x}_0). \tag{29a}$$

Equation (29a) agrees with equation (16a) of Principal Result 1. Similarly, upon substituting (28) into the infinite-order inner expansion (20), we obtain

$$v(\mathbf{y}; \varepsilon) = \nu W_{0H}(\mathbf{x}_0) v_c(\mathbf{y}) \sum_{j=0}^{\infty} [-2\pi R_{d00}\nu]^j = \frac{\nu W_{0H}(\mathbf{x}_0)}{1 + 2\pi\nu R_{d00}} v_c(\mathbf{y}), \tag{30}$$

which recovers equation (16b) of Principal Result 1.

Next, we compare the results of the hybrid method with results obtained either analytically or numerically from the full perturbed problem (1).

We consider flow in a circular pipe Ω of cross-sectional radius r_0 that contains a concentric core Ω_ε of various cross-sectional shapes centered at the origin. We use Table 1 for the logarithmic capacitance d for a square

core, an elliptical core, and an equilateral triangular core. Using the notation in the table, we set the major and minor semi-axes of the ellipse as $a = 2$ and $b = 1$, and both the side of the square and the equilateral triangle as $h = 1$. To compute the hybrid method solution, we readily calculate that the Green's function is $G_d = -(2\pi)^{-1} \log(r/r_0)$ and that the unperturbed solution is $W_{0H} = \beta(r_0^2 - r^2)/4$. The outer hybrid method solution, as obtained from (16a) of Principal Result 1, is simply

$$w(\mathbf{x}; \varepsilon) = \frac{\beta}{4} \left[r_0^2 - r^2 - r_0^2 \frac{\log(r_0/r)}{\log(r_0/[\varepsilon d])} \right] , \qquad r = |\mathbf{x}| . \qquad (31)$$

From (31), we can compute the asymptotic mean flow rate using (2).
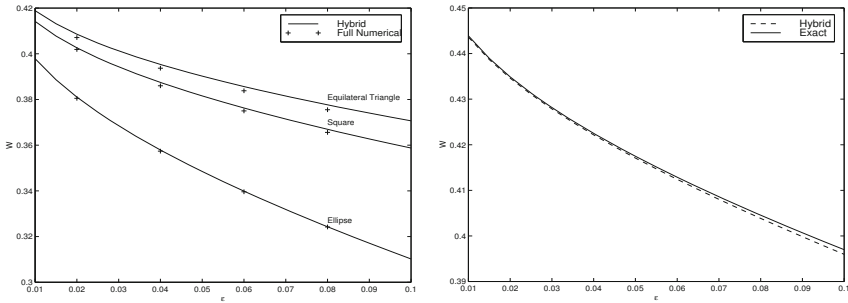
(a) Concentric Geometry: $\bar{w}$ vs. ε (b) Eccentric Geometry: $\bar{w}$ vs. ε

Figure 1. The mean flow velocity $\bar{w}$ versus the cross-sectional 'radius' of an inner core pipe located inside a circular pipe of cross-sectional radius $r_0 = 2$. Left figure: (Concentric annulus geometry). Plots of $\bar{w}$ vs. ε for three different cross-sectional shapes of the inner core pipe. The discrete points are the full numerical results. Right figure (Eccentric Geometry). Plots of $\bar{w}$ versus the circular pipe core cross-sectional radius ε when the inner pipe is centered at $\mathbf{x}_0 = (-1, 0)$. The hybrid and exact results are the dotted and solid curves, respectively.

To validate the asymptotic results for $\bar{w}$, we compare them with corresponding direct numerical results computed from the full problem (1) using the *PDE Toolbox* of MATLAB (1996). For a circular pipe of radius $r_0 = 2$ containing a concentric core and with $\beta = 1$, Fig. 1(a) contains curves of mean flow velocity, $\bar{w}$, versus ε, a measure of the size of the core, for three

different cross-sectional shapes of the core. In the hybrid method solution, the change in shape and size of the core requires only that we vary the product εd, which allows us to compute the entire ε curve very easily. In contrast, for each change of shape and size of the core in the direct numerical solution, we had to re-create the solution geometry and re-mesh the solution grid when using the *PDE Toolbox* of MATLAB (1996). For a core of elliptic cross-section, the figure shows that the hybrid method results agree very well with those of the direct numerical solution. The slight discrepancy in comparing the results for the other two core cross-sectional shapes, the square and equilateral triangle, could be due to the inability of the numerical method to resolve the non-smooth boundary of the core.

Next, we consider flow in a circular pipe Ω of radius $r_0 > 1$ that contains a circular core Ω_ε of radius ε centered at $\mathbf{x}_0 = (-1, 0)$. For this case, the exact mean flow velocity $\bar{w}_E$ for this eccentric annulus geometry can be written as a complicated infinite series as in Ward-Smith (1980). In contrast, we need only calculate three specific quantities for our hybrid formulation in (16). Firstly, the unperturbed solution is again given by $W_{0H}(r) = \beta(r_0^2 - r^2)/4$. Next, since the inner core cross-section is a circle of radius ε, then the logarithmic capacitance is $d = 1$, so that $\nu = -1/\log\varepsilon$. Finally, using the method of images, we solve (13) analytically to obtain the Green's function

$$G_d(\mathbf{x}; \mathbf{x}_0) = -\frac{1}{2\pi} \log\left(\frac{|\mathbf{x} - \mathbf{x}_0| r_0}{|\mathbf{x} - \mathbf{x}_0'||\mathbf{x}_0|} \right). \tag{32}$$

Here the image point $\mathbf{x}_0'$ of $\mathbf{x}_0$ in the circle of radius r_0 lies along the ray containing $\mathbf{x}_0$ and satisfies $|\mathbf{x}_0'||\mathbf{x}_0| = r_0^2$. Comparing (32) with (13b), we can then calculate the self-interaction term as

$$R_{d00} \equiv R_d(\mathbf{x}_0; \mathbf{x}_0) = -\frac{1}{2\pi} \log\left[\frac{r_0}{|\mathbf{x}_0 - \mathbf{x}_0'||\mathbf{x}_0|} \right]. \tag{33}$$

Substituting (32), (33), $\nu = -1/\log\varepsilon$, and $W_{0H}(r)$, into (16a) we obtain the outer solution for the hybrid method. This solution is then used in (2) with $A_\Omega \sim \pi r_0^2$ to compute the mean flow velocity for the hybrid method. The integral in (2) is obtained from a numerical quadrature. For an eccentric annulus with pipe radius $r_0 = 2$, and with $\beta = 1$, in Fig. 1(b) we plot the mean flow velocity $\bar{w}$ versus the circular core radius ε as obtained from the exact solution and from the hybrid solution. This plot shows that the hybrid method results compare rather well with the exact results.

We remark that for an inner pipe core of an arbitrary shape centered at $\mathbf{x}_0 = (-1, 0)$, the hybrid method solution as obtained above for the eccentric annulus still applies, provided that we replace $\nu = -1/\log\varepsilon$ in (16a) with

$\nu = -1/\log(\varepsilon d)$, where d is to be computed from (7). In particular, if there is an ellipse with semi-axes ε and 2ε centered at $\mathbf{x}_0 = (-1, 0)$ instead of the circle of radius ε, then from Table 1 we get $d = 3/2$. Hence, the plot in Fig. 1(b) for the hybrid solution still applies provided that we replace the horizontal axis in this figure by $3\varepsilon/2$.

3 Some Related Steady-State Problems in Bounded Singularly Perturbed Domains

In this section we extend the analysis of §2 to treat some related steady-state problems. The problem in 3.1, which concerns the distribution of oxygen partial pressure in muscle tissue, involves multiple inclusions in a two-dimensional domain. In §3.2 we show how to extend the method of §2 to a nonlinear problem.

3.1 Oxygen Transport From Capillaries to Skeletal Muscle

The analytical study of tissue oxygenation from capillaries dates from the original work of Krogh (1919). In the oxygen distribution process of the micro-circulation, oxygen binds to its carrier, haemoglobin, in red blood cells, which transports it through the arterioles, branching to the capillary networks, to the collecting venules. In the capillaries, the oxygen is released from its carrier and diffuses into the surrounding tissue. The reviews of Popel (1989), Fletcher (1978), and the references in Titcombe and Ward (2000), provide substantial information on theoretical research in this area.
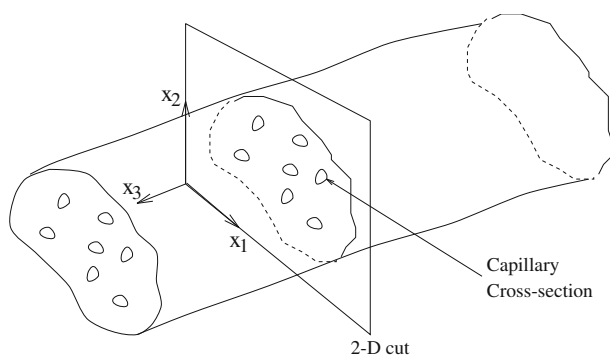
Figure 2. Mathematical idealization of capillary blood supply in skeletal muscle tissue

In this section, we show how to determine the steady-state oxygen partial pressure distribution in a two-dimensional domain representing a transverse section of skeletal muscle tissue that receives oxygen from an array of capillaries of small but arbitrary cross-sectional shape (see Fig. 2). Following the approach of many authors (e.g. Popel (1989)), we model the transport of oxygen from capillaries to tissue by a passive diffusive process. Assuming Fick's law, $J = -D\nabla c$, relating the oxygen flux J to the gradient of oxygen concentration c, and Henry's law, $c = \alpha p$ the dimensionless steady-state oxygen partial pressure p satisfies

$$\triangle p = \mathcal{M}, \quad \mathbf{x} \in \Omega \backslash \Omega_p \qquad \Omega_p \equiv \overset{N}{\underset{j=1}{\cup}} \Omega_{\varepsilon_j}, \qquad (34a)$$

$$\partial_n p = 0, \quad \mathbf{x} \in \partial\Omega. \qquad (34b)$$

$$\varepsilon \partial_n p + \kappa_j (p - p_{cj}) = 0, \quad \mathbf{x} \in \partial\Omega_{\varepsilon_j}, \quad j = 1, \dots, N. \qquad (34c)$$

The condition (34c) models the capillary wall as a finitely permeable membrane, where $\kappa_i > 0$ is the permeability coefficient of the ith capillary and p_{ci} is the oxygen partial pressure within the ith capillary (assumed constant). In (34c) and (34b), ∂_n is the outward normal derivative to the tissue domain. In deriving (34) we have assumed that the oxygen diffusivity is spatially constant, and so the oxygen consumption rate $\mathcal{M}$ has been normalized by this constant value. To incorporate skeletal muscle tissue heterogeneities, such as localized oxygen-consuming mitochondria, we assume that $\mathcal{M}$ is spatially-dependent and has the form

$$\mathcal{M}(\mathbf{x}) = \mathcal{M}_0 + \sum_{i=1}^{m} \mathcal{M}_i \exp\left(-\frac{|\mathbf{x} - \mathbf{x}_i|^2}{\sigma_i^2}\right), \qquad (35)$$

for some positive constants $\mathcal{M}_0$ and $\mathcal{M}_i$ for $i = 1, \dots, m$.

The model (34) is an extension of the well-known Krogh cylinder model Krogh (1919), which consists of one capillary of circular cross-section concentric with a circular cross-section of muscle tissue. For this concentric annulus geometry $\varepsilon < |\mathbf{x}| < 1$, the exact radially symmetric solution p_e is

$$p_e(r) = p_{c1} + \frac{\mathcal{M}}{2} \left[\frac{r^2 - \varepsilon^2}{2} + \frac{\varepsilon^2 - 1}{\kappa_1} + \log\left(\frac{\varepsilon}{r}\right) \right]. \qquad (36)$$

This shows that $p_e = \mathcal{O}(\log \varepsilon)$ as $\varepsilon \to 0$, as induced by the Neumann boundary condition in (34b) on the boundary of the cross-section. In the extended model (34), formulated originally in Titcombe and Ward (2000), one allows for multiple capillaries of arbitrary location, of arbitrary cross-sectional shape, and for the tissue domain to be arbitrary.

Most previous attempts to study the oxygenation of muscle tissue analytically have assumed that the capillaries can be represented as point sources for (34). However, by using the method of matched asymptotic expansions, we show that this type of rough simplification represents only the leading-order term in an infinite asymptotic expansion of the oxygen partial pressure in powers of $-1/\log\varepsilon$, where ε is a measure of the capillary cross-section. From a physiological viewpoint, this type of point-source approximation ignores the effect of the shape of the capillary cross-section and the effect of the interaction between the capillaries. When many capillaries are present, the effect of the capillary interaction should be significant.

Our goal here is to extend the hybrid method of §2 to calculate the asymptotic solution to (34) with an error that is smaller than any power of $-1/\log\varepsilon$. Such an approach, which effectively sums the infinite logarithmic series, takes into account the effect of the capillary interaction.

In the outer region we expand the solution to (34) as

$$p(\mathbf{x};\varepsilon) = P_0(\mathbf{x};\nu_1,\ldots,\nu_N) + \sigma(\varepsilon)P_1(\mathbf{x};\nu_1,\ldots,\nu_N) + \cdots. \qquad (37)$$

Here $\nu_j = \mathcal{O}(1/\log\varepsilon)$ for $j = 1,\ldots,N$ are gauge functions to be chosen, and we assume that $\sigma \ll \nu_j^k$ for any $k > 0$ as $\varepsilon \to 0$. Thus, P_0 contains all of the logarithmic terms in the expansion. Substituting (37) into (34a) and (34b), and letting $\Omega_{\varepsilon_j} \to \mathbf{x}_j$ as $\varepsilon \to 0$, we get that P_0 satisfies

$$\triangle P_0 = \mathcal{M}, \quad \mathbf{x} \in \Omega\backslash\{\mathbf{x}_1,\ldots,\mathbf{x}_N\}, \qquad (38a)$$

$$\partial_n P_0 = 0, \quad \mathbf{x} \in \partial\Omega, \qquad (38b)$$

$$P_0 \quad \text{is singular as } \mathbf{x} \to \mathbf{x}_j. \qquad (38c)$$

The matching of the outer and inner expansions will determine singularity behaviors for P_0 as $\mathbf{x} \to \mathbf{x}_j$ for $j = 1,\ldots,N$.

In the inner region near the jth capillary Ω_{ε_j} we introduce the inner variables

$$\mathbf{y} = \varepsilon^{-1}(\mathbf{x} - \mathbf{x}_j), \qquad p(\mathbf{y};\varepsilon) = q_j(\mathbf{x}_j + \varepsilon\mathbf{y};\varepsilon), \qquad (39)$$

together with the local expansion

$$q_j = p_{cj} + q_{0j}(\mathbf{y};\nu_1,\ldots,\nu_N) + \mu q_{1j}(\mathbf{y};\nu_1,\ldots,\nu_N) + \cdots. \qquad (40)$$

Here we assume that $\mu \ll \nu_j^k$ for any $k > 0$. We then write q_{0j} in the form

$$q_{0j} = A_j q_{cj}(\mathbf{y}), \qquad (41)$$

where $A_j = A_j(\nu_1,\ldots,\nu_N)$ is an unknown constant to be determined, and $q_{cj}(\mathbf{y}) \sim \log|\mathbf{y}|$ as $\mathbf{y} \to \infty$. By substituting (39), (40), and (41), into (34a)

and (34c), we readily derive that q_{cj} is the solution to

$$\triangle_{\mathbf{y}} q_{cj} = 0, \quad \mathbf{y} \notin \Omega_j; \qquad \partial_n q_{cj} + \kappa_j q_c = 0, \quad \mathbf{y} \in \partial\Omega_j, \qquad (42\text{a})$$

$$q_{cj} \sim \log|\mathbf{y}|, \quad \text{as} \quad |\mathbf{y}| \to \infty, \qquad (42\text{b})$$

where $\Omega_j \equiv \varepsilon^{-1}\Omega_{\varepsilon_j}$. The unique solution to (42) has the following far-field asymptotic behavior:

$$q_{cj}(\mathbf{y}) \sim \log|\mathbf{y}| - \log d_j + \mathcal{O}\left(\frac{1}{|\mathbf{y}|}\right), \quad |\mathbf{y}| \gg 1. \qquad (42\text{c})$$

In comparing (42) with (7) for the pipe problem of §2, we observe that here $d_j = d_j(\kappa_j)$. For a particular cross-sectional shape of the capillary and for a given value of κ_j, one must compute $d_j = d_j(\kappa_j)$ numerically from a boundary integral method applied to (42). For a circular capillary of radius ε, for which q_{cj} can be found analytically, we readily calculate that

$$d_j = \exp\left(-1/\kappa_j\right). \qquad (43)$$

Moreover, by comparing (6b) with (41) we observe that here we have introduced a slight change in the definition of the inner solution. In the analysis below, we will show that $A_j = \mathcal{O}(1)$ as $\varepsilon \to 0$ in (41), which is a direct consequence of the Neumann boundary condition in (34b).

By using (40) and (42c), we re-write the far-field form for $|\mathbf{y}| \gg 1$ of the inner solution in terms of the outer variables as

$$q_j \sim p_{cj} + A_j \log|\mathbf{x} - \mathbf{x}_j| + \frac{A_j}{\nu_j}. \qquad (44\text{a})$$

Here we have introduced the logarithmic gauge function ν_j by

$$\nu_j \equiv -\frac{1}{\log(\varepsilon d_j)}. \qquad (44\text{b})$$

The matching condition is that the far-field form (44a) of the inner solution must agree with the near-field behavior of the outer solution for p. Thus, P_0 satisfies (38) subject to the following singularity behavior

$$P_0 \sim p_{cj} + A_j \log|\mathbf{x} - \mathbf{x}_j| + \frac{A_j}{\nu_j}, \quad \text{as} \quad \mathbf{x} \to \mathbf{x}_j, \quad j = 1, \ldots, N. \qquad (45)$$

As remarked in §2, we emphasize that the singularity behavior in (45) specifies both the regular and singular part of a Coulomb singularity at each $\mathbf{x}_j$. As such, the singularity behaviors (45) for $j = 1, \ldots, N$ will

provide N equations for the determination of the unknown constants A_j for $j = 1, \ldots, N$. By using the divergence theorem, it readily follows that (38), together with (45), has a solution if and only if

$$\sum_{j=1}^{N} A_j = -\frac{1}{2\pi} \int_{\Omega} \mathcal{M}(\mathbf{x}) \, d\mathbf{x} \,. \tag{46}$$

This provides one equation for the determination of A_j for $j = 1, \ldots, N$, and shows that $A_j = \mathcal{O}(1)$ as $\varepsilon \to 0$.

Next, we decompose the solution to (38) and (45) in the form

$$P_0 = P_R(\mathbf{x}) - 2\pi \sum_{i=1}^{N} A_i G_N(\mathbf{x}; \mathbf{x}_i) + \chi \,. \tag{47}$$

Here χ is an unknown constant, and $P_R(\mathbf{x})$ is the unique solution of

$$\triangle P_R = \mathcal{M} - \frac{1}{|\Omega|} \int_{\Omega} \mathcal{M}(\mathbf{x}) \, d\mathbf{x} \,, \quad \mathbf{x} \in \Omega \,; \quad \partial_n P_R = 0 \,, \quad \mathbf{x} \in \partial\Omega \,, \tag{48}$$

with $\int_{\Omega} P_R(\mathbf{x}) \, d\mathbf{x} = 0$. Here $|\Omega|$ denotes the area of Ω. When $\mathcal{M}$ is a spatially independent, then $P_R = 0$ for each $\mathbf{x} \in \Omega$. In (47), $G_N(\mathbf{x}; \boldsymbol{\xi})$ is the Neumann Green's function, defined as the solution to

$$\Delta G_N = \frac{1}{|\Omega|} - \delta(\mathbf{x} - \boldsymbol{\xi}) \,, \quad \mathbf{x} \in \Omega \,; \quad \partial_n G_N = 0 \,, \quad \mathbf{x} \in \partial\Omega \,, \tag{49a}$$

$$G_N(\mathbf{x}; \boldsymbol{\xi}) \sim -\frac{1}{2\pi} \log |\mathbf{x} - \boldsymbol{\xi}| + R_N(\boldsymbol{\xi}; \boldsymbol{\xi}) + o(1) \,, \quad \text{as} \quad \mathbf{x} \to \boldsymbol{\xi} \,, \tag{49b}$$

with $\int_{\Omega} G_N(\mathbf{x}; \boldsymbol{\xi}) \, d\mathbf{x} = 0$. The constant $R_N(\boldsymbol{\xi}; \boldsymbol{\xi})$ is called either the self-interaction term or the regular part of G_N. Since G_N and P_R have zero spatial averages, then χ in (47) is the spatial average of P_0.

Finally, we expand the solution (47) as $\mathbf{x} \to \mathbf{x}_j$ and we compare the regular part of the resulting expression with the regular part of the required singularity structure in (45). In this way, we obtain N algebraic equations for the unknowns χ and $A_1, \ldots, A_N$:

$$P_R(\mathbf{x}_j) - 2\pi \left[A_j R_{Njj} + \sum_{\substack{i=1 \\ i \neq j}}^{N} A_i G_{Nji} \right] + \chi = \frac{A_j}{\nu_j} + p_{cj} \,, \quad j = 1, \ldots, N \,. \tag{50}$$

Here we have defined $R_{Njj} \equiv R_N(\mathbf{x}_j; \mathbf{x}_j)$ and $G_{Nji} \equiv G_N(\mathbf{x}_j; \mathbf{x}_i)$. The remaining equation relating these unknowns is (46). We summarize our asymptotic construction as follows:

Principal Result 2: For $\varepsilon \to 0$, the asymptotic solution to (34) near the jth capillary, is

$$p \sim p_{cj} + A_j q_{cj}(\mathbf{y}), \qquad \mathbf{y} = \varepsilon^{-1}(\mathbf{x} - \mathbf{x}_j) = \mathcal{O}(1), \qquad (51a)$$

where q_{cj} satisfies (42). In the outer region, defined at $\mathcal{O}(1)$ distances from the centers of the capillaries, we have

$$p \sim P_R(\mathbf{x}) - 2\pi \sum_{i=1}^{N} A_i G_N(\mathbf{x}; \mathbf{x}_i) + \chi. \qquad (51b)$$

Here $P_R(\mathbf{x})$ satisfies (48), and G_N is the Neumann Green's function, as defined by (49). The constants A_j for $j = 1, \ldots, N$ and χ satisfy the $N + 1$ dimensional linear algebraic system defined by (50) and (46).
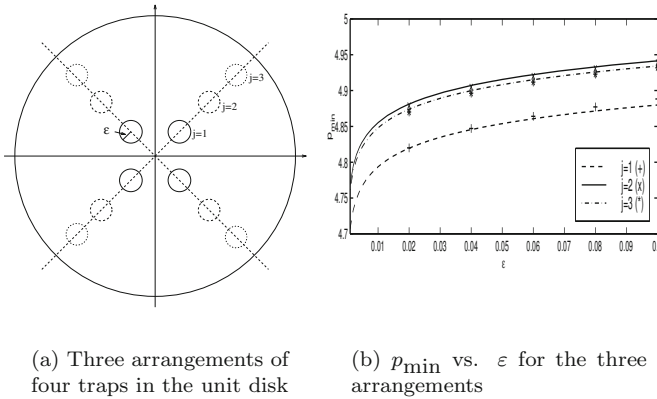
To implement the hybrid method, we must compute the Neumann Green's function G_N and its regular part R_N. This can be done explicitly for the unit disk (see equation (4.3) of Kolokolnikov et al. (2005)) and for a rectangle. In particular, upon representing points as complex numbers, we obtain for the unit disk that

$$G_N(\mathbf{x}; \boldsymbol{\xi}) = \frac{1}{2\pi} \left(-\log|\mathbf{x} - \boldsymbol{\xi}| - \log \left| \mathbf{x}|\boldsymbol{\xi}| - \frac{\boldsymbol{\xi}}{|\boldsymbol{\xi}|} \right| + \frac{1}{2}(|\mathbf{x}|^2 + |\boldsymbol{\xi}|^2) - \frac{3}{4} \right), \tag{52a}$$

$$R_N(\boldsymbol{\xi}; \boldsymbol{\xi}) = \frac{1}{2\pi} \left(-\log \left| \boldsymbol{\xi}|\boldsymbol{\xi}| - \frac{\boldsymbol{\xi}}{|\boldsymbol{\xi}|} \right| + |\boldsymbol{\xi}|^2 - \frac{3}{4} \right). \tag{52b}$$

For more general domains, G_N and its regular part can be computed numerically from a boundary integral method (see Pillay et al. (to appear, 2010)). Then, after specifying $\mathcal{M}$, we can compute the smooth function P_R numerically from (48), and evaluate it at each capillary location $\mathbf{x}_j$. Finally, the effect of the cross-sectional shape of the capillary and the permeability of the capillary wall enters only into the determination of the shape-dependent parameters d_j to be used in $\nu_j = -1/\log(\varepsilon d_j)$ in (50). This information, required in (50) and (46), represents the numerical part of the hybrid algorithm. The numerical solution to the linear system (50) and (46) then determines the strengths, A_i, of the singularities and the average pressure χ as functions of ε.

As an illustration of the theory, we consider $N = 4$ capillaries of circular cross-section, each of radius ε, located inside a circular tissue domain Ω of unit radius. Therefore, $d_i = 1$ for $i = 1, \ldots, 4$. For each fixed j, with $j = 1, 2, 3$, the capillaries are centered at the locations $\mathbf{x}_i^j = j/4 \left(\cos\left((2i-1)\pi/4\right), \sin\left((2i-1)\pi/4\right) \right)$ for $i = 1, \ldots, 4$ (see Fig. 3(a) for

(a) Three arrangements of
four traps in the unit disk

(b) $p_{\min}$ vs. ε for the three
arrangements

Figure 3. Left figure: Locations of four identical circular capillaries, each of
radius ε, centered at $(\pm j/4 \cos(\pi/4), \pm j/4 \sin(\pi/4))$ for $j = 1, 2, 3$ inside the
unit disk. Right figure: Minimum oxygen partial pressure $p_{\min}$ versus the
capillary radius ε for the three arrangements shown in the left figure. The
parameter values are $\mathcal{M} = 0.3$, with $p_{ci} = 5$ and $\kappa_i = \infty$ for $i = 1, \ldots, 4$.
The solid curves for $j = 1, 2, 3$ are from the hybrid-method solution, while
the discrete points are the full numerical results.

the geometry). For simplicity we choose a constant oxygen consumption
rate $\mathcal{M} = 0.3$, with capillary permeability coefficients $\kappa_i = \infty$, and intra-
capillary oxygen partial pressure $p_{ci} = 5$, for $i = 1, \ldots, 4$. In Fig. 3(b) we
plot the minimum oxygen partial pressure $p_{\min} = \min_{\mathbf{x} \in \Omega \backslash \Omega_p} p(\mathbf{x})$ versus ε for
each of the three arrangements of four traps as calculated from the hybrid
formulation (51), (50), and (46). In this figure we also show that the full
numerical results for $p_{\min}$, as computed directly from (34) using the *PDE
Toolbox* of MATLAB (1996), agree very well with the hybrid results.

Additional illustrations of the asymptotic theory are given in Titcombe
and Ward (2000). It is an open problem to extend the asymptotic method-
ology to analyze more biologically realistic models of oxygen transport in
muscle tissue by considering the local fluid flow inside each capillary and to
allow for nonlinear saturation effects on the oxygen consumption rate. More
elaborate mathematical models addressing some of these issues are given in
Mikelić and Primicerio (2006).

3.2   A Nonlinear Elliptic Problem

Next, we show how the method of §2 can be extended to treat a nonlinear elliptic second-order problem on a bounded two-dimensional domain Ω, which contains a small hole Ω_ε, formulated as

$$\triangle w + F(w) = 0, \quad \mathbf{x} \in \Omega \backslash \Omega_\varepsilon, \tag{53a}$$

$$\partial_n w + b(w - w_b) = 0, \quad \mathbf{x} \in \partial\Omega, \tag{53b}$$

$$w = \alpha, \quad \mathbf{x} \in \partial\Omega_\varepsilon. \tag{53c}$$

Here α is constant, $F(w)$ is a smooth function of w, ∂_n denotes the outward normal derivative, $b > 0$, and Ω_ε is a small hole of radius $\mathcal{O}(\varepsilon)$ with $\Omega_\varepsilon \to \mathbf{x}_0 \in \Omega$ uniformly as $\varepsilon \to 0$. Nonlinear problems of this type arise in many applications, including steady-state combustion theory where $F(w)$ is an exponential function (cf. Ward et al. (1993)). The primary difference between the linear problem (1) and the unperturbed problem corresponding to (53) is that, depending on the form of the nonlinearity $F(w)$, the unperturbed problem may have no solution, a unique solution, or multiple solutions. We shall assume that the unperturbed problem has at least one solution, and we will focus on determining how a specific solution to this problem is perturbed by the presence of the subdomain Ω_ε.

In the outer region we expand w as in (3). The leading-order term $W_0(\mathbf{x}; \nu)$ in this expansion satisfies

$$\triangle W_0 + F(W_0) = 0, \quad \mathbf{x} \in \Omega \backslash \{\mathbf{x}_0\}, \tag{54a}$$

$$\partial_n W_0 + b(W_0 - w_b) = 0, \quad \mathbf{x} \in \partial\Omega, \tag{54b}$$

$$W_0 \quad \text{is singular as } \mathbf{x} \to \mathbf{x}_0. \tag{54c}$$

The analysis of the solution in the inner region is the same as that in §2 since the effect of the nonlinear term in the inner region is $\mathcal{O}(\varepsilon^2)$, which is transcendentally small compared to the logarithmic terms. Hence, W_0 must have the following singular behavior (see equation (10)):

$$W_0 = \alpha + \gamma + \gamma\nu \log |\mathbf{x} - \mathbf{x}_0| + o(1), \quad \text{as} \quad \mathbf{x} \to \mathbf{x}_0. \tag{55}$$

Here $\gamma = \gamma(\nu)$ is to be found and ν is defined in terms of the logarithmic capacitance d of (7) by $\nu = -1/\log(\varepsilon d)$.

At this stage, the analysis of (53) differs slightly from its linear counterpart (1). We suppose that for some range of the parameter S we can find a solution to (54) with the singular behavior

$$W_0 \sim S \log |\mathbf{x} - \mathbf{x}_0|, \quad \text{as} \quad \mathbf{x} \to \mathbf{x}_0. \tag{56}$$

Then, in terms of this solution we define the regular part $R = R(S; \mathbf{x}_0)$ of this Coulomb singularity by

$$R(S; \mathbf{x}_0) = \lim_{\mathbf{x} \to \mathbf{x}_0} (W_0 - S \log |\mathbf{x} - \mathbf{x}_0|) . \tag{57a}$$

In general R is a nonlinear function of S at each $\mathbf{x}_0$. Therefore, we have

$$W_0 \sim S \log |\mathbf{x} - \mathbf{x}_0| + R(S; \mathbf{x}_0) + o(1), \quad \text{as} \quad \mathbf{x} \to \mathbf{x}_0 . \tag{57b}$$

By equating (57b) to (55) we get $S = \nu\gamma$ and $R = \alpha + \gamma$, where $\nu = -1/\log(\varepsilon d)$. For fixed εd and α, these relations are two nonlinear algebraic equations for the two unknowns S and γ. Alternatively, we can view these relations as providing a parametric representation of the desired curve $\gamma = \gamma(\nu)$ in the form $\nu = \nu(S)$ and $\gamma = \gamma(S)$, where

$$\gamma = R(S; \mathbf{x}_0) - \alpha, \qquad \nu = \frac{S}{R(S; \mathbf{x}_0) - \alpha} . \tag{58}$$

The equation for ν in (58) is an implicit equation determining S in terms of ε from $\nu = -1/\log(\varepsilon d)$. Therefore, we can analytically sum all of the logarithmic terms in the expansion of the solution to (53) provided that we compute the solution to (54), with singular behavior (56), and then identify $R(S; \mathbf{x}_0)$ from (57a). In general this must be done numerically. However, we now illustrate the method with an example where $R(S; \mathbf{x}_0)$ can be calculated analytically.

Let Ω be the unit disk, and take $b = \infty$, $w_b = 0$, $F(w) = e^w$, and assume that Ω_ε is an arbitrarily-shaped hole centered at the origin. Then, (54) and (56) reduce to a radially symmetric problem for $W_0(r)$, given by

$$W_0'' + \frac{1}{r}W_0' + e^{W_0} = 0, \quad 0 < r \le 1; \quad W_0 = 0, \quad \text{on} \quad r = 1, \tag{59a}$$

$$W_0 \sim S \log r, \quad \text{as} \quad r \to 0, \tag{59b}$$

where $r = |\mathbf{x}|$. This problem (59) can be solved analytically by first introducing the new variables v and η defined by

$$v = W_0 - S \log r, \qquad \eta = r^{1+S/2} . \tag{60}$$

When $S > -2$, we then obtain that $v = v(\eta)$ is smooth and satisfies

$$v'' + \frac{1}{\eta}v' + \left(1 + \frac{S}{2}\right)^{-2} e^v = 0, \quad 0 \le \eta \le 1; \quad v = 0, \quad \text{on} \quad \eta = 1. \tag{61}$$

The well-known solution $v = v(\eta)$ to (61) (see Ward et al. (1993)) can be written in parametric form as

$$v(\eta) = 2\log\left(\frac{1+\rho}{1+\rho\eta^2}\right)\,, \qquad \left(1+\frac{S}{2}\right)^{-2} = \frac{8\rho}{(1+\rho)^2}\,. \qquad (62)$$

The maximum of the right-hand side of the implicit expression for $\rho(S)$ in (62) is 2 and occurs when $\rho = 1$. Therefore, for the existence of a solution to (59) we require that $(1 + S/2)^2 > 1/2$, which yields $S > \sqrt{2} - 2$. When $S > \sqrt{2} - 2$, then $\rho(S)$ from (62) has two roots for ρ, and hence (59) has two solutions. Let us consider the smaller root, labeled by $\rho_-(S)$, given by

$$\rho_-(S) = (S+1)(S+3) - (S+2)\left[(S+2)^2 - 2\right]^{1/2}\,. \qquad (63)$$

Setting $\eta = 0$ in (62), and using (60), we compare with (57a) to obtain

$$v(0) = R(S;0) = 2\log(1 + S/2) + \log\left[8\rho_-(S)\right]\,. \qquad (64)$$

Substituting (64) into (58) gives a parametric representation of the curve $\gamma = \gamma(\nu)$ in the form $\nu = \nu(S)$ and $\gamma = \gamma(S)$.

4   Slow Viscous Flow Over a Cylinder

Next, we consider the classical problem of slow, steady, two-dimensional flow of a viscous incompressible fluid around an infinitely long straight cylinder. For simplicity, we assume that the cross-sectional shape of the cylinder is symmetric about the direction of the oncoming stream, but otherwise is arbitrary. By slow we mean that the Reynolds number $\varepsilon \equiv U_\infty L/\nu$ is small, where U_∞ is the velocity of the fluid at infinity, ν is the kinematic viscosity, and $2L$ is the diameter of the cross-section of the cylinder.

For $\varepsilon \to 0$, the method of matched asymptotic expansions was used systematically in Kaplun (1957) and in Proudman and Pearson (1957) to resolve the well-known Stokes paradox, and to calculate asymptotically the stream function in both the Stokes region, which is near the body, and in the Oseen region, which is far from the body. These pioneering studies showed that, for $\varepsilon \to 0$, the asymptotic expansion for the drag coefficient C_D of a circular cylindrical body starts with $C_D \sim 4\pi\varepsilon^{-1}S(\varepsilon)$, where $S(\varepsilon)$ is an infinite series in powers of $1/\log\varepsilon$. The coefficients in this series are determined in terms of the solutions to certain forced Oseen problems. For a cylinder of arbitrary cross-section, it was shown in Kaplun (1957) that $C_D \sim 4\pi\varepsilon^{-1}S(\varepsilon d_f)$, where d_f is an 'effective' radius of the cylinder. This

result establishes a certain asymptotic equivalence for C_D between cylinders of various cross-sectional shapes and is known as Kaplun's equivalence principle.

In an effort to determine C_D quantitatively, analytical formulae for the first three coefficients in $S(\varepsilon)$ were derived in Kaplun (1957). However, as a result of the slow decay of $1/\log \varepsilon$ with decreasing values of ε, the resulting three-term truncated series for C_D agrees rather poorly with the experimental results of Tritton (1959) unless ε is very small. Owing to the complexity of the calculations required, it is impractical to obtain a closer quantitative determination of the drag coefficient by calculating further coefficients in $S(\varepsilon)$ analytically. As a result of these fundamental long-standing difficulties, the problem of slow viscous flow around a cylinder has served as a paradigm for problems where a matched asymptotic analysis fails to be of much practical use, unless ε is very small. A comprehensive recent survey of asymptotic and renormalization group methods applied to slow viscous flow problems is given in Veysey and Goldenfeld (2007).

In Kropinski et al. (1995), this problem was re-examined and a hybrid asymptotic-numerical method was formulated and implemented to effectively sum the infinite logarithmic expansions that arise from the singular perturbation analysis of slow viscous flow around a cylinder. Our approach differs from the hybrid method employed in Lee and Leal (1986) in which numerical methods are used within the framework of the method of matched asymptotic expansions to calculate the first few coefficients in the logarithmic expansions of the flow field and the drag coefficient. Instead, we show that these entire infinite logarithmic series are contained in the solution to a certain related problem that does not involve the cross-sectional shape of the cylinder. The overall framework of our approach is similar to that done in §2 and §3, and is outlined below.

The model formulation is as follows. Consider steady, incompressible, viscous flow around a cylindrical body with a uniform stream of velocity U_∞ in the x direction at large distances from the body. We assume that the cross-section Ω of the cylinder is symmetric with respect to the oncoming stream. Then, in terms of polar coordinates centered inside the body, it follows from the Navier-Stokes equations that the dimensionless stream function ψ satisfies

$$\triangle^2 \psi + \varepsilon\, J_\rho\left[\psi, \triangle\psi\right] = 0\,, \quad \text{for } \rho > \rho_b(\theta)\,, \tag{65a}$$

$$\psi = \partial_n \psi = 0\,, \quad \text{on } \rho = \rho_b(\theta)\,, \tag{65b}$$

$$\psi \sim y\,, \quad \text{as } \rho = (x^2 + y^2)^{1/2} \to \infty\,. \tag{65c}$$

Here $\varepsilon \equiv U_\infty L/\nu \ll 1$ is the Reynolds number based on the radius L of

Ω, lengths are in units of L, ∂_n denotes the normal derivative, $\triangle$ and $\triangle^2$ denote the Laplacian and Biharmonic operators, respectively, and J_ρ is the Jacobian defined by $J_\rho [a, b] \equiv \rho^{-1} (\partial_\rho a\, \partial_\theta b - \partial_\theta a\, \partial_\rho b)$. The boundary of the scaled cross-section is denoted by $\rho = \rho_b(\theta)$ for $-\pi \le \theta \le \pi$, and the symmetry condition $\rho_b(\theta) = \rho_b(-\theta)$ is assumed to hold. In terms of ψ, the dimensionless negative vorticity ω is $\omega = \triangle\psi$, and the x and y components of the fluid velocity, u and v, are

$$u = \partial_y \psi = \sin\theta\, \partial_\rho \psi + \frac{\cos\theta}{\rho}\, \partial_\theta \psi\,, \quad v = -\partial_x \psi = -\cos\theta\, \partial_\rho \psi + \frac{\sin\theta}{\rho}\, \partial_\theta \psi\,. \tag{66}$$

We first outline the conventional singular perturbation analysis of (65) for $\varepsilon \to 0$ (cf. Kaplun (1957) and Proudman and Pearson (1957)). We then formulate the hybrid method for summing the infinite-order logarithmic expansions that arise from the analysis.

In the Stokes, or inner, region defined by $\rho = \mathcal{O}(1)$, the stream function has an infinite logarithmic expansion of the form

$$\psi_s(\rho,\theta) = \sum_{j=1}^{\infty} \nu^j \psi_j(\rho,\theta) + \cdots\,. \tag{67}$$

Here, we define $\nu = \nu(\varepsilon d_f) \equiv -1/\log\left(\varepsilon d_f e^{1/2}\right)$, where d_f is a shape-parameter that is specified below in terms of the far-field behavior of a Biharmonic problem. For a circular cylinder of radius one then $d_f = 1$. Upon substituting (67) into (65a), we obtain that $\psi_j = a_j \psi_c$, where the a_j for $j \ge 1$ are undetermined constants and $\psi_c \equiv \psi_c(\rho,\theta)$ is the solution to the following canonical inner or Stokes problem:

$$\triangle^2 \psi_c = 0\,, \quad \text{for}\ \ \rho > \rho_b(\theta)\,; \qquad \psi_c(\rho,\theta) = -\psi_c(\rho,-\theta)\,, \tag{68a}$$
$$\psi_c = 0 \quad \text{and} \quad \partial_n \psi_c = 0\,, \quad \text{on}\ \ \rho = \rho_b(\theta)\,. \tag{68b}$$

The asymptotic form of ψ_c as $\rho \to \infty$ involves linear combinations of $\{\rho^3, \rho\log\rho, \rho, \rho^{-1}\}\sin\theta$. However, to match ψ_s with the Oseen expansion below we require that the coefficient of ρ^3 must vanish. Then, to specify ψ_c uniquely, we impose that the coefficient of $\rho\log\rho$ is unity. Therefore, we define ψ_c as the unique solution to (68a) and (68b), with the far-field asymptotic behavior

$$\psi_c \sim \left(\rho\log\rho - \rho\log\left[d_f e^{1/2}\right]\right)\sin\theta\,, \quad \text{as}\ \ \rho \to \infty\,. \tag{68c}$$

The constant d_f, depending on the specific shape of the body, is determined uniquely by the solution to (68). This exterior Biharmonic problem (68) is analogous to the exterior Laplace problem (7) for the pipe problem of §2.

Upon substituting $\psi_j = a_j \psi_c$ into (67), the Stokes expansion becomes

$$\psi_s(\rho, \theta) = \sum_{j=1}^{\infty} \nu^j \, a_j \psi_c(\rho, \theta) + \cdots . \qquad (69a)$$

Then, by using (68c), we obtain the following far-field behavior of (69a):

$$\psi_s(\rho, \theta) \sim \sum_{j=1}^{\infty} \nu^j \, a_j \left(\log \rho - \log \left[d_f e^{1/2} \right] \right) \rho \sin \theta , \quad \text{as} \quad \rho \to \infty . \qquad (69b)$$

Next, we consider the outer or Oseen region defined for $\rho = \mathcal{O}(\varepsilon^{-1})$. In this region, we introduce the new Oseen, or outer, length-scale r by $r = \varepsilon \rho$ with $r = \mathcal{O}(1)$. We then re-write the far-field behavior of the Stokes solution (69b) in terms of the outer Oseen variable r to obtain

$$\psi_s \sim \frac{1}{\varepsilon} \left(a_1 r \sin \theta + \sum_{j=1}^{\infty} \nu^j \left[a_j \log r + a_{j+1} \right] r \sin \theta \right) . \qquad (69c)$$

This expression (69c) yields a singularity structure for the outer Oseen solution as $r \to 0$. This behavior suggests that we introduce the new variable Ψ by $\Psi(r, \theta) = \varepsilon \psi(\varepsilon^{-1} r, \theta)$, and that we expand Ψ as

$$\Psi(r, \theta) = r \sin \theta + \nu \Psi_1(r, \theta) + \sum_{j=2}^{\infty} \nu^j \Psi_j(r, \theta) + \cdots , \qquad (70)$$

in order to satisfy the free-stream condition as $r \to \infty$ in (65c). Upon substituting (70) into (65a), and matching Ψ as $r \to 0$ to the required singular behavior (69c), we find that $a_1 = 1$ and that Ψ_1 and Ψ_j, for $j \geq 2$, satisfy the following Oseen problems on $0 < r < \infty$:

$$L_{0s} \Psi_1 \equiv \triangle^2 \Psi_1 + \left(r^{-1} \sin \theta \, \partial_\theta - \cos \theta \, \partial_r \right) \triangle \Psi_1 = 0 , \qquad (71a)$$

$$\Psi_1 \sim (\log r + a_2) \, r \sin \theta , \quad \text{as} \quad r \to 0 ; \quad \partial_r \Psi_1 \to 0 , \quad \text{as} \quad r \to \infty , \qquad (71b)$$

$$L_{0s} \Psi_j = - \sum_{k=1}^{j-1} J_r \left[\Psi_k, \triangle \Psi_{j-k} \right] , \qquad (71c)$$

$$\Psi_j \sim (a_j \log r + a_{j+1}) \, r \sin \theta , \quad \text{as} \quad r \to 0 ; \quad \partial_r \Psi_j \to 0 , \quad \text{as} \quad r \to \infty . \qquad (71d)$$

Here L_{0s} is referred to as the linearized Oseen operator, and Ψ_1 is the linearized Oseen solution.

The limiting conditions (71b) and (71d) are the required singularity behaviors of Ψ_1 and Ψ_j for $j \geq 2$, respectively, as $r \to 0$. For (71b) the strength of the singular part $r \log r \sin \theta$ is set to unity. In terms of the solution to (71a) with $\Psi_1 \sim r \log r \sin \theta$ as $r \to 0$, we then calculate the constant a_2 of the regular part of the singularity structure from the limiting process $\Psi_1 - r \log r \sin \theta \sim a_2 r \sin \theta$ as $r \to 0$. Then, with a_2 determined in this way, we solve for Ψ_2 from (71c) with singular behavior $\Psi_2 \sim a_2 r \log r \sin \theta$ as $r \to 0$, The constant a_3 in the regular part of (71d) is then determined from the limiting process $\Psi_2 - a_2 r \log r \sin \theta \sim a_3 r \sin \theta$ as $r \to 0$.

Hence, the coefficients a_j for $j = 2, 3, ..$, which are independent of ε and of the shape of the body, are determined recursively from (71), in a similar way as in §2. The first two coefficients are (cf. Kaplun (1957), Proudman and Pearson (1957))

$$a_2 = \gamma_e - \log 4 - 1 \approx -1.8091 \,, \tag{72a}$$

$$a_3 - a_2^2 = -\int_0^\infty \left[r^{-1} I_1(2r) + 1 - 4K_1(r)I_1(r) \right] K_0(r)K_1(r) \, dr \approx -0.8669 \,. \tag{72b}$$

Here K_1, K_0, I_0 and I_1 are the usual modified Bessel functions, and γ_e is Euler's constant. This formula for a_2 was obtained in Kaplun (1957) and Proudman and Pearson (1957), while the expression for a_3 was given in Kaplun (1957). The expression for a_2 was obtained in Proudman and Pearson (1957) in terms of the explicit solution to (71a) with singular behavior $\Psi_1 \sim r \log r \sin \theta$ as $r \to 0$ given by

$$\Psi_1(r, \theta) = -\sum_{n=1}^\infty \frac{c_n(r/2)}{n} r \sin(n\theta) \,, \quad c_n(s) \equiv 2 \left[K_1(s)I_n(s) + K_0(s)I_n'(s) \right] \,. \tag{73}$$

As $r \to 0$, then $c_n(r/2) = \mathcal{O}(r^{n-1})$ for $n > 1$, and $c_1(r/2) \sim 1 - \log(\rho/4) - \gamma_e$, where γ_e is Euler's constant. Therefore, we conclude that $\Psi_1 - r \log r \sin \theta \to r (\gamma_e - \log 4 - 1) \sin \theta$ as $r \to 0$. Hence, from the regular part in (71b), we obtain that $a_2 = \gamma_e - \log 4 - 1$. In contrast, the derivation in Kaplun (1957) of the explicit formula for a_3 given in (72b) is considerably more involved. Explicit analytical formulae for a_j when $j \geq 4$ are not available.

A formula for the drag coefficient C_D is given in Imai (1951) in terms of an arbitrary closed contour around the body. From this formula, and from

the symmetry of the flow, it follows that

$$
C_D = \rho \int_0^\pi \left[\cos\theta \left(\psi_\rho^2 - \frac{1}{\rho^2}\psi_\theta^2 \right) - \frac{2}{\rho}\sin\theta\,\psi_\rho\psi_\theta \right] d\theta
$$
$$
- 2\rho \int_0^\pi \omega\,\psi_\theta \sin\theta\,d\theta - 2\varepsilon^{-1}\rho \int_0^\pi (\rho\omega_\rho - \omega)\sin\theta\,d\theta\,, \quad (74)
$$

where ψ satisfies (65) and $\omega = \triangle\psi$. Here ρ, in terms of the Stokes length-scale, is the radius of an arbitrary circular contour that encloses the body. To derive an asymptotic formula for the drag coefficient, we substitute the far-field form (69b) into (74) and evaluate the resulting expression on a large circle $\rho = \rho_0 \gg 1$. In this way, we obtain for $\varepsilon \to 0$ that the drag coefficient C_D for a cylinder of arbitrary cross-section is given in terms of the coefficients a_j by

$$
C_D \sim 4\pi\varepsilon^{-1}\nu(\varepsilon d_f)\left(\sum_{j=0}^\infty a_{j+1}\nu^j(\varepsilon d_f) + \cdots \right)\,, \quad \nu(\varepsilon d_f) \equiv -\frac{1}{\log\left[\varepsilon d_f e^{1/2}\right]}\,.
$$
$$
(75)
$$

Kaplun's (see Kaplun (1957)) approximation for C_D results from substituting $a_1 = 1$ and (72) for a_2 and a_3 into (75). The resulting three-term expansion, in equivalent asymptotic form, is

$$
C_D \sim \frac{4\pi}{\varepsilon}\hat{\nu}(\varepsilon d_f)\left[1 - 0.8669\,\hat{\nu}^2(\varepsilon d_f)\right]\,, \qquad \hat{\nu}(z) \equiv \left[\log\left(3.7027/z\right)\right]^{-1}\,.
$$
$$
(76)
$$

For a circular cylinder, the explicit form (76) provides a rather poor determination of the experimental drag coefficient unless ε is rather small (cf. Dyke (1975)). One way to overcome this difficulty would be to compute numerically further coefficients a_j, for $j \geq 4$, from the the infinite sequence of PDE's (71c) with singularity structures (71d). This would still require truncating the series (75) at some finite j. As an alternative to series truncation, we now follow Kropinski et al. (1995) and formulate a hybrid asymptotic-numerical method that has the effect of summing all the terms on the right-hand side of (75), but which avoids computing the coefficients a_j for $j \geq 1$ individually.

To do so, we let $A^\star(z)$ denote a function that is asymptotic to the sum of the terms written explicitly in the brackets on the right-hand side of (75):

$$
A^\star(z) \sim \sum_{j=1}^\infty \nu^{j-1}(z)\,a_j\,, \qquad z \equiv \varepsilon d_f\,. \quad (77)
$$

Then, the Stokes expansion (69a) is asymptotic to

$$\psi_s(\rho, \theta) = \nu(z) A^\star(z) \psi_c(\rho, \theta) + \cdots, \qquad z = \varepsilon d_f. \tag{78}$$

Substituting (68c) into (78), and writing the resulting expression in terms of the Oseen variable $r = \varepsilon \rho$, we obtain the far-field form in the Stokes region,

$$\psi_s \sim \varepsilon^{-1} A^\star(z) \left[1 + \nu(z) \log r\right] r \sin \theta. \tag{79}$$

This expression yields the singularity structure for the outer solution.

In the Oseen, or outer region, we do not expand the solution in powers of ν as in (70). Instead, we solve the full problem (65a) and (65c) for $r > 0$ subject to the singularity structure (79), which is to hold as $r \to 0$. Therefore, in analogy with the approach used in §3.2 (see equations (54)–(58) of §3.2) to treat nonlinear elliptic problems in perforated domains, we introduce the parameter-dependent auxiliary streamfunction $\Psi_H \equiv \Psi_H(r, \theta; S)$, with $\Psi_H(r, \theta; S) = -\Psi_H(r, -\theta; S)$, satisfying

$$\triangle^2 \Psi_H + J_r\left[\Psi_H, \triangle \Psi_H\right] = 0, \quad r > 0, \tag{80a}$$

$$\Psi_H \sim r \sin \theta, \quad \text{as} \quad r \to \infty, \tag{80b}$$

$$\Psi_H \sim S r \log r \sin \theta, \quad \text{as} \quad r \to 0. \tag{80c}$$

In Kropinski et al. (1995) (see also Keller and Ward (1996)), this parameter-dependent problem is solved numerically for a range of S values, and in terms of this solution we identify the regular part $R = R(S)$ of this singularity structure by the following limiting process

$$\Psi_H - S r \log r \sin \theta = R(S) r \sin \theta + o(r), \quad \text{as} \quad r \to 0. \tag{81}$$

A plot of the numerically computed function $R = R(S)$ is shown in Fig. 4. Given that the hybrid problem (80) is posed on $0 < r < \infty$, it is an interesting open problem to investigate whether it is possible to find an exact solution of (80), in a similar way as was found in (59)–(64) for the nonlinear elliptic problem of §3.2. In this regard, the class of exact solutions to the full 2-D incompressible Navier-Stokes equations found in Ranger (1995) may be useful.

Finally, since the required singularity behavior from (79) is that

$$\Psi_H = A^\star \left[1 + \nu(z) \log r\right] r \sin \theta + o(r), \quad \text{as} \quad r \to 0, \tag{82}$$

we conclude that $A^\star(z)$ and $\nu(z)$, with $z \equiv \varepsilon d_f$, are given parametrically in terms of the singularity strength S and its regular part $R(S)$ by

$$\nu(z) = -\frac{1}{\log\left[z e^{1/2}\right]} = \frac{S}{R(S)}, \qquad A^\star(z) = R(S). \tag{83}$$
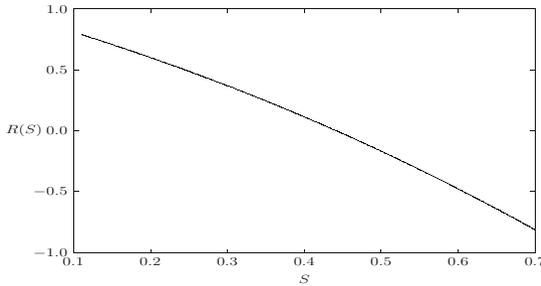
Figure 4. Plot of $R = R(S)$ computed numerically from the hybrid formulation (80) and (81).

The problem (80) is a hybrid asymptotic-numerical formulation of the full problem (65). More specifically, the cylinder in (65) is replaced by the singularity structure (82) that was derived by exploiting the far-field form of the infinite-order logarithmic expansion in the Stokes region. Instead of having to compute solutions to the infinite sequence of problems (71), the hybrid method requires the solution of the parameter-dependent problem (80), with singular behavior (80c) given in terms of the parameter S. Then, the regular part $R = R(S)$ of this singularity behavior is calculated from (81). Finally, (83) determines $A^\star(z)$ in terms of $z = \varepsilon d_f$ implicitly.

In terms of $A^\star$ and d_f, the asymptotic formula for the drag coefficient, valid to within all logarithmic correction terms, is given by

$$C_D = \frac{4\pi}{\varepsilon} \left[\nu(z) A^\star(z) + \cdots \right] , \qquad \nu(z) = \frac{-1}{\log\left[z\, e^{1/2} \right]} , \qquad z = \varepsilon d_f . \quad (84)$$

Kaplun's equivalence principle follows from the fact that the curve $A^\star(z)$ versus z can be used for a cylinder of arbitrary cross-section. To determine $A^\star(\varepsilon d_f)$ for a body of a specific shape, we need only compute the single constant d_f from the numerical solution to the canonical Stokes problem (68). This feature provides a significant advantage over a direct numerical approach on the full problem (65).

For a few simple cross-sectional shapes, the constant d_f can be determined analytically from (68). In particular, for a circular cross-section,

where $\rho_b(\theta) = 1$, then the solution to (68) is

$$\psi_c = \left(\rho \log \rho - \frac{\rho}{2} + \frac{1}{2\rho} \right) \sin\theta , \tag{85}$$

so that $d_f = 1$. Next we consider an elliptical domain defined by $(x/a)^2 + (y/b)^2 = 1$ where $\max(a,b) = 1$. In the case where $a = 1$, for which the major axis is aligned parallel to the oncoming stream, the solution to (68) can be found by introducing elliptic cylinder coordinates (see Kropinski et al. (1995)). In this way, we obtain that

$$d_f = \left(\frac{a+b}{2} \right) \exp \left[\frac{b-a}{2(b+a)} \right] . \tag{86}$$

This formula for d_f also holds for the case when $b = 1$ (the major axis is is aligned perpendicular to the oncoming stream). A plot of d_f for various ellipses is shown in Fig. 5.
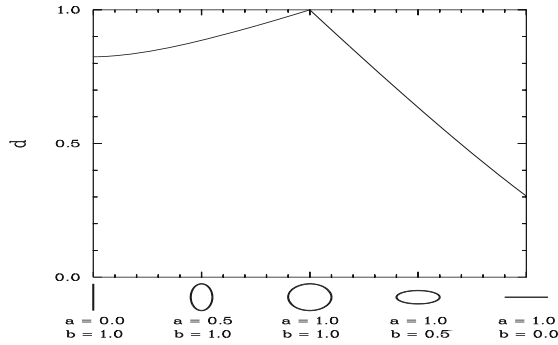
Figure 5. The shape-parameter d_f of (86) for an ellipse with a semi-major axis of unity.

In Kropinski et al. (1995) a numerical conformal mapping method was used to calculate d_f numerically from (68) for other simple cross-sectional shapes that can be mapped to the unit disk. In particular, such an analytical conformal mapping is known for the family of symmetric Karman-Trefftz (KT) airfoils (cf. Milne-Thomson (1958)). The mapping function, $z = z(\sigma)$, for the boundary of these profiles is

$$z(\sigma) = \beta_0 k c \left[\frac{(\xi+c)^k + (\xi-c)^k}{(\xi+c)^k - (\xi-c)^k} \right] , \qquad \xi \equiv \sigma^{-1} + c - 1 , \tag{87a}$$

Table 2. Numerical values for d_f corresponding to the KT airfoils (87). The tail angle (in degrees) is θ_T, and the thickness ratio is δ. The last column gives the value of b for an ellipse, with $a = 1$, that has the same value of d_f as the corresponding airfoil.

δ	θ_T	k	c	d_f	b
.050	0°	2.000	0.961	0.328	0.040
.080	5°	1.972	0.952	0.344	0.066
.100	13°	1.928	0.960	0.354	0.082
.120	16°	1.910	0.954	0.364	0.098
.120	20°	1.889	0.968	0.363	0.096
.200	25°	1.861	0.915	0.410	0.170

where $\sigma = e^{i\theta}$ with $0 \leq \theta \leq 2\pi$. By fixing the length of the airfoil to be 2, we find that the mapping constant β_0 is given in terms of k and c by

$$\beta_0 = \frac{\left[1 - (1 - c)^k\right]}{kc}. \tag{87b}$$

A parametric representation for the airfoil profile is obtained by setting $\sigma = e^{i\theta}$ in (87a). In (87), the parameters k and c, where $1 < k < 2$ and $0 < c < 1$, determine the thickness ratio δ of the airfoil and the tail angle θ_T, given by $\theta_T = (2 - k)\pi$. Numerical values for d_f for some KT airfoils, as computed in Kropinski et al. (1995), are given in Table 2.

For each of the KT airfoil examples given in Table 2 there is an equivalent ellipse with $a = 1$ that has the same value of d_f. The values of b for these equivalent ellipses, which are computed using (86), are given in the last column of Table 2. By Kaplun's equivalence principle each of these equivalent ellipses has the same asymptotic drag coefficient, to within all logarithmic correction terms, as the corresponding KT airfoil. However, it is clear that the transcendentally small terms in the expansion of the drag coefficient, which are smaller than any power of ν, will not satisfy the same equivalence principle. Such terms are not accounted for in our analysis.

We now compare the hybrid results for the drag coefficient of a circular cylindrical body for which $d_f = 1$ and $z = \varepsilon$. In Fig. 6(a) we plot the hybrid drag coefficient C_D versus ε, given by (84) with $d_f = 1$. In this figure we compare our hybrid results with Kaplun's three-term expansion (76), with full numerical results computed directly from (65) (see Kropinski et al. (1995)), and the experimental results of Tritton (1959). We observe

that the hybrid method provides a significantly better determination of C_D over the range $0.50 < \varepsilon < 2.0$ than does the three-term expansion (76).
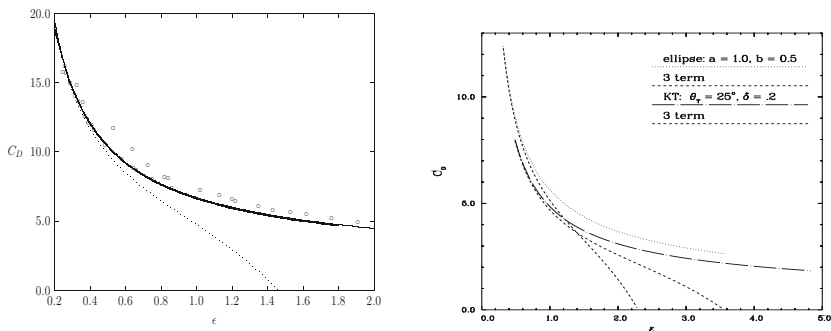
(a) C_D vs. ε: Circular cylindrical cross-section

(b) C_D vs. ε: Two other shapes

Figure 6. The drag coefficient C_D versus the Reynolds number ε. Left figure: for a circular cylinder the hybrid result (84) (solid curve), the full numerical results (heavy solid curve), the three-term result (76) (dotted curve), and the experimental results of Tritton (1959) (discrete points), are compared. Right figure: the hybrid result (84) is compared with the three-term result (76) for a cylindrical body of either an elliptical or a KT airfoil cross-section.

Finally, we consider flow around other cylindrical bodies. In Fig. 6(b) we plot the hybrid drag coefficient for flow around certain cylinders having either elliptical or KT airfoil cross-sections. In this figure, we compare, for an ellipse and an airfoil, the hybrid results for C_D with Kaplun's three-term asymptotic result (76). These results were obtained from (83) and (84), and by using the data from the plot of $R = R(S)$ in Fig. 4. The value of d_f, needed in (83), is given in (86) for the ellipse, and in Table 2 for the KT airfoil.

We now make several remarks concerning some extensions of the analysis. We first remark that our hybrid method does not incorporate the effect of the transcendentally small inertial terms arising from the Stokes region. Therefore, the asymmetry in the flow field near the body, which becomes more prominent as the Reynolds number is increased, is not captured by our

analysis. For a circular cylinder, the leading-order effects of these inertial terms on the flow field and on the drag coefficient were analyzed in Skinner (1975). In §3 of Keller and Ward (1996) an extension of the hybrid approach of Kropinski et al. (1995) was used to calculate these transcendentally small terms for a circular cylinder, and to predict the asymmetry in the flow field near the body.

Secondly, we remark that a similar hybrid method was developed in Titcombe et al. (2000) to calculate the drag and lift coefficient for slow viscous flow over a cylindrical body of arbitrary cross-sectional shape. For this problem, the hybrid method solution involves a 2×2 matrix, depending on the shape of the body, which replaces the single shape-dependent parameter d_f for symmetric cylindrical bodies. In Titcombe et al. (2000) the hybrid results were compared with those of Shintani et al. (1983).

Finally, we remark that our hybrid method can also be adapted to treat some new microfluid flow problems. In Matthews and Hill (2009) (see also Matthews and Hill (2006)) the drag coefficient for steady slow viscous flow over an infinite nanocylinder was analyzed by asymptotically calculating two terms in the infinite logarithmic series for the flow field and drag coefficient. The novel feature of this microfluid flow problem is that, due to the small scales involved, the usual no-slip boundary condition on the cylinder is replaced by the Navier boundary condition, which takes into account the effect of boundary surface roughness. An analysis of this related problem by a hybrid asymptotic-numerical method will, essentially, only require the modification of the boundary condition in (68b).

4.1   Summing Logarithmic Expansions: A Linear Biharmonic Problem

In this subsection we consider a linear Biharmonic problem on a concentric annular domain with a small inner radius ε, formulated as

$$\triangle^2 u = 0 \,, \quad \varepsilon < r < 1 \,, \tag{88a}$$

$$u = \sin\theta \,, \quad u_r = 0 \,, \quad \text{on} \quad r = 1 \,, \tag{88b}$$

$$u = u_r = 0 \,, \quad \text{on} \quad r = \varepsilon \,. \tag{88c}$$

We will calculate the exact solution to this problem, and then show how a hybrid method similar to that used for the low Reynolds number flow problem can be readily formulated and implemented to calculate an approximate solution to (88) that contains all logarithmic correction terms.

The exact solution of (88a), which satisfies (88b), is

$$u = \left(Ar^3 + Br \log r + \left(-2A + \frac{1}{2} - \frac{B}{2}\right) r + \left(\frac{1}{2} + A + \frac{B}{2}\right) \frac{1}{r} \right) \sin\theta \,,$$
(89)

for any constants A and B. Then, imposing that $u = u_r = 0$ on $r = \varepsilon$, we get two equations for A and B:

$$A\varepsilon^3 + B\varepsilon \log \varepsilon + \left(-2A + \frac{1}{2} - \frac{B}{2}\right) \varepsilon + \left(\frac{1}{2} + A + \frac{B}{2}\right) \varepsilon^{-1} = 0 \,, \quad (90a)$$

$$3A\varepsilon^2 + B + B \log \varepsilon + \left(-2A + \frac{1}{2} - \frac{B}{2}\right) - \left(\frac{1}{2} + A + \frac{B}{2}\right) \varepsilon^{-2} = 0 \,. \quad (90b)$$

By comparing the $\mathcal{O}(\varepsilon^{-1})$ and $\mathcal{O}(\varepsilon^{-2})$ terms in (90), it follows that

$$\frac{1}{2} + A + \frac{B}{2} = \kappa\varepsilon^2 \,,$$
(91)

where κ is an $\mathcal{O}(1)$ constant to be found. Substituting (91) into (90), and neglecting the higher order $A\varepsilon^3$ and $3A\varepsilon^2$ terms in (90), we obtain the approximate system

$$B \log \varepsilon + \left(-2A + \frac{1}{2} - \frac{B}{2}\right) \approx -\kappa \,, \quad B + B \log \varepsilon + \left(-2A + \frac{1}{2} - \frac{B}{2}\right) \approx \kappa \,.$$
(92)

By adding the two equations above to eliminate κ, we obtain that

$$B + 2B \log \varepsilon + (-4A + 1 - B) = 0 \,.$$
(93)

From (93), together with $A \sim -(1 + B)/2$ from (91), we obtain that

$$B \sim \frac{3\nu}{2 - \nu} \,, \qquad A = 1 - \frac{3}{2 - \nu} \,, \qquad \text{where} \quad \nu \equiv \frac{-1}{\log\left[\varepsilon e^{1/2}\right]} \,. \qquad (94)$$

Finally, substituting (94) into (89), we obtain that the outer solution has the asymptotics

$$u \sim \left((1 - \tilde{A})r^3 + \nu\tilde{A}r \log r + \tilde{A}r\right) \sin\theta \,, \quad r \gg \mathcal{O}(\varepsilon) \,. \qquad (95a)$$

where $\tilde{A}$ is defined by

$$\tilde{A} \equiv \frac{3}{2 - \nu} \,, \qquad \nu \equiv \frac{-1}{\log\left[\varepsilon e^{1/2}\right]} \,. \qquad (95b)$$

We remark that (95) is an infinite-order logarithmic series approximation to the exact solution. However, it does not contain transcendentally small terms of algebraic order in ε as $\varepsilon \to 0$.

Next, we show how to derive (95) by employing the hybrid formulation used in the low Reynolds number flow problem of §4. In order to sum the infinite logarithmic series we formulate a hybrid method by following (77)–(79). In the inner region, with inner variable $\rho \equiv \varepsilon^{-1}r$, we look for an inner solution in the form (see (78) and (85))

$$v(\rho, \theta) = u(\varepsilon\rho, \theta) \sim \varepsilon\nu\tilde{A}(\nu)\left(\rho\log\rho - \frac{\rho}{2} + \frac{1}{2\rho}\right)\sin\theta\,. \tag{96}$$

Here $\nu \equiv -1/\log\left[\varepsilon e^{1/2}\right]$ and $\tilde{A} \equiv \tilde{A}(\nu)$ is a function of ν to be found. The extra factor of ε in (96) is needed since the solution in the outer region is not algebraically large as $\varepsilon \to 0$. Now letting $\rho \to \infty$, and writing (96) in terms of the outer variable $r = \varepsilon\rho$, we obtain that the far-field form of (96) is

$$v \sim \left(\tilde{A}\nu r\log r + \tilde{A}r\right)\sin\theta\,. \tag{97}$$

Therefore, the approximate outer hybrid solution w_H to (88) that sums all the logarithmic terms must satisfy

$$\triangle^2 w_H = 0\,, \quad 0 < r < 1\,, \tag{98a}$$

$$w_H = \sin\theta\,, \quad w_{Hr} = 0\,, \quad \text{on} \quad r = 1\,, \tag{98b}$$

$$w_H \sim \left(\tilde{A}\nu r\log r + \tilde{A}r\right)\sin\theta\,, \quad \text{as} \quad r \to 0\,. \tag{98c}$$

The solution to (98a) and (98b) is given explicitly by

$$w_H = \left(\alpha r^3 + \beta r\log r + \left(-2\alpha + \frac{1}{2} - \frac{\beta}{2}\right)r + \left(\frac{1}{2} + \alpha + \frac{\beta}{2}\right)\frac{1}{r}\right)\sin\theta\,. \tag{99}$$

The condition (98c) then yields the three equations

$$\beta = \tilde{A}\nu\,, \qquad -2\alpha + \frac{1}{2} - \frac{\beta}{2} = \tilde{A}\,, \qquad \frac{1}{2} + \alpha + \frac{\beta}{2} = 0\,, \tag{100}$$

for α, β, and $\tilde{A}$. We solve this system to obtain

$$\beta = \tilde{A}\nu\,, \qquad \tilde{A} = \frac{3}{2 - \nu}\,, \qquad \alpha = 1 - \tilde{A}\,. \tag{101}$$

Upon substituting (101) into (99), we obtain that the resulting expression agrees exactly with the result (95) obtain from the exact solution.

4.2   A Convection-Diffusion Problem

Convection-diffusion problems in two dimensional regions with obstacles in the low Peclet number limit can be analyzed in a similar way. A recent analytical study of such problems in both the low and high Peclet number limit using a different and highly innovative approach is given in Choi et al. (2005). The following analysis is related to the work in Titcombe and Ward (1997).

Consider the steady-state convection-diffusion equation for $T(\mathbf{X})$, with $\mathbf{X} = (X_1, X_2)$ posed outside two circular disks Ω_j for $j = 1, 2$ of a common radius a, and with a center-to-center separation $2L$ between the two disks:

$$\kappa \triangle T = U \cdot \nabla T\,, \qquad \mathbf{X} \in \mathbb{R}^2 \backslash \cup_{j=1} \Omega_j\,, \tag{102a}$$

$$T = T_j\,, \qquad \mathbf{X} \in \partial \Omega_j\,, \quad j = 1, 2\,, \tag{102b}$$

$$T = T_\infty\,, \qquad |\mathbf{X}| \to \infty\,. \tag{102c}$$

Here $\kappa > 0$ is constant, T_j for $j = 1, 2$ and T_∞ are constants, and $\mathbf{U} = \mathbf{U}(\mathbf{X})$ is a given bounded flow field with $\mathbf{U}(\mathbf{X}) \to (U_\infty, 0)$ as $|\mathbf{X}| \to \infty$, where U_∞ is constant. We introduce the dimensionless variables $\mathbf{x}$, $\mathbf{u}(\mathbf{x})$, and $w(\mathbf{x})$ by

$$\mathbf{x} = \mathbf{X}/\gamma\,, \quad T = T_\infty w\,, \quad \mathbf{u}(\mathbf{x}) = \mathbf{U}(\gamma \mathbf{x})/U_\infty\,, \quad \gamma \equiv \kappa/U_\infty\,. \tag{103}$$

We also define the dimensionless centers of the two circular disks by $\mathbf{x}_j$ for $j = 1, 2$, and their constant boundary temperatures α_j for $j = 1, 2$, by

$$\mathbf{x}_j = \mathbf{X}_j/\gamma\,, \qquad \alpha_j = w_j/T_\infty\,, \qquad j = 1, 2\,. \tag{104}$$

Then, (102) transforms in dimensionless form to

$$\triangle w = \mathbf{u} \cdot \nabla w\,, \qquad \mathbf{x} \in \mathbb{R}^2 \backslash \cup_{j=1}^2 D_{\varepsilon j}\,, \tag{105a}$$

$$w = \alpha_j\,, \qquad \mathbf{x} \in \partial D_{\varepsilon j}\,, \quad j = 1, 2\,, \tag{105b}$$

$$w \sim 1\,, \qquad |\mathbf{x}| \to \infty\,. \tag{105c}$$

Here $D_{\varepsilon j} = \{\mathbf{x} \mid |\mathbf{x} - \mathbf{x}_j| \le \varepsilon\}$ is the circular disk of radius ε centered at $\mathbf{x}_j$. The center-to-center separation is

$$|\mathbf{x}_2 - \mathbf{x}_1| = 2l\varepsilon\,, \qquad l \equiv L/a\,. \tag{106}$$

The dimensionless flow has limiting behavior $\mathbf{u} \sim (1, 0)$ as $|\mathbf{x}| \to \infty$. There are two interesting limiting cases of (105), which can be analyzed.
Case 1: We assume that $l = \mathcal{O}(1)$ as $\varepsilon \to 0$, so that $|\mathbf{x}_2 - \mathbf{x}_1| = \mathcal{O}(\varepsilon)$. This is the case where the bodies are close together. It leads below to a different inner problem, not considered in §2.

We assume without loss of generality that $\mathbf{x}_1 + \mathbf{x}_2 = 0$. We then introduce the inner variables $\mathbf{y}$ and $v(\mathbf{y})$ by

$$\mathbf{y} = \varepsilon^{-1}\mathbf{x}, \qquad v(\mathbf{y}) = w(\varepsilon\mathbf{y}). \tag{107}$$

Then, we obtain that (105a) and (105b) transform to

$$\triangle_{\mathbf{y}}v = \varepsilon\mathbf{u}_0 \cdot \nabla_{\mathbf{y}}v, \qquad \mathbf{y} \in \mathbb{R}^2 \backslash \cup_{j=1}^2 D_j, \tag{108a}$$

$$v = \alpha_j, \qquad \mathbf{y} \in \partial D_j, \quad j = 1,2. \tag{108b}$$

Here $D_j = \{\mathbf{y} \mid |\mathbf{y} - \mathbf{y}_j| \leq 1\}$ is the circular disk centered at $\mathbf{y}_j = \mathbf{x}_j/\varepsilon$ of radius one, and $\mathbf{u}_0 \equiv \mathbf{u}(0)$. The inter-disk separation is

$$|\mathbf{y}_2 - \mathbf{y}_1| = 2l. \tag{109}$$

We then look for a solution to (108) in the form

$$v = v_0 + \nu A v_c, \tag{110}$$

where $\nu = \mathcal{O}(-1/\log\varepsilon)$ and $A = A(\nu)$ is to be found. Here v_0 solves

$$\triangle_{\mathbf{y}}v_0 = 0, \qquad \mathbf{y} \in \mathbb{R}^2 \backslash \cup_{j=1}^2 D_j, \tag{111a}$$

$$v_0 = \alpha_j, \qquad \mathbf{y} \in \partial D_j, \quad j = 1,2, \tag{111b}$$

$$v_0 \text{ bounded as } |\mathbf{y}| \to \infty. \tag{111c}$$

Moreover, $v_c(\mathbf{y})$ is the solution to

$$\triangle_{\mathbf{y}}v_c = 0, \qquad \mathbf{y} \in \mathbb{R}^2 \backslash \cup_{j=1}^2 D_j, \tag{112a}$$

$$v_c = 0, \qquad \mathbf{y} \in \partial D_j, \quad j = 1,2, \tag{112b}$$

$$v_c \sim \log|\mathbf{y}|, \quad \text{as} \quad |\mathbf{y}| \to \infty. \tag{112c}$$

Since D_j for $j = 1,2$ are non-overlapping circular disks, the problem (111) can be solved explicitly using conformal mapping and the introduction of symmetric points. In this way, we can derive that

$$v_0 \sim v_{0\infty} + o(1), \quad \text{as} \quad |\mathbf{y}| \to \infty. \tag{113}$$

The simple calculation of $v_{0\infty}$ is omitted. When $\alpha_1 = \alpha_2 = \alpha_c$, then clearly $v_{0\infty} = \alpha_1$. Next, we can solve (112) exactly by introducing bipolar coordinates as in Appendix B of Coombs et al. (2009). In this way, we calculate that

$$v_c(\mathbf{y}) \sim \log|\mathbf{y}| - \log d + o(1), \quad |\mathbf{y}| \to \infty, \tag{114}$$

where d is given by

$$\log d = \log\left(2\beta\right) - \frac{\xi_c}{2} + \sum_{m=1}^{\infty} \frac{e^{-m\xi_c}}{m\cosh(m\xi_c)}\,. \tag{115}$$

Here β and ξ_c are determined in terms of l by

$$\beta = \sqrt{l^2 - 1}\,; \qquad \xi_c = \log\left[l + \sqrt{l^2 - 1}\right]\,. \tag{116}$$

We remark that in this analysis we have neglected the transcendentally small $\mathcal{O}(\varepsilon)$ term in (108), representing a weak drift in the inner region.

Upon substituting (113) and (114) into (110), and writing $\mathbf{y} = \varepsilon^{-1}\mathbf{x}$, we obtain in terms of outer variables that the far-field behavior of v is

$$v \sim v_{0\infty} + A + \nu A \log|\mathbf{x}|\,, \qquad \nu \equiv \frac{-1}{\log\left(\varepsilon d\right)}\,. \tag{117}$$

The behavior (117) is the singularity behavior for the infinite-logarithmic series approximation $V_0(\mathbf{x};\mu)$ to the outer solution as $\mathbf{x} \to 0$. This approximation satisfies

$$\triangle V_0 = \mathbf{u} \cdot \nabla V_0\,, \qquad \mathbf{x} \in \mathbb{R}^2\backslash\{0\}\,; \qquad V_0 \sim 1\,, \quad |\mathbf{x}| \to \infty\,, \tag{118}$$

with singularity behavior (117) as $\mathbf{x} \to 0$. To solve (118), we introduce the Green's function $G(\mathbf{x};\boldsymbol{\xi})$ satisfying

$$\triangle G = \mathbf{u} \cdot \nabla G - \delta(\mathbf{x} - \boldsymbol{\xi})\,, \qquad \mathbf{x} \in \mathbb{R}^2\,, \tag{119a}$$

$$G(\mathbf{x};\boldsymbol{\xi}) \sim -\frac{1}{2\pi}\log|\mathbf{x} - \boldsymbol{\xi}| + R(\boldsymbol{\xi};\boldsymbol{\xi}) + o(1)\,, \quad \mathbf{x} \to \boldsymbol{\xi}\,, \tag{119b}$$

with $G(\mathbf{x};\boldsymbol{\xi}) \to 0$ as $|\mathbf{x}| \to \infty$. Here $R(\boldsymbol{\xi};\boldsymbol{\xi})$ is the regular part of this Green's function at $\mathbf{x} = \boldsymbol{\xi}$.

The solution to (118) with singular behavior $V_0 \sim \nu A \log|\mathbf{x}|$ as $\mathbf{x} \to 0$ is

$$V_0 = 1 - 2\pi\nu A G(\mathbf{x};0)\,. \tag{120}$$

By expanding (120) as $\mathbf{x} \to 0$, and equating the regular part of the resulting expression with that in (117), we get $1 - 2\pi\nu A R_{00} = A + v_{0\infty}$. This determines $A = A(\nu)$ by

$$A = \frac{1 - v_{0\infty}}{1 + 2\pi\nu R_{00}}\,, \qquad \nu \equiv \frac{-1}{\log(\varepsilon d)}\,, \tag{121}$$

where $R_{00} \equiv R(0;0)$. The outer and inner solutions are then given in terms of A. Finally, one can calculate the Nusselt number, representing

the average heat flux across the bodies, by using the divergence theorem together with the form (117) of the far-field behavior in the inner region. We leave this simple calculation to the reader.

<u>Case 2:</u> We assume that $l = \mathcal{O}(\varepsilon^{-1})$ as $\varepsilon \to 0$, and define $l = l_0/\varepsilon$ with $l_0 = \mathcal{O}(1)$, so that $|\mathbf{x}_2 - \mathbf{x}_1| = 2l_0$. This is the case where the small disks of radius ε are separated by $\mathcal{O}(1)$ distances in (105). In the analysis there are two distinct inner regions; one near $\mathbf{x}_1$ and the other at an $\mathcal{O}(1)$ distance away centered at $\mathbf{x}_2$. Since each separated disk is a circle of radius ε, it has a logarithmic capacitance $d = 1$. Therefore, the infinite-logarithmic series approximation $V_0(\mathbf{x}; \mu)$ to the outer solution satisfies

$$\triangle V_0 = \mathbf{u} \cdot \nabla V_0 \,, \qquad \mathbf{x} \in \mathbb{R}^2 \backslash \{0\} \,; \qquad V_0 \sim 1 \,, \quad |\mathbf{x}| \to \infty \,, \qquad (122a)$$

$$V_0 \sim \alpha_j + A_j + \nu A_j \log |\mathbf{x} - \mathbf{x}_j| \,, \quad \nu \equiv \frac{-1}{\log \varepsilon} \,. \qquad (122b)$$

The solution to (122) is given explicitly by

$$V_0 = 1 - 2\pi\nu \sum_{i=1}^{2} A_i G(\mathbf{x}; \mathbf{x}_i) \,. \qquad (123)$$

We then let $\mathbf{x} \to \mathbf{x}_j$ for $j = 1, 2$ in (123) and equate the nonsingular part of the resulting expression with the regular part of the singularity structure in (122b). This yields that A_1 and A_2 satisfy the linear algebraic system

$$A_1 (1 + 2\pi\nu R_{11}) + 2\pi\nu A_2 G_{12} = 1 - \alpha_1 \,, \qquad (124)$$

$$A_2 (1 + 2\pi\nu R_{22}) + 2\pi\nu A_1 G_{21} = 1 - \alpha_2 \,. \qquad (125)$$

Here $G_{ij} = G(\mathbf{x}_j; \mathbf{x}_i)$ and $R_{jj} = R(\mathbf{x}_j; \mathbf{x}_j)$ are the Green's function and its regular part as defined by (119).

Finally, we remark that for the case of a uniform flow where $\mathbf{u} = (1, 0)$, then the explicit solution to (119) is

$$G(\mathbf{x}; \boldsymbol{\xi}) = \frac{1}{2\pi} \exp\left[\frac{x_1 - \xi_1}{2}\right] K_0 (|\mathbf{x} - \boldsymbol{\xi}|) \,, \qquad (126a)$$

where $\mathbf{x} = (x_1, x_2)$ and $\boldsymbol{\xi} = (\xi_1, \xi_2)$. By letting $\mathbf{x} \to \boldsymbol{\xi}$, and using $K_0(r) \sim -\log r + \log 2 - \gamma_e$, as $r \to 0^+$, where γ_e is Euler's constant, we readily calculate that

$$R(\boldsymbol{\xi}, \boldsymbol{\xi}) = \frac{1}{2\pi} (\log 2 - \gamma_e) \,. \qquad (126b)$$

These results for G and its regular part can be used in the results of either (121) or (125) for Case I or Case II, respectively.

5 The Fundamental Neumann Eigenvalue in a Planar Domain with Localized Traps

In this section we follow Kolokolnikov et al. (2005) and consider an optimization problem for the fundamental eigenvalue of the Laplacian in a planar bounded two-dimensional domain with a reflecting boundary that is perturbed by the presence of K small holes in the interior of the domain. The perturbed eigenvalue problem is

$$\Delta u + \lambda u = 0, \quad \mathbf{x} \in \Omega \backslash \Omega_p; \quad \int_{\Omega \backslash \Omega_p} u^2 \, d\mathbf{x} = 1, \tag{127a}$$

$$\partial_n u = 0, \quad \mathbf{x} \in \partial\Omega; \quad u = 0, \quad \mathbf{x} \in \partial\Omega_p \equiv \cup_{i=1}^{K} \partial\Omega_{\varepsilon_i}. \tag{127b}$$

Here Ω is the unperturbed domain, $\Omega_p = \cup_{i=1}^{K} \Omega_{\varepsilon_i}$ is a collection of K small interior holes Ω_{ε_i}, for $i = 1, \ldots, K$, each of 'radius' $\mathcal{O}(\varepsilon)$, and $\partial_n u$ is the outward normal derivative of u on $\partial\Omega$. We assume that the small holes in Ω are non-overlapping and that $\Omega_{\varepsilon_i} \to \mathbf{x}_i$ as $\varepsilon \to 0$, for $i = 1, \ldots, K$. A schematic plot of the domain is shown in Fig. 7.
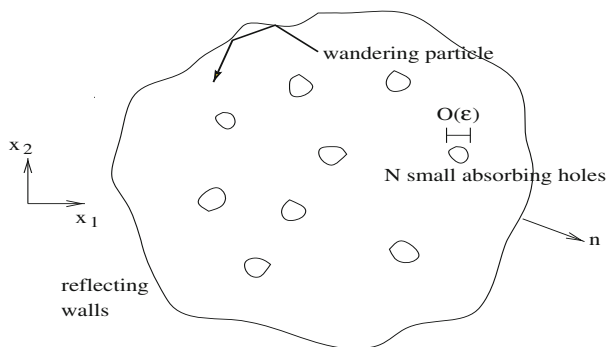
Figure 7. A schematic plot of the perturbed domain for the eigenvalue problem (127).

We let $\lambda_0(\varepsilon)$ denote the first eigenvalue of (127), with corresponding eigenfunction $u(\mathbf{x}, \varepsilon)$. Clearly, $\lambda_0(\varepsilon) \to 0$ as $\varepsilon \to 0$. Our objective is to determine the locations, $\mathbf{x}_i$ for $i = 1, \ldots, K$, of the K holes of a given shape that maximize this fundamental eigenvalue. Asymptotic expansions for the fundamental eigenvalue of related eigenvalue problems in perforated multi-dimensional domains, with various boundary conditions on the

holes and outer boundary, are given in Ozawa (1981), Ward et al. (1993), Ward and Keller (1993), Davis and Llewellyn-Smith (2007), and Lange and Weinitschke (1994) (see also the references therein).

As an application of (127), consider the Brownian motion of a particle in a two-dimensional domain Ω, with reflecting walls, that contains K small traps Ω_{ε_i}, for $i = 1, \ldots, K$, each of 'radius' ε, for $i = 1, \ldots, K$. The traps are centered at $\mathbf{x}_i$, for $i = 1, \ldots, K$. If the Brownian particle starts from the point $\mathbf{y} \in \Omega \backslash \Omega_p$ at time $t = 0$, then the probability density $v(\mathbf{x}, \mathbf{y}, t, \varepsilon)$ that the particle is at point $\mathbf{x}$ at time t satisfies

$$v_t = \Delta v, \quad \mathbf{x} \in \Omega \backslash \Omega_p; \quad \partial_n v = 0, \quad \mathbf{x} \in \partial \Omega; \quad v = 0, \quad \mathbf{x} \in \partial \Omega_p, \quad (128)$$

with $v = \delta(\mathbf{x} - \mathbf{y})$ at time $t = 0$. By calculating the solution to (128) in terms of an eigenfunction expansion, and by assuming that $\mathbf{y}$ is uniformly distributed over $\Omega \backslash \Omega_p$, it is easy to show that the probability $P_0(t, \varepsilon)$ that the Brownian particle is in $\Omega \backslash \Omega_p$ at time t is given by

$$P_0(t, \varepsilon) = e^{-\lambda_0(\varepsilon) t} \left[1 + \mathcal{O}(\nu) \right] . \quad (129)$$

Therefore, the expected lifetime of the Brownian particle is proportional to $1/\lambda_0(\varepsilon)$. In this context, our optimization problem is equivalent to choosing the locations of K small traps to minimize this expected lifetime.

We first consider (127) for the case of one hole. In Ward et al. (1993) (see also Ward and Keller (1993)) it was shown that as $\varepsilon \to 0$ the first eigenvalue λ_0 of (127) has the asymptotic expansion:

$$\lambda_0(\varepsilon) = \lambda_{00} + \nu(\varepsilon) \lambda_{01} + \nu^2(\varepsilon) \lambda_{02} + \cdots .$$

Here, $\nu(\varepsilon) = -1/\log(\varepsilon d)$ where d is the logarithmic capacitance of the hole. For the unperturbed problem with $\varepsilon = 0$, we have $\lambda_{00} = 0$. In the $\mathcal{O}(\nu)$ term, λ_{01} is independent of the location of the hole at $\mathbf{x} = \mathbf{x}_0$ (cf. Ward et al. (1993)). Therefore, we need the higher-order coefficient λ_{02} in order to determine the location of the hole that maximizes λ_0.

For the case of one hole, an infinite logarithmic expansion for $\lambda_0(\varepsilon)$ has the form

$$\lambda_0(\varepsilon) = \lambda^*(\nu) + \mathcal{O}\left(\frac{\varepsilon}{\log \varepsilon} \right), \quad \nu \equiv -\frac{1}{\log(\varepsilon d)} .$$

To calculate $\lambda^*(\nu)$ we use the hybrid method of Kolokolnikov et al. (2005). Near the hole, we identify an inner (local) region in terms of a local spatial variable $\mathbf{y} = \varepsilon^{-1}(\mathbf{x} - \mathbf{x}_0)$, and where the hole is rescaled so that $\Omega_0 \equiv \varepsilon^{-1} \Omega_\varepsilon$. Denoting the inner (local) solution by $v(\mathbf{y}, \varepsilon) = u(\mathbf{x}_0 + \varepsilon \mathbf{y}, \varepsilon)$, we then expand $v(\mathbf{y}, \varepsilon)$ as

$$v(\mathbf{y}, \varepsilon) = A \nu v_c(\mathbf{y}) + \cdots . \quad (130)$$

Here, $A = A(\nu) \sim \mathcal{O}(1)$ as $\varepsilon \to 0$, and $v_c(\mathbf{y})$ is the solution of the canonical inner problem (7), re-written here as

$$\Delta_{\mathbf{y}} v_c = 0, \quad \mathbf{y} \notin \Omega_0; \quad v_c = 0, \quad \mathbf{y} \in \partial\Omega_0, \tag{131a}$$

$$v_c \sim \log |\mathbf{y}| - \log d + \frac{\mathbf{p} \cdot \mathbf{y}}{|\mathbf{y}|^2}, \quad \text{as} \quad |\mathbf{y}| \to \infty. \tag{131b}$$

In (131b), the logarithmic capacitance d and the dipole vector $\mathbf{p} = (p_1, p_2)$ are determined from the shape of the hole.

We expand the eigenvalue λ_0 and the outer (global) solution as

$$\lambda_0(\varepsilon) = \lambda^*(\nu) + \mu\lambda_1 + \cdots, \qquad u(\mathbf{x}, \varepsilon) = u^*(\mathbf{x}, \nu) + \mu u_1(\mathbf{x}, \nu) + \cdots, \tag{132}$$

where $\mu \ll \mathcal{O}(\nu^k)$ for any $k > 0$. Substituting (132) into (127a) and the boundary condition (127b) on $\partial\Omega$, we obtain the full problem in a domain punctured by the point $\mathbf{x}_0$,

$$\Delta u^* + \lambda^* u^* = 0, \quad x \in \Omega \backslash \{\mathbf{x}_0\}; \quad \int_{\Omega} (u^*)^2 \, d\mathbf{x} = 1; \quad \partial_n u^* = 0, \quad \mathbf{x} \in \partial\Omega. \tag{133}$$

The singularity condition for (133) as $\mathbf{x} \to \mathbf{x}_0$ given below arises from matching u^* to the inner solution. Substituting (131b) into (130), and expressing the result in global variables, we obtain

$$v(\mathbf{y}, \varepsilon) \sim A\nu \log |\mathbf{x} - \mathbf{x}_0| + A + \varepsilon A\nu \frac{\mathbf{p} \cdot (\mathbf{x} - \mathbf{x}_0)}{|\mathbf{x} - \mathbf{x}_0|^2} + \cdots, \quad \text{as} \quad \mathbf{y} \to \infty. \tag{134}$$

Here, we have used $\nu \equiv -1/\log(\varepsilon d)$. To match u^* to (134), we require that u^* has the singularity behavior

$$u^*(\mathbf{x}, \nu) \sim A\nu \log |\mathbf{x} - \mathbf{x}_0| + A, \quad \text{as} \quad \mathbf{x} \to \mathbf{x}_0. \tag{135}$$

Comparing the terms in (134) and (132) at the next order, we see that $\mu = \mathcal{O}(\varepsilon\nu)$.

Next, we must determine $u^*(\mathbf{x}, \nu)$ and $\lambda^*(\nu)$ satisfying (133) and (135). To do so, we introduce the Helmholtz Green's function, $G_h(\mathbf{x}; \mathbf{x}_0, \lambda^*)$, and its regular part, $R_h(\mathbf{x}_0; \mathbf{x}_0, \lambda^*)$, satisfying

$$\Delta G_h + \lambda^* G_h = -\delta(\mathbf{x} - \mathbf{x}_0), \quad \mathbf{x} \in \Omega; \quad \partial_n G_h = 0, \quad \mathbf{x} \in \partial\Omega, \tag{136a}$$

$$G_h(\mathbf{x}; \mathbf{x}_0, \lambda^*) \sim -\frac{1}{2\pi} \log |\mathbf{x} - \mathbf{x}_0| + R_h(\mathbf{x}_0; \mathbf{x}_0, \lambda^*) + o(1), \quad \text{as} \quad \mathbf{x} \to \mathbf{x}_0. \tag{136b}$$

In terms of this Green's function, $u^*(\mathbf{x}, \nu)$ is given by

$$u^*(\mathbf{x}, \nu) = -2\pi A \nu G_h(\mathbf{x}; \mathbf{x}_0, \lambda^*).$$

By using (136b), we expand u^* as $\mathbf{x} \to \mathbf{x}_0$ to obtain

$$u^*(\mathbf{x}, \nu) \sim A \nu \log |\mathbf{x} - \mathbf{x}_0| - 2\pi A \nu R_h(\mathbf{x}_0; \mathbf{x}_0, \lambda^*), \quad \text{as} \quad \mathbf{x} \to \mathbf{x}_0. \quad (137)$$

The matching condition is that the expressions in (135) and (137) agree. The $\log |\mathbf{x} - \mathbf{x}_0|$ terms agree automatically, and from the remaining terms, we obtain a transcendental equation for $\lambda^*(\nu)$ given by

$$R_h(\mathbf{x}_0; \mathbf{x}_0, \lambda^*) = -\frac{1}{2\pi\nu}. \quad (138)$$

To obtain the asymptotic behavior for λ_0, we need the solution λ^* of (138) that tends to zero as $\nu \to 0$.

Equation (138) can, in general, only be solved numerically as a function of ν. Below, we only determine an expression for λ^* that is correct to terms of order $\mathcal{O}(\nu^2)$. To obtain this expression, we expand the Helmholtz Green's function, $G_h(\mathbf{x}; \mathbf{x}_0, \lambda^*)$, in terms of $\lambda^* \ll 1$, as

$$G(\mathbf{x}; \mathbf{x}_0, \lambda^*) = \frac{1}{\lambda^*} G_0(\mathbf{x}; \mathbf{x}_0) + G_1(\mathbf{x}; \mathbf{x}_0) + \lambda^* G_2(\mathbf{x}; \mathbf{x}_0) + \cdots. \quad (139)$$

Substituting (139) into (136), we get a series of problems for the $G_j(\mathbf{x}; \mathbf{x}_0)$, $j = 0, 1, 2, \ldots$. At order $\mathcal{O}(1/\lambda^*)$, G_0 satisfies $\Delta G_0 = 0$ in Ω and $\partial_n G_0 = 0$ on $\partial\Omega$, from which we obtain that G_0 is a constant. The higher-order corrections G_j for $j \geq 1$ are readily found to satisfy

$$\Delta G_j = \begin{cases} -\delta(\mathbf{x} - \mathbf{x}_0) - G_0, & j = 1, \\ -G_{j-1}, & j > 1, \end{cases} \quad \mathbf{x} \in \Omega; \quad \partial_n G_j = 0, \quad \mathbf{x} \in \partial\Omega, \quad (140)$$

with $\int_\Omega G_j \, d\mathbf{x} = 0$ for $j \geq 1$. Applying the Divergence Theorem, we obtain that $G_0 = -1/|\Omega|$, where $|\Omega|$ is the area of Ω. The function $G_1(\mathbf{x}; \mathbf{x}_0)$ (which we shall henceforth call G_N) is the Neumann Green's function, with regular part $R_N(\mathbf{x}_0; \mathbf{x}_0)$ defined by (49).

From (139) and (49b), we write the two-term expansion for G when $\lambda^* \ll 1$ as

$$G_h(\mathbf{x}; \mathbf{x}_0, \lambda^*) = -\frac{1}{|\Omega|\lambda^*} + G_N(\mathbf{x}; \mathbf{x}_0) + \mathcal{O}(\lambda^*). \quad (141)$$

A similar two-term expansion for the regular part R_h of the Helmholtz Green's function in terms of the regular part of the Neumann Green's function is

$$R_h(\mathbf{x}_0; \mathbf{x}_0, \lambda^*) = -\frac{1}{|\Omega|\lambda^*} + R_N(\mathbf{x}_0; \mathbf{x}_0) + \mathcal{O}(\lambda^*). \quad (142)$$

Substituting this expression into (138), we get the following two-term asymptotic result:

Principal Result 3:(One Hole) For $\varepsilon \to 0$, the first eigenvalue λ_0 of (127) has the two-term asymptotic behavior

$$\lambda_0(\varepsilon) = \frac{2\pi\nu}{|\Omega|\,(1 + 2\pi\nu R_N(\mathbf{x}_0; \mathbf{x}_0))} + \mathcal{O}(\nu^3) = \frac{2\pi\nu}{|\Omega|} - \frac{4\pi^2\nu^2}{|\Omega|} R_N(\mathbf{x}_0; \mathbf{x}_0) + \mathcal{O}(\nu^3)\,.$$

$$(143)$$

Here $\nu = -1/\log(\varepsilon d)$, and d is the logarithmic capacitance determined from the inner problem (131). An infinite-order logarithmic expansion for λ_0 is given by $\lambda_0 \sim \lambda^*$, where λ^* is the first positive root of (138).

Next, we extend the asymptotic framework to the case of K holes. Much of the analysis above remains the same, except that now the single hole $\mathbf{x}_0$ is replaced by $\mathbf{x}_i$, for $i = 1, \ldots, K$. The hybrid formulation for K holes is

$$\Delta u^* + \lambda^* u^* = 0\,, \quad x \in \Omega \backslash \{\mathbf{x}_1, \ldots, \mathbf{x}_K\}\,; \quad \partial_n u^* = 0\,, \quad \mathbf{x} \in \partial\Omega\,, \quad (144\text{a})$$

$$u^* \sim A_i\,\nu_i\,\log|\mathbf{x} - \mathbf{x}_i| + A_i\,, \quad \text{as} \quad \mathbf{x} \to \mathbf{x}_i\,, \ i = 1, \ldots, K\,,$$

$$(144\text{b})$$

with normalization condition $\int_\Omega (u^*)^2\, d\mathbf{x} = 1$. Here, $\nu_i = -1/\log(\varepsilon d_i)$, where d_i is the logarithmic capacitance of the ith hole. In this formulation, we have the K unknowns, A_i, for $i = 1, \ldots, K$, and one normalization condition for u^*. The normalization condition effectively sets one relation between the A_i, for $i = 1, \ldots, K$.

We write u^* in terms of the Helmholtz Green's function defined in (136), and then take the limit $\mathbf{x} \to \mathbf{x}_i$ to get

$$u^* = -2\pi \sum_{j=1}^{K} A_j \nu_j G_h(\mathbf{x}; \mathbf{x}_j, \lambda^*) \sim A_i \nu_i \left(\log|\mathbf{x} - \mathbf{x}_i| - 2\pi\nu_i R_h(\mathbf{x}_i; \mathbf{x}_i, \lambda^*) \right)$$

$$- 2\pi \sum_{\substack{j=1 \\ j \neq i}}^{K} A_j \nu_j G_h(\mathbf{x}_i; \mathbf{x}_j, \lambda^*)\,. \quad (145)$$

The matching condition is that the expressions in (144b) and (145) agree. The logarithmic terms agree, and from the remaining terms, we obtain a $K \times K$ homogeneous linear system to solve for the A_i, given by

$$A_i \left(1 + 2\pi\nu_i R_h(\mathbf{x}_i; \mathbf{x}_i, \lambda^*) \right) + 2\pi \sum_{\substack{j=1 \\ j \neq i}}^{K} A_j \nu_j G_h(\mathbf{x}_i; \mathbf{x}_j, \lambda^*) = 0\,, \ i = 1, \ldots, K\,.$$

$$(146)$$

A solution to (146) exists only when the determinant associated with the linear system (146) vanishes. This condition provides an expression for $\lambda^*(\nu_1, \ldots, \nu_K)$ that sums all the logarithmic terms in the asymptotic expansion of $\lambda_0(\varepsilon)$.

As with the case for one hole in the domain, we can derive an asymptotic formula for λ^* that has an error of $\mathcal{O}(\nu^3)$. This formula is again determined in terms of the Neumann Green's function G_N and its regular part R_N, defined in (49). By using (141) and (142) in (146), we obtain a homogeneous linear system for the A_i for $i = 1, \ldots, K$, given by

$$A_i \left[1 + 2\pi\nu_i R_N(\mathbf{x}_j; \mathbf{x}_j) - \frac{2\pi\nu_i}{|\Omega|\lambda^*} \right] + 2\pi \sum_{\substack{j=1 \\ j \neq i}}^{K} A_j \nu_j \left[-\frac{1}{|\Omega|\lambda^*} + G_N(\mathbf{x}_j; \mathbf{x}_i) \right] = 0 \,.$$

$$(147)$$

It is convenient to write (147) in matrix form as

$$\mathcal{C}\boldsymbol{a} = \frac{2\pi}{|\Omega|\lambda^*} \mathcal{B}\mathcal{V}\boldsymbol{a} \,, \qquad \mathcal{C} \equiv I + 2\pi\mathcal{G}_N\mathcal{V} \,, \qquad (148\text{a})$$

where

$$\mathcal{V} \equiv \begin{pmatrix} \nu_1 & 0 & \cdots & 0 \\ 0 & \ddots & \cdots & 0 \\ \vdots & \vdots & \ddots & \vdots \\ 0 & 0 & \cdots & \nu_K \end{pmatrix}, \quad \mathcal{B} \equiv \begin{pmatrix} 1 & 1 & \cdots & 1 \\ 1 & \ddots & \cdots & 1 \\ \vdots & \vdots & \ddots & \vdots \\ 1 & 1 & \cdots & 1 \end{pmatrix}, \quad \boldsymbol{a} \equiv \begin{pmatrix} A_1 \\ \vdots \\ A_K \end{pmatrix}.$$

$$(148\text{b})$$

In (148a), the Neumann Green's function matrix $\mathcal{G}_N$ is the $K \times K$ symmetric matrix with entries

$$(\mathcal{G}_N)_{ij} \equiv G_N(\mathbf{x}_i; \mathbf{x}_j) \,, \quad i \neq j \,; \qquad (\mathcal{G}_N)_{jj} = R_N(\mathbf{x}_j; \mathbf{x}_j) \,. \qquad (148\text{c})$$

Let $\nu_m = \max_{j=1,\ldots,K} \nu_j$. Then, for ν_m sufficiently small, we can invert $\mathcal{C}$ approximately, to obtain that λ^* is an eigenvalue of the matrix eigenvalue problem

$$\mathcal{A}\boldsymbol{a} = \lambda^*\boldsymbol{a} \,, \qquad \mathcal{A} = \frac{2\pi}{|\Omega|} \mathcal{C}^{-1}\mathcal{B}\mathcal{V} \,. \qquad (149)$$

By using this representation of λ^* we obtain the following result:

Principal Result 4:(K Holes) For $\varepsilon \to 0$, the first eigenvalue λ_0 of (127) has the explicit two-term asymptotic behavior

$$\lambda_0(\varepsilon) \sim \lambda^* \,, \qquad \lambda^* = \frac{2\pi}{|\Omega|} \left(\sum_{j=1}^{K} \nu_j - 2\pi \sum_{j=1}^{K} \sum_{i=1}^{K} \nu_j \nu_i \left(\mathcal{G} \right)_{Nij} \right) + \mathcal{O}(\nu_m^3) \,.$$

$$(150)$$

Here $(\mathcal{G})_{Nij}$ are the entries of the Neumann Green's function matrix $\mathcal{G}_N$ defined in (148c).

Proof. We first notice that the matrix $\mathcal{B}\mathcal{V}$ has rank one, since $\mathcal{V}$ is diagonal and $\mathcal{B} = e_0 e_0^t$, where $e_0^t = (1, 1, \ldots, 1)$. This implies that $\mathcal{A}$ has rank one, and so λ^* is the unique nonzero eigenvalue of $\mathcal{A}$. Hence, $\lambda^* = \text{Trace}\mathcal{A}$. By using the structure of $\mathcal{A}$ in (149), we readily calculate that

$$\lambda^* = \frac{2\pi}{|\Omega|} \sum_{j=1}^{K} \nu_j \left(\sum_{i=1}^{K} c_{ij} \right), \qquad c_{ij} \equiv \left(\mathcal{C}^{-1} \right)_{ij} . \qquad (151)$$

Finally, we use the asymptotic inverse $\mathcal{C}^{-1} \sim I - 2\pi\mathcal{G}_N\mathcal{V} + \cdots$ for $\nu_m \ll 1$ to calculate c_{ij}. Substituting this result into (151) we obtain (150). ∎

As a Corollary to this result, we obtain the following simplification for the case of K identical holes:

Corollary 5:(K Identical Holes) Suppose that the K holes are identical, in the sense that εd_j is independent of j. Then, (150) can be written as the explicit two-term expansion

$$\lambda_0(\varepsilon) \sim \lambda^*, \qquad \lambda^* = \frac{2\pi K \nu}{|\Omega|} - \frac{4\pi^2 \nu^2}{|\Omega|} p(\mathbf{x}_1, \ldots, \mathbf{x}_K) + \mathcal{O}(\nu^3), \qquad (152)$$

where $\nu \equiv -1/\log(\varepsilon d)$, and the function $p(\mathbf{x}_1, \ldots, \mathbf{x}_K)$ is defined by

$$p(\mathbf{x}_1, \ldots, \mathbf{x}_K) = \sum_{j=1}^{K} \sum_{i=1}^{K} (\mathcal{G})_{Nij} = \sum_{i=1}^{K} \left(R_N(\mathbf{x}_i; \mathbf{x}_i) + \sum_{\substack{j=1 \\ j \neq i}}^{K} G_N(\mathbf{x}_j; \mathbf{x}_i) \right) .$$
$$(153)$$

Here $(\mathcal{G})_{Nij}$ are the entries in the matrix $\mathcal{G}_N$ in (148c). For K circular holes of radius ε, then $d_j = 1$ for $j = 1, \ldots, K$, and so $\nu = -1/\log \varepsilon$.

When Ω is the unit disk, the optimal spatial configurations of the centers $\{\mathbf{x}_1, \ldots, \mathbf{x}_K\}$ of K distinct traps of a common radius ε were computed numerically in Kolokolnikov et al. (2005) by optimizing the function $p(\mathbf{x}_1, \ldots, \mathbf{x}_K)$ in (153). For the unit disk, the Neumann Green's function $G_N(\mathbf{x}; \boldsymbol{\xi})$ and its regular part $R_N(\boldsymbol{\xi}; \boldsymbol{\xi})$ are explicitly available (see equation (52)). By using this Green's function, it is readily shown that the problem of minimizing the function $p(\mathbf{x}_1, \ldots, \mathbf{x}_K)$ is equivalent to the discrete

variational problem of minimizing the function $\mathcal{F}(\mathbf{x}_1, \ldots, \mathbf{x}_K)$ defined by

$$
\mathcal{F}(\mathbf{x}_1, \ldots, \mathbf{x}_K) = -\sum_{j=1}^{K} \sum_{\substack{k=1 \\ k \neq j}}^{K} \log |\mathbf{x}_j - \mathbf{x}_k| - \sum_{j=1}^{K} \sum_{k=1}^{K} \log |1 - \mathbf{x}_j \bar{\mathbf{x}}_k| + K \sum_{j=1}^{K} |\mathbf{x}_j|^2 \,,
$$

(154)

for $|xij| = 1$ and $\mathbf{x}_j \neq \mathbf{x}_k$ when $j \neq k$. Here $\bar{\mathbf{x}}_k$ denotes the complex conjugate of $\mathbf{x}_k$.

An interesting open problem is to determine the optimal arrangement of $K \gg 1$ traps in the dilute fraction limit $K\varepsilon^2 \ll 1$. In particular, does the optimal arrangement approach a hexagonal lattice structure with a boundary layer near the rim of the unit disk?

6   Conclusion

In this article we have surveyed the development and application of a hybrid asymptotic-numerical method for solving linear and nonlinear PDE models in two-dimensional domains that have small inclusions or obstructions. Related theoretical approaches have also been developed to treat similar strongly localized perturbation problems including, an eigenvalue perturbation problem in a three-dimensional domain (cf. Ward and Keller (1993)), cell-signaling problems in mathematical biology (cf. Bressloff et al. (2008), Straube and Ward (2009)), the narrow escape problem from a sphere or a disk that has small absorbing windows on its boundary (cf. Cheviakov et al. (to appear, 2010), Pillay et al. (to appear, 2010)), and the mean first passage time in a three-dimensional domain with interior traps (cf. Cheviakov and Ward (to appear, 2010)).

Acknowledgments

Bibliography

C. Bandle and M. Flucher. Harmonic radius and concentration of energy; hyperbolic radius and liouville's equation. *SIAM Review*, 38(2):191–238,

1996.

P. C. Bressloff, D. Earnshaw, and M. J. Ward. Diffusion of protein receptors on a cylindrical dendritic membrane with partially absorbing traps. *SIAM J. Appl. Math.*, 68(5):1223–1246, 2008.

A. Cheviakov and M. J. Ward. Optimizing the fundamental eigenvalue of the laplacian in a sphere with interior traps. *Mathematical and Computer Modeling*, to appear, 2010.

A. Cheviakov, M. J. Ward, and R. Straube. An asymptotic analysis of the mean first passage time for narrow escape problems: Part ii: The sphere. *SIAM J. Multiscale Modeling*, to appear, 2010.

J. Choi, D. Margetis, T. M. Squires, and M. Z. Bazant. Steady advection-diffusion around finite absorbers in two-dimensional potential flows. *J. Fluid Mech.*, 536:155–184, 2005.

D. Coombs, R. Straube, and M. J. Ward. Diffusion on a sphere with localized traps: Mean first passage time, eigenvalue asymptotics, and fekete points. *SIAM J. Appl. Math.*, 70(1):302–332, 2009.

A. M. Davis and S. G. Llewellyn-Smith. Perturbation of eigenvalues due to gaps in two-dimensional boundaries. *Proc. Roy. Soc. A*, 463:759–786, 2007.

W. W. Dijkstra and M. E. Hochstenbach. Numerical approximation of the logarithmic capacity. *CASA Report 08-09, Technical U. Eindhoven*, 2008.

M. Van Dyke. *Perturbations Methods in Fluid Mechanics*. Parabolic Press, 1975.

J. E. Fletcher. Mathematical modeling of the microcirculation. *Math Biosciences*, 38:159–202, 1978.

I. Imai. On the asymptotic behavior of viscous fluid flow at a great distance from a cylindrical body, with special reference to filon's paradox. *Proc. Roy. Soc. A*, 208:487–516, 1951.

S. Kaplun. Low reynolds number flow past a circular cylinder. *J. Math. Mech.*, 6(5):52–60, 1957.

J. B. Keller and M. J. Ward. Asymptotics beyond all orders for a low reynolds number flow. *J. Engrg. Math.*, 30(1-2):253–265, 1996.

J. Kevorkian and J. Cole. *Multiple Scale and Singular Perturbation Methods*. Applied Mathematical Sciences, Vol. 114, Springer-Verlag, 1993.

T. Kolokolnikov, M. Titcombe, and M. J. Ward. Optimizing the fundamental neumann eigenvalue for the laplacian in a domain with small traps. *Europ. J. Appl. Math.*, 16(2):161–200, 2005.

A. Krogh. The number and distribution of capillaries in muscles with calculations of the oxygen pressure head necessary for supplying the tissue. *J. Physiology (London)*, 52:409–415, 1919.

M. C. Kropinski, M. J. Ward, and J. B. Keller. A hybrid asymptotic-numerical method for calculating low reynolds number flows past symmetric cylindrical bodies. *SIAM J. Appl. Math.*, 55(6):1484–1510, 1995.

P. A. Lagerstrom. *Matched Asymptotic Expansions*. Applied Mathematical Sciences, Vol. 76, Springer-Verlag, 1988.

C. Lange and H. Weinitschke. Singular perturbations of elliptic problems on domains with small holes. *Stud. Appl. Math.*, 92(1):55–93, 1994.

S. H. Lee and L. G. Leal. Low reynolds number flow past cylindrical bodies of arbitrary cross-sectional shape. *J. Fluid Mech.*, 164:401–427, 1986.

MATLAB. *Partial Differential Equations Toolbox, User's Guide*. The Math-Works, Inc., 1996.

M. Matthews and J. Hill. Flow around nanospheres and nanocylinders. *Q. J. Mech. Appl. Math.*, 59(2):191–210, 2006.

M. Matthews and J. Hill. Asymptotic analysis of the viscous micro/nano pump at low reynolds number. *J. Engrg. Math.*, 63(2-4):279–292, 2009.

A. Mikelić and M. Primicerio. A diffusion-consumption problem for oxygen in a living tissue perfused by capillaries. *Nonlinear Diff. Eq. Appl.*, 13(3): 349–367, 2006.

L. M. Milne-Thomson. *Theoretical Aerodynamics*. Dover Publications Inc., 1958.

S. Ozawa. Singular variation of domains and eigenvalues of the laplacian. *Duke Math. J.*, 48(4):767–778, 1981.

S. Pillay, M. J. Ward, A. Peirce, and T. Kolokolnikov. An asymptotic analysis of the mean first passage time for narrow escape problems: Part i: Two-dimensional domains. *SIAM J. Multiscale Modeling*, to appear, 2010.

A. S. Popel. Theory of oxygen transport to tissue. *Critical Reviews in Biomedical Engrg.*, 17:257–321, 1989.

I. Proudman and J. Pearson. Expansions at small reynolds number for the flow past a sphere and a circular cylinder. *J. Fluid Mech.*, 2:237–262, 1957.

K. B. Ranger. Explicit solutions of the steady two-dimensional navier-stokes equations. *Stud. Appl. Math.*, 94(2):169–181, 1995.

T. Ransford. *Potential Theory in the Complex Plane*. London Mathematical Society Student Texts Vol. 28, Cambridge University Press, 1995.

K. Shintani, A. Umemura, and A. Takano. Low reynolds number flow past an elliptic cylinder. *J. Fluid Mech.*, 136:277–289, 1983.

L. A. Skinner. Generalized expansions for slow flow past a cylinder. *Q. J. Mech. Appl. Math.*, 28(3):333–340, 1975.

R. Straube and M. J. Ward. Intraceulluar signalling gradients arising from multiple compartments: A matched asymptotic expansion approach. *SIAM J. Appl. Math.*, 70(1):248–269, 2009.

M. Titcombe and M J. Ward. Convective heat transfer past small cylindrical bodies. *Stud. Appl. Math.*, 99(1):81–105, 1997.

M. Titcombe and M J. Ward. Summing logarithmic expansions for elliptic equations in multiply-connected domains with small holes. *Canadian Appl. Math. Quart.*, 7(3):313–343, 1999.

M. Titcombe and M J. Ward. An asymptotic study of oxygen transport from multiple capillaries to skeletal muscle tissue. *SIAM J. Appl. Math.*, 60(5):1767–1788, 2000.

M. Titcombe, M J. Ward, and M. C. Kropinski. A hybrid asymptotic-numerical solution for low reynolds number flow past an asymmetric cylindrical body. *Stud. Appl. Math.*, 105(2):165–190, 2000.

D. J. Tritton. Experiments on the flow past a circular cylinder at low reynolds numbers. *J. Fluid Mech.*, 6:547–567, 1959.

J. Veysey and N. Goldenfeld. Simple viscous flows: From boundary layers to the renormalization group. *Reviews of Modern Physics*, 79:883–927, 2007.

M. J. Ward, W. D. Henshaw, and J. B. Keller. Summing logarithmic expansions for singularly perturbed eigenvalue problems. *SIAM J. Appl. Math.*, 53(3):799–828, 1993.

M. J. Ward and J. B. Keller. Strong localized perturbations of eigenvalue problems. *SIAM J. Appl. Math.*, 53(3):770–798, 1993.

A. J. Ward-Smith. *Internal Fluid Flow.* Clarendon Press, Oxford, 1980.

Exponential Asymptotics and Generalized Solitary Waves

Roger Grimshaw [*]

[*] Loughborough University, UK

Abstract Many problems in fluid mechanics involve asymptotic expansions in the form of a power series for a suitable small parameter. Such expansions necessarily fail to find terms which are exponentially small with respect to this parameter. Although small these missing terms are often of physical importance. This chapter will describe how to find such exponentially small terms, using as the main tool matched asymptotic expansions in the complex plane and Borel summation. The techniques are developed in the context of model problems related primarily to the theory of weakly nonlocal solitary waves (also called generalized solitary waves) which arise in the study of gravity-capillary waves, internal waves and in several other physical contexts. These waves have a central core of finite amplitude, but are accompanied by co-propagating oscillatory tails whose amplitude is exponentially small. Special interest lies in the possibility that for certain parameter values, the amplitude of the oscillatory tails may be zero, leading to the important concept of embedded solitary waves.

1 Introduction

An inverse power series is asymptotic to a function $f(x)$ if, for *fixed N* and *sufficiently large $x > 0$*,

$$f(x) - \sum_{n=0}^{N} \frac{a_n}{x^n} = O(\frac{1}{x^{N+1}}). \tag{1}$$

This formal definition, due to Poincare, describes the limit when $x \to \infty$ for a fixed integer N. When (1) holds, we write

$$f(x) \sim \sum_{n=0}^{\infty} \frac{a_n}{x^n}. \tag{2}$$

Importantly the series expansion in (2) need not converge as $N \to \infty$ in order for it to be asymptotic. Our concern here is that when the series is asymptotic, but diverges, it fails to detect terms proportional to $\exp(-Kx)$, where $K > 0$ is a constant. Such terms are smaller than x^{-N} for any integer N as $x \to \infty$. The detection of such terms requires *exponential asymptotics*, or *asymptotics beyond all orders*, see Bender and Orzsag (1978) or Boyd (1998) for instance.

1.1 Stieltjes Integral

To begin, let us consider the function defined by the integral

$$I(x) = \int_0^\infty \frac{\exp(-xt)}{1+t} dt. \tag{3}$$

This function is well-defined for all $x > 0$. Now integrate by parts N times, to get that

$$I(x) = \sum_{n=0}^{N} (-1)^n \frac{n!}{x^{n+1}} + \epsilon_N(x), \tag{4}$$

$$\epsilon_N(x) = (-1)^{N+1} \frac{(N+1)!}{x^{N+1}} \int_0^\infty \frac{\exp(-xt)}{(1+t)^{N+1}} dt. \tag{5}$$

Since the integral term in (5) is bounded by $1/x$, it is easily shown that $\epsilon_N(x) = O(x^{-N-2})$ for each fixed N, and so

$$I(x) \sim \sum_{n=0}^{\infty} (-1)^n \frac{n!}{x^{n+1}}. \tag{6}$$

Note that the series diverges for all $x > 0$, but nonetheless is a useful approximation to $I(x)$ as $x \to \infty$.

For each fixed x, as $x \to \infty$, we can minimize $|\epsilon_N(x)|$ with respect to N. Using Stirling's formula for large N, $N! \approx (2\pi)^{1/2} \exp(-N) N^{N+1/2}$, we find that the minimum occurs when $N \approx x$, and then the error

$$\epsilon_N(x) = O(\exp(-x))$$

is *exponentially small*. The plot shows $x = 5, 10, 15$ (red, blue, black) and the exponential error (dots). This crucial observation leads to the well-developed theories for *optimal truncation, superasymptotics and hyperasymptotics*, see Berry and Howls (1990), (Berry, 1992, 11-14), Boyd (1998) or Boyd (1999) for instance.
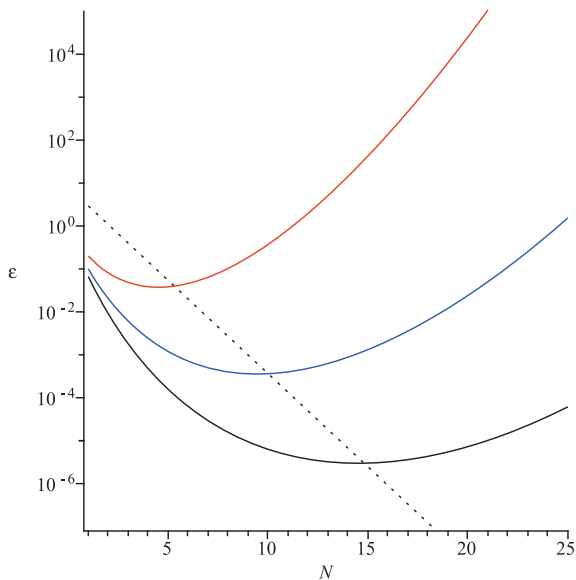
Figure 1. Plot of the error (5) as a function of N; the dashed line is proportional to $\exp(-x)$

1.2 Fourier Integral

Suppose that the function $F(x)$ is defined by

$$F(x) = \int_{-\infty}^{\infty} \hat{F}(k) \exp(ikx)\, dk\,, \tag{7}$$

where $\hat{F}^*(-k) = \hat{F}(k)$ for all real k, in order that $F(x)$ is real-valued (the superscript * denotes the complex conjugate). Suppose that the Fourier transform $\hat{F}(k)$ and all its derivatives vanish as $k \to \pm\infty$. Then we can estimate $F(x)$ as $x \to \pm\infty$ by integrating (7) by parts. The outcome is

$$F(x) = O(x^{-N})\,, \quad \text{as} \quad x \to \pm\infty\,, \tag{8}$$

for *all integers* N. The asymptotic series (2) has zero coefficients, and we infer that $F(x)$ is *exponentially small*. For $x > 0$, the contour of integration is moved into the upper half of the complex k-plane, that is $\operatorname{Im} k > 0$. Then if the nearest singularity of $\hat{F}(k)$ to the real k-axis is at $k = a + ib, b > 0$ we can estimate that $F(x) = O(\exp(-bx))$ as $x \to \infty$. An analogous procedure

is used if $x < 0$, when the contour is moved into the lower half of the complex k-plane.

For example, suppose that $\hat{F}(k) = \text{sech}(\gamma k)$ so that

$$F(x) = \int_{-\infty}^{\infty} \text{sech}(\gamma k) \exp(ikx) \, dk . \tag{9}$$

There are poles at $k = \pm i\pi/2\gamma, \pm 3i\pi/2\gamma, \cdots$. Evaluating the residue at the nearest pole to the real axis yields

$$F(x) \sim \frac{2\pi}{\gamma} \exp\left(-\frac{\pi|x|}{2\gamma}\right) . \tag{10}$$

Indeed, in this case the integral (9) can be explicitly evaluated to give

$$F(x) = \frac{\pi}{\gamma} \text{sech}\left(\frac{\pi x}{2\gamma}\right) ,$$

from which the estimate (10) readily follows.

1.3   Airy Functions

Airy's differential equation is

$$\frac{d^2 w}{dz^2} = zw , \tag{11}$$

expressed here for a complex-valued function $w(z)$ of the *complex variable* $z = x + iy$. Note that on the real positive-axis, $z = x > 0$, we expect the two linearly independent solutions to be either exponentiall growing or exponentially decaying, but on the real negative-axis, $z = x < 0$, both solutions will be oscillatory. The task is to connect these contrasting behaviours, and we will show that this can be accomplished using ideas of exponential asymptotics in the complex z-plane. On the real axis $z = x$, the Airy function of the first kind can be defined by

$$Ai(x) = \frac{1}{\pi} \int_0^{\infty} \cos\left(xt + \frac{t^3}{3}\right) dt . \tag{12}$$

This is real-valued on the real axis, and is extended to all complex z by

$$Ai(z) = \frac{1}{2\pi i} \int_C \exp\left(\frac{t^3}{3} - zt\right) dt , \tag{13}$$

where the contour C runs from $\infty e^{-i\pi/3}$ to $\infty e^{i\pi/3}$.

To obtain the second solution, define $\sigma = e^{2i\pi/3}$, Then if $w(z)$ is any solution of (11), so are $w(\sigma z)$ and $w(\sigma^{-1}z)$. Any two of these three functions are linearly independent, and further

$$w(z) + \sigma w(\sigma z) + \sigma^{-1}w(\sigma^{-1}) = 0. \qquad (14)$$

Hence we now define the Airy function of the second kind as

$$Bi(z) = e^{-i\pi/6}Ai(\sigma z) + e^{i\pi/6}Ai(\sigma^{-1}z). \qquad (15)$$

Note that, like $Ai(z)$, $Bi(z)$ (15) is real-valued on the real axis. Our interest here is in the asymptotic expansions of $Ai(z)$, $Bi(z)$ in the complex z-plane. These can be obtained from the integral (13) using the method of steepest descent. Here we shall combine that with WKB asymptotic expansions directly from Airy's differential equation (11) in order to exhibit the *Stokes phenomenon*. First, from the integral (13) we find that (using the saddle point at $t = z^{1/2}$)

$$Ai(z) \sim \frac{1}{2\pi^{1/2}z^{1/4}} \exp\left(-\frac{2z^{3/2}}{3}\right), \quad \text{as} \quad |z| \to \infty, \quad |\arg(z)| < \pi. \qquad (16)$$

1.4   WKB Solutions and Stokes Phenomenon

Although this asymptotic expression (16), combined with the relation (14) can be used to get the desired connection formulas, it is instructive to take a different approach based on finding WKB asymptotic solutions of the differential equation (11) directly. Hence, seek a solution of the form

$$w(z) = \exp\left(\phi(z)\right). \qquad (17)$$

Substitution into (11) ($w_{zz} = zw$) yields

$$\phi_{zz} + \phi_z^2 = z, \qquad (18)$$

which is a Riccati equation for ϕ_z. The WKB procedure for the limit $|z| \to \infty$ yields the solutions

$$\phi_z = \mp z^{1/2} - \frac{1}{4z} + O(z^{-5/2}). \qquad (19)$$

The outcome are the WKB asymptotic solutions,

$$w_{1,2} = \frac{1}{z^{1/4}} \exp\left(\mp\frac{2z^{3/2}}{3}\right)(1 + O(z^{-3/2})). \qquad (20)$$

It follows that we can write that

$$Ai(z) = a_1 w_1(z) + a_2 w_2(z), \quad \text{where} \quad w_{1,2} \sim \frac{1}{z^{1/4}} \exp\left(\mp \frac{2z^{3/2}}{3}\right). \quad (21)$$

The issue is to find the *constants* $a_{1,2}$. The key requirement is to find the regions where $w_{1,2}$ are either exponentially decaying or growing. These regions are defined by *anti-Stokes lines* where the exponential is purely oscillatory, while the *Stokes lines* are where the exponent is real-valued. Here the anti-Stokes lines are arg $= \pm\pi/3, \pm\pi$ (shown in red), and the Stokes lines are arg $= 0, \pm 2\pi/3$ (shown in blue).
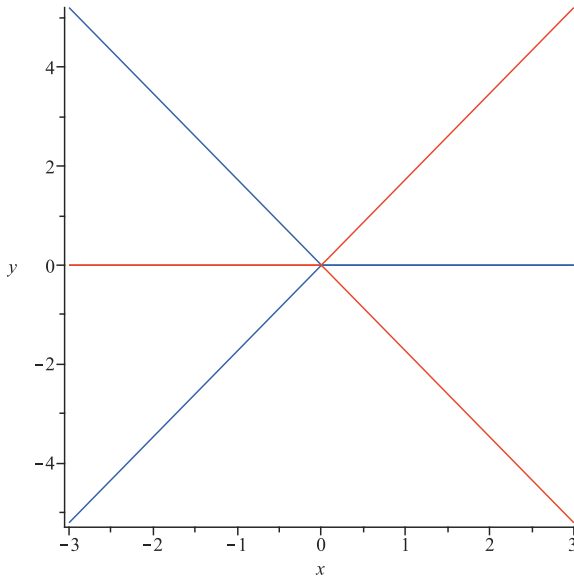
Figure 2. Plot of the ant-Stokes lines (red) and the Stokes lines (blue).

Thus $w_{1,2}(z)$ is exponentially small (large) (*subdominant, dominant*) in the sector $|\arg(z)| < \pi/3$, but is exponentially large (small) in the sectors $\pi/3 < |\arg(z)| < \pi$. It follows that *in the sector $|\arg(z)| < \pi/3$, $a_2 = 0$* since we require that $Ai(z)$ is to be the solution which is exponentially small for $z = x > 0$. *But $a_2 \neq 0$ in the sectors $\pi/3 < |\arg(z)| < \pi$*. This discontinuity in the constant a_2 is the *Stokes phenomenon*.

The constant a_1 must be real-valued in order for $Ai(z)$ to be real-valued when $z = x > 0$; it is found by comparison with the asymptotic formula

(16) and so $a_1 = 1/2\pi^{1/2}$. The final task then is to find the value of a_2 in terms of a_1. The fact that $a_2 \neq 0$ when we evaluate the asymptotic expression (21) for $Ai(z)$ as $z \to x < 0$ is crucial. The evaluation of a_2 can be achieved by recourse to the integral expression (13), or more simply by the requirement that $Ai(z)$ should be real-valued when $z = x < 0$. This latter yields $a_2 = \pm ia_1$ as $z = x < 0$, $\arg(z) = \pm i\pi$. Substitution into (21) yields the asymptotic expression

$$Ai(x) \sim \frac{1}{\pi^{1/2}(-x)^{1/4}} \sin\left(\frac{2(-x)^{3/2}}{3} + \frac{\pi}{4}\right), \quad \text{as} \quad x \to -\infty. \tag{22}$$

The corresponding expressions for $Bi(z)$ can now be found from the formula (15). Thus, the counterparts of (16, 22) for $Ai(z)$ are

$$Bi(z) \sim \frac{1}{\pi^{1/2}z^{1/4}} \exp\left(\frac{2z^{3/2}}{3}\right), \quad \text{as} \quad |z| \to \infty, \quad |\arg(z)| < \frac{\pi}{3}, \tag{23}$$

$$Bi(x) \sim \frac{1}{\pi^{1/2}(-x)^{1/4}} \cos\left(\frac{2(-x)^{3/2}}{3} + \frac{\pi}{4}\right), \quad \text{as} \quad x \to -\infty. \tag{24}$$

2 Wave Scattering and Reflection

2.1 Forced Harmonic Oscillator

The classical D'Alembert wave equation is

$$U_{tt} - c^2 U_{xx} = -c^2 F(x,t), \tag{25}$$

where c is the constant wave speed, and $F(x,t)$ is a specified forcing term. Suppose $F(x,t) = f(x)\exp(-i\omega t)$ and seek a time-harmonic solution $U(x,t) = u(x)\exp(-i\omega t)$. Then we get a forced harmonic oscillator equation for $u(x)$,

$$u_{xx} + k^2 u = f(x), \tag{26}$$

where $k = \omega/c$. We shall suppose that $f(x)$ *is localized*, so that $f(x)$ and all its derivatives vanish as $x \to \pm\infty$. In the absence of any forcing, the general solution is

$$u = a\exp(ikx) + b\exp(-ikx), \tag{27}$$

for some constants a, b, describing a wave to the right or left respectively. This is also the general asymptotic solution at infinity, since $f(x) \to 0$ there, where now in general $a = a_\pm, b = b_\pm$ according as we take the limit

$x \to \pm\infty$. They correspond to incident, reflected or transmitted waves. The aim now is to determine these constants, and in particular, which may be taken equal to zero.

Although the forced equation (26) can be explicitly solved, it is instructive to consider the limit $k \to \infty$. Then we can construct an asymptotic expansion

$$u(x) \sim \frac{f(x)}{k^2} - \frac{f_{xx}(x)}{k^4} + O(k^{-6}) \,. \qquad (28)$$

Clearly, this can be continued to all orders in k^{-2N}, and no free waves are obtained. We infer that the wave amplitudes at infinity are exponentially small. The general solution of (26) is

$$u(x) = a \exp(ikx) + b \exp(-ikx) + \frac{1}{2ik} \int_{-\infty}^{\infty} \exp(ik|x - \hat{x}|) f(\hat{x}) d\hat{x} \,, \qquad (29)$$

where a, b are arbitrary constants. We now impose the boundary conditions all waves should be *outgoing*, so that as $x \pm \infty$, $u \to a_+ \exp(ikx)$, $b_- \exp(-ikx)$ for some constants a_+, b_-; note this implies there is a Stokes phenomenon. Now let $x \pm \infty$ in (29),

$$u(x) \to a \exp(ikx) + b \exp(-ikx) + \alpha_\pm \exp(\pm ikx) \,,$$
$$\alpha_\pm = \frac{1}{2ik} \int_{-\infty}^{\infty} \exp(\mp ik\hat{x}) f(\hat{x}) d\hat{x} \,. \qquad (30)$$

Hence we must choose $a = b = 0$ in (29). It follows that the radiated outgoing waves are given by

$$u(x) \to \alpha_\pm \exp(\pm ikx) \,, \quad \alpha_\pm = \frac{1}{2ik} \int_{-\infty}^{\infty} \exp(\mp ik\hat{x}) f(\hat{x}) d\hat{x} \,. \qquad (31)$$

The radiation coefficients $\alpha_\pm(k)$ are not zero, but are *exponentially small* as $k \to \infty$. Note that $\alpha_- = -\alpha_+^*$ (the superscript * denotes the complex conjugate). Hence it is sufficient to evaluate α_+. The contour of integration is moved into the lower half of the complex $\hat{x}$-plane, that is Im $\hat{x} < 0$. Then if the nearest singularity of $f(\hat{x})$ to the real $\hat{x}$-axis is at $\hat{x} = K - iL, L > 0$ we can estimate that $\alpha_+ = O(\exp(-kL))$ as $k \to \infty$. For example, $\hat{f}(\hat{x}) = sech(\gamma\hat{x})$ has poles at $\hat{x} = \pm i\pi/2\gamma, \pm 3i\pi/2\gamma, \cdots$. Evaluating the residue at the nearest pole to the real axis yields

$$\alpha_+ \sim \frac{\pi}{ik\gamma} \exp\left(-\frac{\pi k}{2\gamma}\right) \,. \qquad (32)$$

Indeed, in this case the integral (31) can be explicitly evaluated to give

$$\alpha_+ = \frac{\pi}{2ik\gamma}\operatorname{sech}(\frac{\pi k}{2\gamma})\,,$$

from which the estimate (32) readily follows.

Suppose now that

$$f(\hat{x}) = \exp\left(-\gamma^2\hat{x}^2\right).$$

This has no singularities in the complex $\hat{x}$-plane, and so the scattering coefficients must be estimated in a different way. Indeed, this Gaussian function, while decaying exponentially on the real axis, is only subdominant in the sectors $|\arg\hat{x}| < \pi/4, 3\pi/4 < |\arg\hat{x}| < \pi$, and is dominant in $\pi/4 < |\arg\hat{x}| < 3\pi/4$. Thus the contour of integration in (31)

$$\alpha_\pm = \frac{1}{2ik}\int_{-\infty}^{\infty}\exp\left(\mp ik\hat{x}\right)f(\hat{x})d\hat{x}$$

cannot easily be moved from the real axis. Instead, in this case, we can evaluate the integrals explicitly to get that

$$\alpha_\pm = \frac{\pi^{1/2}}{2ik\gamma}\exp\left(-\frac{k^2}{4\gamma^2}\right).$$

2.2 Balanced Flow and Slow Manifold

Consider the system, introduced by Lorenz (1986), see also Lorenz and Krishnamurthy (1987) and Vanneste (2003), as a model of large-scale atmospheric flow interacting with internal-inertial gravity waves,

$$u_t = -vw + bvy\,, \quad v_t = uw - buy\,, \quad w_t = -uv\,, \tag{33}$$

$$x_t = -y\,, \quad y_t = x + buv\,. \tag{34}$$

The variables (u, v, w) represent the large-scale flow, and the variables (x, y) represent the internal gravity waves. The parameter b represents a Froude number, and we shall consider the case when $b \ll 1$. When $b = 0$, the system uncouples into a set of equations describing the *slow manifold*, a resonant triad of large-scale planetary (Rossby) waves, and an equation for *fast oscillations*, representing gravity waves. Hence, seek an asymptotic expansion

$$(u, v, w) \sim \sum_{n=0}^{\infty}(u_n, v_n, w_n)b^n\,, \quad (x, y) \sim \sum_{n=1}^{\infty}(x_n, y_n)b^n\,. \tag{35}$$

Then at the leading order, the system (33, 34) reduce to

$$u_{0t} = -v_0 w_0 \,, v_{0t} = u_0 w_0 \,, w_{0t} = -u_0 v_0 \,, \quad x_{1tt} + x_1 = -u_0 v_0 \,. \tag{36}$$

We take a solution for the slow manifold as

$$u_0 = F\mathrm{sech}(Ft) \,, v_0 = F \tanh (Ft) \,, w_0 = F\mathrm{sech}(Ft) \,. \tag{37}$$

Then the equation for the leading-order fast oscillations is

$$x_{1tt} + x_1 = f_1 = F^2\mathrm{sech}(Ft) \tanh(Ft) \,, \tag{38}$$

which has the general solution

$$x_1 = A \exp (it) + B \exp (-it) + \frac{1}{2i} \int_{-\infty}^{\infty} \exp (i|t - \hat{t}|) f_1(\hat{t}) d\hat{t} \,. \tag{39}$$

The arbitrary constants A, B are now determined by the requirement that there should be no oscillations as $t \to -\infty$. Then we can show that

$$x_1 \sim -C_1 \cos t \,, \quad C_1 = \int_{-\infty}^{\infty} \sin (\hat{t}) f_1(\hat{t}) d\hat{t} = \pi \mathrm{sech}(\frac{\pi}{2F}) \quad x \to \infty \,. \tag{40}$$

Thus there is *no pure slow manifold*, as gravity waves are inevitably generated as $t \to \infty$. Note that the oscillations are *exponentially small* as the parameter $F \to 0$.

2.3   Waves in a Variable Medium

The classical D'Alembert wave equation in a variable medium is

$$U_{tt} - \{c^2(x)U_x\}_x = 0 \,, \tag{41}$$

where the speed $c = c(x)$ varies spatially. Now seek a time-harmonic solution $U(x, t) = u(x) \exp (-i\omega t)$ and then (41) becomes

$$\{c^2(x)u_x\}_x + \omega^2 u = 0 \,. \tag{42}$$

We shall seek *high-frequency ($\omega \to \infty$) WKB solutions*. For this purpose we make the transformation

$$X = \int_{x_0}^{x} \frac{d\hat{x}}{c(\hat{x})} \,, \quad v(X) = c(x)^{1/2} u(x) \,, \tag{43}$$

$$\text{so that} \quad v_{XX} + \omega^2 v = Q(X)v \,, \tag{44}$$

$$Q(X) == \frac{(c^{-1/2}c_X)_X}{2c^{1/2}} = \frac{c_{XX}}{2c} - \frac{c_X^2}{4c^2}.\tag{45}$$

In the limit $\omega \to \infty$, the right-hand side of (2.3) can be ignored at the leading order, assuming that $Q(X)$ is a smooth function. Then WKB solutions are found by putting

$$v(X) = \exp\left(i\omega\Phi(X)\right),\tag{46}$$

$$i\omega\Phi_{XX} - \omega^2\Phi_X^2 + \omega^2 = Q(X).\tag{47}$$

At the leading order $\Phi \sim \pm X$, corresponding to a wave to the right, or a wave to the left respectively. The leading terms are

$$\Phi \sim \pm X \mp \frac{\tilde{Q}(X)}{2\omega^2} - \frac{iQ(X)}{4\omega^3} + \cdots, \quad \tilde{Q}(X) = \int_{-\infty}^{X} Q(\hat{X})d\hat{X}.\tag{48}$$

Thus the WKB asymptotic solutions are

$$v_\pm(X) = \exp\left(\pm i[\omega X - \frac{\tilde{Q}(X)}{2\omega}]\right)\{1 + \frac{Q}{4\omega^2} + O(\omega^{-3})\}.\tag{49}$$

The general solution of (42) is

$$v(X) = A_+v_+(X) + A_-v_-(X).\tag{50}$$

Now suppose that $Q(X)$ (45) is a localized function such that $Q(X) \to 0$ as $X \pm\infty$. That is, the variable speed $c(x)$ is such that $c \to c_\pm$ as $x \to \pm\infty$, where $c_\pm$ are constants. Then consider a wave incident on the variable medium from the left. That is, we impose the boundary conditions that

$$v(X) \to \exp\left(i\omega X\right) + R\exp\left(-i\omega X\right) \quad \text{as} \quad X \to -\infty,$$
$$v(X) \to T\exp\left(i\omega X\right), \quad \text{as} \quad X \to \infty,\tag{51}$$

where the reflection and transmission coefficients R, T are constants to be determined; again this formulation implies the presence of a Stokes phenomenon. Also note that in terms of $u(x)$ the transmission coefficient is $T(c_-/c_+)^{1/2}$.

Then from the WKB solution (50) we infer that $A_+ = 1, A_- = 0$, noting that as $x \to -\infty, \Phi \sim \pm X$ and as $x \to \infty, \Phi \sim \pm X \mp \tilde{Q}(\infty)/2\omega^2$. Hence

$$v(X) \sim v_+(X).\tag{52}$$

Thus, $T \sim \exp\left(i\tilde{Q}(\infty)/2\omega\right), |T| \sim 1, R \sim 0$ in this WKB approximation, and we infer that to all orders in ω^{-N}, there is no reflected wave. The

reflection coefficient R must be exponentially small as $\omega \to \infty$, and its calculation needs *exponential asymptotics*, see Meyer (1975) and Grimshaw (1976).

First note that from the exact equation for $v(X)$ (44), we find that

$$v^* v_X - v v_X^* = \text{constant} , \tag{53}$$

which is an expression of conservation of wave energy flux. Then, substitution of the boundary conditions at infinity (51) into (53) yields

$$|R|^2 + |T|^2 = 1 . \tag{54}$$

Next, again from the the exact equation for $v(X)$ (44) we can show that

$$
\begin{aligned}
v(X) &= A \exp\left(i\omega X\right) + B \exp\left(-i\omega X\right) \\
&+ \frac{1}{2i\omega} \int_{-\infty}^{\infty} \exp\left(i\omega |X - \hat{X}|\right) Q(\hat{X}) v(\hat{X}) d\hat{X} ,
\end{aligned}
\tag{55}
$$

The constants A, B are found by applying the boundary conditions at infinity (51), so that $A = 1, B = 0$, and then

$$R, T - 1 = \mp \frac{1}{2i\omega} \int_{-\infty}^{\infty} \exp\left(\pm i\omega \hat{X}\right) Q(\hat{X}) v(\hat{X}) d\hat{X} . \tag{56}$$

Equation (55) is an integral equation for $v(X)$, while the expressions (56) allow the determination of the reflection coefficients. Since $v(X) \sim v_+(X)$ to all orders $O(\omega^{-N})$ (52), it follows that the reflection coefficient R can now be obtained from (56). Keeping just the leading term for $v_+(X) \sim \exp\left(i\omega X\right)$,

$$R \sim -\frac{1}{2i\omega} \int_{-\infty}^{\infty} \exp\left(2i\omega \hat{X}\right) Q(\hat{X}) d\hat{X} . \tag{57}$$

Since we are assuming that $Q(\hat{X})$ is a smooth function of X we can infer that R is $O(\omega^{-N})$, and is exponentially small, determined by the singularities of $Q(\hat{X})$ in the complex $\hat{X}$-plane. This if the nearest singularity to the real axis is at $\hat{X} = K + iL, L > 0$, then $R = O(\exp\left(-2\omega L\right)$ as $\omega \to \infty$.

Now recall that

$$Q(X) = \frac{(c^{-1/2} c_X)_X}{2c^{1/2}} = \frac{c_{XX}}{2c} - \frac{c_X^2}{4c^2} , \qquad X = \int_{x_0}^{x} \frac{d\hat{x}}{c(\hat{x})} ,$$

$$\text{or} \quad Q(x) = \frac{c^{1/2} (c^{1/2} c_x)_x}{2} = \frac{c c_{xx}}{2} + \frac{c_x^2}{4} .$$

As an example, suppose that

$$c(X) = \alpha + \beta \tanh{(\gamma X)}, \quad \text{so that} \quad x = \alpha X + \frac{\beta}{\gamma}\ln{(\cosh{(\gamma X)})},$$

where $\alpha > |\beta|, \gamma > 0$. It follows that as $X \to \pm\infty, x \sim (\alpha \pm \beta)x$ and $c_\pm = \alpha \pm \beta, 2(\alpha, \beta) = c_+ \pm c_-$. Evaluating $Q(X)$ we find that the relevant poles are double poles at $\hat{X} = i\pi/2, i\pi/2 + \ln{(c_+/c-)}$. Since,

$$R \sim -\frac{1}{2i\omega}\int_{-\infty}^{\infty} \exp{(2i\omega\hat{X})}Q(\hat{X})d\hat{X},$$

evaluation at these dominant poles gives

$$R \sim -\frac{i\pi}{2}\exp{(-\frac{\pi\omega}{\gamma})}\{1 + \exp{[2i\omega\ln{(\frac{c_+}{c_-})}]}\}.$$

3 Borel Summation: Forced Nonlinear Harmonic Oscillator

We now consider the forced harmonic oscillator with a nonlinear term

$$\mu^2 u_{xx} + u - \epsilon u^2 = f(x),\tag{58}$$

where ϵ, μ are *small parameters*. We shall suppose that $f(x)$ is *localized*, so that $f(x)$ and all its derivatives vanish as $x \to \pm\infty$. In this limit, $f(x) \to 0$ and the general solution of (58) includes a family of periodic solutions, which in the limit of small amplitude take the form

$$u \approx a_\pm \cos{(x/\mu)} + b_\pm \sin{(x/\mu)},\tag{59}$$

for some constants $a_\pm, b_\pm$.

We shall now further suppose that $f(x) = f(-x)$ is *symmetric* and an analytic function of x in the complex x-plane. Then we seek the solutions of (58) which are also *symmetric*, that is $u(x) = u(-x)$. In particular, it then follows that $a_+ = a_-, b_+ = -b_-$. To be explicit, we shall consider two representative examples:

$$\begin{aligned}(a): \quad &f(x) = \text{sech}^2(x),\\ (b): \quad &f(x) = \text{sech}(x),\end{aligned}\tag{60}$$

A balance is now required between the two small parameters, and this depends on the form of $f(x)$. Since we expect that the structure of the

solution is related to the singularities of $f(x)$ in the complex x-plane nearest to the real axis. We note that for cases (a,b) these are poles at $x = \pm i\pi/2$. Near each pole,

$$(a): \quad f(x) \approx \frac{-1}{(x - i\pi/2)^2}, \qquad (b): \quad f(x) \approx \frac{-i}{(x - i\pi/2)}, \tag{61}$$

respectively. Hence we write

$$x = \frac{i\pi}{2} + \lambda q, \quad v(q) = \epsilon u(x), \tag{62}$$

so that equation (58) becomes

$$\frac{\mu^2}{\lambda^2} v_{qq} + v - v^2 = \frac{-\epsilon}{\lambda^2 q^2} \text{ for case } (a), \quad \frac{-i\epsilon}{\lambda q} \text{ for case } (b), \tag{63}$$

respectively. In this *inner equation* all terms must be in balance, and so

$$(a): \quad \lambda = \mu = \epsilon^{1/2}, \qquad (b): \quad \lambda = \mu = \epsilon. \tag{64}$$

Each of these cases will now be examined using exponential asymptotics and Borel summation to calculate the small tails (59), see Pomeau et al (1988), Kruskal and Segur (1991) and Grimshaw and Joshi (1995) for the development and application of this approach. An alternative approach using Fourier transforms was developed by Akylas and Yang (1995).

3.1   Case (a)

Equation (58) is now

$$\epsilon u_{xx} + u - \epsilon u^2 = \text{sech}^2(x). \tag{65}$$

First consider the *outer expansion*

$$u \sim u_s = \sum_{n=0}^{\infty} u_n(x)\epsilon^n, \quad u_0 = \text{sech}^2(x), u_{n+1} = \sum_{j=0}^{n} u_j u_{n-j} - u_{nxx}. \tag{66}$$

As expected, for real x this asymptotic solution is symmetric, and no tail oscillations emerge to all orders in ϵ^n. Instead, these are found from the singularties of u_s in the complex x-plane, which are located at $x = \pm i\pi/2, \pm 3i\pi/2, \cdots$. It will be sufficient to consider just the singularity at $x = i\pi/2$ closest to the real axis in the upper half-plane, and write, see (62),

$$x = \frac{i\pi}{2} + \epsilon^{1/2} q. \tag{67}$$

Substitution into (66) and evalaution in the limit $\epsilon^{1/2}q \to 0$ yields

$$u_s \sim \frac{1}{\epsilon}\left(-\frac{1}{q^2} + \frac{7}{q^4} + \cdots\right) + \left(\frac{1}{3} - \frac{2}{3q^2} + \cdots\right) + O(\epsilon). \tag{68}$$

Next we consider the *inner expansion*, where we replace x with q (67), and put $v(q) = \epsilon u(x)$ (62), so that

$$v_{qq} + v - v^2 = -\frac{\epsilon}{\sinh^2(\epsilon^{1/2}q)} \sim -\frac{1}{q^2} + \frac{\epsilon}{3} + \cdots. \tag{69}$$

The symmetry condition becomes

$$\operatorname{Im} v(q) = 0, \quad \text{on} \quad \operatorname{Re} q = 0. \tag{70}$$

Equation (69) is exact, and we seek the expansion

$$v(q) \sim \sum_{n=0}^{\infty} v_n(q)\epsilon^n, \tag{71}$$

so that $\quad v_{0qq} + v_0 - v_0^2 = -\frac{1}{q^2}. \quad v_{1qq} + v_1 - 2v_0v_1 = -\frac{1}{3}. \tag{72}$

Matching with the outer expansion (68) for u_s yields

$$v_0 \sim -\frac{1}{q^2} + \frac{7}{q^4} + \cdots, \quad v_1 \sim \frac{1}{3} - \frac{2}{3q^2} + \cdots, \tag{73}$$

taken in the limit $q \to \infty$ for $\operatorname{Re} q > 0, \operatorname{Im} q < 0$.

$$v_{0qq} + v_0 - v_0^2 = -\frac{1}{q^2}$$

Now seek an asymptotic solution

$$v_0 \sim \sum_{n=1}^{\infty} \frac{b_n}{q^{2n}}, \quad \text{as} \quad q \to \infty, \ \operatorname{Re} q > 0, \operatorname{Im} q < 0 \tag{74}$$

Substitution into equation (72) yields $b_1 = -1, b_2 = 7$ as required by (73) and then

$$b_{n+1} + 2n(n+1)b_n - \sum_{j=0}^{n-1} b_{j+1}b_{n-j} = 0, \quad n = 1, 2, \cdots. \tag{75}$$
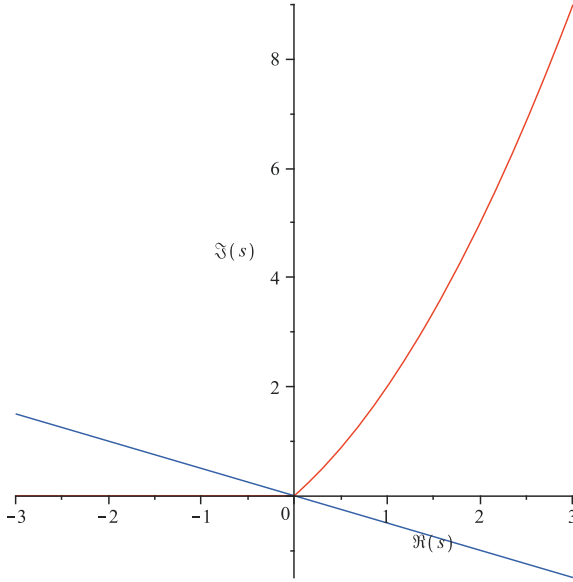
Figure 3. The complex s-plane for $\mathrm{Re}\,q > 0, \mathrm{Im}\,q < 0$. The line $\mathrm{Re}\,(sq) = 0$ is blue, and the contour Γ is red.

The aim now is to sum the series (74) using *Borel summation* We seek a solution of equation (72) in the form of a *Laplace transform*

$$v_0 = \int_\Gamma \exp\left(-sq\right) V(s)\, ds\,, \qquad (76)$$

where the contour Γ runs from zero to infinity in the complex s-plane such that $\mathrm{Re}(sq) > 0$.

Substitution of the Laplace transform into equation (72) for v_0 yields a Fredholm integral equation for $V(s)$,

$$(s^2 + 1)V(s) - \int_0^s V(\hat{s})V(s - \hat{s})\, d\hat{s} = -s\,. \qquad (77)$$

To solve this we seek a solution as a power series

$$V(s) = \sum_{n=0}^{\infty} a_n s^{2n+1}\,. \qquad (78)$$

Substitution of (78) into equation (77) shows that $a_0 = -1$ and

$$a_n + a_{n-1} - \sum_{j=0}^{n-1} a_j a_{n-j} \frac{(2j+1)!(2n-2j-1)!}{(2n+1)!} = 0, \quad n = 1, 2, \cdots. \quad (79)$$

Next, substitution of (78) into the Laplace transform (76) recovers the asymptotic series (74) with

$$b_{n+1} = (2n+1)!a_n. \quad (80)$$

Thus solving the recurrence relation (79) for a_n effectively sums the asymptotic series (74) and yields the solution of equation (72) for v_0 as a Laplace transform. Examination of the recurrence relation (79)

$$a_n + a_{n-1} - \sum_{j=0}^{n-1} a_j a_{n-j} \frac{(2j+1)!(2n-2j-1)!}{(2n+1)!} = 0, \quad n = 1, 2, \cdots.$$

shows that as $n \to \infty$, $a_n \sim (-1)^n K$ where $K = 1.55...$ is a constant found numerically. Hence the series (78)

$$V(s) = \sum_{n=0}^{\infty} a_n s^{2n+1}.$$

converges for $|s| < 1$. Analytic continuation into the complex s-plane, using the integral equation (77), yields a complete solution for $V(s)$ and hence $v_0(q)$ as the Laplace transform (76).

Since $a_n \sim (-1)^n K$ as $n \to \infty$ we see that $V(s) = \sum_{n=0}^{\infty} a_n s^{2n+1}$ has singularities at $s = \pm i$ given by

$$V(s) \approx \frac{Ks}{s^2 + 1}, \quad \text{for} |s| \approx 1. \quad (81)$$

There are similar poles at $s = 2i, 3i, \cdots$, but these will be seen to generate higher harmonics in the tail oscillations, and so are not our immediate concern. We must know make a specific choice of the contour Γ in the Laplace transform (76). Since we are seeking a symmeric solution, which satisfies the condition (70), it is sufficient to suppose that at first $\operatorname{Re} q > 0$ and $\operatorname{Im} q < 0$. Then choose the contour Γ to lie initially in $\operatorname{Re} s > 0, \operatorname{Im} s \geq 0$, so that $\operatorname{Re} sq > 0$ and the Laplace transform is well defined for the allowed values of q. In particular, since $V(s)$ can be represented by the power series (78), which generates the asymptotic series (74), which in turn is equivalent to the asymptotic series (66), we conclude that $v_0 \sim v_s = \epsilon u_s$.

The next step is to deform the contour Γ onto the imaginary s-axis. in this process we will need to deform around the poles at $s = i, 2i, 3i, \cdots$ and collect the (half) residues. Hence we find that (76) becomes, on putting $s = iy$ on the deformed contour Γ,

$$v_0 = \int_0^\infty \exp\left(-iyq\right) V(iy)\, i\, dy + \frac{i\pi K}{2} \exp\left(-iq\right) + \cdots, \qquad (82)$$

where the dots denote terms proportional to $\exp\left(-2iq\right), \exp\left(-3iq\right), \cdots$. The integral is interpreted as a principal value integral at the singularities at $y = 1, 2, 3, \cdots$. This holds in $\operatorname{Re} q > 0, \operatorname{Im} q < 0$. To apply the *symmetry condition* (70) that v_0 should be real-valued on the imaginary q-axis, we must now let $\operatorname{Re} q \to 0$, and put $q = -iQ, Q > 0$ in the expression (82). From the series (78), $V(iy) = i \sum_{n=0}^\infty a_n (-1)^n y^{2n}$ is pure imaginary since the coefficients a_n are all real-valued. Hence the integral term is real-valued as required. But the contributions from the poles are pure imaginary, and hence the expression (82) cannot satisfy the symmetry condition. The remedy is to note that the term $\exp\left(-iq\right)$ is exponentially small in the sector $\operatorname{Re} q > 0, \operatorname{Im} q < 0$ and hence is *subdominant*, so that we are allowed to add such terms asymptotically to (82).

Thus we replace (82) with

$$v_0 = \int_0^\infty \exp\left(-iyq\right) V(iy)\, i\, dy + \frac{i\pi K}{2} \exp\left(-iq\right) + \frac{ib}{2} \exp\left(-iq + i\delta\right) + \cdots, \qquad (83)$$

where b, δ are real constants. Now application of the symmetry condition shows that

$$b \cos \delta = -\pi K. \qquad (84)$$

Thus the final solution for v_0 in $\operatorname{Re} q > 0, \operatorname{Im} q < 0$ is

$$v_0 \sim \int_\Gamma \exp\left(-sq\right) V(s)\, ds + + \frac{ib}{2} \exp\left(-iq + i\delta\right) + \cdots, \qquad (85)$$

where b is determined in terms of δ by (84). It remains to bring this solution back to the real x-axis, for $x > 0$, using (67), $x = i\pi/2 + \epsilon^{1/2} q$. Here we must also collect a similar contribution from the singularities in the lower half of the complex x-plane. Thus the full solution consists of a *central core and an exponentially small tail oscillation*.

The final result is that, for $x > 0$ (the case $x < 0$ follows from the imposed symmetry),

$$u \sim u_s + \frac{b}{\epsilon} \exp\left(-\frac{\pi}{2\epsilon^{1/2}}\right) \sin\left(\frac{x}{\epsilon^{1/2}} - \delta\right), \quad b \cos \delta = -\pi K, \qquad (86)$$

where $u_s \sim \operatorname{sech}^2(x) + O(\epsilon)$ is given by (66). The tail oscillations form a one-parameter family characterized by the phase shift $\delta, 0 \leq \delta < \pi/2$, where the minimum amplitude occurs for $\delta = 0$.
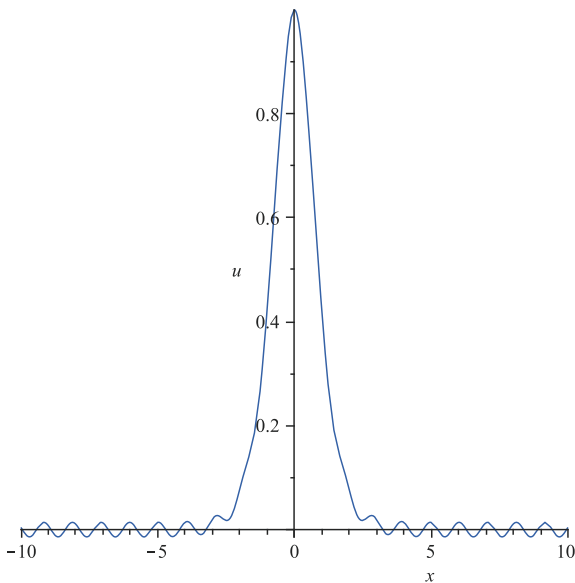
Figure 4. Plot of the asymptotic solution (86) for $\delta = 0$ and $\epsilon = 1/36$.

Suppose that instead of the symmetry condition (70) we look for *one-sided solutions* such that $u(x) \to 0$ as $x \to \infty$. The same procedure can be followed, and again the solution for $\operatorname{Re} q > 0$ is given by the Laplace transform (76), with the same contour Γ, which ensures that there are no oscillations as $x \to \infty$. But now, to find the behaviour as $x \to -\infty$, the contour Γ must be moved across the imaginary q-axis to $\operatorname{Re} q < 0$, and in doing so the solution collects the residue at the poles $s = i, 2i, 3i, \cdots$. The residue at $s = i$ is $i\pi K \exp(-iq)$, exactly twice the contribution from the half residue shown in (82). Then, bringing the solution back to the real x-axis, in $x < 0$, we find that

$$u \sim u_s + \frac{2\pi K}{\epsilon} \exp\left(-\frac{\pi}{2\epsilon^{1/2}}\right) \sin\left(\frac{x}{\epsilon^{1/2}}\right). \tag{87}$$

For these one-sided solutions there are no free parameters.

3.2   Case(b): Outer expansion

Equation (58) is now

$$\epsilon^2 u_{xx} + u - \epsilon u^2 = \operatorname{sech}(x) \,. \tag{88}$$

The outer expansion is again (66), $u \sim u_s = \sum_{n=0}^{\infty} u_n(x)\epsilon^n$, but now

$$u_0 = \operatorname{sech}(x) \,, \quad u_1 = u_0^2 \,, \quad u_{n+2} = \sum_{j=0}^{n+1} u_j u_{n-j} - u_{nxx} \,. \tag{89}$$

Again, for real x this asymptotic solution is symmetric, and no tail oscillations emerge to all orders in ϵ^n. The singularties of u_s in the complex x-plane, are again located at $x = \pm i\pi/2, \pm 3i\pi/2, \cdots$, and we now write in place of (67), see (62),

$$x = \frac{i\pi}{2} + \epsilon q \,. \tag{90}$$

Substitution into (89) and evalaution in the limit $\epsilon q \to 0$ yields

$$u_s \sim \frac{1}{\epsilon}\left(-\frac{i}{q} - \frac{1}{q^2} + \cdots\right) + \epsilon\left(\frac{iq}{6} - \frac{1}{3q} + \cdots\right) + O(\epsilon^3) \,. \tag{91}$$

Here we replace x with q (90), and put $v(q) = \epsilon u(x)$ (62), so that

$$v_{qq} + v - v^2 = -\frac{i\epsilon}{\sinh(\epsilon q)} \sim -\frac{i}{q} + \frac{\epsilon i q}{6} + \cdots \,. \tag{92}$$

The symmetry condition (70) is unchanged. Instead of (71) we write

$$v(q) \sim \sum_{n=0}^{\infty} v_n(q)\epsilon^{2n} \,, \tag{93}$$

so that $\quad v_{0qq} + v_0 - v_0^2 = -\dfrac{i}{q} \,. v_{1qq} + v_1 - 2v_0 v_1 = -\dfrac{1}{3} \,. \tag{94}$

Matching with the outer expansion (91) for u_s yields

$$v_0 \sim -\frac{i}{q} - \frac{1}{q^2} + \cdots \,, \quad v_1 \sim \frac{1}{3} - \frac{2}{3q^2} + \cdots \,, \tag{95}$$

taken in the limit $q \to \infty$ for $\operatorname{Re} q > 0, \operatorname{Im} q < 0$.

$$v_{0qq} + v_0 - v_0^2 = -\frac{i}{q}$$

Now seek an asymptotic solution

$$v_0 \sim \sum_{n=1}^{\infty} \frac{b_n}{q^n}\,, \qquad \text{as} \quad |q| \to \infty\,, \ \operatorname{Im} q < 0 \tag{96}$$

Substitution into equation (72) yields $b_1 = -i, b_2 = -1$ as required by (73) and then

$$b_{n+2} + n(n+1)b_n - \sum_{j=1}^{n+1} b_j b_{n+2-j} = 0\,, \quad n = 1, 2, \cdots. \tag{97}$$

The aim now is to sum the series (96) using *Borel summation* We again seek a solution of equation (94) in the form of a *Laplace transform* (76).

As before, we substitute the Laplace transform into equation (94) to get now the Fredholm integral equation

$$(s^2 + 1)V(s) - \int_0^s V(\hat{s})V(s - \hat{s})\, d\hat{s} = -i\,. \tag{98}$$

To solve this we seek a solution as a power series

$$V(s) = \sum_{n=0}^{\infty} (-i)^{n+1} a_n s^n\,. \tag{99}$$

Substitution of (99) into equation (98) shows that $a_0 = 1, a_1 = 1$ and

$$a_n - a_{n-2} - \sum_{j=1}^{n} a_{j-1} a_{n-j} \frac{(j-1)!(n-j)!}{n!} = 0\,, \quad n = 2, 3, \cdots. \tag{100}$$

Next, again as before, substitution of (99) into the Laplace transform (??) recovers the asymptotic series (96) with

$$b_{n+1} = n!(-i)^{n+1} a_n\,. \tag{101}$$

Examination of the recurrence relation (100) shows that

$$a_n \sim Cn + O(n^{-1})\,, \quad \text{as} \quad n \to \infty\,,$$

where $C = 0.94$ is a constant found numerically. Hence the series (99) *converges* for $|s| < 1$, and so as in case (a), we can obtain a complete solution for $V(s)$ and $v_0(q)$. There is a singularity at $s = i$, given by

$$V(s) \approx \frac{C}{(s-i)} + \frac{iC}{(s-i)^2}\,, \quad \text{for} \quad s \approx i\,. \tag{102}$$

The essential difference here from case (a) is the *double pole at $s = i$*. This leads to a half-residue of

$$\pi C(q + i) \exp(-iq) \tag{103}$$

where the new feature is the non-uniform factor "q".

To explain the origin of this new secularity, we return to the basic equation (94) and seek a solution of the form

$$v_0 \sim v_s + v_w, \tag{104}$$

where as $|q| \to \infty$, v_s is given by the asymptotic expansion (96) and is the dominant term. Substitution into (94) and linearization yields

$$v_{wqq} + v_w - 2v_w v_s \approx 0. \tag{105}$$

Then, as $|q| \to \infty$,

$$v_w \sim B(q + i) \exp(-iq + i\delta), \tag{106}$$

for some real constants B, δ. The secular term arises, because in contrast to case (a), $v_s \sim q^{-1}$ rather than q^{-2}.

Then we choose the same contour Γ as in case (a), move the contour to the imaginary q-axis, collect the half-residues and add the allowed subdominant terms. The outcome is that (83) is replaced by

$$v_0 \sim v_{int} + \pi C(q + i) \exp(-iq) + B(q + i) \exp(-iq + i\delta) + \cdots. \tag{107}$$

$$v_{int} = \int_0^\infty \exp(-iyq) V(iy) i \, dy. \tag{108}$$

To apply the symmetry condition (70), we let $q = -iQ$, $Q > 0$ in (107). The series (99) is $V(iy) = i \sum_{n=0}^\infty a_n (-1)^n y^n$ is pure imaginary since the coefficients a_n are all real-valued. Hence v_{int} is real-valued, and as in case (a) we must choose the constants B, δ to ensure that v_0 is real-valued on the imaginary q-axis. The outcome is

$$B \cos \delta = -\pi C. \tag{109}$$

Thus the final solution for v_0 in $\operatorname{Re} q > 0, \operatorname{Im} q < 0$ is

$$v_0 \sim \int_\Gamma \exp(-sq) V(s) \, ds + + B(q + i) \exp(-iq + i\delta) + \cdots, \tag{110}$$

where the integral term is just the asymptotic series $v_s = \epsilon u_s$.

It remains to bring this solution back to the real x-axis, for $x > 0$, using (90), $x = i\pi/2 + \epsilon q$. Here we must also collect a similar contribution from the singularities in the lower half of the complex x-plane. The outcome will be

$$u \sim u_s + u_w \,, \tag{111}$$

where $u_s \sim sech(x) + O(\epsilon)$ is given by (89). Substitution into (88) and linearization yields

$$\epsilon^2 u_{wxx} + u_w - 2\epsilon u_w u_s \approx 0 \,. \tag{112}$$

Just as for the corresponding equation (105) for v_w, a WKB analysis yields

$$u_w \sim A(x) \exp\left(i\phi(x)\right) + A(x) \exp\left(-i\phi(x)\right), \tag{113}$$

where both $A(x), \phi(x)$ are real-valued for real x. We find that

$$\phi_x \sim \frac{1}{\epsilon} - u_s + O(\epsilon) \,, \quad A \sim A_0 + O(\epsilon) \,, \tag{114}$$

Using the leading expression for u_s,

$$\phi \sim \frac{x}{\epsilon} - 2\tan^{-1}\left(\exp\left(x\right)\right) + \phi_0 + O(\epsilon) \,. \tag{115}$$

In order to find the constants A_0, ϕ_0, the WKB expression for u_w (113) should be matched with the corresponding expression for $v_w = \epsilon u_w$ (106) when $x = i\pi/2 + \epsilon q$, for $\operatorname{Re} q > 0, \operatorname{Im} q < 0$. Thus, we find that

$$\phi \sim \frac{i\pi}{2\epsilon} + q - \pi + i\ln\left[\tanh\left(\frac{\epsilon q}{2}\right)\right] + \phi_0 + O(\epsilon) \,,$$

so that, as $|q| \to \infty$,

$$u_w \sim -\frac{A_0 \epsilon q}{2} \exp\left(\frac{\pi}{2\epsilon} - iq - i\phi_0\right), \tag{116}$$

noting that in $\operatorname{Im} q > 0$, $\exp\left(-iq\right)$ is dominant over $\exp\left(iq\right)$. The matching condition now shows that

$$A_0 = -\frac{2B}{\epsilon^2} \exp\left(-\frac{\pi}{2\epsilon}\right), \quad \phi_0 = -\delta \,. \tag{117}$$

Finally we get that, as $x \to \infty$, the tail oscillations are given by

$$u_w \sim \frac{4B}{\epsilon^2} \exp\left(-\frac{\pi}{2\epsilon}\right) \cos\left(\frac{x}{\epsilon} - \delta\right), \tag{118}$$

where $B\cos\delta = -\pi C$ (109). Again, they form a one-parameter family.

4   Generalized Solitary Waves

4.1   Korteweg-de Vries equation

Solitary waves are steady localized traveling waves of permanent form. In the weakly nonlinear long wave regime, the canonical equation describing solitary waves is the famous *Korteweg-de Vries (KdV)* equation, first derived in the water-wave context in 1895, and subsequently found to hold in many physical systems,

$$u_t + c_0 u_x + \mu u u_x + \delta u_{xxx} = 0 \,. \tag{119}$$

The dominant term is $u_t + c_0 u_x \approx 0$, showing that the wave propagates approximately with a speed c_0. At the next order weak dispersion due to the term δu_{xxx} is balanced by weak nonlinearity due to the term $\mu u u_x$, The speed c_0 (linear long wave phase speed), and the coefficients μ, δ depend on the particular physical system being considered. For water waves

$$c_0 = (gh)^{1/2} \,, \quad \mu = \frac{3c_0}{2h} \,, \quad \delta = \frac{c_0 h^2}{6} \,,$$

when $u(x,t)$ is the elevation of the water surface above the undisturbed depth h, and g is the acceleration due to gravity. The KdV equation is, in the reference frame moving with speed c_0 (transform $x \to x - c_0 t$),

$$u_t + \mu u u_x + \delta u_{xxx} = 0 \,. \tag{120}$$

This is an *integrable* equation, a result first established in the 1960's by Kruskal and collaborators. Its principal solutions are *solitons*. A single soliton is the *solitary wave*, given by

$$u = a \operatorname{sech}^2(\gamma(x - Vt)) \,, \quad V = \frac{\mu a}{3} = 4\delta\gamma^2 \,. \tag{121}$$

Note that it solves the second order ordinary differential equation

$$\delta u_{xx} - Vu + \frac{\mu}{2} u^2 = 0 \,. \tag{122}$$

The solution (121) is a one-parameter family of solutions, parametrized by the amplitude a say. The speed V is proportional to the amplitude a and is positive (negative) as $\delta > 0 (< 0)$, and is also proportional to the square of the wavenumber γ; thus large waves are thinner and travel faster. They are waves of elevation (depression) when $\mu\delta > 0 (< 0)$. Integrability means that the general initial-value problem for a localized initial condition can be solved through the *Inverse Scattering Transform*, with the generic outcome of a finite number of solitons propagating in the positive x-direction, and some dispersing radiation, propagating in the negative x-direction (when $\mu\delta > 0$).
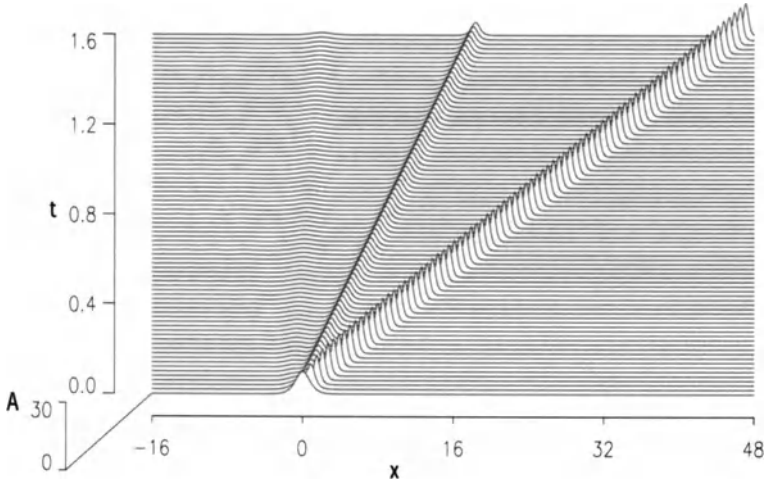
Figure 5. The generation of three solitons from a localized initial condition for the KdV equation $A_t + 6AA_x + A_{xxx} = 0$.

4.2   Linear spectrum

The basic paradigms for solitary waves, at least for weakly nonlinear long wave regime, is the central role played by model equations, such as the KdV equation. Our aim now is to describe how small-amplitude solitary waves can be found by an *asymptotic perturbation procedure* directly from the full system, rather than from a model equation.

Because solitary waves are required to *decay in their tail regions*, some information about their possible existence or otherwise, can be obtained by an examination of these tail regions. Here, except in certain exceptional cases, a *linearized analysis* is applicable. One-dimensional steady solitary waves, propagating in the x-direction with speed c are functions of $\xi = x - ct$, together with a set of other spatial transverse variables which define the modal structure. For instance, for water waves, the dependence is on ξ and z (x is horizontal and z is vertical), and there is no dependence on the remaining horizontal variable y.

In the tail region, where we assume that a linearized analysis holds, we seek solutions proportional to

$$Re\left\{\exp\left(ik(x - ct)\right)\right\}. \tag{123}$$

The linearized equations will then yield the linear dispersion relation

$$c = c(k) \,, \tag{124}$$

written here for the phase speed c rather than the frequency $\omega = ck$. Whereas usually this dispersion relation (which may have several branches) is considered as an equation for c given a real wavenumber k, for solitary wave tails it needs to be considered as an equation for a *complex-valued k given a real speed c*. Indeed, it is immediately clear that if there exist real-valued solutions of (124) for the given value of c, then it is unlikely that the solitary wave can decay to zero in its tail region. Instead, it will probably be accompanied by a non-decaying co-propagating oscillatory wave field. This consideration leads to the notion that solitary waves generally can only exist in the *gaps* in the linear spectrum.
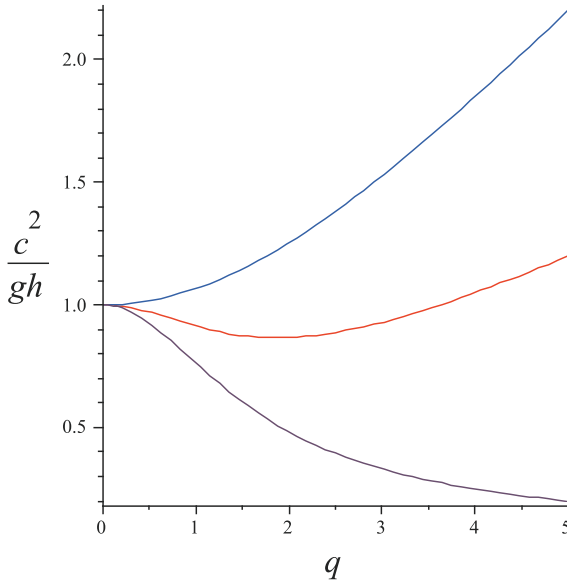
Figure 6. Plot of the water wave dispersion relation (125) for $B = 0$ (violet), $B = 0.2$ (red), $B = 0.4$ (blue).

For instance, for water waves, the dispersion relation in the presence of *surface tension* is

$$\frac{c^2}{gh} = \frac{(1 + Bq^2)}{q} \tanh q \,, \qquad q = kh \,, \tag{125}$$

where the Bond number $B = \sigma/gh^2$ and $\rho\sigma$ is the coefficient of surface tension (ρ is density), and has a value of $74\,dynes/cm$ at 20^oC. It may then be shown that solitary waves of the KdV type can exist only when either $B = 0, c^2 > gh$ or when $B > 1/3, c^2 < gh$ with a bifurcation from wavenumber zero ($k = 0$) and $c^2 = gh$ in both cases. Otherwise when $0 < B < 1/3$ solitary waves can exist for $|c| < c_m$ where c_m^2 is the minimum value that c^2 can take in (125) as q takes all real values. In deep water, $|q| \to \infty$, $c_m^2 = 2(g\sigma)^{1/2}$ and occurs at $|k| = k_m = (g\sigma)^{1/2}$, a wavelength $2\pi/k_m = 0.23\,cm$. These solitary waves bifurcate at a finite wavenumber k_m and from the speed c_m, and have decaying oscillations in their tail regions. They are *envelope solitary waves*, of a quite different kind from the afore-mentioned KdV-type solitary waves, and closely related to the nonlinear Schrodinger (NLS) equation.

4.3   Reformulation as a dynamical system

This approach has recently been developed into the basis of a rigorous approach to finding solitary waves, often called the "dynamical-systems" method, see Dias and Iooss (2003), Grimshaw and Iooss (2003) and Grimshaw (2007) for recent reviews. Since here we are considering only solitary waves which occur in *conservative* systems, which is the common and traditional scenario for solitary waves, we shall suppose that the underlying physical system is *Hamiltonian* (energy-conserving) and *reversible* (symmetry under the transformation $\xi \to -\xi$). In this case it can be shown the the solutions k of the dispersion relation $c = c(k)$ (124) for each real value of c have the property that $-k$ and k^* (complex conjugate) are also solutions. It follows that generically the solutions form a *quartet* $(k, k^*, -k, -k^*)$, with an associated four-dimensional subspace for the corresponding wave mode. For solitary waves we require solutions with $Im(k) > 0(< 0)$ when $\xi \to \infty(\to -\infty)$, in order to ensure that the solution decays to zero in its tail region. In the general case when $Im(k) \neq 0$ we see that there are generically two such roots available as $\xi \to \infty$ and, due to the reversible symmetry, two other roots available as $\xi \to -\infty$. Thus, for the corresponding wave mode, as $\xi \to \infty$ two boundary conditions are needed at each of $\pm\infty$. This count is consistent with the existence of a solitary wave solution, which from this dynamical systems point of view, is a *homoclinic orbit*.

Next, consider how this quartet structure may change as some system parameter is varied. Bifurcations arise when two solutions for k coalesce, for which the necessary condition is that $\partial c/\partial k = 0$ simultaneously with the dispersion relation (124). When this occurs at a real value of k, it is

equivalent to the condition that $c = c_g$ where

$$c_g = \frac{\partial \omega}{\partial k} = \frac{\partial (ck)}{\partial k} = c + k \frac{\partial c}{\partial k}$$

is the group velocity. Generically, there are four possibilities:

(1) $(0, 0, i\gamma, -i\gamma)$ where $\gamma > 0$ is real-valued.
(2) $(0, 0, \beta, -\beta)$ where $\beta > 0$ is real-valued.
(3) $(\beta, \beta, -\beta, -\beta)$ where $\beta > 0$ is real-valued.
(4) $(i\gamma, i\gamma, -i\gamma, -i\gamma)$ where $\gamma > 0$ is real-valued.

Case (1) corresponds to a KdV-type solitary wave, and case (3) corresponds to an envelope (NLS) solitary wave. Case (2) corresponds to a so-called *generalized solitary wave*, which does not decay at infinity, but instead is accompanied there be small-amplitude co-propagating oscillations. Case (4) has only rarely been studied and corresponds to a transition from a KdV-type solitary wave to an envelope solitary wave.

The full system is now projected onto the appropriate four-dimensional subspace, and the resulting bifurcation analyzed within the framework of this subspace. Of course, rigorous results require a delicate and sophisticated justification of this process. Here we shall instead briefly describe the structure of the subspace, which we suppose is represented by the 4-vector $\mathbf{W}(\xi)$. It satisfies an equation of the form

$$\mathbf{W}_\xi = L(\mathbf{W}; \epsilon) + N(\mathbf{W}). \tag{126}$$

Here $L(\mathbf{W}; \epsilon)$ is a linear operator and $N(\mathbf{W})$ contains all the nonlinear terms. The bifurcation parameter is ϵ, and is such that the spectrum of L at $\epsilon = 0$ reproduces one of the cases (1) to (4) describe above. That is, the eigenvalues $\lambda = ik$ of the linear operator $L(\mathbf{W}; 0)$ are respectively :

(1) $(0, 0, -\gamma, \gamma)$.
(2) $(0, 0, i\beta, -i\beta)$.
(3) $(i\beta, i\beta, -i\beta, -i\beta)$
(4) $(-\gamma, -\gamma, \gamma, \gamma)$.

4.4   Case (1)

Let us first consider case (1). At the bifurcation point ($\epsilon = 0$) the linearized system (126) has a double-zero eigenvalue. Then, without loss

of generality, we can transform the *linear operator* $L(\mathbf{W}; \epsilon)$ so that its projection onto the two-dimensional is represented by the matrix

$$\begin{bmatrix} 0 & 1 \\ \epsilon & 0 \end{bmatrix}. \tag{127}$$

Generically there is a corresponding single eigenvector $\mathbf{V}_0$, and a single generalized eigenvector $\mathbf{V}_1$, chosen orthogonal to $\mathbf{V}_0$. Small-amplitude solutions are then sought in the form

$$\mathbf{W} = A(\xi)\,\mathbf{V}_0 + B(\xi)\,\mathbf{V}_1 + \mathbf{W}^{(2)}. \tag{128}$$

Here A, B are real variables of $O(\alpha)$, measuring wave amplitude, while $\mathbf{W}^{(2)}$, is orthogonal to $\mathbf{V}_0$, $\mathbf{V}_1$ and of $O(\alpha^2)$. The two remaining eigenvalues $\mp\gamma$ play no role at the leading order here, since they correspond to strong exponential decay at infinity, and their effects are included in $\mathbf{W}^{(2)}$. Projection onto the two-dimensional subspace yields

$$A_\xi = B + a_1 A^2 + a_2 AB + a_3 B^2 + O(\alpha^3), \tag{129}$$
$$B_\xi = \epsilon A + b_1 A^2 + b_2 AB + b_3 B^2 + O(\alpha^3). \tag{130}$$

The next step is to make a *near-identity transformation*

$$\tilde{A} = A + \alpha_1 A^2 + \beta_1 AB + \gamma_1 B^2, \quad \tilde{B} = B + \alpha_2 A^2 + \beta_2 AB + \gamma_2 B^2, \tag{131}$$

Substitution into (129, 130) and choosing the coefficients so that

$$\alpha_1 = \beta_2 = -a_2, \beta_1 = 2a_1 + b_2, \gamma_1 = -a_2 + b_3, \alpha_2 = a_1, \gamma_2 = 2a_1 + a_3 + b_2,$$

where we show only the leading order terms as $\epsilon \to 0$, enables the elimination of all the quadratic nonlinear terms in (129, 130) except A^2 in (130) with coefficient b_1. Hence, omitting the superscript we find the *normal form*,

$$A_\xi = B + \cdots,$$
$$B_\xi = \epsilon A + \mu A^2 + \cdots, \tag{132}$$

where $\mu = b_1$ is a real-valued coefficient, specific to the system being considered, and the omitted terms are $O(\alpha^3)$. The coefficient ϵ yields the perturbed eigenvalues $\pm\epsilon^{1/2}$ for $\epsilon > 0$, and $\pm i|\epsilon|^{1/2}$ for $\epsilon < 0$; the former case yields the solitary wave solution. Comparison with the dispersion relation (124) leads to the identification of ϵ as

$$\epsilon = -\frac{2(c - c(0))}{c_{kk}(0)}. \tag{133}$$

It follows that for solitary waves, $c > (<)c(0)$ according as $c_{kk}(0) < (>)0$, as expected. When the error terms in (132) are omitted, it becomes the *steady-state KdV equation* (122) with the *"sech²" solution* (121) It is then a delicate and intricate task to establish that this solitary wave solution persists when the error terms are restored.

4.5   Case (2)

Next consider case (2). At the bifurcation point ($\epsilon = 0$) the linearized system (126) again has a double-zero eigenvalue, with a corresponding single eigenvector $\mathbf{V}_0$, and a single generalized eigenvector $\mathbf{V}_1$. However, account must now be taken of the other two eigenvalues $\pm i\beta$, with their associated eigenvectors $\mathbf{V}_2$, $\mathbf{V}_2^*$, since they do not now lead to decaying solutions at infinity. Small-amplitude solutions are sought in the form

$$\mathbf{W} = A(\xi)\, \mathbf{V}_0 + B(\xi)\, \mathbf{V}_1 + C(\xi)\, \mathbf{V}_2 + C^*(\xi)\, \mathbf{V}_2^* + \mathbf{W}^{(2)}\,. \qquad (134)$$

Here C is a complex-valued variable, and the leading terms form a four-dimensional subspace (A, B, C), while $\mathbf{W}^{(2)}$ is again a small error term. Projection onto this four-dimensional subspace, and a normal form analysis reveals that (A, B, C) satisfy the system

$$\begin{aligned}
A_\xi &= B + \cdots, \\
B_\xi &= \epsilon A + \mu A^2 + \nu |C|^2 \cdots, \\
C_\xi &= i\gamma(1 + \delta A)C + \cdots.
\end{aligned} \qquad (135)$$

Here μ, ν, δ are real-valued coefficients specific to the system being considered, and the omitted terms are small error terms as before.

When the error terms are omitted the system is integrable. Indeed in that limit, $|C| = C_0$ is a constant, and after a change of origin, the system reduces to the same form as (132) in case (1). Thus, for the case $\epsilon > 0$ (when case (1) is a KdV-type solitary wave), the solution is a one-parameter family of homoclinic-to-periodic solutions, with $|C| = C_0$ constant and $(A, B) \to (A_0,)$ as $\xi \to \pm\infty$ where A_0 is a real constant, given by $\epsilon A_0 + \mu A_0^2 + \nu C_0^2 = 0$. The solution is a *generalized solitary wave* which typically has a *"sech²" core, and decays at infinity to non-zero oscillations of constant amplitude C_0 and wavenumber γ*, see Figure 4. A delicate analysis of the full system (126) with the the small error terms shows that at least two of these solutions persist; the minimal amplitude C_0 being *exponentially small*, that is $O(\exp(-K/|\epsilon|^{1/2}))$ where K is a positive real constant. Although such waves are permissible as solutions of the steady-state equations, they have infinite energy and their associated group velocity is

inevitably inward at one end and outward at the other end. Hence, they cannot be realised in a physical system from any localized initial condition. Instead localized initial conditions will typically generate a one-sided generalized solitary wave, whose central core is accompanied by small-amplitude outgoing waves on one side only. Such waves cannot be steady, and instead will slowly decay with time.

4.6 Case (3)

Finally we consider case (3), when there is a double eigenvalue $\lambda = i\beta$ with generically a corresponding single eigenvector $\mathbf{V}_0$, and a single generalized eigenvector $\mathbf{V}_1$, while the complex conjugate double eigenvalue $\lambda = -i\beta$ has corresponding complex conjugate eigenvectors. Small-amplitude solutions are now sought in the form

$$\mathbf{W} = A(\xi)\,\mathbf{V}_0 + B(\xi)\,\mathbf{V}_1 + A^*(\xi)\,\mathbf{V}_0^* + B^*(\xi)\,\mathbf{V}_1^* + \mathbf{W}^{(2)}\,. \tag{136}$$

Here A, B are complex-valued variables, forming a four-dimensional subspace while $\mathbf{W}^{(2)}$ is again a small error term. Projection onto this subspace and a normal form analysis reveals that

$$A_\xi = i\beta A + B + iAP(\epsilon, |A|^2, K) + \cdots\,,$$
$$B_\xi = i\beta B + iBP(\epsilon, |A|^2, K) + AQ(\epsilon, |A|^2, K) + \cdots\,. \tag{137}$$
$$\text{where} \quad K = i(AB^* - A^*B)\,, \tag{138}$$

Here P, Q are real-valued polynomials of degree 1, that is we may write

$$P(\epsilon, |A|^2, K) = \epsilon + \nu_1 |A|^2 + \nu_2 K\,,$$
$$Q(\epsilon, |A|^2, K) = 2\epsilon\beta + \mu_1 |A|^2 + \mu_2 K \tag{139}$$

where all coefficients are real-valued.

The truncated system, obtained when the error terms are omitted, is integrable. There are two integrals, K, H both constants, where

$$H = |B|^2 - \left(2\epsilon\beta|A|^2 + \frac{\mu_1}{2}|A|^4 + \mu_2 K|A|^2\right)\,. \tag{140}$$

For a solitary wave solution we must have $K = H = 0$ and it then follows that

$$|A|_\xi^2 = 2\epsilon\beta|A|^2 + \frac{\mu_1}{2}|A|^4\,. \tag{141}$$

Thus solitary wave solutions exist provided that $\epsilon > 0$, and that the nonlinear coefficient $\mu_1 < 0$. The condition $\epsilon > 0$ implies that the perturbed

eigenvalues, $\lambda \approx i\beta + (2\epsilon\beta)^{1/2}$ have split off the imaginary axis, and so provide the conditions needed for exponential decay at infinity; the condition $\mu_1 < 0$ depends on the particular physical system being considered.

   The solution of the truncated system is

$$A = a \exp\left(i[\beta + \epsilon]\xi\right)\text{sech}(\gamma\xi)\,, \quad \text{where } \gamma = (2\epsilon\beta)^{1/2}\,, \ |a|^2 = -\frac{4\epsilon\beta}{\mu_1}\,. \quad (142)$$

This solution describes an *envelope solitary wave*, with a carrier wavenumber $\beta + \epsilon$ and an envelope described by the "sech"-function. These solitary waves can also be obtained from the *soliton solutions of the nonlinear Schrodinger equation (NLS) equation*, for that special case when the phase velocity equals the group velocity, $c = c_g$, or more precisely when $c + \Omega/K = c_g + V$, where V is the soliton speed and Ω, K are the frequency and wavenumber corrections. Note that the solution (142) contains an arbitrary phase in the complex amplitude a, meaning that the location of the crests of the carrier wave *vis-a-vis* the maximum of the envelope (here located at $\xi = 0$) is arbitrary. However, restoration of the error terms leads to the result that *only two of these solutions persist*, namely, those for which a carrier wave crest or trough is placed exactly at $\xi = 0$, so that the resulting solitary wave is either one of *elevation or depression*. This result requires very delicate analysis, but could be anticipated by noting that these are the only two solutions which persist under the symmetry transformation $\xi \to -\xi$.

   For water waves, for which the dispersion relation is (125), these two cases (1) and (2) imply that pure solitary waves of elevation exist for $B = 0$, and of depression for $B > 1/3$, while generalized solitary waves arise whenever $0 < B < 1/3$. Concerning case (3) the conditions are met for capillary -gravity waves with $0 < B < 1/3$, where it can be shown that the coefficient $\mu_1 < 0$ as required. Hence we find envelope solitary waves.

   For the case of generalized solitary waves, there is always the possibility that the amplitude of the oscillations is zero, and the solution then reduces to a pure solitary, called an *"embedded"* solitary wave. There are now many examples of such embedded solitary waves arising in various physical systems, notably for internal waves, but from various numerical and analytical studies, it would seem that they do not arise in the water wave context. This "dynamical-systems" approach to finding solitary waves has also been applied to interfacial waves, where again the linear dispersion relation holds the key to where solitary waves can be found.

5   Fifth-order Korteweg-de Vries equation

5.1   Formulation and outer expansion

In the next two sections we shall look at how generalized solitary waves arise in two illustrative model systems, one in this section representing gravity-capillary waves, and one in the next section representing internal waves. First, for gravity-caplillary waves, we shall consider a model equation, valid when $B \approx 1/3$ and for small amplitudes. This is the usual KdV equation supplemented by a fifth-order linear dispersive term, known as the fifth-order Korteweg-de Vries (5KdV) equation,

$$u_t + c_0 u_x + \mu u u_x + \delta u_{xxx} + \delta_1 u_{xxxxx} = 0 \,. \tag{143}$$

where, for gravity-capillary waves

$$c_0 = (gh)^{1/2} \,, \quad \mu = \frac{3c_0}{2h} \,, \quad \delta = \frac{c_0 h^2 \tau}{6} \,, \quad \delta_1 = c_0 h^4 \{ \frac{1}{90} + \frac{\tau}{18} - \frac{\tau^2}{72} \} \,,$$

where $\tau = 1 - 3B$. When $B = 1/3, \tau = 0$, and then $\delta = 0, \delta_1 > 0$. We are concerned here with the case when $0 < \tau << 1$, when $\delta > 0, \delta_1 > 0$. With appropriate changes of variable, we replace (143) with

$$u_t + 6u u_x + u_{xxx} + \epsilon^2 u_{xxxxx} = 0 \,. \tag{144}$$

When $\epsilon = 0$ this is the standard KdV equation. But when $\epsilon \neq 0$ it has a linear dispersion relation

$$c = -k^2 + \epsilon^2 k^4 \,, \tag{145}$$

and so there is a resonance at $c = 0$ between $k = 0$ and $k = \pm \epsilon^{-1}$.

We seek solutions of the form

$$u = u(x - ct) \,, \tag{146}$$

so that the 5KdV equation (144) becomes

$$-cu + 3u^2 + u_{xx} + \epsilon^2 u_{xxxx} = 0 \,, \tag{147}$$

A constant of integration have been set to zero, essentially by imposing solitary wave boundary conditions, or better, by translating u by a constant. Equation (147) is a fourth order ordinary differential equation. We shall seek a *symmetric generalized solitary wave* solution, that is $u(x) = u(-x)$, with a co-propagating oscillatory tail of small amplitude. This amplitude will be found using exponential asymptotics and Borel summation, in an analogous manner to that used in section 3, see Pomeau et al (1988) and Grimshaw and Joshi (1995) for more details.

First consider the *outer expansion*

$$u \sim u_s = \sum_{n=0}^{\infty} u_n(x)\epsilon^{2n}, \quad c \sim \sum_{n=0}^{\infty} \epsilon^{2n} c_{2n}, \tag{148}$$

$$u_0 = 2\gamma^2 \mathrm{sech}^2(\gamma x), \quad c_0 = 4\gamma^2, \tag{149}$$

$$u_1 = -10\gamma^2 u_0 + \frac{15}{2}u_0^2, \quad c_1 = c_0^2. \tag{150}$$

For real x this asymptotic solution can be continued to all orders in ϵ^{2n}. As expected, it is symmetric, and no tail oscillations emerge. Instead, these are found from the singularties of u_s in the complex x-plane, which are located at $x = \pm i\pi/2\gamma, \pm 3i\pi/2\gamma, \cdots$. It will be sufficient to consider just the singularity at $x = i\pi/2\gamma$ closest to the real axis in the upper half-plane, and write

$$x = \frac{i\pi}{2\gamma} + \epsilon q. \tag{151}$$

Substitution into (148) and evalaution in the limit $\epsilon q \to 0$ yields

$$u_s \sim \frac{1}{\epsilon^2}\{-\frac{2}{q^2} + \frac{30}{q^4} + O(q^{-6})\} + 2\gamma^2\{\frac{1}{3} + O(q^{-6})\} + \epsilon^2\{-\frac{2\gamma^2 q^2}{15}\}. \tag{152}$$

5.2   Inner expansion and Borel summation

Next we replace x with q (151), and put $v(q) = \epsilon^2 u(x)$, so that (147) becomes

$$v_{qqqq} + v_{qq} + 3v^2 - \epsilon^2 cv = 0. \tag{153}$$

The symmetry condition becomes

$$\mathrm{Im}\, v(q) = 0, \quad \text{on} \quad \mathrm{Re}\, q = 0. \tag{154}$$

Equation (153) is exact, and we seek the expansion

$$v(q) \sim \sum_{n=0}^{\infty} v_n(q)\epsilon^{2n}, \tag{155}$$

so that $v_{0qqqq} + v_{0qq} + 3v_0^2 = 0. \tag{156}$

Matching with the outer expansion (152) for u_s yields

$$v_0 \sim -\frac{2}{q^2} + \frac{30}{q^4} + O(q^{-6}), \tag{157}$$

taken in the limit $q \to \infty$ for $\mathrm{Re}\, q > 0, \mathrm{Im}\, q < 0$. Note that the speed c does not appear at the leading order.

$$v_{0qq} + v_0 + 3v_0^2 = 0$$

Now seek an asymptotic solution

$$v_0 \sim \sum_{n=1}^{\infty} \frac{b_n}{q^{2n}}, \quad \text{as} \quad q \to \infty, \; \text{Re}\, q > 0 \, \text{Im}\, q < 0. \tag{158}$$

Substitution into equation (156) yields $b_1 = -2, b_2 = 30$ as required by (157) and then

$$(2n - 3)(2n + 4)b_n + (2n - 2)(2n - 1)n(2n + 1)b_{n-1}$$
$$+ 3\sum_{j=2}^{n-1} b_j b_{n+1-j} = 0, \quad n = 1, 2, \cdots. \tag{159}$$

The aim now is to sum the series (158) using *Borel summation* We seek a solution of equation (156) in the form of a *Laplace transform*

$$v_0 = \int_{\Gamma} \exp\left(-sq\right) V(s)\, ds, \tag{160}$$

where the contour Γ runs from zero to infinity in the complex s-plane such that $\text{Re}(sq) > 0$, see Figure 3.

Substitution of the Laplace transform into the equation (156) for v_0 yields the Fredholm integral equation for $V(s)$,

$$(s^2 + 1)V(s) + 3\int_0^s V(\hat{s})V(s - \hat{s})\, d\hat{s} = 0. \tag{161}$$

To solve this we seek a solution as a power series

$$V(s) = \sum_{n=0}^{\infty} a_n s^{2n+1}. \tag{162}$$

Substitution of (162) into equation (161) shows that $a_0 = -2, a_1 = 5$ and

$$\frac{(2n - 1)(2n + 6)}{(2n + 2)(2n + 3)} a_n + a_{n-1} +$$
$$3\sum_{j=1}^{n-1} a_j a_{n-j} \frac{(2j + 1)!(2n - 2j + 1)!}{(2n + 3)!} = 0, \quad n = 1, 2, \cdots. \tag{163}$$

Next, substitution of (162) into the Laplace transform (160) recovers the asymptotic series (158) with

$$b_{n+1} = a_n(2n+1)!, \quad n = 0, 1, 2, \cdots. \tag{164}$$

Thus solving the recurrence relation (163) for a_n effectively sums the asymptotic series (158) and yields the solution of equation (156) for v_0 as a Laplace transform. Examination of the recurrence relation (163) shows that as $n \to \infty$, the nonlinear terms drop out, and so $a_n \sim (-1)^n K$ where $K = -19.97$ is a constant found numerically. Hence the series (162)

$$V(s) = \sum_{n=0}^{\infty} a_n s^{2n+1}.$$

converges for $|s| < 1$. Analytic continuation into the complex s-plane, using the integral equation (161), yields a complete solution for $V(s)$ and hence $v_0(q)$ as the Laplace transform (160).

Since $a_n \sim (-1)^n K$ as $n \to \infty$ we see that $V(s) = \sum_{n=0}^{\infty} a_n s^{2n+1}$ has singularities at $s = \pm i$ given by

$$V(s) \approx \frac{Ks}{s^2 + 1}, \quad \text{for} |s| \approx 1. \tag{165}$$

There are similar poles at $s = 2i, 3i, \cdots$, but these generate higher harmonics in the tail oscillations, and so are not our immediate concern. We must know make a specific choice of the contour Γ in the Laplace transform (160)

$$v_0 = \int_{\Gamma} \exp{(-sq)} V(s) \, ds.$$

Since we are seeking a symmeric solution, which satisfies the condition (154), it is sufficient to suppose that at first $\operatorname{Re} q > 0$ and $\operatorname{Im} q < 0$. Then choose the contour Γ to lie initially in $\operatorname{Re} s > 0, \operatorname{Im} s \geq 0$, so that $\operatorname{Re} sq > 0$ and the Laplace transform is well defined for the allowed values of q. In particular, since $V(s)$ can be represented by the power series (162), which generates the asymptotic series (158), which in turn is equivalent to the asymptotic series (148), we conclude that $v_0 \sim v_s = \epsilon^2 u_s$.

The next step is to deform the contour Γ onto the imaginary s-axis. In this process we will need to deform around the poles at $s = i, 2i, 3i, \cdots$ and collect the (half) residues. Hence we find that (160) becomes, on putting $s = iy$ on the deformed contour Γ,

$$v_0 = \int_0^{\infty} \exp{(-iyq)} V(iy) \, i \, dy + \frac{i\pi K}{2} \exp{(-iq)} + \cdots, \tag{166}$$

where the dots denote terms proportional to $\exp(-2iq), \exp(-3iq), \cdots$. The integral is interpreted as a principal value integral at the singularities at $y = 1, 2, 3, \cdots$. This holds in $\operatorname{Re} q > 0, \operatorname{Im} q < 0$. To apply the *symmetry condition (154) that v_0 should be real-valued on the imaginary q-axis*, we must now let $\operatorname{Re} q \to 0$, and put $q = -iQ, Q > 0$ in the expression (166). From the series (162), $V(iy) = i \sum_{n=0}^{\infty} a_n(-1)^n y^{2n}$ is pure imaginary since the coefficients a_n are all real-valued. Hence the integral term is real-valued as required. But the contributions from the poles are pure imaginary, and hence the expression (166) cannot satisfy the symmetry condition. The remedy is to note that the term $\exp(-iq)$ is exponentially small in the sector $\operatorname{Re} q > 0, \operatorname{Im} q < 0$ and hence is *subdominant*, so that we are allowed to add such terms asymptotically to (166).

Thus we replace (166) with

$$
\begin{aligned}
v_0 = \int_0^\infty \exp(-iyq)\, V(iy)\, i\, dy + \frac{i\pi K}{2} \exp(-iq) \\
+ \frac{ib}{2} \exp(-iq + i\delta) + \cdots,
\end{aligned}
\tag{167}
$$

where b, δ are real constants. Now application of the symmetry condition shows that

$$
b \cos \delta = -\pi K.
\tag{168}
$$

Thus the final solution for v_0 in $\operatorname{Re} q > 0, \operatorname{Im} q < 0$ is

$$
v_0 \sim \int_\Gamma \exp(-sq)\, V(s)\, ds + + \frac{ib}{2} \exp(-iq + i\delta) + \cdots,
\tag{169}
$$

where b is determined in terms of δ by (168). It remains to bring this solution back to the real x-axis, for $x > 0$, using (151), $x = i\pi/2 + \epsilon q$. Here we must also collect a similar contribution from the singularities in the lower half of the complex x-plane. Thus the full solution consists of a *central core and an exponentially small tail oscillation*.

The final result is that, for $x > 0$ (the case $x < 0$ follows from the imposed symmetry),

$$
u \sim u_s + \frac{b}{\epsilon^2} \exp\left(-\frac{\pi}{2\epsilon\gamma}\right) \sin\left(\frac{x}{\epsilon} - \delta\right), \quad b \cos \delta = -\pi K,
\tag{170}
$$

where $u_s \sim 2\gamma^2 \operatorname{sech}^2(\gamma x) + O(\epsilon^2)$ is given by (149). The tail oscillations form a *one-parameter family* characterized by the phase shift $\delta, 0 \leq \delta < \pi/2$. The minimum amplitude occurs for $\delta = 0$ and then the generalized solitary wave has the structure shown in Figure 4. This result agrees with Pomeau

et al (1988) (for the case $\delta = 0$), and with the numerical solutions of Boyd (1991). Amick and Toland (1992) have established theoretically that the nonlocal solutions of the fourth order ordinary differential equation (147) form a one-parameter family homoclinic to periodic solutions for (147).

5.3   One-sided oscillations

Suppose that instead of the symmetry condition (154) we look for *one-sided solutions* such that $u(x) \to 0$ *as* $x \to -\infty$. This choice is motivated by the observation that for the fifth-order KdV equation (144) the group velocity $c_g = 2\epsilon^{-2} > 0$ at the resonant wavenumber $k = \epsilon^{-2}$ and hence the radiation is emitted into $x > 0$ The same procedure can be followed, and again the solution for $\mathrm{Re}\, q > 0, \mathrm{Im}\, q < 0$ is given by the Laplace transform (160), with the contour Γ now chosen to lie in $\mathrm{Re}\, s < 0, \mathrm{Im}\, s > 0$ (that is, to the left of the imaginary axis in Figure 3), which ensures that there are no oscillations as $x \to -\infty$. But now, to find the behaviour as $x \to \infty$, the contour Γ must be moved across the imaginary s-axis in order to evaluate the solution when $\mathrm{Re}\, q > 0$. In doing so the solution collects the residue at the poles $s = i, 2i, 3i, \cdots$. The residue at $s = i$ is $-i\pi K \exp(-iq)$, exactly twice the contribution and oppositely-signed from the half residue shown in (166). Then, bringing the solution back to the real x-axis, in $x > 0$, we find that

$$u \sim u_s - \frac{2\pi K}{\epsilon^2} \exp\left(-\frac{\pi}{2\epsilon}\right) \sin\left(\frac{x}{\epsilon}\right). \tag{171}$$

For these one-sided solutions there are no free parameters. A schematic example of a one-sided oscillation is shown in Figure 7. Further, these waves are unsteady and slowly *decay* due to this radiation.

5.4   Higher-order terms

We now return to the inner expansion (155)

$$v(q) \sim \sum_{n=0}^{\infty} v_n(q)\epsilon^{2n},$$

and examine the effect of the next term v_1, where we recall from (152) that the matching condition is that $v_1 \to 2\gamma^3/3$ as $q \to \infty$ in $\mathrm{Re}\, q > 0, \mathrm{Im}q < 0$. First, we re-examine the tail oscillations and seek a solution of (147) of the form

$$u \sim u_s + u_w, \tag{172}$$
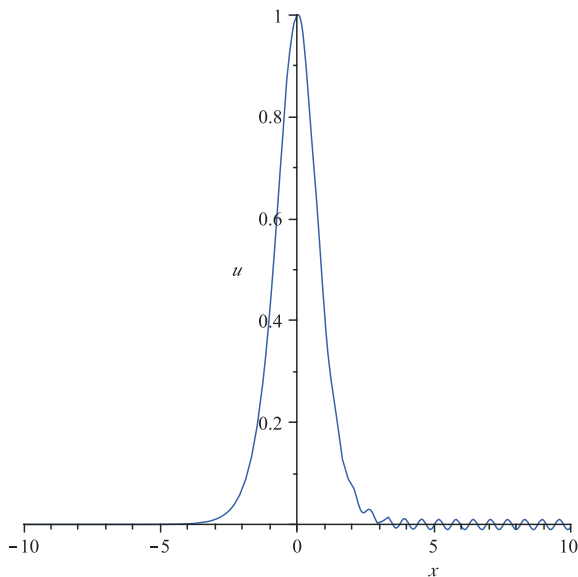
Figure 7. A schematic plot of a one-sided oscillation.

where u_s is the outer expansion (148) and u_w are the tail oscillations. Substitution into (147) and linearization about u_s yields

$$-cu_w + 6u_su_w + u_{wxx} + \epsilon^2 u_{wxxxx} = 0. \tag{173}$$

When $x \to \infty$, the term $6u_su_w$ can be omitted, and we find that

$$u_w \sim \alpha \sin\left(\frac{kx}{\epsilon} - \delta\right), \quad k^4 - k^2 = \epsilon^2 c. \tag{174}$$

for some constants α, δ. Since $c = 4\gamma^2 + 16\epsilon^2\gamma^4 + O(\epsilon^4)$, we find that $k = 1 + 2\epsilon^2\gamma^2 + O(\epsilon^4)$.

To obtain the higher-order terms, we put

$$u_w \sim \alpha(1 + \epsilon^2 R(x)) \sin\left(\frac{kx}{\epsilon} - \delta + \epsilon\phi(x)\right). \tag{175}$$

Substitution into (173) yields

$$R(x) = 15\gamma^2 \text{sech}^2(\gamma x) + O(\epsilon^2), \quad \phi(x) = -6\tanh(\gamma x) + O(\epsilon^2). \tag{176}$$

Then, to match with he inner solution, we use $x = i\pi/2\gamma + \epsilon q$ (151) to get

$$u_w \sim \frac{i\alpha}{2} \exp\left(\frac{k\pi}{2\epsilon\gamma}\right) \exp\left(-iq + \delta\right)[1 + \frac{6i}{q} + O(q^{-2})]. \tag{177}$$

Next, we re-examine the inner solution and replace (160) with

$$v_0 \sim v_s + w_0, \quad v_s = \int_\Gamma \exp\left(-sq\right) V(s) ds, \tag{178}$$

where the contour Γ runs from zero to infinity in $\operatorname{Re} q > 0$, $\operatorname{Im} q < 0$, as before. Substitution into equation (153) and linearization about v_s gives

$$w_{0qqqq} + w_{0qq} + 6v_s w_0 = 0. \tag{179}$$

As $q \to \infty$, the term $6v_s w_0$ can be omitted, and we get that $w_0 \propto \exp\left(-iq\right)$ in agreement with (167). But a more careful analysis which takes account of the term $6v_s w_0$ yields

$$w_0 \sim \frac{ib}{2} \exp\left(-iq + i\delta\right)\{1 + \frac{6i}{q} + O(q^{-2})\}. \tag{180}$$

The reaming analysis proceeds as before, with deformation of the contour Γ onto the imaginary axis, and we again get (168) that $b\cos\delta = -\pi K$. The expression (180) can now be matched successfully with u_w (177) to leading order in ϵ^2.

Next, consider the term $\epsilon^2 v_1$ in the expansion (155) for v, which satisfies the equation

$$v_{1qqqq} + v_{1qq} + 6v_0 v_1 - 4\gamma^2 v_0 = 0, \tag{181}$$

where we have used the leading order expression (149) for $c_0 = 4\gamma^2$. From the outer expansion (152) for u_s expressed in terms of q we find that the matching condition is that

$$v_1 \sim \frac{2\gamma^2}{3}, \quad \text{as} \quad q \to \infty, \operatorname{Re} q > 0, \operatorname{Im} q < 0. \tag{182}$$

But now we see that $v_1 = 2\gamma^2/3$ *is an exact solution* of (181), and hence there is no need for any Borel summation. But again, we need to insert a subdominant term, and so write

$$v_1 = \frac{2\gamma^2}{3} + w_1, \tag{183}$$

It is then readily shown that w_1 satisfies the *same equation* (179 *as that for* w_0, and hence can be absorbed into the same solution (180) by allowing the

constants b, δ to be expanded in powers of ϵ^2. Matching between u_w and w_0 then yields

$$\alpha = \frac{b}{\epsilon^2} \exp\left(-\frac{k\pi}{2\epsilon\gamma}\right). \tag{184}$$

Here we recall that $b\cos\delta = -\pi K$, and that the wavenumber k is given by (174), so that $k = 1 + 2\epsilon^2\gamma^2 + O(\epsilon^4)$, while u_w is then given by (175). As $x \to \infty$, we get

$$u_w \sim \alpha \sin\left(\frac{kx}{\epsilon} - \delta - 6\epsilon\right). \tag{185}$$

Hence the main effect of the higher-order terms is to replace $k = 1$ with the full expression (174) for k.

6   Coupled Korteweg-de Vries Equations

6.1   Internal waves

Generalized solitary waves also occur for interfacial waves when there is a free surface, and for all internal waves with mode numbers $n \geq 2$, see Akylas and Grimshaw (1992) and Boyd (1998). The underlying reason is that there is a resonance between a long wave with wavenumber $k \approx 0$ and a short wave with a finite wavenumber k, see the dispersion curves shown in Figure 8. In the absence of the surface mode, only mode 1 supports a genuine solitary wave. In the presence of the surface mode, all internal modes support only generalized solitary waves. When the amplitude of the central core is small, $O(\epsilon^2)$, the amplitude of the oscillations with wavenumber k is *exponentially small*, typically $O(\exp(-K/\epsilon))$ where K is a positive constant. Hence they cannot usually be found by conventional asymptotic expansions, and again we need *exponential asymptotics*.

Steady generalized solitary waves are necessarily symmetric. But this means they cannot be realized physically as then the group velocity of the small oscillations is the same at both ends, which implies that energy sources and sinks are needed. In practice, they are generated with a core and small oscillations only on *one side*, determined by the group velocity, as shown for gravity-capillary waves in Figure 7. However, for internal waves, unlike gravity-capillary waves, the group velocity is less than the phase velocity, and so the tail oscillations occur on the opposite side to those shown in Figure 7. An example of an observation of a mode-2 internal wave with a mode 1-tail is shown in Figure 2 of Akylas and Grimshaw (1992).

The technique we use to find the tail oscillations is again based on extending the usual asymptotic expansion into the complex plane, and using *Borel summation*. It is similar to the techniques used by Pomeau et al
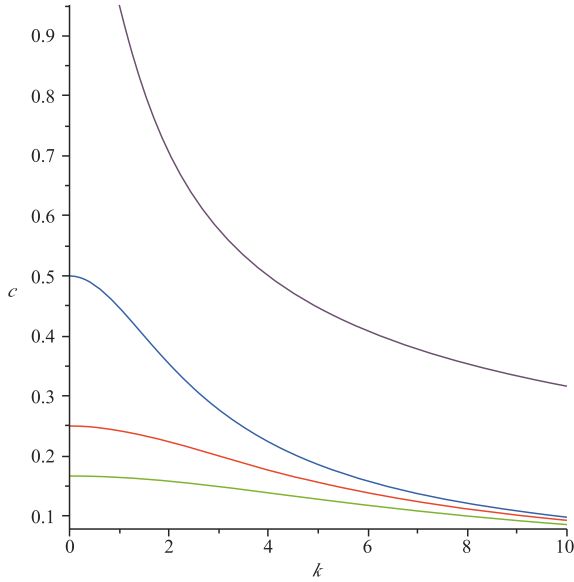
Figure 8. Plot of a typical set dispersion curves for internal waves for the phase speed $c = c(k)$ in terms of wavenumber k: mode 1 (blue), mode 2 (red), mode 3 (green) and the surface mode (violet).

(1988) and Kruskal and Segur (1991). The full system was analyzed using this approach by Akylas and Grimshaw (1992). Here, for simplicity, we consider instead two *coupled Korteweg-de Vries (KdV) equations*, which can be shown to describe the interaction between two weakly nonlinear long internal waves whose linear long wave speeds are nearly equal,

$$u_t + 6uu_x + u_{xxx} + (pv_{xx} + quv + \frac{1}{2}rv^2)_x = 0 \,, \qquad (186)$$

$$v_t + \Delta v_x + 6vv_x + v_{xxx} + \lambda(pu_{xx} + ruv + \frac{1}{2}qu^2)_x = 0 \,. \qquad (187)$$

This system is Hamiltonian, and conserves the "mass" u, v, the "momentum" $\lambda u^2 + v^2$, and the Hamiltonian. For stability we choose the coupling parameter $\lambda > 0$. Δ is the detuning parameter, proportional to the difference between the two linear long wave speeds; without loss of generality we take $\Delta > 0$.

First examine the linear spectrum, for waves of wavenumber k and phase

speed $c = c(k)$,

$$c = \frac{\Delta}{2} - k^2 \pm \{\lambda p^2 k^4 + \frac{\Delta^2}{4}\}^{1/2}. \tag{188}$$

If we let the coupling parameter $\lambda \to 0$ these linear modes uncouple into a u-mode with spectrum $c = -k^2$ and a v-mode with spectrum $c = \Delta - k^2$. This situation persists for $\lambda > 0$, and there is a *resonance* between the long wave (u-mode, in red) and a short wave (v-mode, in blue), with a resonant wavenumber $k_0 = (\Delta/1 - \lambda p^2)^{1/2}$ provided that $\lambda p^2 < 1$, see Figure 9.
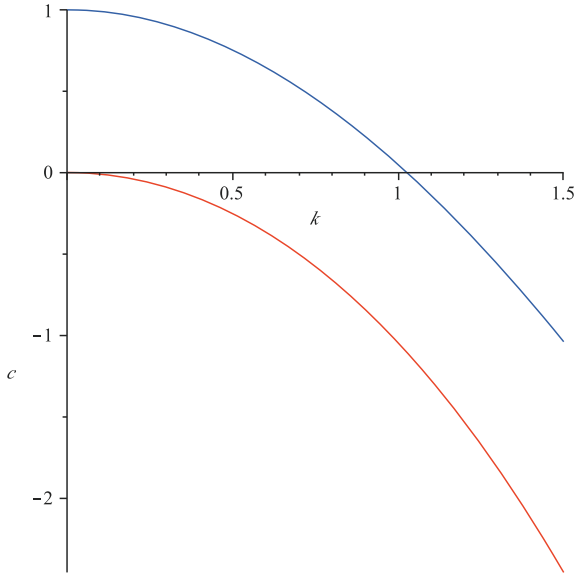
Figure 9. A plot of the dispersion relation (188) for $\Delta = 1, p = 0.5, \lambda = 0.2$

We seek solutions of the form

$$u = u(x - ct), \quad v = v(x - ct), \tag{189}$$

so that the coupled KdV system (186, 187) becomes

$$-cu + 3u^2 + u_{xx} + pv_{xx} + quv + \frac{1}{2}rv^2 = 0, \tag{190}$$

$$-cv + \Delta v + 3v^2 + v_{xx} + \lambda(pu_{xx} + ruv + \frac{1}{2}qu^2) = 0. \tag{191}$$

The two constants of integration have been set to zero, essentially by imposing solitary wave boundary conditions, or better, by translating u, v by

constants. Equations (190, 191) form a fourth order ordinary differential equations system. We shall show that they have symmetric generalized solitary wave solutions, with co-propagating oscillatory tails of small amplitude. This amplitude will be found using either exponential asymptotics, or more directly by expanding in λ.

6.2   Outer expansion

First, expand around $k = 0$ for the long (u-mode) wave. Thus, we introduce a small parameter $\epsilon << 1$, and seek a solution as an asymptotic expansion,

$$u_s(\epsilon x) = \sum_{n=1}^{\infty} \epsilon^{2n} u_n\,, \quad v_s(\epsilon x) = \sum_{n=1}^{\infty} \epsilon^{2n} v_n\,, \quad c = \sum_{n=1}^{\infty} \epsilon^{2n} c_n\,. \tag{192}$$

Substitution into (190, 191) yields

$$u_1 = 2\gamma^2 \text{sech}^2(\epsilon\gamma x)\,, \quad v_1 = 0\,, \quad c_1 = 4\gamma^2\,, \tag{193}$$

$$u_2 = \frac{\lambda}{\Delta}\{(20p^2 + q^2 - 8pq)c_1 u_1 - (q - 6p)(q - 10p)u_1^2\}\,, \tag{194}$$

$$v_2 = -\frac{\lambda}{\Delta}\{pc_1 u_1 + \frac{1}{2}(q - 6p)u_1^2\}\,, \tag{195}$$

$$c_2 = -\frac{\lambda}{\Delta}p^2 c_1^2\,. \tag{196}$$

This expansion can be continued to all orders in ϵ^2 without any oscillatory tail being detected.

To find the tail oscillations, we observe that u_n, v_n are singular in the complex plane at $x = \pm i\pi/2\epsilon\gamma, \pm 3i\pi/2\epsilon\gamma, \cdots$. This motivates us to examine this singularity by the change of variables

$$x = \frac{i\pi}{2\epsilon\gamma} + z\,, \tag{197}$$

Then as $\epsilon z \to 0$, $\text{sech}^2(\epsilon\gamma x) \sim -1/\epsilon^2\gamma^2 z^2$, and so

$$u_s \sim -\frac{2}{z^2} - \frac{\lambda}{2\Delta z^4}(q - 6p)(q - 10p) + \cdots + O(\epsilon^2)\,, \tag{198}$$

$$v_s \sim -\frac{2\lambda}{\Delta z^4}(q - 6p) + \cdots + O(\epsilon^2)\,. \tag{199}$$

6.3   Inner expansion and Borel summation

Next, we consider the *inner problem* in which we seek solutions of (190, 191) in the form $u = u(z), v = v(z)$, for which the expressions (198, 199)

form an *outer boundary condition*. The outcome is just the same system (190, 191) with x replaced by z. Note that $c = O(\epsilon^2)$, and can be omitted at the leading order.

We seek a solution of this inner problem as a Laplace transform

$$[u, v] = \int_\Gamma \exp{(-zs)}[U(s), V(s)] \, ds , \qquad (200)$$

where the contour Γ runs from 0 to ∞ in the half-plane $\mathrm{Re}(sz) > 0$, see Figure 3 and note that here z replaces q. We seek a power series solution

$$[U(s), V(s)] = \sum_{n=1}^{\infty} [a_n, b_n] s^{2n-1} , \qquad (201)$$

where $a_1 = -2$, $b_1 = 0$, $a_2 = -\lambda(q-6p)(q-10p)/12\Delta$, $b_2 = -\lambda(q-6p)/3\Delta$. In general, substitution of (201) into the Laplace transform (200) generates the asymptotic series

$$[u, v] \sim \sum_{n=1}^{\infty} [\alpha_n, \beta_n] z^{-2n} , \quad [\alpha_n, \beta_n] = (2n-1)! [a_n, b_n] . \qquad (202)$$

This agrees with the asymptotic series (198, 199), and in effect the Laplace transform is a *Borel summation* of the asymptotic series.

Substitution of the Laplace transform (200) and the series (201) into the differential equation system (190, 191) yields a recurrence relation for $[a_n, b_n]$. Putting $\Delta[A_n, B_n)] = (-k_0^2)^n[a_n, b_n]$, we get

$$\frac{(n+1)(2n+5)}{(n-1)(2n-1)} A_{n-1} + \{p - \frac{q}{(n-1)(2n-1)}\} B_{n-1} = F_n , \qquad (203)$$

$$(1 - \lambda p^2) B_n - B_{n-1} - \lambda p A_{n-1} + \lambda \frac{r B_{n-1} + q A_{n-1}}{(n-1)(2n-1)} = G_n , \qquad (204)$$

where F_n, G_n are quadratic convolution expressions in $A_2, \cdots A_{n-2}, B_2 \cdots , B_{n-2}$. As $n \to \infty$, these nonlinear terms can be neglected, and we find that

$$[A_n, B_n] \to [-p, 1]K \quad \text{as} \quad n \to \infty , \qquad (205)$$

where K is a constant whose value depends on λ, p, q, r. It now follows that the series (201) *converges for* $|s| < k_0$, $k_0^2 = \Delta/(1 - \lambda p^2)$. The result (205) shows that as $s \to ik_0$ there is a pole singularity given by

$$[U(s), V(s)] \approx \Delta \frac{[p, -1]K}{2(s - ik_0)} . \qquad (206)$$

We have now established that the solution in the z-variable is given by

$$[u, v] = \int_\Gamma \exp\left(-zs\right)[U(s), V(s)]\, ds\,,$$

where $[U(s), V(s)]$ has a pole singularity at $s = ik_0$, also at the complex conjugate point $s = -ik_0$ and at all their harmonics $s = \pm ink_0$, $n = 2, 3$ etc. Hence the contour Γ should be chosen to avoid the imaginary s-axis, and to be explicit we choose it to lie in $\operatorname{Re} s > 0$. But we seek a *symmetric solution*, which in the z-variable requires that $\operatorname{Im}[u.v] = 0$ when $\operatorname{Re} z = 0$. But the presence of the pole prevents (200) from satisfying this condition, and so, as in section 5, we must correct it by adding a subdominant term

$$[u, v] = \int_\Gamma \exp\left(-zs\right)[U(s), V(s)]\, ds + \frac{ib}{2}[p, -1]\exp\left(-ik_0 z + i\delta\right). \quad (207)$$

Here b, δ are real constants, and note that $|\exp\left(-ik_0 z\right)|$ is smaller than of z^{-n} as $z \to \infty$ in $\operatorname{Re} z > 0$, $\operatorname{Im} z < 0$, recalling that $x = (i\pi/2\epsilon\gamma) + z$. The symmetry condition is now applied by bringing the contour Γ onto $\operatorname{Re} s = 0$ and deforming around the pole at $s = ik_0$.

The outcome is

$$b\cos\delta = \pi K\,. \quad (208)$$

which is substituted into

$$[u, v] = \int_\Gamma \exp\left(-zs\right)[U(s), V(s)]\, ds + \frac{ib}{2}[p, -1]\exp\left(-ik_0 z + i\delta\right).$$

The final step is to bring this solution (207) back to the real axis, using $x = (i\pi/2\epsilon\gamma) + z$. Taking account of the corresponding singularity at $s = -ik_0$, we finally get that

$$[u, v] \sim [u_s, v_s] + b\Delta[-p, -1]\exp(-\pi k_0/2\epsilon\gamma)\sin(k_0|x| - \delta)\,. \quad (209)$$

Here we recall (193) that $u_s \sim 2\epsilon^2\gamma^2\operatorname{sech}^2(\gamma\epsilon x)$, $v_s \sim O(\epsilon^4)$. This is a two-parameter family, the parameters being $\epsilon\gamma, \delta, 0 < \delta < \pi/2$. The minimum tail amplitude occurs at $\delta = 0$. Note that the constant in the exponential term is determined by the location of the singularity, but the amplitude needs the exponential asymptotics.

The constant K is determined by the recurrence relations (203, 204). It is a function of the system parameters λ, p, q, r and in general is found numerically. But $K = 0$ for $q = 6p$ (see (193, 194)), and in general it was found by Grimshaw and Cook (1996) that there are many parameter combinations where $K = 0$, see their Figures 1-4. In particular

$$K \approx \frac{\lambda(6p - q)}{3\Delta} \quad \text{as} \quad \lambda \to 0\,. \quad (210)$$

These special values imply that the solitary wave decays to zero at infinity, even although its speed lies inside the linear spectrum, at least in this asymptotic limit. These are called *embedded solitons*. They are usually not stable, but are instead *metastable*, or are said to exhibit *semi-stability*. Nevertheless they are found useful in several applications, such as nonlinear optics and solid state physics. For water waves with surface tension, generalized solitary waves exist for Bond numbers $0 < B < 1/3$, but from numerical simulations it seems there are no embedded solitons.

These symmetric solitary waves cannot be realized in practice, since they require an energy source and sink at infinity. Instead, they are replaced by *solitary waves with radiating tails on one side only*, determined by the group velocity. That is, in $x > 0$ for $c_g > c$, or in $x < 0$ for $c_g < c$, where c_g is the group velocity at the resonant wavenumber. For the present case, the linear dispersion relation is (188) and so for the relevant u-mode, $c_g = \Delta - 3k^2 < c = \Delta - k^2$. Hence there are no oscillations in $x > 0$, but they will appear in $x < 0$. Thus, in this case for one-sided oscillations, in $x > 0$, or more generally in Re $z > 0$, the solution is completely defined by the Laplace transform integral (200), with the contour Γ lying in Re $s > 0$. Then for $x < 0$, or Re $z < 0$, the contour Γ must be moved to Re $z < 0$ across the axis Re $s = 0$. In this process the solution collects a contribution from the pole at $s = ik_0$, which generates the tail oscillation. The final outcome is that (209) is replaced by

$$[u, v] \sim [u_s, v_s] - H(-x)2\pi K\Delta[-p, -1]\exp(-\pi k_0/2\epsilon\gamma)\sin(k_0 x) \quad (211)$$

where $H(\cdot)$ is the Heaviside function. That is, in effect the phase shift $\delta = 0$, there are no oscillations in $x > 0$ and *the amplitude in $x < 0$ is exactly twice the amplitude of the symmetric solution.*

6.4   Weak coupling approximation

In the system (190, 191) suppose that $0 < \lambda << 1$ and expand,

$$[u, v] \sim \sum_{n=0}^{\infty} \lambda^n [u_n, v_n], \quad c \sim \sum_{n=0}^{\infty} \lambda^n c_n. \quad (212)$$

$$u_0 = 2\beta^2 \mathrm{sech}^2(\beta x), \quad v_0 = 0, \quad c_0 = 4\beta^2. \quad (213)$$

This leading term is a u-mode solitary wave. Note that in comparison with the previous expansion (192) $\beta = \epsilon\gamma$, but now the amplitude can be order unity. At the next order

$$-c_0 u_1 + 6u_0 u_1 + u_{1xx} + pv_{1xx} + qu_0 v_1 - c_1 u_0 = 0, \quad (214)$$

$$(\Delta - c_0)v_1 + v_{1xx} + pu_{0xx} + \frac{q}{2}u_0^2 = 0 \,. \tag{215}$$

$$(\Delta - c_0)v_1 + v_{1xx} = f(x) = -pc_0u_0 + (6p - q)\frac{u_0^2}{2} \,. \tag{216}$$

Note that in this limit $\lambda \to 0$, the resonant wavenumber $k_0 \approx (\Delta - c_0)^{1/2}$ and takes account of the *finite speed* of the wave. We must now take $c_0 < \Delta$ to get tail oscillations, and for $c_0 > \Delta$ the expansion yields a genuine solitary wave. The general solution of (216) is

$$v_1 = A\sin k_0 x + B\cos k_0 x + \frac{1}{2k_0}\int_{-\infty}^{\infty} f(x')\sin(k_0|x - x'|)dx' \,. \tag{217}$$

To determine the constants A, B we impose a symmetry condition on v_1, so that $A = 0$, and then

$$v_1 \sim b_1\sin(k_0|x| - \delta) \quad \text{as} \quad |x| \to \infty \,, \tag{218}$$

$$b_1\cos\delta = L = \frac{1}{2k_0}\int_{-\infty}^{\infty} f(x)\cos(k_0x)dx \,. \tag{219}$$

With v_1 known, we can find u_1 from (214), and

$$u_1 \sim -p\frac{(\Delta - c_0)}{\Delta}b_1\sin(k_0|x| - \delta) \,, \quad \text{as} \quad |x| \to \infty \,, \tag{220}$$

$$[u_1, v_1] \sim [-p\frac{(\Delta - c_0)}{c_0}, 1]\,b_1\sin(k_0|x| - \delta) \,, \quad \text{as} \quad |x| \to \infty \,,$$

$$v_1 \sim b_1\sin(k_0|x| - \delta) \quad \text{as}|x| \to \infty \,,$$

$$b_1\cos\delta = L = \frac{1}{2k_0}\int_{-\infty}^{\infty} f(x)\cos(k_0x)dx \,,$$

$$f(x) = -pc_0u_0 + (6p - q)\frac{u_0^2}{2} \,.$$

We find that

$$L = -\frac{6k_0}{\beta^2}\{k_0^2(q - 6p) + 4\beta^2 q\}\int_{-\infty}^{\infty} \text{sech}^2(\beta x)\cos(k_0x)dx \,. \tag{221}$$

Then as $\beta = \epsilon\gamma \to 0$, this reduces to

$$L \sim \frac{\pi k_0^2}{3}(6p - q)\exp(-\pi k_0/2\epsilon\gamma) \,, \tag{222}$$

which agrees with the previous result (210) from the exponential asymptotics, since $L = \pi K$. The one-sided solutions are obtained by setting $\delta = 0$, and replacing b_1 in (218, 220) by $0, 2b_1$ for $x > 0, x < 0$.

Bibliography

T. R. Akylas and R. H. J. Grimshaw *Solitary internal waves with oscillatory tails J.Fluid Mech.*, vol 242, 279-298, 1992.

T. R. Akylas and T-S. Yang *On short-scale oscillatory tails of long-wave disturbances Stud. Appl. Math.*, vol 94, 1-20, 1995.

C. Amick and J. Toland *Solitary waves with surface tension I: trajectories homoclininic to periodic orbits in four dimensions Arch. Rat. Mech. Anal.*, vol 118, 37-69, 1992.

C.M. Bender and S. A. Orzsag, *Advanced mathematical methods for scientists and engineers, McGraw-Hill*, (ISBN 0-07-066173-1) 1978,

M.V. Berry and C. J. Howls, *Hyperasymptotics, Proc. Roy. Soc.*, vol A 430, 653-668,1990.

M. V. Berry, *Asymptotics, superasymptotics, hyperasymptotics, "Asymptotics beyond all orders" , ed. H Segur and S Tanveer, Plenum*, 1-14, 1992.

J. Boyd *Weakly nonlocal solitons for capillary-gravity waves: fifth-degree Korteweg-de Vries equation Physica D*, vol 48, 37-69, 1991.

J. P. Boyd *Weakly nonlocal solitary waves and beyond-all-order asymptotics, Kluwer, Amsterdamr*, (ISBN 0-7923-5072-3), 1998.

J.P. Boyd *The devils invention: asymptotic, superasymptotic and hyperasymptotic series Acta Applicandae Mathematicae*, vol 56, 1-98, 1999.

F. Dias and G. Iooss *Water waves as a spatial dynamical system Handbook of Mathematical Fluid Dynamics, ed, S.Friedlander and D.Serre Elsevier, North Holland*, Chapter 10, 443 -499, 2003.

R. Grimshaw *The reflection of internal gravity waves from a shear layer Quart. J. Appl. Math.*, vol 29, 511-525, 1976.

R. Grimshaw *Solitary Waves in Fluids, Advances in Fluid Mechanics, ed. R. Grimshaw, vol 47, WIT press, UK*, Ch. 1 1-17, Ch. 7 159-179, 2007.

R. Grimshaw and P. Cook *Solitary waves with oscillatory tails Proceedings of Second International Conference on Hydrodynamics, Hong Kong, 1996, "Hydrodynamics: Theory and Applications", Vol. 1, ed. A.T. Chwang, J.H.W. Lee and D.Y.C. Leung, A.A. Balkema, Rotterdam*, 327-336, 1996.

R. Grimshaw and G. Iooss *Solitary waves of a coupled Korteweg-de Vries system Mathematics and Computers in Simulation*, vol 62, 31 - 40. 2003.

R. Grimshaw and N. Joshi *Weakly nonlocal solitary waves in a singularly perturbed Korteweg-de Vries equation SIAM J. Math.*, vol 55, 124-135, 1995.

M. D. Kruskal and H. Segur *Asymptotics beyond all orders in a model of crystal growth Stud. Appl. Math.*, vol 85, 129181, 1991.

E.N. Lorenz *On the existence of a slow manifold J. Atmos. Sci.*, vol 43, 1547-1557, 1986.

E. N. Lorenz and V. Krishnamurthy *On the nonexistence of a slow manifold J. Atmos. Sci.,*, vol 44, 2940-2950, 1987.

R. E. Meyer *Gradual Reflection of Short Waves SIAM J. Appl. Math.*, vol 29, 481-492, 1975.

Y. Pomeau, A. Ramani and B. Grammaticos *Structural stability of the Korteweg-de Vries solitons under a singular perturbation Physica D*, vol 31, 127-134, 1988.

J. Vanneste *Inertia-gravity wave generation by balanced motion: revisiting the Lorenz-Krishnamurthy model J. Atmos. Sci.*, vol 61, 224-23, 2003.

Exponential Asymptotics and Stokes Line Smoothing for Generalized Solitary Waves

Philippe H. Trinh

University of Oxford, UK

Abstract In another paper of this volume, Grimshaw has demonstrated how techniques of Borel summation can be used to elucidate the exponentially small terms that lie hidden *beyond all orders* of a divergent asymptotic expansion. Here, we provide an alternative derivation of the generalized solitary waves of the fifth-order Korteweg-de Vries equation. We will first optimally truncate the asymptotic series, and then smooth the Stokes line. Our method provides an *explicit* view of the switching-on mechanism, and thus increased understanding of the Stokes Phenomenon.

1 Introduction

The *Stokes Phenomenon* describes the puzzling event in which exponentially small terms can suddenly appear or disappear when an asymptotic expansion is analytically continued across key lines *(Stokes lines)* in the Argand plane— *"as it were into a mist,"* Stokes once remarked in 1902.

Fortunately, much of the inherent vagueness of this phenomenon, as well as its deep implications for the study of asymptotic approximations has been examined since Stokes' time (see Boyd (1999) for a comprehensive review). In another paper of this volume by Grimshaw—henceforth referred to as [Grimshaw]—it was shown how Borel summation can be used to reveal the exponentially small waves found in the fifth-order Korteweg-de Vries equation (5KdV).

In this review paper, we will show how the methodology outlined in Olde Daalhuis et al. (1995) and Chapman et al. (1998) can be used as an alternative treatment of the 5KdV equation. The procedure is as follows: (1) Expand the solution as a typical asymptotic expansion, (2) find the behaviour of the late-order terms $(n \to \infty)$, and (3) optimally truncate the expansion and examine the remainder as the Stokes lines are crossed.

The location of the Stokes lines, as well as the details of the Stokes Phenomenon and resultant exponentials are intrinsically linked to the late-

order terms of the asymptotic approximation—thus, as we proceed through Steps 1 to 3, we are effectively deriving the beyond-all-orders contributions by *decoding* the divergent tails of the expansion. The novelty in this approach (in contrast to the one shown in [Grimshaw]) is that all the analysis is done in the (complexified) physical space, rather than in Borel-transformed space. This provides us with a special vantage point—to see the *smooth* switching-on of the exponentially small terms as each Stokes line is crossed (see Figure 1). Come, let us stare into Stokes' mist.
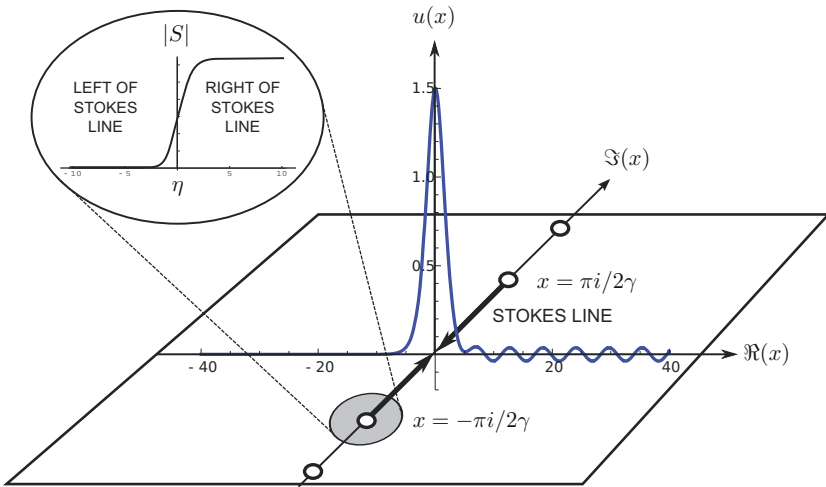
Figure 1. The analytic continuation of the traditional asymptotic solution (the classical solitary wave) contains singularities up and down the imaginary axis, with Stokes lines emanating from each of these singularities. By re-scaling near the singularities and optimally truncating, we will be able to observe the smooth switching-on of the exponentially small terms (top-left).

2 Generalized Solitary Waves and the 5KdV

We will consider the existence of solutions to the 5KdV equation,

$$\epsilon^2 u_{xxxx} + u_{xx} + 3u^2 - cu = 0 \tag{1}$$

with $u \to 0$ as $x \to \pm\infty$. Although the problem is for $x \in \mathbb{R}$, it will be important to consider the effects of allowing u and x to be complex.

2.1 Initial Asymptotic Analysis and Late Terms

We begin as usual by substituting the asymptotic expansions,

$$u = \sum_{n=0}^{\infty} \epsilon^{2n} u_n \quad \text{and} \quad c = \sum_{n=0}^{\infty} \epsilon^{2n} c_n$$

into Equation (1). This yields the first two orders as,

$$u_0 = 2\gamma^2 \text{sech}^2(\gamma x) \qquad\qquad c_0 = 4\gamma^2 \qquad (2)$$

$$u_1 = -10\gamma^2 u_0 + \left(\frac{15}{2}\right) u_0^2 \qquad\qquad c_1 = c_0^2 \qquad (3)$$

while at $O(\epsilon^{2n})$,

$$u_{(n-1)xxxx} + u_{nxx} + 6u_0 u_n - c_0 u_n + \ldots = 0. \qquad (4)$$

Here, the key observation is that there exists *singularities* in the analytic continuation of the leading order solution, $u_0(x)$ at $x = \pm\pi i/2\gamma, \pm 3\pi i/2\gamma, \ldots$ This use of *ill-defined* approximations in order to represent perfectly well-defined phenomena is one of the caveats of singular asymptotics, but one would feverishly hope that a singularity far from the region of interest (in this case, $x \in \mathbb{R}$) has little effect on the approximations!

Unfortunately this is not the case. We see from Equation (4) that at each order, u_n is partly determined by differentiating u_{n-1} twice and thus each additional order adds to the power of the singularities in the early terms. We would therefore expect the late terms of the asymptotic expansion to exhibit *factorial over power* divergence of the form,

$$u_n \sim \frac{Q(z)\Gamma(2n+\gamma)}{[\chi(z)]^{2n+\gamma}}, \quad \text{as } n \to \infty. \qquad (5)$$

Here, γ is a constant, while $Q(z)$ and $\chi(z)$ are functions to be determined. Substituting this ansatz into Equation (4) yields at leading order,

$$-\left(\frac{d\chi}{dz}\right)^4 + \left(\frac{d\chi}{dz}\right)^2 = 0, \quad \text{as } n \to \infty. \qquad (6)$$

Now from the above discussion, we would expect that $\chi = 0$ at the relevant singularities, $x = \sigma_i$ for some i; we then conclude that $\chi' = \pm 1$ and thus without loss of generality, $\chi = x - \sigma_i$. In general, u_n will be a sum of terms of the form (5), one for each singularity. However along the real axis, the behaviour of u_n will be dominated by those singularities closest to

the axis and thus we need only concern ourselves with the singularities at $x = \pm\sigma \equiv \pm i\pi/2\gamma$. Finally, at next order as $n \to \infty$, we find that $Q(z) = \Lambda$, a constant.

The determination of γ, Λ, and in fact, the Stokes line smoothing in the next section will require an analysis near each of the two singularities, $x = \pm\sigma$; for brevity, we will henceforth focus on the singularity at $x = \sigma$ in the upper-half plane.

First, since by Equation (2), $u_0 \sim -2/(x-\sigma)^2$ as $x \to \sigma$, we must require that $\gamma = 2$. Second, in order to determine the final constant Λ, we need to re-scale near the singularity $x = \sigma$, express the leading-order inner solution as a power series (in inner coordinates) and match with the outer solutions. In the end, however, Λ is determined by the numerical solution of a canonical *inner* problem. As was shown in [Grimshaw], $\Lambda \approx -19.97$.

Finally, let us discuss the significance of χ. Following Dingle (1973), we expect there to be a Stokes line wherever u_n and u_{n+1} have the same phase as $n \to \infty$, or in this case where,

$$\Im\left[-\chi^2\right] = 0 \text{ and } \Re\left[-\chi^2\right] \geq 0. \tag{7}$$

Thus there exist Stokes lines from $x = \pi i/2\gamma$ *down* the imaginary axis and from $x = -\pi i/2\gamma$ *up* the imaginary axis (as illustrated in Figure 1). In the next section, we will optimally truncate the asymptotic expansion and examine the switching-on of exponentially small terms as these two Stokes lines are crossed.

2.2   Optimal Truncation and Stokes Smoothing

By now we have entirely determined the late terms of the asymptotic expansion. In order to identify the exponentially small waves, we truncate the expansion and study its remainder,

$$u = \sum_{n=0}^{N-1} \epsilon^{2n} u_n + R_N(x).$$

Substitution into Equation (1) yields the equation

$$\epsilon^2 R_N'''' + R_N'' + 6u_0 R_N - c_0 R_N + \ldots \sim \epsilon^{2N} u_N'', \tag{8}$$

which, using Stirling's formula, we can write the right-hand side as

$$\epsilon^{2N} u_N'' \sim \epsilon^{2N} \frac{\Lambda(-1)^N \Gamma(2N+\gamma+2)\chi'}{\chi^{2N+\gamma+2}}$$

$$\sim \epsilon^{2N} \frac{\Lambda(-1)^N \left\{ \sqrt{2\pi} e^{-(2N+\gamma+2)}(2N+\gamma+2)^{2N+\gamma+3/2} \right\}}{\chi^{2N+\gamma+2}} \quad (9)$$

We can see now that the remainder is only *algebraically* small unless $N \sim |\chi|/2\epsilon$ (where the ratio of consecutive terms are equal) and thus we set $N = r/2\epsilon + \rho$ where ρ is bounded as $\epsilon \to 0$.

Although there are four homogeneous solutions to Equation (8) as $\epsilon \to 0$, we will show that one in particular,

$$R_N(x) \sim S(x) e^{-i(x-\sigma)/\epsilon} \quad (10)$$

is switched on as the Stokes line is crossed. We will call the function $S(x)$ the *Stokes multiplier*, and we expect it to vary smoothly from one constant to another across the Stokes line. We write

$$\chi = x - \sigma = r e^{i\theta} \quad \text{and} \quad \frac{d}{dx} = -\frac{i e^{-i\theta}}{r} \frac{d}{d\theta}, \quad (11)$$

where now, since N is fixed (and thus also the modulus, r), we are only interested in the "fast" variation in θ across the Stokes line. Then using Equations (9) and (11) in (8) gives

$$\frac{dS}{d\theta} \sim \frac{\Lambda \sqrt{r\pi}}{\sqrt{2}\epsilon^{\gamma+1/2}} e^{-r/\epsilon} e^{ire^{i\theta}/\epsilon} \left(e^{-i\theta}\right)^{r/\epsilon+2\rho+\gamma+2} \left(e^{-\pi i/2}\right)^{r/\epsilon+2\rho} e^{i\theta}$$

$$= \frac{\Lambda \sqrt{r\pi}}{\sqrt{2}\epsilon^{\gamma+1/2}} \times \exp\left[-\frac{r}{\epsilon}\left\{1 - ie^{i\theta} + i\theta + \frac{\pi i}{2}\right\}\right.$$

$$\left. + i\left\{-2\rho\left(\theta + \frac{\pi}{2}\right) - \theta(\gamma+1)\right\}\right] \quad (12)$$

From the terms within the curly braces, we see that the change in S is exponentially small, except near the Stokes line $\theta = -\pi/2$. Here, we will re-scale $\theta = -\pi/2 + \sqrt{\epsilon}\eta$ and integrate Equation (12) from left ($\eta \to -\infty$) to right to show that

$$S \sim \text{const} + \frac{\Lambda \sqrt{\pi}}{\sqrt{2}\epsilon^{\gamma}} e^{\pi i(\gamma+1)/2} \int_{-\infty}^{\sqrt{r}\eta} e^{-s^2/2} \, ds. \quad (13)$$

This integral (the error function) precisely illustrates the *smoothing* of the Stokes line in Figure 1. Thus the jump in the Stokes multiplier and consequently, the remainder is

$$\left[S\right]_{\text{Stokes}} \sim \frac{\Lambda\pi}{\epsilon^\gamma} e^{3\pi i/2} \implies \left[R_N\right]_{\text{Stokes}} \sim \frac{\Lambda\pi}{\epsilon^2} e^{3\pi i/2} e^{-i(x-\sigma)/\epsilon}. \qquad (14)$$

We must remember that the analysis must be repeated for analytic continuation into the lower-half x-plane and thus near the singularity at $x = -\pi i/2\gamma$. The result is another exponentially small contribution which is the complex conjugate of Equation (14) and thus along the real axis, the sum of contributions from crossing the pair of Stokes lines is,

$$u_{\text{exp}} \sim -\frac{2\Lambda\pi}{\epsilon^2} e^{-\pi/2\gamma\epsilon} \sin\left(x/\epsilon\right). \qquad (15)$$

Let us recap our analysis: (1) The *singular* nature of the 5KdV equation produces singularities in the early terms, (2) As more and more terms are taken, the effects of the singularities grow, eventually producing factorial over power divergence in the late terms, (3) Stokes lines emerge from each of the singularities, and (4) By optimally truncation and examining the jump in the remainder as the Stokes lines are crossed, we see the Stokes Phenomenon and thus the appearance of exponentially small terms.

So finally, we are ready to answer the original question: *Do there exist classical solitary wave solutions of the 5KdV equation?* No. For suppose that we did impose the condition that only the base (non-oscillatory) asymptotic solution applies at $x = -\infty$. Then as we pass through $x = 0$, the term in Equation (15) necessarily switches on and $u \sim u_0 + u_{\text{exp}}$ for $x > 0$.

We have thus passed through Stokes' mist and subsequently, realized that *there do not exist classical solitary wave solutions of the 5KdV.*

Bibliography

J.P. Boyd. The Devil's invention: Asymptotics, superasymptotics and hyperasymptotics. *Acta Applicandae*, 56:1–98, 1999.

S.J. Chapman, J.R. King, and K.L. Adams. Exponential asymptotics and Stokes lines in nonlinear ordinary differential equations. *Proc. R. Soc. Lond. A*, 454:2733–2755, 1998.

R.B. Dingle. *Asymptotic Expansions: Their Derivation and Interpretation.* Academic Press, London, 1973.

A.B. Olde Daalhuis, S.J. Chapman, J.R. King, J.R. Ockendon, and R.H. Tew. Stokes Phenomenon and matched asymptotic expansions. *SIAM J. Appl. Math.*, 55(6):1469–1483, 1995.

G.G. Stokes. On the discontinuity of arbitrary constants that appear as multiples of semi-convergent series. *Acta. Math. Stockholm*, 26:393–397, 1902.

Multiple scales methods in meteorology

Rupert Klein [‡], Stefan Vater [‡], Eileen Paeschke [‡],
and Daniel Ruprecht [‡]

[‡] FB Mathematik & Informatik, Freie Universität Berlin, Germany

Abstract With emphasis on meteorological applications, we discuss here the fluid dynamical fundamental governing equations, their nondimensionalization including the identification of key nondimensional parameters, and a general approach to meteorological modelling based on multiple scales asymptotics.

1 Overview

In Chapter 2 we will derive the fluid mechanical conservation laws. We explore the basic principles considering "pure" fluid mechanics, i.e., we neglect the influences of gravity, Earth's rotation (Coriolis force), molecular transport, and of the so called "diabatic effects". The latter subsume all processes that involve external energy supply by radiation or conversion of energy due to condensation, chemical reactions, etc.. Gravity and the Coriolis force will be included in subsequet sections. The chapter concludes with a summary of the governing equations, now extended to also include a general set of species transport equations. These will be important, e.g., in describing (atmospheric) chemistry or moist processes.

Chapter 3 introduces the technique of multiple scales asymptotics using the (almost trivial) example of a linear oscillator. After deriving analytical solutions, we will focus on a situation which, in many ways, resembles situations arising frequently in geophysical problems: a slow background motion caused by an external force is accompanied by rapid oscillations around it, with the oscillation amplitudes generally not being small. To give some meaning to the notions of "smallness" and "rapidity", we will first nondimensionalize the oscillator equations and identify small parameters that lend themselves for comparison. By means of single and multiple scales analyses we will then try to derive simplified approximate solutions that become more and more accurate as the small parameters vanish.

One important aim of theoretical meteorology is the development of simplified model equations that describe the large variety of scale-dependent

phenomena observed in atmospheric flows. Chapter 4 summarizes the basic scaling arguments that justify a unified approach to the derivation of such models based on multiple scales asymptotic techniques. We note that Keller and Ting (1951) already anticipated the foundations of this approach in an internal report of the Institute for Mathematics and Mechanics of New York University. In particular, Chapter 4 non-dimensionalization to the equations of compressible flows on a rotating sphere as a first step in building the unified multiscale modelling framework. The subsequent steps are the introduction of a quite generally applicable set of distinguished limits, and multiple-scales asymptotics. For simplicity, diabatic effects, such as radiation, water phase transitions, or turbulent transport are represented as lumped terms in the governing equations to be specified later. For extensions see Klein and Majda (2006).

Chapter 5 employs the general asymptotics-based approach to rederive the classical quasi-geostrophic model, see Pedlosky (1987).

The reader may want to consult Klein (2010) for further references.

2   Fluid mechanical conservation laws

In this chapter we will derive the fluid mechanical conservation laws. In section 2.1 we explore the basic principles considering "pure" fluid mechanics, i.e., we neglect the influences of gravity, Earth's rotation (Coriolis force), molecular transport, and of the so called "diabatic effects". The latter subsume all processes that involve external energy supply by radiation or conversion of energy due to condensation, chemical reactions, etc.. Gravity and the Coriolis force will be included later in Sections 2.3 and 2.4. Section 2.6 provides a summary of the governing equations, now extended to also include a general set of species transport equations. These will be important, e.g., in describing (atmospheric) chemistry or moist processes.

Remark: *In the present context, some quantity, say U, is conserved if the total content of U within a given, fixed control volume in space can change in time only by exchange of U across the control volume's interface.*

2.1   Pure fluid dynamics

Mass conservation   During the motion of a mass parcel its mass is conserved while, in general, the parcel's volume can change. The change of density (mass per unit volume) caused by this change of volume is expressed in the law of mass conservation. The mass M of a fixed control volume Ω
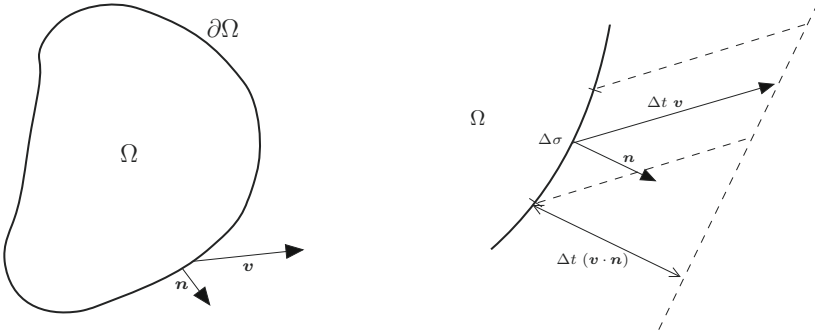
Figure 1. Change of a volume's mass with time

at time t can be expressed as an integral over the density,

$$M(t; \Omega) = \int_{\Omega} \varrho(t, \boldsymbol{x}) \, dV \, . \tag{1}$$

This mass will change during a time interval Δt if mass parcels cross interface $\partial \Omega$, being carried along by the flow velocity, $\boldsymbol{v}$ (see Fig. 1). The change of mass, ΔM, associated with the passage of parcels across a control surface segment $\Delta \sigma \subset \partial \Omega$, is then equal to $-\varrho \, (\Delta t \, \boldsymbol{v}) \cdot \boldsymbol{n} \, \Delta \sigma$, where $\boldsymbol{n}$ is the outward pointing normal on $\Delta \sigma$. The scalar multiplication $\boldsymbol{v} \cdot \boldsymbol{n}$ selects the component of $(\Delta t \, \boldsymbol{v})$ perpendicular to $\Delta \sigma$ as the one relevant for mass transport across the surface element. By summation (integration) along the entire boundary of the control volume, and for time increments covering a finite interval $t \in [t_1, t_2]$ we find

$$M(t_2; \Omega) - M(t_1; \Omega) = - \int_{t_1}^{t_2} \int_{\partial \Omega} (\varrho \boldsymbol{v}) \cdot \boldsymbol{n} \, d\sigma \, dt \, . \tag{2}$$

This is the most general formulation of the law of mass conservation which holds for arbitrary control volumes for which the integrals in (1), (2) are meaningfully defined. Notice that the above definitions merely require suitable *integrability* for the mass and momentum densities, ϱ and $\varrho \boldsymbol{v}$. These quantities need not be differentiable in either space or time for the mass balance in (2) to make sense!

If, however, we may assume differentiability of $M(t; \Omega)$ w.r.t. time, t, we may let $(t_2 - t_1) \to 0$ to find

$$\frac{dM}{dt} = - \int_{\partial \Omega} (\varrho \boldsymbol{v}) \cdot \boldsymbol{n} \, d\sigma \, . \tag{3}$$

If, in addition, $\varrho\boldsymbol{v}$ satisfies the conditions of Gauß' integral theorem, (see appendix 5.6), then $\int_{\partial\Omega}(\varrho\boldsymbol{v})\cdot\boldsymbol{n}\ d\sigma = \int_{\Omega}\nabla\cdot(\varrho\boldsymbol{v})\ dV$, and

$$\int_{\Omega}\Big(\varrho_t + \nabla\cdot(\varrho\boldsymbol{v})\Big)\ dV = 0 \qquad \text{for arbitrary Gauß domains } \Omega. \qquad (4)$$

This equation can hold, for continuously differentiable fields $\varrho, \boldsymbol{v}$ and for arbitrary control volumes Ω, only if pointwise the following partial differential equation is satisfied:

$$\varrho_t + \nabla\cdot(\varrho\boldsymbol{v}) = 0\,. \qquad (5)$$

Adopting this differential form restricts solutions to the class of continuously differentiable fields. Yet, in practice one uses (5) as a short-hand for (2), thereby implying that whereever ϱ_t and $\nabla\cdot(\varrho\boldsymbol{v})$ are singular, their spacio-temporal integrals remain well defined. For discussions of such *weak solutions of conservation laws* see, e.g., LeVeque (1990) and Kröner (1997); for a measure theoretical approach to conservation laws see Temam and Miranville (2000).

General conservation laws   The considerations of the last section lead us to the following general formal pattern of a conservation law: Let U denote an extensive conserved quantity. For extensive quantities, their "total amount", $U(t,\Omega)$, is well defined for arbitrary control volumes, Ω, that are Gauß domains, and they are additive in that

$$U\left(t; [\Omega_1 \cup \Omega_2]\right) = U(t; \Omega_1) + U(t; \Omega_2) \quad \forall \quad \Omega_1, \Omega_2\ :\ \Omega_1 \cap \Omega_2 = \emptyset. \qquad (6)$$

Let $u(t,\boldsymbol{x})$ denote the density field associated with U, so that

$$U(t; \Omega) = \int_{\Omega} u(t,\boldsymbol{x})\ dV\,, \qquad (7)$$

and $\boldsymbol{f}$ its flux density. Then conservation of U in time is expressed by the <u>Integral Conservation Law</u>

$$U(t_2; \Omega) - U(t_1; \Omega) = -\int_{t_1}^{t_2}\int_{\partial\Omega}\boldsymbol{f}\cdot\boldsymbol{n}\ d\sigma\ dt\,. \qquad (8)$$

If, in addition, u and $\boldsymbol{f}$ are sufficiently smooth, then they satisfy the <u>Partial Differential Equation in Conservation Form</u>

$$u_t + \nabla\cdot\boldsymbol{f} = 0\,. \qquad (9)$$

Remark: *The integral form of the conservation law in (8) is the most general basis for the formulation of numerical methods for problems in continuum mechanics because, by construction, it allows for the correct representation of non-smooth, e.g., discontinuous, solutions. See, e.g., LeVeque (1990), Kröner (1997).*

Remark: *Partial differential equations which, in addition to divergence terms, include other expressions that have no equivalent divergence form cannot be cast in the more general integral form (8). Such equations do not describe conservation in the present sense.*

Energy conservation   The conservation of energy follows the same pattern just described, yet here the conserved quantity can not only be exchanged by the motion of fluid parcels. Rather, the energy contained in a control volume is also changed by the work done by the pressure and other stresses when the fluid moves across or along the boundary of the considered control volume, or when heat is added through thermal conduction, radiation, and the like. Further effects, such as those due to changes in potential energy in the Earth's gravity field will be discussed in the next chapter. The energy contained in some control volume Ω is

$$E(t) = \int_\Omega \varrho e(t, \boldsymbol{x}) \; dV \,, \tag{10}$$

where e is the total energy per unit mass, or *specific total energy*, and ϱ is again the mass density.

Energy is transported by the motion of fluid parcels in analogy with the flux of mass considered in section 2.1. The associated contribution to the energy flux density is $\varrho e \, \boldsymbol{v}$. In addition, there are forces acting within a fluid between adjacent fluid parcels. Those forces are represented by means of a second order tensor field $(p \, \boldsymbol{id} + \boldsymbol{\tau})$, where p is the thermodynamic pressure, and $\boldsymbol{id}, \boldsymbol{\tau}(t, \boldsymbol{x}) \in \boldsymbol{R}^{3 \times 3}$ are the unit tensor and the viscous stress tensor, respectively. The interpretation of this tensor, $(p \, \boldsymbol{id} + \boldsymbol{\tau})$, and its two contributions to the energy flux is as follows:

Consider the boundary, $\partial\Omega$, of a control volume (or some similar surface embedded in the flow domain). At any location $\boldsymbol{x} \in \partial\Omega$ the vector $(p \, \boldsymbol{id} + \boldsymbol{\tau}) \cdot \boldsymbol{n}$, with $\boldsymbol{n}$ the outward pointing normal on $\partial\Omega$, denotes the force per unit area, i.e., the stress, which the fluid within the control volume exerts onto the fluid outside. If the fluid is in motion, with flow velocity $\boldsymbol{v}(t, \boldsymbol{x})$, then $\boldsymbol{v} \cdot (p \, \boldsymbol{id} + \boldsymbol{\tau}) \cdot \boldsymbol{n}$ is the work per unit time and unit area done by the fluid inside the control volume on the fluid outside. This is the second contribution to the energy flux density to be considered here. It consists

of (i) the work done by the thermodynamic pressure forces, $p\,\boldsymbol{v}\cdot\boldsymbol{n}$, and (ii) the work done by the viscous stresses, $\boldsymbol{v}\cdot\boldsymbol{\tau}\cdot\boldsymbol{n}$.

We know from experience that two bodies of finite mass and different temperature tend to exchange thermal energy so as to eventually approach states of equal temperature. Let us denote the associated energy flux per unit area by $\boldsymbol{\jmath}$.

Combining the three effects just discussed we obtain the energy conservation law, written here in its differential form as

$$(\varrho e)_t + \nabla \cdot \left([\varrho e + p]\,\boldsymbol{v} + \boldsymbol{v}\cdot\boldsymbol{\tau} + \boldsymbol{\jmath} \right) = 0\,. \tag{11}$$

In much of the subsequent discussions we will neglect the terms, $(\boldsymbol{v}\cdot\boldsymbol{\tau}+\boldsymbol{\jmath})$, which are associated with molecular transport processes, for simplicity of exposition.

Momentum conservation   The momentum of the fluid contained in a control volume is defined as

$$\boldsymbol{I}(t) = \int_\Omega \varrho\boldsymbol{v}(t,\boldsymbol{x})\ dV\,, \tag{12}$$

so that $\varrho\boldsymbol{v}$ is the momentum density. Fluxes of momentum arise again through advection, i.e., through transport by the fluid motion, and the associated flux density across a surface with unit normal $\boldsymbol{n}$ is $\varrho\boldsymbol{v}(\boldsymbol{v}\cdot\boldsymbol{n})$.

Newton's law of motion then states that the forces acting on some finite mass equal the rate of change of its momentum. In the present continuum mechanics we have seen that $(p\,\boldsymbol{id} + \boldsymbol{\tau})\cdot\boldsymbol{n}$ is the force per unit area which some mass of fluid within our control volume Ω exerts onto the fluid outside it (when $\boldsymbol{n}$ is the outward-pointing normal unit vector). Thus, $(p\,\boldsymbol{id}+\boldsymbol{\tau})\cdot\boldsymbol{n}$ represents a flux of momentum from the control volume to its environment, and the momentum conservation law reads

$$(\varrho\boldsymbol{v})_t + \nabla \cdot (\varrho\boldsymbol{v}\circ\boldsymbol{v} + p\,\boldsymbol{id} + \boldsymbol{\tau}) = 0\,, \tag{13}$$

where $\circ$ denotes the tensorial product.

Remark: *The divergence of $(p\,\boldsymbol{id})$ equals the pressure gradient. In cartesian co-ordinates we have*

$$\left(\nabla\cdot(p\,\boldsymbol{id})\right) = \left(\frac{\partial}{\partial x},\frac{\partial}{\partial y},\frac{\partial}{\partial z}\right)\cdot\begin{pmatrix} p & 0 & 0 \\ 0 & p & 0 \\ 0 & 0 & p \end{pmatrix} = \left(\frac{\partial p}{\partial x},\frac{\partial p}{\partial y},\frac{\partial p}{\partial z}\right)\,. \tag{14}$$

In the notation of co-ordinate-free tensor analysis,

$$\nabla\cdot(p\,\boldsymbol{id}) = \nabla p\,. \tag{15}$$

2.2   Equations of state

The system of mass, momentum, and energy conservation laws, (5), (13), and (11), is not closed, as the pressure, p, the stress tensor, $\boldsymbol{\tau}$, and the heat flux density, $\boldsymbol{\jmath}$, have not yet been related to the primary variables, $(\varrho, \varrho\boldsymbol{v}, \varrho e)$. For the present purposes it suffices to take the model of an ideal gas with constant specific heat capacities, endowed with Newtonian friction and Fourier-type heat conduction as an example. For this case, we introduce the temperature,

$$T = \frac{p}{\varrho R} \tag{16}$$

where $R = R^*/M$, $R^* = 8.3141$ J mol^{-1} K^{-1} is the idal gas constant, and M the gas' molecular weight. Then we express the total energy density, ϱe, as the sum of the internal (or thermal) and the kinetic energy via

$$\varrho e = \varrho(e_{\text{th}} + e_{\text{kin}}) = \varrho c_v T + \frac{\varrho \boldsymbol{v}^2}{2} . \tag{17}$$

Here the coefficient c_v is known as the *specific heat capacity at constant volume* and it is assumed constant below.

From the ideal gas law (16) we obtain

$$\varrho e = \frac{c_v}{R} p + \frac{1}{2}\varrho\boldsymbol{v}^2 = \frac{p}{\gamma - 1} + \frac{1}{2}\varrho\boldsymbol{v}^2 , \tag{18}$$

where $\gamma \equiv 1 + \frac{R}{c_v} = \frac{c_p}{c_v}$ is the isentropic exponent of the gas (and c_p is its heat capacity at constant pressure). For atmospheric air a good estimate is $\gamma = 1.4 = const.$ with variations due to admixtures of water vapor and other trace gases being of the order of a few percent at most (see the subsequent remarks).

Remark: *Generalization of these constitutive laws for mixtures of ideal gases with molecular weights $(M_1, M_2, \ldots M_n)$ and mass fractions $(Y_1, Y_2, \ldots Y_n)$ maintains (16) and (17) but replaces the gas constant and specific heat capacity at constant volume with*

$$(R, c_v) = \sum_{i}^{n} Y_i(R_i, c_{v,i}) .$$

See also section 2.6.

Remark: *For an ideal gas with non-constant specific heat capacities,*

$$e_{th} = \int_0^T c_v(T') \, dT'$$

with the specific heat capacity at constant volume, $c_v(T)$, being a known function of temperature. The ideal gas law from (16) is maintained in this case with R remaining independent of temperature.

For the stress tensor $\boldsymbol{\tau}$, we assume Newton's law

$$\boldsymbol{\tau} = -\mu \left(\nabla \boldsymbol{v} + (\nabla \boldsymbol{v})^T - \hat{\mu} \left(\nabla \cdot \boldsymbol{v} \right) \boldsymbol{id} \right), \tag{19}$$

where the *dynamic viscosity*, μ, and the dimensionless coefficient of bulk viscosity, $\hat{\mu}$, depend on the fluid considered, and on the thermodynamic state through the temperature (quite generally) and the pressure (for some fluids). For air, $\mu \approx 1.7 \times 10^{-5}$ kg m^{-1}s^{-1} at typical atmospheric conditions, Gill (1982). The coefficient $\hat{\mu}$ is very difficult to measure experimentally, and for lack of more precise information one often assumes $\hat{\mu} = \frac{2}{3}$, which simplifies the equations to some extent by eliminiating trace($\boldsymbol{\tau}$).

For the thermal energy flux density we adopt Fourier's law of heat conduction, so that

$$\boldsymbol{\jmath} = -\lambda \cdot \nabla T \quad . \tag{20}$$

Here λ is the thermal conductivity which again depends on the medium as well as possibly on temperature and pressure. For instance, in water we have $\lambda_{H_2O} = 0.6$ Wm^{-1}K^{-1}, while in air $\lambda_{air} = 0.023$ Wm^{-1}K^{-1}, Gill (1982)).

The constitutive laws (16)–(20), when added to the conservation laws for mass, momentum, and energy in (5), (13), and (11), yield the desired closed set of partial differential equations for the flow of an ideal gas.

2.3   The influence of gravity

In the previous section we neglected Earth's gravity. Gravity exerts a bulk force, which cannot be directly expressed as a flux divergence (although in a broad range of applications in meteorology it can!). The change of momentum caused by this bulk force is proportional to the fluid density, ϱ, and directed oppositely to some unit vector $\hat{\boldsymbol{g}}$ that points away from the Earth's center of mass. In the present notes, we will restrict to flows covering sufficiently small domains, so that we may safely assume $\hat{\boldsymbol{g}} \equiv \boldsymbol{k}$, where $\boldsymbol{k}$ is the "vertical" unit vector, perpendicular to a suitably chosen tangent plane to the Earth's surface. The factor of proportionality is the acceleration of gravity,

$$g \approx 9.81 \, \frac{\text{m}}{\text{s}^2} \,, \tag{21}$$

which may be considered constant here.

Remark: *Because of the shape of the earth, g actually varies at sea level around ±0.3 percent in north-south direction and around 0.3 percent with a change of height of 10 km Gill (1982).*

To account for the influence of gravity, we must endow the momentum balance in (13) with a source term,

$$(\varrho \boldsymbol{v})_t + \nabla \cdot (\varrho \boldsymbol{v} \circ \boldsymbol{v} + p\, \boldsymbol{id} + \boldsymbol{\tau}) = -\varrho\, g\, \boldsymbol{k}\,. \tag{22}$$

In the energy balance, (11), we must account for the potential energy associated with the position of the fluid mass in the Earths gravity field. This is done by extending the constitutive law from (17), to include a potential energy term, viz.,

$$\varrho e = \varrho(e_{\text{th}} + e_{\text{kin}} + e_{\text{pot}}) = \varrho c_v T + \frac{\varrho \boldsymbol{v}^2}{2} + \varrho \Phi(\boldsymbol{x})\,. \tag{23}$$

Here $\Phi(\boldsymbol{x})$ is the Earth's geopotential, which in the present setting (tangent plane approximation) we approximate by

$$\Phi(\boldsymbol{x}) = gz \tag{24}$$

with z denoting height above sea level.

Remark: *For the present setting of flows in a tangential plane with g, $\boldsymbol{k} \equiv const.$, even the momentum equation is effectively in conservative form, too. By introducing the hydrostatic pressure P_{hy}, defined by*

$$P_{hy}(z) = g \int_z^\infty \varrho(z')\, dz' \qquad \text{and} \qquad \frac{\partial P_{hy}}{\partial z} = -g\, \varrho \tag{25}$$

we rewrite the right hand side of the momentum equation to become

$$-(\varrho\, g\, \boldsymbol{k}) = (0, 0, -\varrho\, g) = \left(0, 0, \frac{\partial P_{hy}}{\partial z}\right) = \nabla \cdot \begin{pmatrix} 0 & 0 & 0 \\ 0 & 0 & 0 \\ 0 & 0 & P_{hy} \end{pmatrix}, \tag{26}$$

or

$$-\varrho\, g\, \boldsymbol{k} = -\nabla \cdot \boldsymbol{\Pi}_{hy}\,. \tag{27}$$

We thus obtain the momentum equation in conservative form

$$(\varrho \boldsymbol{v})_t + \nabla \cdot (\varrho \boldsymbol{v} \circ \boldsymbol{v} + p\, \boldsymbol{id} + \boldsymbol{\tau} + \boldsymbol{\Pi}_{hy}) = 0\,. \tag{28}$$
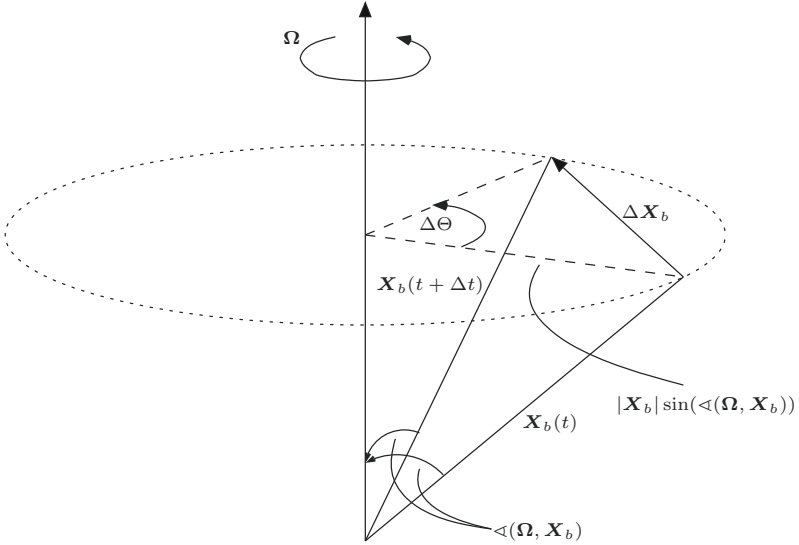
Figure 2. $\boldsymbol{X}_b$ at times t and $t + \Delta t$

2.4   The effects of Earth's rotation

Rotating frame of reference   Up to now we have considered a non-accelerating coordinate system and neglected the effects of Earth's rotation. Physical phenomena are independent of the choice of a coordinate system, but their description depends on the observer and, in particular, on his choice of a coordinate system. For obvious reasons, we are interested in observers that follow Earth's rotation.

Consider some point on the Earth's surface with position vector $\boldsymbol{X}_b = \boldsymbol{X}_b(t)$ in an absolute, inertial frame of reference. Because of Earth's rotation, $\boldsymbol{X}_b$ is rotating with angular velocity $\boldsymbol{\Omega}$. In a small time interval Δt the vector $\boldsymbol{X}_b$ turns by an angle $\Delta\theta = |\boldsymbol{\Omega}|\Delta t$, where $|\boldsymbol{\Omega}|$ is the absolute value of $\boldsymbol{\Omega}$ (figure 2, see also Pedlosky (1987)). This small change of $\boldsymbol{X}_b$ is described by

$$\boldsymbol{X}_b(t+\Delta t) - \boldsymbol{X}_b(t) \equiv \Delta\boldsymbol{X}_b = \boldsymbol{n}\, |\boldsymbol{X}_b|\, \sin(\sphericalangle(\boldsymbol{\Omega}, \boldsymbol{X}_b))\, \Delta\theta + O\big((\Delta\theta)^2\big) \quad (29)$$

with the unit vector

$$\boldsymbol{n} = \frac{\boldsymbol{\Omega} \times \boldsymbol{X}_b}{|\boldsymbol{\Omega} \times \boldsymbol{X}_b|}, \quad\quad\quad\quad\quad (30)$$

pointing in direction of the change of $\boldsymbol{X}_b$ (perpendicular to $\boldsymbol{X}_b$ and $\boldsymbol{\Omega}$). As

$\Delta t \to 0$ we find

$$\lim_{\Delta t \to 0} \frac{\Delta \boldsymbol{X}_b}{\Delta t} = \frac{d\boldsymbol{X}_b}{dt} = |\boldsymbol{X}_b| \ \sin(\sphericalangle(\boldsymbol{\Omega}, \boldsymbol{X}_b)) \ \frac{d\theta}{dt} \ \frac{\boldsymbol{\Omega} \times \boldsymbol{X}_b}{|\boldsymbol{\Omega} \times \boldsymbol{X}_b|}, \qquad (31)$$

and, using $|\boldsymbol{\Omega} \times \boldsymbol{X}_b| = |\boldsymbol{\Omega}| \ |\boldsymbol{X}_b| \ \sin(\sphericalangle(\boldsymbol{\Omega}, \boldsymbol{X}_b))$,

$$\dot{\boldsymbol{X}}_b = \boldsymbol{\Omega} \times \boldsymbol{X}_b \,. \qquad (32)$$

Both observers see the same vector $\boldsymbol{X}_b$ but their perception of how it changes is completely different.

Remark: *The length of $\boldsymbol{X}_b$ is constant, independent of the used coordinate system. Because of $\boldsymbol{X}_b \perp (\boldsymbol{\Omega} \times \boldsymbol{X}_b)$ it follows that*

$$\frac{d|\boldsymbol{X}_b|^2}{dt} = 2 \ \boldsymbol{X}_b \cdot \frac{d\boldsymbol{X}_b}{dt} = 2 \ \boldsymbol{X}_b \cdot (\boldsymbol{\Omega} \times \boldsymbol{X}_b) = 0 \,. \qquad (33)$$

To describe the time-dependent vector $\boldsymbol{X}_b(t)$ in a non-rotating coordinate system, the vector $\boldsymbol{X}_b(t)$ is split into a vector that describes the distance of the circle of latitude on which $\boldsymbol{X}_b(t)$ moves to the equator and two other vectors that define the position on this circle of latitude. Let $\boldsymbol{e}_\Omega$ be the unit vector in direction of the earth rotation vector $\boldsymbol{\Omega}$, then the vector describing its circle of latitude is

$$\cos[\sphericalangle(\boldsymbol{\Omega}, \boldsymbol{X}_b(0))] \ |\boldsymbol{X}_b(0)|\boldsymbol{e}_\Omega = (\boldsymbol{e}_\Omega \cdot \boldsymbol{X}_b(0))\boldsymbol{e}_\Omega \,. \qquad (34)$$

The position of $\boldsymbol{X}_b(t)$ on the circle of latitude can be determined by the linear combination of a distance vector $\boldsymbol{X}_b(0)$, expressing the distance to the axis of rotation and the vector perpendicular to it. The distance vector can be computed by

$$\boldsymbol{X}_b(0) - (\boldsymbol{e}_\Omega \cdot \boldsymbol{X}_b(0))\boldsymbol{e}_\Omega = (\boldsymbol{id} - \boldsymbol{e}_\Omega \circ \boldsymbol{e}_\Omega)\boldsymbol{X}_b(0) \,. \qquad (35)$$

The vector perpendicular to it with same length is (because of $\boldsymbol{e}_\Omega \times \boldsymbol{e}_\Omega = 0$)

$$[\boldsymbol{X}_b(0) - (\boldsymbol{e}_\Omega \cdot \boldsymbol{X}_b(0))\boldsymbol{e}_\Omega] \times \boldsymbol{e}_\Omega = \boldsymbol{X}_b(0) \times \boldsymbol{e}_\Omega \,. \qquad (36)$$

Thus we get

$$\boldsymbol{X}_b(t) = (\boldsymbol{e}_\Omega \cdot \boldsymbol{X}_b(0))\boldsymbol{e}_\Omega + \cos(|\boldsymbol{\Omega}|t)(\boldsymbol{id} - \boldsymbol{e}_\Omega \circ \boldsymbol{e}_\Omega)\boldsymbol{X}_b(0) + \sin(|\boldsymbol{\Omega}|t)(\boldsymbol{X}_b(0) \times \boldsymbol{e}_\Omega) \,. \tag{37}$$

Governing equations in a rotating frame of reference   With help
of some tedious but straightforward computations we transform our con-
servation laws. In this section we use cartesian coordinates throughout,
representing vectors as 3-columns, tensors as 3×3-matrices, etc.. In par-
ticular, rotation by the Earth rotation vector $\boldsymbol{\Omega}$ is represented by matrix-
multiplication with the skewsymmetric matrix $\underline{\underline{\boldsymbol{\Omega}}}$ built from the components
$(\Omega_x, \Omega_y, \Omega_z)^t$ of the rotation vector:

$$
\underline{\underline{\boldsymbol{\Omega}}} \times \underline{\boldsymbol{u}} = \left(\begin{array}{ccc} 0 & -\Omega_z & \Omega_y \\ \Omega_z & 0 & -\Omega_x \\ -\Omega_y & \Omega_x & 0 \end{array}\right) \left(\begin{array}{c} u_x \\ u_y \\ u_z \end{array}\right) = \left(\begin{array}{c} \Omega_y u_z - \Omega_z u_y \\ \Omega_z u_x - \Omega_x u_z \\ \Omega_x u_y - \Omega_y u_x \end{array}\right) . \quad (38)
$$

Here vectors and tensors are represented by their coordinate tupels and
matrices as indicated, and $\underline{\boldsymbol{u}}$ is the column of cartesian coordinates of $\boldsymbol{u}$.

   With this notation, the mass balance in the intertial frame reads

$$
\varrho_t + \underline{\nabla} \cdot (\varrho \underline{\boldsymbol{v}}) = 0 . \quad (39)
$$

We transform the time derivative $(\partial \varrho / \partial t)$ according to (226) as

$$
\frac{\partial \varrho(x,t)}{\partial t} = \frac{\partial \tilde{\varrho}}{\partial \tilde{t}} + \underline{\tilde{\boldsymbol{x}}}^T \underline{\underline{\boldsymbol{\Omega}}} (\tilde{\nabla} \tilde{\varrho})^T , \quad (40)
$$

and the divergence term, following (228), as

$$
\begin{aligned}
\underline{\nabla} \cdot (\varrho \underline{\boldsymbol{v}}) &= \underline{\nabla} \cdot \left(\varrho [\underline{\boldsymbol{v}}^{\mathrm{rel}} + \underline{\underline{\boldsymbol{\Omega}}} \, \underline{\boldsymbol{x}}] \right) \\
&= (\underline{\nabla} \varrho) \underline{\boldsymbol{v}}^{\mathrm{rel}} + (\underline{\nabla} \varrho)(\underline{\underline{\boldsymbol{\Omega}}} \, \underline{\boldsymbol{x}}) + \varrho \underline{\nabla} \cdot \underline{\boldsymbol{v}}^{\mathrm{rel}} + \varrho \underline{\nabla} \cdot (\underline{\underline{\boldsymbol{\Omega}}} \, \underline{\boldsymbol{x}}) \quad (41) \\
&= (\underline{\tilde{\nabla}} \tilde{\varrho}) \underline{\tilde{\boldsymbol{v}}}^{\mathrm{rel}} + (\underline{\tilde{\nabla}} \tilde{\varrho})(\underline{\underline{\boldsymbol{\Omega}}} \, \underline{\tilde{\boldsymbol{x}}}) + \tilde{\varrho} \underline{\tilde{\nabla}} \cdot \underline{\tilde{\boldsymbol{v}}}^{\mathrm{rel}} .
\end{aligned}
$$

   For the *scalar* quantity $\underline{\tilde{\boldsymbol{x}}}^T \underline{\underline{\boldsymbol{\Omega}}} (\tilde{\nabla} \tilde{\varrho})^T$ we have

$$
\underline{\tilde{\boldsymbol{x}}}^T \underline{\underline{\boldsymbol{\Omega}}} (\tilde{\nabla} \tilde{\varrho})^T = \left(\underline{\tilde{\boldsymbol{x}}}^T \underline{\underline{\boldsymbol{\Omega}}} (\tilde{\nabla} \tilde{\varrho})^T \right)^T = (\tilde{\nabla} \tilde{\varrho}) \underline{\underline{\boldsymbol{\Omega}}}^T \underline{\tilde{\boldsymbol{x}}} \quad (42)
$$

and, as $\underline{\underline{\boldsymbol{\Omega}}}$ is skew symmetric, with $\underline{\underline{\boldsymbol{\Omega}}}^T = -\underline{\underline{\boldsymbol{\Omega}}} = -\underline{\underline{\tilde{\boldsymbol{\Omega}}}}$, the mass conservation
law in the rotating frame becomes

$$
\begin{aligned}
\varrho_t + \underline{\nabla} \cdot (\varrho \underline{\boldsymbol{v}}) &= \frac{\partial \tilde{\varrho}}{\partial \tilde{t}} + (\underline{\tilde{\nabla}} \tilde{\varrho}) \underline{\tilde{\boldsymbol{v}}}^{\mathrm{rel}} + \tilde{\varrho} \underline{\tilde{\nabla}} \cdot \underline{\tilde{\boldsymbol{v}}}^{\mathrm{rel}} + \left((\underline{\tilde{\nabla}} \tilde{\varrho}) \underline{\underline{\boldsymbol{\Omega}}} \, \underline{\tilde{\boldsymbol{x}}} + (\underline{\tilde{\nabla}} \tilde{\varrho})(-\underline{\underline{\boldsymbol{\Omega}}}) \underline{\tilde{\boldsymbol{x}}} \right) \\
&= \frac{\partial \tilde{\varrho}}{\partial \tilde{t}} + \tilde{\nabla} \cdot (\tilde{\varrho} \underline{\tilde{\boldsymbol{v}}}^{\mathrm{rel}}) .
\end{aligned}
$$

$$
(43)
$$

Thus the equation for mass conservation is invariant under the present coordinate transformation into a rotating frame.

The momentum balance, in the present notation, reads

$$(\varrho\underline{v})_t + \left[\underline{\nabla}\cdot(\varrho\ \underline{v}\,\underline{v}^T)\right]^T + \underline{\nabla}p = -\varrho\underline{\nabla}\Phi - \underline{\nabla}\cdot\underline{\underline{\tau}}\,. \tag{44}$$

As only the first two terms do change under coordinate transformations (the reader may want to verify this), we can neglect the others for the time being. For the first two terms we use the product rule to obtain

$$(\varrho\underline{v})_t \;=\; \varrho_t\ \underline{v} + \varrho\ \underline{v}_t \quad \text{and} \tag{45}$$

$$\left[\underline{\nabla}\cdot(\varrho\underline{v}\,\underline{v}^T)\right]^T \;=\; (\underline{\nabla}\cdot(\varrho\underline{v}))\underline{v} + \varrho(\underline{v}^T\underline{\nabla}^T)\underline{v}\,. \tag{46}$$

Using mass conservation, we further have

$$(\varrho\underline{v})_t + \left[\underline{\nabla}\cdot(\varrho\underline{v}\,\underline{v}^T)\right]^T \;=\; (\varrho_t + \underline{\nabla}\cdot(\varrho\underline{v}))\,\underline{v} \;+\; \varrho\left(\underline{v}_t + (\underline{v}^T\underline{\nabla}^T)\underline{v}\right)$$

$$=\; 0 \;+\; \varrho\left(\underline{v}_t + (\underline{v}^T\underline{\nabla}^T)\underline{v}\right), \tag{47}$$

and the transformation of these terms into the rotating coordinate system yields

$$\varrho\left(\frac{\partial\tilde{\underline{v}}^{\mathrm{rel}}}{\partial t} + ((\tilde{\underline{v}}^{\mathrm{rel}})^T\underline{\nabla}^T)\tilde{\underline{v}}^{\mathrm{rel}} + 2\,(\underline{\underline{\Omega}}\,\tilde{\underline{v}}^{\mathrm{rel}}) + \underline{\underline{\Omega}}(\underline{\underline{\Omega}}\,\underline{x})\right) + \tilde{\underline{\nabla}}p = -\varrho\tilde{\underline{\nabla}}\Phi - \tilde{\underline{\nabla}}\cdot\tilde{\underline{\underline{\tau}}} \quad. \tag{48}$$

Physically, the term $2\,(\underline{\underline{\Omega}}\,\tilde{\underline{v}}^{\mathrm{rel}})$ represents the Coriolis acceleration.

The term $\underline{\underline{\Omega}}(\underline{\underline{\Omega}}\,\underline{x})$ expresses the centripetal acceleration due to the rotation of the reference frame. As this term can be written as the density times the gradient of a potential (namely which one?), it is often combined with gravity term, thereby inducing a modified effective gravitational potential. The order of magnitude of the centripetal inertia may be estimated by

$$(10^{-4}\mathrm{s}^{-1})^2\cdot 6\cdot 10^6\ \mathrm{m} \approx 10^{-2}\ \frac{\mathrm{m}}{\mathrm{s}^2}\,. \tag{49}$$

In contrast, the acceleration of gravity is of the order of $g \approx 10\ \mathrm{m\ s^{-2}}$, and the centripetal acceleration may be neglected for most practical purposes in meteorology. Notice, however, that this may be a different issue in climate models, because in long-time simulations, even small effects can accumulate and eventually induce leading-order changes.

Like the equation for the mass conservation, the equation of energy conservation does not change when introducing a rotating coordinate system. We leave the verification of this claim to the reader.

2.5   Adiabatic motions and the concept of potential temperature

Consider a flow field that is sufficiently smooth so that the differential form of the mass, momentum, and energy balances are valid, i.e.,

$$
\begin{aligned}
\varrho_t + \nabla \cdot (\varrho \boldsymbol{v}) &= 0 \\
(\varrho \boldsymbol{v})_t + \nabla \cdot (\varrho \boldsymbol{v} \circ \boldsymbol{v} + p\,\boldsymbol{id}) + 2\boldsymbol{\Omega} \times \varrho \boldsymbol{v} &= -\nabla \cdot \boldsymbol{\tau} - \varrho\,(g\nabla\Phi + \boldsymbol{\Omega} \times \boldsymbol{\Omega} \times \boldsymbol{x}) \\
(\varrho e)_t + \nabla \cdot ([\varrho e + p]\boldsymbol{v}) &= -\nabla \cdot (\boldsymbol{v} \cdot \boldsymbol{\tau} + \boldsymbol{\jmath})
\end{aligned}
\tag{50}
$$

and they are closed by the equation of state connecting the pressure p with the conserved quantities, $(\varrho, \varrho\boldsymbol{v}, \varrho e)$,

$$
\varrho e = \frac{p}{\gamma - 1} + \varrho \frac{\boldsymbol{v}^2}{2} + \varrho(\Phi + \Phi_\Omega),
\tag{51}
$$

with Φ_Ω defined such that $\nabla\Phi_\Omega = \boldsymbol{\Omega} \times \boldsymbol{\Omega} \times \boldsymbol{x}$.

In these equations, the (molecular) stress tensor, $\boldsymbol{\tau}$, and heat flux density vector, $\boldsymbol{\jmath}$, represent transport processes of momentum and energy within the fluid that occur without any mass being exchanged. When these terms are absent, control volumes within the fluid are restricted to exchange mechanical energy only, either by advection of total energy, as represented by the flux term $\varrho e \boldsymbol{v}$, or by mechanical work, as represented by the energy flux $p\boldsymbol{v}$. Flows of this kind are called *adiabatic*.

Remark: *When considering mixtures of different fluid species, we will also require diffusion, i.e., the molecular-level transport of the individual species relative to the mean flow, to be zero for the notion of an adiabatic process to apply.*

For adiabatic, smooth flows, the conservation laws may be linearly combined to yield an evolution equation for the pressure field. Together with the equation for density, it reads

$$
\begin{aligned}
\varrho_t + \boldsymbol{v} \cdot \nabla\varrho + \varrho\nabla \cdot \boldsymbol{v} &= 0 \\
p_t + \boldsymbol{v} \cdot \nabla p + \gamma p\nabla \cdot \boldsymbol{v} &= 0\,.
\end{aligned}
\tag{52}
$$

By eliminating the velocity divergence, we obtain

$$
\frac{1}{\varrho}\frac{D\varrho}{Dt} - \frac{1}{\gamma p}\frac{Dp}{Dt} = 0,
\tag{53}
$$

where

$$
\frac{D}{Dt} = (\partial_t + \boldsymbol{v} \cdot \nabla)
\tag{54}
$$

is the time derivative which an observer moving with the fluid (at velocity $\boldsymbol{v}$) will measure.

The above is equivalent to

$$\frac{D\Theta}{Dt} = 0 \qquad \text{where} \qquad \Theta = T_0 \left(\frac{(p/p_0)^{1/\gamma}}{\varrho/\varrho_0} \right) \tag{55}$$

is the *potential temperature*. Here ϱ_0, T_0, and $p_0 = \varrho_0 R T_0$ are some arbitrary, yet for any given flow fixed, reference values. They are introduced to render the expression of taking a non-integer power of some quantity mathematically meaningful by first non-dimensionalizing it.

If we pick ϱ_0, T_0, p_0 to denote the standard reference values of typical conditions at sea level, i.e., $p_0 = 10^5$ N/m^2, $T_0 = 273$ K, then Θ has a neat interpretation: Take any parcel of air at thermodynamic conditions p, ϱ, and let it undergo an adiabatic process that brings its pressure up or down to the reference pressure p_0. Then Θ is the temperature the parcel will acquire when that process is finished.

Remark: *The potential temperature is closely related to thermodynamic entropy. In the present case, one can directly be expressed as a function of the other. Thus, (55) is where our coefficient γ received its name isentropic exponent from.*

Remark: *Mixtures of different fluid species may undergo changes of composition when the pressure and temperature adjust during an adiabatic process. In that case, the notion of a potential temperature with exactly the same physical meaning as given above remains valid. Yet the formula in (55) becomes more involved.*

2.6   Summarizing the equations

In the sequel, we will study (i) the conservation of mass, momentum, and energy, extented by a set of species balance equations. This extension will allows us to later account for moist processes.

$$\varrho_t + \nabla \cdot (\varrho \boldsymbol{v}) = 0 \tag{56a}$$

$$(\varrho \boldsymbol{v}_{\shortparallel})_t + \nabla \cdot (\varrho \boldsymbol{v} \circ \boldsymbol{v}_{\shortparallel}) + 2(\boldsymbol{\Omega} \times \varrho \boldsymbol{v})_{\shortparallel} + \nabla_{\shortparallel} p = -(\nabla \cdot \boldsymbol{\tau})_{\shortparallel} \tag{56b}$$

$$(\varrho w)_t + \nabla \cdot (\varrho \boldsymbol{v} w) + 2(\boldsymbol{\Omega} \times \varrho \boldsymbol{v})_{\perp} + p_z = -(\nabla \cdot \boldsymbol{\tau})_{\perp} - \varrho g \tag{56c}$$

$$(\varrho e)_t + \nabla \cdot (\boldsymbol{v} \left[\varrho e + p \right]) = -\nabla \cdot \left(\boldsymbol{\jmath} + \boldsymbol{v} \cdot \boldsymbol{\tau} + \sum_{i=1}^{n_{\mathrm{sp}}} h_i \boldsymbol{d}_i \right) . \tag{56d}$$

$$(\varrho Y_i)_t + \nabla \cdot (\varrho Y_i \boldsymbol{v}) = \varrho \omega_i - \nabla \cdot \boldsymbol{d}_i . \qquad (i = 1, \ldots, n_{\mathrm{sp}} - 1) \qquad (56e)$$

Here we have split the momentum equations into their horizontal "$_\parallel$" and vertical "$_\perp$" components anticipating that the vertical direction in meteorological applications usually plays a mathematically special role.

Also, we have added a set of transport equations for n_{sp} energy-carrying (chemical) species. The composition of the gas is described by the species' mass fractions Y_i. Potential species conversion processes, such as chemical reactions or the formation of cloud water from water vapor are represented by the source terms ω_i. The flux terms $\boldsymbol{d}_i$ cover the diffusion of species relative to the mean flow. (Why does the counter in the last equation run up to $n_{\mathrm{sp}} - 1$ only?)

The system is closed by adding the equations of state

$$\varrho e = \varrho \int_0^T c_v(T) dT' + \varrho \, \Phi + \frac{1}{2} \varrho v^2 + \sum_{i=1}^{n\mathrm{spec}} \varrho Y_i Q_i , \quad \text{and} \quad p = \varrho R T \quad (57)$$

where

$$c_v(T) = \sum_{i=1}^{n\mathrm{spec}} Y_i \, c_{v,i}(T) , \qquad R = \sum_{i=1}^{n\mathrm{spec}} Y_i \, R_i , \qquad (58)$$

and

$$h_i = \int_0^T c_{p,i}(T) dT' + Q_i . \qquad (59)$$

Here the constants R_i, Q_i are the gas constants and formation enthalpies of the species, $c_{v,i}, c_{p,i}$ are their specific heat capacities at constant volume and at constant pressure, respectively.

In addition, we have to adopt appropriate expressions for the stress tensor, heat flux density, and species diffusion fluxes, $\boldsymbol{\tau}$, $\boldsymbol{\jmath}$, and $\boldsymbol{d}$, respectively. For a Navier-Stokes fluid, the former two are given by (19) and (20). However, in practical meteorological modelling applications involving turbulence, one often replaces these fluxes with effective turbulent closure schemes so as to describe not the transport due to molecular motions but rather the transport due to turbulent fluctuations. In that case, the functional form of these "subscale" momentum and heat flux terms may take a wide variety of forms which we will not address here in detail.

3   Introduction to multiple scales asymptotics

To motivate the mathematical techniques we are going to apply to the atmospheric flow equations in later chapters, we will now analyze the simple

example of a linear oscillator. After deriving analytical solutions, we will focus on a situation that in many ways resembles situations arising frequently in geophysical problems: a slow background motion caused by an external force is accompanied by rapid oscillations around it. The oscillation amplitudes are generally not small! To give some meaning to the notions of "smallness" and "rapidity", we will first nondimensionalize the oscillator equations and identify small parameters that lend themselves for comparison. By means of single and multiple scales analyses we will then try to derive simplified approximate solutions that become more and more accurate as the small parameters vanish.

3.1 Exact solutions for the linear oscillator

A typical example of a linear oscillator is a (small) piece of material with mass m attached to a spring with stiffness c. The stronger the spring, the higher the spring constant c. At time t, the mass is located at position $x = x(t)$ (see Fig. 3). If we displace it away from its equilibrium position, at which the spring's force just balances the weight of the piece, and then let the system evolve freely, it will oscillate around its equilibrium with constant amplitude. If we let the mass dive into some not-too-viscous fluid, the system will perform a damped oscillation. If the viscosity of the fluid is sufficiently high, the mass will not oscillate anymore but just move back monotonically to its equilibrium position.
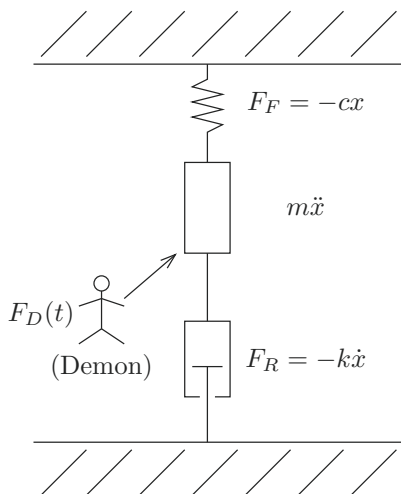
Figure 3. Damped spring–mass system

There are two forces acting *within* the system: the restoring force of the spring in the direction opposite to the *displacement* of the mass, and the frictional force $F_R = -k\dot{x}$ of the viscous fluid which acts in the direction opposite to the *motion* of the mass. Newton's law, which says that the temporal change of momentum equals the sum of all acting forces, yields an equation of motion for the system,

$$m\ddot{x} = -cx - k\dot{x} + F_D(t) \,. \tag{60}$$

Here we have included a general external force $F_D = F_D(t)$ which some demon may exert on the mass.

The solution to this second-order ordinary differential equation (ODE) is uniquely determined once initial conditions $x(0) = x_0$ and $\dot{x}(0) = \dot{x}_0$ are prescribed. Following the theory of linear ODEs [Walter (1996)] we can construct all solutions $x(t)$ as a superposition of the general solution of the homogenous problem and one so-called *particular solution* of the inhomogenous equation, i.e.,

$$x(t) = x_h(t) + x_p(t) \,. \tag{61}$$

Free oscillations   We will now derive the general solution of the spring-mass system's homogenous ODE ((60) with $F_D \equiv 0$),

$$m\ddot{x} + k\dot{x} + cx = 0 \,. \tag{62}$$

To solve this equation, we choose an exponential ansatz,

$$x(t) = \exp(\omega t) \,. \tag{63}$$

Inserting, we have

$$m\left(\omega^2 \exp(\omega t)\right) + k\left(\omega \exp(\omega t)\right) + c\left(\exp(\omega t)\right) = 0 \,, \tag{64}$$

and after division by $\exp(\omega t) \neq 0$ we find

$$m\omega^2 + k\omega + c = 0 \,, \tag{65}$$

which is the system's *characteristic equation*. The solutions are

$$\omega_{1/2} = -\frac{1}{2}\frac{k}{m} \pm \sqrt{D} \qquad \text{with} \qquad D := \frac{k^2}{4m^2} - \frac{c}{m} \,. \tag{66}$$

If $\omega_1 = \omega_2$, i.e., if the discriminant $D = 0$, the solutions differ qualitatively from those obtained when $\omega_1 \neq \omega_2$. Generally, if ω is a k-fold multiple solution of the characteristic equation, it corresponds to k linearly independent solutions of the form

$$e^{\omega t}, \; te^{\omega t}, \ldots, \; t^{k-1}e^{\omega t} \tag{67}$$

of the associated differential equation (Walter, 1996, S.173ff). One impor-
tant property of linear homogenous differential equations is that the sum of
two solutions is again a solution. Using this for the case $D \neq 0$ we obtain
the general solution to (62),

$$x(t) = A \exp(\omega_1 t) + B \exp(\omega_2 t), \tag{68}$$

where A and B are constants that remain to be determined. For the case
$D = 0$ we have

$$x(t) = A \exp(\omega t) + Bt \exp(\omega t) = (A + Bt) \exp(\omega t) \tag{69}$$

again with yet unknown constants A und B.

Next we will distinguish several cases that differ w.r.t. the relative mag-
nitudes of the spring constant, c, the damping coefficient, k and the mass,
m:

1st case: $k = 0; c > 0$.

Thus we consider an inviscid oscillator for which

$$\omega_{1,2} = \pm i\omega_0 \qquad \text{with} \qquad \omega_0 = \sqrt{\frac{c}{m}}, \tag{70}$$

and

$$x(t) = A \exp(i\omega_0 t) + B \exp(-i\omega_0 t). \tag{71}$$

The solution $x(t)$ is now complex-valued, but since we seek real-valued so-
lutions, we allow $A, B \in \mathbb{C}$ to be complex as well,

$$A = A_r + iA_i, \quad B = B_r + iB_i. \tag{72}$$

Later we will choose A and B in such a way that the final result is again
real valued and phyiscally meaningful.

Using Euler's formula, $e^{ix} = \cos x + i \sin x$, respectively, $e^{-ix} = \cos x -
i \sin x$, and splitting A and B into their real and an imaginary parts, we
transform (71) into

$$\begin{aligned} x(t) \quad &= \quad \Big((A_r + B_r)\cos(\omega_0 t) + (-A_i + B_i)\sin(\omega_0 t)\Big) \\ &\quad i\,\Big((A_r - B_r)\sin(\omega_0 t) + (A_i + B_i)\cos(\omega_0 t)\Big). \end{aligned} \tag{73}$$

Because sine and cosine are linearly independent, the solution is real valued
if the coefficients $(A_r - B_r)$ and $(A_i + B_i)$ satisfy

$$\begin{aligned} (A_r - B_r) &= 0 & \Leftrightarrow & \quad A_r &= B_r \\ (A_i + B_i) &= 0 & \Leftrightarrow & \quad A_i &= -B_i. \end{aligned} \tag{74}$$
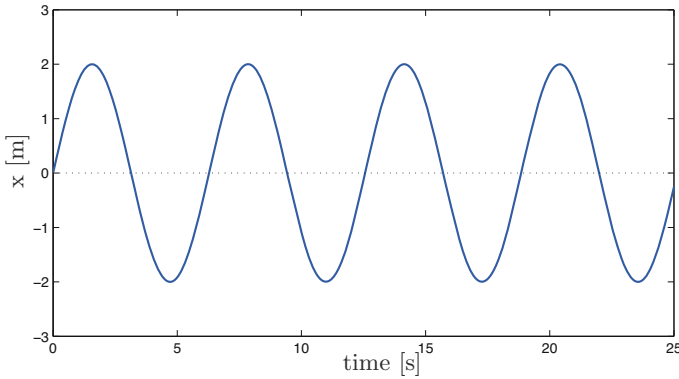
Figure 4. Exact solution for the oscillator without friction $(k = 0)$ with $C = 2$ and $\omega_0 = 1$.

Now (73) can be reduced to

$$
\begin{aligned}
x(t) &= 2B_r \cos(\omega_0 t) + 2B_i \sin(\omega_0 t) \\
     &= a \cos(\omega_0 t) + b \sin(\omega_0 t)
\end{aligned}
\tag{75}
$$

The constants a and b in (75) can be determined from the given initial conditions and we obtain a particular solution for the considered system.

Example: *Let us chose $x_0 = x(0) = 0$, so that the mass is at its equilibrium at time $t = 0$, and $\dot{x}_0 = \frac{dx}{dt}(0) = C\omega_0$, so that it has initial velocity $C\omega_0$. Inserting, we find from (75)*

$$
a = 0 \quad und \quad b = \frac{\dot{x}_0}{\omega_0} = C ,
\tag{76}
$$

and the solution reads

$$
x(t) = C \sin(\omega_0 t) .
\tag{77}
$$

See Fig. 4.

2nd case: $k > 0; c > 0$.

In this case with non-zero friction, the discriminant, D, in the general solution for ω in (66) has to be examined in more detail. It may be greater than, equal, or less than zero.

a) $D < 0$ $\qquad \left(\frac{k^2}{4m^2} < \frac{c}{m} \;\Rightarrow\; \omega_{1,2} = -\frac{k}{2m} \pm i \sqrt{\frac{c}{m} - \frac{k^2}{4m^2}} \right)$

Inserting $\omega_{1,2}$ into (68) and using Euler's formula provides

$$x(t) = \exp\left(-\frac{k}{2m}t\right)\left(\tilde{a}\cos(\tilde{\omega}_a t) + \tilde{b}\sin(\tilde{\omega}_a t)\right), \tag{78}$$

where

$$\tilde{\omega}_a = \sqrt{\frac{c}{m} - \frac{k^2}{4m^2}}. \tag{79}$$

The coefficients $\tilde{a}$ and $\tilde{b}$ again have to be determined so as to satisfy the required initial conditions. The mass now performs a damped oscillation around its equilibrium position with a modified frequency compared to first case. See Fig. 5.

b) $D > 0$ $\qquad \left(\frac{k^2}{4m^2} > \frac{c}{m} \;\Rightarrow\; \omega_{1,2} = -\frac{k}{2m} \pm \sqrt{\frac{k^2}{4m^2} - \frac{c}{m}} \right)$

Again, we insert into (68), and A and B are constants that have to be computed using given initial conditions. We find

$$x(t) = \exp\left(-\frac{k}{2m}t\right)\left(A\exp(\tilde{\omega}_b t) + B\exp(-\tilde{\omega}_b t)\right) \tag{80}$$
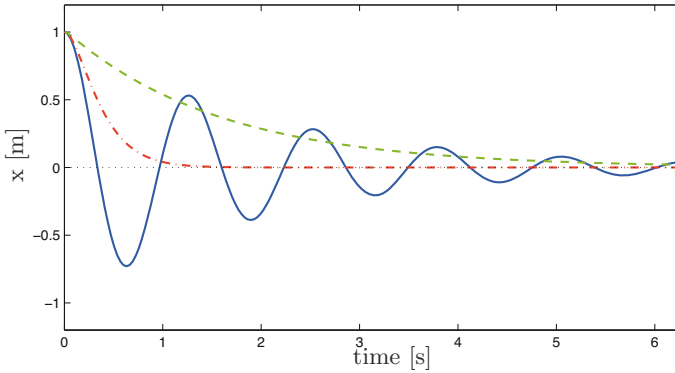
where

$$\tilde{\omega}_b = \sqrt{\frac{k^2}{4m^2} - \frac{c}{m}}. \tag{81}$$

Comparison of the solutions in (78) and (80) shows that both cases describe a damped motion, the term $\exp(\tilde{\omega}_b t)$ "losing" against $\exp(-\frac{k}{2m}t)$ for $t \to \infty$, but there is a fundamental difference: in case a), the system with the exponential function $\exp(-\frac{k}{2m}t)$ performs a damped harmonic oscillation and passes the origin several times. In case b), however, the damping is so strong that the mass is not oscillating at all and just moves back monotonically to its equilibirium (creeping case).

c) $D = 0$ $\qquad \left(\frac{k^2}{4m^2} = \frac{c}{m} \;\Rightarrow\; \omega_{1,2} = -\frac{k}{2m} \right)$

The solution in this case is in line with the one in the case already mentioned above with general solution (69). We find

$$x(t) = \exp\left(-\frac{k}{2m}t\right)(A + Bt), \tag{82}$$

Figure 5. Exact solution for the oscillator with friction ($k > 0$): a) $D < 0$ (blue, line), b) $D > 0$ (green,dashed), c) $D = 0$ (red, point-dashed).

where again the constants A and B have to be determind from the initial conditions.

Thus, case c) is exactly "between" cases a) and b). It is called *aperiodic limiting case.* In case b) the damping is still stronger and faster than in case c) but in both cases there is no oscillation in the system.

Forced oscillations   Now we account for an external force $F_D = F_D(t)$ acting on the linear oscillator by computing the particular part $x_p(t)$ of the solution of the inhomogeneous differential equation (60). We will restrict to the case of a periodic force

$$F_D(t) = F_0 \cos(\Omega t)\,. \tag{83}$$

(Why is this not a severe restriction?). Experiments show that an oscillator exposed to such a force performs a forced harmonic oscillation after some adjustment time has elapsed. The frequency of this oscillation equals that of the driving force, $F_D(t)$. Let us verify that this will in fact be a valid particular solution. We let

$$x_p(t) = A_p \sin(\Omega t) + B_p \cos(\Omega t) \tag{84}$$

with coefficients A_p and B_p remaining to be determined.   Inserting the corresponding time derivatives

$$
\begin{aligned}
\dot{x}_p(t) &= A_p \Omega \cos(\Omega t) - B_p \Omega \sin(\Omega t) \\
\ddot{x}_p(t) &= -A_p \Omega^2 \sin(\Omega t) - B_p \Omega^2 \cos(\Omega t)
\end{aligned}
\tag{85}
$$
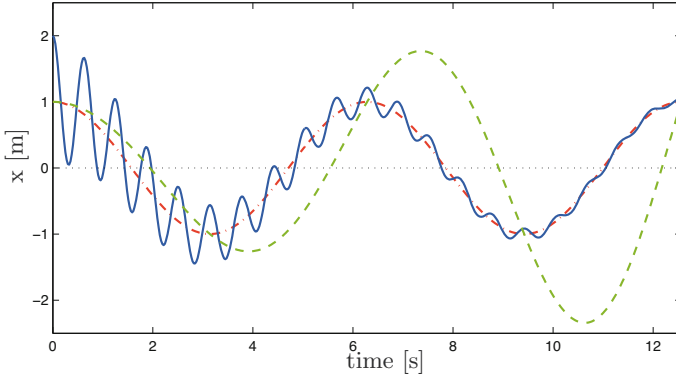
Figure 6. Exact solution for the oscillator driven by an external force. a) Superposition of fast oscillations and slow background movement (blue line) b) resonance (green dashed line) c) driving external force (red dashed-pointed line)

into equation (60) we obtain

$$
\begin{aligned}
F_0 \cos(\Omega t) \quad = \quad & -m(A_p \Omega^2 \sin(\Omega t) + B_p \Omega^2 \cos(\Omega t)) + \\
& k(-B_p \Omega \sin(\Omega t) + A_p \Omega \cos(\Omega t)) + \\
& c(A_p \sin(\Omega t) + B_p \cos(\Omega t)).
\end{aligned}
\tag{86}
$$

Linear independence of the sine and cosine functions allows us to split this equation, such that

$$
\begin{aligned}
(c - m\Omega^2)A_p - k\Omega B_p \quad &= \quad 0 \\
(c - m\Omega^2)B_p + k\Omega A_p \quad &= \quad F_0.
\end{aligned}
\tag{87}
$$

This is a system of two equations with two unknowns A_p and B_p that is easily solved. If $k \neq 0$ (2nd case), then

$$
\begin{aligned}
B_p \quad &= \quad \frac{c - m\Omega^2}{k\Omega} A_p \\
A_p \quad &= \quad \frac{F_0}{k\Omega} \left(1 + \left(\frac{c - m\Omega^2}{k\Omega} \right)^2 \right)^{-1}.
\end{aligned}
\tag{88}
$$

If $k = 0$ and $(c - m\Omega^2) \neq 0$, then

$$
A_p = 0 \qquad \text{and} \qquad B_p = \frac{F_0}{c - m\Omega^2}
\tag{89}
$$

and the case $k = 0$ and $(c - m\Omega^2) = 0$ yields the *resonant* solution (see for example Walter (1996)) with time-dependent coefficients

$$A_p(t) = \frac{F_0}{2m\Omega}t \qquad \text{and} \qquad B_p = 0\,. \tag{90}$$

We have found particular solutions that satisfy the inhomogenous equation for each of the parameter regimes. The sum of the homogenous and the particular solution is the general solution of the oscillator equation with external periodic forcing. For example, in case 2a) this solution reads

$$x(t) = \exp\left(-\frac{k}{2m}t\right)\left(\tilde{a}\cos(\tilde{\omega}_a t) + \tilde{b}\sin(\tilde{\omega}_a t)\right) + A_p\sin(\Omega t) + B_p\cos(\Omega t) \tag{91}$$

The constants A_p and B_p have to be defined according to equation (88) and only $\tilde{a}$ and $\tilde{b}$ are to be computed from the intial conditions. The solutions for the other cases can be derived analogously.

3.2   Dimensionless representation and small parameters

In the preceding section we were able to derive the general solution for the linear oscillator with the equation of motion

$$m\ddot{x} + k\dot{x} + cx = F_0\cos(\Omega t) \tag{92}$$

and initial conditions $x(0) = x_0$ and $\dot{x}(0) = \dot{x}_0$. This solution consists of a homogeneous and an inhomogenous part. As we have seen in the second case, the homogenous solution is decaying exponentially when there is non-zero damping, so that in the longtime motion only the inhomogenous (particular) part of the solution prevails.

In the present section, we will continue our analysis by studying situations in which the free oscillation, damping, and forcing act on very different characteristic time scales. (The notion of a *characteristic scale* will hopefully be reasonably clear by the end of the section. The reader may trust her or his intuition for the time being.) An important tool for deriving concise mathematical descriptions of such *scale-separated* processes is Multiple-Scales Asymptotics, the main ideas and techniques of which will be explained here using the linear oscillator as an example.

To determine the different time scales of the system we will nondimensionalize the general equation of motion (92) in the first step.

Remarks on dimensional analysis   Within the governing equation for the linear oscillator, we identify three fundamental physical dimensions

$\{\mathcal{X}_i\}_{i=1}^3$: Length $\mathcal{L}$, Time $\mathcal{T}$, and Mass $\mathcal{M}$. Each physical quantity ϕ_j that appears in this governing equation has a physical dimension that is a product of these fundamental ones, so that

$$\text{Dim}(\phi_j) = \prod_{i=1}^{3} (\mathcal{X}_i)^{b_j^i} . \tag{93}$$

For the linear oscillator, we have

quantity ϕ	**physical dimension Dim**(ϕ)

dependent and independent variables

x	$\mathcal{L}$
t	$\mathcal{T}$

parameters of governing equation

m	$\mathcal{M}$	
k	$\mathcal{M}/\mathcal{T}$	(94)
c	$\mathcal{M}/\mathcal{T}^2$	
F_0	$\mathcal{M}\mathcal{L}/\mathcal{T}^2$	
Ω	$1/\mathcal{T}$	

initial data

x_0	$\mathcal{L}$
$\dot{x}_0$	$\mathcal{L}/\mathcal{T}$

Once a system of concrete units is chosen based on which these fundamental dimensions shall be measured, each of the physical quantities and coefficients in the governing equations can be quantified by a sole number. The familiar SI-system is one example, where $(\mathcal{T}, \mathcal{L}, \mathcal{M})$ are measured in terms of (Seconds, Meter m, Kilogram kg).

Knowing a quantity's physical dimension and the underlying system of units one can always transform these non-dimensional numbers back into measurable physical values. Obviously, there is a one-to-one map between any two different systems of units, so that the exact solutions of the governing equations will not depend on which system is chosen.

As it stands, the oscillator equation in (60) does not reveal anything besides what was built into it to begin with: Newton's law of motion for the particular case of the mechanical system in Fig. 3. To obtain a somewhat improved intuition about possible solutions one may study classes of solutions distinguished by some particular global mathematical characterization.

For any given solution of the equations one can identify "characteristic values" $[\phi_{j,\mathrm{ref}}]_{j=1}^{N}$ of the total of N physical quantities in the system which roughly describe their orders of magnitude throughout the solution or at least during a certain time interval (and within a selected region in space for pdes). These dimensional characteristic quantities may be combined into non-dimensional characteristic numbers

$$\Pi_k = \prod_{j=1}^{N} (\phi_{j,\mathrm{ref}})^{a_k^j} , \qquad (95)$$

with the exponents a_k^j chosen so as to guarantee that the Π_k do not have a physical dimension as will be explained shortly.

These numbers are extremely useful as they provide a comparison between various quantities that may have the same physical dimension but very different physical origin. An example is the ratio of the oscillator's frequency of free, undamped oscillations, $\sqrt{c/m}$, and that of its harmonic excitation,

$$\Pi_* = \frac{\sqrt{c/m}}{\Omega} . \qquad (96)$$

For the non-dimensional Π's to be actually non-dimensional, all the physical dimensions have to cancel exactly in the product. Using (93), we may rephrase this statement as

$$\mathrm{Dim}(\Pi_k) = \prod_{j=1}^{N} \left[\prod_{i=1}^{3} (\mathcal{X}_i)^{b_j^i} \right]^{a_k^j} = \prod_{i=1}^{3} \left[\prod_{j=1}^{N} (\mathcal{X}_i)^{b_j^i \, a_k^j} \right] = \prod_{i=1}^{3} (\mathcal{X}_i)^{\left[\sum\limits_{j=1}^{N} b_j^i \, a_k^j \right]} \equiv 1 . \qquad (97)$$

For this equation to hold, the respective powers of each of the fundamental dimensions $\mathcal{X}_i$ must vanish independently, so that

$$\sum_{j=1}^{N} b_j^i \, a_k^j \equiv 0 \qquad (i = 1 \ldots 3, \quad k \text{ arbitrary}) . \qquad (98)$$

These are 3 linear constraints on the N-tuples $\boldsymbol{a}_k = (a_k^1, \ldots, a_k^N)$, which therefore span a total space of dimension $N - 3$. This, in turn, is equivalent to the existence of a set of $N - 3$ independent characteristic numbers $\{\Pi_k\}_{k=1}^{N-3}$, which is the key statement of the famous *Buckingham's π-theorem*.

Remark: *Often this theorem is quoted from E. Buckingham (1914) as* Buckingham's Theorem. *Yet, Barenblatt (1996) acknowledges a A. Federmann*

(St. Petersburg 1911) for the first proof, and Görtler (1975) for a concise formulation.

Remark: *For further aspects of dimensional analysis, the reader may want to consult Barenblatt (1996).*

Dimensionless representation of the oscillator problem With the nine quantities from (94) we have 9-3=6 linear independent dimensionless combinations. Two of these are our new dimensionless dependent and independent variables, y and τ. Four of them are dimensionless real numbers which relate and characterize all those quantities that influence the solution in one way or the other. A possible specific choice of these quantities is

Dependent and independent variables

$$y \;=\; \frac{x}{F_0/c} \;\; ; \quad \mathrm{Dim}\,(y) \;=\; \mathcal{L} \cdot \frac{\mathcal{T}^2}{\mathcal{ML}} \cdot \frac{\mathcal{M}}{\mathcal{T}^2} \;=\; 1$$

$$\tau \;=\; \Omega t \;\; ; \quad \mathrm{Dim}\,(\tau) \;=\; \frac{1}{\mathcal{T}} \cdot \mathcal{T} \;=\; 1$$

Characteristic numbers

(99)

$$\mu \;=\; m\frac{\Omega^2}{c} \;\; ; \quad \mathrm{Dim}\,(\mu) \;=\; \mathcal{M} \cdot \frac{1}{\mathcal{T}^2} \cdot \frac{\mathcal{T}^2}{\mathcal{M}} \;=\; 1$$

$$\kappa \;=\; k\frac{\Omega}{c} \;\; ; \quad \mathrm{Dim}\,(\kappa) \;=\; \frac{\mathcal{M}}{\mathcal{T}} \cdot \frac{1}{\mathcal{T}} \cdot \frac{\mathcal{T}^2}{\mathcal{M}} \;=\; 1$$

$$y_0 \;=\; \frac{x_0}{F_0/c} \;\; ; \quad \mathrm{Dim}\,(y_0) \;=\; \mathcal{L} \cdot \frac{\mathcal{T}^2}{\mathcal{ML}} \cdot \frac{\mathcal{M}}{\mathcal{T}^2} \;=\; 1$$

$$y_0' \;=\; \frac{\dot{x}_0}{\Omega F_0/c} \;\; ; \quad \mathrm{Dim}\,(y_0') \;=\; \frac{\mathcal{L}}{\mathcal{T}} \cdot \mathcal{T} \cdot \frac{\mathcal{T}^2}{\mathcal{ML}} \cdot \frac{\mathcal{M}}{\mathcal{T}^2} \;=\; 1$$

Here μ characterizes the system's inertia, κ its damping, and y_0, y_0' the initial data that allow us to select a specific solution. In interpreting these quantities, notice that F_0/c is the static displacement of a spring with stiffness c under the effect of a (constant) force F_0.

Notice that $y : I\!\!R^+ \to I\!\!R$, is a *function*, not just a number, and τ varies all over $I\!\!R^+$. The original unknowns $x(t), t$ and the new ones, $y(\tau), \tau$, must
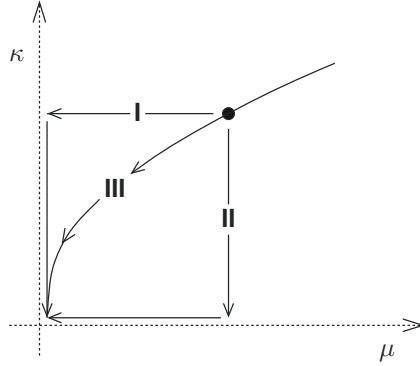
Figure 7. Different possibilities of performing a limit in an asymptotic system with small parameters μ and κ

satisfy

$$\frac{x(t)}{F_0/c} = y(\Omega t) \qquad \text{and} \qquad \Omega t = \tau. \tag{100}$$

Using this identity, we have

$$\dot{x}(t) \quad = \quad \frac{F_0}{c}\frac{dy}{d\tau}\frac{d\tau}{dt} = \frac{F_0\Omega}{c}\, y'(\tau) \tag{101}$$

$$\ddot{x}(t) \quad = \quad \frac{F_0}{c}\frac{d^2y}{d\tau^2}\left(\frac{d\tau}{dt}\right)^2 = \frac{F_0\Omega^2}{c}\, y''(\tau), \tag{102}$$

and (92) then allows us to specify a differential equation for $y(\tau)$,

$$\frac{m\Omega^2}{c}\, y'' + \frac{k\Omega}{c}\, y' + y = \cos\tau \tag{103}$$

or

$$\mu y'' + \kappa y' + y = \cos\tau. \tag{104}$$

The appropriate initial conditions read

$$y(0) = y_0 = \frac{x_0 c}{F_0} \qquad \text{and} \qquad y'(0) = y_0' = \frac{\dot{x}_0 c}{F_0\Omega}. \tag{105}$$

Oscillators with small mass and small damping – exact solutions
Here we examine the behavior of the (dimensionless) oscillator system

$$y = y(\tau; \mu, \kappa, y_0, y_0') \tag{106}$$

for fixed initial data, but for smaller and smaller values of the inertia and damping parameters μ, κ (i.e., $\mu, \kappa \in \mathbb{R}^+$; $\mu, \kappa \ll 1$).

Distinguished limits Letting μ, $\kappa \to 0$ it turns out to be important just *how* these values tend to zero: For example, if we let μ vanish first, following path I in Fig. 7, we formally get rid of the second derivative in (104) and obtain a first-order ordinary differential equation. But if we let $\kappa \to 0$ first (path II), then the system formally reduces to the undamped oscillator equation. Along the first path, we expect non-oscillatory, purely damped motions, whereas along the second, oscillations of constant amplitude about some slow mean harmonic motion should arise. To verify or reject the stated hypotheses regarding paths I and II, or to decide what behavior will emerge for some path in between, such as III, requires some deeper analyses.

The first ansatz that may come to mind when looking for solutions in the vicinity of the location $\mu = 0; \kappa = 0$ in parameter space might be a Taylor expansion with respect to the μ-κ-dependence of the solution. This would promise to provide the best-possible linear, quadratic, or higher-order polynomial approximations as long as the dependence of the solution on these parameters is sufficiently smooth.

In fact, when such an expansion exists at all, it reads

$$y = y|_{\mu,\kappa=0} + \left(\mu \frac{\partial y}{\partial \mu} \bigg|_{\mu,\kappa=0} + \kappa \frac{\partial y}{\partial \kappa} \bigg|_{\mu,\kappa=0} \right) + o(\mu, \kappa) \qquad (\mu, \kappa \to 0)\,, \quad (107)$$

where

$$\left(\frac{\partial y}{\partial \mu}, \frac{\partial y}{\partial \kappa} \right) = \mathrm{grad}_{(\mu,\kappa)} y \qquad\qquad (108)$$

is the gradient (or (*Fréchet*-) derivative) of the solution with respect to our two small parameters. (For the definition of a Fréchet-derivative see, e.g., (Werner, 2000, S. 113)).

However, from our previous considerations regarding the path-dependence of the solution behavior as $\mu \to 0$ and $\kappa \to 0$ we conclude that even though there is a limit solution, $y|_{\mu,\kappa=0}(\tau) = \cos(\tau)$, it is *not* the limit of either solution found along paths I or II in the parameter space of Fig. 7. Thus we cannot decide whether the "proper behaviour" for very small μ, κ should be purely oscillatory, purely damped, or something in between. We are led to conclude that the gradient in (108) *does not exist*!

Fortunately, not all is lost. Analysis has it that even if a Fréchet-derivative does not exist, linear approximations to the solution *along straight lines*, i.e., directional derivatives, may still be well-defined. This would lead

us to consider coupling μ, κ in such a way that $\kappa = \alpha\mu$ as $\mu \to 0$ for some fixed α.

We allow here for more general μ-κ–relationships which include this former one by letting (μ, κ) approach the origin of their parameter space along some parameterized trajectory. To this end, we introduce a new expansion parameter $\varepsilon \ll 1$, and two functions $\hat{\mu}(\varepsilon), \hat{\kappa}(\varepsilon)$ that should satisfy

$$(\hat{\mu}(\varepsilon), \hat{\kappa}(\varepsilon)) = o(1) \qquad (\varepsilon \to 0). \tag{109}$$

Then, dropping the solution's explicit dependence on the initial data in the notation for the moment, we Taylor-expand w.r.t. ε,

$$y(\tau; \mu, \kappa) = \hat{y}(\tau; \varepsilon) = \hat{y}(\tau; \hat{\mu}(\varepsilon), \hat{\kappa}(\varepsilon)) = \hat{y}(\tau; 0) + \varepsilon \frac{\partial \hat{y}}{\partial \varepsilon}(\tau; 0) + o(\varepsilon) \qquad (\varepsilon \to 0). \tag{110}$$

The mappings

$$\begin{aligned}(\hat{\mu}, \hat{\kappa}) \quad &: \quad \mathbb{R} \to \quad \mathbb{R}^2 \\ \varepsilon &\mapsto \quad (\hat{\mu}(\varepsilon), \hat{\kappa}(\varepsilon))\end{aligned} \tag{111}$$

comprise a *distinguished limit*.

Remark: *Here $\partial\hat{y}/\partial\varepsilon(\tau; 0)$ is a generalization of the directional or Gâteaux derivative*

$$\frac{\partial}{\partial \varepsilon} \left(y(\tau; \alpha\varepsilon, \beta\varepsilon) \right)_{\varepsilon=0} \quad \alpha, \beta = const. \tag{112}$$

In general we know from functional analysis that for some mapping f

$$f \text{ Fréchet-differentiable} \quad \overset{\Rightarrow}{\underset{\nLeftarrow}{}} \quad f \text{ Gâteaux-differentiable}. \tag{113}$$

We conclude that asymptotic expansions based on an approximation in ε with respect to appropriate distinguished limits are more general than a multi-parameter expansions, because–as pointed out above–the latter correspond to classical Taylor-expansions in μ, κ and would require the existence of the Fréchet-derivative $\text{grad}_{\mu,\kappa} y$ at $\mu = \kappa = 0$.

Time scales In analyzing distinguished limits below, we will pay special attention to the timescales on which oscillation, damping, and background forcing will act as ε vanishes. The expressions m/k and $\sqrt{m/c}$ determine the timescales of damping and free oscillation of the system: In our solution from (91), the damping is described by $\exp(-\frac{k}{2m}t)$. Thus, t has to change by $O(m/k)$ to change the argument of the exponential function by $O(1)$. For an undamped, free oscillation, t has to change by $O(1/\omega_0) = O\left(\sqrt{m/c}\right)$

to change the arguments of sine and cosine by $O(1)$. The dimensionless quantities

$$\mathrm{K_D} = \Omega \frac{m}{k} = \mu/\kappa \qquad \text{and} \qquad \mathrm{K_O} = \Omega \sqrt{\frac{m}{c}} = \sqrt{\mu} \qquad (114)$$

allow us to compare the internal damping and oscillation time scales of the oscillator with that of the external forcing. Notice that both are functions of our dimensionless mass and damping parameters, (μ, κ).

Three examples shall underline the consequences of picking particular distinguished limits in the oscillator problem:

1st case: $\mu \sim \kappa$ $\qquad (\mu = \varepsilon$ and $\kappa = \varepsilon \hat{\kappa}$ with $\hat{\kappa} = \text{const. as } \varepsilon \to 0)$

Here we have $\mathrm{K_D} = 1/\hat{\kappa} = \text{const.}$ and $\mathrm{K_O} = \sqrt{\varepsilon}$. Thus, as $\varepsilon \to 0$, the timescale of free oscillation becomes much shorter than that of the external forcing, while the damping timescale remains comparable to it. We verify this considering the upper graph in Fig. 8. The frequency of oscillation increases as we reduce ε from 10^{-2} to $5 \cdot 10^{-4}$, whereas the time which the oscillation needs to decay remains the same.

2nd case: $\mu \sim \kappa^2$ $\qquad (\mu = \varepsilon$ and $\kappa = \sqrt{\varepsilon}\hat{\kappa}$ with $\hat{\kappa} = \text{const. as } \varepsilon \to 0)$

Here, since $\mathrm{K_O} = \sqrt{\varepsilon}$ and $\mathrm{K_D} = \sqrt{\varepsilon}/\hat{\kappa}$, the oscillation and damping time-scales remain comparable in the limit. As a consequence, the number of oscillations which the system performs before the oscillation is essentially damped away remains nearly independent of ε. We corroborate this by inspecting the centred graph in Fig. 8.

3rd case: $\mu \sim \kappa^3$ $\qquad (\mu = \varepsilon$ and $\kappa = \varepsilon^{\frac{1}{3}}\hat{\kappa}$ with $\hat{\kappa} = \text{const. as } \varepsilon \to 0)$

For this case, Fig. 8 reveals that the system does no longer oscillate at all. For small ε, the damping timescale $\mathrm{K_D} = \varepsilon^{\frac{2}{3}}/\hat{\kappa}$ is always much smaller than the timescale of oscillation $\mathrm{K_O} = \sqrt{\varepsilon}$. Therefore, the inertial motion of the oscillator is already damped before the first overshoot due to the incipient oscillation can take place. After a short initial transient, the mass is essentially "slaved" by the external forcing.

It turns out that the regime $\mu \sim \kappa^2$ is precisely the threshold that separates the regions in μ-κ–space in which, as $\varepsilon \to 0$, either an oscillatory or a purely damped motion prevails. If μ vanishes slower than κ^2, the system will oscillate, otherwise it is strongly damped as summarized in figure 9.
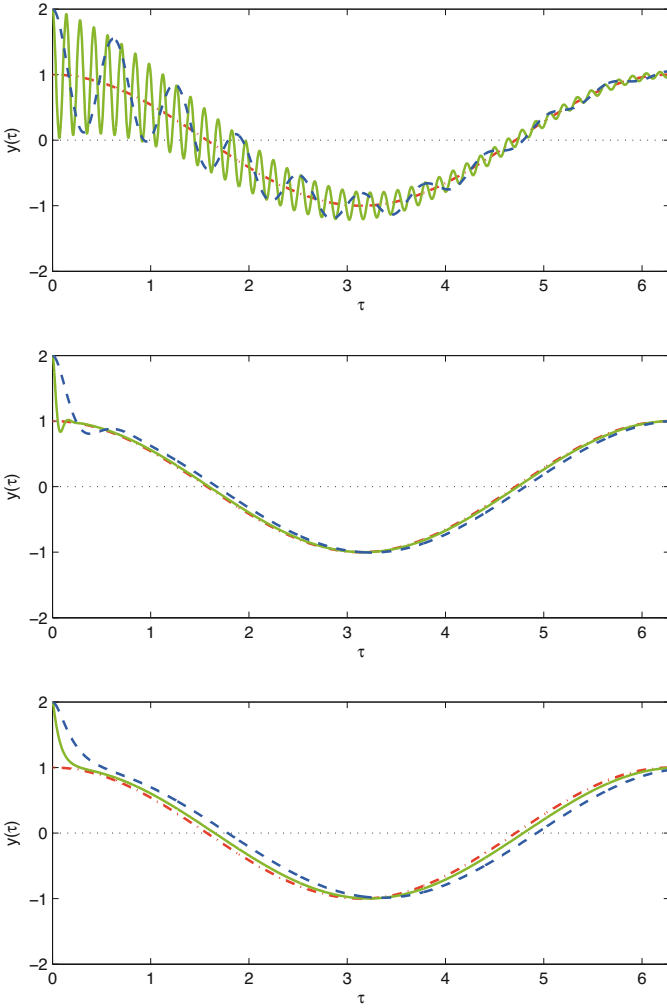
Figure 8. Impact of different choices for the distinguished limit. Exact solutions for $\varepsilon = 0.01$ (blue dashed lines), $\varepsilon = 0.0005$ (green lines) and background oscillation (red dashed-pointed lines). $\mu = \kappa = \varepsilon$ (upper), $\mu = \kappa^2 = \varepsilon$ (centre), and $\mu = \kappa^3 = \varepsilon$ (lower graph).
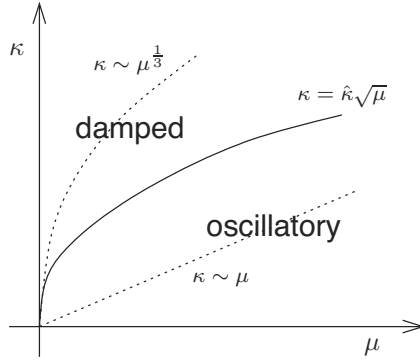
Figure 9. Ratio between mass and damping in the problem and the resulting behaviour of the solution.

If there exist solutions for which y' and y'' remain bounded while $\mu \to 0$ and $\kappa \to 0$, equation (104) reduces to

$$y = \cos\tau. \qquad (115)$$

in the limit. The solution written in dimensional terms becomes

$$x(t) = \frac{F_0}{c}\, y(\tau) = \frac{F_0}{c}\, \cos(\Omega t)\,. \qquad (116)$$

This is in line with "experimental observations" (and with the exact solution, of course). After a certain initial period of adjustment, the oscillator with external force $F_D(t) = F_0 \cos(\Omega t)$ performs a periodic oscillation with angular frequency Ω. This is a limiting long-time behavior to be expected from any approximate (asymptotic) solution below, as long as $\kappa > 0$.

3.3 Regular perturbation analysis for small mass and damping

In the sequel we will derive approximate solutions to the dimensionless equation of motion (104) using techniques of asymptotic analysis. To do so, we choose case 1 from the last section, i.e., we let

$$\mu = \varepsilon, \quad \kappa = \varepsilon\hat{\kappa} \quad \text{with} \quad \hat{\kappa} = \text{const.} \quad \text{as} \quad \varepsilon \to 0. \qquad (117)$$

Remark: *Choosing a different distinguished limit would yield different asymptotic results!*

With this distinguished limit fixed, the oscillator's governing equation reduces to

$$\varepsilon y'' + \varepsilon\hat{\kappa} y' + y = \cos\tau. \qquad (118)$$

We consider the solution to explicitly depend only on τ and ε and denote it by $y(\tau; \varepsilon)$, dropping the "hat" notation used earlier in (110).

Slow-time asymptotic expansion For the solution $y = y(\tau; \varepsilon)$ of (118), we choose here an asymptotic ansatz of the form

$$y(\tau; \varepsilon) = y^{(0)}(\tau) + \varepsilon y^{(1)}(\tau) + \varepsilon^2 y^{(2)}(\tau) + o(\varepsilon^2) . \tag{119}$$

Remark: *Generally, a series of the form*

$$\sum_{n=1}^{N} \phi_n(\varepsilon) \, u_n(\boldsymbol{x}) \tag{120}$$

with $\phi_{n+1}(\varepsilon) = o(\phi_n(\varepsilon))$ for $\varepsilon \to 0$ is called an asymptotic N-term expansion of the function u if

$$u(\boldsymbol{x}; \varepsilon) - \sum_{n=1}^{N} \phi_n(\varepsilon) \, u_n(\boldsymbol{x}) = o(\phi_N(\varepsilon)) \tag{121}$$

for $\varepsilon \to 0$ (see for example Kevorkian and Cole (1996) and Schneider (1978)). Notice that the result of the analysis will depend on the choice of the asymptotic sequence $\{\phi_n(\varepsilon)\}_{n \in \mathbf{N}}$.

The chosen ansatz is a Taylor expansion in $\varepsilon = 0$ of the desired solution $y = y(\tau; \varepsilon)$, i.e., we look for the coefficients of $\varepsilon, \varepsilon^2$ etc. in

$$
\begin{aligned}
y(\tau; \varepsilon) &= \sum_{n=0}^{N} \frac{1}{n!} \varepsilon^n \left(\frac{\partial^n y}{\partial \varepsilon^n} \right)(\tau; 0) + o(\varepsilon^N) \\
&= y(\tau; 0) + \varepsilon(\partial_\varepsilon y)(\tau; 0) + \frac{\varepsilon^2}{2}(\partial_\varepsilon^2 y)(\tau; 0) + o(\varepsilon^2)
\end{aligned}
\tag{122}
$$

Letting $y^{(0)}(\tau) := y(\tau; 0)$, $y^{(1)}(\tau) := (\partial_\varepsilon y)(\tau; 0)$ etc. naturally leads to (119). We proceed to determine the asymptotic behaviour of the solution y for a fixed τ and an arbitrary but small ε. Depending on the power of ε considered, one speaks of the behaviour of the solution *at a certain order*. Thus, $y^{(0)}(\tau)$ describes the behaviour at leading or zeroeth order, $y^{(1)}(\tau)$ the behaviour at first order, etc.

Inserting the time derivatives from (119) (time means the dimensionless time τ)

$$
\begin{aligned}
y'(\tau; \varepsilon) &= y^{(0)'}(\tau) + \varepsilon y^{(1)'}(\tau) + \varepsilon^2 y^{(2)'}(\tau) + o(\varepsilon^2) \\
y''(\tau; \varepsilon) &= y^{(0)''}(\tau) + \varepsilon y^{(1)''}(\tau) + \varepsilon^2 y^{(2)''}(\tau) + o(\varepsilon^2)
\end{aligned}
\tag{123}
$$

into (118) we find

$$
\begin{aligned}
0 \;=\; & \varepsilon \left(y^{(0)''} + \varepsilon y^{(1)''} + \varepsilon^2 y^{(2)''} + o(\varepsilon^2) \right) + \\
& \varepsilon \hat{\kappa} \left(y^{(0)'} + \varepsilon y^{(1)'} + \varepsilon^2 y^{(2)'} + o(\varepsilon^2) \right) + \\
& \left(y^{(0)}(\tau) + \varepsilon y^{(1)} + \varepsilon^2 y^{(2)} + o(\varepsilon^2) \right) - \cos\tau
\end{aligned}
\tag{124}
$$

or

$$
\left(y^{(0)} - \cos\tau \right) + \varepsilon \left(y^{(0)''} + \hat{\kappa} y^{(0)'} + y^{(1)} \right) + \varepsilon^2 \left(y^{(1)''} + \hat{\kappa} y^{(1)'} + y^{(2)} \right) = o(\varepsilon^2) \;.
\tag{125}
$$

If this equation is to hold for arbitrary (but small) ε, each of the coefficients of ε^i for $(i = 1, 2, \ldots)$ (the expressions in brackets) has to be zero individually. Therefore,

$$
\begin{aligned}
y^{(0)} \;&=\; \cos\tau \\
y^{(1)} \;&=\; -y^{(0)''} - \hat{\kappa} y^{(0)'} \;=\; \cos\tau + \hat{\kappa}\sin\tau \\
y^{(2)} \;&=\; -y^{(1)''} - \hat{\kappa} y^{(1)'} \;=\; (1 - \hat{\kappa}^2)\cos\tau + 2\hat{\kappa}\sin\tau \;.
\end{aligned}
\tag{126}
$$

Our second-order accurate asymptotic solutions thus reads

$$
y(\tau;\varepsilon) = \cos\tau + \varepsilon\left(\cos\tau + \hat{\kappa}\sin\tau\right) + \varepsilon^2\left((1 - \hat{\kappa}^2)\cos\tau + 2\hat{\kappa}\sin\tau\right) + o(\varepsilon^2) \,,
\tag{127}
$$

and this is compared with the exact solution in Fig. 10.

Discussion For $\varepsilon \to 0$, the approximate asymptotic solution in (127) reduces to

$$
y(\tau; 0) = y^{(0)}(\tau) = \cos\tau \,,
\tag{128}
$$

and the asymptotic solution in the limit coincides with (115). Yet, there is a severe catch:

We have no degrees of freedom to meet the initial data!

Instead, the initial displacement and velocity from the leading-order asymptotics are $y^{(0)}(\tau) = 1$ and $y^{(0)'}(0) = 0$. Any different values for y_0 and y_0' can nowhere be accounted for. The reason is that with the present ansatz we can only see the solution after any initial transient, which *would be* determined by the initial data, has already decayed.
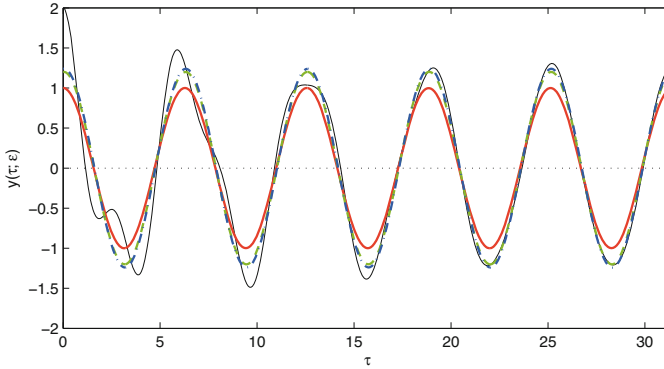
Figure 10. Asymptotic expansion of the solution in τ with $y_0 = 2$, $y_0' = 0$, $\varepsilon = 0.2$ and $\hat{\kappa} = 0.2$. Exact solution: black line, $y(\tau; \varepsilon) = y^{(0)}$: red line, $y(\tau; \varepsilon) = y^{(0)} + \varepsilon y^{(1)}$: green dashed, $y(\tau; \varepsilon) = y^{(0)} + \varepsilon y^{(1)} + \varepsilon^2 y^{(2)}$: blue dash-pointed

This can be verified in Fig. 10, even when the next two higher-order terms are included. Adding the first- and second-order contributions, makes merely a slight difference for the asymptotic approximation. It can do no more than reproduce with better accuracy the background oscillation as more and more expansion terms are included.

Fast-time asymptotic expansion   Using the time coordinate $\tau = \Omega t$ we miss the fast oscillatory motions associated with the free oscillation time scale $\sqrt{m/c}$. The rescaled time variable

$$\vartheta = \frac{t}{\sqrt{m/c}} = \frac{\tau}{\sqrt{m\Omega^2/c}} = \frac{\tau}{\sqrt{\varepsilon}} \tag{129}$$

would remedy this problem. We will try out a new expansion scheme in which the unknowns will depend on ϑ instead of on τ. Since each time derivative $d/d\tau$ that appears in the governing equation in that case will produce a factor $1/\sqrt{\varepsilon}$ by the chain rule, we should expand the solution in powers of $\sqrt{\varepsilon}$ instead of in powers of ε. (What happens if we don't but use ϑ as the independent variable while expanding in powers of ε?) Thus we choose the new asymptotic expansion scheme

$$y(\tau; \varepsilon) =: y^{(0)}(\vartheta) + \sqrt{\varepsilon} y^{(1)}(\vartheta) + \varepsilon y^{(2)}(\vartheta) + o(\varepsilon) , \tag{130}$$

which is equivalent to

$$y(\tau; \varepsilon) = y^{(0)}\left(\frac{\tau}{\sqrt{\varepsilon}}\right) + \sqrt{\varepsilon}y^{(1)}\left(\frac{\tau}{\sqrt{\varepsilon}}\right) + \varepsilon y^{(2)}\left(\frac{\tau}{\sqrt{\varepsilon}}\right) + o(\varepsilon) . \qquad (131)$$

We will need to be aware of the latter form of writing the expansion when we insert into the governing equation in (118), which is written in terms of τ. In preparation, we compute the τ-derivatives of (131) for fixed ε,

$$\left.\frac{\partial y}{\partial \tau}\right|_{\varepsilon} (\vartheta; \varepsilon) = \frac{dy^{(0)}}{d\vartheta}\frac{d\vartheta}{d\tau} + \sqrt{\varepsilon}\frac{dy^{(1)}}{d\vartheta}\frac{d\vartheta}{d\tau} + \varepsilon\frac{dy^{(2)}}{d\vartheta}\frac{d\vartheta}{d\tau} + o\left(\varepsilon\frac{d\vartheta}{d\tau}\right)$$

$$= \frac{1}{\sqrt{\varepsilon}}\frac{dy^{(0)}}{d\vartheta} + \frac{dy^{(1)}}{d\vartheta} + \sqrt{\varepsilon}\frac{dy^{(2)}}{d\vartheta} + o\left(\sqrt{\varepsilon}\right) \qquad (132)$$

$$\left.\frac{\partial^2 y}{\partial \tau^2}\right|_{\varepsilon} (\vartheta; \varepsilon) = \frac{1}{\varepsilon}\frac{d^2y^{(0)}}{d\vartheta^2} + \frac{1}{\sqrt{\varepsilon}}\frac{d^2y^{(1)}}{d\vartheta^2} + \frac{d^2y^{(2)}}{d\vartheta^2} + o(1) . \qquad (133)$$

The notation $\left.\frac{\partial y}{\partial \tau}\right|_{\varepsilon}$ shall underline that, for any solution of the oscillator problem, ε is a fixed parameter and thus held constant when differentiating. If, instead, we were to consider ε as varying in time, then the time scales, and thus the mass, spring stiffness, and the damping coefficient, would change in time, too.

We express the forcing term in (118) in terms of ϑ, and then Taylor-expand w.r.t. $\sqrt{\varepsilon}$,

$$\cos \tau = \cos(\sqrt{\varepsilon}\vartheta) = 1 - \frac{\varepsilon}{2}\vartheta^2 + O\left(\varepsilon^2\right) . \qquad (134)$$

Inserting the appropriate derivatives and expansions into (118) we find

$$\begin{aligned}\frac{d^2y^{(0)}}{d\vartheta^2} + \sqrt{\varepsilon}\frac{d^2y^{(1)}}{d\vartheta^2} + \varepsilon\frac{d^2y^{(2)}}{d\vartheta^2} & \\ + \hat{\kappa}\sqrt{\varepsilon}\frac{dy^{(0)}}{d\vartheta} + \hat{\kappa}\varepsilon\frac{dy^{(1)}}{d\vartheta} & \\ + y^{(0)} + \sqrt{\varepsilon}y^{(1)} + \varepsilon y^{(2)} & = 1 - \varepsilon\frac{\vartheta^2}{2} + o(\varepsilon) .\end{aligned} \qquad (135)$$

This yields, after collection of like powers of ε, the following hierarchy of

perturbation equations,

$$O(1): \qquad \frac{d^2 y^{(0)}}{d\vartheta^2} + y^{(0)} \;=\; 1$$

$$O(\sqrt{\varepsilon}): \qquad \frac{d^2 y^{(1)}}{d\vartheta^2} + y^{(1)} \;=\; -\hat{\kappa}\frac{dy^{(0)}}{d\vartheta} \qquad\qquad (136)$$

$$O(\varepsilon): \qquad \frac{d^2 y^{(2)}}{d\vartheta^2} + y^{(2)} \;=\; -\hat{\kappa}\frac{dy^{(1)}}{d\vartheta} - \frac{\vartheta^2}{2}\,.$$

At leading order (i.e., at $O(1)$) we find the equation for an undamped oscillator with time-independent forcing. The solution is

$$y^{(0)} = a_0 \sin\vartheta + b_0 \cos\vartheta + 1\,. \qquad\qquad (137)$$

Here a_0 and b_0 are constants that depend on the initial conditions.

Next we solve the first-order equation (at $O(\sqrt{\varepsilon})$) in the expansion, which becomes

$$\frac{d^2 y^{(1)}}{d\vartheta^2} + y^{(1)} = -\hat{\kappa}\left(a_0 \cos\vartheta - b_0 \sin\vartheta\right) \qquad\qquad (138)$$

The solution is a superposition of the homogeneous solution, $y_h^{(1)} = a_1 \sin\vartheta + b_1 \cos\vartheta$, and a particular solution that takes care of the right-hand side. The coefficients a_1 and b_1 will have to be computed from the initial conditions as before. To derive a particular solution, we use the technique of variation of coefficients, i.e.,

$$y_p^{(1)} = f(\vartheta)\sin\vartheta + g(\vartheta)\cos\vartheta\,, \qquad\qquad (139)$$

where f and g remain to be determined. Inserting this ansatz into the differential equation (138) yields

$$(\ddot{f} - 2\dot{g})\sin\vartheta + (\ddot{g} + 2\dot{f})\cos\vartheta = -\hat{\kappa}\left(a_0 \cos\vartheta - b_0 \sin\vartheta\right)\,. \qquad (140)$$

Comparing coefficients, we find the constraints

$$\ddot{f} - 2\dot{g} = \hat{\kappa}b_0 \quad \text{and} \quad \ddot{g} + 2\dot{f} = -\hat{\kappa}a_0\,. \qquad\qquad (141)$$

The desired solutions are polynomials in ϑ of degree less than two, and we let $f(\vartheta) = A_f\vartheta + B_f$ and $g(\vartheta) = A_g\vartheta + B_g$. Without loss of generality, we may also assume $B_f \equiv 0$ and $B_g \equiv 0$, as these terms can be covered by the homogenous part of the solution. Solving (141), yields

$$y_p^{(1)} = -\vartheta\frac{\hat{\kappa}}{2}\left(a_0 \sin\vartheta + b_0 \cos\vartheta\right) \qquad\qquad (142)$$

so that

$$y^{(1)} = y_h^{(1)} + y_p^{(1)} = a_1 \sin \vartheta + b_1 \cos \vartheta - \vartheta \frac{\hat{\kappa}}{2} \left(a_0 \sin \vartheta + b_0 \cos \vartheta \right) . \quad (143)$$

In the same way one may compute higher-order solutions.

It turns out that this ansatz based on the short-time variable is still not satisfactory. As seen in figure 11, although the solution improves with increasing order, this is true only for the early stages of the evolution. With increasing time the solution deteriorates dramatically, and this gets worse the higher the approximation order!
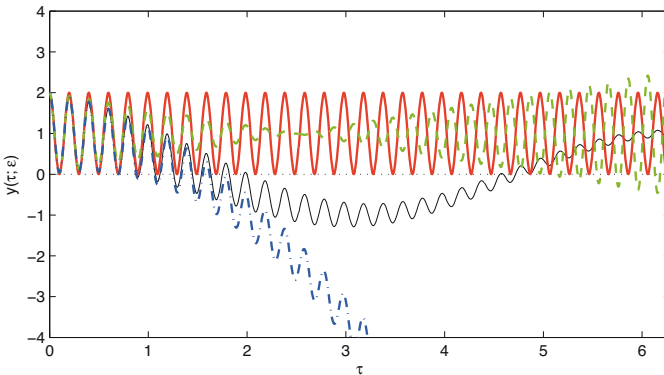
Figure 11. Asymptotic expansion of the solution in ϑ with $y_0 = 2$, $y_0' = 0$, $\varepsilon = 0.001$ and $\hat{\kappa} = 0.8$. $y(\tau; \varepsilon)$ (exact solution): black line; $y^{(0)}$: red line; $y^{(0)} + \sqrt{\varepsilon} y^{(1)}$: green dashed line; $y^{(0)} + \sqrt{\varepsilon} y^{(1)} + \varepsilon y^{(2)}$: blue dash-pointed line

Remark: *For the present short-time expansion we could have chosen an ansatz similar to (119) (i.e. with $\phi_n(\varepsilon) = \varepsilon^n$). It is easy to verifiy that this yields only the trivial solution $y(\tau; \varepsilon) \equiv 0$. This shows that the choice of the asymptotic sequence $\{\phi_n(\varepsilon)\}_{n \in N}$ is crucial when looking for an asymptotic solution.*

Remark: *As we have seen, the differential equation for $y^{(1)}$ has a resonant, amplifying solution. After some time, the term $\sqrt{\varepsilon} y^{(1)}$ becomes comparable to the previous one, $y^{(0)}$, and the whole idea of building a series with smaller and smaller corrections as the order of approximation increases fails badly. In fact, the present asymptotic approximate solution is valid only for $\vartheta = O(1)$ or, equivalently, $\tau = O(\sqrt{\varepsilon})$, i.e., for asymptotically short times on the time scale of the background forcing.*

3.4   Multiple scales analysis

The analyses based on single timescale representations, with $\tau = O(\sqrt{\varepsilon})$ and $\tau = O(1)$, respectively, were at best partially successful. They did allow us to cover the early, respectively, late development of the solution, but were definitely not valid uniformly in time. Here we consider an asymptotic expansion scheme that accounts for both of these timescales in a single sweep,

$$
\begin{aligned}
y(\tau;\varepsilon) &= y^{(0)}\left(\frac{\tau}{\sqrt{\varepsilon}},\tau\right) + \sqrt{\varepsilon}\, y^{(1)}\left(\frac{\tau}{\sqrt{\varepsilon}},\tau\right) + \varepsilon y^{(2)}\left(\frac{\tau}{\sqrt{\varepsilon}},\tau\right) + O(\varepsilon) \\
&= y^{(0)}(\vartheta,\tau) + \sqrt{\varepsilon}\, y^{(1)}(\vartheta,\tau) + \varepsilon y^{(2)}(\vartheta,\tau) + O(\varepsilon)\ .
\end{aligned}
\tag{144}
$$

Including both the time variables considered in our previous expansions, we expect this scheme to allow us to fulfill the initial conditions, $y(0;\varepsilon) = y_0$ and $y'(0;\varepsilon) = y'_0$, but to also capture the long-time behavior of the solution without resonant growth.
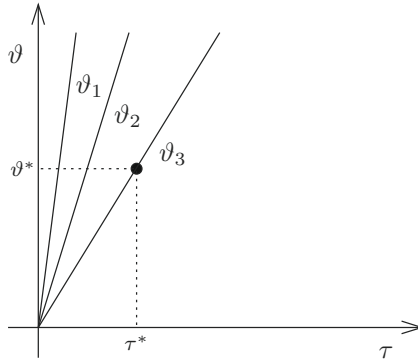
Remark: *The key challenge, of course, will be to find the dependencies of the expansion functions, $y^{(i)}(\vartheta,\tau)$, on two time variables, even though our orginal govering equation involves merely a single independent variable, τ. In fact, we will have to determine the variation of the expansion functions within the entire (ϑ,τ)–plane, because we want to obtain solutions that are valid for small, but otherwise arbitrary values of ε. Varying ε, the ratio between ϑ and τ changes, as indicated in Fig. 12. Thus, for any fixed value of τ we may be interested in $y^{(i)}(\vartheta,\tau)$ within a range of values of ϑ, and vice versa, the range being determined by the range of realistic values of ε.*

To proceed, we need to work out the time derivatives needed in (144) taking into account that the $y^{(i)}(\vartheta,\tau)$ are functions of two independent variables. Using the chain rule, we find

$$
\begin{aligned}
\left.\frac{\partial y}{\partial \tau}\right|_{\varepsilon} &= y^{(0)}_{\vartheta}\vartheta_{\tau} + y^{(0)}_{\tau} + \sqrt{\varepsilon}\, y^{(1)}_{\vartheta}\vartheta_{\tau} + \sqrt{\varepsilon}\, y^{(1)}_{\tau} + \varepsilon y^{(2)}_{\vartheta}\vartheta_{\tau} + \varepsilon y^{(2)}_{\tau} + o(\varepsilon\vartheta_{\tau}) \\
&= \frac{1}{\sqrt{\varepsilon}} y^{(0)}_{\vartheta} + \left(y^{(0)}_{\tau} + y^{(1)}_{\vartheta}\right) + \sqrt{\varepsilon}\left(y^{(1)}_{\tau} + y^{(2)}_{\vartheta}\right) + o\left(\sqrt{\varepsilon}\right) \\
\left.\frac{\partial^2 y}{\partial \tau^2}\right|_{\varepsilon} &= \frac{1}{\varepsilon} y^{(0)}_{\vartheta\vartheta} + \frac{1}{\sqrt{\varepsilon}}\left(2 y^{(0)}_{\vartheta\tau} + y^{(1)}_{\vartheta\vartheta}\right) + \left(y^{(0)}_{\tau\tau} + 2 y^{(1)}_{\vartheta\tau} + y^{(2)}_{\vartheta\vartheta}\right) + o(1)
\end{aligned}
\tag{145}
$$

Inserting into (118) one has

$$
\left(y^{(0)}_{\vartheta\vartheta} + y^{(0)} - \cos\tau\right) + \sqrt{\varepsilon}\left(2 y^{(0)}_{\vartheta\tau} + y^{(1)}_{\vartheta\vartheta} + \hat{\kappa} y^{(0)}_{\vartheta} + y^{(1)}\right) + o\left(\sqrt{\varepsilon}\right) = 0\ . \tag{146}
$$

Figure 12. Relation between the time coordinates τ and ϑ for chosen ε, where $\vartheta_i = \tau/\sqrt{\varepsilon_i}$ ($\varepsilon_1 < \varepsilon_2 < \varepsilon_3$). For every τ^* there is exactly one ϑ^*.

For this equation to hold for arbitrary $\varepsilon \ll 1$ it is sufficient that the different terms in brackets vanish. Considering that, through the dependence of the $y^{(i)}$ on τ and $\vartheta = \tau/\sqrt{\varepsilon}$, these brackets implicitly do depend on ε, it is not immediately clear that the vanishing of the brackets is also necessary. But, if we *can* make all the coefficients disappear for arbitrary (ϑ, τ), then our equation is in any case satisfied. Let's give it a try!

For the different orders in $\sqrt{\varepsilon}$ this leads to

$$
\begin{aligned}
O(1): \quad & y^{(0)} + y^{(0)}_{\vartheta\vartheta} = \cos\tau \\
O(\sqrt{\varepsilon}): \quad & y^{(1)} + y^{(1)}_{\vartheta\vartheta} = -2y^{(0)}_{\vartheta\tau} - \hat{\kappa}y^{(0)}_{\vartheta} .
\end{aligned}
\tag{147}
$$

It is of crucial importance that the first of these equations is an ODE for the ϑ–depencence of $y^{(0)}$, and that any τ–derivative of this leading-order function appears only at the next order. Thus, if the first equation is solved for the ϑ–dependence, τ remains as a parameter the influence of which will remain to be determined.

Following the same procedures as earlier in this section, we find the general solution in terms of ϑ for $(147)_1$ to be

$$
y^{(0)}(\vartheta, \tau) = A(\tau)\cos\vartheta + B(\tau)\sin\vartheta + \cos\tau .
\tag{148}
$$

This is the superposition of a slow background motion and an oscillation with increasing frequency as $\varepsilon \to 0$. In addition, when $A(\tau) \equiv B(\tau) \equiv 0$ we just retrieve the leading-order solution $y^{(0)}$ from the single-scale analysis. Thus, the present result includes the previous solutions, and has extended

the description of the fast oscillations to arbitrary τ. (Remember that the fast-time analysis restricted us to considering $\tau = O(\sqrt{\varepsilon})$ only!)

Considering $(147)_2$ and inserting the partial derivatives of (148) we have,

$$y_{\vartheta\vartheta}^{(1)} + y^{(1)} = (2A' + \hat{\kappa}A)(\tau)\sin\vartheta - (2B' + \hat{\kappa}B)(\tau)\cos\vartheta. \qquad (149)$$

This equation has a resonant solution (compare the remarks in the section 3.1):

$$y^{(1)} = y_h^{(1)} - \vartheta\left(\left(A' + \frac{\hat{\kappa}}{2}A\right)(\tau)\cos\vartheta + \left(B' + \frac{\hat{\kappa}}{2}B\right)(\tau)\sin\vartheta\right) =: y_h^{(1)} + \vartheta\tilde{y}_p^{(1)}. \qquad (150)$$

If $\tilde{y}_p^{(1)} \neq 0$, the term $\sqrt{\varepsilon}y^{(1)}(\vartheta,\tau) = \sqrt{\varepsilon}y_h^{(1)} + \tau\tilde{y}_p^{(1)}$ in the asymptotic ansatz (144) is no longer negligible compared to the term $y^{(0)}(\vartheta,\tau)$ if $\tau = O(1)$. To exclude resonant solutions like this and thus to make sure that successive terms in our approximation yield systematically smaller and smaller corrections even if $\tau = \sqrt{\varepsilon}\vartheta = O(1)$, we demand that, for fixed τ

$$\sqrt{\varepsilon}y^{(i)}\left(\frac{\tau}{\sqrt{\varepsilon}},\tau\right) \to 0 \qquad \text{as} \qquad \varepsilon \to 0. \qquad (151)$$

Remark: *The condition (151) is known as sub-linear growth condition. In general we impose the condition*

$$\frac{\phi_n(\varepsilon)}{\phi_{n-1}(\varepsilon)}\, u^{(n)}\left(\frac{x_1}{\psi(\varepsilon)}, x_1, x_2, \ldots, x_m\right) \to 0 \quad \text{as} \quad \varepsilon \to 0,\, x_i, i = 1, \ldots, m \text{ fixed} \qquad (152)$$

on the coefficients $u^{(n)}(\eta, x_1, x_2, \ldots, x_m)$ of an asymptotic expansion of (121) (with $\eta = x_1/\psi(\varepsilon) \to \infty$ for $\varepsilon \to 0$ at fixed x_1). The name "sub-linear growth condition" is motivated by the above condition for $\eta = x_1/\varepsilon$ and $\phi_n(\varepsilon) = \varepsilon^n$. In this case,

$$\lim_{\eta\to\infty} \frac{u^{(n)}(\eta, x_1, x_2, \ldots, x_m)}{\eta} = 0 \quad , \quad x_i, i = 1, \ldots, m \text{ fixed.} \qquad (153)$$

and this means the $u^{(n)}$ grow slower (sub-linear) than η for $\eta \to \infty$, or for $\varepsilon \to 0$ at fixed x_1.

Demanding that $y^{(1)}$ contain no "resonant terms" of the type $\vartheta\tilde{y}_p^{(1)}$ leads to

$$A'(\tau) + \frac{\hat{\kappa}}{2}\, A(\tau) = 0 \quad \text{and} \quad B'(\tau) + \frac{\hat{\kappa}}{2}\, B(\tau) = 0. \qquad (154)$$

These equations are solved by

$$A(\tau) = A(0)\exp\left(-\frac{\hat{\kappa}}{2}\tau\right) \quad \text{and} \quad B(\tau) = B(0)\exp\left(-\frac{\hat{\kappa}}{2}\tau\right). \qquad (155)$$

At this point it is reasonable to continue with the expansion of the initial conditions $y(0) = y_0$, $y'(0) = y_0'$. This will provide us with some additional information that will be needed to determine $A(0)$ and $B(0)$. The expansion of the initial conditions is done by inserting $\tau = 0$ and $\vartheta = 0$ into (144). This results in

$$
\begin{aligned}
y_0 &= y^{(0)}(0,0) + \sqrt{\varepsilon}\, y^{(1)}(0,0) + \varepsilon y^{(2)}(0,0) + o(\varepsilon) & (156) \\
y_0' &= \left(\frac{1}{\sqrt{\varepsilon}} y_\vartheta^{(0)} + (y_\tau^{(0)} + y_\vartheta^{(1)}) + \sqrt{\varepsilon}(y_\tau^{(1)} + y_\vartheta^{(2)}) \right)(0,0) + o\!\left(\sqrt{\varepsilon}\right) & (157)
\end{aligned}
$$

Assuming initial conditions of type $y_0 = O(1)$ and $y_0' = O(1)$ and an allowing for small but otherwise arbitrary ε, we conclude that

$$
\begin{aligned}
y^{(0)}(0,0) &= y_0 \\
y^{(i)}(0,0) &= 0 \qquad (i = 1,2,...) \\
y_\vartheta^{(0)}(0,0) &= 0 \qquad\qquad\qquad\quad . \qquad (158) \\
(y_\tau^{(0)} + y_\vartheta^{(1)})(0,0) &= y_0' \\
(y_\tau^{(i)} + y_\vartheta^{(i+1)})(0,0) &= 0 \qquad (i = 1,2,...)
\end{aligned}
$$

Inserting these results into the leading-order solution from (148), and using

$$
y_\vartheta^{(0)} = -A(\tau)\sin\vartheta + B(\tau)\cos\vartheta , \qquad (159)
$$

we derive initial data for A and B,

$$
\begin{aligned}
y^{(0)}(0,0) &= A(0) + 1 & \Rightarrow \quad A(0) &= y_0 - 1 \\
y_\vartheta^{(0)}(0,0) &= B(0) & \Rightarrow \quad B(0) &= 0 \, .
\end{aligned} \qquad (160)
$$

Thus, with (155) and (148) we obtain the leading-order multiple-scales solution,

$$
y^{(0)}(\vartheta, \tau) = (y_0 - 1)\exp\left(-\frac{\hat{\kappa}}{2}\tau \right)\cos\vartheta + \cos\tau \, . \qquad (161)
$$

Remark: *We have used the initial conditions exclusively at $\vartheta = \tau = 0$, but not for $\vartheta = 0$ and arbitrary τ. The latter would be incorrect, because in the ϑ,τ–plane, for fixed system parameters μ, κ, i.e., for fixed ε, the solution evolves along a straight line through the origin in the ϑ, τ–plane as shown*
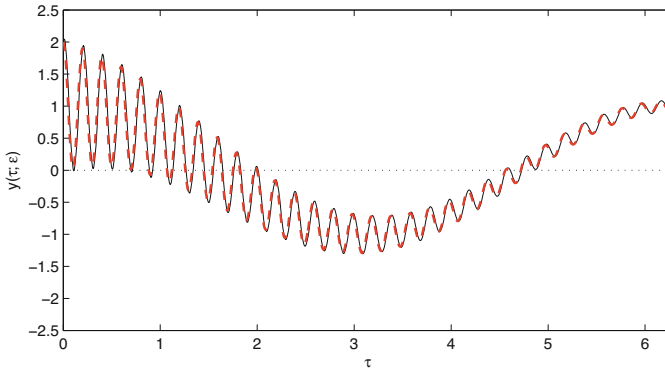
Figure 13. Asymptotic multiscale expansion of the solution in τ and ϑ with $\varepsilon = 0.001$, $\hat{\kappa} = 0.8$ and initial conditions $y_0 = 2$ and $y_0' = 10$. Exact solution: black line, $y^{(0)}(\tau; \varepsilon)$: red dashed line

in Fig. 12. Obviously, at physical time $t = 0$, we access the asymptotic solutions $y^{(i)}(\vartheta, \tau)$ at $\vartheta = \tau = 0$.

Figure 13 displays the leading-order and exact solutions for $y_0 = 2; y_0' = 0$, i.e., for a setting in which $y_0 = O_s(1)$ and $y_0' = O_s(1)$. The agreement is convincing, even after many of the fast oscillation cycles, and for times $\tau = O(1)$.

Remark: *We observe that the leading-order multiple scales solution from Fig. 13 nowhere makes explicit use of the velocity initial datum, $y(0) = y_0'$. This raises several questions:*

1. *Why is that?*
2. *How will we account for this second initial condition in the present expansion scheme?*
3. *What kind of initial data would be required to make the initial velocity show up in the leading-order solution?*

3.5   Some comments and a question

Multiple-Scales Asymptotics is
- a direct, constructive approach to approximate model reduction,
- first of all a *formal* approach; rigorous justification of any specific asymptotic expansion must generally be handled on a case-by-case basis,
- a means to systematically describe scale interactions,

Multiple-Scales Asymptotics is *not*
- a techique for deriving "the" general solution to any given pde- or related problem,
- a cure to all multiscale problems; problems involving a continuous range of interacting scales as observed, e.g., in turbulent flows, cannot be handled by multiple scales asymptotics (at least not in a straightforward fashion.

Having read this section, how would you describe a "scale", and how would you mathematically describe scale-separation in a class of problems?

4 Universal parameters, distinguished limits, and non-dimensionalization

One important aim of theoretical meteorology is the development of simplified model equations that describe the large variety of scale-dependent phenomena observed in atmospheric flows. Here we summarize the basic scaling arguments that justify a unified approach to the derivation of such models based on multiple scales asymptotic techniques. The approach was proposed by Klein (2004) and has led to or been an important part of several recent new developments, Majda and Klein (2003), Klein et al. (2004), Majda and Biello (2004), Mikusky et al. (2005), Biello and Majda (2006), Klein and Majda (2006), and references therein. Remarkably, Keller and Ting (1951) already anticipated the foundations of this approach in an internal report of the Institute for Mathematics and Mechanics of New York University.

To elucidate our main points, we restrict the discussion here to inviscid compressible flows on a rotating sphere. Diabatic effects, such as radiation, water phase transitions, or turbulent transport will be represented as lumped terms in the governing equations to be specified later. Extensions of the framework to include moist processes have been developed by Klein and Majda (2006).

4.1 Universal parameters and distinguished limits

Table 1 displays several physical variables that are characteristic of atmospheric flows, and that are valid independently of the typical length and time scales of any specific flow phenomenon: The mean sea level pressure p_{ref} is set by the requirement that it balance the weight of a vertical column of air. Thus, it is directly given by the total mass of the atmosphere which, to a very good approximation, is evenly distributed over the sphere. A reference temperature T_{ref} is set roughly by the global radiation balance which, even

Earth's radius	a	$=$	$6 \cdot 10^6$	m
Earth's rotation rate	Ω	$\sim$	10^{-4}	s^{-1}
Acceleration of gravity	g	$=$	9.81	ms^{-2}
Sea level pressure	p_{ref}	$=$	10^5	Pa
Water freezing temperature	T_{ref}	$\sim$	273	K
Equator–pole temperature difference	$\Delta T|_{\mathrm{eq}}^{\mathrm{p}}$	$\sim$	50	K
Dry air gas constant	R	$=$	287	$\mathrm{ms}^{-2}/\mathrm{K}$
Dry air isentropic exponent	γ	$=$	1.4	

Table 1. Universal characteristics of atmospheric motions.

without greenhouse gases, would render the mean near-surface air temperature near 250K. The actual value in Table 1 is the freezing temperature of water under standard conditions, i.e., $T_{\mathrm{ref}} \sim 273$K, which is about midway between the observed maximal and minimal near-surface air temperatures. The equator-to-pole air temperature difference near the surface, $\Delta T|_{\mathrm{eq}}^{\mathrm{p}}$, is a consequence of the latitudinal variation of the sun's irradiation. The dry air gas constant, R, and isentropic exponent, γ, as thermodynamic properties are also universally characteristic for atmospheric flows, because their variations due to admixtures of water vapor, trace gases, and the like are no larger than a few percent in general.

Based on these eight basic reference quantities, four independent dimensionless combinations can be composed. To define combinations with intuitive interpretations, we introduce as auxiliary quantities the pressure scale height, h_{sc}, the characteristic speed c_{ref} of barotropic[1] gravity waves, and a reference density, ϱ_{ref}, via

$$
\begin{aligned}
h_{\mathrm{sc}} &= p_{\mathrm{ref}}/(g\,\rho_{\mathrm{ref}}) & \sim & \quad 10 & \text{km} \\
c_{\mathrm{ref}} &= \sqrt{gh_{\mathrm{sc}}} & \sim & \quad 300 & \mathrm{ms}^{-1} \\
\rho_{\mathrm{ref}} &= p_{\mathrm{ref}}/(R\,T_{\mathrm{ref}}) & \sim & \quad 1 & \mathrm{kgm}^{-3}.
\end{aligned}
\tag{162}
$$

---

[1] Atmospheric flow modes are called "barotropic" if their structure is homogeneous in the vertical direction.

Then we let

$$\Pi_1 \;=\; \frac{h_{\mathrm{sc}}}{a} \quad\sim\quad 1.67\cdot 10^{-3}\,,$$

$$\Pi_2 \;=\; \frac{\Delta T|_{\mathrm{eq}}^{\mathrm{p}}}{T_{\mathrm{ref}}} \quad\sim\quad 0.18\,, \tag{163}$$

$$\Pi_3 \;=\; \frac{c_{\mathrm{ref}}}{\Omega a} \quad\sim\quad 0.5\,.$$

The interpretations of Π_1 and Π_2 should be obvious, while the parameter Π_3 compares a typical barotropic gravity wave speed with the tangential speed of points on the equator as induced by Earth's rotation.

Remark: *The sound speed,* $\sqrt{\gamma p_{\mathrm{ref}}/\rho_{\mathrm{ref}}}$ *is comparable to the barotropic wave speed,* $c_{\mathrm{ref}} = \sqrt{g h_{\mathrm{sc}}}$ *according to (162).*

The parameter Π_1 is definitely quite small. Π_2 is not extremely small, yet, many successful developments in theoretical meteorology have relied on scale analysis (asymptotics) in terms of, e.g., Rossby numbers or internal wave Froude numbers with values in a similar range. Finally, for Π_3 one may argue that, even though it is less than unity, one may be hard pressed to consider it "asymptotically small". Deviating somewhat from our earlier work cited above, we will consider $\Pi_3 \ll 1$ in the present notes.

There is little hope for success with asymptotic expansions that would allow Π_1, Π_2, and Π_3 to vary *independently* in a limit process: even for the simple example of a linear oscillator such expansions in two independent parameters were found in section 3 not to exist! Thus, for the present parameters we need to adopt a distinguished limit, and we investigate the following scaling relationships below,

$$\Pi_1 \sim \varepsilon^3\,, \qquad \Pi_2 \sim \varepsilon\,, \qquad \Pi_3 \sim \sqrt{\varepsilon}\,, \qquad \text{as} \qquad \varepsilon \to 0\,. \tag{164}$$

These limits are compatible with the estimates in (163) for actual values of $\varepsilon \in [1/7 \ldots 1/8]$. We will adopt ε as the reference expansion parameter for asymptotic analyses below, and any additional small or large non-dimensional parameter that may be associated with singular perturbations in the governing equations is subsequently tied to ε through suitable further distinguished limits.

Remark: *Before we proceed to do so, we notice that Keller and Ting (1951) already proposed to use the acceleration ratio,* $\varepsilon \sim (a\Omega^2/g)^{1/3} = (\Pi_1/\Pi_3^2)^{1/3}$, *as a basic expansion parameter for meteorological modelling. When* $\Pi_3 = O(1)$, *this is equivalent to (164) above.*

Remark: *In contrast to (164), in my earlier work I have usually let $\Pi_3 = O(1)$. The present, slightly modified limit I introduce because it appears to unify current developments of planetary balanced models by my colleague Stamen Dolaptchiev with Pedlosky's derivations of the quasi-geostrophic theory in (Pedlosky (1987)).*

4.2   Nondimensionalization and general multiple scales ansatz

With p_{ref} and T_{ref}, and through the ideal gas equation of state, $\rho = p/RT$, Table 1 immediately suggests reference values for the nondimensionalization of pressure, temperature, and density. But what about velocity, length, and time?

Hydrostatic–geostrophic velocity scale   Most theories for atmospheric flows rely on the assumption that typical flow speeds are small compared with the speed of barotropic gravity waves c_{ref} which, except for a factor of $\sqrt{\gamma}$, matches the speed of sound. Here and in the rest of this section we make this assumption explicit by introducing a reference speed

$$u_{\mathrm{ref}} = \frac{g h_{\mathrm{sc}}}{\Omega a} \frac{\Delta T|_{\mathrm{eq}}^{\mathrm{p}}}{T_{\mathrm{ref}}} = c_{\mathrm{ref}} \Pi_2 \Pi_3 \sim \varepsilon^{\frac{3}{2}} c_{\mathrm{ref}} \qquad (165)$$

for the nondimensionalization of the flow velocity. (What is a typical value for u_{ref}?) The reader may verify that the above expression has in fact the dimension of a velocity, but what is the motivation for this choice? We will resolve this question later when we (re-)derive the quasi-geostrophic theory (QG). (See also the **Remark** at the end of this section!)

The choice of a velocity scale in (165) allows us to express two classical non-dimensional parameters of theoretical meteorology (and fluid dynamics), the (barotropic) Froude and Mach numbers, in terms of our small parameter,

$$\overline{\mathrm{Fr}} = \frac{\mathrm{M}}{\sqrt{\gamma}} = \frac{u_{\mathrm{ref}}}{c_{\mathrm{ref}}} \sim \varepsilon^{\frac{3}{2}} \qquad \text{as} \qquad \varepsilon \to 0 \,. \qquad (166)$$

Scaling of space and time   As we are interested in multiple scales problems, and will consistently take into account different characteristic lengths in our analyses, the specific choice of reference length and time scales for non-dimensionalization should not make much of a difference. We opt here to use, h_{sc}, i.e., the smallest length scale that suggests itself just from the fundamental parameters in Table 1 via equation (162), to non-dimensionalize all lengths. The associated advection time serves as a

reference time. Thus,

$$\ell_{\mathrm{ref}} = h_{\mathrm{sc}} \qquad \text{and} \qquad t_{\mathrm{ref}} = \frac{h_{\mathrm{sc}}}{u_{\mathrm{ref}}} . \tag{167}$$

Questions
- What would be the scaling in terms of ε of the Froude number based on a typical internal gravity wave speed*?
- What would be the scaling of the Rossby number based on our reference length, h_{sc}*?
- By what power of $1/\varepsilon$ is the internal Rossby radius larger than h_{sc}*?
- By what power of $1/\varepsilon$ is the Obhoukhov or *external* Rossby radius larger than h_{sc}?
- By what power of $1/\varepsilon$ is the Obhoukhov or *external* Rossby radius larger than the internal Rossby radius? — Compare your result with a related remark in Pedlosky (1987).
- Does the Oboukhov or *external* Rossby radius come out larger, comparable or smaller than the Earth radius, a, which is representative of the planetary scale?

* It is safe to assume that the variation of potential temperature across the troposphere is comparable to the equator-pole temperature difference, $\Delta T|_{\mathrm{eq}}^{\mathrm{p}}$.

4.3 Scaled governing equations and general multiple scales expansion scheme

With these scalings, the nondimensional governing equations in the rotating earth system may be written as

$$\boldsymbol{v}_{\|,t} + \boldsymbol{v}_{\|} \cdot \nabla_{\|} \boldsymbol{v}_{\|} + w \boldsymbol{v}_{\|,z} + \varepsilon\, 2(\boldsymbol{\Omega} \times \boldsymbol{v})_{\|} + \frac{1}{\varepsilon^3}\, \frac{1}{\rho} \nabla_{\|} p \;=\; \boldsymbol{Q}_{\boldsymbol{v}_{\|}} ,$$

$$w_t + \boldsymbol{v}_{\|} \cdot \nabla_{\|} w + w w_z + \varepsilon\, 2(\boldsymbol{\Omega} \times \boldsymbol{v})_{\perp} + \frac{1}{\varepsilon^3}\, \frac{1}{\rho} p_z \;=\; Q_w - \frac{1}{\varepsilon^3} ,$$

$$p_t + \boldsymbol{v}_{\|} \cdot \nabla_{\|} p + w p_z + \gamma p\, \nabla \cdot \boldsymbol{v} \;=\; Q_p ,$$

$$\Theta_t + \boldsymbol{v}_{\|} \cdot \nabla_{\|} \Theta + w \Theta_z \;=\; Q_\Theta ,$$

$$\tag{168}$$

where

$$\Theta = \frac{p^{1/\gamma}}{\rho} \tag{169}$$

is the dimensionless potential temperature, $\boldsymbol{k}$ is the local vertical unit vector indicating the direction of the acceleration of gravity. The terms $\boldsymbol{Q}_{\boldsymbol{v}}, Q_p,$

and Q_Θ represent additional effects which in a concrete application may stem from turbulence closures or similar models for the net influence of non-resolved scales.

Klein (2004) suggested to consider the small parameter ε as introduced above as *the* general singular asymptotic expansion parameter for theoretical developments in meteorology (although suggesting a slightly different distinguished limit for Π_3 from (163)). To this end, the solution vector $\mathcal{U} = (p, \Theta, \boldsymbol{v})$ is expanded in powers of ε (or some fractional power thereof), and all expansion functions would depend on a series of space-time coordinates that are scaled again by powers of ε. The most straightforward version of such a scheme reads

$$\mathcal{U}(u, z, t, ; \varepsilon) = \sum_i \varepsilon^i \mathcal{U}^{(i)}\left(\ldots, \frac{t}{\varepsilon}, t, \varepsilon t, \ldots, \frac{\boldsymbol{x}}{\varepsilon}, \boldsymbol{x}, \varepsilon \boldsymbol{x}, \ldots \frac{z}{\varepsilon}, z, \ldots\right). \quad (170)$$

In practical applications it might be necessary to work with fractional powers of ε for the scaling of the coordinates, or more general asymptotic sequences, $\phi^{(i)}(\varepsilon)$, as explained in the context of (121) in section 3.

In a number of publications, e.g., Majda and Klein (2003); Klein (2004); Klein et al. (2004); Klein (2005), we have demonstrated that a wide range of known simplified model equations of theoretical meteorology can be rederived in a unified fashion starting from the full compressible flow equations in (168) and suitable specializations of the multi-scale ansatz in (170). To derive a typical existing model, one would maintain one scaled time, one scaled horizontal coordinate, and one pair of scaled vertical coordinates, respectively, and this we consider a welcome "validation" of the approach. We will demonstrate the procedure in the next chapter.

Of course, such "validation studies" are but a first step, as (170) strongly suggests itself as the basis for systematic studies of multiple scales interactions. See Majda and Klein (2003), Majda and Biello (2004), Klein et al. (2004), Biello and Majda (2006), Klein and Majda (2006) for related developments.

Remark: *The particular choice of a reference velocity in (165) does in no way restrict our degrees of freedom in constructing simplified asymptotic models. If, for example, we were to consider flows that are inherently compressible, so that systematically $|\boldsymbol{v}| \sim c_{\text{ref}}$, then the asymptotic expansion scheme for the (dimensionless) flow velocity would simply have to read*

$$\boldsymbol{v} = \frac{1}{\varepsilon^{\frac{3}{2}}}\left(\sum_i \varepsilon^i \boldsymbol{v}^{(i)}(\ldots, \frac{u}{\varepsilon}, u, \varepsilon u, \ldots \frac{z}{\varepsilon}, z, \ldots \frac{t}{\varepsilon}, t, \varepsilon t, \ldots)\right). \quad (171)$$

5 (Re-)derivation of the quasi-geostrophic (QG) theory

In this chapter, we employ the general asymptotics-based approach from section 4 to rederive the quasi-geostrophic model, see Pedlosky (1987).

5.1 Asymptotic expansion scheme

For the derivation of this theory, we will take the dimensionless form of the compressible flow equations from (168) as our point of departure. For simplicity of the exposition we assume adiabatic flow, dropping the source and transport terms in the governing equations. Then (168) simplifies to

$$
\begin{aligned}
\varrho_t + \boldsymbol{v}_{\shortparallel} \cdot \nabla_{\shortparallel} \varrho \; + \; w\varrho_z \quad + \quad \varrho\,(\nabla_{\shortparallel} \cdot \boldsymbol{v}_{\shortparallel} + w_z) \qquad\qquad &= \; 0\,, \\[4pt]
\boldsymbol{v}_{\shortparallel,t} + \boldsymbol{v}_{\shortparallel} \cdot \nabla_{\shortparallel} \boldsymbol{v}_{\shortparallel} + w\boldsymbol{v}_{\shortparallel,z} \; + \; \varepsilon\,2(\boldsymbol{\Omega} \times \boldsymbol{v})_{\shortparallel} + \frac{1}{\varepsilon^3}\,\frac{1}{\rho}\nabla_{\shortparallel} p &= \; 0\,, \\[4pt]
w_t + \boldsymbol{v}_{\shortparallel} \cdot \nabla_{\shortparallel} w \; + \; ww_z \quad + \; \varepsilon\,2(\boldsymbol{\Omega} \times \boldsymbol{v})_{\perp} + \frac{1}{\varepsilon^3}\,\frac{1}{\rho}p_z &= \; -\frac{1}{\varepsilon^3}\,, \\[4pt]
\Theta_t + \boldsymbol{v}_{\shortparallel} \cdot \nabla_{\shortparallel} \Theta \; + \; w\Theta_z \qquad\qquad &= \; 0\,,
\end{aligned}
\tag{172}
$$

and

$$
\Theta = \frac{p^{1/\gamma}}{\rho}\,. \tag{173}
$$

The quasi-geostrophic theory is designed to address flows on length scales comparable to the *internal Rossby radius*, and on time scales corresponding to horizontal advection across such distances. How can we access these length and time scales within our multiple scales asymptotic scheme?

The *internal Rossby radius* is defined as the distance which an internal gravity wave would travel during a characteristic Earth rotation time. This is equivalent to requiring

$$
L_{\mathrm{Ro}} = \frac{Nh_{\mathrm{sc}}}{\Omega}\,, \tag{174}
$$

where

$$
N = \sqrt{\frac{g}{\Theta}\frac{\partial\Theta}{\partial z'}} \tag{175}
$$

is the so-called Brunt-Väisälä or buoyancy frequency, and

$$
Nh_{\mathrm{sc}} = \sqrt{gh_{\mathrm{sc}}}\,\sqrt{\frac{h_{\mathrm{sc}}}{\Theta}\frac{\partial\Theta}{\partial z'}} = c_{\mathrm{ref}}\,\sqrt{\frac{h_{\mathrm{sc}}}{\Theta}\frac{\partial\Theta}{\partial z'}} \tag{176}
$$

is a typical travelling speed of internal gravity waves. The reader may want to consult the established literature for corroboration.

Remark: *Here and below, primes mark dimensional variables!*

Remark: *Another interpretation of the internal Rossby radius considers it the characteristic distance which an internal gravity wave would have to travel to become affected by the Coriolis effect.*

Non-dimensionalizing L_{Ro} by our reference length, $\ell_{\mathrm{ref}} = h_{\mathrm{sc}}$, and using the above we find

$$\frac{L_{\mathrm{Ro}}}{h_{\mathrm{sc}}} = \frac{N}{\Omega} = \frac{c_{\mathrm{ref}}}{\Omega h_{\mathrm{sc}}} \sqrt{\frac{h_{\mathrm{sc}}}{\Theta} \frac{\partial \Theta}{\partial z'}} \sim \frac{c_{\mathrm{ref}}}{\Omega a} \frac{a}{h_{\mathrm{sc}}} \sqrt{\frac{\Delta T|_{\mathrm{eq}}^{\mathrm{p}}}{T_{\mathrm{ref}}}} = \Pi_3\,\Pi_1\,\sqrt{\Pi_2} \qquad (177)$$

or, using the distinguished limits introduced earlier for the Π_i,

$$\frac{L_{\mathrm{Ro}}}{h_{\mathrm{sc}}} = O\left(\varepsilon^{\frac{1}{2}}\, \frac{1}{\varepsilon^3}\, \varepsilon^{\frac{1}{2}} \right) = O\left(\frac{1}{\varepsilon^2} \right), \qquad (178)$$

Here we have used the scalings of our fundamental parameters from Table 1 as discussed in (162)–(164), and the well established observation, [Schneider (2006); Frierson (2008)], that the equator-to-pole temperature differences are comparable to the vertical potential temperature variations across the troposphere, so that

$$\frac{h_{\mathrm{sc}}}{\Theta} \frac{\partial \Theta}{\partial z} \sim \frac{\Delta T|_{\mathrm{eq}}^{\mathrm{p}}}{T_{\mathrm{ref}}}. \qquad (179)$$

With the estimate in (178), if we want to describe horizontal variations on scales comparable to L_{Ro}, we should use the dimensionless horizontal coordinate

$$\boldsymbol{\xi} = \frac{\boldsymbol{x}'}{L_{\mathrm{Ro}}} = \frac{h_{\mathrm{sc}}}{L_{\mathrm{Ro}}} \frac{\boldsymbol{x}'}{h_{\mathrm{sc}}} = \varepsilon^2\, \boldsymbol{x}. \qquad (180)$$

We will be interested here in phenomena associated with advection over distances of L_{Ro}, so we will use the time variable

$$\tau = \frac{t'}{L_{\mathrm{Ro}}/u_{\mathrm{ref}}} = \frac{h_{\mathrm{sc}}}{L_{\mathrm{Ro}}} \frac{t'}{h_{\mathrm{sc}}/u_{\mathrm{ref}}} = \varepsilon^2\, t. \qquad (181)$$

Finally, in order to study phenomena which occupy the full depth of the troposphere, we will use a vertical coordinate non-dimensionalized by the pressure scale height, h_{sc}, i.e., we use our original dimensionless coordinate

$$z = \frac{z'}{h_{\mathrm{sc}}}. \qquad (182)$$

These scalings are summarized in Fig. 14.
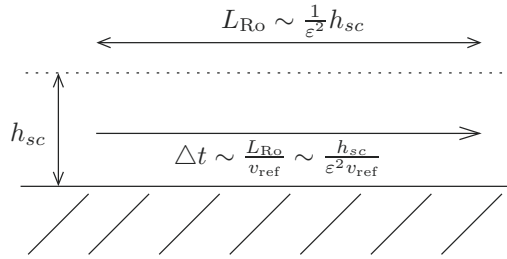
Figure 14. Length and time scales addressed by quasi-geostrophic theory.

Our asymptotic expansion scheme for the solution written in terms of non-dimensional variables will thus read

$$\mathcal{U}(t, \boldsymbol{x}, z; \varepsilon) = \sum_i \varepsilon^i \mathcal{U}^{(i)}(\varepsilon^2 t, \varepsilon^2 \boldsymbol{x}, z), \qquad \mathcal{U} = (p, \Theta, \boldsymbol{v}_{\shortparallel}, w)^t, \qquad (183)$$

which is the announced specialization of the general multiple scales expansion scheme in (170) adapted to resolve advection phenomena on the length scale of the internal Rossby radius.

5.2 Some preliminaries

When inserting this expansion into the governing equations in (172) we will have to account for the following transformation rules for the partial derivatives,

$$\left.\frac{\partial}{\partial t}\right|_{\boldsymbol{x}, z; \varepsilon} = \varepsilon^2 \left.\frac{\partial}{\partial \tau}\right|_{\boldsymbol{\xi}, z; \varepsilon}, \qquad \nabla_{\boldsymbol{x}}\big|_{t, z; \varepsilon} = \varepsilon^2 \nabla_{\boldsymbol{\xi}}\big|_{\tau, z; \varepsilon} . \qquad (184)$$

Here the subscripts indicate which variables are to be held constant when carrying out the partial differentiations.

We also anticipate the following properties of the background stratification of the atmosphere in order to save us some tedious calculations:

$$\begin{aligned}
\varrho(t, \boldsymbol{x}, z; \varepsilon) &= \varrho_0(z) + \varepsilon \varrho_1(z) + \varepsilon^2 \varrho^{(2)}(\tau, \boldsymbol{\xi}, z) + o(\varepsilon^2) , \\[4pt]
p(t, \boldsymbol{x}, z; \varepsilon) &= p_0(z) + \varepsilon p_1(z) + \varepsilon^2 p^{(2)}(\tau, \boldsymbol{\xi}, z) + o(\varepsilon^2) , \\[4pt]
\Theta(t, \boldsymbol{x}, z; \varepsilon) &= 1 + \varepsilon \Theta_1(z) + \varepsilon^2 \Theta^{(2)}(\tau, \boldsymbol{\xi}, z) + o(\varepsilon^2) , \\[4pt]
w(t, \boldsymbol{x}, z; \varepsilon) &= \varepsilon^3 w^{(3)}(\tau, \boldsymbol{\xi}, z) + o(\varepsilon^3) .
\end{aligned} \qquad (185)$$

Remark: *That the leading-order thermodynamic variables are independent of time and do not vary horizontally can actually be derived within the*

present framework rather than having to be anticipated. The same is true for the vanishing of the leading two orders of vertical velocity, $w^{(0)}, w^{(1)}$.

Remark: *The leading-order potential temperature must be a constant, because of the order-of-magnitude analyses of the previous subsection which restrict variations of potential temperature to $\Delta\Theta/T_{ref} = O(\varepsilon)$. We may set this leading-order constant to $\Theta^{(0)} \equiv 1$ by choosing an appropriate reference temperature.*

5.3   Expansions of the governing equations

The next steps are standard procedure. We insert the expansion scheme, collect like powers of ε, and separately equate the sum of these terms to zero, so as to create the usual hierarchy of perturbation equations.

Mass conservation   Expanding the mass conservation law, $(172)_1$, we find

$$
\begin{aligned}
O\!\left(\varepsilon^0\right) &: & \varrho_0\,\nabla_{\boldsymbol{\xi}}\cdot\boldsymbol{v}_{\scriptscriptstyle\|}^{(0)} &= 0\,, \\[4pt]
O(\varepsilon) &: & \varrho_0\,\nabla_{\boldsymbol{\xi}}\cdot\boldsymbol{v}_{\scriptscriptstyle\|}^{(1)} + \frac{\partial}{\partial z}\!\left(\varrho_0 w^{(3)}\right) &= 0\,.
\end{aligned}
\tag{186}
$$

In writing down the terms of $O(\varepsilon)$ we have already neglected $\varrho^{(1)}\nabla_{\boldsymbol{\xi}}\cdot\boldsymbol{v}_{\scriptscriptstyle\|}^{(0)}$ on account of (186).

Horizontal momentum balance

Splitting the Coriolis term   Before expanding the momentum balances, we need to explicitly split the Coriolis term into its horizontal a vertical components.

$$
\begin{aligned}
\boldsymbol{\Omega}\times\boldsymbol{v} &= (\boldsymbol{\Omega}_{\scriptscriptstyle\|} + \boldsymbol{k}\Omega_{\perp})\times(\boldsymbol{v}_{\scriptscriptstyle\|} + \boldsymbol{k}w) \\[4pt]
&= \underbrace{(\boldsymbol{\Omega}_{\scriptscriptstyle\|}\times\boldsymbol{v}_{\scriptscriptstyle\|})}_{=(\boldsymbol{\Omega}\times\boldsymbol{v})_{\perp}} + \underbrace{(\Omega_{\perp}\boldsymbol{k}\times\boldsymbol{v}_{\scriptscriptstyle\|} + w\boldsymbol{\Omega}_{\scriptscriptstyle\|}\times\boldsymbol{k})}_{=(\boldsymbol{\Omega}\times\boldsymbol{v})_{\scriptscriptstyle\|}} + \underbrace{(\Omega_{\perp}w\boldsymbol{k}\times\boldsymbol{k})}_{=0,\text{ as }\boldsymbol{k}\times\boldsymbol{k}=0}\,.
\end{aligned}
\tag{187}
$$

We will need the vertical component of $\boldsymbol{\Omega}$ (see Fig. 15), which we expand
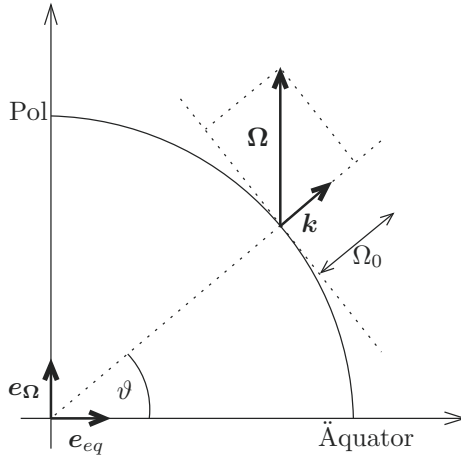
Figure 15. Splitting of the coriolis term into a horizontal and a vertical component.

as

$$
\begin{aligned}
\Omega_\perp &= \boldsymbol{k} \cdot \boldsymbol{\Omega} \\
&= (\boldsymbol{e}_{eq} \cos \vartheta + \boldsymbol{e}_{\boldsymbol{\Omega}} \sin \vartheta) \cdot \boldsymbol{e}_{\boldsymbol{\Omega}} |\boldsymbol{\Omega}| \\
&= |\boldsymbol{\Omega}| \sin \vartheta \\
&= |\boldsymbol{\Omega}| \sin \left(\vartheta_0 + \frac{y'}{a} \right) \\
&= |\boldsymbol{\Omega}| \sin(\vartheta_0 + \varepsilon\, \xi_2) \\
&= \underbrace{|\boldsymbol{\Omega}| \sin(\vartheta_0)}_{=:\Omega_0} + \varepsilon\, \underbrace{|\boldsymbol{\Omega}| \cos(\vartheta_0)}_{=:\beta} \xi_2 + o(\varepsilon) \\
&= \Omega_0 + \varepsilon \beta \xi_2 + o(\varepsilon) \; .
\end{aligned}
\tag{188}
$$

Here we have taken into account that ϑ is the arclength along a longitudinal circle divided by the radius of the reference sphere, a, introduced deviations from a reference latitude, so that $\vartheta = \vartheta_0 + y'/a$, and recalled that $h_{\mathrm{sc}}/a = \varepsilon^3$ and $\xi_2 = \varepsilon^2 y'/h_{\mathrm{sc}}$. The rest is Taylor expansion of the sine function about the reference latitude.

Since $w^{(0)} \equiv w^{(1)} \equiv 0$ we also know that $w \boldsymbol{\Omega}_{\shortparallel} \times \boldsymbol{k} = o(\varepsilon)$ and, in

summary, we find

$$
\begin{aligned}
(\boldsymbol{\Omega} \times \boldsymbol{v})_{\shortparallel} &= (\Omega_0 + \varepsilon\beta\xi_2)\boldsymbol{k} \times \boldsymbol{v}_{\shortparallel} + o(\varepsilon)\,, \\
(\boldsymbol{\Omega} \times \boldsymbol{v})_{\perp} &= \boldsymbol{\Omega}_{\shortparallel} \times \boldsymbol{v}_{\shortparallel}\,.
\end{aligned}
\tag{189}
$$

Expansion of the horizontal momentum balance Consider now the horizontal momentum balance, written in terms of the new variables, $(\tau, \boldsymbol{\xi}, z)$,

$$
\boldsymbol{v}_{\shortparallel\tau} + (\boldsymbol{v}_{\shortparallel} \cdot \nabla_{\boldsymbol{\xi}})\boldsymbol{v}_{\shortparallel} + \frac{1}{\varepsilon^2}\, w\boldsymbol{v}_{\shortparallel z} + \frac{1}{\varepsilon^3}\, \frac{\nabla_{\boldsymbol{\xi}}p}{\varrho} + \frac{1}{\varepsilon}\, (\hat{\boldsymbol{\Omega}} \times \boldsymbol{v})_{\shortparallel} = 0\,.
\tag{190}
$$

Using $w^{(0)} \equiv w^{(1)} \equiv 0$, and that $p^{(0)} \equiv p_0(z)$ and $p^{(1)} \equiv p_1(z)$, we immediately move to the equation at $O(\varepsilon^{-1})$ where we find the *geostrophic balance*,

$$
\Omega_0\, \boldsymbol{k} \times \boldsymbol{v}_{\shortparallel}^{(0)} + \nabla_{\boldsymbol{\xi}}\pi^{(2)} = 0\,, \qquad \text{where} \qquad \pi^{(2)} = \frac{p^{(2)}}{\varrho_0}\,,
\tag{191}
$$

i.e., the balance of the horizontal Coriolis and pressure gradient forces. Geostrophic balance implies that, at leading order, the horizontal flow direction is perpendicular to the horizontal pressure gradient.

We verify for later purposes that

$$
\nabla_{\boldsymbol{\xi}} \cdot \boldsymbol{v}_{\shortparallel}^{(0)} = 0 \qquad \text{and} \qquad \boldsymbol{v}_{\shortparallel}^{(0)} = \frac{1}{\Omega_0}\, \boldsymbol{k} \times \nabla_{\boldsymbol{\xi}}\pi^{(2)}
\tag{192}
$$

by, respectively, applying $(\boldsymbol{k} \cdot (\nabla_{\boldsymbol{\xi}} \times [\cdot]))$ and $(\boldsymbol{k} \times [\cdot])$ to $(191)_1$.

Remark: *With (191) we have found a time-independent constraint on the leading order velocity and second order pressure fields. Such constraints did not exist for the original system of the compressible flow equations! The constraint implies that only if the initial data for a given flow problem satisfy the constraint, at least at the given orders, can we hope that the approximate asymptotic solution will remain close to the exact solution. This kind of "change of type" of the asymptotic limit problem relative to the original one is typical of singular perturbation problems. Also, we recall that we encountered a similar issue with the slow-time expansion for the linear oscillator in chapter 3.*

Vertical momentum balance From the vertical momentum balance we obtain at orders ε^{-5} to ε^{-2}

$$
\frac{\partial p^{(i)}}{\partial z} = -\varrho^{(i)} \qquad (i = 0, 1, 2, 3)\,.
\tag{193}
$$

Expanding the defining equation for the potential temperature, i.e., $\varrho\Theta = p^{\frac{1}{\gamma}}$ into

$$O(\varepsilon^0): \qquad\qquad \varrho_0 = p_0^{\frac{1}{\gamma}}$$

$$O(\varepsilon): \qquad\qquad \varrho_1 + \varrho_0\Theta_1 = p_0^{\frac{1}{\gamma}}\frac{p_1}{\gamma p_0} \qquad\qquad (194)$$

$$O(\varepsilon^2): \qquad \varrho^{(2)} + \varrho_1\Theta_1 + \varrho_0\Theta^{(2)} = p_0^{\frac{1}{\gamma}}\left(\frac{p^{(2)}}{\gamma p_0} + \frac{(1-\gamma)p_1^2}{2\gamma^2 p_0^2}\right)$$

we obtain from (193)

$$p^{(0)-\frac{1}{\gamma}}\frac{\partial p^{(0)}}{\partial z} = -1 \qquad\qquad (195)$$

with the exact solution

$$p_0(z) = \left(1 - \frac{\gamma-1}{\gamma}z\right)^{\frac{\gamma}{\gamma-1}}. \qquad\qquad (196)$$

In a similar way one solves the first order equation explicitly for given $\Theta_1(z)$. We leave this as an exercise.

Evolution of the potential temperature The first non-trivial asymptotic equation is extracted from the potential temperature transport equation at $O(\varepsilon)$, and it reads

$$\left(\frac{\partial}{\partial\tau} + \boldsymbol{v}_{\shortparallel}^{(0)}\cdot\nabla_\xi\right)\Theta^{(2)} + w^{(3)}\frac{d\Theta_1}{dz} = 0. \qquad\qquad (197)$$

5.4 Summary of the leading-order balances

Using the expansion scheme in (185), we have found first that the background structure is in hydrostatic balance, i.e.,

$$\frac{dp_i}{dz} = -\varrho_i \qquad (i = 0, 1). \qquad\qquad (198)$$

The remaining primary unknowns for description of the flow field are then

$$\left(\pi^{(2)}, \boldsymbol{v}_{\shortparallel}^{(0)}, w^{(3)}, \Theta^{(2)}\right)(\tau, \boldsymbol{\xi}, z), \qquad\qquad (199)$$

where $\pi^{(2)} = p^{(2)}/\varrho_0$, and they satisfy the following balance and transport equations:

Hydrostatic Balance

$$\frac{\partial \pi^{(2)}}{\partial z} = \Theta^{(2)} \tag{200}$$

Geostrophic Balance

$$\Omega_0\, \boldsymbol{k} \times \boldsymbol{v}_{\shortparallel}^{(0)} + \nabla_{\boldsymbol{\xi}} \pi^{(2)} = 0 \tag{201}$$

Anelastic Constraint

$$\varrho_0\, \nabla_{\boldsymbol{\xi}} \cdot \boldsymbol{v}_{\shortparallel}^{(1)} + \frac{\partial}{\partial z}\left(\varrho_0 w^{(3)}\right) = 0 \tag{202}$$

Potential Temperature Transport

$$\left(\frac{\partial}{\partial \tau} + \boldsymbol{v}_{\shortparallel}^{(0)} \cdot \nabla_{\boldsymbol{\xi}}\right)\Theta^{(2)} + w^{(3)}\frac{d\Theta_1}{dz} = 0 \tag{203}$$

If it were not for the appearance of the first-order divergence, $\nabla_{\boldsymbol{\xi}} \cdot \boldsymbol{v}_{\shortparallel}^{(1)}$ in (202), we would have the same number of equations as we have unknowns. As it is, the system is as yet unclosed. We will extract additional information on $\nabla_{\boldsymbol{\xi}} \cdot \boldsymbol{v}_{\shortparallel}^{(1)}$ from the next higher order horizontal momentum equation in the next section in the form of a *solvability condition* that may be interpreted as a vorticity transport equation,

First-Order Solvability Condition / Vorticity Transport Equation

$$\left(\partial_\tau + \boldsymbol{v}_{\shortparallel}^{(0)} \cdot \nabla_{\boldsymbol{\xi}}\right)(\zeta^{(0)} + \beta\xi_2) + \Omega_0 \nabla_{\boldsymbol{\xi}} \cdot \boldsymbol{v}_{\shortparallel}^{(1)} = 0\,. \tag{204}$$

where,

$$\zeta^{(0)} = \boldsymbol{k} \cdot (\nabla_{\boldsymbol{\xi}} \times \boldsymbol{v}_{\shortparallel}^{(0)})\,, \tag{205}$$

is the vorticity of the leading-order velocity field.

This completes the summary of the quasi-geostrophic model equations.

Remark: *We have given the QG equations here in a somewhat unusual form, sticking as closely as possible to the original equations. In this way, it remains transparent that (200) and (201) are direct consequences of the vertical and horizontal momentum balances, respectively, (202) emerges from mass conservation, and (203) from the potential temperature transport*

equation. These equations can all directly be read off the original equations at the appropriate orders in the asymptotic expansion.

The closure for $\nabla_{\boldsymbol{\xi}} \cdot \boldsymbol{v}_{\parallel}^{(1)}$ in (204) emerges as a solvability condition at $O(\varepsilon^0)$ in the horizontal momentum balance as will be shown in the next section.

Remark: *As can see clearly in the present summary of our asymptotic limit equations, considering large spacial and long time scales only implies strong constraints on the solutions. Instead of evolution equations for the primary unknowns in the compressible flow equations (the densities of mass, momentum, and energy) we find three time independent constraints or balances! Only the potential temperature evolution equation in (203) and the vorticity transport equation in (204) have maintained the original "prognostic" (time evolution) character.*

5.5   First-order solvability condition / existence of $\nabla_{\boldsymbol{\xi}} p^{(3)}$

Consider the scaled horizontal momentum balance from (190), which we had already written in terms of our new coordinates, $(\tau, \boldsymbol{\xi}, z)$, at $O(\varepsilon^0)$,

$$(\boldsymbol{v}_{\parallel}^{(0)})_\tau + (\boldsymbol{v}_{\parallel}^{(0)} \cdot \nabla_{\boldsymbol{\xi}})\boldsymbol{v}_{\parallel}^{(0)} + \left[\frac{\nabla_{\boldsymbol{\xi}} p}{\varrho}\right]^{(3)} + \Omega_0 \, \boldsymbol{k} \times \boldsymbol{v}_{\parallel}^{(1)} + \beta\xi_2 \boldsymbol{k} \times \boldsymbol{v}_{\parallel}^{(0)} = 0 \,. \quad (206)$$

Using the fact that ϱ_0, ϱ_1 depend on z only, so that $\nabla_{\boldsymbol{\xi}} \varrho_0 = \nabla_{\boldsymbol{\xi}} \varrho_1 = 0$, and $\pi^{(i)} = p^{(i)}/\varrho_0$ we rewrite the pressure gradient term as

$$\left[\frac{\nabla_{\boldsymbol{\xi}} p}{\varrho}\right]^{(3)} = \frac{1}{\varrho_0}\nabla_{\boldsymbol{\xi}} p^{(3)} - \frac{\varrho_1}{\varrho_0^2}\nabla_{\boldsymbol{\xi}} p^{(2)} = \nabla_{\boldsymbol{\xi}} \pi^{(3)} - \nabla_{\boldsymbol{\xi}}\left(\frac{\varrho_1}{\varrho_0}\, \pi^{(2)}\right). \quad (207)$$

Next we regroup (206) into first-order "geostrophic terms" on left-hand side and terms that distort the geostrophic balance, i.e., "ageostrophic terms", on the right,

$$\nabla_{\boldsymbol{\xi}} \pi^{(3)} + \Omega_0 \, \boldsymbol{k} \times \boldsymbol{v}_{\parallel}^{(1)} =$$
$$-\left((\boldsymbol{v}_{\parallel}^{(0)})_\tau + (\boldsymbol{v}_{\parallel}^{(0)} \cdot \nabla_{\boldsymbol{\xi}})\boldsymbol{v}_{\parallel}^{(0)} + \beta\xi_2 \boldsymbol{k} \times \boldsymbol{v}_{\parallel}^{(0)} - \nabla_{\boldsymbol{\xi}}\left(\frac{\varrho_1}{\varrho_0}\pi^{(2)}\right)\right). \quad (208)$$

We know that any gradient of a scalar is curl-free. In particular,

$$\boldsymbol{k} \cdot (\nabla_{\boldsymbol{\xi}} \times \nabla_{\boldsymbol{\xi}} \phi) \equiv 0 \quad (209)$$

for any scalar function $\phi(\boldsymbol{\xi})$ that is sufficiently smooth. By applying the operator $\boldsymbol{k} \cdot (\nabla_{\boldsymbol{\xi}} \times [\,\cdot\,])$ to (208) we thus eliminate the terms involving $\pi^{(2)}$

and $\pi^{(3)}$. The remaining terms become

$$
\begin{aligned}
\boldsymbol{k} \cdot \left(\nabla_{\boldsymbol{\xi}} \times \left(\Omega_0 \, \boldsymbol{k} \times \boldsymbol{v}_{\shortparallel}^{(1)} \right) \right) &= \Omega_0 \boldsymbol{k} \cdot \left(\boldsymbol{k} \left(\nabla_{\boldsymbol{\xi}} \cdot \boldsymbol{v}_{\shortparallel}^{(1)} \right) \right) \\
&= \Omega_0 \, \nabla_{\boldsymbol{\xi}} \cdot \boldsymbol{v}_{\shortparallel}^{(1)} \,,
\end{aligned}
$$

$$
\boldsymbol{k} \cdot \left(\nabla_{\boldsymbol{\xi}} \times (\boldsymbol{v}_{\shortparallel}^{(0)})_{\tau} \right) = \zeta_{\tau}^{(0)} \,,
$$

$$
\boldsymbol{k} \cdot \left(\nabla_{\boldsymbol{\xi}} \times \left((\boldsymbol{v}_{\shortparallel}^{(0)} \cdot \nabla_{\boldsymbol{\xi}}) \boldsymbol{v}_{\shortparallel}^{(0)} \right) \right) = \boldsymbol{v}_{\shortparallel}^{(0)} \cdot \nabla_{\boldsymbol{\xi}} \zeta^{(0)} \,, \tag{210}
$$

$$
\begin{aligned}
\boldsymbol{k} \cdot \left(\nabla_{\boldsymbol{\xi}} \times \left(\beta \xi_2 \, \boldsymbol{k} \times \boldsymbol{v}_{\shortparallel}^{(0)} \right) \right) &= \beta \, \boldsymbol{k} \cdot \boldsymbol{k} \left(\nabla_{\boldsymbol{\xi}} \xi_2 \cdot \boldsymbol{v}_{\shortparallel}^{(0)} \right) \\
&= \beta v^{(0)} \\
&= \beta \left(\frac{\partial}{\partial \tau} + \boldsymbol{v}_{\shortparallel}^{(0)} \cdot \nabla_{\boldsymbol{\xi}} \right) \xi_2 \,.
\end{aligned}
$$

Collecting, we find the vorticity transport equation,

$$
\left(\partial_{\tau} + \boldsymbol{v}_{\shortparallel}^{(0)} \cdot \nabla_{\boldsymbol{\xi}} \right) (\zeta^{(0)} + \beta \xi_2) + \Omega_0 \nabla_{\boldsymbol{\xi}} \cdot \boldsymbol{v}_{\shortparallel}^{(1)} = 0 \,, \tag{211}
$$

as announced in (204).

5.6   Classical formulation of the QG-theory and PV transport

In (201)–(204) we have taken care to display the quasi-geostrophic balance equations in a form that reveals their close connection to the mass, momentum, and potential temperature evolution equations. This may not be the most practicable description in many applications, and it hides the central role of *potential vorticity (PV)* in the quasi-geostrophic regime.

In fact, one can rewrite (211) as a transport equation for the QG-potential vorticity,

$$
q = \zeta^{(0)} + \beta \, \xi_2 + \frac{\Omega_0}{\varrho_0} \frac{\partial}{\partial z} \left(\frac{\varrho_0 \Theta^{(2)}}{\Theta_1'} \right) \qquad \text{with} \qquad \Theta_1' = d\Theta_1/dz \,, \tag{212}
$$

which then reads

$$
\left(\partial_{\tau} + \boldsymbol{v}_{\shortparallel}^{(0)} \cdot \nabla_{\boldsymbol{\xi}} \right) q = 0 \,. \tag{213}
$$

Equipped with the additional constitutive relations

$$
\begin{aligned}
\boldsymbol{v}_{\shortparallel}^{(0)} &= \frac{1}{\Omega_0}\boldsymbol{k} \times \nabla_{\xi} p^{(2)} \,, \\
\Theta^{(2)} &= \frac{\partial \pi^{(2)}}{\partial z} \,, \\
\zeta^{(0)} &= \boldsymbol{k} \cdot \left(\nabla_{\xi} \times \boldsymbol{v}_{\shortparallel}^{(0)} \right) = \frac{1}{\Omega_0}\nabla_{\xi}^2 \pi^{(2)}
\end{aligned}
\tag{214}
$$

we have the QG theory in its classical form (Pedlosky (1987)): Equation (213) describes advection of potential vorticity by the leading order velocity field $\boldsymbol{v}_{\shortparallel}^{(0)}$, which can be expressed in terms of the pressure gradient $\nabla_{\xi}\pi^{(2)}$ according to $(214)_1$. Given the (advected) PV-field, one can retrieve the pressure field solving the ellliptic equation that results from inserting $(214)_{2,3}$ into (212), viz.

$$
\nabla_{\xi}^2 \pi^{(2)} + \frac{\Omega_0^2}{\varrho_0}\frac{\partial}{\partial z}\left(\frac{\varrho_0}{\Theta_1'}\frac{\partial \pi^{(2)}}{\partial z} \right) = q - \beta \, \xi_2 \,.
\tag{215}
$$

Appendix

Gauß' Integral Theorem

Let $\Omega \subset \boldsymbol{R}$ be a compact subset with a smooth boundary, $\boldsymbol{n} : \partial\Omega \to \boldsymbol{R}^n$ the field of outer unit normal vectors and $U \supset \Omega$ an open subset of $\boldsymbol{R}^n$. Then for every continuous differentiable vector field $F : U \to \boldsymbol{R}^n$ the following is true

$$
\int_{\Omega} \nabla \cdot F(x) \; dV = \int_{\partial\Omega} F(x) \cdot \boldsymbol{n} \; d\sigma
$$

Proof see (Forster, 1984, S. 155)

The symbols $O()$ and $o()$ (Landau's symbols)

The symbol $O()$ is used in this text in two ways. One formulation is based on the so called Landau symbol. Here, for functions f and g the equity holds

$$
f(x) = O(g(x)) \qquad \text{as} \qquad x \to a
$$

if and only if $f(x)/g(x) \to const.$ for $x \to a$ (in the asymptotic sense). On the other hand the symbol is often used in the way that the statement „the quantity X is $O(\epsilon)$" means that X is of the same order of magnitude as ϵ. The particular meaning of $O(\,\cdot\,)$ will be clear from the context.

The second Landau symbol $o(\,\cdot\,)$ ("little oh"). For functions f and g we have

$$f(x) = o(g(x)) \quad \text{as} \quad x \to a \quad,$$

if and only if $f(x)/g(x) \to 0$ for $x \to a$.

If for some function f we not only have $f(x) = O(g(x))$ but also $g(x) = O(f(x))$ as $x \to a$, then $f(x) = O_s(g(x))$ as $x \to a$.

Vector identities

For vectors $\boldsymbol{A}, \boldsymbol{B}, \boldsymbol{C} \in \boldsymbol{R}^n$ and scalars $\varphi, \ \psi \in \boldsymbol{R}$ the following general identities are true :

$$\boldsymbol{A} \times (\boldsymbol{B} \times \boldsymbol{C}) \;=\; (\boldsymbol{C} \times \boldsymbol{B}) \times \boldsymbol{A} = \boldsymbol{B}(\boldsymbol{A} \cdot \boldsymbol{C}) - \boldsymbol{C}(\boldsymbol{A} \cdot \boldsymbol{B}) \quad (216)$$

$$\nabla \cdot (\varphi \, \boldsymbol{A}) \;=\; \varphi \nabla \cdot \boldsymbol{A} + \boldsymbol{A} \cdot \nabla \varphi \quad (217)$$

$$\nabla \times (\varphi \, \boldsymbol{A}) \;=\; \varphi \nabla \times \boldsymbol{A} + \nabla \varphi \times \boldsymbol{A} \quad (218)$$

$$\nabla \cdot (\boldsymbol{A} \times \boldsymbol{B}) \;=\; \boldsymbol{B} \cdot \nabla \times \boldsymbol{A} - \boldsymbol{A} \cdot \nabla \times \boldsymbol{B} \quad (219)$$

$$\nabla \times (\boldsymbol{A} \times \boldsymbol{B}) \;=\; \boldsymbol{A}(\nabla \cdot \boldsymbol{B}) - \boldsymbol{B}(\nabla \cdot \boldsymbol{A}) + (\boldsymbol{B} \cdot \nabla)\boldsymbol{A}$$
$$- (\boldsymbol{A} \cdot \nabla)\boldsymbol{B} \quad (220)$$

$$\nabla(\boldsymbol{A} \cdot \boldsymbol{B}) \;=\; \boldsymbol{A} \times (\nabla \times \boldsymbol{B}) + \boldsymbol{B} \times (\nabla \times \boldsymbol{A})$$
$$+ (\boldsymbol{A} \cdot \nabla)\boldsymbol{B} + (\boldsymbol{B} \cdot \nabla)\boldsymbol{A} \quad (221)$$

$$\nabla \times \nabla \varphi \;=\; 0 \quad (222)$$

$$\nabla \cdot \nabla \times \boldsymbol{A} \;=\; \operatorname{div}(\operatorname{rot}\boldsymbol{A}) = 0 \quad (223)$$

$$\nabla \cdot (\boldsymbol{A} \circ \boldsymbol{B}) \;=\; (\nabla \cdot \boldsymbol{A})\boldsymbol{B} + (\boldsymbol{A} \cdot \nabla)\boldsymbol{B} \quad (224)$$

Pressure scale height

The atmosphere is in hydrostatic balance if the vertical pressure gradient is equal to the gravity acceleration, i.e.,

$$\frac{\partial p}{\partial z} = -\varrho g$$

Starting from a reference pressure p_{ref} (e.g. a mean pressure on sea level) we can define the *pressure scale height* by the height difference at which the pressure in an atmosphere in hydrostatic balance and with constant density changes of an order of magnitude of p_{ref}

$$h_{\mathrm{sc}} := \frac{p_{\mathrm{ref}}}{\varrho_{\mathrm{ref}}\, g} \quad .$$

The thermal wind

The equation of the *thermal wind*

$$-\Omega_0\, \boldsymbol{k} \times \frac{\partial \boldsymbol{v}_{\parallel}^{(0)}}{\partial z} = \frac{1}{\Theta_\infty} \nabla_{\parallel} \Theta^{(3)}$$

does not give any information about the geostrophic wind itself, but only about it's vertical variation. The thermal wind denotes the velocity differences that result from geostrophic balance across some vertical distance, say, $\triangle z : \boldsymbol{v}_T = \triangle \boldsymbol{v} = \boldsymbol{v}(z_1) - \boldsymbol{v}(z_2)$.

Some details of the transformations into a rotating reference frame

We switch from $\boldsymbol{R}^3$ to a Cartesian system of coordinates $Z = \boldsymbol{R} \times \boldsymbol{R} \times \boldsymbol{R}$ in which $\boldsymbol{\Omega}$ and $\boldsymbol{X}_b(t)$ are defined by

$$\underline{\boldsymbol{\Omega}} := \begin{pmatrix} \Omega_1 \\ \Omega_2 \\ \Omega_3 \end{pmatrix} \quad , \quad \underline{\boldsymbol{X}}_b(t) := \begin{pmatrix} X_{b1} \\ X_{b2} \\ X_{b3} \end{pmatrix} \quad .$$

With the additional definition of

$$\underline{\underline{\boldsymbol{\Omega}}} := \begin{pmatrix} 0 & -\Omega_3 & \Omega_2 \\ \Omega_3 & 0 & -\Omega_1 \\ -\Omega_2 & \Omega_1 & 0 \end{pmatrix}$$

the change with time of $\underline{\boldsymbol{X}}_b(t)$ can also be written as a matrix vector product, namely

$$\underline{\dot{\boldsymbol{X}}}_b(t) = \underline{\boldsymbol{\Omega}} \times \underline{\boldsymbol{X}}_b(t) = \underline{\underline{\boldsymbol{\Omega}}}\, \underline{\boldsymbol{X}}_b(t) = \begin{pmatrix} -\Omega_3 X_{b2}(t) + \Omega_2 X_{b3}(t) \\ \Omega_3 X_{b1}(t) - \Omega_1 X_{b3}(t) \\ -\Omega_2 X_{b1}(t) + \Omega_1 X_{b2}(t) \end{pmatrix} . \quad (225)$$

With the knowledge from the theory of ordinary differential equations we can derive equation (37) in a different way. We know that the solution of the initial value problem

$$\underline{\dot{\boldsymbol{X}}}_b(t) = \underline{\underline{\boldsymbol{\Omega}}}\, \underline{\boldsymbol{X}}_b(t) \quad , \quad \underline{\boldsymbol{X}}_b(0) = \underline{\boldsymbol{X}}_{b0}$$

is

$$\underline{\boldsymbol{X}}_b(t) = \exp(\underline{\underline{\boldsymbol{\Omega}}}t) \; \underline{\boldsymbol{X}}_b(0) \qquad \text{, wobei } \exp(\underline{\underline{\boldsymbol{\Omega}}}t) := \sum_{\nu=0}^{\infty} \frac{t^\nu}{\nu!} (\underline{\underline{\boldsymbol{\Omega}}})^\nu \quad .$$

Because of

$$\underline{\underline{\boldsymbol{\Omega}}}^2 = \begin{pmatrix} -\Omega_2^2\Omega_3^2 & \Omega_1^2\Omega_2^2 & \Omega_1^2\Omega_3^2 \\ \Omega_1^2\Omega_2^2 & -\Omega_1^2\Omega_3^2 & \Omega_2^2\Omega_3^2 \\ -\Omega_1^2\Omega_3^2 & \Omega_2^2\Omega_3^2 & -\Omega_1^2\Omega_2^2 \end{pmatrix} = |\underline{\boldsymbol{\Omega}}|^2(\underline{\boldsymbol{e}}_\Omega\underline{\boldsymbol{e}}_\Omega^T - \underline{\underline{\boldsymbol{1}}}) \quad ,$$

$$\underline{\underline{\boldsymbol{\Omega}}}^3 = -|\underline{\boldsymbol{\Omega}}|^2\underline{\underline{\boldsymbol{\Omega}}} \quad , \quad \underline{\underline{\boldsymbol{\Omega}}}^4 = -|\underline{\boldsymbol{\Omega}}|^4(\underline{\boldsymbol{e}}_\Omega\underline{\boldsymbol{e}}_\Omega^T - \underline{\underline{\boldsymbol{1}}}) \quad , \quad \underline{\underline{\boldsymbol{\Omega}}}^5 = -|\underline{\boldsymbol{\Omega}}|^2\underline{\underline{\boldsymbol{\Omega}}}^3 = |\underline{\boldsymbol{\Omega}}|^4\underline{\underline{\boldsymbol{\Omega}}} \quad \text{etc.}$$

With $\underline{\boldsymbol{e}}_\Omega = \frac{\underline{\boldsymbol{\Omega}}}{|\underline{\boldsymbol{\Omega}}|}$ and $|\underline{\boldsymbol{\Omega}}| = \sqrt{\Omega_1^2 + \Omega_2^2 + \Omega_3^2}$ we then have

$$\begin{aligned}
\underline{\boldsymbol{X}}_b(t) &= \left[\underline{\underline{\boldsymbol{1}}} + t\,\underline{\underline{\boldsymbol{\Omega}}} + \frac{t^2}{2!}|\underline{\boldsymbol{\Omega}}|^2(\underline{\boldsymbol{e}}_\Omega\underline{\boldsymbol{e}}_\Omega^T - \underline{\underline{\boldsymbol{1}}}) - \frac{t^3}{3!}|\underline{\boldsymbol{\Omega}}|^2\underline{\underline{\boldsymbol{\Omega}}} \right. \\
&\qquad \left. - \frac{t^4}{4!}|\underline{\boldsymbol{\Omega}}|^4(\underline{\boldsymbol{e}}_\Omega\underline{\boldsymbol{e}}_\Omega^T - \underline{\underline{\boldsymbol{1}}}) + \frac{t^5}{5!}|\underline{\boldsymbol{\Omega}}|^4\underline{\underline{\boldsymbol{\Omega}}} + ... \right] \underline{\boldsymbol{X}}_b(0) \\
&= \left[(\underline{\boldsymbol{e}}_\Omega\underline{\boldsymbol{e}}_\Omega^T) + \left(1 - \frac{|\underline{\boldsymbol{\Omega}}|^2 t^2}{2!} + \frac{|\underline{\boldsymbol{\Omega}}|^4 t^4}{4!} - ... \right) (\underline{\underline{\boldsymbol{1}}} - \underline{\boldsymbol{e}}_\Omega\underline{\boldsymbol{e}}_\Omega^T) \right. \\
&\qquad \left. + \left(|\underline{\boldsymbol{\Omega}}|t - \frac{|\underline{\boldsymbol{\Omega}}|^3 t^3}{3!} + \frac{|\underline{\boldsymbol{\Omega}}|^5 t^5}{5!} - ... \right) \frac{\underline{\boldsymbol{\Omega}}}{|\underline{\boldsymbol{\Omega}}|} \right] \underline{\boldsymbol{X}}_b(0) \\
&= \left[(\underline{\boldsymbol{e}}_\Omega\underline{\boldsymbol{e}}_\Omega^T) + \cos(|\underline{\boldsymbol{\Omega}}|t)(\underline{\underline{\boldsymbol{1}}} - \underline{\boldsymbol{e}}_\Omega\underline{\boldsymbol{e}}_\Omega^T) + \sin(|\underline{\boldsymbol{\Omega}}|t)\frac{\underline{\boldsymbol{\Omega}}}{|\underline{\boldsymbol{\Omega}}|} \right] \underline{\boldsymbol{X}}_b(0)
\end{aligned}$$

and this, because of the representation in coordinates, is just the same as the previously derived result from (37). As (225), $\underline{\underline{\boldsymbol{\Omega}}}\,\underline{\boldsymbol{X}}_b$ can be represented as $\underline{\boldsymbol{\Omega}} \times \underline{\boldsymbol{X}}_b$ and we obtain

$$\underline{\boldsymbol{X}}_b(t) = (\underline{\boldsymbol{e}}_\Omega^T\underline{\boldsymbol{X}}_b(0))\underline{\boldsymbol{e}}_\Omega + \cos(|\underline{\boldsymbol{\Omega}}|t)(\underline{\underline{\boldsymbol{1}}} - \underline{\boldsymbol{e}}_\Omega\underline{\boldsymbol{e}}_\Omega^T)\underline{\boldsymbol{X}}_b(0) + \sin(|\underline{\boldsymbol{\Omega}}|t)(\underline{\boldsymbol{X}}_b(0) \times \underline{\boldsymbol{e}}_\Omega) \quad .$$

Defining $\underline{\underline{\boldsymbol{R}}}(t) := \exp(\underline{\underline{\boldsymbol{\Omega}}}t)$, $\underline{\underline{\boldsymbol{R}}}(t)$ has the following properties:

- $\underline{\underline{\boldsymbol{R}}}(-t) = \underline{\underline{\boldsymbol{R}}}^T(t)$

  As $\underline{\underline{\boldsymbol{\Omega}}}$ is skew symmetric, i.e., it is $\underline{\underline{\boldsymbol{\Omega}}}^T = -\underline{\underline{\boldsymbol{\Omega}}}$, and as the $\cos(\,\cdot\,)$ is an even while the $\sin(\,\cdot\,)$ is an uneven function, we have

$$\begin{aligned}
\underline{\underline{\boldsymbol{R}}}^T(t) &= (\underline{\boldsymbol{e}}_\Omega\underline{\boldsymbol{e}}_\Omega^T)^T + \cos(|\underline{\boldsymbol{\Omega}}|t)(\underline{\underline{\boldsymbol{1}}} - \underline{\boldsymbol{e}}_\Omega\underline{\boldsymbol{e}}_\Omega^T)^T + \sin(|\underline{\boldsymbol{\Omega}}|t)\frac{\underline{\underline{\boldsymbol{\Omega}}}^T}{|\underline{\boldsymbol{\Omega}}|} \\
&= (\underline{\boldsymbol{e}}_\Omega\underline{\boldsymbol{e}}_\Omega^T) + \cos(-|\underline{\boldsymbol{\Omega}}|t)(\underline{\underline{\boldsymbol{1}}} - \underline{\boldsymbol{e}}_\Omega\underline{\boldsymbol{e}}_\Omega^T) - \sin(-|\underline{\boldsymbol{\Omega}}|t)\frac{-\underline{\underline{\boldsymbol{\Omega}}}}{|\underline{\boldsymbol{\Omega}}|} = \underline{\underline{\boldsymbol{R}}}(-t)
\end{aligned}$$

- $\underline{\underline{R}}(-t) = \underline{\underline{R}}^{-1}(t)$

We will now analyze how the different terms of our conservation laws change when we switch to a rotating coordinate system. To this end, we represent an arbitrary fixed vector with respect to the inertial basis $\{\underline{e}_1, \underline{e}_2, \underline{e}_3\}$ as

$$\underline{e}_1 = \begin{pmatrix} 1 \\ 0 \\ 0 \end{pmatrix} \quad , \quad \underline{e}_2 = \begin{pmatrix} 0 \\ 1 \\ 0 \end{pmatrix} \quad , \quad \underline{e}_3 = \begin{pmatrix} 0 \\ 0 \\ 1 \end{pmatrix}$$

in the basis $\{\tilde{\underline{e}}_1, \tilde{\underline{e}}_2, \tilde{\underline{e}}_3\}$ of the rotating coordinate system. The interrelation between the coordinate systems is given in the following form :

$$\tilde{\underline{e}}_i = \underline{\underline{R}}(t)\underline{e}_i \ , \qquad i = 1, 2, 3 \quad .$$

Then $\underline{x}$ can be represented by the two bases as

$$\underline{x} = \sum_{i=1}^{3} x_i \underline{e}_i = \sum_{i=1}^{3} \tilde{x}_i \tilde{\underline{e}}_i = \sum_{i=1}^{3} \tilde{x}_i \underline{\underline{R}}(t)\underline{e}_i \quad .$$

Multiplication from left with $\underline{e}_k^T$ yields

$$x_k = \sum_{i=1}^{3} \tilde{x}_i (\underline{e}_k^T \underline{\underline{R}}(t))\underline{e}_i = \sum_{i=1}^{3} \tilde{x}_i (\underline{\underline{R}}(t))_{ki} \quad .$$

Hence,

$$\underline{x} = \underline{\underline{R}}(t)\tilde{\underline{x}} \quad \text{und} \quad \tilde{\underline{x}} = \underline{\underline{R}}^{-1}(t)\underline{x} \quad .$$

Furthermore we analyze the differential operators under the present a transformation of coordinates. For the transformation $(t, \underline{x}) \rightarrow (\tilde{t}, \tilde{\underline{x}})$ with $\tilde{t} = t$ it holds for a function f that

$$f(t, x) = \tilde{f}(\tilde{t}, \tilde{\underline{x}}) = \tilde{f}(\tilde{t}(t, \underline{x}), \tilde{\underline{x}}(t, \underline{x})) \quad .$$

This yields

$$
\begin{aligned}
\left(\frac{\partial f}{\partial t}\right)_{\underline{x}} &= \left(\frac{\partial \tilde{t}}{\partial t}\right)_{\underline{x}}\left(\frac{\partial \tilde{f}}{\partial \tilde{t}}\right)_{\underline{\tilde{x}}} &&+ \sum_{i=1}^{3}\left(\frac{\partial \tilde{x}_i}{\partial t}\right)_{\underline{x}}\left(\frac{\partial \tilde{f}}{\partial \tilde{x}_i}\right)_{\tilde{t},x_j(j\neq i)} \\
&= \frac{\partial \tilde{f}}{\partial \tilde{t}} &&+ \sum_{i=1}^{3}(-\underline{\underline{\Omega}}\,\underline{\tilde{x}})_i\frac{\partial \tilde{f}}{\partial \tilde{x}_i} \\
&= \frac{\partial \tilde{f}}{\partial \tilde{t}} &&+ \sum_{i,j=1}^{3}(-\Omega_{ij}\tilde{x}_j)\frac{\partial \tilde{f}}{\partial \tilde{x}_i} &&& (226)\\
&= \frac{\partial \tilde{f}}{\partial \tilde{t}} &&+ \sum_{i,j=1}^{3}(\tilde{x}_j\Omega_{ji})\frac{\partial \tilde{f}}{\partial \tilde{x}_i} \\
&= \frac{\partial \tilde{f}}{\partial \tilde{t}} &&+ \underline{\tilde{x}}^T\underline{\underline{\Omega}}(\tilde{\nabla}\tilde{f})^T
\end{aligned}
$$

and

$$
\begin{aligned}
\left(\frac{\partial f}{\partial x_i}\right)_{\tilde{t},x_k(k\neq i)} &= \left(\frac{\partial \tilde{t}}{\partial x_i}\right)_{t,x_k(k\neq i)}\left(\frac{\partial \tilde{f}}{\partial \tilde{t}}\right)_{\underline{\tilde{x}}}+ \\
&\quad +\sum_{j=1}^{3}\left(\frac{\partial \tilde{x}_j}{\partial x_i}\right)_{t,x_k(k\neq i)}\left(\frac{\partial \tilde{f}}{\partial \tilde{x}_j}\right)_{\tilde{t},\tilde{x}_k(k\neq j)} \\
&= \sum_{j=1}^{3}(\underline{\underline{R}}^{-1}(t))_{ji}\frac{\partial \tilde{f}}{\partial \tilde{x}_j} \\
&= \sum_{j=1}^{3}(\underline{\underline{R}}(t))_{ij}\frac{\partial \tilde{f}}{\partial \tilde{x}_j}
\end{aligned}
$$

or

$$
(\nabla f)^T = \underline{\underline{R}}(t)(\tilde{\nabla}\tilde{f})^T \quad .
$$

Consider now the transformation of the velocity of a particle: The position of a particle in both coordinate systems can be expressed by

$$
\underline{x}_p(t) = \sum_{i=1}^{3} x_{pi}(t)\underline{e}_i = \sum_{j=1}^{3} \tilde{x}_{pj}(t)\underline{\tilde{e}}_j(t)
$$

and its velocity is

$$
\begin{aligned}
\frac{d\underline{x}_p}{dt} = \sum_{i=1}^{3} \dot{x}_{pi}(t)\underline{e}_i &= \sum_{j=1}^{3}(\dot{\tilde{x}}_{pj}(t)\underline{\tilde{e}}_j(t) + \tilde{x}_{pj}(t)\dot{\underline{\tilde{e}}}_j(t)) \\
&= \underline{\dot{x}}_p^{\text{rel}}(t) + \sum_{j=1}^{3} \tilde{x}_{pj}(t)\underline{\underline{\Omega}}\,\underline{\tilde{e}}_j(t) \\
&= \underline{\dot{x}}_p^{\text{rel}}(t) + \underline{\underline{\Omega}}\,\underline{x}_p(t) \quad .
\end{aligned}
$$

Thus, if p denotes a particle of the fluid we look at, then $\underline{\dot{x}}_p^{\text{rel}} = \underline{v}_p^{\text{rel}}$ is the relevant *wind speed* and the local flow velocity $\underline{v}(\underline{x},t)$ can be splitted

$$
\begin{aligned}
\underline{v} = \underline{\dot{x}} &= \underline{v}^{\text{rel}} + \underline{\underline{\Omega}}\,\underline{x} \\
&= \sum_{i=1}^{3} \tilde{v}_i^{\text{rel}}\underline{\tilde{e}}_i + \underline{\underline{\Omega}}\,\underline{x}
\end{aligned}
\tag{227}
$$

into a part arising from earth's rotation and the relative wind speed. When transforming the velocity divergence we find

$$
\nabla \cdot \underline{v} = \nabla \cdot (\underline{v}^{\text{rel}} + \underline{\underline{\Omega}}\,\underline{x}) = \nabla \cdot \underline{v}^{\text{rel}} + \nabla \cdot (\underline{\underline{\Omega}}\,\underline{x}) \quad ,
$$

whereas because of the zeros on the diagonals of the rotation matrix $\underline{\underline{\Omega}}$

$$
\nabla \cdot (\underline{\underline{\Omega}}\,\underline{x}) = \sum_{i,j=1}^{3} \frac{\partial}{\partial x_i}(\Omega_{ij}x_j) = \sum_{i,j=1}^{3} \Omega_{ij}\delta_{ij} = 0 \,,
$$

(the symbol $\delta_{ij} = 1$ if $i = j$, 0 otherwise, denotes the Kronecker-Symbol). As also $\underline{e}_i^T \underline{\tilde{e}}_j = \underline{e}_i^T \underline{\underline{R}}\underline{e}_j = R_{ij}$ and $\frac{\partial}{\partial x_i} = \sum_{j=1}^{3} R_{ij}\frac{\partial}{\partial \tilde{x}_i}$, one has

$$
\begin{aligned}
\nabla \cdot \underline{v}^{\text{rel}} = \sum_{i=1}^{3} \frac{\partial v_i^{\text{rel}}}{\partial x_i} &= \sum_{i=1}^{3} \frac{\partial}{\partial x_i}(\underline{e}_i^T \sum_{j=1}^{3} \tilde{v}_j^{\text{rel}}\underline{\tilde{e}}_j) \\
&= \sum_{i,j=1}^{3} \frac{\partial}{\partial x_i}\left(\tilde{v}_j^{\text{rel}}(\tilde{t}(t,\underline{x}),\underline{\tilde{x}}(t,\underline{x}))\right)\underline{e}_i^T\,\underline{\tilde{e}}_j \\
&= \sum_{i,j,k=1}^{3} R_{ik}\frac{\partial}{\partial \tilde{x}_k}\tilde{v}_j^{\text{rel}}R_{ij} \\
&= \sum_{j,k=1}^{3} \delta_{ik}\frac{\partial}{\partial \tilde{x}_k}\tilde{v}_j^{\text{rel}} = \sum_{k=1}^{3} \frac{\partial \tilde{v}_k^{\text{rel}}}{\partial \tilde{x}_k} = \tilde{\nabla} \cdot \underline{\tilde{v}}^{\text{rel}} \quad .
\end{aligned}
\tag{228}
$$

Furthermore, because of $\underline{\underline{R}}^{-1}(t) = \underline{\underline{R}}^T(t) = \underline{\underline{R}}(-t)$ we have $(\underline{\underline{R}}^T\underline{\underline{R}})_{kj} = \sum_{i=1}^{3} R_{ik}R_{ij} = \delta_{kj}$.

For momentum conservation the following auxiliary calculations might be useful: Transforming $(\underline{v}_t + (\underline{v}^T\nabla^T)\underline{v})$ into the rotating system of coordinates and using (226) and (227) yields for the derivative with respect to time

$$
\begin{aligned}
\underline{v}_t &= \left(\frac{\partial}{\partial t}\right)_{\underline{x}} (\underline{v}^{\mathrm{rel}} + \underline{\underline{\Omega}}\,\underline{x}) \\
&= \left(\frac{\partial}{\partial t}\right)_{\underline{x}} \left(\sum_{i=1}^{3} \tilde{v}_i^{\mathrm{rel}}\underline{\tilde{e}}_i\right) \qquad\qquad\qquad + \left(\frac{\partial}{\partial t}\right)_{\underline{x}} (\underline{\underline{\Omega}}\,\underline{x}) \\
&= \sum_{i=1}^{3} \left(\frac{\partial \tilde{v}_i^{\mathrm{rel}}}{\partial \tilde{t}} + \underline{\tilde{x}}^T\underline{\underline{\Omega}}(\tilde{\nabla}\tilde{v}_i^{\mathrm{rel}})^T\right) \underline{\tilde{e}}_i + \sum_{i=1}^{3} \tilde{v}_i^{\mathrm{rel}}\underline{\underline{\Omega}}\,\underline{\tilde{e}}_i \quad + \qquad 0 \\
&= \sum_{i=1}^{3} \frac{\partial \tilde{v}_i^{\mathrm{rel}}}{\partial \tilde{t}}\underline{\tilde{e}}_i + \left(\underline{\tilde{x}}^T\underline{\underline{\Omega}}\tilde{\nabla}^T\right)\underline{\tilde{v}}^{\mathrm{rel}} + \underline{\underline{\Omega}}\,\underline{\tilde{v}}^{\mathrm{rel}}
\end{aligned}
$$

Because of

$$
(\underline{v}^{\mathrm{rel}^T}\nabla^T)\underline{v}^{\mathrm{rel}} = \sum_{i=1}^{3} ((\underline{\tilde{v}}^{\mathrm{rel}})^T\tilde{\nabla}^T)\tilde{v}_i^{\mathrm{rel}}\underline{\tilde{e}}_i \quad ,
$$

$$
\left((\underline{\underline{\Omega}}\,\underline{x})^T\nabla^T\right)\underline{v}^{\mathrm{rel}} = (\underline{\tilde{x}}^T\underline{\underline{\Omega}}^T\tilde{\nabla}^T)\underline{\tilde{v}}^{\mathrm{rel}} = -(\underline{\tilde{x}}^T\underline{\underline{\Omega}}\tilde{\nabla}^T)\underline{\tilde{v}}^{\mathrm{rel}} \quad ,
$$

$$
\begin{aligned}
(\underline{v}^{\mathrm{rel}^T}\nabla^T)\underline{\underline{\Omega}}\,\underline{x} &= \left(\sum_{i=1}^{3} v_i^{\mathrm{rel}}\frac{\partial}{\partial x_i}\right)\underline{\underline{\Omega}}\left(\sum_{i=1}^{3} x_i\underline{e}_i\right) = \sum_{i,j=1}^{3} \tilde{v}_j^{\mathrm{rel}}\frac{\partial}{\partial \tilde{x}_j}(\underline{\underline{\Omega}}\,\underline{e}_i\tilde{x}_i) \\
&= \sum_{i,j=1}^{3} \underline{\underline{\Omega}}\tilde{v}_j^{\mathrm{rel}}\delta_{ij}\underline{e}_i = \underline{\underline{\Omega}}\,\underline{\tilde{v}}^{\mathrm{rel}}
\end{aligned}
$$

and

$$
\begin{aligned}
\left((\underline{\underline{\Omega}}\,\underline{x})^T\nabla^T\right)(\underline{\underline{\Omega}}\,\underline{x}) &= -(\underline{x}^T\underline{\underline{\Omega}}\nabla^T)\underline{\underline{\Omega}}\,\underline{x} \\
&= -\sum_{i,j,k,l=1}^{3} x_i\Omega_{ik}\frac{\partial}{\partial x_k}\Omega_{jl}x_l\underline{e}_j = \sum_{i,j,k=1}^{3} x_i\Omega_{ki}\Omega_{jk}\underline{e}_j \\
&= \left(\underline{x}^T\underline{\underline{\Omega}}^T\underline{\underline{\Omega}}^T\right)^T = \underline{\underline{\Omega}}(\underline{\underline{\Omega}}\,\underline{x}) = \underline{\underline{\Omega}} \times (\underline{\underline{\Omega}} \times \underline{x})
\end{aligned}
$$

we obtain

$$
\begin{aligned}
\underline{\boldsymbol{v}}_t + (\underline{\boldsymbol{v}}^T\nabla^T)\underline{\boldsymbol{v}} &= \underline{\boldsymbol{v}}_t + \left((\underline{\boldsymbol{v}}^{\mathrm{rel}} + \underline{\underline{\boldsymbol{\Omega}}}\,\underline{\boldsymbol{x}})^T\nabla^T\right)\left(\underline{\boldsymbol{v}}^{\mathrm{rel}} + \underline{\underline{\boldsymbol{\Omega}}}\,\underline{\boldsymbol{x}}\right) \\
&= \underline{\boldsymbol{v}}_t + (\underline{\boldsymbol{v}}^{\mathrm{rel}^T}\nabla^T)\underline{\boldsymbol{v}}^{\mathrm{rel}} + \left((\underline{\underline{\boldsymbol{\Omega}}}\,\underline{\boldsymbol{x}})^T\nabla^T\right)\underline{\boldsymbol{v}}^{\mathrm{rel}} \\
&\quad + (\underline{\boldsymbol{v}}^{\mathrm{rel}^T}\nabla^T)(\underline{\underline{\boldsymbol{\Omega}}}\,\underline{\boldsymbol{x}}) + \left((\underline{\underline{\boldsymbol{\Omega}}}\,\underline{\boldsymbol{x}})^T\nabla^T\right)(\underline{\underline{\boldsymbol{\Omega}}}\,\underline{\boldsymbol{x}}) \\
&= \sum_{i=1}^{3}\frac{\partial \tilde{v}_i^{\mathrm{rel}}}{\partial t}\underline{\tilde{\boldsymbol{e}}}_i + \sum_{i=1}^{3}((\underline{\tilde{\boldsymbol{v}}}^{\mathrm{rel}})^T\tilde{\nabla}^T)\tilde{v}_i^{\mathrm{rel}}\underline{\tilde{\boldsymbol{e}}}_i \\
&\quad + 2\,\underline{\underline{\boldsymbol{\Omega}}}\,\underline{\tilde{\boldsymbol{v}}}^{\mathrm{rel}} + \underline{\underline{\boldsymbol{\Omega}}}(\underline{\underline{\boldsymbol{\Omega}}}\,\underline{\boldsymbol{x}})
\end{aligned}
$$

Multiplication with $\underline{\tilde{\boldsymbol{e}}}_k^T$ yields

$$
\left(\underline{\boldsymbol{v}}_t + (\underline{\boldsymbol{v}}^T\nabla)\underline{\boldsymbol{v}}\right)_k = \frac{\partial \tilde{v}_k^{\mathrm{rel}}}{\partial t} + ((\underline{\tilde{\boldsymbol{v}}}^{\mathrm{rel}})^T\nabla^T)\tilde{v}_k^{\mathrm{rel}} + 2\,(\underline{\underline{\boldsymbol{\Omega}}}\,\underline{\tilde{\boldsymbol{v}}}^{\mathrm{rel}})_k + \left(\underline{\underline{\boldsymbol{\Omega}}}(\underline{\underline{\boldsymbol{\Omega}}}\,\underline{\boldsymbol{x}})\right)_k
$$

Bibliography

G. I. Barenblatt. *Scaling, self-similarity, and intermediate asymptotics.* Cambridge Texts in Applied Mathematics. Cambridge University Press, Cambridge, New York, Melbourne, 1996.

J.A. Biello and A.J. Majda. Transformations for temperature flux in multiscale models of the tropics. *Theor. Comp. Fluid Dyn.*, under revision, 2006.

O. Forster. *Analysis 3.* Vieweg & Sohn Verlagsgesellschaft, Braunschweig, Wiesbaden, 3. edition, 1984.

D. M. W. Frierson. Midlatitude static stability in simple and comprehensive general circulation models. *J. Atmos. Sci.*, 65:1049–1062, 2008.

A.E. Gill. *Atmosphere-Ocean Dynamics*, volume 30 of *International geophysics series.* Academic Press, New York, 1982.

H. Görtler. *Dimensionsanalyse: Theorie der physikalischen Dimensionen mit Anwendungen.* Ingenieurwissenschaftliche Bibliothek. Springer, Berlin, Heidelberg, New York, 1975.

J.B. Keller and L. Ting. Approximate equations for large scale atmospheric motions. Internal Report, http://www.arxiv.org/abs/physics/0606114, Inst. for Mathematics & Mechanics (renamed to *Courant Institute of Mathematical Sciences* in 1962), NYU, 1951.

J. Kevorkian and J.D. Cole. *Multiple Scale and Singular Perturbation Methods*, volume 114 of *Applied Mathematical Sciences.* Springer-Verlag, New York, 1996.

R. Klein. An applied mathematical view of meteorological modelling. In *Applied Mathematics Entering the 21st century; Invited talks from the ICIAM 2003 Congress*, volume 116. SIAM Proceedings in Applied Mathematics, 2004.

R. Klein. Multiple spacial scales in engineering and atmospheric low mach number flows. *ESAIM: Math. Mod. & Num. Analysis (M2AN)*, 39:537–559, 2005.

R. Klein. Scale-dependent models for atmospheric flows. *Ann. Rev. Fluid Mech.*, 42:249–274, 2010.

R. Klein and A.J. Majda. Systematic multiscale models for deep convection on mesoscales. *Theor. Comp. Fluid Dyn.*, accepted, 2006.

R. Klein, E. Mikusky, and A. Owinoh. Multiple scales asymptotics for atmospheric flows. In A. Laptev, editor, *4th European Conference of Mathematics, Stockholm, Sweden*, pages 201–220. European Mathematical Society Publishing House, 2004.

D. Kröner. *Numerical Schemes for Conservation Laws*. J. Wiley & Sons und B.G. Teubner-Verlag, Chichester, Stuttgart, 1997.

R.J. LeVeque. *Numerical Methods for Conservation Laws*. Lectures in Mathematics, ETH Zürich. Birkhäuser Verlag, Basel, Boston, Berlin, 1990.

A. J. Majda and R. Klein. Systematic multiscale models for the tropics. *Journal of the Atmospheric Sciences*, 60(2):393–408, 2003.

A.J. Majda and J.A. Biello. A multiscale model for tropical intraseasonal oscillations. *Proc. Natl. Acad. Sci. USA*, 101:4736–4741, 2004.

E. Mikusky, A. Owinoh, and R. Klein. On the influence of diabatic effects on the motion of 3D-mesoscale vortices within a baroclinic shear flow. In *Computational Fluid and Solid Mechanics 2005*, pages 766–768. Elsevier, Amsterdam, 2005.

J. Pedlosky. *Geophysical Fluid Dynamics*. Springer-Verlag, New York, 2. edition, 1987.

T. Schneider. The general circulation of the atmosphere. *Ann. Rev. Earth Planet. Sci.*, 34:655–688, 2006.

W. Schneider. *Mathematische Methoden der Strömungsmechanik*. Vieweg & Sohn Verlagsgesellschaft, Braunschweig, 1978.

R. Temam and A. Miranville. *Mathematical Modeling in Continuum Mechanics*. Cambridge University Press, Cambridge, UK, 2000.

W. Walter. *Gewöhnliche Differentialgleichungen*. Springer-Verlag, Berlin, Heidelberg, New York, 6. edition, 1996.

D. Werner. *Funktionalanalysis*. Springer-Verlag, Berlin, Heidelberg, New York, 3rd edition, 2000.

Multiple Scales Analysis of the Turbulent Undular Hydraulic Jump

Herbert Steinrück[*]

[*] Vienna University of Technology, Institute of Fluid Mechanics and Heat Transfer, Vienna, Austria

Abstract The undular hydraulic jump in turbulent open channel flow is considered in the double limit of very large Reynolds numbers, and Froude numbers approaching the critical value, i.e. $Fr = 1 + \frac{3}{2}\varepsilon$ with $\varepsilon \to 0+$.

The undular jump is associated with a distinguished limit, which is characterized by the similarity parameters A and a. The square root of the first parameter $\sqrt{A}$ is essentially the ratio of the dimensionless friction velocity and the difference of the Froude number to its critical value. The second parameter a is a scaled measure of the difference of the incident turbulent flow to the fully developed turbulent flow.

Since a wavy solution with a slowly varying amplitude is expected, a multiple scales expansion is performed. A new independent variable is introduced such that the wave length becomes constant and normalized to one. The perturbation equations of the orders ε, $\varepsilon^{3/2}$, ε^2, and $\varepsilon^{5/2}$ have to be considered in order to obtain a complete first-order solution.

In case of fully developed incident flow analytical results for the amplitude and wave length of the first wave are obtained. They are compared with measured data and reasonable agreement is observed.

1 Introduction

The undular hydraulic jump is a peculiar change of state that can be observed in steady open channel flows if the upstream Froude number is slightly above the critical value 1, cf. Böß (1927), Chow (1959), Hager and Hutter (1984), Hager (1992), Henderson (1966), Chanson (1993), Chanson and Montes (1995), Reinauer and Hager (1995), Ohtsu et al. (2001).

As far as the observations are concerned, the undular hydraulic jump is characterized by a wavy shape of the free surface, with wave lengths that

are much larger than the depth of the liquid and amplitudes that decay
slowly in main flow direction.

From a theoretical point of view there is the difficulty that, though the
viscosity effects are very weak, an inviscid-flow solution does not exist, cf.
Benjamin and Lighthill (1954).

For laminar flow, Johnson (1972) was able to cope with these difficulties
and provide an asymptotic analysis in terms of Froude numbers near 1 and
large Reynolds numbers. His main result is a steady-state version of the
Korteweg-de Vries-Burgers equation that governs the perturbations of the
surface elevation.

For turbulent flow, attempts have been made to analyze the undular
hydraulic jump on the basis of various ad-hoc approximations, e.g. An-
dersen (1978), Hager and Hutter (1984), Kaufmann (1934), Lauffer (1935),
Chanson and Montes (1995). More detailed comments on those previous
investigations can be found in Grillhofer (2002).

In Grillhofer (2002), Grilllhofer and Schneider (2003) and Steinrück et al.
(2003) an asymptotic analysis of the undular jump in turbulent flow was
given. Plane flow over a bottom of constant slope was considered in the
double limit of very large Reynolds numbers, i.e. $Re_\tau \to \infty$, and Froude
numbers approaching the critical value, i.e. $Fr = 1 + \frac{3}{2}\varepsilon$ with $\varepsilon \to 0$.

Here we will follow the analysis in Steinrück et al. (2003) to study the
influence of small viscosity effects on near critical open channel flow. Based
on the shallow water approximation we will employ the method of multiple
scales to derive equations for the change of amplitude and wave length of
the undulated surface.

2   Governing equations and scaling

We consider a plane open channel flow of a fluid with constant density ρ and
constant kinematic viscosity ν over a plane bottom with constant angle of
inclination α, cf. Figure 1. The coordinate system is such that the x-axis is
in the bottom plane and the y-axis is perpendicular to it. The corresponding
velocity components are u and v, respectively.

As reference state we chose the volumetric mean velocity $\bar{u}_r$, the height
of the free surface $\bar{h}_r$ at some appropriate location x_r and and wall shear
stress τ_{wr} of a locally fully developed open channel flow with volumetric
mean velocity $\bar{u}_r$ and height of the free surface $\bar{h}_r$.

Having a shallow water approximation in mind we choose a typical wave
length l to nondimensionalize the x-coordinate. The velocity components
are scaled accordingly. The pressure p is referred to the hydrostatic pressure
$\rho g h_r$ at the bottom of the channel.
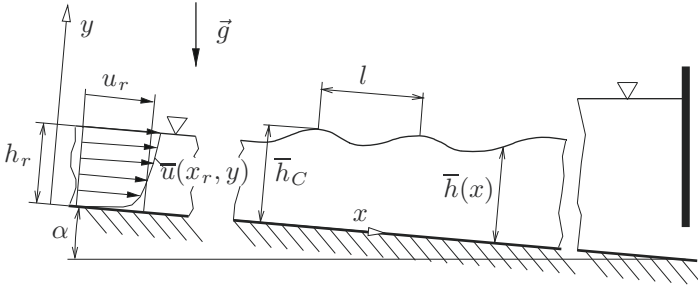
Figure 1. The undular hydraulic jump in turbulent open channel flow

The Reynolds stresses $(\overline{u'^2})$, $(\overline{u'v'})$ and $(\overline{v'^2})$ are scaled with the square of the reference friction velocity, which is given by:

$$u_{\tau r}^2 = \frac{\tau_{wr}}{\rho}. \qquad (1)$$

We introduce the following dimensionless variables:

$$X = \frac{x}{l}, \quad Y = \frac{y}{h_r}, \quad \bar{U} = \frac{\bar{u}}{u_r}, \quad \bar{V} = \frac{\bar{v}}{\delta u_r}, \quad \bar{P} = \frac{\bar{p}\, Fr^2}{\rho u_r^2}, \quad \bar{H} = \frac{\bar{h}}{h_r}, \quad (2a)$$

$$(\overline{U'^2}) = \frac{(\overline{u'^2})}{u_{\tau r}^2}, \quad (\overline{U'V'}) = \frac{(\overline{u'v'})}{u_{\tau r}^2}, \quad (\overline{V'^2}) = \frac{(\overline{v'^2})}{u_{\tau r}^2}, \quad U_\tau = \frac{u_\tau}{u_{\tau r}}, \quad (2b)$$

where the dimensionless parameters

$$Fr = \frac{u_r}{\sqrt{gh_r}}, \quad \delta = \frac{h_r}{l}, \quad \alpha, \quad \gamma = \frac{u_{\tau r}}{\bar{u}_r} \qquad (3)$$

are the Froude number, the shallow water parameter, the angle of inclination and the ratio of the reference wall friction velocity and the volumetric mean velocity, respectively. The later is a function of the Reynolds number $Re = u_r h_r / \nu$ only. If the fully developed flow in an open channel with the inclination α is chosen as reference state the force balance yields $\sin \alpha = \gamma^2\, Fr^2$.

For high Reynolds numbers the flow field can be decomposed into a defect layer and a viscous sub-layer. Since a universal solution exists for the viscous sub-layer, cf. Kluwick (1998), Schlichting and Gersten (2000), it is sufficient to consider the defect layer only.

Using the scalings (2a) and (2b), the continuity equation for the dimensionless Reynolds averaged velocities becomes:

$$\bar{U}_X + \bar{V}_Y = 0. \tag{4}$$

The momentum equations for the defect layer in dimensionless form are:

$$Fr^2 \left(\bar{U}\bar{U}_X + \bar{V}\bar{U}_Y\right) = -\bar{P}_X + \frac{\sin\alpha}{\delta} - Fr^2\frac{\gamma^2}{\delta}\left(\delta(\overline{U'^2})_X + (\overline{U'V'})_Y\right), \tag{5a}$$

$$\delta^2 Fr^2 \left(\bar{U}\bar{V}_X + \bar{V}\bar{V}_Y\right) = -\bar{P}_Y - \cos\alpha - Fr^2\gamma^2\left(\delta(\overline{U'V'})_X + (\overline{V'^2})_Y\right). \tag{5b}$$

We define the averaged free surface $Y = \bar{H}(X)$ by a particular streamline of the Reynolds averaged velocity field $(\bar{u}, \bar{v})$. This particular streamline corresponds to the averaged volume flow rate

$$\bar{\bar{V}} := \overline{\int_0^{H(X,Z,t)} U(X,Y,t)\ dY} = \int_0^{\bar{H}(X)} \bar{U}(X,Y)\ dY. \tag{6}$$

Using the above definition of the mean free surface, the common kinematic boundary condition for the averaged velocities holds:

$$\bar{V}(X,\bar{H}(X)) = \bar{U}(X,\bar{H}(X))\,\bar{H}_X(X). \tag{7}$$

In the absence of a general theory of turbulent free surfaces, the dynamic boundary conditions are also formulated following common approaches, cf. Rodi (1993). Thus

$$\gamma^2 Fr^2 \begin{pmatrix} (\overline{U'^2}) & (\overline{U'V'}) \\ (\overline{U'V'}) & (\overline{V'^2}) \end{pmatrix} \cdot \begin{pmatrix} -\delta\bar{H}_X \\ 1 \end{pmatrix} = \bar{P}\begin{pmatrix} \delta H_X \\ -1 \end{pmatrix} \quad \text{at} \quad Y = \bar{H}. \tag{8}$$

2.1 The friction law

Matching with respect to the viscous sub-layer is accomplished by requiring

$$\bar{V}(X,0) = 0 \tag{9}$$

and, furthermore, making use of the logarithmic friction law (cf. Schlichting and Gersten (2000), p. 524, eq. (17.54)), which may be written as follows:

$$\bar{U}_S(X) = \gamma\bar{U}_\tau \left[\frac{1}{\kappa}\ln\left(Re\gamma\bar{U}_\tau\bar{H}\right) + C^+ + \bar{C}(X)\right], \tag{10}$$

where $\bar{U}_S = \bar{U}(X, \bar{H}(X))$ is the surface velocity, $\bar{U}_\tau^2 = -(\overline{U'V'})_{Y=0}$ is the dimensionless wall shear stress and the function $\bar{C}(X)$ is given by

$$\bar{C}(X) = \int_0^{\bar{H}} \left(\frac{1}{\gamma U_\tau} \frac{d\bar{U}}{dY} - \frac{1}{\kappa Y} \right) \, dY,$$

where κ is von Karman's constant. C^+ is another empirical constant, which, as it will turn out, does not appear in the final results.

Let us denote $\Delta \bar{U}_S = \bar{U}_S - \bar{U}_{Sr}$, $\Delta \bar{U}_\tau = \bar{U}_\tau - 1$, and $\Delta \bar{H} = \bar{H} - 1$ the difference of the dimensionless surface velocity, friction velocity and surface height to its reference values at $X = X_r$, respectively. Using the friction law (10) the surface velocity $\bar{U}_{Sr}$ at the reference state, $X = X_r$, is given by

$$\bar{U}_{Sr} = \gamma \left[\frac{1}{\kappa} \ln(Re\gamma) + C^+ + \bar{C}(X_r) \right] \tag{11}$$

and we can rewrite the friction law as

$$\Delta \bar{U}_S = \bar{U}_{Sr} \Delta \bar{U}_\tau + (1 + \Delta \bar{U}_\tau)\gamma \left(\frac{1}{\kappa} \ln(1 + \Delta \bar{H}) + \bar{C}(X) - \bar{C}(X_r) \right). \tag{12}$$

Expanding (12) for small changes we obtain

$$-(\overline{U'V'})_{Y=0} = (1 + \Delta \bar{U}_\tau)^2 \sim 1 + 2\Delta \bar{U}_S. \tag{13}$$

2.2   External forces

In order to motivate the scaling assumptions we consider the external forces: the component of the gravity force in flow direction integrated over the fluid height $\bar{H} \sin \alpha / \delta$ and the shear stress $Fr^2 \gamma^2 (\overline{U'V'})_{Y=0} / \delta$ at the bottom of the channel. Using the expansion (13) of the friction law the external net force on a cross section of the flow can be written as

$$F_{ext} = \bar{H} \frac{\sin \alpha}{\delta} + \frac{Fr^2 \gamma^2}{\delta} (\overline{U'V'})_{Y=0}$$

$$\sim -\frac{1}{\delta} (\, Fr^2 \gamma^2 - \sin \alpha) + \frac{Fr^2 \gamma^2}{\delta} 3\Delta \bar{H}. \tag{14}$$

Here we have already used $\Delta \bar{U}_S = -\Delta \bar{H} + o(\Delta \bar{H})$ which follows from the shallow water approximation and will be shown later.

The difference $\gamma^2 \, Fr^2 - \sin \alpha$ measures the deviation of the reference state from the fully developed turbulent flow. The second parameter $\gamma^2 Fr^2 / \delta$ measures the change of the wall shear stress due to changes of the fluid depth $\bar{H}$.

2.3   Scaling assumptions

Our intention is to study the flow for slightly supercritical upstream flow conditions. Thus we introduce the small perturbation parameter ε according to the relation

$$Fr = 1 + \frac{3}{2}\varepsilon, \tag{15}$$

where the coefficient $\frac{3}{2}$ serves for later convenience.

We perform an asymptotic analysis with respect to the small parameters α, δ, ε and γ. The relative sizes of these parameters have to be chosen such that one can use the shallow water approximation and take turbulence effects into account, but limit their magnitude in such a way that the well-known results for fully developed flow can be applied locally to the disturbed flow. Thus no turbulence model will be required to derive the results for the free surface.

We choose the shallow water parameter δ to be

$$\delta = 3\varepsilon^{1/2}, \tag{16}$$

where the coefficient 3 is introduced for the sake of simplifying the final equations.

In order to define a distinguished limit we have to couple the angle of inclination α and the wall shear stress γ to the perturbation parameter ε in such a way that to the leading order the shallow water equation will be recovered. Therefore we introduce the two similarity parameters a and A, which are assumed to be of order one as

$$a = \frac{\gamma^2 \ Fr^2 - \sin\alpha}{\delta\varepsilon^{5/2}}, \quad A = \frac{3\gamma^2 \ Fr^2}{\delta\varepsilon^{3/2}}. \tag{17}$$

As mentioned above the parameter a measures the deviation of the reference state from the fully developed flow. With other words if the flow in the reference state is fully developed the parameter a vanishes. This assumption has been made in Grilllhofer and Schneider (2003) and Steinrück et al. (2003). The other parameter A is a measure for the change of the wall shear stress due to a change of the fluid height.

The reference state   We assume that the reference state state is attained at X_r and the flow is a locally fully developed turbulent open channel flow. Thus in the defect layer the velocity profile can be written as

$$\bar{U}(X_r) = 1 + \gamma\bar{U}_D = 1 + \varepsilon\sqrt{A}\bar{U}_D \quad \text{with} \quad \int_0^1 \bar{U}_D(Y) \ dY = 0, \tag{18}$$

where $\bar{U}_D$ is the velocity defect.

3 Asymptotic Analysis

3.1 Shallow water approximation

In a first attempt we try to use a regular expansion of the form

$$\bar{U} = 1 + \varepsilon\bar{U}_1 + \varepsilon^2\bar{U}_2 + \cdots, \tag{19a}$$

$$\bar{P} = 1 - y + \varepsilon\bar{P}_1 + \varepsilon^2\bar{P}_2 + \cdots, \tag{19b}$$

$$\bar{H} = 1 + \varepsilon\bar{H}_1 + \varepsilon^2\bar{H}_2 + \cdots \tag{19c}$$

$$(\overline{U'V'}) = (\overline{U'V'})_0 + \varepsilon(\overline{U'V'})_1 \cdots. \tag{19d}$$

Inserting into the Y-momentum equation and the dynamic boundary condition yields

$$\bar{P}_1 = \bar{H}_1. \tag{20}$$

Using the X-momentum equation and the continuity equation we obtain

$$\bar{U}_1 = -\bar{H}_1 + \sqrt{A}\bar{U}_D, \quad \bar{V}_1 = \bar{H}_{1,X}\, Y. \tag{21}$$

However the perturbation $\bar{H}_1$ of the fluid height remains undetermined from the analysis of the $O(\varepsilon)$-terms.

The component of the gravity term in flow direction is of order $O(\varepsilon^{3/2})$. Due to the scaling assumptions the derivative of the Reynolds' shear stress is of the same order. Using the dynamic boundary condition we obtain

$$(\overline{U'V'})_0 = 1 - Y. \tag{22}$$

Considering the $O(\varepsilon)^2$-terms the Y-momentum equation yields

$$\bar{P}_2 = \bar{H}_2 + \frac{9}{2}\bar{H}_{1,XX}(1 - Y^2) - A(\overline{V'^2})_0 \tag{23}$$

Using the X-momentum equation and integration of the continuity equation yields the second order term of the vertical velocity component.

$$\bar{V}_2(X, 1) = \bar{H}_{2,X} + 3\bar{H}_{1,XXX} +$$
$$+ \left(-3 + \bar{H}_1 + \sqrt{A}\bar{U}_D - 2\sqrt{A}\int_0^1 \bar{U}_D\ dY\right)\bar{H}_{1,X}. \tag{24}$$

Employing the kinematic boundary condition a second expression for $\bar{V}_2(X, 1)$ can be obtained

$$\bar{V}_2(X, 1) + \bar{V}_{1,Y}\bar{H}_1 = \bar{H}_{2,x} + (-\bar{H}_1 + \sqrt{A}\Delta\bar{U}_D)\bar{H}_{1,x}. \tag{25}$$

Comparing both expressions for $\bar{V}_2(X,1)$ we obtain the third order differential equation for $\bar{H}_1$

$$\bar{H}_{1,XXX} + \bar{H}_{1,X}(\bar{H}_1 - 1) = 0. \tag{26}$$

Integrating (26) once we obtain

$$\bar{H}_{1,XX} + \frac{1}{2}\bar{H}_1^2 - \bar{H}_1 = R. \tag{27}$$

Multiplying (27) by $\bar{H}_{1,X}$ and integration yields

$$-3\bar{H}_{1,X}^2 = p(\bar{H}_1, R, S) := \bar{H}_1^3 - 3\bar{H}_1^2 - 6R\bar{H}_1 - 6S, \tag{28}$$

where R and S are constants of integration. With the help of a phase plane analysis it can be easily verified that (28) has periodic solutions if the polynomial $p(\bar{H}_1)$ has three different real roots. That is the case if the discriminant $D = 8R^3 + 3R^2 - 18RS - 9S^2 - 6S$ is positive. Now let $h_1 = h_1(R,S)$, $h_2 = h_2(R,S)$ and $h_3 = h_3(R,S)$ be the three roots of $p(\bar{H}_1, R, S)$ with $h_1 \leq h_2 \leq h_3$. Then the solution (28) can be written as

$$\bar{H}_1(X) = \begin{cases} h_2 + (h_2 - h_3)\operatorname{cn}^2\left(\frac{X\sqrt{h_2 - h_1}}{2\sqrt{3}}\Big|\nu\right) & \text{for} \quad \nu < 1 \\ h_2 + (h_2 - h_3)\operatorname{sech}^2\left(\frac{X\sqrt{h_2 - h_1}}{2\sqrt{3}}\right) & \text{for} \quad \nu = 1 \end{cases} \tag{29}$$

with $\nu = \frac{h_3 - h_2}{h_2 - h_1}$.

If $D < 0$ the polynomial $p(\bar{H}_1)$ has only one real root and the solution of (28) is unbounded. Of special interest is the case when the reference state at $X = -\infty$ is a fully developed turbulent flow. Then we seek for a solution which connects the fully developed flow with a flow with an undulated surface. A candidate might be the solution of (28) for the case that the $p(\bar{H}_1)$ has a double root (D=0 or $\nu = 1$). Then $\bar{H}_1$ has a single hump and for $X \to \infty$ the flow will return to the fully developed state again. Thus none of the described solutions of (28) can be used to describe an undular hydraulic jump.

3.2   Multiple Scales Expansion

Considering our goal to describe the undulated surface of the fluid in an open channel we look for a solution which is almost periodic. The amplitude and wave length of the surface are expected to change slowly by virtue of dissipative effects. Of course such a solution structure is not possible with a regular expansion discussed in the preceeding section. However, if we allow

the constants of integration R and S in (28) to vary slowly we can achieve our goal.

Thus we expect to have two longitudinal length scales. The wave length and a scale on which the wave length changes. Thus we have a typical multiple scales problem.

Our strategy will be the following: First we define two length scales. The original length scale X and a slow variable $\mathcal{X} = \varepsilon^{1/2}(X - X_0(\varepsilon))$. Here X_0 is an appropriate shift of the origin of the coordinate system. Thus we will allow all functions to depend on both length scales independently. For example

$$\bar{H} = \bar{H}(X, \mathcal{X}). \tag{30}$$

Thus a derivative with respect to X becomes a sum of two partial derivatives

$$\frac{d}{dX}\bar{H} = \frac{\partial}{\partial X}\bar{H} + \frac{\partial}{\partial \mathcal{X}}\bar{H}\frac{d\mathcal{X}}{dX} = \frac{\partial}{\partial X}\bar{H} + \varepsilon^{1/2}\frac{\partial}{\partial \mathcal{X}}\bar{H}. \tag{31}$$

The derivatives with respect to the slow variable of terms of order $O(\varepsilon)$ are of order $O(\varepsilon^{3/2})$ and the derivatives of terms of the order $O(\varepsilon^2)$ are of the order $O(\varepsilon^{5/2})$. Equations for the constants of integration R and S as functions of the slow variable $\mathcal{X}$ will be obtained from the requirement that all functions are periodic with respect to the fast variable X. Thus we have to include terms of the order $\varepsilon^{3/2}$ and $\varepsilon^{5/2}$ additionally to the terms of order ε and ε^2 in the expansion of the dependent variables (19). However, to facilitate the formulation of the periodicity condition with respect to the fast variable X we introduce a transformed fast variable ξ

$$\xi = \frac{1}{\varepsilon^{1/2}}\Omega(\mathcal{X}), \quad \text{with} \quad \mathcal{X} = \varepsilon^{1/2}(X - X_0(\varepsilon)), \tag{32}$$

such that all function have period 1 with respect to the new fast variable ξ. We have

$$d\xi = \omega(\Omega) \ dX, \quad \text{with} \quad \omega = \Omega'. \tag{33}$$

Thus $1/\omega$ is the wave length in terms of the original fast variable X and part of the solution.

Representative for all dependent state variables the expansion of the pressure is given by:

$$\bar{P} \sim \bar{P}_0(Y) + \varepsilon\bar{P}_1(\xi, \Omega, Y) + \varepsilon^{3/2}\bar{P}_{3/2}(\xi, \Omega, Y) +$$

$$\varepsilon^2\bar{P}_2(\xi, \Omega, Y) + \varepsilon^{5/2}\bar{P}_{5/2}(\xi, \Omega, Y) + \cdots . \tag{34}$$

Terms of order $O(\varepsilon)$ Using the Y-momentum equation (5b) and the dynamic boundary condition (8) we obtain

$$\bar{P}_1(\xi, \Omega, Y) = \bar{H}_1(\xi, \Omega). \tag{35}$$

The X-momentum equation (5a) yields

$$\bar{U}_{1,\xi} = -\bar{P}_{1,\xi}, \tag{36}$$

with the solution

$$\bar{U}_1(\xi, \Omega, Y) = -\bar{H}_1(\xi, \Omega) + \sqrt{A}\bar{U}_D(Y, \Omega). \tag{37}$$

Note that the asymptotic analysis allows the velocity 'defect' to depend on the slowly varying variable Ω. From the continuity equation (4) we get the Y-component of the velocity:

$$\bar{V}_1(\xi, \Omega, Y) = \omega \bar{H}_{1,\xi}(\xi, \Omega)Y. \tag{38}$$

From the dynamic boundary condition (8) and the relation for the surface velocity (13) the perturbation of the Reynolds shear stress is obtained:

$$(\overline{U'V'})_1(\xi, \Omega, 1) = -\bar{H}_1(\xi, \Omega), \quad (\overline{U'V'})_1(\xi, \Omega, 0) = 2\bar{H}_1(\xi, \Omega). \tag{39}$$

The comparison of terms of order $O(\varepsilon)$ leaves, however, the perturbation $\bar{H}_1$ of the height of the free surface undetermined. An equation for $\bar{H}_1$ has to be derived from equations for the higher–order terms.

Terms of order $O(\varepsilon^{3/2})$ The analysis of the $O(\varepsilon^{3/2})$ terms follows the same lines as the analysis of the $O(\varepsilon)$ terms. Formally in equations (35)-(39) the subscript '1' has to be replaced by the subscript '3/2'. We note that in order to avoid secular terms $\Delta\bar{U}_{1,\Omega}$ has to vanish. Thus we have $\bar{U}_D(Y, \Omega) = \bar{U}_D(Y)$.

Up to now we have not used the kinematic boundary condition at all. Inspection shows that it is already satisfied.

In what follows the discussion of the terms of order $O(\varepsilon^2)$ and $O(\varepsilon^{5/2})$, respectively, will run along the same lines, with the exception that the kinematic boundary condition will provide solvability conditions that will serve as equations to determine the perturbation quantities $\bar{H}_1$ and $\bar{H}_{3/2}$, respectively.

Terms of order $O(\varepsilon^2)$ Using the Y-momentum equation (5b) the $O(\varepsilon^2)$ pressure perturbation $\bar{P}_2$ can be expressed in terms of $\bar{H}_2$ as

$$\bar{P}_2(\xi, \Omega, Y) = \bar{H}_2 + \frac{9}{2}\bar{H}_{1,\xi\xi}(1 - Y^2)\omega^2 - A(\overline{V'^2})_0. \tag{40}$$

Inserting $\bar{P}_2$ into the X-momentum equation (5a), using the continuity equation (4) and integrating with respect to Y gives:

$$\bar{V}_2(X, \Omega, 1) = \left(-3 + \bar{H}_1 + \sqrt{A}\bar{U}_D - 2\sqrt{A}\int_0^1 \bar{U}_D \ dY\right)\omega\bar{H}_{1,\xi}$$
$$+3\omega^3\bar{H}_{1,\xi\xi\xi} + \omega\bar{H}_{2,\xi} + \omega\bar{H}_{3/2,\Omega} \qquad (41)$$

However, $\bar{V}_2$ has to satisfy the kinematic boundary condition as well, i.e.

$$\bar{V}_2 + \bar{V}_{1,Y}\bar{H}_1 = (\bar{H}_{2,\xi} + \bar{U}_1\bar{H}_{1,\xi} + \bar{H}_{3/2\Omega})\omega. \qquad (42)$$

Thus we obtain the solvability condition

$$\omega^3\bar{H}_{1,\xi\xi\xi} + \omega\bar{H}_{1,\xi}\left(\bar{H}_1 - 1\right) = 0, \qquad (43)$$

which is a third order differential equation for $\bar{H}_1$ as a function of the fast variable ξ. It is essentially the same differential equation (26) which we have obtained in our first approach. Integrating (43) with respect to ξ we obtain

$$\omega^2\bar{H}_{1,\xi\xi} + \frac{1}{2}\bar{H}_1^2 - \bar{H}_1 = R, \qquad (44)$$

where $R = (\Omega)$ is a constant of integration which may depend on the slowly varying variable Ω. Multiplying it with $\bar{H}_{1,\xi}$ and integrating with respect to ξ again yields

$$-3\omega^2\bar{H}_{1,\xi}^2 = p(\bar{H}_1, R(\Omega), S(\Omega)), \qquad (45)$$

where $S = S(\Omega)$ is another slowly varying constant of integration. We have recovered equation (28) again. The only difference is that the constants of integration are allowed to vary on the slow variable Ω. Differential equations for both R and S as functions of the slow variable Ω will be obtained by avoiding secular terms in the equation for the $O(\varepsilon^{5/2})$ terms.

Terms of order $O(\varepsilon^{5/2})$ Using the Y-momentum equation (5b) and the dynamic boundary condition (8) we obtain the $O(\varepsilon^{5/2})$ pressure perturbation $\bar{P}_{5/2}$:

$$\bar{P}_{5/2} = \bar{H}_{5/2} + \frac{9}{2}\left(\omega^2\bar{H}_{3/2,\xi\xi} + \omega^2\bar{H}_{1,\xi\Omega} + \bar{H}_{1,\xi}\omega\frac{d\omega}{d\Omega}\right)\left(1 - Y^2\right). \qquad (46)$$

In the balance of the $O(\varepsilon^{5/2})$ terms of the X-momentum equation the Reynolds shear stress has to be taken into account, i.e.

$$(\bar{U}_{5/2,\xi} + \bar{U}_{2,\Omega})\omega + 3(\bar{U}_{3/2,\xi} + \bar{U}_{1,\Omega})\omega =$$

$$-(\bar{P}_{5/2,\xi} + \bar{P}_{2,\Omega})\omega - a(\overline{U'V'})_{0,Y} - \frac{1}{3}A(\overline{U'V'})_{1,Y} \qquad (47)$$

$$-\bar{U}_1\bar{U}_{1,\Omega}\omega - \bar{U}_1\bar{U}_{3/2,\xi}\omega - \bar{U}_{3/2}\bar{U}_{1,\xi}\omega - \bar{V}_{3/2}\bar{U}_{1,Y} - \bar{V}_1\bar{U}_{3/2,Y}.$$

Using the continuity equation (4), the dynamic boundary condition (8) and equation (39) we obtain

$$-\bar{V}_{5/2} - 3(\bar{H}_{3/2,\xi} + \bar{H}_{1,\Omega})\omega =$$

$$= -\bar{H}_{5/2,\xi}\omega - 3\bar{H}_{3/2,\xi\xi\xi}\omega^3 - \bar{H}_{2,\Omega}\omega-$$

$$-6\bar{H}_{1,\xi\xi\Omega}\omega^3 - 9\omega^2\frac{d\omega}{d\Omega}\bar{H}_{1,\xi\xi} - \frac{1}{2}(\bar{H}_1^2)_\Omega\omega + (\bar{H}_1\bar{H}_{3/2})_\xi\omega-$$

$$-(\bar{H}_{1,\Omega} + \bar{H}_{3/2,\xi})\sqrt{A}\bar{U}_D + 2\left(\bar{H}_{3/2,\xi} + \bar{H}_{1,\Omega}\right)\omega\sqrt{A}\int_0^1 \bar{U}_D\ dy+ \qquad (48)$$

$$+a(\overline{U'V'})_0|_{Y=0} - \frac{A}{3}\left((\overline{U'V'})_1|_{Y=1} - (\overline{U'V'})_1|_{Y=0}\right).$$

Finally, with the help of the kinematic boundary condition for the $O(\varepsilon^{5/2})$ terms, i.e.

$$\bar{V}_{5/2} + \bar{V}_{1,Y}\bar{H}_{3/2} + \bar{V}_{3/2,Y}\bar{H}_1 =$$

$$= \bar{H}_{5/2,\xi}\omega + \bar{H}_{2,\Omega}\omega + \bar{U}_1\bar{H}_{3/2,\xi}\omega + \bar{U}_{3/2}\bar{H}_{1,\xi}\omega + \bar{U}_1\bar{H}_{1,\Omega}\omega, \qquad (49)$$

we obtain the following equation for $\bar{H}_{3/2}$:

$$\omega^2\bar{H}_{3/2,\xi\xi} + \bar{H}_{3/2}\bar{H}_1 - \bar{H}_{3/2} = r \qquad (50)$$

with

$$\omega r_\xi = \frac{A}{3}\bar{H}_1 - \frac{a}{3} - \bar{H}_{1,\xi\xi\Omega}\omega^3 - \bar{H}_{1,\xi\xi}\omega^2\frac{d\omega}{d\Omega} - R_\Omega. \qquad (51)$$

where we have used $(\overline{U'V'})_{0,Y=0} = 1$ and $(\overline{U'V'})_{1,Y=0} - (\overline{U'V'})_{1,Y=1} = 3\bar{H}_1$.

In the following we derive differential equations for the slowly varying 'constants' R and S. Integrating (51) with respect to ξ over one period gives the following differential equation for R:

$$\omega R_\Omega = -\frac{a}{3} + \frac{A}{3}\int_0^1 \bar{H}_1(\xi, \Omega)\ d\xi. \qquad (52)$$

Multiplying equation (44) with $\bar{H}_{3/2,\xi}$ and adding (50) multiplied by $\bar{H}_{1,\xi}$ we get

$$\left(\omega^2 \bar{H}_{3/2,\xi\xi} + \bar{H}_{3/2}\bar{H}_1 - \bar{H}_{3/2} - r\right)\bar{H}_{1,\xi}+$$
$$+\left(\omega\bar{H}_{1,\xi\xi} + \frac{1}{2}\bar{H}_1^2 - \bar{H}_1 - R\right)\bar{H}_{3/2,\xi} = 0. \tag{53}$$

Integrating (53) with respect to ξ over one period, and integrating the result by parts yields

$$\int_0^1 r_\xi \, \bar{H}_1 \, d\xi = 0. \tag{54}$$

Taking the derivative of (44) with respect to Ω and using (51) and (54) we obtain the following differential equation for S:

$$\omega \, S_\Omega = \frac{a}{3}\int_0^1 \bar{H}_1 \, d\xi - \frac{A}{3}\int_0^1 \bar{H}_1^2 \, d\xi. \tag{55}$$

Thus we have derived a set of differential equations for the slowly varying constants of integration R and S. As we will discuss later the wave length and amplitude of the undulated surface can be determined from R and S.

The main result of the multiple scales analysis can now be summarized as follows: Let $\mathcal{H}(X; R, S)$ be the solution of

$$\mathcal{H}_X^2 + \frac{1}{3}\mathcal{H}^3 - \mathcal{H}^2 = 2R\,\mathcal{H} + 2S, \quad \mathcal{H}_X(0, R, S) = 0, \quad \mathcal{H}_{XX}(0, R, S) > 0, \tag{56}$$

where $R = R(\Omega)$ and $S = S(\Omega)$ are the solutions of (52), (55). If $\bar{H}_1(0)$, $\bar{H}_1'(0)$ and $\bar{H}_1''(0)$ is given initial conditions for R and S are obtained from (27) and (28). Then the first-order perturbation of the free surface, i.e. $\bar{H}_1$, is given by:

$$\bar{H}_1(X) = \mathcal{H}\left(\frac{\xi - \frac{1}{2}}{\omega}; R, S\right), \quad \mathcal{X} = \int_0^\Omega \frac{d\Omega}{\omega}, \quad \xi = \frac{\Omega}{\sqrt{\varepsilon}}, \tag{57}$$

with

$$X(\xi, \varepsilon) = \frac{1}{\sqrt{\varepsilon}}\mathcal{X} + X_0, \tag{58}$$

where X_0 is chosen such that $\mathcal{H}(-X_0, R(0), S(0)) = \bar{H}_1(0)$.

3.3   Uniformly valid differential equation

In Jurisits et al. (2007) and Grilllhofer and Schneider (2003) the following third order differential equation

$$\hat{H}_{XXX} + \hat{H}_X(\hat{H} - 1) = \frac{\sqrt{\varepsilon}}{3}\left(-a + A\hat{H}\right) \tag{59}$$

has been derived to describe the perturbation of the free surface of an open channel flow near critical flow conditions. The equations is written here in a form such that the parameters a, A and ε are the same as defined in (15), (16, (17), respectively. In the derivation of (59) terms resulting from the unbalanced external forces, which are of the order $O(\varepsilon^{5/2})$ have been included in the balance of the order $O(\varepsilon^2)$. As a result the perturbation parameter ε appears in the equation for the leading order terms. However, equation (59) can be taken as a the starting point of a multiple scales analysis. We want to show here that the leading order terms for the fast and slowly varying quantities agree with the results presents in the previous section. Since equation (59) contains all the information of the multiple scales analysis we call it a uniformly valid differential equation.

Equation (59) is equivalent to the first order system of differential equation

$$3\hat{H}_X^2 = p(\hat{H}, \hat{R}, \hat{S}), \tag{60a}$$

$$\hat{R}_X = \frac{\sqrt{\varepsilon}}{3}\left(-a + A\hat{H}\right), \quad \hat{S}_X = -\frac{\sqrt{\varepsilon}}{3}\left(-a + A\hat{H}\right)\hat{H}, \tag{60b}$$

where $p(\hat{H}, \hat{R}, \hat{S})$ is the third order polynomial defined in (28). In order to study the asymptotic behavior of the solution (59) in the limit $\varepsilon \to 0$ we can perform a multiple scale expansion according to the same lines as in preceeding subsection

$$\hat{H} \sim \hat{H}_1(\hat{\xi}, \hat{\Omega}) + \dots, \quad \hat{R} \sim \hat{R}_1(\hat{\xi}, \hat{\Omega}) + \dots, \quad \hat{S} \sim \hat{S}_1(\hat{\xi}, \hat{\Omega}) + \dots, \tag{61}$$

where $\hat{H}_1$, $\hat{R}_1$, $\hat{S}_1$ are assumed to be periodic function with period 1 of the fast variable $\hat{\xi}$. The slow variable $\hat{\Omega}$ and the fast variable $\hat{\xi}$ are defined analogously to (32). Now it is easy to see that the leading order terms $\hat{H}_1$, $\hat{R}_1$, $\hat{S}_1$ satisfy exactly the same differential equations as $\bar{H}$, R and S. In particular $\hat{R}_1$ and $\hat{S}_1$ are functions of the slow variable $\hat{\Omega}$ only.

We remark that one of the two perturbations terms on the right hand side of (59) can be eliminated by setting

$$\hat{H}(X) = 1 + b\left(G(X/c) - 1\right), \quad b = \left|1 - \frac{a}{A}\right| \quad c = 1/\sqrt{b}. \tag{62}$$

We obtain

$$G''' \pm G'(G - 1) = \frac{\sqrt{\varepsilon}}{3}\tilde{A}G, \quad \tilde{A} = \frac{c}{b}, \tag{63}$$

provided that $A \neq a$ and $A \neq 0$. The plus sign holds for $A > a$ and the minus sign for $A < a$.

If $A = a$ we set $b = A^{2/3}$, $c = 1/\sqrt{b}$ and obtain

$$G''' \pm G'G = \frac{\sqrt{\varepsilon}}{3}\tilde{A}G, \quad \tilde{A} = \frac{c}{b}. \tag{64}$$

3.4   The equations for the slowly varying variables

We have already derived the differential equations for the slowly varying quantities R and S. Here we want to indicate how the integrals on the right hand side can be considered as functions of R and S. It is obvious that $\bar{H}_1$ is a periodic function of the fast variable if the polynomial $p(\bar{H}_1, R, S)$ has three real roots, $h_1(R, S) \leq h_2(R, S) \leq h_3(R, S)$. Now let

$$I_j(R, S) = \int_{h_2(R,S)}^{h_3(R,S)} \frac{h^j\ dh}{\sqrt{(h - h_1(R, S))(h - h_2(R, S))(h_3(R, S) - h)}}, \quad (65)$$

with $j = 0, 1, 2$. Then the equations for R, S and ω are

$$R_\Omega = -\frac{a}{3\omega} + \frac{2A}{\sqrt{3}} I_1(R, S), \qquad (66a)$$

$$S_\Omega = \frac{2a}{\sqrt{3}} I_1(R, S) - \frac{2A}{\sqrt{3}} I_2(R, S), \qquad (66b)$$

$$\omega = \frac{1}{2\sqrt{3}I_0(R, S)}. \qquad (66c)$$

We can state a sufficient condition for the existence of a solution of (66) for all $\Omega > 0$: Let $A > a$, and $R(0) > 0$ and $S(0) < 0$ such that the polynomial $p(H, R(0), S(0))$ has three real roots then the solution of the initial value problem (66) for the slow variables exists for all $\Omega > 0$.

Proof
(i) It is sufficient to consider the case $A > 0$. If $a \neq 0$ the transform

$$\bar{H}_1(\xi, \Omega), = 1 + b\,\bar{G}_1(\xi/c, \Omega/c), \quad b = 1 - \frac{a}{A}, \quad c = 1/\sqrt{b} \qquad (67)$$

can be used to eliminate a.
(ii) We consider the polynomial $p(H)$ defined in (28). If $R > 0$ it has a local maximum at $H^*_{max} = 1 - \sqrt{1 + 2R} < 0$ and a local minimum at $H^*_{min} = 1 - \sqrt{1 + 2R} > 0$. If $p(h, R, S)$ has three roots: $h_1 < H^*_{max} < 0$ and $h_3 > H^*_{min} = 1 - \sqrt{1 + 2R} > 0$. Thus $h_2 = 6S/(h_1 h_3) > 0$.
(iii) Since h_2 and h_3 are positive the integrals I_j, $j = 0, 1, 2$ are also positive. With $A > 0$ it follows that $R_\Omega > 0$ and $S_\Omega < 0$. Thus zero is a lower bound for R and an upper bound for S. It can be shown that the integrals I_j can be estimated by

$$0 < I_j < C_R(1 + \sqrt{R})^j, \quad j = 0, 1, 2, \qquad (68)$$

for some constant C_R. Thus we obtain $R < \tilde{C}\Omega^2$ for an appropriate constant $\tilde{C}$. Furthermore, S_Ω can be estimated from below independently of S. Integration yields a lower bound for S. It remains to show that the right hand side of the differential equation is well defined for $\Omega > 0$. Thus we have to show that h_2 and h_3 never coalesce.

(iv) The differential equations for R and S can be reformulated as differential equations for

$$h_m = \frac{h_2 + h_3}{2}, \quad \Delta h = \frac{h_3 - h_2}{2}. \tag{69}$$

(v) The solution of the differential equations for h_m, Δh can be discussed in the h_m, Δh-plane. It turns out that on line $\Delta h = 0$, $\Delta h_\Omega = 0$, but $h_{m,\Omega} > 0$ holds. Thus Δh cannot become zero at a finite Ω and this completes the proof.

Asymptotic behavior far downstream $(\Omega, \mathcal{X} \to \infty)$ To discuss the behavior for $\mathcal{X} \to \infty$ it is appropriate to consider h_m and Δh defined in (69) instead of R, S. Expanding the integrals I_j for $\Delta h/h_m \ll 1$ we obtain the following differential equations for Δh and h_m:

$$\Delta h_\mathcal{X} \sim -A\frac{\Delta h}{4h_m}, \quad h_{m,\mathcal{X}} \sim \frac{A}{3}\left(1 + \frac{1}{h_m}\right) \tag{70}$$

with the solution

$$h_m \sim \frac{A}{3}\mathcal{X} + \ln\left(1 + \frac{A}{3}\mathcal{X}\right), \quad \Delta h = O(\mathcal{X}^{-3/4}). \tag{71}$$

Thus the amplitude of the oscillation decays and the mean value over an oscillation period increases linearly with increasing $\mathcal{X}$.

Breakdown of the multiple scales approximation   If $a > A$ the roots h_1 and h_2 may coalesce and thus the multiple scale solution may terminate at a finite value of Ω. This has been observed by Jurisits et al. (2007). They solved the uniformly valid differential equation (59) numerically for the case $a = 3A$ and compared the solution with the multiple scales approximation, see figure 2. The solution of the uniformly valid differential equation behaves at first almost periodically and is in excellent agreement with multiple scales approximation. Representative for the slowly varying quantities the zeros h_2 and h_3 of the polynomial $p(\bar{H}_1)$ are shown.

All of a sudden the solution of the uniformly valid differential equation terminates in a singularity. At first glance h_2 and h_3 are almost constant.
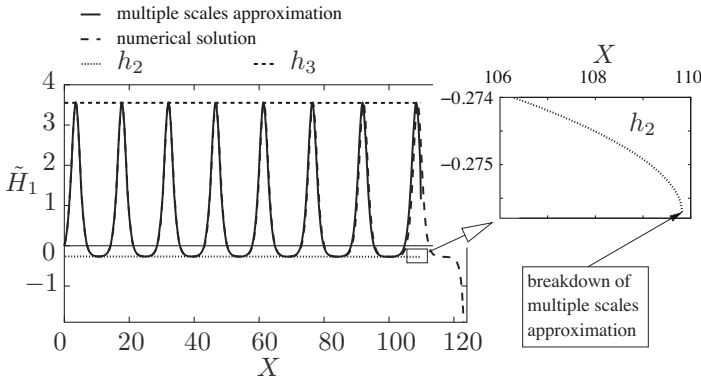
Figure 2. Breakdown of solution: Comparison of a numerical solution of the uniformly valid differential equation (59) with the multiple scales approximation. Parameter values: $\varepsilon 3 \times 10^{-12}$, $A = 1$, $a = 3$, Inital conditions $\bar{H}_1(0) = 0$, $\bar{H}_1'(0) = 0.3$, $\bar{H}_1''(0) = 0.314$. The zero h_2 of the ploynomial p is shown in the insert to the right, see Jurisits et al. (2007).

But a detailed view of h_2 shows that it terminates in a square-root singularity shortly before the breakdown of the numerical solution. Considering the multiple scales approximation it turns out that the two zeros h_1 and h_2 coalesce. Thus the multiple scales approximation terminates at a final value of Ω.

3.5   Initially fully developed flow

Here we focus on a flow which is fully developed far upstream. Thus the external forces are in equilibrium, i.e. $a = 0$.

It remains to determine appropriate initial conditions for R and S. As the origin of the X-axis we choose the location of the first crest of the free surface, i.e. the first maximum of $\bar{H}_1$. Since $\bar{H}_1$ has to decay to zero for $X \to -\infty$, the period becomes infinite as $X \to -\infty$.

This gives the following initial conditions for R and S:

$$R(0) = S(0) = 0. \tag{72}$$

In this case the shift of the origin X_0 has to depend on ε. It is chosen such that the first wave crest is at $X = 0$. We have

$$X(\xi, \varepsilon) = \frac{1}{\sqrt{\varepsilon}} \mathcal{X} + X_0(\varepsilon), \quad X_0(\varepsilon) = -\int_0^{1/2} \frac{1}{\omega(\sqrt{\varepsilon}\xi)} \, d\xi. \tag{73}$$
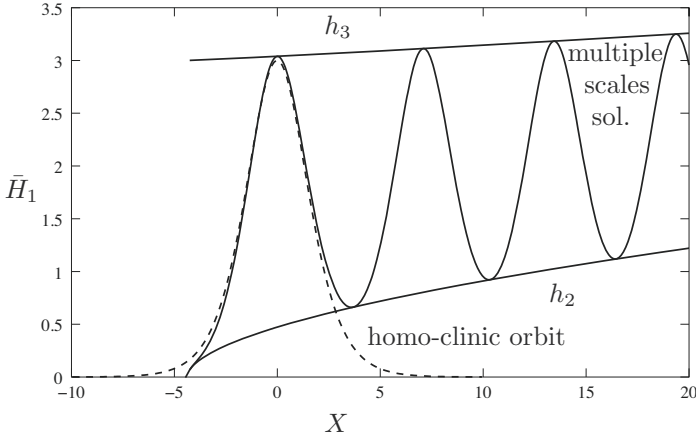
Figure 3. Multiple scales solution (57) for $A = 3$, $\varepsilon = 10^{-4}$ and the homo-clinic orbit $(A = 0)$ according to eq. (74). The solution for the slowly varying variables is represented by h_2 and h_3, i.e. the local minima and maxima, respectively.

We will see later that $\mathcal{X}(0) = 0$ and X_0 is finite. Thus the multiple scales approximation (57) fails for $X \to -\infty$. However, an asymptotic analysis using the original coordinate X yields the inviscid solution

$$\bar{H}_1(X) = \mathcal{H}(X; 0, 0), \tag{74}$$

which is a homo-clinic orbit in the phase plane. It is the limiting solution for the first elevation and describes the behavior for $X \to -\infty$ correctly, but fails to approximate the undular behavior.

In Figure 3 the multiples scales solution (57), evaluated for $\varepsilon = 10^{-4}$, $A = 3$ and the homo-clinic orbit are plotted. Moreover the solution of the equations for the slowly varying variables represented by the zeros h_2 and h_3 of the polynomial $p(h; R, S)$ are also shown in Figure 3. In Figure 4 the multiple scales solution (57) and the homo-clinic orbit (74) are shown in the phase plane.

Behavior near the origin ($\Omega \ll 1$) Although the polynomial $p(h)$, which occurs in the denominator of I_1 and I_2, respectively, has a double root at $h_2 = h_1 = 0$ for $R = S = 0$, these integrals exist for $R = S = 0$:

$$I_1(0, 0) = 2\sqrt{3}, \quad I_2(0, 0) = 4\sqrt{3}. \tag{75}$$
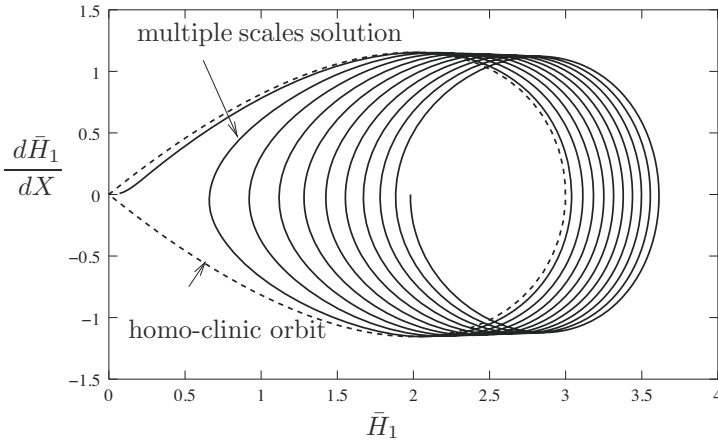
Figure 4. Phase portrait of the multiple scales solution (57) for $A = 3$, $\varepsilon = 10^{-4}$ and the homo-clinic orbit $(A = 0)$ according to eq. (74).

Using

$$R \sim R_\Omega(0)\Omega = 4A\,\Omega, \quad S \sim S_\Omega(0)\Omega = -8A\,\Omega \tag{76}$$

we obtain for the zeros of the polynomial $p(h)$:

$$h_1 \sim -4\sqrt{A\Omega}, \quad h_2 \sim 4\sqrt{A\Omega}, \quad h_3 \sim 3 + \frac{8}{3}A\Omega + ... \quad . \tag{77}$$

Expanding I_0 for $\Omega \ll 1$ gives

$$\frac{1}{\omega} \sim \ln\frac{1}{A\Omega} + 2\ln 6. \tag{78}$$

With

$$\mathcal{X}(\Omega) = \int_0^\Omega \frac{1}{\omega}\; d\Omega \sim \Omega\left(\ln\frac{1}{A\Omega} + 1 + 2\;\ln 6\right) \tag{79}$$

we get $\mathcal{X}(0) = 0$ and obtain the shift

$$X_0(\varepsilon) = -\frac{1}{\sqrt{\varepsilon}}\mathcal{X}(\frac{\sqrt{\varepsilon}}{2}) = -\int_0^{1/2} \frac{1}{\omega(\sqrt{\varepsilon}\xi)}\; d\xi \sim \frac{1}{2}\;\ln A\sqrt{\varepsilon} - \frac{3}{2}\;\ln 2 - \;\ln 3 - \frac{1}{2}. \tag{80}$$
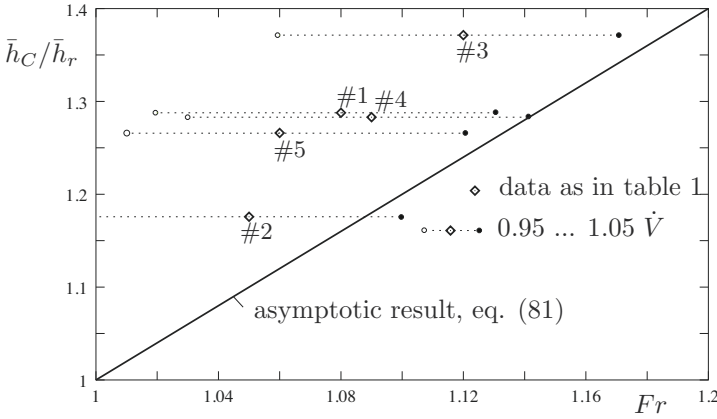
Figure 5. Comparison of calculated and measured amplitudes $\overline{h}_C/\overline{h}_r$ of the first elevation. The dotted lines indicate how the non-dimensionalized height of the first crest changes for a variation of the volume flow rate within $\pm 5\%$ around the value given in table 1.
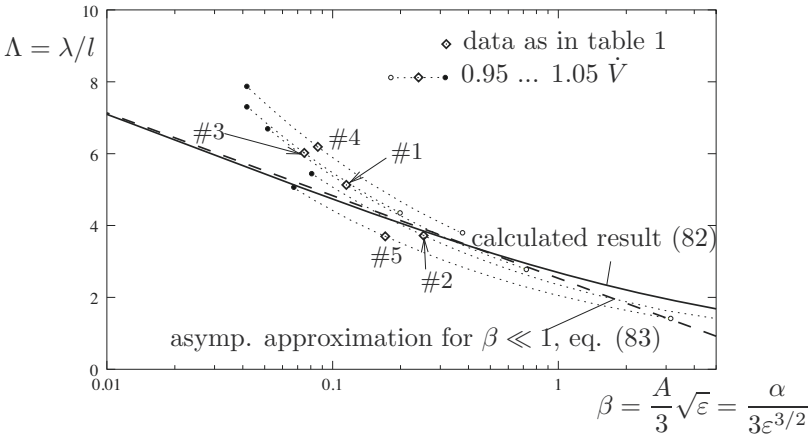
Figure 6. Comparison of calculated and measured distances λ/l between the first two maxima. The dotted lines indicate how the non-dimensionalized first wave length changes for a variation of the volume flow rate within $\pm 5\%$ around the value given in table 1.

#	Exp.	V $[\,m^2/s\,]$	α $[rad]$	$\bar{h}_r$ $[\,m\,]$	w $[\,m\,]$
1	HCUJ8e	0.028	4.10×10^{-3}	0.041	0.25
2	HCUJ10c	0.080	3.99×10^{-3}	0.084	0.25
3	HCUJ4b	0.119	4.99×10^{-3}	0.105	0.25
4	HCUH1b	0.0416	3.7×10^{-3}	0.053	0.25
5	HCUJ4a	0.120	4.33×10^{-3}	0.109	0.25

#	Exp.	λ $[\,m\,]$	$\bar{h}_C$ $[\,m\,]$	Fr $[-]$	β $[-]$	$\dfrac{\lambda_{as}}{\lambda_{ex}}$ $[-]$
1	HCUJ8e	0.310	0.052	1.077	0.115	0.94
2	HCUJ10c	0.600	0.100	1.049	0.225	1.07
3	HCUJ4b	0.750	0.144	1.119	0.075	0.87
4	HCUH1b	0.450	0.068	1.088	0.086	0.83
5	HCUJ4a	0.660	0.138	1.062	0.171	1.20

Table 1. Experimental data, selected from Chanson (1993)

Comparison with experiments   In the literature there is a large amount of experimental data for the undular hydraulic jump, but to obtain a meaningful comparison with the present analysis the experiments have to satisfy the following criteria:

  (i) A fully developed flow far upstream is required. This is only possible in an inclined channel.
 (ii) The theory is based on an asymptotic expansion in terms of the small parameter ε. Thus we consider only experiments with $0 < \varepsilon < 0.1$, i.e. $1 < Fr < 1.15$.
(iii) The relative error of neglected terms has to be small. The smallest terms that influence the leading order result for the wave length are of order $O(A\varepsilon^{5/2}) = O(\alpha\sqrt{\varepsilon})$, whereas terms of order $O(\varepsilon^3)$ are neglected. Thus the relative truncation error is of $O(\varepsilon^{5/2}/\alpha)$, and only experiments with $\varepsilon^{5/2}/\alpha$ being sufficiently small are considered.
 (iv) The height of the first crest and the first wave-length, i.e. the distance between two successive crests, must be among the measured quantities.

In Table 1 experiments selected to meet these criteria are listed. The experiments have been performed in a channel of width w.

In the analysis the maxima of the surface elevation occur at $\xi = \frac{1}{2}, \frac{3}{2}, ...$, and so on. Thus the first maximum is $\bar{H}_{1,max} = h_3(\frac{\sqrt{\varepsilon}}{2}) = 3 + 4\frac{A\sqrt{\varepsilon}}{3}$, cf. (77), and for the height $\bar{h}_C$ of the first crest we obtain:

$$\bar{h}_C/h_r \sim 1 + \frac{2}{3}(\,Fr - 1)\bar{H}_{1,max} = 1 + 2(\,Fr - 1)(1 + \frac{8}{3}\beta). \quad (81)$$

The parameter $\beta = \frac{A\sqrt{\varepsilon}}{3}$ has been introduced in Grillhofer (2002) and Grillhofer and Schneider (2003) and is used also here for convenience.

Let Λ be the scaled first wave lengths. It is referred to reference $l\bar{h}_r/\delta = \bar{h}_r/3\sqrt{\varepsilon}$, see (2a), (3). Thus we obtain from

$$\Lambda(\varepsilon) = \frac{1}{\sqrt{\varepsilon}} \left(\mathcal{X}(\frac{3\sqrt{\varepsilon}}{2}) - \mathcal{X}(\frac{\sqrt{\varepsilon}}{2}) \right) = \int_{1/2}^{3/2} \frac{1}{\omega(\sqrt{\varepsilon}\xi)} \ d\xi. \qquad (82)$$

In the limit $\varepsilon \to 0$ eq. (82) becomes

$$\Lambda(\varepsilon) \sim \ \ln \frac{8\sqrt{3}}{A\sqrt{\varepsilon}} + 1 = \ \ln \frac{8}{\sqrt{3}\beta} + 1. \qquad (83)$$

In Figures 5 and 6 a comparison of measured data with the results (81), (82) and (83), respectively, is given. The volume flux in the experiments is measured with an accuracy of 5% (cf Chanson (1993), p. 2-1). Therefore the effect of a variation of the volume flux by $\pm 5\%$ is also shown in the figures. It can be seen that the results are very sensitive with respect to uncertainties in the volume flux. In Figure 6 results are given for both a numerical evaluation of Λ and the asymptotic approximation for small values of $\beta = A\sqrt{\varepsilon}/3$.

Taking into account that the aspect ration w/h_r, where w is the width of the channel, is larger than 0.16 in all experiments, so that side wall effects may influence the results considerably, the agreement between the measured data and the theoretical results for plane flow is reasonable.

4   Conclusions

The multiple scaling approach as proposed in this paper permits a self-consistent asymptotic analysis of the undular hydraulic jump in turbulent flow. Results for the perturbation of the height of the fluid are obtained without making use of a turbulence model. Ordinary differential equations have been derived for the slowly varying quantities, i.e. the amplitude and the wave-length, as well as for the rapidly varying height of the free surface.

The price for the rigorous analysis is a limited range of parameters where the requirements for the analysis are satisfied. In view of the high sensitivity of the the wave length and the amplitude, the agreement with experimental data appears reasonable.

Bibliography

V.M. Andersen. Undular hydraulic jump. *J. Hydraulics Div.*, 104(HY8): 1185–1188, 1978.

T.B. Benjamin and M.J. Lighthill. On cnoidal waves and bores. *Proc. Roy. Soc.*, A224:448–460, 1954.

P. Böß. Berechnung der Wasserspiegellage. *Forschungsarbeiten VDI*, 284, 1927.

H. Chanson. Characteristics of undular hydraulic jumps. *University of Queensland, Department of Civil Engineering Research Report Series*, CE146, 1993.

H. Chanson and J.S. Montes. Characteristics of undular hydraulic jumps: Experimental apparatus and flow patterns. *J. Hydraulic Eng.*, 121:129–144, 1995.

V.T. Chow. *Open-Channel Hydraulics.* McGraw-Hill, 1959.

W. Grillhofer. *Der wellige Wassersprung in einer turbulenten Kanalströmung mit freier Oberfläche.* Dissertation, Technische Universität Wien, 2002.

W. Grilllhofer and W. Schneider. The undular hydraulic jump in turbulent open channel flow at large reynolds numbers. *Phys. Fluids*, 15:730–735, 2003.

W. Hager. *Energy Dissipators and Hydraulic Jump.* Kluwer, 1992.

W.H. Hager and K. Hutter. On pseudo-uniform flow in open channel hydraulics. *Acta Mechanica*, 53:183–200, 1984.

F.M. Henderson. *Open Channel Flow.* Macmillan Company, 1966.

R.S. Johnson. Shallow water waves on a viscous fluid - the undular bore. *Phys. Fluids*, 15:1693–1699, 1972.

R. Jurisits, W. Schneider, and Y.S. Bae. A multiple scales solution to the undular hydraulic jump problem. *PAMM*, 7:4120007 – 4120008, 2007.

K. Kaufmann. *Hydromechanik II.* Springer, 1934.

H. Lauffer. Wassersprung bei kleinen Sprunghöhen. *Wasserwirtschaft und Technik*, pages 137–140, 1935.

I. Ohtsu, Y. Yasuda, H. Gotoh, and M. Iahr. Hydraulic condition for undular-jump formations. *J. Hydraulic Res.*, 39:203–209, 2001.

R. Reinauer and W. Hager. Non-breaking undular hydraulic jump. *J. Hydraulic Res.*, 33:683–698, 1995.

H. Steinrück, W. Schneider, and W. Grillhofer. A multiple scales analysis of the undular hydraulic jump in turbulent open channel flow. *Fluid Dyn. Res.*, 33:41–55, 2003.

Modern Aspects of High-Reynolds-Number Asymptotics of Turbulent Boundary Layers
From Fully Attached to Marginally Separated Flows

Bernhard Scheichl[†‡*]

† Institute of Fluid Mechanics and Heat Transfer, Vienna University of Technology, Vienna, Austria
‡ AC²T research, Austrian Center of Competence for Tribology, Wiener Neustadt, Austria

Abstract This contribution reports on recent efforts with the ultimate goal to obtain a fully self-consistent picture of turbulent boundary layer separation. To this end, it is shown first how the classical theory of turbulent boundary layers having an asymptotically small streamwise velocity deficit can be generalised rigorously to boundary layers with a slightly larger, i.e. moderately large, velocity defect and, finally, to situations where the velocity defect is of $O(1)$. In the latter case, the formation of short recirculation zones describing marginally separated flows is found possible, as described in a rational manner.

1   Introduction

Despite the rapid increase of computer power in the recent past, the calculation of turbulent wall-bounded flows still represents an extremely challenging and sometimes insolvable task. Direct-Numerical-Simulation computations based on the full Navier–Stokes equations are feasible for moderately large Reynolds numbers only. Flows characterised by much higher Reynolds numbers can be investigated if one resorts to turbulence models for the small scales, as accomplished by the method of Large Eddy Simulation, or for all scales, as in computer codes designed to solve the Reynolds-averaged Navier–Stokes equations. Even then, however, the numerical efforts rapidly

---

increase with increasing Reynolds number. This strongly contrasts the use
of asymptotic theories, the performance of which improves as the values of
the Reynolds number become larger and, therefore, may be considered to
complement purely numerically based work.

With a few exceptions (e.g. Deriat, 1986; Walker, 1998; Scheichl and
Kluwick, 2008a), studies dealing with the high-Reynolds-number properties
of turbulent boundary layers start from the time- or, equivalently, Reynolds-
averaged equations. By defining non-dimensional variables in terms of a
representative length $\tilde{L}$ and flow speed $\tilde{U}$ and assuming incompressible nom-
inally steady two-dimensional flow they take on the form

$$\frac{\partial u}{\partial x} + \frac{\partial v}{\partial y} = 0 \,, \tag{1a}$$

$$u\frac{\partial u}{\partial x} + v\frac{\partial u}{\partial y} = -\frac{\partial p}{\partial x} + \frac{1}{Re}\nabla^2 u - \frac{\partial \overline{u'^2}}{\partial x} - \frac{\partial \overline{u'v'}}{\partial y} \,, \tag{1b}$$

$$u\frac{\partial v}{\partial x} + v\frac{\partial v}{\partial y} = -\frac{\partial p}{\partial y} + \frac{1}{Re}\nabla^2 v - \frac{\partial \overline{u'v'}}{\partial x} - \frac{\partial \overline{v'^2}}{\partial y} \,. \tag{1c}$$

Herein $\nabla^2 = \partial^2/\partial x^2 + \partial^2/\partial y^2$, and (x,y), (u,v), (u',v'), $-\overline{u'^2}$, $-\overline{u'v'}$, $-\overline{v'^2}$,
and p are Cartesian coordinates measuring the distance along and perpen-
dicular to the wall, the corresponding time mean velocity components, the
corresponding velocity fluctuations, the components of the Reynolds stress
tensor, and the pressure, respectively. The Reynolds number is defined by
$Re := \tilde{U}\tilde{L}/\tilde{\nu}$, where $\tilde{\nu}$ is the (constant) kinematic viscosity. Equations (1)
describe flows past flat impermeable walls when supplemented with the
usual no-slip and no-penetration conditions $u = v = u' = v' = 0$. Effects of
wall curvature can be incorporated without difficulty but are beyond the
scope of the present analysis.

When it comes down to the solution of the simplified version of these
equations provided by asymptotic theory in the limit $Re \to \infty$, one is, of
course, again faced with the closure problem. The point, however, is that
these equations and the underlying structure represent closure-independent
basic physical mechanisms characterising various flow regions, identified by
asymptotic reasoning. This has been shown first in the seminal studies
by Yajnik (1970), Bush (1972), Fendell (1972), Mellor (1972), and more
recently and in considerable more depth and breath by Walker (1998) and
Schlichting and Gersten (2000) for the case of small-defect boundary layers,
which are subject of Section 2. Those exhibiting a slightly larger, i.e. a
moderately large, velocity defect are treated in Section 3. Finally, Section 4
deals with situations where the velocity defect is of $O(1)$ rather than small.

2   Classical Theory of (Small-Defect) Turbulent Boundary Layers

We first outline the basic ideas underlying an asymptotic description of turbulent boundary layers.

2.1   Preliminaries

Based on dimensional reasoning put forward by L. Prandtl and Th. von Kármán, a self-consistent time-mean description of firmly attached fully developed turbulent boundary layers holding in the limit of large Reynolds numbers Re, i.e. for $Re \to \infty$, has been proposed first in the aforementioned early asymptotic work (Yajnik, 1970; Bush, 1972; Fendell, 1972; Mellor, 1972). One of the main goals of the present investigation is to show that this rational formulation can be derived from a minimum of assumptions:

(A) all the velocity fluctuations are of the same order of magnitude in the limit $Re \to \infty$, so that all Reynolds stress components are equally scaled by a single velocity scale u_{ref}, non-dimensional with a global reference velocity $\tilde{U}$ (hypothesis of locally isotropic turbulence);

(B) the pressure gradient does not enter the flow description of the viscous wall layer to leading order (assumption of firmly attached flow);

(C) the results for the outer predominantly inviscid flow region can be matched directly with those obtained for the viscous wall layer (assumption of "simplest possible" flow structure).

In those outstanding papers (Yajnik, 1970; Bush, 1972; Fendell, 1972; Mellor, 1972), u_{ref} is taken to be of the same order of magnitude in the fully turbulent main portion of the boundary layer and in the viscous wall layer and, hence, equal to the skin-friction velocity

$$u_\tau := \left[Re^{-1} (\partial u / \partial y)_{y=0} \right]^{1/2} . \tag{2}$$

This in turn leads to the classical picture, according to which (i) the streamwise velocity defect with respect to the external impressed flow is small and of $O(u_\tau)$ across most of the boundary layer, while (ii) the streamwise velocity is itself small and of $O(u_\tau)$ inside the (exponentially thin) wall layer, and, finally, (iii) $u_\tau / U_e = O(1/\ln Re)$. Furthermore, then (iv) the celebrated universal logarithmic velocity distribution

$$u/u_\tau \sim \kappa^{-1} \ln y^+ + C^+ , \quad y^+ := y \, u_\tau \, Re \to \infty . \tag{3}$$

is found to hold in the overlap of the outer (small-defect) and inner (viscous wall) layer. Here κ denotes the von Kármán constant; in this connection we note the currently accepted empirical values $\kappa \approx 0.384$, $C^+ \approx 4.1$, which

refer to the case of a perfectly smooth surface (see Österlund et al., 2000) and have been obtained for a zero pressure gradient.

This might be considered to yield a stringent derivation of the logarithmic law of the wall (3), anticipating the existence of an asymptotic state and universality of the wall layer flow as $Re \to \infty$; a view which, however, has been increasingly challenged in more recent publications (e.g. Barenblatt and Goldenfeld, 1995; Barenblatt et al., 2000; Barenblatt and Chorin, 2000). It thus appears that – as expressed by Walker (1998) – "...although many arguments have been put forward over the years to justify the logarithmic behaviour, non are entirely satisfactory as a proof, ...". As a result, one has to accept that matching (of inner and outer expansions), while ensuring self-consistency, is not sufficient to uniquely determine (3). In the following, from the viewpoint of the time-averaged flow description the logarithmic behaviour (3), therefore, will be taken to represent an experimentally rather than strictly theoretically based result holding in situations where the assumption (B) applies. The description of the boundary layer in the limit $Re \to \infty$ can then readily be formalised.

In passing, we mention that in the classical derivations (see Yajnik, 1970; Bush, 1972; Fendell, 1972; Mellor, 1972) the assumption (B) is not adopted, in favour of rather heuristic dimensional arguments already put forward by (among other authors) Clauser (1956) that constitute the scalings of the thicknesses of both the entire boundary and the wall layer. In view of assumption (A) and dimensional notation, these are given by $\tilde{L}\,u_{\mathrm{ref}}$ and $\tilde{\nu}/(\tilde{U}u_{\mathrm{ref}})$, respectively. As demonstrated in detail by Mellor (1972), then (3) results from matching, which decisively contrasts the present study where it is imposed. However, this procedure additionally requires to anticipate *a priori* that in the outer layer $u \sim u_0 + O(u_{\mathrm{ref}})$, $u_0 = O(1)$. On balance, we thus render that classical approach less generic than that proposed here and elucidated in the following.

2.2   Leading-Order Approximation

Inside the wall layer where $y^+ = y\,u_\tau Re = O(1)$ the streamwise velocity component u, the Reynolds shear stress $\tau := -\overline{u'v'}$ and the pressure p are expanded in the form

$$u \sim u_\tau(x; Re)\,u^+(y^+) + \cdots , \tag{4a}$$

$$\tau \sim u_\tau^2(x; Re)\,t^+(y^+) + \cdots , \tag{4b}$$

$$p \sim p_0(x) + \cdots , \tag{4c}$$

where u^+ exhibits the limiting behaviour implied by (3):

$$u^+(y^+) \sim \kappa^{-1}\ln y^+ + C^+ , \quad y^+ \to \infty . \tag{5}$$

Assumption (C), quoted in Subsection 2.1, then uniquely determines the asymptotic expansions of, respectively, u, τ, and p further away from the wall where the Reynolds stress τ is predominant. Let $\delta_o(x; Re)$ characterise the thickness of this outer main layer, i.e. of the overall boundary layer. In turn, one obtains

$$u \sim U_e(x) - u_\tau(x; Re)\, F_1'(x, \eta) + \cdots \;, \tag{6a}$$

$$\tau \sim u_\tau^2(x; Re)\, T_1(x, \eta) + \cdots \;, \tag{6b}$$

$$p \sim p_e(x) + \cdots \;, \tag{6c}$$

where $\eta := y/\delta_o$ and F_1, T_1 represent a perturbation stream function and a shape function for the Reynolds shear stress, respectively. Here and in the following primes denote differentiation with respect to η. Furthermore, U_e and p_e stand for the velocity and the pressure, respectively, at the outer edge $\eta = 1$ of the boundary layer (here taken as a sharp line with sufficient asymptotic accuracy) imposed by the external irrotational flow. The asymptotic structure of the boundary layer is sketched in Figure 1.
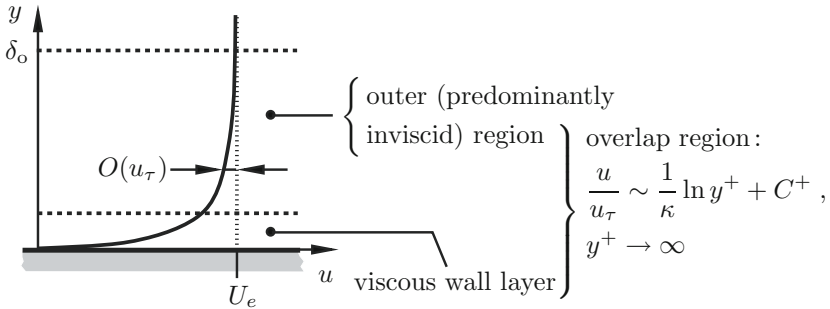
Figure 1: Structure of classical two-tiered boundary layer.

Matching of the expansions (4) and (6) by taking into account (5) forces a logarithmic behaviour of F_1',

$$F_1' \sim -\kappa^{-1} \ln \eta + C_0(x) \;, \quad \eta \to 0 \;, \tag{7}$$

yields $p_0(x) = p_e(x)$, and is achieved provided $\gamma := u_\tau/U_e$ satisfies the skin-friction relationship

$$\kappa/\gamma \sim \ln(Re\,\gamma\,\delta_o U_e) + \kappa(C^+ + C_0) + O(\gamma) \;. \tag{8}$$

From substituting (4) into the x-component (1b) of the Reynolds equations (1) one obtains the well-known result that the total stress inside the

wall layer is constant to leading order,

$$\mathrm{d}u^+/\mathrm{d}y^+ + t^+ = 1 \ . \tag{9}$$

Moreover, the expansions (6) lead to a linearisation of the convective terms in the outer layer, so that there Bernoulli's law holds to leading order,

$$\mathrm{d}p_e/\mathrm{d}x = -U_e \, \mathrm{d}U_e/\mathrm{d}x \ . \tag{10}$$

The necessary balance with the gradient of the Reynolds shear stress then determines the magnitude of the thickness of the outer layer, i.e. $\delta_{\mathrm{o}} = O(u_\tau)$. As a consequence, the expansions (6) are supplemented with

$$\delta_{\mathrm{o}} \sim \gamma \, \Delta_1(x) + \cdots \ , \tag{11}$$

which in turn gives rise to the leading-order outer-layer streamwise momentum equation. After integration with respect to η and employing the matching condition $T_1(x,0) = 1$, the latter is conveniently written as

$$(E + 2\beta_0)\eta F_1' - E F_1 - \Delta_1 F_{1,e} \, \partial F_1/\partial x = F_{1,e}(T_1 - 1) \ , \tag{12a}$$

$$F_{1,e} := F_1(x,1) \ , \quad \beta_0 := -\Delta_1 F_{1,e}(\mathrm{d}U_e/\mathrm{d}x)/U_e \ , \tag{12b}$$

$$E := (F_{1,e}/U_e^3)\mathrm{d}(\Delta_1 U_e^3)/\mathrm{d}x = 1 - \Delta_1 \mathrm{d}F_{1,e}/\mathrm{d}x \ . \tag{12c}$$

The last equality is due to the usual boundary or patching conditions imposed, $T_1(x,1) = F_1'(x,1) = 0$. The boundary layer equation (12a) is unclosed, and in order to complete the flow description to leading order, turbulence models for t^+ and T_1 have to be adopted. Integration of (12) then provides the velocity distribution in the outer layer and determines the yet unknown function $C_0(x)$ entering (7) and the skin-friction law (8).

As a main result, inversion of (8) with the aid of (11) yields

$$\gamma \sim \kappa\sigma[1 - 2\sigma\ln\sigma + O(\sigma)], \quad \sigma := 1/\ln Re \ , \quad \partial\gamma/\partial x = O(\gamma^2) \ . \tag{13}$$

Finally, the skin-friction law (13) implies the scaling law (iii), already mentioned in Subsection 2.1, which is characteristic of classical small-defect flows.

2.3   Second-Order Outer Problem

Similar to the description of the leading-order boundary layer behaviour, the investigation of higher-order effects is started by considering the wall layer first. By substituting (4a), (4b), (8) into (1b) and taking into account

the slow variation of γ, cf. (13), one obtains upon integration (cf. Walker, 1998),

$$\frac{1}{Re}\frac{\partial u}{\partial y} + \tau \sim \gamma^2 U_e^2 - \frac{dU_e/dx}{\gamma\, Re}\, y^+ + \frac{\gamma\, dU_e/dx}{Re} \int_0^{y^+} u^{+2}\, dy^+ \cdots \, . \quad (14)$$

Herein the second and the third term on the right-hand side account for, respectively, the effects of the (imposed) pressure gradient, cf. (10), and the convective terms, which have been neglected so far. By using (5) and (12), one can easily derive the asymptotic behaviour of τ as $y^+ \to \infty$ (e.g. Walker, 1998). When rewritten in terms of the outer-layer variable η, this is found to be described by

$$\frac{\tau}{(\gamma U_e)^2} \sim 1 + 2\frac{\delta_o\, dU_e/dx}{\gamma\kappa U_e}\eta \ln \eta + \cdots + \gamma\left[\frac{\Delta_1 dU_e/dx}{\kappa^2 U_e}\eta(\ln\eta)^2 + \cdots\right] + \cdots ,$$
$$(15)$$

as $\eta \to 0$ and $Re \to \infty$, which immediately suggests the appropriate generalisation of the small-defect expansions (6a), (6b), (11):

$$u/U_e \sim 1 - \gamma F_1' - \gamma^2 F_2' + \cdots , \quad (16a)$$
$$\tau/(\gamma U_e)^2 \sim T_1 + \gamma T_2 + \cdots , \quad (16b)$$
$$\delta_o/\gamma \sim \Delta_1(x) + \gamma\Delta_2(x) + \cdots . \quad (16c)$$

On the basis of these second order results, here matching with the wall layer is achieved if

$$F_1' \sim -\kappa^{-1}\ln\eta + C_0(x) , \quad F_2' \sim C_1(x) , \quad (17a)$$
$$T_1 \sim 1 + \frac{2\Delta_1}{\kappa U_e}\frac{dU_e}{dx}\eta\ln\eta , \quad T_2 \sim \frac{dU_e/dx}{\kappa U_e}\eta\ln\eta\left[\frac{\Delta_1}{\kappa}\ln\eta + 2\Delta_2\right] , \quad (17b)$$

as $\eta \to 0$, provided that the skin-friction relationship (8) is modified to explicitly include an additional term of $O(\gamma)$,

$$\kappa/\gamma \sim \ln(Re\gamma\delta_o U_e) + \kappa(C^+ + C_0 + \gamma C_1) + \cdots . \quad (18)$$

Similar to $C_0(x)$, the function $C_1(x)$ depends on the specific turbulence model adopted, as well as the upstream history of the boundary layer.

2.4   Can Classical Small-Defect Theory Describe Boundary Layer Separation?

An estimate of the thickness δ_w of the viscous wall layer is readily obtained from the definition of y^+, see (3), and the (inverted) skin-friction

relationship (13): $\delta_{\mathrm{w}} = O[\gamma^{-1}\exp(-\kappa/\gamma)]$. In the limit $Re \to \infty$, therefore, the low-momentum region close to the wall is exponentially thin as compared to the outer layer, where Reynolds stresses cause a small $O(\gamma)$-reduction of the fluid velocity with respect to the mainstream velocity $U_e(x)$. This theoretical picture of a fully attached turbulent small-defect boundary layer has been confirmed by numerous comparisons with experimental data for flows of this type (e.g. Walker, 1998; Afzal, 1995; Monkewitz et al., 2007). However, it also indicates that attempts based on this picture to describe the phenomenon of boundary layer separation, frequently encountered in engineering applications, will face serious difficulties. Since the momentum flux in the outer layer, which comprises most of the boundary layer, differs only slightly from that in the external flow region, an $O(1)$-pressure rise almost large enough to cause flow reversal even there appears to be required to generate negative wall shear, which hardly can be considered as flow separation. This crude estimate is confirmed by a more detailed analysis dealing with the response of a turbulent small-defect boundary layer to a surface-mounted obstacle, carried out, among others, by Sykes (1980). Moreover, to date no self-consistent theory of flow separation compatible with the classical concept of a turbulent small-defect boundary layer has been formulated.

The above considerations strikingly contrast the case of laminar boundary layer separation, where the velocity defect is of $O(1)$ across the whole boundary layer and the associated pressure increase tends to zero as $Re \to \infty$. It, however, also indicates that a turbulent boundary layer may become more prone to separation by increasing the velocity defect. That this is indeed a realistic scenario can be inferred by seeking self-preserving solutions of (12), i.e. by investigating equilibrium boundary layers. Such solutions, where the functions F_1, T_1, characterising the velocity deficit and the Reynolds shear stress in the outer layer, respectively, solely depend on η, exist if the parameter β_0 in the outer-layer momentum equation (12a) is constant, i.e. independent of x. Equation (12a) then assumes the form

$$(1 + 2\beta_0)\eta F_1' - F_1 = F_{1,e}(T_1 - 1) , \qquad (19)$$

where

$$U_e \propto (x-x_{\mathrm{v}})^m , \quad m = -\beta_0/(1+3\beta_0) , \quad \Delta_1 F_{1,e} = (1+3\beta_0)(x-x_{\mathrm{v}}) . \quad (20)$$

Herein $x = x_{\mathrm{v}}$ denotes the virtual origin of the boundary layer flow. In the present context flows associated with large values of β_0 are of most interest. By introducing suitably (re)scaled quantities in the form $F_1 = \beta_0^{1/2}\hat{F}(\hat{\eta})$,

$T_1 = \beta_0 \hat{T}(\hat{\eta})$, $\eta = \beta_0^{1/2} \hat{\eta}$, the momentum equation (19) reduces to

$$2\hat{\eta}\hat{F}' = \hat{F}_e \hat{T} , \quad \hat{F}_e := \hat{F}(1) \tag{21}$$

in the limit $\beta_0 \to \infty$. Solutions of (21) describing turbulent boundary layers having a velocity deficit measured by $u_{\text{ref}} := \beta_0^{1/2} u_\tau \gg u_\tau$ have been obtained first in Mellor and Gibson (1966). Unfortunately, however, it was not realised that this increase of the velocity defect no longer allows for a direct match of the flow quantities in the outer and inner layer, which has significant consequences, to be elucidated below.

We note that in general $\beta_0(x)$ can be regarded as the leading-order contribution to the so-called Rotta–Clauser pressure-gradient parameter (e.g. Schlichting and Gersten, 2000), formed with the pressure gradient given by (10) and the displacement thickness δ^*,

$$\beta := -U_e \frac{\mathrm{d}U_e}{\mathrm{d}x} \frac{\delta^*}{u_\tau^2} , \quad \delta^* := \delta_\mathrm{o} \int_0^\infty \left(1 - \frac{u}{U_e}\right) \mathrm{d}\eta . \tag{22}$$

As already mentioned by Mellor and Gibson (1966), the quantity β allows for the appealing physical interpretation that u_{ref} is independent of the wall shear stress u_τ^2 for $\beta_0 \gg 1$.

3   Moderately Large Velocity Defect

Following the considerations summarised in the preceding section, we now seek solutions of (1) describing a relative velocity defect of $O(\epsilon)$, where the newly introduced perturbation parameter ϵ is large compared to γ but still small compared to one: $\gamma \ll \epsilon \ll 1$. From assumption (A), see Subsection 2.1, we then have $-\overline{u'v'} \sim \epsilon^2$, and the linearised x-momentum equation immediately yields the estimate $\delta_\mathrm{o} = \epsilon\Delta$ for the boundary layer thickness, where Δ is of $O(1)$ and accounts for its streamwise variation. However, since $-\overline{u'v'} \sim \epsilon^2$ with $\epsilon \gg u_\tau^2$, here the solution describing the flow behaviour in the outer velocity defect region no longer matches with the solution for the universal wall layer as in the classical case. As a consequence, the leading-order approximation to the Reynolds shear stress must vanish in the limit $\eta = y/\delta_\mathrm{o} \to 0$. This indicates that the flow having a velocity defect of $O(\epsilon)$ in the outer main part of the boundary layer exhibits a wake-type behaviour, leading to a finite wall slip velocity at its base and, therefore, forces the emergence of a sublayer, termed intermediate layer, where the magnitude of $-\overline{u'v'}$ reduces to $O(u_\tau^2)$, being compatible with the wall layer scaling.

3.1 Intermediate Layer

Here the streamwise velocity component u is expanded about its value at the base $\eta = 0$ of the outer defect region: $u/U_e \sim 1 - \epsilon W - \gamma U_i + \cdots$, so that the quantities W, U_i, assumed to be of $O(1)$, account, respectively, for the wall slip velocity, given by $u = U_e(1 - \epsilon W)$ with $W > 0$, and the dominant contribution to u that varies with distance y from the wall. Integration of the x-momentum balance then shows that the Reynolds shear stress increases linearly with distance y for $y/\delta_o \ll 1$:

$$\tau \sim \tau_w - \epsilon y \, \mathrm{d}(U_e^2 W)/\mathrm{d}x , \quad y/\delta_i = O(1) . \tag{23}$$

Herein δ_i denotes the thickness of the intermediate layer and τ assumes its near-wall value τ_w as $y/\delta_i \to 0$. Matching with the wall layer then requires that $\tau_w \sim u_\tau^2$, which immediately yields $\delta_i = O(u_\tau^2/\epsilon)$. By taking into account (22), we then infer that $\delta_i/\delta_o = O(\beta^{-1})$ and recover the relationship $\epsilon = O(u_\tau \beta^{1/2})$, already suggested by the final considerations of Subsection 2.4. Formal expansions of u and $-\overline{u'v'}$ in the intermediate layer, therefore, are written as

$$u/U_e \sim 1 - \epsilon W(x; \epsilon, \gamma) - \gamma U_i(x, \zeta) , \tag{24a}$$
$$-\overline{u'v'}/(\gamma U_e)^2 \sim T_i(x, \zeta; \epsilon, \gamma) \sim 1 + \lambda\zeta , \tag{24b}$$

where $\zeta := y/\delta_i = y\epsilon/(\Delta\gamma^2)$ and $\lambda := -(\Delta/U_e^2) \, \mathrm{d}(U_e^2 W)/\mathrm{d}x$.

To close the problem for U_i, we adopt the common mixing length concept,

$$-\overline{u'v'} := \ell^2 \frac{\partial u}{\partial y} \left| \frac{\partial u}{\partial y} \right| , \tag{25}$$

by assuming that the mixing length ℓ behaves as $\ell \sim \kappa y$ for $y = O(\delta_i)$, which is the simplest form allowing for a match with the adjacent layers. Integration of (24b), supplemented with (25), then yields

$$\kappa U_i = -\ln\zeta + 2\ln\left[(1 + \lambda\zeta)^{1/2} + 1\right] - 2(1 + \lambda\zeta)^{1/2} , \tag{26}$$

from which the limiting forms

$$\kappa U_i \sim -2(\lambda\zeta)^{1/2} + (\lambda\zeta)^{-1/2} + O(\zeta^{-3/2}) , \quad \zeta \to \infty , \tag{27a}$$
$$\kappa U_i \sim -\ln(\lambda\zeta/4) - 2 - \lambda\zeta/2 + O(\zeta^2) , \quad \zeta \to 0 , \tag{27b}$$

can readily be inferred.

The behaviour (27a) holding at the base of the outer defect layer is recognised as the square-root law deduced first by Townsend (1961) in his study

of turbulent boundary layers exhibiting vanishingly small wall shear stress; the outermost layer so to speak "anticipates" the approach to separation as the velocity defect increases to a level larger than u_τ. We remark that Townsend (1961) identified the intermediate region as the so-called "equilibrium layer", where convective terms in (1b) are (erroneously within the framework of asymptotic high-Reynolds-number theory) considered to be negligibly small. Equation (27b) provides the logarithmic variation of U_i as $\zeta \to 0$, required by the match with the wall layer, which gives rise to the generalised skin-friction relationship

$$\frac{\kappa}{\gamma} \sim \ln\left(\frac{Re\gamma^2 U_e^3}{\beta_0^{1/2}}\right) + \beta_0\kappa W + O(\gamma\beta_0) \sim (1 + \epsilon W)\ln Re \ . \qquad (28)$$

Note that (28) reduces to (8) when $\beta_0 = O(1)$.

Having demonstrated that the classical theory of turbulent boundary layers in the limit of large Reynolds number can – in a self-consistent manner – be extended to situations where the velocity defect is asymptotically large as compared to u_τ but still $o(1)$, we now consider the flow behaviour in the outer wake-type region in more detail.

3.2 Outer Defect Region: Quasi-Equilibrium Flows and Non-Uniqueness

We first introduce the stream function ψ by $u = \partial\psi/\partial y$, $v = -\partial\psi/\partial x$, so that the continuity equation (1a) is satisfied identically. Following the arguments put forward at the beginning of Section 3, we write the flow quantities in the outer layer in the form

$$p \sim p_e(x) + \epsilon^2 P(x, \eta; \epsilon, \gamma) \ , \qquad (29a)$$

$$\psi/U_e \sim y - \epsilon\delta_o F(x, \eta; \epsilon, \gamma) \ , \qquad (29b)$$

$$\left[-\overline{u'^2}, -\overline{v'^2}, -\overline{u'v'}\right] \sim U_e^2\epsilon^2[R_x, R_y, T](x, \eta; \epsilon, \gamma) \ . \qquad (29c)$$

As before, here $\eta = y/\delta_o$ and we accordingly expand

$$Q \sim Q_1 + \epsilon Q_2 + \cdots \ , \quad Q := F, P, R_x, R_y, T, W \ , \qquad (30a)$$

$$\delta_o \sim \epsilon\Delta_1 + \epsilon^2\Delta_2 + \cdots \ , \qquad (30b)$$

$$\beta/\beta_v \sim B_0(x) + \epsilon B_1(x) + \cdots \ , \quad \beta_v \to \infty \ , \qquad (30c)$$

where we require (without any loss of generality) that β_v equals β_0 at $x = x_v$, so that $\beta_0 = \beta_v B_0$ and $B_0(x_v) = 1$, $B_i(x_v) = 0$, $i = 1, 2, \dots$. In analogy

to (12), the first-order problem then reads

$$[U_e^2 \mathrm{d}(U_e \Delta_1)/\mathrm{d}x]\eta F_1' - \partial(U_e^3 \Delta_1 F_1)/\partial x = U_e^3 T_1 \;, \tag{31a}$$

$$F_1(x,0) = F_1'(x,1) = F_1''(x,1) = T_1(x,1) = 0 \;, \tag{31b}$$

$$\eta \to 0: \quad T \sim (\kappa \eta F_1'')^2 \;, \quad F_1' \sim W_1(x) - (2/\kappa)(\lambda\eta)^{1/2} \;. \tag{31c}$$

In the following we concentrate on solutions which are self-similar up to second order, i.e. $\partial F_1/\partial x \equiv \partial T_1/\partial x \equiv 0$ and $\partial F_2/\partial x \equiv \partial T_2/\partial x \equiv 0$. By again adopting the notations $F_1 = \hat{F}(\eta)$, $T_1 = \hat{T}(\eta)$, and setting $\Delta_1 = \hat{\Delta}(x)$, $U_e = \hat{U}(x)$, we recover the requirements (20), (21) for self-similarity at first order resulting from classical small-defect theory in the limit of large values of β_v, in agreement with (30b) and the definition of β provided by (22):

$$B_0 \equiv 1 \;, \quad \hat{\Delta}\hat{F}_e = 3(x - x_v) \;, \quad \hat{U} = (C/3)^{1/3}(x - x_v)^{-1/3} \;, \tag{32}$$

with a constant C, and

$$2\eta\hat{F}' = \hat{F}_e\hat{T} \;, \quad \hat{F}(0) = \hat{T}(0) = \hat{F}'(1) = \hat{F}''(1) = \hat{T}(1) = 0 \;. \tag{33}$$

If, as in the discussion of the flow behaviour in the intermediate layer, a mixing length model $\hat{T} = [l(\eta)\hat{F}''(\eta)]^2$, $l := \ell/\delta_o$, in accordance with (25) is chosen to close the problem, integration of (33) yields the analytical expressions

$$\hat{F}'(\eta) = \frac{1}{2\hat{F}_e}\left[\int_\eta^1 \frac{z^{1/2}}{l(z)}\,\mathrm{d}z\right]^2 \;, \quad \hat{F}_e = \left\{\frac{1}{2}\int_0^1\left[\int_\eta^1 \frac{z^{1/2}}{l(z)}\,\mathrm{d}z\right]^2 \mathrm{d}\eta\right\}^{1/2} \;. \tag{34}$$

Equations (34) have been evaluated numerically by using a slightly generalised version of the mixing length closure originally suggested by Michel et al. (1969),

$$l = \ell/\delta_o = c_\ell I(\eta)^{1/2} \tanh(\kappa\eta/c_\ell) \;, \quad I = 1/(1 + 5.5\eta^6) \;, \quad c_\ell = 0.085 \;. \tag{35}$$

Herein $I(\eta)$ represents the well-known intermittency factor proposed by Klebanoff (1955). One then obtains $W_1 = \hat{F}'(0) \doteq 13.868$, $\hat{F}_e \doteq 5.682$, and $\mathrm{d}\hat{\Delta}/\mathrm{d}x \doteq 0.528$, cf. (32). As seen in Figure 2(a), both $\hat{F}'$ and $\hat{T}$ vanish quadratically as $\eta \to 1$ as a result of the boundary conditions expressing vanishing vorticity, $\hat{T}(1) = \hat{T}'(1) = 0$, cf. (33). Also, note that $\hat{F}'$ exhibits the square-root behaviour required from the match with the intermediate layer as $\eta \to 0$.

Turning now to the second-order problem, we consider the most general case that the wall shear enters the description of the flow in the outer layer at this level of approximation (principle of least degeneracy). Therefore, we

require $\epsilon^3 T_2(0) \sim \gamma^2$, which finally determines the yet unknown magnitude of ϵ relative to γ, namely that $\epsilon = O(\gamma^{2/3})$. Since, as pointed out before and indicated by (22) and (32), here setting $B_0 \equiv 1$ yields $\epsilon \sim \gamma\beta_0^{1/2}$, this estimate for ϵ implies that $\epsilon\beta_0 = \Gamma := 1/T_2(0) = O(1)$. Inspection of the resulting second-order problem then indicates that self similar solutions exist only if the external velocity distribution (32) predicted by classical theory is slightly modified in the form

$$\hat{U}(x) = (C/3)^{1/3}(x - x_{\mathrm{v}})^{-1/3+\mu}, \quad \mu \sim \gamma^{2/3}\mu_1 + \cdots , \tag{36}$$

where the $O(1)$-parameter μ_1 satisfies a solvability condition that represents the integral momentum balance obtained from integrating the second-order x-momentum equation from $\eta = 0$ to $\eta = 1$. It can be cast into the canonical form

$$9\hat{D}^2\hat{\mu} = 1 + \hat{D}^3 , \tag{37a}$$

$$\hat{D} = r^{1/3}\Gamma^{1/3} , \quad \hat{\mu} = r^{-2/3}\mu_1 , \quad r = \hat{F}_e^{-1} \int_0^1 (\hat{F}'^2 - \hat{R}_x + \hat{R}_y)\, \mathrm{d}\eta . \tag{37b}$$

A graph of the relationship (37a) which represents the key result of the analysis dealing with boundary layers that are in quasi-equilibrium (i.e. self-similar to first and second order) having a moderately large velocity defect is shown in Figure 2(b). Most interesting, it is found that solutions describing flows of this type exist for $\hat{\mu} \geq \hat{\mu}^* = 2^{1/3}/6$ only and form two branches, associated with non-uniqueness of the quantity $\hat{D}$, which serves as a measure of velocity defect, for a specific value of the pressure gradient. Along the lower branch, $\hat{D} \leq \hat{D}^* = 2^{1/3}$ and decreases with increasing values of $\hat{\mu}$, so that the classical small-defect theory is recovered in the limit $\hat{\mu} \to \infty$, where $\hat{D} \sim (9\hat{\mu})^{-1/2}$. In contrast, this limit leads to an unbounded growth of values $\hat{D} \geq \hat{D}^*$ associated with the upper branch: $\hat{D} \sim 9\hat{\mu}$ as $\hat{\mu} \to \infty$. This immediately raises the question if it is possible to formulate a general necessarily nonlinear theory which describes turbulent boundary layers having a finite velocity defect in the limit of infinite Reynolds number. We also note that the early experimental observations made by Clauser (1956) seem to strongly point to this type of non-uniqueness.

The non-uniqueness is intrinsically tied to the nonlinearity of the inertia terms in (1b). For small-defect boundary layers, these come into play as inhomogeneities in the second-order flow description, as reflected by the term $\hat{D}^3$ in (37a). It is, therefore, instructive to seek for double-valued self-preserving flows for various values of m by starting from an *ad-hoc* boundary layer approximation of the governing equations (1). We hence assume that
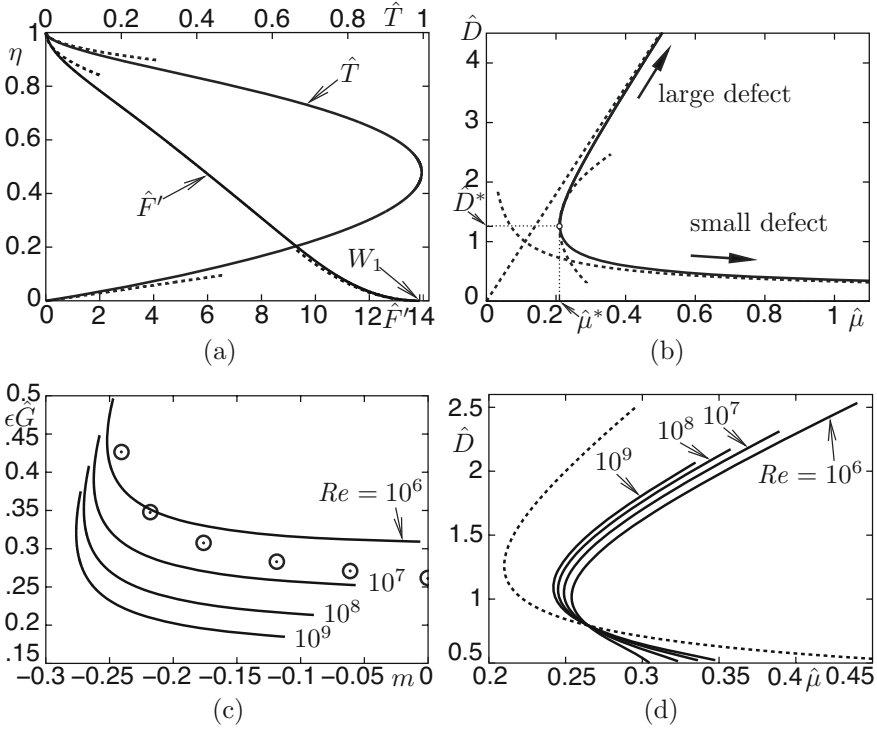
Figure 2: Non-unique quasi-equilibrium flows; (a) $\hat{F}'(\eta)$, $\hat{T}(\eta)$, *dashed*: asymptotes found from (31b), (31c); (b) canonical representation (37a), *dashed*: asymptotes (see text) and osculating parabola in the point $(\mu^*, \hat{D}^*)$; (c), (d) *solid*: solutions of (38) for various values of Re; (c) *circles*: experimental data; (d) *dashed*: asymptote (37a) for $Re \to \infty$.

$\psi = \delta_{\mathrm{o}} U_e g(\eta)$, $\tau = U_e^2 t(\eta)$, with U_e given by (20), and $\delta_{\mathrm{o}} = a(x - x_{\mathrm{v}})$, to end up with the boundary-value problem

$$t'/a = m(g'^2 - 1) - (m+1)gg'' , \tag{38a}$$

$$\eta \to 0: \quad g \to 0 , \quad \gamma\eta g'' \to \kappa , \quad t \to \gamma^2 , \tag{38b}$$

$$\eta = 1: \quad g' = 1 , \quad g'' = t = 0 . \tag{38c}$$

The boundary conditions (38b) and (38c) account for the behaviour of F_1, F_2, T_1, T_2 entering the expansions (16), even in case of a moderately small defect still formally valid in the entire small-defect region, near the base and the outer edge of the latter, respectively. When supplemented with an

asymptotically correct closure for t, i.e. one consistent with these conditions, for sufficiently small values of γ and external flows represented by m the quantities g, t, a represent an asymptotically accurate description of small-defect flows that are in equilibrium up to second order with respect to the expansions (16).

We again adopt (25) by setting $t = (lg'')^2$, with l satisfying (35). In order to detect non-uniqueness, (38) was solved numerically for $g(\eta)$, $t(\eta)$, and m by prescribing values of Re and a. Then γ is computed from (8), and increasing the value of a means increasing the boundary layer thickness at some position x. The approximation $\beta_0 \sim -ma[1 - g(1)]/\gamma^2 + O(\gamma^2)$ inferred from (22) is used to evaluate $\epsilon \sim \gamma\beta_0^{1/2}$, $\Gamma^{1/3} = \gamma^{1/3}\beta_0^{1/2}$, and, in turn, $\hat{\mu}$ and $\hat{D}$ from (37b). Here we set $\hat{R}_x = \hat{R}_y = 0$, owing to the lack of reliable closures for these stress components but in agreement with the boundary layer approximation adopted, so that r is identified with the so-called shape factor $\hat{G}$ (cf. Schlichting and Gersten, 2000). Also, the estimates $\hat{F}' \sim (1 - g')/\epsilon + O(\epsilon^2)$, $\hat{F}_e \sim [1 - g(1)]/\epsilon + O(\epsilon^2)$ are employed.

Figure 2(c) shows the comparison of the resulting relationship $m(\epsilon\hat{G}; Re)$ with data extracted from the measurements by Simpson et al. (1981) of a massively separating boundary layer under the action of an adverse pressure gradient (Schlichting and Gersten, 2000, p. 590): here U_e is found to obey a power law according to (20) with m being a slowly varying function of x, and the value of Re is estimated roughly as 3×10^6. Notwithstanding this uncertainty, the neglect of effects due to Reynolds normal stresses, and the fact that the experimental flow is in equilibrium only locally, the agreement with the results that are consistent with the asymptotic theory is encouraging. Figure 2(d) uncovers the rather slow convergence of the function $\hat{\mu}(\hat{D}; Re)$ towards the canonical relationship (37), cf. Figure 2(b), attained for $Re \to \infty$, which originates from the logarithmic dependence of γ on Re.

4   Large Velocity Deficit

As in the cases of small and moderately small velocity defect we require the boundary layer to be slender. However, in contrast to the considerations of Sections 2 and 3, the validity of this requirement can no longer be inferred from assumption (A) and the balance between convective and Reynolds stress gradient terms in the outer predominantly inviscid region of the boundary layer which now yields $\partial\tau/\partial y = O(1)$, rather than $\partial\tau/\partial y \ll 1$ as earlier. A hint how this difficulty can be overcome is provided by the observation that the transition from a small to a moderately large velocity defect is accompanied with the emergence of a wake-type flow in this outer

layer. One expects that this effect will become more pronounced as the velocity defect increases further, suggesting in turn that the outer part of the boundary layer, having a velocity defect of $O(1)$, essentially behaves as a turbulent free shear layer. An attractive strategy then is to combine the asymptotic treatment of such flows, (see Schneider, 1991) in which the experimentally observed slenderness is enforced through the introduction of a Reynolds-number-independent parameter $\alpha \ll 1$ with the asymptotic theory of turbulent wall bounded flows.

4.1   Outer Wake Region

Let the parameter $\alpha \ll 1$ measure the lateral extent of the outer wake region, so that $\bar{y} := y/\alpha = O(1)$. Appropriate expansions of the various field quantities then are

$$p \sim p_e(x) + O(\alpha) , \quad q \sim \alpha\, q_0(x, \bar{y}) + o(\alpha) , \tag{39}$$

where q stands for Δ, ψ, $\tau = -\overline{u'v'}$ (as well as the remaining components $-\overline{u'^2}$, $-\overline{v'^2}$ of the Reynolds stress tensor). From substitution into (1b–1c) the leading order outer wake problem is found to be

$$\frac{\partial \psi_0}{\partial \bar{y}} \frac{\partial^2 \psi_0}{\partial \bar{y} \partial x} - \frac{\partial \psi_0}{\partial x} \frac{\partial^2 \psi_0}{\partial \bar{y}^2} = -U_e \frac{\mathrm{d}U_e}{\mathrm{d}x} + \frac{\partial \tau_0}{\partial \bar{y}} , \tag{40a}$$

$$\bar{y} = 0 : \quad \psi_0 = \tau_0 = 0 , \tag{40b}$$

$$\bar{y} = \Delta_0(x) : \quad \partial\psi_0/\partial\bar{y} = U_e , \quad \tau_0 = 0 . \tag{40c}$$

As in the case of a moderately large velocity defect, we expect a finite wall slip $U_s(x) := \partial\psi_0/\partial\bar{y}$ at the base $\bar{y} = 0$ of this outer layer, which yields the limiting behaviour

$$\partial\psi_0/\partial\bar{y} \sim U_s(x) + O(\bar{y}^{3/2}) , \quad \tau_0 \sim \Lambda_0\, \bar{y} + O(\bar{y}^{3/2}) , \tag{41}$$

with $\Lambda_0 := U_s\, \mathrm{d}U_s/\mathrm{d}x - U_e\, \mathrm{d}U_e/\mathrm{d}x > 0$.

It is easily verified that the various layers introduced so far in the description of turbulent boundary layers share the property that their lateral extent is of the order of the mixing length ℓ, defined by (25), characteristic of the respective layer. In contrast, the scalings given by (39) imply that ℓ is much smaller than the thickness of the outer wake region: $\ell \sim \alpha^{3/2} \ll \alpha$. This is a typical feature of free shear layers, of course, but also indicates that the outer wake region "starts to feel" the presence of the confining wall at distances $y \sim \alpha^{3/2}$, which in turn causes the emergence of an inner wake region.

4.2   Inner Wake Region

By introducing the stretched wall distance $Y = y/\alpha^{3/2} = O(1)$, inspection of (41) suggests the expansions

$$\psi \sim \alpha^{3/2} U_s(x) + \alpha^{9/4} \bar\psi(x, Y) + \cdots , \tag{42a}$$

$$\tau \sim \alpha^{3/2} \bar T(x, Y) + \cdots , \quad \ell \sim \alpha^{3/2} \bar L(x, Y) + \cdots , \tag{42b}$$

which leads to

$$\bar T = \Lambda_0 Y . \tag{43}$$

Furthermore, $\bar T$ and $\bar\psi$ are subject to the boundary conditions

$$T(x, 0) = \bar\psi(x, 0) = 0 , \tag{44a}$$

$$\bar\psi_Y \sim \frac{2}{3} \frac{\Lambda_0^{1/2}}{\bar L_0} Y^{3/2} , \quad Y \to \infty , \quad \bar L_0 = \lim_{Y \to \infty} \bar L . \tag{44b}$$

The solution of the inner wake problem posed by (43), (44) can be obtained in closed form. It exhibits the expected square-root behaviour of $\bar\psi_Y$,

$$\bar\psi_Y \sim \bar U_s(x) + 2 \frac{(\Lambda_0 Y)^{1/2}}{\chi(x)}, \quad \bar L \sim \chi(x) \bar Y , \quad Y \to 0 . \tag{45}$$

Here $\bar U_s(x)$ denotes the correction of the slip velocity $U_s(x)$ caused by the inner wake region,

$$u_s \sim U_s(x) + \alpha^{3/4} \bar U_s(x) + \cdots , \tag{46a}$$

$$\bar U_s(x) = - \int_0^\infty \left(\frac{1}{\bar L} - \frac{1}{\bar L_0} \right) (\Lambda_0 Y)^{1/2} \, \mathrm{d}Y \quad (< 0) . \tag{46b}$$

At this point it is important to recall the basic assumption made at the beginning of this section, namely, that the slenderness parameter α is independent of Re, or more generally, asymptotes to a small but finite value as $Re \to \infty$. As a consequence, the outer and inner wake regions provide a complete description of the boundary layer flow in the formal limit $Re^{-1} = 0$. If, however, $0 < 1/Re \ll 1$ an additional sublayer forms at the base of the inner wake region. This sublayer plays a similar role as the intermediate layer discussed in Subsection 3.1: there the magnitude of the Reynolds shear stress, still varying linearly with distance from the wall, is reduced to $O(u_\tau^2)$, which is necessary to provide the square-root behaviour expressed in (45) and, finally, to allow for the match with the universal wall layer (see Scheichl and Kluwick, 2007b).

4.3   Numerical Solution of the Leading-Order Outer-Wake Problem

As in Subsection 3.2, here again (25) and (35) shall be adopted to close the outer wake problem posed by (40). Numerical calculations were carried out for a family of retarded external flows controlled by two parameters m_s, k, with $m_s < 0$, $0 \le k < 1$:

$$U_e(x; m_s, k) = (1 + x)^{m(x; m_s, k)} \,, \tag{47a}$$

$$\frac{m}{m_s} = 1 + \frac{k}{1 - k}\,\Theta(2 - x)\big[1 - (1 - x)^2\big]^3 \,. \tag{47b}$$

Herein Θ denotes the Heaviside step function. Self-similar solutions of the form $\psi_0 = \Delta_0 f(\xi)$, $\xi := Y/\Delta_0$, $\Delta_0 = b(1 + x)$, where b is a constant and the position $x = -1$ defines the virtual origin of the flow, exist for $k = 0$ if $m_s > -1/3$ and are used to provide initial conditions at $x = 0$ for the downstream integration of (40) with U_e given by (47). As a specific example, we consider the case $F'(0) = 0.95$ of a relatively small velocity defect, imposed at $x = 0$, for which the requirement of self-similarity for $-1 < x < 0$ yields $b \doteq 0.3656$ and $m_s \doteq -0.3292$. The key results which are representative for the responding boundary layer and, most important, indicate that the present theory is capable of describing the approach to separation are displayed in Figure 3. If k is sufficiently small, the distribution of the wall slip velocity U_s is smooth and $U_s > 0$ throughout. However, when k reaches a critical value $k_M \doteq 0.84258$, the slip velocity U_s is found to vanish at a single location $x = x_M$, but is positive elsewhere. A further increase of k provokes a breakdown of the calculations, accompanied with the formation of a weak singularity slightly upstream of x_M at $x = x_G$. A similar behaviour is observed for the scaled boundary layer thickness Δ_0, which is smooth in the subcritical case $k < k_M$, exhibits a rather sharp peak $\Delta_{0,M}$ for $k = k_M$ at $x = x_M$, and approaches a finite limit $\Delta_{0,G}$ in an apparently singular manner in the supercritical case $k > k_M$.

Following the qualitatively similar behaviour of the wall shear stress that replaces U_s in the case of laminar boundary layers (see Ruban, 1981, 1982; Stewartson et al., 1982) the critical solution with $k = k_M$ is termed a marginally separating boundary layer solution. However, in vivid contrast to its laminar counterpart, is is clearly seen to be locally asymmetric with respect to $x = x_M$ where it is singular. This numerical finding is supported by a local analysis of the flow behaviour near $x = x_M$, carried out by Scheichl and Kluwick (2007a): it indicates that U_s decreases linearly with x upstream
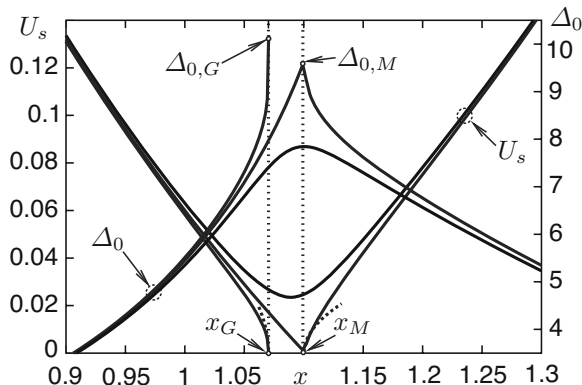
Figure 3: Solutions of (40) for $|x - x_M| \ll 1$, $|k - k_M| \ll 1$, *dashed*: asymptotes expressed by (48b) and (49).

of $x = x_M$ but exhibits a square-root singularity as $x - x_M \to 0_+$,

$$U_s/P_{00}^{1/2} \sim -B(x - x_M) , \qquad x - x_M \to 0_- , \tag{48a}$$

$$U_s/P_{00}^{1/2} \sim U_+(x - x_M)^{1/2} , \quad x - x_M \to 0_+ , \tag{48b}$$

where $P_{00} = (\mathrm{d}p_e/\mathrm{d}x)(x_M)$. It is found that $P_{00} \doteq 0.02272$ in case of the specific choice (47) of the external-flow speed U_e. Also, U_+ takes on an universal value, $U_+ \doteq 1.1835$, whereas the constant B remains arbitrary in the local investigation and has to be determined by comparison with the numerical results for $x \leq x_M$.

This local analysis also shows that a square-root singularity forms at a position $x = x_G < x_M$ for $k > k_M$,

$$U_s/P_{00}^{1/2} \sim U_-(x_G - x)^{1/2} , \quad x - x_G \to 0_- , \tag{49}$$

with some U_- to be determined numerically, and that the solution cannot be extended further downstream. This behaviour, which has been described first by Melnik (1989), is reminiscent of the Goldstein singularity well-known from the theory of laminar boundary layers and, therefore, will be termed the turbulent Goldstein singularity. As shown in the next section, the bifurcating behaviour of the solutions for $k - k_M \to 0$ is associated with the occurrence of marginally separating flow.

4.4   Marginal Separation

According to the original boundary layer concept, pressure disturbances caused by the displacement of the external inviscid flow due to the momentum deficit, which is associated with the reduced velocities close to the

wall, represent a higher order effect. Accordingly, higher-order corrections
to the leading-oder approximation of the flow quantities inside and out-
side the boundary layer can be calculated in subsequent steps. However,
as found first for laminar flows, this so-called hierarchical structure of the
perturbation scheme breaks down in regions where the displacement thick-
ness changes so rapidly that the resulting pressure response is large enough
to affect the lowest-order boundary layer approximation (e.g. Stewartson,
1974). A similar situation is encountered for the type of turbulent flows dis-
cussed in the preceding section. Indeed, the slope discontinuity of Δ_0 and,
in turn, of the displacement thickness forces a singularity in the response
pressure, indicating a breakdown of the hierarchical approach to boundary
layer theory. As for laminar flows (see Ruban, 1981, 1982; Stewartson et al.,
1982) this deficiency can be overcome by adopting a local interaction strat-
egy, so that the induced pressure disturbances enter the description of the
flow in leading rather than higher order (see Scheichl and Kluwick, 2007a).
We subsequently present the essential results of this theory.

Again, similar to laminar flows, three layers (decks) characterising re-
gions of different flow behaviour have to be distinguished inside the local
interaction region, see Figure 4. Effects of Reynolds stresses are found to
be confined to the lower deck region (LD), having a streamwise and lateral
extent of $O(\alpha^{3/5})$ and $O(\alpha^{6/5})$, respectively. Here the flow is governed by
equations of the form (40). The majority of the boundary layer, i.e. the
main deck (MD), behaves passively in the sense that it transfers displace-
ment effects caused by the lower deck region unchanged to the external flow
region taking part in the interaction process, the so-called upper deck (UD),
and transfers the resulting pressure response unchanged to the lower deck.
Solutions to the leading-order main and upper deck problems can be ob-
tained in closed form which finally leads to the fundamental lower deck
problem. By using suitably stretched variables, it can be written in terms
of a stream function $\hat{\psi}(\hat{X}, \hat{Y})$ as

$$\frac{\partial \hat{\psi}}{\partial \hat{Y}} \frac{\partial^2 \hat{\psi}}{\partial \hat{Y} \partial \hat{X}} - \frac{\partial \hat{\psi}}{\partial \hat{X}} \frac{\partial^2 \hat{\psi}}{\partial \hat{Y}^2} = -1 - \hat{\Lambda}(\hat{\Gamma}) \frac{\mathrm{d}\hat{P}'}{\mathrm{d}\hat{X}} + \frac{\partial \hat{T}}{\partial \hat{Y}} \, , \tag{50a}$$

$$\hat{T} = \frac{\partial^2 \hat{\psi}}{\partial \hat{Y}^2} \left| \frac{\partial^2 \hat{\psi}}{\partial \hat{Y}^2} \right| \, , \tag{50b}$$

$$\hat{P}(\hat{X}) = \frac{1}{\pi} \fint_{-\infty}^{\infty} \frac{\hat{A}'(\hat{S})}{\hat{X} - \hat{S}} \, \mathrm{d}\hat{S} \, , \tag{50c}$$

$$\hat{Y} = 0 : \quad \hat{\psi} = \hat{T} = 0 \, , \tag{50d}$$

$$\hat{Y} \to \infty : \quad \hat{T} - \hat{Y} \to \hat{A}(\hat{X}) \, , \tag{50e}$$

$$\hat{X} \to -\infty : \ \hat{\psi} \to (4/15)\hat{Y}^{5/2} + \hat{\Gamma}\hat{Y} \ , \quad 0 \le \hat{\Gamma} \le 1 \ , \tag{50f}$$

$$\hat{X} \to \infty : \ \hat{\psi} \to \hat{X}^{5/6}F_{+}(\hat{\eta}) \ , \quad \hat{\eta} := \hat{Y}/\hat{X}^{1/3} \ . \tag{50g}$$

The first and the second term on the right-hand side of (50a) account for the imposed and the induced pressure, respectively. The latter is given by the Hilbert integral (50c), where $\hat{A}$ characterises the displacement effect exerted by the lower deck region. The far-field condition (50e) expresses the passive character of the main deck mentioned before, whereas the conditions (50f), (50g) follow from the match with regions LD_{-}, LD_{+} immediately upstream and downstream of the local interaction zone. The analysis of region LD_{+} determines the function $F_{+}(\hat{\eta})$. Finally, the parameter $\hat{\Gamma}$ measures the intensity of the interaction process as the monotonically increasing but otherwise arbitrary function $\hat{\Lambda}(\hat{\Gamma})$ expresses the magnitude of the induced pressure gradient. The distinguished limit underlying the interacting-flow description is given by $\alpha^{3/10} \ln|k - k_M| = O(1)$ as $k \to k_M$, $\alpha \to 0$.
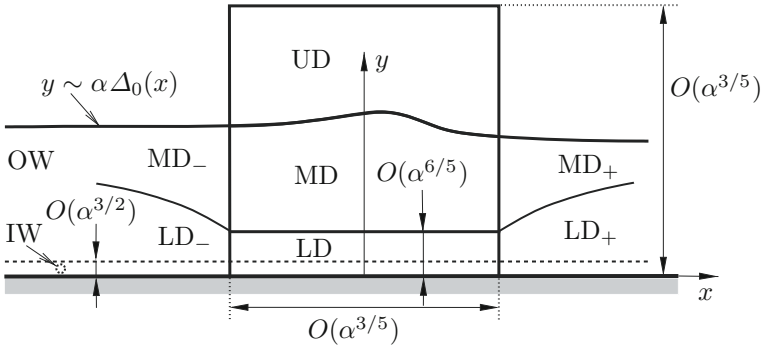
Figure 4: Triple-deck structure, for captions see text, subscripts "$-$" and "$+$" refer to the continuation of flow regions up- and downstream of the local interaction zone, *dashed* line indicates inner wake.

As a representative example of flows encountering separation, the distributions of $\hat{A}$, $\hat{P}$, and the wall slip $\hat{U}_s := (\partial\hat{\psi}/\partial\hat{Y})(\hat{X}, \hat{Y} = 0)$, obtained by numerical solution of the triple-deck problem (50) for $\hat{\Gamma} = 0.019$, $\hat{\Lambda} = 3$, are depicted in Figure 5(a). Here the upstream and downstream asymptotes for $\hat{A}$, $\hat{P}$, $\hat{U}_s$ have been obtained from the analysis of the flow behaviour in the pre- and post-interaction regions (subscripts "$-$" and "$+$" in Figure 4), and $\hat{X}_D$ and $\hat{X}_R$ denote the $\hat{X}$-positions of, respectively, detachment and

reattachment. For example, under the assumption $\hat{A}(\hat{\Gamma}) \equiv 3$, reversed-flow regions are observed for $\hat{\Gamma}_{\min} \leq \hat{\Gamma} \leq \hat{\Gamma}_{\max}$, $\hat{\Gamma}_{\min} \doteq 0.017$, $\hat{\Gamma}_{\max} \doteq 0.205$. It is interesting to note that the passage of $\hat{U}_s$ into the reversed-flow region where $\hat{U}_s < 0$ causes the interaction pressure $\hat{P}$ to drop initially before it rises sharply, overshoots and finally tends to zero in the limit $\hat{X} \to \infty$. This is in striking contrast to laminar flows, where flow separation always is triggered by an initial pressure rise, and reflects the fact that – in the case of turbulent flows considered here – the streamwise velocity component at the base $\hat{Y} = 0$ of the lower deck region is allowed to take on finite values, whereas the no-slip condition is enforced in its laminar counterpart.
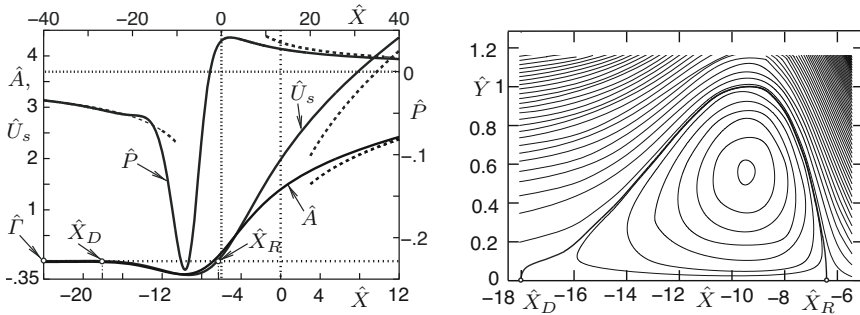
Figure 5: Specific solution of (50); (a) key quantities, bottom abscissa: $\hat{X}$-values for $\hat{A}(\hat{X})$, $\hat{U}_s(\hat{X})$, top abscissa: $\hat{X}$-values for $\hat{P}(\hat{X})$, *dashed*: asymptotes; (b) streamlines, *bold*: separating streamline $\hat{\psi} = 0$.

The streamlines inside the lower-deck region (constant values of $\hat{\psi}$) are displayed in Figure 5(b), which clearly shows the formation of a recirculating eddy. Also, we draw attention to the increasing density of streamlines further away from the wall and downstream of reattachment, associated with the strong acceleration of the fluid there as evident from the rapid increase of $\hat{U}_s$.

The interaction process outlined so far describes the (local) behaviour of marginally separated turbulent flows in the formal limit $1/Re = 0$. As in the case of conventional, i.e. hierarchical, boundary layers having a velocity of defect of $O(1)$, additional sublayers form closer to the wall if $1/Re \ll 1$ but finite. Their analysis, outlined in detail by Scheichl and Kluwick (2007b), provides the skin-friction relationship in generalised form to include the effects of vanishing and negative wall shear – treated first in a systematic way by Schlichting and Gersten (2000) – but also shows that these layers behave passively insofar as the lower deck problem (50) remains intact.

5   Conclusions and Outlook

In this presentation an attempt has been made to derive the classical two-layer structure of a turbulent small-defect boundary layer from a minimum of assumptions. As in the overview given by Walker (1998), but in contrast to earlier investigations (e.g. Mellor, 1972), the (logarithmic) law of the wall is taken basically as an empirical observation rather than a consequence of matching inner and outer layers, as the latter is not felt rich enough to provide a stringent foundation of this important relationship reflecting the dynamics of the flow close to the wall, which is not understood in full at present. Probably the first successful model that describes essential aspects of this dynamics is provided by Prandtl's mixing length concept, proposed more than 50 years before the advent of asymptotic theories in fluid mechanics. Significant progress has been achieved in more recent years and, in particular, by the pioneering work of Walker (e.g. Walker, 1998), whose untimely death ended a line of thought which certainly ought to be taken up again.

Following the brief outline of the classical small-defect theory, it is shown how a description of turbulent boundary layers having a slightly larger (i.e. moderately large) velocity defect, where the outer predominantly inviscid layer starts to develop a wake-type behaviour, can be formulated. Further increase of the velocity defect to values of $O(1)$ causes the wake region to become even more pronounced and is seen to allow for the occurrence of reversed-flow regions close to the wall, resulting in what we believe to be the first fully self-consistent theory of marginally separated turbulent flows.

Unfortunately, however, this success seemingly does not shed light on the phenomenon of global or gross separation associated with flows past (more-or-less) blunt bodies or, to put it more precisely, flows which start at a stagnation point rather than a sharp leading edge. Indeed, a recent careful numerical investigation for the canonical case of a circular cylinder, presented, among others, by Scheichl et al. (2008b), Scheichl and Kluwick (2008c), undoubtedly indicates that the boundary layer approaching separation exhibits a small rather than a large velocity defect, leading in turn to the dilemma addressed in Subsection 2.4. The accompanying asymptotic analysis based on the turbulence intensity gauge model introduced by Neish and Smith (1992), however, strongly suggests that a boundary layer forming on a body of finite extent and originating in a front stagnation point does not reach a fully developed turbulent state, even in the limit $Re \to \infty$. Specifically, it is found that the boundary layer thickness δ and the Reynolds shear stress are slightly smaller than predicted by classical small-defect theory, while, most important, the thickness of the wall layer is slightly larger.

In fact, δ varies predominantly algebraically with Re, whereas the velocity defect measure γ in the outer region is still of $O(1/\ln Re)$, conforming to the matching condition (8) decisive for the classical flow description. As a consequence, the outer large-momentum region does not penetrate to distances from the wall which are transcendentally small. In turn, this situation opens the possibility to formulate a local interaction mechanism that describes the detachment of the boundary layer from the solid wall within the framework of free-streamline theory at pressure levels which are compatible with experimental observation. This is a topic of intense current investigations; for preliminary results see Scheichl et al. (2009) or Scheichl et al. (2010).

Bibliography

N. Afzal. Scaling of Power Law Velocity Profile in Wall-Bounded Turbulent Shear Flows. Meeting paper 2005-109, AIAA, 2005.

G. I. Barenblatt and A. J. Chorin. A note on the intermediate region in turbulent boundary layers. *Phys. Fluids*, 12(9):2159–2161, 2000. Letter.

G. I. Barenblatt, A. J. Chorin, and V. M. Prototoskin. Self-similar intermediate structures in turbulent boundary layers at large Reynolds numbers. *J. Fluid Mech.*, 410:263–283, 2000.

G. I. Barenblatt and N. Goldenfeld. Does fully developed turbulence exist? Reynolds number independence versus asymptotic covariance. *Phys. Fluids*, 7(12):3078–3082, 1995.

W. B. Bush and F. E. Fendell. Asymptotic analysis of turbulent channel and boundary-layer flow. *J. Fluid Mech.*, 56(4):657–681, 1972.

F. H. Clauser. The Turbulent Boundary Layer. In H. L. Dryden and Th. von Kármán, editors, *Advances in Applied Mechanics*, volume 4, pages 1–51. Academic Press, New York, 1956.

E. Deriat and J.-P. Guiraud. On the asymptotic description of turbulent boundary layers. *J. Theor. Appl. Mech.*, 109–140, 1986. Special Issue on Asymptotic Modelling of Fluid Flows. Original French article in *J. Méc. Théor. Appl.*

F. E. Fendell. Singular Perturbation and Turbulent Shear Flow near Walls. *J. Astronaut. Sci.*, 20(11):129–165, 1972.

P. S. Klebanoff. Characteristics of turbulence in a boundary layer with zero pressure gradient. NACA Report 1247, NASA – Langley Research Center, Hampton, VA, 1955. See also NACA Technical Note 3178, 1954.

A. Kluwick and B. Scheichl. High-Reynolds-Number Asymptotics of Turbulent Boundary Layers: From Fully Attached to Marginally Separated Flows. Invited Paper. In A. F. Hegarty, N. Kopteva, E. O'Riordan, and M. Stynes, editors, *BAIL 2008 – Boundary and Interior Layers.*

Proceedings of the International Conference on Boundary and Interior Layers – Computational and Asymptotic Methods, Limerick, July 2008, volume 69 of Lecture Notes in Computational Science and Engineering, pages 3–22. Springer-Verlag, Berlin, Heidelberg, 2009.

G. L. Mellor. The Large Reynolds Number, Asymptotic Theory of Turbulent Boundary Layers. *Int. J. Engng Sci.*, 10(10):851–873, 1972.

G. L. Mellor and D. M. Gibson. Equilibrium turbulent boundary layers. *J. Fluid Mech.*, 24(2):225–253, 1966.

R. E. Melnik. An Asymptotic Theory of Turbulent Separation. *Computers & Fluids*, 17(1):165–184, 1989.

R. Michel, C. Quémard, and R. Durant. Hypothesis on the mixing length and application to the calculation of the turbulent boundary layers. In S. J. Kline, M. V. Morkovin, G. Sovran, and D. J. Cockrell, editors, *Proceedings of Computation of Turbulent Boundary Layers – 1968 AFOSR-IFP-Stanford Conference*, volume 1, pages 195–207. Stanford University, CA, 1969.

P. A. Monkewitz, K. A. Chauhan, and H. M. Nagib. Self-consistent high-Reynolds-number asymptotics for zero-pressure-gradient turbulent boundary layers. *Phys. Fluids*, 19(11):115101-1–115101-12, 2007.

A. Neish and F. T. Smith. On turbulent separation in the flow past a bluff body. *J. Fluid Mech.*, 241:443–467, August 1992.

J. M. Österlund, A. V. Johansson, H. M. Nagib, and M. Hites. A note on the overlap region in turbulent boundary layers. *Phys. Fluids*, 12(1):1–4, 2000. Letter.

A. I. Ruban. Singular Solutions of the Boundary Layer Equations Which Can Be Extended Continuously Through the Point of Zero Surface Friction. *Fluid Dyn.*, 16(6):835–843, 1981. Original Russian article in *Izvestiya Akademii Nauk SSSR, Mekhanika Zhidkosti i Gaza* (6), 42–52, 1981.

A. I. Ruban. Asymptotic Theory of Short Separation Regions on the Leading Edge of a Slender Airfoil. *Fluid Dyn.*, 17(1):33–41, 1982. Original Russian article in *Izvestiya Akademii Nauk SSSR, Mekhanika Zhidkosti i Gaza* (1), 42–51, 1982.

B. Scheichl and A. Kluwick. Turbulent Marginal Separation and the Turbulent Goldstein Problem. *AIAA J.*, 45(1):20–36, 2007a. See also *AIAA Meeting paper 2005-4936*.

B. Scheichl and A. Kluwick. On turbulent marginal boundary layer separation: how the half-power law supersedes the logarithmic law of the wall. *Int. J. Computing Science and Mathematics (IJCSM)*, 1(2/3/4):343–359, 2007b. Special Issue on Problems Exhibiting Boundary and Interior Layers.

B. Scheichl and A. Kluwick. Asymptotic theory of bluff-body separation: a novel shear-layer scaling deduced from an investigation of the unsteady motion. *J. Fluids Struct.*, 24(8):1326–1338, December 2008. Special Issue on the IUTAM Symposium on Separated Flows and their Control.

B. Scheichl, A. Kluwick, and M. Alletto. "How turbulent" is the boundary layer separating from a bluff body for arbitrarily large Reynolds numbers? *Acta Mech.*, 201(1–4):131–151, 2008b. Special Issue dedicated to Professor Wilhelm Schneider on the occasion of his 70th birthday.

B. Scheichl and A. Kluwick. Level of Turbulence Intensities Associated with Bluff-Body Separation for Large Values of the Reynolds number. Meeting paper 2008-4348, AIAA, 2008c.

B. Scheichl, A. Kluwick, and F. T. Smith. Time-mean description of turbulent bluff-body separation in the high-Reynolds-number limit. In B. Eckhardt, editor, *Advances in Turbulence XII. Proceedings of the 12th EUROMECH European Turbulence Conference, September 7-10, 2009, Marburg, Germany*, volume 132 of Springer Proceedings in Physics, pages 577–580. Springer-Verlag, Berlin, Heidelberg, New York, 2009.

B. Scheichl, A. Kluwick, and F. T. Smith. Break away separation for high turbulence intensity and large Reynolds number. *J. Fluid Mech.*, submitted in revised form, 2010.

H. Schlichting and K. Gersten. *Boundary-Layer Theory*. Springer-Verlag, Berlin, Heidelberg, New York, 8th edition, 2000.

W. Schneider. Boundary-layer theory of free turbulent shear flows. *Z. Flugwiss. Weltraumforsch. (J. Flight Sci. Space Res.)*, 15(3):143–158, 1991.

R. L. Simpson, Y.-T. Chew, and B. G. Shivaprasad. The structure of a separating turbulent boundary layer. Part 1. Mean flow and Reynolds stresses. *J. Fluid Mech.*, 113(2):23–51, 1981.

K. Stewartson. Multistructured Boundary Layers on Flat Plates and Related Bodies. In Y. Chia-Sun, editor, *Advances in Applied Mechanics*, volume 14, pages 145–239. Academic Press, New York, San Francisco, London, 1974.

K. Stewartson, F. T. Smith, and K. Kaups. Marginal Separation. *Studies in Applied Mathematics*, 67(1):45–61, 1982.

R. I. Sykes. An asymptotic theory of incompressible turbulent boundary-layer flow over a small hump. *J. Fluid Mech.*, 101(3):631–646, 1980.

A. A. Townsend. Equilibrium layers and wall turbulence. *J. Fluid Mech.*, 11(1):97–120, 1961.

J. D. A. Walker. Turbulent Boundary Layers II: Further Developments. In A. Kluwick, editor, *Recent Advances in Boundary Layer Theory*, volume 390 of CISM Courses and Lectures, pages 145–230. Springer-Verlag, Vienna, New York, 1998.

K. S. Yajnik. Asymptotic theory of turbulent shear flows. *J. Fluid Mech.*, 42(2):411–427, 1970.

Interactive Boundary Layer (IBL)

P.-Y. Lagrée

CNRS & UPMC Univ Paris 06, UMR 7190,
Institut Jean Le Rond d'Alembert, Boîte 162, F-75005 Paris, France
pierre-yves.lagree@upmc.fr ; www.lmm.jussieu.fr/~lagree

Abstract We present here the Interacting Boundary Layer Equations. It is called Inviscid-Viscous Interactions as well. This is a way to solve an approximation of the Navier Stokes equations at large Reynolds number using the Ideal Fluid / Boundary Layer decomposition. But, instead of solving first the ideal Fluid and second the Boundary Layer, both are solved together. This "strong coupling" (or this Viscous-Inviscid Interaction) allows to compute separated flows. This was impossible in the classical Boundary Layer framework, because in this framework, the boundary layer is constrained by the Ideal Fluid which imposes its slip velocity at the wall. This coupling is justified in the Triple Deck theory which is the rational explanation of IBL. We present some numerical experiments showing some simple academic examples of interactions such as flows over bumps or wedges in subsonic, supersonic, subcritical and supercritical external flows and in pipes. Some examples from the literature are then presented.

1 Introduction

The concept of Ideal Fluid/ Boundary Layer decomposition is classical (see Schlichting books (42), (41) (17) or Prandtl (37)). The rational technique of expansion has been presented by Van Dyke (48) and is explained in its book (51). The procedure is as follows, starting from Navier Stokes equations we put first $1/Re = 0$; this gives the Euler description (called "outer problem" see (51)). In this non viscous description, the flow slips at the wall. This gives an "outer velocity" at the wall, parallel to the wall. This singular behavior is removed by the introduction of a thin layer of relative thickness $1/\sqrt{Re}$, the boundary layer (called "inner problem" see (51)). The velocity at the upper bound of this layer (at infinity in local inner boundary layer variables) is by matching the ideal fluid velocity at the wall. In this boundary layer, viscous effects act in order to decrease this slip velocity to full fit the no slip condition.
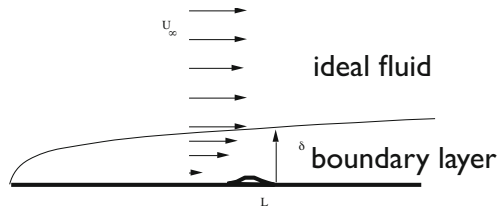
Figure 1. The typical problem a plane plate (neglect curvature) with a small bump on it. The position L is used to scale x and y, the velocity U_∞ is used to scale the velocities

From a practical aeronautical point of view, the ideal fluid description gives the lift of the wing, the viscous layer gives the drag (we are aware of the induced drag on finite span wings which is a ideal fluid effect).

But, everything is not so simple as just described here and in section 2 were we present classical notations and solutions (Falkner Skan, Von Kármán...). There are problems when computing the boundary layer. The first most important problem is the boundary layer separation problem. It is introduced in section 3. We introduce in this same section an other important problem which is the "upstream influence problem". We will show in the section 4 that to solve those two problems, the good strategy is a strategy of "strong interaction" between the boundary layer and the ideal fluid, furthermore, to obtain boundary layer separation one has to solve the boundary layer in an inverse way. So in section 5 is presented what is called "Interactive Boundary Layer" or "Viscous Inviscid Interaction", or "Viscid-Inviscid coupling" or "Inviscid Viscous Interaction", see (3), (7), (12), (28), (9) and (44)). The strategy of coupling is presented. Some practical examples with boundary layer separation from literature and for various flows régimes are then presented in the final section 6.

2 Classical Boundary Layer Equations

2.1 Prandtl Boundary Layer equations

Let us consider a simple semi infinite flat plate with a kind of bump on it (see figure 1). Using L and U_∞ as scales ($x = L\bar{x}$, $y = L\bar{y}$, $u = U_\infty\bar{u}$, and $v = U_\infty\bar{v}$), first, we compute the ideal fluid solution. We obtain the "slip velocity", written $\bar{u}_e$ the value of the ideal fluid velocity at the wall (the transverse velocity is zero). Near the wall, the ideal fluid solution is no more valid as the velocity should be zero at a wall. We have to introduce a "Boundary Layer". To obtain this we use the "least degeneracy principle"

or "dominant balance" (Van Dyke (51), Darrozès & François (11)): we want the convective terms and at least re hook one diffusive term (as $\bar{y} = \tilde{y}\delta/L$):

$$\tilde{u}\frac{\partial \tilde{u}}{\partial \bar{x}} \propto \frac{1}{Re(\delta/L)^2}\frac{\partial^2 \tilde{u}}{\partial \tilde{y}^2},$$

we then say that the boundary layer is of relative order $Re^{-1/2}$. So we classically define

$$x = L\bar{x},\ y = Re^{-1/2}L\tilde{y},\ u = U_\infty \tilde{u},\ v = U_\infty Re^{-1/2}\tilde{v},\ p = \rho U_\infty^2 \tilde{p},$$

in those new scales, the Navier Stokes equation are the Prandtl equations:

$$\frac{\partial \tilde{u}}{\partial \bar{x}} + \frac{\partial \tilde{v}}{\partial \tilde{y}} = 0, \qquad \tilde{u}\frac{\partial \tilde{u}}{\partial \bar{x}} + \tilde{v}\frac{\partial \tilde{u}}{\partial \tilde{y}} = \bar{u}_e\frac{d\bar{u}_e}{d\bar{x}} + \frac{\partial^2 \tilde{u}}{\partial \tilde{y}^2}, \tag{1}$$

with no slip boundary conditions $\tilde{u} = \tilde{v} = 0$ on the wall, and the matching

$$\tilde{u}(\bar{x}, \tilde{y} \to \infty) \to \bar{u}_e(\bar{x}, \bar{y} \to 0);$$

at the first position in $\bar{x}$, a initial profile of $\tilde{u}$ should be given to start the resolution which is marching in $\bar{x}$. With a given external velocity, those equations are in principle solvable.

2.2   Blowing Velocity Induced by the Boundary Layer

But, before going further, let us present a useful relation for the sequel. Let us look at the transverse velocity in the Boundary Layer, in fact, we do not match the transverse velocity (at initial order). The reason is that it is of order $Re^{-1/2}$, which is negligible for the Ideal Fluid. Starting from the incompressibility equation and adding and substracting the same derivative of the velocity $\frac{\partial \bar{u}_e}{\partial \bar{x}}$ (in the spirit of Von Kármán integral equations see thereafter), we obtain, after integration up to an $\tilde{y}$ ($\bar{x}$ and $\tilde{y}$ are independent variables), that the transverse velocity is:

$$\tilde{v}(\tilde{y}) - \tilde{v}(0) = -\frac{\partial}{\partial \bar{x}}\int_0^{\tilde{y}}(\tilde{u} - \bar{u}_e)d\tilde{y} - \tilde{y}\frac{\partial \bar{u}_e}{\partial \bar{x}}.$$

So, if $\tilde{y}$ is large enough and as $\tilde{v}(0) = 0$, we obtain the behavior for large enough $\tilde{y}$, with the help of the displacement thickness $\tilde{\delta}_1$:

$$\tilde{v}(\tilde{y}) \simeq \frac{d}{d\bar{x}}(\bar{u}_e\tilde{\delta}_1) - \tilde{y}\frac{\partial \bar{u}_e}{\partial \bar{x}} \ \ \text{with } \tilde{\delta}_1 = \int_0^\infty (1 - \frac{\tilde{u}}{\bar{u}_e})d\tilde{y}. \tag{2}$$

This velocity must be expressed in outer variables, so it is multiplied by $Re^{-1/2}$, and $\bar{y} = Re^{-1/2}\tilde{y}$ is used. Now, we write the outer velocity in the

ideal fluid as a Taylor expansion near the wall for small $\bar{y}$ (and taken into account the incompressibility of the ideal fluid):

$$\bar{v} = \bar{v}(\bar{x}, 0) + \bar{y}\frac{\partial \bar{v}}{\partial \bar{y}} + ... = \bar{v}(\bar{x}, 0) - \bar{y}\frac{\partial \bar{u}_e}{\partial \bar{x}} + ...$$

matching this velocity and the boundary layer velocity 2 shows that:

$$\bar{v}(\bar{x}, 0) = Re^{-1/2}\frac{d}{dx}(\bar{u}_e\tilde{\delta}_1).$$

Hence the boundary layer disturbs the ideal fluid at order $Re^{-1/2}$. It is called the "blowing velocity". So the velocity in the ideal fluid (called transpiration boundary condition as well) induces perturbations at the order $Re^{-1/2}$ in the fluid:

$$\bar{u} = \bar{u}_1 + Re^{-1/2}\bar{u}_2, \quad \bar{v} = \bar{v}_1 + Re^{-1/2}\bar{v}_2, \quad \bar{p} = \bar{p}_1 + Re^{-1/2}\bar{p}_2...$$

with $\bar{u}_1(x, 0) = \bar{u}_e(x)$. The classical asymptotic sequence (as described by Van Dyke (51)) is then: the ideal fluid at order $O(1)$ drives the boundary layer at order $O(1)$. In turn the boundary layer disturbs the ideal fluid at order $O(Re^{-1/2})$, then this perturbation creates a corrective boundary layer at this $O(Re^{-1/2})$ order, and so on. There is a cascade of disturbances at increasing order (see figure from Van Dyke 10 left for this classical sequence).

The analysis was presented for a flat plate, but we will present in section 6 examples of flows over a flat plate with a small bump. The bump is defined by the function $\bar{f}(\bar{x})$. Before going further, we have to present the "Prandtl transform" which consists to change the transverse velocity and variable: $\tilde{v} \rightarrow \tilde{v} - \bar{f}'(\bar{x})\tilde{u}$ and $\tilde{y} \rightarrow \tilde{y} - \bar{f}(\bar{x})$ and keep $\bar{x}$ and $\tilde{u}$. With this transformation, the Prandtl system is invariant, and now the position on the wall is 0 again. The blowing velocity is then corrected by $\bar{f}'(\bar{x})\bar{u}_e$. This is a trick which allows to change the bumpy wall in a flat one.

2.3 Self Similar Solutions of Prandtl Equations

There is a simple class of solution of the boundary layer equations which correspond to the flow along a wedge of half angle $\beta\pi/2$ (see figure 6 left). The ideal fluid slip velocity is then a power law $\bar{x}$, the suitably non-dimensional longitudinal velocity is:

$$\bar{u}_e = \bar{x}^n \quad \text{with} \quad n = \frac{\beta}{2 - \beta}, \quad \beta = \frac{2n}{n + 1}.$$

This is the so called Falkner Skan problem (41). There is a self similar solution in the boundary layer, the longitudinal velocity is $f'(\eta)\bar{x}^n$ with $\eta = (\sqrt{\frac{n+1}{2}})\frac{\tilde{y}}{\bar{x}^{(1-n)/2}}$. The selfsimilar stream function equation $f(\eta)$ is from Prandt Equation 1:

$$f''' + ff'' + \beta(1 - f'^2) = 0, \ f(0) = f'(0) = 0 \text{ and } f'(\infty) = 1. \qquad (3)$$

The Blasius solution is the solution of the flow over a flat plate, it corresponds to $n = 0$ and $\beta = 0$, and $f''(0) = 0.332\sqrt{2}$ and $\int_0^\infty (1-f')d\eta = 1.732$. The Hiemenz stagnation point solution is the solution of the flow against a flat plate, it corresponds to $n = 1$ and $\beta = 1$ and $f''(0) = 0.92$ and $\int_0^\infty (1 - f')d\eta = 0.8$. In principle, for a given geometry (β), one solves the ideal fluid and obtains n. Then the equation is solved, one finds the value of $f''(0)$ which allows to suit all the boundary conditions. See figure 6 where $f''(0)$ is plotted as a function of β (we will see section 4.1 that the $f''(0)$ function of β is in fact multivalued in $\beta < 0$. One other result is the displacement thickness $\int_0^\infty (1 - f')d\eta$. In fact, this naive direct resolution gives a very stiff problem, and in practice, for a given β and a negative $f''(0)$ it is impossible to solve the system (eq. 3) in the case of separated flows.

2.4   Von Kármán Equation Integral Relation

Boundary layer equations are a 2D PDE which is not so simple to solve. Nevertheless, the velocity profile is sometimes self similar (as just seen). It means that there is a kind of unique profile and that all the profiles are deduced by stretching it (Pohlhausen introduced simple poynomia). The velocity of the ideal fluid at the wall and the thickness of the profile are two fundamental parameters which stretch the fundamental profile.

In this part we present the Von Kármán-Pohlhausen (1921) equation which consists in writing only the global dependance between $\bar{u}_e$ and the displacement thickness δ_1 supposing that in fact all the profiles are nearly similar. An other equivalent interpretation of δ_1 (linked closely to the "blowing veloicity" just defined) is that the flux of mass trough an enough large y is the same than the flux of a constant velocity across a smaller section reduced by the amount of δ_1 so that:

$$\delta_1 u_e = \int_0^\infty (u_e - u)dy.$$

This gives the physical definition of the displacement thickness, it is the distance by which the external stream lines are shifted due to the boundary layer development. To define the Von Kármán equation, we write the total

derivative in conservative form and in a "defect formulation" (Le Balleur (28)), so the momentum equation is:

$$\frac{\partial}{\partial \bar{x}}(\tilde{u}\bar{u}_e - \tilde{u}^2) + (\bar{u}_e - \tilde{u})\frac{\partial \bar{u}_e}{\partial \bar{x}} - \frac{\partial}{\partial \tilde{y}}(\tilde{v}(\tilde{u} - \bar{u}_e)) = -\frac{\partial^2 \tilde{u}}{\partial \tilde{y}^2}.$$

Using the displacement thickness (eq. 2), and defining the momentum thickness $\tilde{\delta}_2$ and the shape factor H:

$$\tilde{\delta}_2 = \int_0^\infty \frac{\tilde{u}}{\bar{u}_e}(1 - \frac{\tilde{u}}{\bar{u}_e})d\tilde{y} \text{ and } H = \frac{\tilde{\delta}_1}{\tilde{\delta}_2},$$

and defining a function f_2 linked to the skin friction as: $\frac{\partial \tilde{u}}{\partial \tilde{y}} = f_2 \frac{H\bar{u}_e}{\tilde{\delta}_1}$ gives the following equation where the ideal fluid promotes the boundary layer:

$$\frac{d}{d\bar{x}}(\frac{\tilde{\delta}_1}{H}) + \frac{\tilde{\delta}_1}{\bar{u}_e}(1 + \frac{2}{H})\frac{d\bar{u}_e}{d\bar{x}} = \frac{f_2 H}{\tilde{\delta}_1 \bar{u}_e}, \qquad i.e. \ \tilde{\delta}_1 = F(\bar{u}_e). \tag{4}$$

Initial condition is for example $\tilde{\delta}_1(0) = 0$ (but the Hiemenz value may be a good first guess) and $\bar{u}_e(0) = 1$. In the classical approach, $\tilde{\delta}_1$ is obtained through the knowledge of $\bar{u}_e$, which we write formaly $\tilde{\delta}_1 = F(\bar{u}_e)$.

To solve this boundary layer equation, a closure relationship linking H and f_2 to the velocity and the displacement thickness is needed. This is of course a strong hypothesis. Defining $\Lambda_1 = \tilde{\delta}_1^2 \frac{d\bar{u}_e}{d\bar{x}}$, the system is closed from the resolution of the Falkner Skan system using the following fit (fig. 2):

$$H = \left\{ \begin{array}{ll} 2.5905e^{-0.37098\Lambda_1} & \text{if } \Lambda_1 < 0.6 \\ 2.074 & \text{if } \Lambda_1 > 0.6 \end{array} \right\}, \quad f_2 = 1.05(-\frac{1}{H} + \frac{4}{H^2}). \tag{5}$$

It means that we suppose that each profile remains a Falkner Skan one in the boundary layer. We used this crude solution in exponential with the value of the sink solution $H = 2.074$ as a limiting value (Lorthois & Lagrée (32)). We tested it to be enough good, other closures may be found in the literature. Some closures use the concept of entrainment. The closure may be done with other families of profiles, and Pohlhausen profiles are good candidates (the solution is part of a polynomia). With those profiles the reverse flow is over estimated compared to Falkner Skan.

In general, the Von Kármán equation is written with the momentum thickness $\tilde{\delta}_2$:

$$\frac{d}{d\bar{x}}(\tilde{\delta}_2 \bar{u}_e^2) + \tilde{\delta}_1 \bar{u}_e \frac{d\bar{u}_e}{d\bar{x}} = \frac{\partial \tilde{u}}{\partial \tilde{y}}\Big|_{\tilde{y}=0}$$
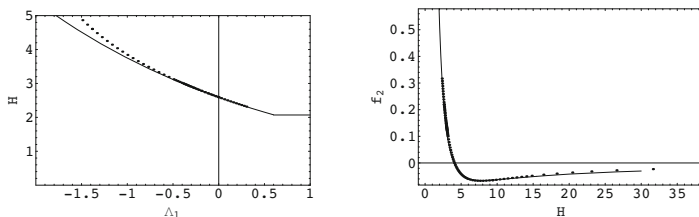
Figure 2. An example of closure of the integral relations. The dots are the Falkner Skan values and the line the proposed function. Anticipating problems of boundary layer separation f_2 may be negative.

(often the symbol $\tilde{\theta}$ is taken), we prefer to write it with $\tilde{\delta}_1$ as we we have seen that this value has a real physical interpretation: the displacement thickness and the "blowing velocity". The reason why mainly $\tilde{\delta}_2$ is used is that its derivative is clearly linked to the skin friction (this gives a technique to deduce the skin friction from even crude measurements of the boundary layer profile.

Up to now, we have all the classical ingredients of the Boundary Layer obtained from the ideal fluid solution. Let us examine some of the problems of this theory.

3   Problems Associated with the Boundary Layer

3.1   Separation

The first problem of the boundary layer is the the problem of separation. The point of separation is the point defined by $\frac{\partial \tilde{u}}{\partial \tilde{y}} = 0$. After this point, the flow is reversed, see an example of representation on figure 3 taken from Prandtl himself (37).

On figure 4 is presented an example of boundary layer computation with an external flow $\bar{u}_e = sin(\bar{x})$ corresponding to the flow on a cylinder of unit radius. An Integral resolution of the equations is compared with a complete boundary layer resolution showing that the Von Kármán approach is enough precise.

The flow is accelerated from $\bar{x} = 0$ to $\pi/2$, near $x = 0$ we have an Hiemenz linear flow. The flow is decelerated for $\bar{x} > \pi/2$, this deceleration promotes an increase of the boundary layer thickness and a decrease of the skin friction. At the point where $\frac{\partial \tilde{u}}{\partial \tilde{y}} = 0$, the boundary layer is singular, we
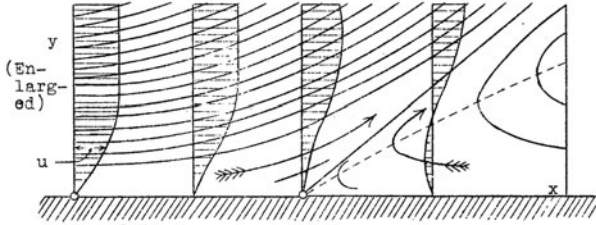
Figure 3. A sketch from Prandtl (37) of the flow near the point of vanishing shear stress.

can not compute numerically (here by finite difference) the boundary layer. Using the Von Kármán equation (Eq. 4 and closure 5) gives the same behavior. It fails nearly at the same point (not exactly, but not so bad).

A simple way to see the problem is to observe the Von Kármán equation linearised around a decelerating flow. Linearizing the velocity near the point of separation is say $\bar{u}_e = sin(\bar{x}_s) - a(\bar{x} - \bar{x}_s)$ with $a = cos(\bar{x}_s)$ and linearizing around small Λ_1 (which is not true but is a enough good approximation) gives $H = H_0 - H_p\Lambda_1$ where $H_0 = 2.59$ and $H_p \simeq -0.96$, so the variation of δ_1/H with respect to $\bar{x}$ is:

$$\frac{d}{d\bar{x}}(\frac{\tilde{\delta}_1}{H}) = \frac{1}{H}(\frac{d}{d\bar{x}}\tilde{\delta}_1)(1 - \frac{\tilde{\delta}_1}{H}\frac{dH}{d\Lambda_1}\frac{d\Lambda_1}{d\tilde{\delta}_1}) \simeq (\frac{1}{H_0}\frac{d}{d\bar{x}}\tilde{\delta}_1)(1 - \frac{2H_p a\tilde{\delta}_1^2}{H_0}),$$

therefore $\frac{d}{d\bar{x}}\tilde{\delta}_1$ is infinite, we can not march in $\bar{x}$ anymore. This crude estimation shows that the separation point is impossible to cross, but direct numerical finite difference solution of the boundary layer equations gives the same result (figure 4).

This difficult problem has been examined, among others by Landau (in the classical text book (25)) and by Goldstein (18). Landau (25) noticed that as in the boundary layer $v \ll u$, so the transverse velocity must increase a lot to be as large as the longitudinal one. It is apparently the case when the flow is separated (stream lines are ejected from the wall). In boundary layer variables Landau infer that $v = \infty$ and $\partial v/\partial y = \infty$ so that $\partial u/\partial x = -\infty$. The velocity is strongly decelerated near the point of separation x_s. So he proposes to work with the inverse of the function $(\frac{\partial x}{\partial u})$ which is zero at separation and proposes a reciprocal expansion of x in u near x_s as (where
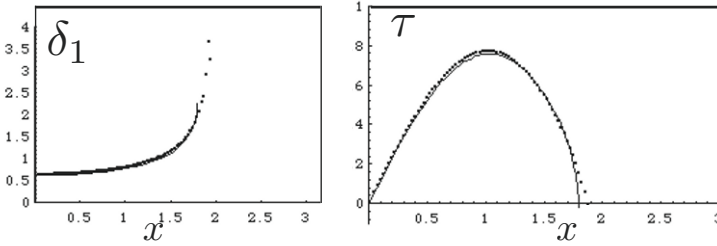
Figure 4. Boundary layer separation on a cylinder, the outer velocity is $\bar{u}_e = sin(\bar{x})$, points are numerical finite difference solution of the Boundary Layer equations, line is the integration of Von Kármán equation with the proposed closure (Eq. 4 and 5). Separation occurs for an angle of 104°.

β is an ad hoc function linked to $\partial_x^2 u$):

$$x - x_s = \frac{\partial x}{\partial u}(u - u_s) + \frac{1}{2}\frac{\partial^2 x}{\partial u^2}(u - u_s)^2 + ... = 0(u - u_s) + \frac{1}{4\beta'(y)^2}(u - u_s)^2 + ...$$

so that one may write the velocity u and by the continuity equation v as:

$$u = u_s(y) + 2\beta'(y)\sqrt{x_s - x} + ... \text{ and } v = \frac{\beta(y)}{\sqrt{x_s - x}} + ...$$

Injecting it in the momentum equation, neglecting the viscosity and writing the total derivative as $u^2(\partial_y(\frac{v}{u}))$ shows that v/u does not depend on y, an hint for the profile near separation may be deduced as :

$$u = u_s(y) + \frac{\partial u_s}{\partial y}A(x) \quad v = -\frac{\partial A}{\partial x}u_s \quad \text{with } A(x) \propto \sqrt{x_s - x}.$$

Unfortunately this description does not fit the good boundary conditions at the wall....

Goldstein showed that for a given external flow, one can not compute the boundary layer if the skin friction vanishes (which is consistent to Landau approach), the skin friction behaves as:

$$\tau_p = \sqrt{48a_4(x_s - x))},$$

one of the problem being an impossible match of the constant a_4 before and after the point of separation. He obtained the same square root singularity. This is called Goldstein singularity, close to the point of separation.

So, for a given external decreasing velocity, there is a possibility of separation with a singularity. The computation can not pass the separation. Most of classical text book of fluid mechanics do the same and end their course on boundary layers by this dead end, for example one can read in Kundu (19): "the boundary layer equations are valid only far downstream as the point of separation. Beyond it the boundary layer becomes so thick that the basic underlying assumptions become invalid. Moreover, the parabolic character of the boundary layer equations requires that a numerical integration is possible only in the direction of advection (along which information are propagated), which is *upstream* within the reversed flow region. A forward (downstream) integration of the boundary layer equations therefore breaks down after the separation point. Last, we can no longer apply potential theory to find the pressure distribution in the separation region, as the effective boundary of the irrotational flow is no longer the solid surface but some unknown shape encompassing part of the body plus the separation region."

3.2   The Problem of the Influence of Downstream on Upstream

One other strange problem appeared in the 50' at the time of the supersonic conquest: the problem of "Upstream Influence". A model configuration for a supersonic wing was the aligned flat plate in a compressible supersonic flow. In various experiments in supersonic flows (Ackeret Chapman and others, see (45)), it was observed that an impinging shock wave on a boundary layer produces perturbations far upstream the point of reflexion of the wave. The boundary layer deviates from its basic state upstream of the impinging shock, see photos on figure 5 from Stewartson 64 book (45). On this figure we even see that three different accidents (an impinging shock, a forward facing step and a wedge) produce the same upstream flow. The deviation occurs far away (in boundary layer thickness units) from the accident.

In the classical supersonic framework this is impossible (figure 5 lower left). First the ideal fluid is supersonic (hyperbolic) so perturbations move downstream in the Mach cone. Second, the boundary layer is parabolic, so perturbations move downstream and across the boundary layer. No disturbance can theoretically move upstream against the flow. This is the upstream influence paradox.

Is it a dead end? No!
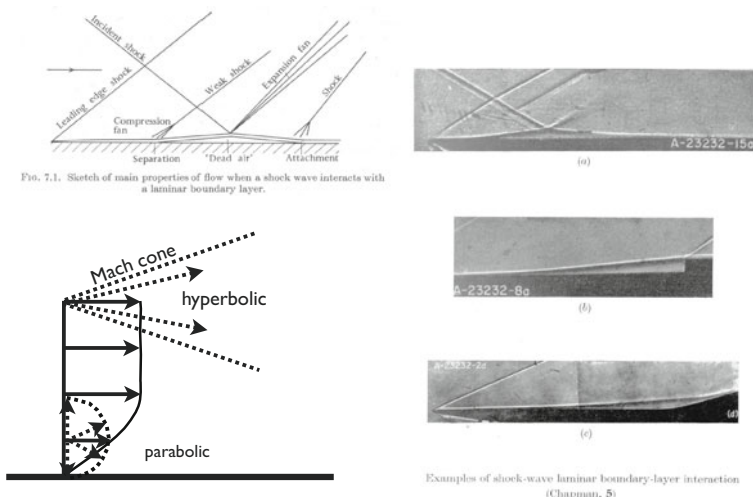
Figure 5. The "upstream influence" in supersonic flows. Figures from Stewartson book (45): upper left, a sketch of the shock wave boundary layer interaction. Right, the three different accidents (an impinging shock, a forward facing step and a wedge) produce the same upstream flow. Lower left: upstream influence paradox: the ideal fluid is supersonic (hyperbolic, perturbations move downstream in the Mach cone), the boundary layer is parabolic (perturbations move downstream and across the boundary layer).

4   Solutions of the paradoxes

4.1   Inverse Boundary Layer

In fact computing the reverse flow within a boundary layer is possible with the Prandtl equations. The good idea is: impose the displacement thickness and solve for pressure gradient. This was the idea of Catherall and Mangler (6) in 66, and they were the first to succeeded to pass the point of flow separation while solving the steady boundary-layer equations with a prescribed displacement thickness (a kind of parabolic shape). With an imposed

$$\tilde{\delta}_1 = \int_0^\infty (1 - \frac{\tilde{u}}{\bar{u}_e})d\tilde{y}$$

it is possible to compute $\bar{u}_e$ and to obtain a negative skin friction.

Is it surprising? Not so much, we previously spoke about a simple class of solution of the boundary layer equations (3) which corresponds to the flow

along a wedge of half angle $\beta\pi/2$ (see figure 6 left), the so called Falkner
Skan problem (41). A naive direct resolution gives a very stiff problem, and
in practice, for a given β it is impossible to find the $f''(0)$ which solves the
system 3 in the direct way when there is separation. We can nevertheless
obtain flow separation for some values of β. To obtain it, we have to solve in
an inverse way, we impose the thickness $\int_0^\infty (1-f')d\eta$, and we find the value
of β associated. Hence, a simple way to feel that the boundary layer must be
solved in inverse way is really the Falkner Skan case. It is representative by
many aspects of the boundary layer behavior: for a given external velocity
one has a given β and one computes the corresponding profile. But, we see
on figure 6 that if the external velocity is with a β to much negative, there
is no solution. Only for an ad hoc external velocity we have solution(s).
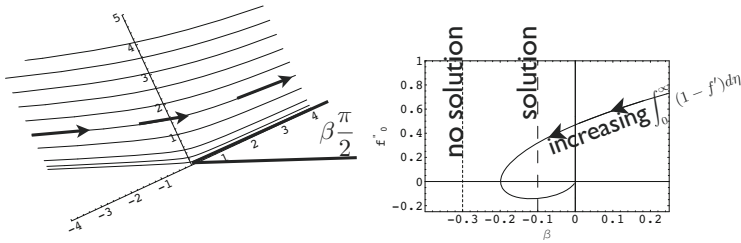
Figure 6. Left the Falkner Skan problem: self similar flow on a wedge. Right,
the numerical solution, value of $f''(0)$ as a function of β. Not every external
velocity is compatible with the boundary layer, for example in the Falkner Skan
case, too small β (less than -0.199) are not relevant (small dashing). A larger
value of the outer velocity gradient (large dashing) gives solutions.

On figure 7 we present an example of inverse boundary layer computation
using the Keller Box method (21). The displacement δ_1 is given, the velocity
is deduced. For enough large values of the increase of the boundary layer
displacement thickness, we have separation with reverse flow. The outer
velocity decreases and reincreases.

4.2   Some Explanations of the Upstream Influence Problem

Now, we have some responses with the inverse solution for Boundary
Layer. But we have not finished. The upstream influence paradox is still to
explain. It puzzled people.
• Some people think that there is always a subsonic part in the boundary
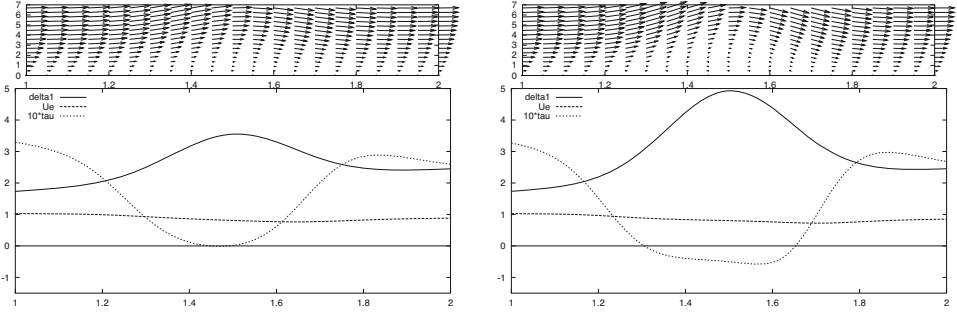
Figure 7. Examples of inverse boundary layer computation. Separation is not an issue when displacement is prescribed. Here given $\tilde{\delta}_1 = 1.73\bar{x}^{1/2} + \alpha e^{-25(\bar{x}-1.5)^2}$, we compute the associated external velocity, and the skin friction. For $\alpha = 1.43$ (left) is the incipient separation, for smaller increase of $\tilde{\delta}_1$, there is no separation just a decrease of velocity. For larger values (right $\alpha = 2.8$) we have separation with reverse flow. The outer velocity decreases and reincreases.

layer, so that the retroaction can travel back in this subsonic layer. In fact it is not the good mechanism as the upstream influence would be of same length than this subsonic layer is thick. But on the experiments, the longitudinal scale is far larger than the boundary layer thickness.

• Garvine (16) proposed a simplified boundary layer model linearising around $u = 1$ the supersonic boundary layer (neglecting thermal effects):

$$\partial_{\bar{x}}\tilde{u} = -\partial_{\bar{x}}\bar{p} + \partial_{\tilde{y}}^2\tilde{u}, \quad \tilde{v} = -\int_0^{\tilde{y}} \partial_{\bar{x}}\tilde{u}d\tilde{y}$$

and writing the Ackeret formula (linking the pressure and the blowing velocity) as:

$$\bar{p} = \frac{1}{\sqrt{Re}\sqrt{M^2 - 1}}\tilde{v}(\tilde{\delta})$$

he obtains after claiming $\tilde{\delta} = cst$ (yes he did!) that the pressure gradient is $-\frac{1}{\sqrt{Re}\sqrt{M^2-1}}\int_0^{\tilde{\delta}} \tilde{u}_{\bar{x}\bar{x}}d\tilde{y}$ so that a model equation of the interaction is:

$$\partial_{\bar{x}}\tilde{u} = \frac{1}{\sqrt{Re}\sqrt{M^2 - 1}}\int_0^{\delta} u_{\bar{x}\bar{x}}d\tilde{y} + \partial_{\tilde{y}}^2\tilde{u}.$$

He pointed out the come back of ellipticity due to this $u_{\bar{x}\bar{x}}$ term. He then obtained a set of eigen solutions with Laplace transform, in fact the exponentially growing one of those solutions can be obtained in looking to $e^{K\bar{x}}$

solutions, so that solution behaves as:

$$e^{\frac{\sqrt{Re}\sqrt{M^2-1}}{\tilde{\delta}}\tilde{x}}.$$

So the coupling of the two equations produces self induced explosive solutions.

• Numerically those explosive solutions were obtained by Werle Dwoyer, and Hankey (54) (among others). On figure 8 we have a clear example of what happens when solving in a marching way the coupled system. Starting from a given initial location they solved the coupled boundary layer system with the so called tangent wedge law (valid for stronger shocks than the linearised Ackeret formula). They showed that changing a bit one parameter may cause different solutions. Those are called "branching solutions".
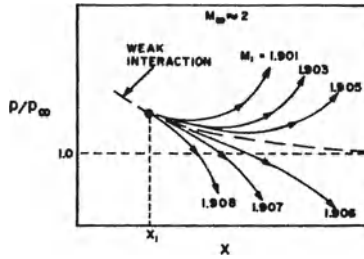
Figure 8. Branching solutions (54): changing a bit one parameter may cause different solutions while solving the equations with a marching scheme.

• One may consider the most simple argument, see Le Balleur (26). He considers the strong coupling of the boundary layer in Von Kármán form (neglecting again thermal effects) with the Ackeret formula (linking the perturbation of pressure at $M > 1$ due to the variations of the effective wall (represented by δ_1) as:

$$\frac{d}{d\bar{x}}(\frac{\tilde{\delta}_1}{H}) + \frac{\tilde{\delta}_1}{\bar{u}_e}(1 + \frac{2}{H})\frac{d\bar{u}_e}{d\bar{x}} = \frac{f_2 H}{\tilde{\delta}_1 \bar{u}_e}, \quad \bar{p} = \frac{1}{\sqrt{Re}\sqrt{M^2-1}}\frac{d\tilde{\delta}_1}{d\bar{x}}, \tag{6}$$

so that, supposing that $\bar{u}_e$ is nearly one and $\partial_{\bar{x}}\bar{u}_e = -\partial_{\bar{x}}\bar{p}$

$$\frac{d}{d\bar{x}}(\frac{\tilde{\delta}_1}{H}) = \frac{\tilde{\delta}_1}{\bar{u}_e}(1 + \frac{2}{H})\frac{1}{\sqrt{Re}\sqrt{M^2-1}}\frac{d^2\tilde{\delta}_1}{d\bar{x}^2} + \frac{f_2 H}{\tilde{\delta}_1 \bar{u}_e},$$

this equation is "not so far" from from the basic flow with subscript 0 and $\bar{u}_e \sim 1$, so after linearisation.

$$\frac{d}{d\bar{x}}\tilde{\delta}_1 = \frac{\tilde{\delta}_{10}}{\bar{u}_e}(H_0+2)\frac{1}{\sqrt{Re}\sqrt{M^2-1}}\frac{d^2\tilde{\delta}_1}{d\bar{x}^2}+....$$

where we forget the contribution of the skin friction. So again, we obtain exponential solutions (called supercritical by Crocco and Lees in 52) for the disturbance of the displacement thickness δ_1:

$$e^{\frac{\sqrt{Re}\sqrt{M^2-1}}{\tilde{\delta}_{10}(H_0+2)}\bar{x}}.$$

It is nearly the same result than Garvine and than the one obtained numerically by Werle et al.

• In fact, Lighthill in 53 (30) proposed a pre-theory of triple deck explaining most of the mechanism (see in Stewartson 64 book as well) based on steady perturbations of the Orr Sommerfeld equation.

• The real definitive theory is the Triple Deck (see Ruban's contribution). In this framework, those kind of explosive solutions are called "self induced solution" (see Neiland (35), Messiter (34) and Stewartson (46)).
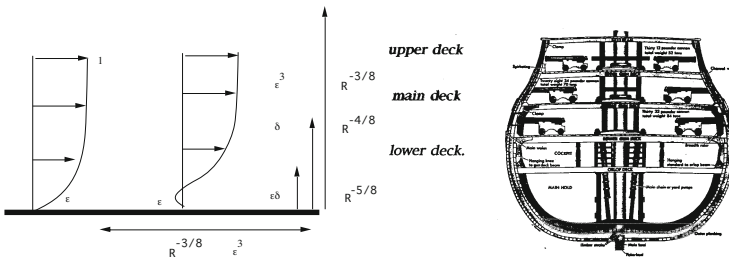
Figure 9. Left, the Triple Deck scales. Right, "triple decker ship of the line" from HMS victory brochure Porthmouth ("vaisseau de ligne à trois ponts"). In german "Dreierdeck-Theorie", a french translation of Triple Deck Theory may be "Triple Pont" instead of "Triple Couche".

To present is quickly, we have the basic non dimensional Blasius profile $U_B(\tilde{y})$ in the boundary layer, where $\tilde{y}$ is the transverse variable scaled by $1/\sqrt{Re}$ (referred as ε^4 and anticipating that $\varepsilon = Re^{-1/8}$). Now suppose that at longitudinal scale say x_3 (referred as ε^3) there is a perturbation of this basic profile. We will call "Main Deck" the region considered which is of relative scale x_3 but which is of boundary layer scale in the transverse direction. As this scale is small, the boundary layer has not evolved, and at

first order there is no transverse velocity. At the longitudinal scale x_3 there is a perturbation of this basic profile of magnitude ε, then retaining all the terms in the incompressibility and in the total derivative equation and as pressure is $O(\varepsilon^2)$ gives the solution in the Main Deck (former Boundary Layer)

$$\tilde{u} = U_B(\tilde{y}) + \varepsilon A(x) U_B'(\tilde{y}) \ \ \tilde{v} = -\varepsilon^2 A'(x) U_B(\tilde{y}), \text{ and } \frac{\partial \tilde{p}}{\partial \tilde{y}} = 0.$$

Note that this function $-A$ is reminiscent to the Landau analysis of section 3. With this description, the velocity is not zero but $\varepsilon A(x) U_B'(0)$ on the wall, so we have to introduce a new layer to full fit the no slip condition. We reobtain Prandtl equations but with a new transverse scale $\delta_3 = \varepsilon^5$ associated to the longitudinal one $x_3 = \varepsilon^3$, in which the longitudinal velocity is scalled by ε. In this new layer, the Lower Deck, the final system is then:

$$\frac{\partial u}{\partial x} + \frac{\partial v}{\partial y} = 0, \ \ u\frac{\partial u}{\partial x} + v\frac{\partial u}{\partial y} = -\frac{dp}{dx} + \frac{\partial^2 u}{\partial y^2}. \tag{7}$$

With no slip condition at the wall ($u = v = 0$), the entrance velocity profile $u(x \to -\infty, y) = U_B'(0)y$, and the matching condition with the Main Deck: $u(x, y \to \infty) = (y + A)U_B'(0)$. Note, that the system is parabolic, there is no output condition needed to solve it.

Going back in the Main Deck, the disturbed velocity at the top of the Main Deck, for $\tilde{y} \to \infty$:

$$\tilde{u} = 1; \ \tilde{v} = -\varepsilon^2 A'(x),$$

there is no more longitudinal perturbation of the velocity at order ε, but there is a transverse velocity, a kind of "blowing velocity" at the edge of the Main Deck. Note that the pressure remains of the same order ε^2.

The final layer is the Upper Deck of longitudinal size $x_3 = \varepsilon^3$ and of same thickness in which we have a blowing velocity at the wall of order ε^2. The velocity at the top of the Main Deck is then the velocity at the bottom of the upper deck: $-A'$. Depending on the ideal fluid régime, one may compute the pressure (of order ε^2). For a incompressible flow one has the Hilbert relation:

$$p = \frac{1}{\pi} \int \frac{\frac{dA}{dx}}{x - \xi} d\xi.$$

For a compressible supersonic flow, one has to use the Ackeret formula:

$$p = -\frac{1}{\sqrt{M^2 - 1}} \frac{dA}{dx}.$$

So one has to couple this relation linking a pressure and a displacement to the Lower Deck problem 7.

One may linearize the Triple Deck around the Basic Flow $u = U'_B(0)y$, say that u_1 and v_1 are the perturbations, the lower Deck :

$$\frac{\partial u_1}{\partial x} + \frac{\partial v_1}{\partial y} = 0, \ \ U'_B(0)y\frac{\partial u_1}{\partial x} + v_1 U'_B(0) = -\frac{dp_1}{dx} + \frac{\partial^2 u_1}{\partial y^2}.$$

With at the wall ($u_1 = v_1 = 0$), at the entrance $u_1(x \to -\infty, y) = 0$, and at the infinity $u_1(x, y \to \infty) = U'_B(0)A_1$. We test e^{Kx} solutions on the linearized system, with $K > 0$.

$$u_1 = e^{Kx}\phi'(y), \quad v_1 = -e^{Kx}\phi(y), \quad p_1 = e^{Kx}P,$$

with $\phi(0) = \phi'(0) = 0$ and say $\phi'(\infty) = U'_B(0)$ so that $A_1 = e^{Kx}$; as the incompressibility is fulfilled, the momentum gives (see Stewartson (47) or Sychev et al. (49) for details):

$$\frac{\partial^2 \phi''(y)}{\partial y^2} = U'_B(0)Ky\phi''(y), \ \text{with} \ \phi''(0) = KP,$$

and $p_1 = -\frac{KA_1}{\sqrt{M^2-1}}$ so that we deduce that the supersonic case allows then an eigen solution

$$K = (-3Ai'(0)(\sqrt{M^2 - 1})U'_B(0)^2)^{3/4}.$$

This exponential behavior at the longitudinal Triple Deck scale is the rational explanation of the observed self induced separation. This upstream influence is then understood as a not well posed problem. In fact, even if each part of the flow seems hyperbolic/ parabolic, due to the interaction one recovers the output influence.

This is the case in the supersonic flows, in shallow water flows at small Froude number, in mixed convection. But there exist flows with no upstream influence: for example in the symmetrical pipe flows.

As a conclusion of this section, we see that we need two two ingredients. First we need to solve the Boundary Layer in an inverse way. And second, the Boundary Layer is no more driven by the Ideal Fluid. The Boundary Layer can retroact on the Ideal Fluid. The retroaction explains the observed self induced interaction. So we now introduce the concept of Interactive Boundary Layer (IBL) which uses those ingredients.

5   Interactive Boundary Layer

5.1   Examples of Users

So it became clear that the interaction with the ideal fluid is not weak but strong. In the early 60 Gad and Curle employed Von Kármán -Pohlhausen method to try to solve the shock waves-boundary layer interaction, "without much success" (as quoted by Lees and Reeves (29). Lees and Reeves in 64 (29) did computations with integral methods, with more success, but the details are not so clear. Reyhner Flügge Lotz 68 (38) did finite differences on the Boundary layer and succeed by iteration to compute the supersonic wedge interaction.

Among people working for applications in the aerospace area, some names and teams are to be associated to Interactive Boundary Layer IBL/ Inviscid Viscous Interaction IVI. Among them:

• Le Balleur, from 1977 ((26), (27)) understood the interaction and using Von Kármán profiles did a lot of practical computations at ONERA, in supersonic and transsonic régimes.

• Veldman ((53), (52)) as well has is own codes at the National Aerospace Laboratory NLR in Amsterdam,

• Carter (4), (14), Jameson (20) at Stanford.

• Cebeci did a huge work (several books on the interactive boundary layer for example (7) (3)) and applied IBL at Boeing.

• Drela (13) and (12) developed a integral boundary layer code which is now free: XFOIL.

• Lock & Williams in a review (31), present the english RAE point of view.

• And last but not least Neiland and Sychev (49) at the TsAGI in USSR. Of course, this is again a very very partial list.

5.2   Interactive Boundary Layer

So the way to bypass Goldstein singularity is to adopt the Interactive Boundary Layer point of view. It means that we use the classical Prantdl boundary layer equations :

$$\frac{\partial \tilde{u}}{\partial \bar{x}} + \frac{\partial \tilde{v}}{\partial \tilde{y}} = 0, \;\; \tilde{u}\frac{\partial \tilde{u}}{\partial \bar{x}} + \tilde{v}\frac{\partial \tilde{u}}{\partial \tilde{y}} = \bar{u}_e \frac{d\bar{u}_e}{d\bar{x}} + \frac{\partial^2 \tilde{u}}{\partial \tilde{y}^2},$$

with no slip boundary conditions ($\tilde{u} = \tilde{v} = 0$ on the body $\bar{f}(\bar{x})$), a first given velocity profile: Blasius. The matching $\tilde{u}(\bar{x}, \tilde{y} \to \infty) \to \bar{u}_e(\bar{x})$.

A result of this computation is the transverse velocity at infinity,we ob-

tained the "blowing velocity".

$$\bar{v}_e = Re^{-1/2}\frac{d(\tilde{\delta}_1\bar{u}_e)}{d\bar{x}}.$$

Hence, the outer flow is no more only given by the wall $\bar{f}(\bar{x})$ (so that the blowing velocity is $\bar{f}'\bar{u}_e$) but, the wall is "thickened" by the boundary layer thickness (or "blowing velocity", or "transpiration boundary condition"), so that for a subsonic flow:

$$\bar{u}_e = 1 + \frac{1}{\pi}\int \frac{\bar{f}'(\bar{x})\bar{u}_e + Re^{-1/2}\frac{d(\tilde{\delta}_1\bar{u}_e)}{d\bar{x}}}{x-\xi}d\xi$$

or in a supersonic flow

$$\bar{u}_e = 1 - \frac{1}{\sqrt{M^2-1}}[\frac{d}{d\bar{x}}\bar{f}(\bar{x})\bar{u}_e + Re^{-1/2}\frac{d(\tilde{\delta}_1\bar{u}_e)}{d\bar{x}}].$$

Instead of the usual weak coupling with the hierarchy (figure 10 left), the boundary layer retroacts on the ideal fluid (figure 10 right). So even if $\bar{u}_e$ appears in the definition of himself through $\frac{d(\tilde{\delta}_1\bar{u}_e)}{dx}$, it is not an issue because of the iterations involved in the solution. The boundary layer thickness $\tilde{\delta}_1$ acts as a fictive wall, it disturbs the ideal fluid, the pressure (pressure and velocity $\bar{u}_e(\bar{x})$ are linked) develops the boundary layer itself. It is a strong interaction. The two layers are coupled. It explains the term "Interactive Boundary Layer", or "Viscous Inviscid Interaction".

Most of the separation problems are then solved...

5.3   Link between Interactive Boundary Layer and Triple Deck

At separation, the displacement boundary layer thickness becomes very thick. It is then not counterintuitive to think that the ideal fluid will be drastically changed by the viscous layer. That is the picture for "Triple Deck", but the scales are changed. In fact it is easy to show the that the IBL equations give at large Reynolds number the Triple Deck structure. The $-A$ is the disturbance of the displacement thickness.

The IBL formulation emphasizes on the displacement thickness,

$$\delta_1 = (Re^{-1/2})\int_0^\infty (1 - u(x,\tilde{y}))d\tilde{y}$$

we have to decompose it into two parts as we cross the Lower and the Main Decks. Let us introduce $\tilde{Y}$ so that we cut the integral in two parts
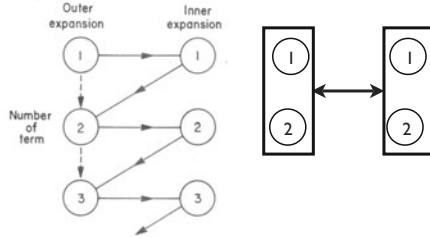
Figure 10. Left the Classical sequence, image taken from Van Dyke's book (51). Right the Interactive Boundary Layer, we do not follow the classical asymptotic sequence (from left): the ideal fluid at order $O(1)$ drives the boundary layer at order $O(1)$, in turn the boundary layer disturbs at the ideal fluid at order $O(Re^{-1/2})$, then this perturbation creates a corrective boundary layer at this $O(Re^{-1/2})$ order, *etc.* But, right, we couple the boundary layer and the ideal fluid at first order.

$(\int_0^{\tilde{Y}} + \int_{\tilde{Y}}^{\infty})$. The first integral is estimated near the wall, so the Lower Deck description ($\tilde{y} = \varepsilon y$) is valid there, but a good idea is to write the velocity $u(x, y) = U_B'(0)(y + A) + u_c$ where u_c is a correction, so the first integral:

$$(\int_0^{\tilde{Y}} (1 - \tilde{u}(\bar{x}, \tilde{y}))d\tilde{y}) = \varepsilon(\int_0^{\tilde{Y}/\varepsilon} (1 - \varepsilon(U_B'(0)(y + A)))dy - \int_0^{\tilde{Y}/\varepsilon} \varepsilon u_c dy)$$

the second integral is in the Main Deck

$$\int_{\tilde{Y}}^{\infty} (1 - u(x, \tilde{y}))d\tilde{y} = \int_{\tilde{Y}}^{\infty} (1 - U_B(\tilde{y}) - \varepsilon A(x)U_B'(\tilde{y}))d\tilde{y}.$$

Re summing the two integrals and changing the order of the terms allows to recognise :

$$\delta_1 = (Re^{-1/2})\{\int_0^{\infty} (1 - U_B(\tilde{y}))d\tilde{y} + \int_0^{\infty} (-\varepsilon A(x)U_B'(\tilde{y}))d\tilde{y} - \varepsilon^2 \int_0^{\tilde{Y}/\varepsilon} u_c dy)\}.$$

or

$$\delta_1 = (Re^{-1/2})\{\int_0^{\infty} (1 - U_B(\tilde{y}))d\tilde{y} - \varepsilon A(x) - O(\varepsilon^2)\}.$$

the $-\varepsilon A$ contribution of the Triple Deck is the perturbation of the displacement thickness $\int_0^{\infty} (1 - U_B(\tilde{y}))d\tilde{y}$. The IBL equations (based on δ_1) even if they seem to be ill posed as they mix different order of magnitude may be justified by the Triple Deck analysis (based on $-A$).

Recently, starting from NS equations, Dechaume Mauss and Cousteix (10) and Cousteix & Mauss (9) showed that we may obtain the IBL system using an other technique than "Matched Asymptotic Expansion". They rather used the so called "Successive Complementary Expansions Method" (MASC in french).

5.4   Reduced Navier Stokes Prandtl, RNSP equations

In this subsection we focus on internal flows (in axi symmetrical pipes or between two plates in 2D). Interestingly enough, we may write the Prandt equations across the pipe itself and obtain a system that we call "Reduced Navier Stokes Prandtl" system (RNSP). This system, just as the Navier Stokes system, degenerates in IBL and in various Double Deck or Triple Deck descriptions. For example, in a pipe we scale the transverse derivative by the radius (R_0) of the pipe itself. In this case the non-dimensional variables are given by :

$x = \tilde{x} R_0 Re$, $r = \tilde{r} R_0$, $u = U_0 \tilde{u}$, $v = \frac{U_0}{Re} \tilde{v}$, $p = p_0 + \rho_0 U_0^2 \tilde{p}$, and $Re = U_0 R_0 / \nu$. p_0 denoting the entry pressure. With these new variables, the following partial differential system is obtained from the Navier-Stokes equations as $Re \to \infty$, the RNSP system

$$\frac{\partial}{\partial \tilde{x}} \tilde{u} + \frac{\partial \tilde{r} \tilde{v}}{\tilde{r} \partial \tilde{r}} = 0, \qquad \tilde{u} \frac{\partial \tilde{u}}{\partial \tilde{x}} + \tilde{v} \frac{\partial \tilde{u}}{\partial \tilde{r}} = -\frac{\partial \tilde{p}}{\partial \tilde{x}} + \frac{\partial}{\tilde{r} \partial \tilde{r}} (\tilde{r} \frac{\partial \tilde{u}}{\partial \tilde{r}}), \qquad 0 = -\frac{\partial \tilde{p}}{\partial \tilde{r}}. \quad (8)$$

The associated boundary conditions are:
- the condition of axial symmetry : $\partial_{\tilde{r}} \tilde{u} = 0$ and $\tilde{v} = 0$ at $\tilde{r} = 0$,
- no-slip condition at the wall : $\tilde{u} = \tilde{v} = 0$ at $\tilde{r} = 1 - f(\tilde{x})$. Of course, in order to be consistent $\tilde{f}$ is of order one, but smaller than one, and the longitudinal scale has to be compatible.
- the entry velocity profiles ($\tilde{u}(0, \tilde{r})$ and $\tilde{v}(0, \tilde{r})$) are given : flat profile or Poiseuille flow, but other profile is also possible,
- there is *no* outflow boundary condition because the system is parabolic. The equations are solved by marching in the stream wise direction, even if there is flow separation.

Rubin & Himansu (39) and Tannehil et al. (50) kept a transversal pressure variation linked with the transverse velocity with $O(Re^{-2})$ terms, but as noted by Fletcher (15), this system contains a mix of orders of magnitude, and is not coherent from an asymptotical point of view. In Lagrée & Lorthois (24) or (33), this system (8) is used to obtain most of the degeneracies of the full NS equations in an axisymmetrical pipe :

• this system allows to compute the entry problem in an unconstricted pipe. This set of equations has been already used for studying entry effects by Cebeci & Cousteix (7) and in Schlichting (42).

• this system, in a case of a constriction (of relative shape $\varepsilon \bar{f}$) situated near the pipe entry, where the velocity profile is flat gives again the Interacting Boundary Layer equations. This RNSP system may be itself splited in an invisicid core and a boundary layer. This inviscid core interacts with boundary layers near the wall. In fact, after rescaling: $r = 1 - \varepsilon \bar{y}$, $u = \bar{u}$, $v = -\varepsilon^{-1} \bar{v}$, $x = \varepsilon^2 \bar{x}$ and $p = \bar{p}$ and assuming a flat entry velocity profile, the RNSP leads to the final IBL formulation as follows:

$$\frac{\partial \bar{u}}{\partial \bar{x}} + \frac{\partial \bar{v}}{\partial \bar{y}} = 0, \, (\bar{u}\frac{\partial \bar{u}}{\partial \bar{x}} + \bar{v}\frac{\partial \bar{u}}{\partial \bar{y}}) = \bar{u}_e \frac{d\bar{u}_e}{d\bar{x}} + \frac{\partial^2 \bar{u}}{\partial \bar{y}^2}, \tag{9}$$

$$\bar{u}_e = \frac{1}{(1 - 2\varepsilon(\bar{\delta}_1 + \bar{f}))} \tag{10}$$

where $\bar{\delta}_1 = \int_0^\infty (1 - \frac{\bar{u}}{\bar{u}_e})d\bar{y}$, where $\bar{f}$ represents the shape of a constriction of the pipe and with the following boundary conditions:
$\bar{u}(\bar{x}, 0) = 0$, $\bar{v}(\bar{x}, 0) = 0$ and $\bar{u}(\bar{x}, \infty) = \bar{u}_e$.

This case leads as well to a special Triple Deck case with $p = A$ identified by Ruban & Timoshin (40).

• this system is used as well in a case of a constriction situated far from the pipe entry, where the flow is fully developed. In this region, the Double Deck theory, also known as Smith's theory of viscous perturbation on a Poiseuille flow in a pipe, is valid ((43)). In this case $A = 0$, and it is shown in (24) that the system (8) contains the Double Deck.

• Finally, it is shown in (24) that if the constriction is short compared to $R_0 Re$, the velocity profile at the entry is not important. In that case, the Interacting Boundary Layer theory proves to be valid again: acceleration is so high that the profile flattens, recreating an inviscid core and a thin boundary layer near the wall.

The same system may be written in 2D, see (23) and (8) and see Barrenechea & Chouly (2) for a finite difference resolution.

5.5   Coupling the Solvers

Boxes   We now have to solve numerically the problem which consists in a coupling between a Boundary Layer and the Ideal Fluid response. As there are two problems coupled, it is natural to define kind of "boxes". A first "box" is the Euler Solver. Given a wall, it computes the pressure and the slip velocity. This box may be a subsonic, supersonic... a linear or not solver. It does not matter, the input is the wall geometry, the output is the

slip velocity.

The second "box" is of course the boundary layer box, given an outer velocity, it computes the displacement thickness. The equations may be laminar or turbulent with any turbulent model. It may be full finite differences resolution or Von Kármán integral method. This box may be used in standard direct way: for a given slip velocities, it computes a displacement thickness. This box may be used in reverse, given a displacement thickness it computes what outer velocity produces it.

Coupling Now, we couple the boxes and present the various possibilities. In fact we will use δ_1 and u in the following figures (we forget all the tildes in this section). We may use $\frac{d\delta_1}{dx}$ instead of δ_1, and instead of u we may use $-p$ (by Bernoulli linearised) or we may use $\frac{dp}{dx}$. There is no real influence of the choice of δ_1 instead of his slope, nor in u, p or his gradient (as we deal with small perturbations).

• Now, having those boxes, we have to branch them. First, the classical boundary layer theory may be represented as a ideal fluid box followed by a boundary layer box, figure 11.

Figure 11. Classical Boundary layer, the geometry gives the velocity which gives the boundary layer.

• But as mentioned previously, branching the output of the boundary layer to the input of the ideal fluid will give the second order effects but will not allow the separation, figure 12.

Figure 12. "Direct method": the geometry gives the velocity which gives the boundary layer, the rebranching will give the second order effects.

• The good way to solve the boundary layer, is to solve it in inverse, we can imagine that we solve the ideal fluid in inverse as well. This is the "inverse

method" figure 13. in fact it is not a good idea as it is difficult to rewrite the Euler codes.

Figure 13. "Inverse method", the total geometry (boundary layer thickness and effective geometry) give the velocity which gives a total geometry, and so on.

• The good way to solve the boundary layer, is to solve it in inverse, the good way to solve the ideal fluid is in the direct way. So we have to relax the input depending on the difference of the outputs. This is the semi-inverse coupling by Le Balleur (figure 14).
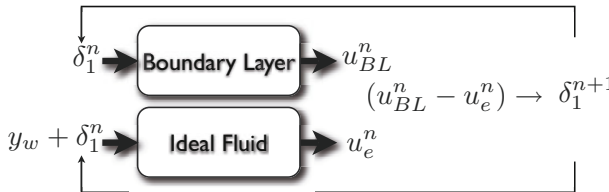
Figure 14. "Semi Inverse method", inverse boundary layer, direct ideal fluid. The difference of the two output velocities is used to update the displacement thickness, and so on.

• There are other possibilities, one is the "quasisimultaneous method" (52). It means that during the coupling values computed downstream are reinjected, which is more useful in the subsonic case.

Semi inverse coupling The point to be clarified is how to update the new δ_1^{n+1} from δ_1^n and the difference $(u_{BL}^n - u_e^n)$, the simplest way is to write:

$$\delta^{n+1} = \delta^n + \lambda(u_{BL}^n - u_e^n)$$

One has to notice that by the Bernoulli relation variation of velocity are opposite of variation of pressure so that we can write as well:

$$\delta^{n+1} = \delta^n - \lambda(p_{BL}^n - p_e^n).$$

The choice of λ is such as we obtain stability for the iterative method.
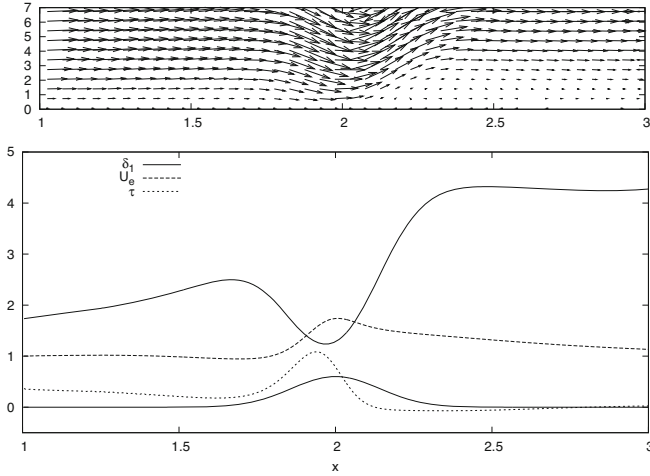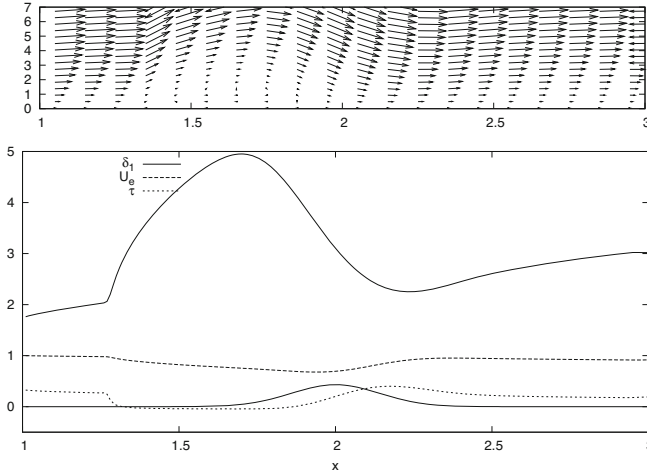
Figure 15. Incompressible flow. Top the velocity field $\tilde{u}, \tilde{v}$ (Prandtl transform), bottom the wall, here a bump, the displacement thickness $\tilde{\delta}_1$ (starting from Blasius value 1.7 in $\bar{x} = 1$), the skin friction (starting from Blasius value 0.3 in $\bar{x} = 1$) and the outer velocity starting from Ideal Fluid value 1 in $\bar{x} = 1$. A positive disturbance of the wall increases the velocity and decreases the displacement. Separation occurs after the bump.

Le Balleur (see (27) and Wigton and Holt (55)) analysis consist to linearize the equation. He defines two operators, one for each box, first B^* defined as $\delta^n = B^* p_{BL}^n$ and for the ideal fluid, he defines in the same vein a linear response $\delta^n = B p_e^n$. Then the update is as:

$$\delta^{n+1} = \delta^n - \lambda(1/B^* - 1/B)\delta^n$$

To make it clear, we use Fourier analysis for all the frequencies between π/L and $\pi/\Delta x$ (the smallest linked to the domain size, and the highest linked to the discretisation step). Furthermore, the B operator may be obtained in subsonic flow we have $B = -1/k$. The analysis is then very simple, defining a "gain" $G = \delta^{n+1}/\delta^n$:

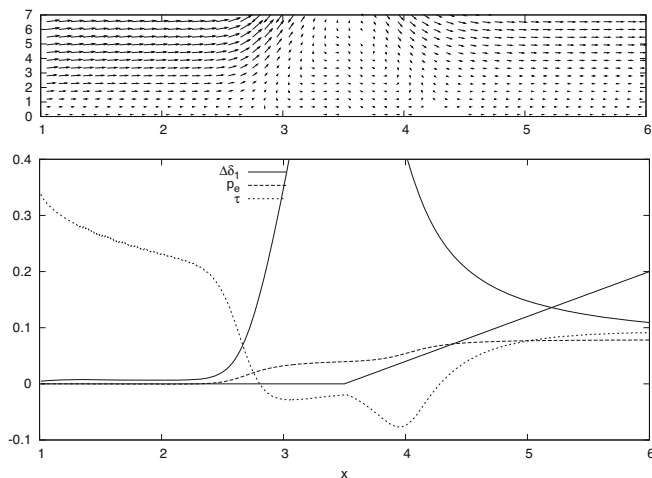$$G = 1 - \lambda(\frac{1}{B^*} + k),$$
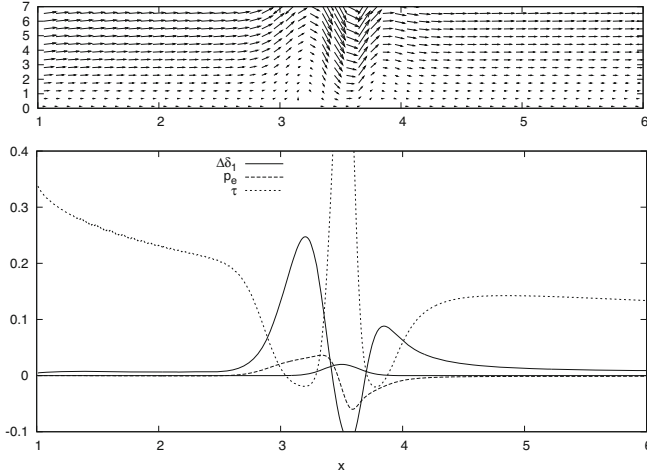
Figure 16. Supersonic flow on a flat plate with a bump. Top, the velocity field $\tilde{u}, \tilde{v}$ (Prandtl transform), bottom the wall, here a bump, the perturbation of displacement thickness from Blasius $\Delta\tilde{\delta}_1$ (starting from 0 in $\bar{x} = 1$), the skin friction (starting from Blasius value 0.3 in $\bar{x} = 1$) and the outer pressure starting from Ideal Fluid value 0 in $\bar{x} = 1$. Note the pressure plateau (here tiny) associated to separation.

we want $|G| < 1$ for $\pi/L < k < \pi/\Delta x$. Often ((27), (55)), it was considered that B^* was real (which is not true), so we can find an optimal λ.

For a supersonic flow we have $B = (ik/(M^2 - 1))^{-1}$. It is easy to show that in this case it is impossible to find an optimal λ. The coupling is always unstable. The good coupling is in fact with the derivative of the pressure:

$$\delta^{n+1} = \delta^n - \mu(\frac{d}{dx}p^n_{BL} - \frac{d}{dx}p^n_e)$$

then again we have:

$$\delta^{n+1} = \delta^n - \mu ik(1/B^* - 1/B)\delta^n$$

which allows to define a "gain" $G = \delta^{n+1}/\delta^n$. We want $|G| < 1$ for all the space frequencies $\pi/L < k < \pi/\Delta x$. We can find an optimal μ.
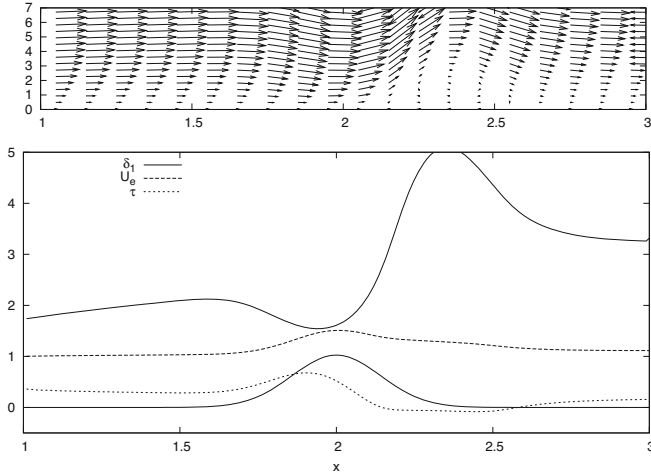
Figure 17. Subcritical flow on a flat plate. Top, the velocity field $\tilde{u}, \tilde{v}$ (Prandtl transform), bottom the wall, here a bump, the displacement thickness $\tilde{\delta}_1$ (starting from Blasius value 1.7 in $\bar{x} = 1$), the skin friction (starting from Blasius value 0.3 in $\bar{x} = 1$) and the outer velocity starting from Ideal Fluid value 1 in $\bar{x} = 1$. A positive disturbance of the wall increases the velocity and decreases the displacement. Separation takes place after the bump. There is no upstream influence.

In the following examples, we use this semi-inverse coupling. In the examples taken from literature (paragraph 6.3) there is a mix between computations in direct way when the flow is attached, and in indirect way when the flow is near separation.

6   Examples

6.1   Some Numerical Examples of IBL

Bump on a Flat Plate in an Incompressible (Subsonic) Flow.   As a first example (fig 15), we present the results for the IBL on a flat plate with a bump defined by $\bar{f}(\bar{x}) = \alpha e^{-25(\bar{x}-2)^2}$; with α increasing by steps of

Figure 18. Supercritical flow on a flat plate. Top, the velocity field $\tilde{u}, \tilde{v}$ (Prandtl transform), bottom the wall, here a bump, the displacement thickness $\tilde{\delta}_1$ (starting from Blasius value 1.7 in $\bar{x} = 1$), the skin friction (starting from Blasius value 0.3 in $\bar{x} = 1$) and the outer velocity starting from Ideal Fluid value 1 in $\bar{x} = 1$. A positive disturbance of the wall decreases the velocity and decreases the displacement. Separation occurs far before the bump, note the long upstream influence and the large increase of $\tilde{\delta}_1$.

0.01 and $Re = 10000$. The velocity is:

$$\bar{u}_e = 1 + \frac{1}{\pi} \int \frac{\bar{f}'(\bar{x}) + Re^{-1/2} \frac{d(\tilde{\delta}_1 \bar{u}_e)}{d\bar{x}}}{x - \xi} d\xi$$

Before the bump there is a small decrease of the $\bar{u}_e$ velocity. In a pure Hilbert case, the response in $\bar{u}_e$ is perfectly symmetrical, but here, due to the boundary layer, the velocity is no more symmetrical. Due to the acceleration on the bump, the displacement thickness first decreases and increases again after the bump. It increases more. So, there is a small overshoot of the thickness associated with the boundary layer separation. This makes the outer velocity non symmetrical. The skin friction increases before the crest, and decreases after. This is consistent with the fact that, for instance, before the crest, the velocity increases, and the boundary layer thickness decreases,

Figure 19. Supersonic flow on a flat plate with a wedge. Top, the velocity field $\tilde{u}, \tilde{v}$ (Prandtl transform), bottom the wall, here a wedge in $\bar{x} = 3.5$, the perturbation of displacement thickness $\Delta\tilde{\delta}_1$ (starting from 0 in $\bar{x} = 1$), the skin friction (starting from Blasius value 0.3 in $\bar{x} = 1$) and the outer pressure starting from Ideal Fluid value 0 in $\bar{x} = 1$. Note the plateau pressure: the pressure is nearly constant in the separated bulb before the wedge, and note the separation occurs far upstream of the wedge.

so the slope of the velocity in the boundary layer increases (it is more or less the ratio of $\bar{u}_e$ and $\tilde{\delta}_1$), the reverse happens after. We notice that the maximum of the skin friction is before the crest, after the inflexion point of the bump, the velocity increases less, but the boundary layer continues to decrease because of the inertia of the fluid, so the maximum of skin friction is between the inflexion point of the bump and the crest. There is eventually a separated bulb with negative skin friction.

Bump on a Flat Plate in a Supersonic Flow.   As a second example (fig 16), we present the results for the IBL on a flat plate with a bump defined by $\bar{f}(\bar{x}) = \alpha e^{-25(\bar{x}-3.5)^2}$; but in the compressible supersonic case,

so that the edge velocity is:

$$\bar{u}_e = 1 - \frac{1}{\sqrt{M^2 - 1}}[\frac{d}{d\bar{x}}\bar{f}(\bar{x}) + Re^{-1/2}\frac{d(\tilde{\delta}_1 \bar{u}_e)}{d\bar{x}}].$$

The bump creates upstream influence and a separated bulb far upstream. The skin friction reincreases and then redecreases to create a second separated bulb.

Bump on a Flat Plate in Subcritical Flow. Nearly the same occurs in the case of the subcritical flow ($F < 1$) or in the case of symmetrical pipe flows. The edge velocity is:

$$\bar{u}_e = 1 + \frac{1}{1 - F}[\bar{f}(\bar{x}) + \tilde{\delta}_1 Re^{-1/2}]$$

It means that the velocity increases and decreases after the crest (see figure 17). The skin friction is extremal just before the crest, and there may be flow separation on the lee side. The behaviour is nearly the same than in the incompressible case but there is no influence of the bump before the beginning of it. In the incompressible case there was some small effect due to the Hilbert integral, but here there is no effect before the bump.

Bump on a Flat Plate in a Supercritical Flow. In the supercritical flow, the equation is the same for the edge velocity, but the story is completely different as $F > 1$. We observe a strong upstream influence on figure 18. The velocity decreases due to the bump, and the skin friction is negative upstream of the bump, the extremum is on the lee side, after the bump. There is a huge jump in $\tilde{\delta}_1$, a kind of hydraulic jump.

Wedge on a Flat Plate in a Supersonic Flow. As final example (fig 19), we present the results for the IBL on a flat plate with a wedge defined by $\bar{f}(\bar{x}) = \alpha(\bar{x} - 3.5)_+$; with α increasing by steps of 0.01 and $Re = 100000$. For enough large α we observe the "plateau" of pressure which is the signature of the self induced interaction and upstream influence. This increase of pressure before the wedge creates a region of reverse flow.

6.2 Example in Internal Flows: Axi- symmetrical Flows, symmetrical and non symmetrical 2D Flows

The system RNSP 8 which is like a Boundary Layer in a whole pipe degenerates in IBL equations like Navier Stokes. Figure 20 from (24), shows
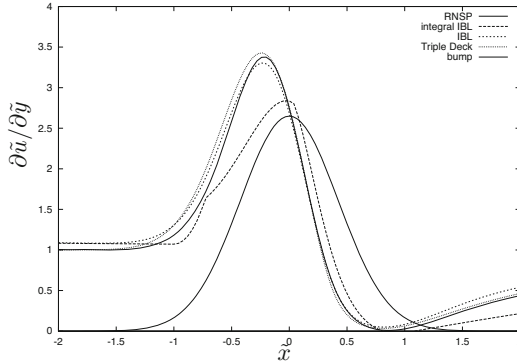
Figure 20. Longitudinal evolution of the wall shear stress near the incipient separation case, in an axis symmetrical flow with a stenosis (a constriction). Reduced Navier Stokes Prandtl model, integral IBL, full IBL resolution (in RNSP variables, the bump is located in $x = 0.02$, and its width is 0.00125), and Triple Deck resolution. All the curves are rescaled in Triple Deck scales.

that the result from system (8) compares to IBL with integral resolution and with full equations and triple Deck (case $p = A$).

The set of RNSP equations in 2D may be solved and compared with Interactive Boundary Layer equations. This has been done for example in (23). On figure 21 is the 2D symmetrical flow between two plates with a constriction. We compare Navier Stokes solved with Castem2000 (5), IBL (Integral resolution) and RNSP (finite differences). Pressures are nearly the same.

If now, we relax the hypothesis of symmetry (see (22)), we compare the solution of the integral IBL and Navier Stokes between two plates, the upper one being flat, and the lower one with a bump (figure 21). In this case two boundary layers, the upper and the lower interact (using twice eq. 4) we just write the difference of pressures between the top and the bottom $p^h - p^b$ which is proportional to:

$$\left(\frac{\left((\delta_1'^h)^2 - (f_b' + \delta_1'^b)^2\right)}{1 - (f_b + \delta_1^b) - (\delta_1^h)} + \frac{\left(\delta_1''^h - f_b'' - \delta_1''^b\right)}{2} \right).$$

We note that this coupling relation produces upstream influence, it means that before the bump, the flow "knows" what is coming. This creates solutions in e^{kx} with $k > 0$ (see figure 22). The pressure on the flat plate
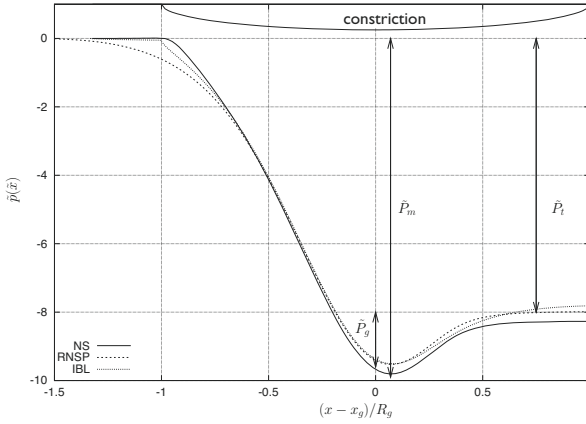
Figure 21. 2D symmetrical flow between two plates with a constriction. A comparison between computed non-dimensional pressure for the three models (NS with Castem 2000 (5), IBL integral and RNSP finite differences, in this last case the wall has been smoothed in $x = \pm 1$ to avoid an infinite slope, this was not the case for NS and IBL), here $\alpha = 0.75$, $Re = 500$. The upper half geometry is plotted as well (the smoothed one is not plotted). It is observed that the ratio: pressure at the glottis divided by maximum pressure drop is nearly constant ($K_e = \tilde{P}_t/\tilde{P}_m \simeq 0.82$). Likewise, the ratio: pressure at the output divided by the pressure drop betwen the output and the glottis is nearly constant ($K_t = \tilde{P}_t/(\tilde{P}_t - \tilde{P}_g) \simeq 0.86$).
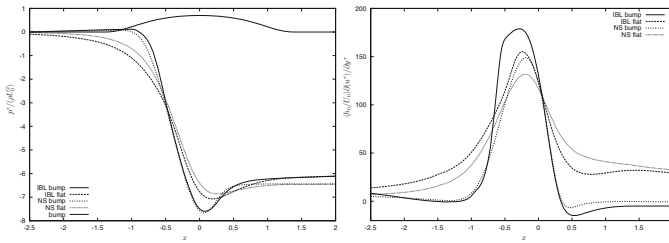
Figure 22. Left Right Comparison of integral IBL and NS (with Castem 2000) pressures. The IBL approach well predicts the over pressure on the flat wall and the positions of the minima of of the pressures after the throat. Skin friction, comparison of integral IBL and NS. The integral IBL over predicts the maximum of skin friction but well predicts the position of the point of separation. The incipient separation before the bump is well predicted.
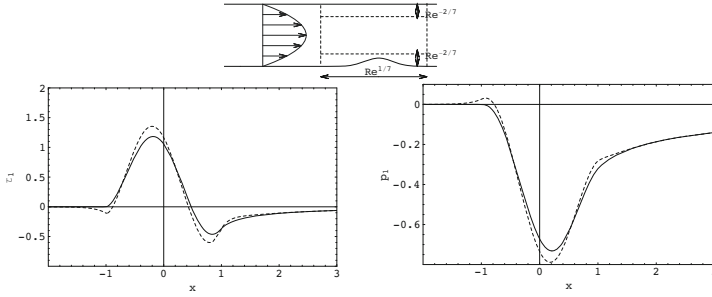
Figure 23. A bump in a Poiseuille flow at the lower will disturb the core flow, the pressure changes across the core flow, perturbations are induced at the upper wall. Linear perturbation of skin friction τ_1 (left) and pressure p_1 (right) over a bump $f_1(x) = cos(\pi x/2)^2$, for $-1 < x < 1$ in the Triple Deck framework. The $A = 0$ is in plain line and the A'' case is in dashed line.

(on the top) decreases before the bump, and pressure on the bumpy wall increases before the bump).

Note that we recover a result that looks like Smith (43) (or Sobey (44)) result in pipe flow, the transversal perturbation of pressure in a perturbed Poiseuille flow is $p_h - p_b = A''/30$ where $-A$ is a displacement of the stream lines as $\delta_1^b - \delta_1^h$ is. Of course the two configurations are very different. On figure 23 we plot the perturbation of a Poiseuille skin friction in the linear case for the $A = 0$ symmetrical case and the non symmetrical A'' case (see Smith (43)). We see the that the case $A = 0$ presents no upstream influence as already mentioned, but we clearly see that the case with A'' promotes upstream response of the flow (before the first position of the bump, the pressure has increased and the skin friction has decreased).

6.3   Some other Numerical Examples

We just reproduce here some examples from literature using this IBL theory. We select among others comparisons of experiments, IBL and Ideal Fluid over an airfoil. On the curves, the experimental and the computation are displayed showing a very good concordance. We present Drela & Giles (12) on figure 24, comparisons from Le Balleur computations of figure 25, and comparisons from Lock & Williams (31) on figure 26. On figure 27, Aftosmis et al. (1) successfully compare IBL strategy with a Navier Stokes solver.
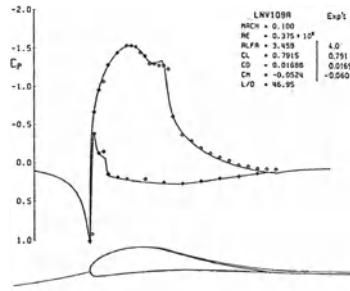
Fig. 9 LNV109A calculated and experimental pressure distribu-
tions.

Figure 24. Example of comparison of IBL computation, Drela & Giles (12)
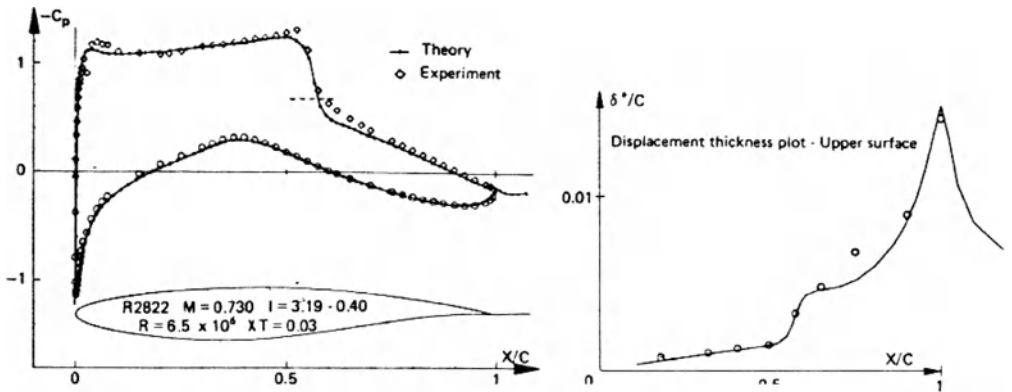
Figure 6. Transonic viscous solver at supercritical conditions (RAE 2822, $M =$
0.730, $\alpha = 2.79°$, $R = 6.5 \times 10^6$, $x_t = 0.03$).

Figure 25. Example of comparison of IBL computation, Le Balleur.
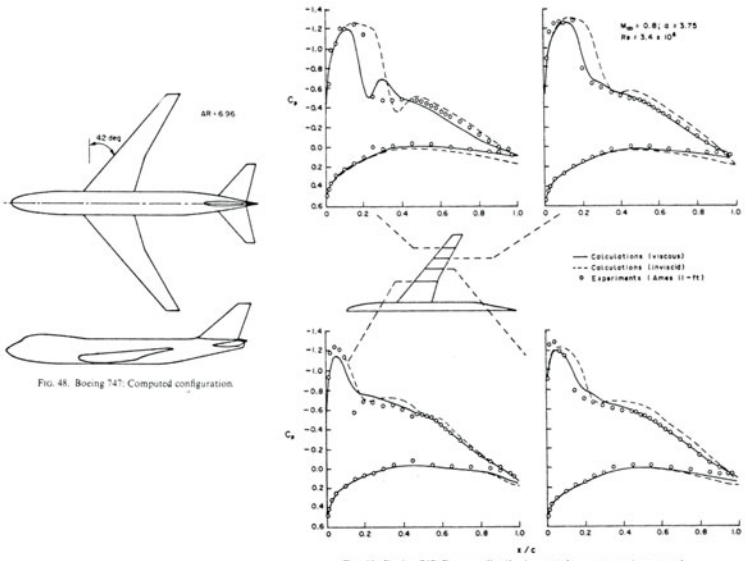
Figure 26. Example of comparison of IBL computation, Lock & Williams (31)
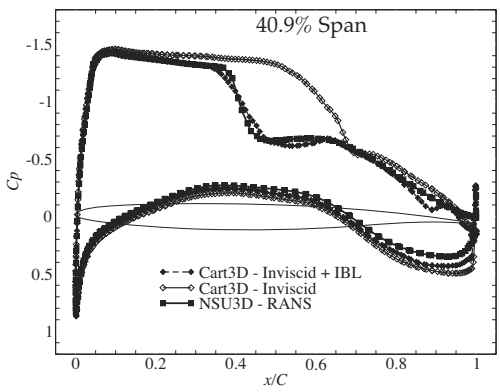
Figure 27. Example of comparison of IBL computation, pressures from (1) (coupled-IBL approach) compared with results from the pure inviscid solver and published data using the NSU3D RANS solver (see (1) for details).

7   Conclusion
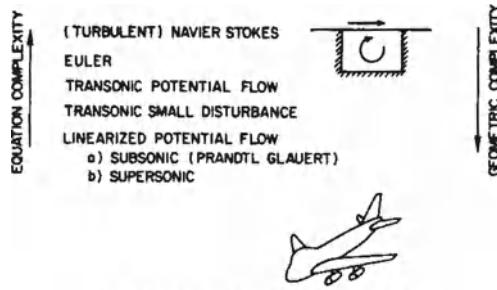
Fig. 2.1   Hierarchy of mathematical models

Figure 28. Complexity and models from Jameson (20)

So we now know that the Boundary Layer equations are more than useful. They can handle flow separation and compute reverse flow bubbles. The strong coupling between the Ideal Fluid and the Boundary Layer allows this. The explanation of this lies in the Triple Deck theory which couples a thin wall layer (the Lower Deck) with the Ideal Fluid (Upper Deck) trough a displacement of the stream lines in the Boundary Layer (the Main Deck).

Further more, the IBL allows as well some upstream influence. It means that in some special régimes such as supersonic, hypersonic, supercritical flows, in non-symmetrical 2D pipe flows, disturbances in the Boundary Layer influence the flow pattern far upstream the position of the disturbance. In axisymmetrical pipe flows, in symmetrical 2D pipe flows, in subcritical flows, there is no upstream influence at all. In the subsonic case, there is only a small influence due to the elliptic character of the flow (seen with the Hilbert integral which is global).

The methodology of IBL, or Inviscid Viscous Interactions, may be summarized in the figure 28 extracted from Jameson (20). Even if this paper was written in 1983, it seems that most of the flying aircraft have been defined since by Viscous Inviscid interactions. The Airbus A380 is one of the first aircraft designed with "full Navier Stokes" (in fact certainly crude RANS models). In the late 90', before the end of the century, a large effort has been done on Navier Stokes solvers. Lot of people are working on this equation. Tremendous progress have been done, and with Navier Stokes, the complexity of the geometry is a problem with lot of solutions. So Navier Stokes solvers are very promising, and give a lot of practical results.

To a certain extent, IBL-IVI methods are less versatile and require spe-

cific methods, they need a kind of *savoir faire* (Aftosmis et al. (1) point some difficulties of the IBL). But when used, they are very good. For example Le Balleur has codes which may compute even large stall on wings, giving results very close to experiments. NS solver have difficulties to reproduce those results. XFOIL free code from Drela allows now everybody to do quick computations of flows over airfoils.

The review of Piomelli & Balaras (36), shows that up to now only very simple models are used for boundary layer near the wall. They suggest a coupling of a Large Eddy Simulation Navier Stokes with a boundary layer code near the wall.

Bibliography

[1] Michael J. Aftosmis Marsha J. Berger, Juan J. Alonso, (2006) "Applications of a Cartesian Mesh Boundary-Layer Approach for Complex Configurations", 44th AIAA Aerospace Sciences Meeting, Reno NV, January 9-12, 2006 AIAA 2006-0652

[2] G.R. Barrenechea, F. Chouly (2009) "A finite element method for the resolution of the Reduced Navier-Stokes/Prandtl equations" ZAMM - Volume 89 Issue 1, Pages 54 - 68

[3] P. Bradshaw, T. Cebecci & J.H. Whitelaw (1981): "Engineering calculation methods for turbulent flow" Academic Press.

[4] J.E. Carter (1979) "A new boundary layer inviscid iteration technique for separated flow". AIAA-79-1450, Jul 1979.

[5] Castem 2000 `http://www-cast3m.cea.fr/cast3m/index.jsp`

[6] D. Catherall and K.W. Mangler (1966) "The integration of the two-dimensional laminar boundary-layer equations past the point of vanishing skin friction. "J. Fluid Mech. 26 (1966) pp.163182.

[7] Cebeci T. & Cousteix J. (2005): "Modeling and computation of boundary layer flows", Springer Verlag 502p.

[8] F. Chouly, A. Van Hirtum, X. Pelorson, Y. Payan, and P.-Y. Lagre (2008): "Numerical and experimental study of expiratory flow in the case of major upper airway obstructions with fluid-structure interaction" Journal of Fluids and Structures 24 (2008) pp. 250 -269

[9] Cousteix J., & Mauss J. (2007): "Asymptotic analysis and boundary layers", Scientific Computations Springer, 432 p.

[10] A. Dechaume, J. Cousteix, J. Mauss, An interactive boundary layer model compared to the triple deck theory, Eur. J. Mech. B Fluids 24 (4)(2005) 439 447

[11] Darrozès J.S. et François C. "Mécanique des fluides incompressibles". Berlin : Springer Verlag, 1982. 461 p. Lecture notes in Physics 163. ISBN 3-540-11578-1

[12] Drela, M. and Giles, M. B. (1987). Viscous-inviscid analysis of transonic and low reynolds number flows. AIAA J., vol 25:13471355.

[13] M. Drela. "XFOIL: An analysis and design system for low Reynolds number airfoils." In T. J. Mueller, editor, Low Reynolds Number Aerodynamics. Springer-Verlag, Jun 1989. Lecture Notes in Engineering, No. 54.

[14] D.E. Edwards and J.E. Carter (1985) "A quasi-simultaneous finite difference approach for strongly interacting flow." In Third Symposium on Numerical and Physical Aspects of Aerodynamic Flows, Long Beach, California, Jan 1985.

[15] Fletcher C.A.J. (1991): "Computational techniques for fluid dynamics, vol II", Springer Verlag.

[16] R W Garvine (1968) " Upstream influence in Viscous Interaction Problems" Phys of Fluids V 11 N 7,pp. 413 1423

[17] Gersten, K. and Hervig, H. (1992): "Strömungsmechanik : Grundlagen der Impuls-Wärme-und Stoffübertragung aus asymptotischer Sicht", Vieweg, Wiesbaden.

[18] S. Goldstein (1948) "On laminar boundary-layer flow near a position of separation". Quarterly J. Mech. and Appl. Math., 1 pp. 4369

[19] Kundu P.K. Cohen I.M. (2008) "Fluid Mechanics Fourth Edition", Academic Press.

[20] A. Jameson, The Evolution of Computational Methods in Aerodynamics. ASME J. Appl . Mech. 50 (1983) 1052-1070.

[21] Keller H.B. (1978): "Numerical methods in Boundary Layer theory", Ann. Rev. Fluid Mech, vol 10, pp. 417-433.

[22] P.-Y. Lagrée, A. Van Hirtum & X. Pelorson (2007): "Asymmetrical effects in a 2D stenosis". European Journal of Mechanics - B/Fluids, Volume 26, Issue 1, January-February 2007, Pages 83-92

[23] Lagrée P.-Y., Berger E., Deverge M., Vilain C. & Hirschberg A. (2005): "Characterization of the pressure drop in a 2D symmetrical pipe: some asymptotical, numerical and experimental comparisons", ZAMM, 5, No. 2, pp. 141-146.

[24] P.-Y. Lagrée & Sylvie Lorthois (2005),"The RNS/Prandtl equations and their link with other asymptotic descriptions: application to the wall shear stress scaling in a constricted pipe", International Journal of Engineering Sciences, Vol 43/3-4 pp 352-378

[25] Landau L. & Lifshitz E. (1997) "Fluid Mechanics" Butterworth-Heinemann, 539 pages

[26] J.C. Le Balleur (1977), Couplage visqueux non-visqueux: Analyse du problme incluant décollements et ondes de choc. La Recherche Aérospatiale. no 6pp. 349-358.

[27] J.C. Le Balleur (1978), Couplage visqueux non-visqueux: Méthode numérique et applications aux écoulements bidimensionnels transsoniques et supersoniques. La recherche Aérospatiale. 1978-2, Eng Trans ESA TT-496 (1978), pp. 6576.

[28] J.C. Le Balleur (1982),"Viscid-Inviscid coupling calculations for txo or three dimensional flows" Von Kármán Institute for Fluid Dynamics LEcture serires 1982-04.

[29] Lees L. & Reeves B.L. "Supersonic Separated and reattaching Laminar Flows", AIAA Journal, Vol 2 11, 1964 pp 1907-1920.

[30] M. J. Lighthill (1953) "On Boundary Layers and Upstream Influence. II. Supersonic Flows without Separation" Proceedings of the Royal Society of London. Series A, Mathematical and Physical Sciences, Vol. 217, No. 1131 (May 21, 1953), pp. 478-507

[31] R. Lock and B. Williams. (1987) "Viscous-inviscid interactions in external aerody- namics. "Prog. Aerospace Science, 24:51171, 1987.

[32] Lorthois S. & Lagrée P.-Y. (2000): "Écoulement dans un convergent axisymétrique: calcul de la contrainte de cisaillement pariétal maximale/ Flow in a axisymmetric convergent: evaluation of maximum wall shear stress", C. R. Acad. Sci. Paris, t328, Série II b, p33-40.

[33] Lorthois S., Lagrée P.-Y., Marc-Vergnes J.-P., & Cassot. F. (2000): "Maximal wall shear stress in arterial stenoses: Application to the internal carotid arteries", Journal of Biomechanical Egineering, Volume 122, Issue 6, pp. 661-666.

[34] A.F. Messiter (1970): Boundarylayer flow near the trailing edge of a flat plate. SIAM J. Appl. Math., 18 :241257,

[35] Neiland V. Ya (1969): "Propagation of perturbation upstream with interaction between a hypersonic flow and a boundary layer", Mekh. Zhid. Gaz., Vol. 4, pp. 53-57.

[36] Piomelli U, Balaras E. (2002) "Wall-layer models for large-eddy simulations." Annual Rev. Fluid Mech. 34:34974

[37] Prandtl L. (1928) "Motion of fluids with little viscosity/ Vier Abhandlungen zur Hydrdynamik und Aerodynamik Göttingen 1927", NACA report 452.

[38] Reyhner, T.A. and & Flügge-Lotz, I., (1968). The interaction of a shock wave with a laminar boundary layer. Int. J. Non-linear Mech. 3, pp. 173199.

[39] Rubin S.G. & Himansu A. (1989): "Convergence properties of high Reynolds number separated flow calculations", Int J. Num Meth Fluids vol 9 1395-1411.

[40] Ruban A.I. & Timoshin S.N. (1986): "Propagation of perturbations in the boundary layer on the walls of a flat channel", MZG 2, pp. 74-79.

[41] H. Schlichting (1987): "Boundary Layer Theory", 7th edition Mac Graw Hill.

[42] H. Schlichting K. Gersten (2000): "Boundary Layer Theory", 8th edition Springer.

[43] Smith F. T. (1976): "Flow through constricted or dilated pipes and channels", part 1 and 2, Q. J. Mech. Appl. Math. vol 29, pp 343- 364 & 365- 376.

[44] I.J. Sobey (2000): "Introduction to interactive boundary layer theory", Oxford applied and engineering mathematics, 256 p.

[45] Stewartson K. (1964) "the Theory of Laminar Boundary Layers in Compressible Fluids", Oxford University Press, London (1964).

[46] Stewartson K. & Williams P.G. (1969): "Self - induced separation",Proc. Roy. Soc. London, A 312, pp 181-206.

[47] Stewartson K. (1974): "Multistructured boundary layer on flat plates and related bodies" Advances Appl. Mech. 14 p145-239.

[48] Van Dyke M. (1962): 'Higher approximations in boundary layer theory", JFM 14, pp 161-177.

[49] Sychev V. V. , Ruban A. I. , Sychev V. V. & Korolev G. L. (1998): "Asymptotic theory of separated flows", Cambridge University Press.

[50] Tannehil J. C., Anderson D. A. & Plettcher R. H. (1997): 'Computational fluid mechanics and heat transfer", Taylor & Francis.

[51] Van Dyke M. (1975): "Perturbation Methods in Fluid Mechanics" Parabolic Press.

[52] A.E.P. Veldman (2001): "Matched asymptotic expansions and the numerical treatment of viscous-inviscid interaction", Journal of Engineering Mathematics, Volume 39, Issue 1, March, pp. 189 - 206

[53] A.E.P. Veldman. The calculation of incompressible boundary layers with strong viscous-inviscid interaction. In Conference on Computation of Viscous-Inviscid In- teractions, 1980. AGARD-CP-291.

[54] Werle, M. J., ; Dwoyer, D. L., ; Hankey W. L., (1973) "Initial conditions for the hypersonic-shock/boundary-layer interaction problem." AIAA Journal 1973 0001-1452 vol.11 no.4 (525-530) doi: 10.2514/3.6780

[55] L.B. Wigton and M. Holt. (1981) "Viscous-inviscid interaction in transonic flow". AIAA-81- 1003, 1981.

Interaction mechanisms in the mixed convection flow past a horizontal plate

Herbert Steinrück[*]

[*] Vienna University of Technology, Institute of Fluid Mechanics and Heat Transfer, Vienna, Austria

Abstract Two different interaction mechanisms arise in the asymptotic analysis of mixed convection flow past a horizontal plate in the limit of large Reynolds and Grashof numbers. A global interaction mechanism between the wake flow and the potential flow and a local triple deck interaction mechanism at the trailing edge. Both interaction mechanisms will be analyzed in the framework of matched asymptotic expansions.

1   Introduction

Two different interaction mechanisms will be investigated by considering the flow past a horizontal heated plate which is aligned under a small angle of attack ϕ to the oncoming parallel flow with velocity $\tilde{U}_\infty$ in a distinguished limit of large Reynolds Re and large Grashof number Gr. The global structure of the flow field is shown in figure 1. According to the method of matched asymptotic expansions in the limit of large Reynolds numbers the flow field can be decomposed into the outer inviscid potential flow, the boundary-layer flow along the plate, the wake behind the plate and several sub-layers near the trailing edge of the plate.

However, the asymptotic approximation in the different layers cannot be determined in a hierarchical order. The following two different interaction mechanism can be identified:

Global interaction: The wake and the potential flow have to be determined simultaneously since the temperature perturbation in the wake causes a pressure difference across the wake which influences the global flow field. On the other hand the potential flow determines the inclination of the wake and thus the velocity and temperature distribution in the wake.

Local interaction: Near the trailing edge of the plate the boundary-layer interacts with the potential flow according to the well known triple-deck mechanism, see Stewartson (1969). Here the influence of buoyancy

forces on the interaction mechanism will be analyzed. In the context of a sudden change of the temperature perturbation local interaction problems of mixed convection flow have been studied by Lagree (1999).
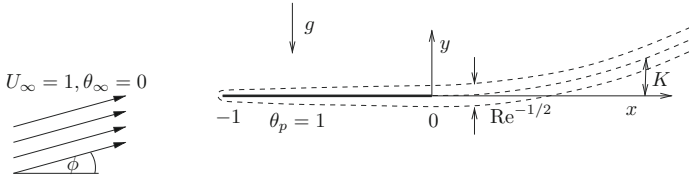
Figure 1. Mixed convection flow past a horizontal plate.

The starting point of the analysis are the Navier Stokes equations for an incompressible fluid using Boussinesq's approximation to take buoyancy forces into account and the energy equation. We introduce a Cartesian coordinate system such that its x-axis is horizontal and its origin is at the trailing edge of the plate. In the following we will use dimensionless variables. All lengths (if not stated otherwise) are scaled with the plate length $\tilde{L}$. Velocities are scaled with the velocity $\tilde{U}_\infty$ of the unperturbed parallel flow. The dimensionless velocity components u, v in x and y direction and the dimensionless temperature perturbation $\theta = (\tilde{T} - \tilde{T}_\infty)/(\tilde{T}_p - \tilde{T}_\infty)$ satisfy the equations of motion, the energy equation and the continuity condition

$$uu_x + vu_y = -p_x + \frac{1}{Re}(u_{xx} + u_{yy}), \tag{1a}$$

$$uv_x + vv_y = -p_y + \frac{1}{Re}(v_{xx} + v_{yy}) + \frac{Gr}{Re^2}\theta, \tag{1b}$$

$$u\theta_x + v\theta_y = \frac{1}{Re\,Pr}(\theta_{xx} + \theta_{yy}), \tag{1c}$$

$$u_x + u_y = 0, \tag{1d}$$

subject to the asymptotic boundary conditions

$$u = 1, \quad v = \phi, \quad \theta = 0 \quad \text{as} \quad x^2 + y^2 \to \infty \tag{2}$$

and the no-slip boundary conditions at the plate

$$u(x,0) = v(x,0) = 0, \quad \theta(x,0) = 1, \quad -1 < x < 0. \tag{3}$$

The dimensionless parameters Reynolds number $Re = \tilde{U}_\infty \tilde{L}/\tilde{\nu}$, Grashof number $Gr = \tilde{g}\tilde{\beta}\Delta\tilde{T}\tilde{L}^3/\tilde{\nu}^2$ and Prandtl number $Pr = \tilde{\nu}/\tilde{a}$ are defined as usual. Here $\tilde{\beta}$, $\tilde{\nu}$ and $\tilde{a}$ denote the isobaric expansion coefficient, the kinematic viscosity and the thermal diffusivity, respectively. Additionally to the above mentioned dimensionless parameters the angle of attack ϕ enters the problem. Although the Reynolds number is assumed to be large, we restrict the analysis to laminar flow conditions. Data for the physical quantities satisfying this assumption can be found in Savić and Steinrück (2007).

In order to define a meaningful interaction parameter we estimate the order of magnitude of the physical quantities involved in the global interaction mechanism. The temperature perturbations are limited to the boundary-layer and the wake, which are both of the thickness $\tilde{L}/\sqrt{Re}$. The temperature perturbation in the wake causes a vertical hydro-static pressure gradient in the wake which is of the order $\tilde{\rho}\tilde{g}\tilde{\beta}\Delta\tilde{T}$. Thus there is a pressure difference of order $\Delta\tilde{p}_h = \tilde{\rho}\tilde{g}\tilde{\beta}\Delta\tilde{T}\tilde{L}/\sqrt{Re}$ across the wake, cf. Schneider (2005). This pressure difference induces a velocity perturbation of the outer potential flow field of the order $\Delta\tilde{p}_h/\tilde{\rho}\tilde{U}_\infty$. This in turn causes a small inclination of the wake of order $K = \Delta\tilde{p}_h/\tilde{\rho}\tilde{U}_\infty^2 = Gr\,Re^{-5/2}$, (see table 1).

From the viewpoint of the outer (potential) flow the wake is located around the streamline starting from the trailing edge of the plate. Due to the (small) inclination of the wake there is a non-vanishing component of the hydro-static pressure gradient in the main flow direction of the wake flow. It is of the order $\tilde{\rho}\tilde{g}\tilde{\beta}\Delta\tilde{T}K$. Referring this pressure gradient in main flow direction to the reference value for a pressure gradient $\tilde{\rho}\tilde{U}_\infty^2/\tilde{L}$ we obtain the interaction parameter

$$\kappa^2 = \frac{\tilde{g}\tilde{\beta}\Delta\tilde{T}\tilde{L}}{\tilde{u}_\infty^2}K = Gr^2 Re^{-9/2}. \tag{4}$$

Thus the velocity profile and the temperature profile in the wake depend on the potential flow, namely on the inclination of the streamline emanating from the trailing edge. As a consequence the wake flow problem and the potential flow problem form an interaction problem and thus both problems have to be solved simultaneously. This problem has been first formulated by Savić and Steinrück (2005) and solved numerically. However, solutions of the potential flow problem exist only if the pressure perturbation across the wake decay downstream. This is the case if the oncoming flow has a positive angle of attack ϕ which is of the order of the induced inclination of the wake. Thus an inclination parameter $\lambda = \phi K\sqrt{Re}$ is introduced. The global interaction problem is formulated in section 2 and and numerical

thickness of the wake	$\tilde{L}\,Re^{-1/2}$
hydro-static pressure gradient in the wake	$\tilde{\rho}\tilde{g}\tilde{\beta}\Delta\tilde{T}$
hydro-static pressuure jump across the wake	$\Delta\tilde{p}_h = \tilde{\rho}\tilde{g}\tilde{\beta}\Delta\tilde{T}\tilde{L}Re^{-1/2}$
velocity perturbation induced by $\Delta\tilde{p}_h$	$\dfrac{\Delta\tilde{p}_h}{\tilde{\rho}\tilde{U}_\infty}$
inclination of the wake centerline induced by $\Delta\tilde{p}_h$	$K = \dfrac{\Delta\tilde{p}_h}{\tilde{\rho}\tilde{U}_\infty^2} = Gr\,Re^{-5/2}$
hydro-static pressure gradient in direction of the wake centerline	$\tilde{\rho}\tilde{g}\tilde{\beta}\Delta\tilde{T}K$
interaction parameter	$\kappa^2 = \dfrac{\tilde{g}\tilde{\beta}\Delta\tilde{T}\tilde{L}}{\tilde{U}_\infty^2}K = Gr^2 Re^{-9/2}$

Table 1. Magnitudes of physical quantities involved in the interaction mechanism

solutions are discussed. Keeping the inclination parameter λ constant it turns out that solutions exist only for interaction parameters κ below a critical value κ_c. At $\kappa = \kappa_c$ a singularity in the wake is observed which will be discussed.

Near the trailing edge of the plate the boundary layer interacts (locally) with the potential flow and sub-layers according to triple deck theory, cf. Stewartson (1969); Messiter (1970). It will be analyzed in section 3. As we will see the inclination parameter λ will play no role in the trailing edge analysis. The local interaction problem will be analyzed and a numerical solution reveals that the interaction pressure is discontinuous at the trailing edge. Thus new sub-layers are introduced to resolve the discontinuity.

2   The global interaction problem

2.1   The potential flow

Using the notation of complex valued functions of a complex variable $z = x + iy$ the potential flow can be written as

$$u - iv = 1 - i\phi\sqrt{\frac{z}{z+1}} + K(u_1 - i\,v_1). \tag{5}$$

The first two terms on the right side of equation (5) describe the potential flow past a horizontal plate of a free stream with an angle ϕ to the horizontal axis. The third term on the right side of (5) takes the buoyancy effects into

account. Along the plate the vertical velocity component v_1 has to vanish.

From the view point of the potential flow the scaled pressure has a jump discontinuity of size γ_w across the wake. Using the linearized Bernoulli equation we have

$$-u_1(x, 0+) + u_1(x, 0-) = \gamma_w(x), \quad x > 0, \tag{6}$$

where γ_w is the dimensionless pressure jump across the wake, see (11). If $\gamma_w(x)$ is given, following Savić and Steinrück (2005), we obtain for the dimensionless inclination of the wake

$$y'_w(x) = \phi \sqrt{\frac{x}{x+1}} + K v_1(x, 0), \tag{7}$$

with

$$v_1(x, 0) = \frac{1}{2\pi} \int_0^\infty \sqrt{\frac{x\,\xi + 1}{\xi\,x + 1}} \frac{\gamma_w(\xi)\ d\xi}{x - \xi}. \tag{8}$$

2.2 The wake flow

In the wake we introduce the vertical coordinate $Y = (y - y_w(x))\sqrt{Re}$ referred to the centerline $y = y_w(x)$ of the wake. Thus the equations for the flow $u \sim U(x, Y)$, $v \sim Re^{-1/2}V(x, Y)$, pressure $p \sim K P(x, Y)$ and temperature field $\theta = \Theta(x, Y)$ are

$$U_x + V_Y = 0, \tag{9a}$$

$$U U_x + V U_Y = Y'_w\Theta + U_{YY}, \quad U_Y(x, 0) = 0, \quad U(x, \infty) = 1, \tag{9b}$$

$$P_Y = \Theta, \tag{9c}$$

$$U\Theta_x + V\Theta_Y = \frac{1}{Pr}\Theta_{YY}, \quad \Theta_Y(x, 0) = 0, \quad \Theta(x, \infty) = 0. \tag{9d}$$

Note that $-p_x = -K(P_x - P_Y y'_w\sqrt{Re})$. Using (9c) and with $Y_w = K\sqrt{Re}\,y_w$ denoting the appropriately scaled centerline of the wake the momentum equation in x-direction (9b) is obtained. If the wake is inclined the hydrostatic pressure gradient has a non-vanishing component in the main flow direction. Thus the fluid in the wake is accelerated in case of positive inclination $Y'_w > 0$ and decelerated in case of negative inclination $Y'_w < 0$.

At the trailing edge, $x = 0$, the velocity and temperature profiles are given by the Blasius velocity profile $U_B(Y)$ and the corresponding temperature profile $\Theta_B(Y)$ for the case of forced convection,

$$U(0, Y) = U_B(Y), \quad \Theta(0, Y) = \Theta_B(Y). \tag{10}$$

The scaled hydro-static pressure difference across the wake is given by

$$\gamma_w(x) = 2 \int_0^\infty \Theta(x, Y) \ dY. \tag{11}$$

From the viewpoint of the potential flow γ_w can be interpreted as a vortex distribution along the wake centerline, see Schneider (2005).

The inclination condition (7) can be rewritten as

$$Y_w'(x) = \lambda \sqrt{\frac{x}{x+1}} + \kappa^2 v_1(x, 0), \tag{12}$$

with $\lambda = \phi K \sqrt{Re}$. From equation (12) it becomes evident when the wake inclination influences the flow and temperature field in the wake. If λ is of order one and $\kappa^2 \ll 1$, the velocity and temperature profile in the wake is affected by the wake inclination. The hydrostatic pressure difference across the wake is also influenced and thus the outer potential flow $u_1 + iV_1$. However, in that case there is no interaction.

Wake-potential flow interaction is only present if κ is of the order one. In the following we assume $\lambda = 1$ fixed and vary the interaction parameter κ.

2.3   Numerical solution

A necessary condition for the existence of the integral in (8), such that v_1 exists, is that $\gamma_w(x)$ decays to zero for $x \to \infty$. Since the total enthalpy flux $\int_0^\infty u\theta \ dy$ in the wake is constant, γ_w can only vanish, if the velocity u in the wake tends to infinity. This is the case when $\lambda > 0$. Then in the far field a similarity solution of the form

$$U \sim \lambda^{2/5} x^{1/5} F'(\eta), \quad \Theta \sim \frac{1}{\lambda^{1/5} x^{3/5}} D(\eta), \quad \eta = \lambda^{1/5} \frac{Y}{x^{2/5}} \tag{13}$$

exists, see Savić and Steinrück (2005), where F and D are the solutions of the similarity equations

$$F''' + \frac{3}{5} F F'' - \frac{1}{5} F'F' + D = 0, \quad \frac{1}{\mathrm{Pr}} D' + \frac{3}{5} FD = 0, \tag{14}$$

with the boundary conditions

$$F(0) = F''(0) = F'(\infty) = 0, \quad \int_0^\infty F'D \ d\eta = \int_0^\infty U_B\Theta_B \ dY. \tag{15}$$

Thus in the far field the velocity and temperature profiles of the wake flow tend to the velocity and temperature profiles of a two-dimensional

laminar plume. Since the flow and temperature profile of the wake flow is symmetric with respect to the centerline, it is sufficient to integrate the enthalpy flux only over one half of the wake.

For the numerical solution of the coupled wake (9), (10), (11), and potential flow equations (8) and the interaction or inclination condition (12) an iterative method is proposed.

i) First a suitable wake centerline $Y_w^{(0)'} = \lambda\sqrt{\frac{x}{x+1}}$ is chosen.

ii) The wake equations are integrated for a velocity $U^{(i)}$ and temperature field $\Theta^{(i)}$ by a marching technique for a prescribed inclination $Y_w^{(i-1)'}$ of the wake.

iii) Then the pressure jump $\gamma_w^{(i)} = 2\int_0^\infty \theta^{(i)} \; dy$ across the wake is determined

iv) Evaluating (8) a new centerline $Y_w^{(i)}$ of the wake is determined and steps ii) -iv) are repeated until convergence is obtained.

We note that for $\kappa = 0$ no iterations are necessary. In the following we keep the inclination parameter $\lambda = 1$ and the Prandtl number $Pr = 0.71$ fixed. The interaction parameter κ will be increased starting from zero.

In figure 2 the velocity at the centerline of the wake and the pressure jump across the wake are shown. For $\kappa = 0$ the shape of the wake is given by the well known 2-d potential flow solution of the flow past an inclined plate Schneider (1978). The centerline velocity increases from $u = 0$ at the trailing edge due to viscosity. Then buoyancy leads to further acceleration and a velocity overshoot forms. Accordingly the vortex distribution $\gamma_w(x)$ (or the pressure jump across the wake) decreases.

Evaluating the integral (8) shows that the induced vertical velocity component v_1 is negative. Thus for κ sufficiently large the wake turns downwards about a plate length behind the trailing edge. After attaining a minimum the wake turns upwards again. Accordingly the graph of centerline velocity first becomes flat. Increasing κ further a minimum forms. When κ attains a critical value $\kappa = \kappa_c$ this minimum becomes zero. Since this solution is singular at the zero of the centerline velocity a further increase of κ is not possible. The physical mechanism which causes the singularity is the following: In the parts of the wake with downward inclination the wake flow is decelerated. The deceleration of the wake causes the wake to broaden there. The increase of the wake thickness causes finally an increase of the hydro-static pressure jump across the wake. In the limiting case $\kappa = \kappa_c$, the wake thickness becomes infinite in wake coordinates and thus γ_w also tends to infinity.

In order to compute solutions with κ close to the critical value κ_c a different strategy has to be employed. First a value $U_{\min}$ for the minimum

of the centerline velocity is prescribed. We chose a suitable vertical velocity perturbation $v_1^{(n)}$ and determine κ such that the minimum of centerline velocity has the prescribed value. This has to be done iteratively. Then a new vorticity distribution is computed and a new vertical velocity $v_1^{(n+1)}$ is determined. The process is repeated until convergence is obtained.

2.4   Analysis of the wake singularity

In order to study the singularity it is convenient to transform the wake equations to the von Mises coordinates and use $W = u^2$ as dependent variable. We define

$$u(x, Y) = \sqrt{W(s, \psi(x, Y))}, \quad \Theta(x, Y) = \tilde{\Theta}(s, \psi(x, Y)) \tag{16}$$

with

$$s = x - x_0, \quad \psi(x, Y) = \int_0^Y u(x, Y') \ dY', \tag{17}$$

where x_0 is the location of the singularity for $\kappa = \kappa_c$ and ψ is the stream function of the wake flow. Thus we obtain

$$W_s = 2Y'_w \tilde{\Theta} + \sqrt{W} W_{\psi\psi}, \quad \tilde{\Theta}_s = \left(\sqrt{W} \tilde{\Theta}_\psi\right)_\psi \tag{18}$$

with the boundary conditions $W_\psi(s, 0) = \tilde{\Theta}_\psi(s, 0) = 0$ and $W(s, \infty) = 1$, $\tilde{\Theta}(s, \infty) = 0$. The pressure jump across the wake is given by

$$\gamma_w = 2 \int_0^\infty \frac{\tilde{\Theta}(s, \psi)}{\sqrt{W(s, \psi)}} \ d\psi. \tag{19}$$

At $s = 0$ for $|\kappa - \kappa_c| \ll 1$ we have $W(0, \psi) \sim \varepsilon + W_0(\psi)$ with $W_0(0) = W_0'(0) = 0$. The parameter ε represents the value of the minimum of W. In the limit $\kappa = \kappa_c$ it vanishes.

We expand W asymptotically for $|s| \ll 1$, $\varepsilon \ll 1$:

$$\begin{aligned} W(s, \psi) &\sim \varepsilon + W_0(\psi) + \hat{Y}_w(s) W_1(\psi) + s W_2(\psi) + \cdots, \\ \tilde{\Theta}(s, \psi) &\sim \tilde{\Theta}_0(\psi) + s \tilde{\Theta}_1(\psi) + \cdots \end{aligned} \tag{20}$$

with $\hat{Y}_w(s) = Y_w(x) - Y_w(x_0)$. The local behavior of the centerline $\hat{Y}_w$ is not known a priorily and thus a corresponding term in the expansion of W is added. Inserting into the differential equation (18) we obtain

$$W_1 = 2\tilde{\Theta}_0, \quad W_2 = \sqrt{W_0} W_0'', \quad \tilde{\Theta}_1 = (\sqrt{W_0} \tilde{\Theta}_0')'. \tag{21}$$
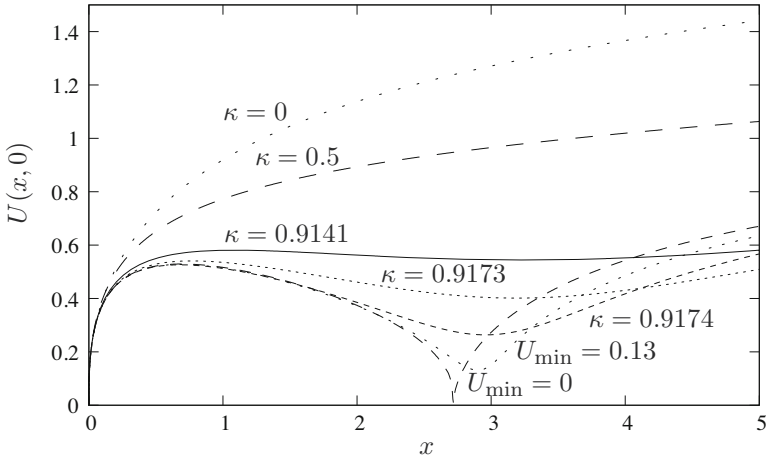
a) Centerline velocity in the wake
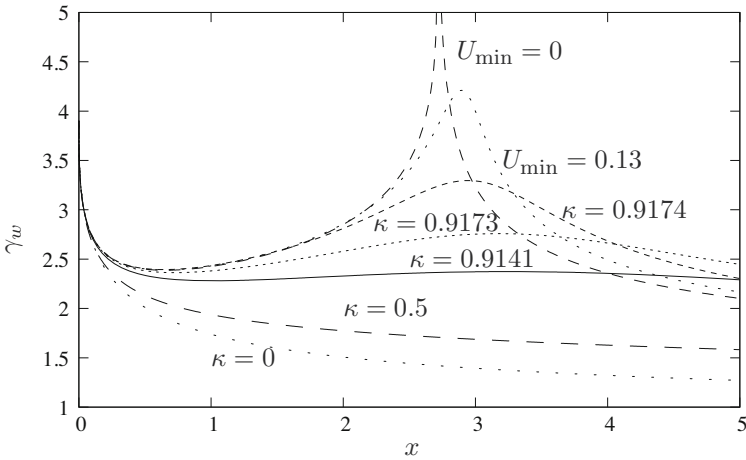
b) Pressure jump across the wake

Figure 2. Numerical solution of the wake problem for $\lambda = 1$, $Pr = 0.71$.

However, W_1, W_2 and $\tilde{\Theta}_1$ do not satisfy the boundary condition at $\psi = 0$. Thus a sub-layer has to be introduced. It turns out that the sub-layer does not influence the leading order equations and thus it will not be discussed here. Note that $W_2(0) = 0$.

Using the local asymptotic expansion we can determine the local be-havior of γ_w. We choose some value $\psi^* > 0$ and approximate $W \sim \varepsilon + W_0''\psi/2 + \hat{Y}_w(s)W_1(0)$ and $\tilde{\Theta} \sim \tilde{\Theta}_0(0)$ for $\psi < \psi^*$ and obtain

$$
\gamma_w(s) = 2\int_0^\infty \frac{\tilde{\Theta}}{\sqrt{W}}\, d\psi \sim 2\int_0^{\psi^*} \frac{\tilde{\Theta}_0(0)}{\sqrt{\varepsilon + W_0''\psi^2/2 + \hat{Y}_w(s)W_1(0)}}\, d\psi \tag{22}
$$

$$
\sim -\frac{\sqrt{2}\tilde{\Theta}_0(0)}{\sqrt{W_0''(0)}} \ln|\varepsilon + \hat{Y}_w(s)W_1|.
$$

It can be shown that the singular part of $\gamma(s)$ is independent of the choice of ψ^*.

Considering that $u_1 - iv_1$ is a potential flow, using the complex valued function theory and $u_1 = -\gamma_w/2$ we conclude

$$
u_1 - i\, v_1 = \frac{\tilde{\Theta}_0(0)}{\sqrt{2W_0''(0)}} \ln F(z, \varepsilon), \tag{23}
$$

where $F(z; \varepsilon)$ is a complex valued function of z with

$$
|F(s)| = |\varepsilon + \hat{Y}_w(s)\, W_1|, \quad -\frac{\tilde{\Theta}_0(0)}{\sqrt{2W_0''(0)}} \arg F(s) = \hat{Y}_w' \quad \text{for } s \text{ real}, \tag{24}
$$

and $\hat{Y}_w(0) = 0$, $\hat{Y}_w'(0) = 0$. This constitutes a problem for finding $F(z, \varepsilon)$ and $\hat{Y}_w(s, \varepsilon)$ simultaneously.

We can express the solution $F(z, \varepsilon) = \varepsilon \tilde{F}(z/\varepsilon)$, $\hat{Y}_w(s, \varepsilon) = \varepsilon \tilde{Y}_w(s/\varepsilon)$ of (24) for arbitrary values of ε by the solution $\tilde{F}$ and $\tilde{Y}_w$ of (24) for $\varepsilon = 1$. In the limiting case $\varepsilon = 0$ we can guess the solution $F(z, 0) = -i\pi\frac{\tilde{\Theta}_0(0)}{2\sqrt{2W_0''(0)}}z$. Thus in that case the centerline of the wake has a corner of size

$$
[Y_w'] = \frac{\tilde{\Theta}_0\pi}{\sqrt{2W_0''(0)}}. \tag{25}
$$

As a consequence the centerline velocity behaves in the limiting case $U_{\min} = 0$ locally like $U \sim \sqrt{|s|}$, see figure 2a and the hydro-static pressure difference γ_w has a logarithmic singularity, see figure 2b. For $\varepsilon > 0$ the corner is smoothed.

3   Local Interaction at the Trailing-Edge

For the analysis of the flow field near the trailing-edge the velocities, pressure and temperature are decomposed into a symmetric and anti-symmetric part

$$\bar{u}(x,y) = \frac{u(x,y) + u(x,-y)}{2}, \quad \Delta u = \frac{u(x,y) - u(x,-y)}{2Re^{-1/4}\kappa}. \tag{26}$$

All other dependent variables, with the exception of the vertical velocity component v, are decomposed accordingly. We decompose the vertical velocity v as

$$\bar{v}(x,y) = \frac{v(x,y) - v(x,-y)}{2}, \quad \Delta v = \frac{v(x,y) + v(x,-y)}{2Re^{-1/4}\kappa}. \tag{27}$$

We rewrite the basic equations for mixed convection flow in terms of the symmetric and anti-symmetric part using the boundary-layer coordinates x, $y = Re^{-1/2}Y$, $u = U(x,Y)$, $v = Re^{-1/2}V(x,Y)$

$$\bar{U}\frac{\partial\bar{U}}{\partial x} + \bar{V}\frac{\partial\bar{U}}{\partial Y} + \frac{\kappa^2}{Re^{1/2}}\left(\Delta U\frac{\partial\Delta U}{\partial x} + \Delta V\frac{\partial\Delta U}{\partial Y}\right) =$$
$$-\frac{\partial\bar{P}}{\partial x} + \frac{\partial^2\bar{U}}{\partial Y^2} + \frac{1}{Re}\frac{\partial^2\bar{U}}{\partial x^2}, \tag{28a}$$

$$\frac{1}{Re}\left(\bar{U}\frac{\partial\bar{V}}{\partial x} + \bar{V}\frac{\partial\bar{V}}{\partial Y}\right) + \frac{\kappa^2}{Re^{3/2}}\left(\Delta U\frac{\partial\Delta V}{\partial x} + \Delta V\frac{\partial\Delta V}{\partial Y}\right) =$$
$$-\frac{\partial\bar{P}}{\partial Y} + \frac{\kappa^2}{Re^{1/2}}\Delta\theta + \frac{1}{Re}\frac{\partial^2\bar{V}}{\partial Y^2} + \frac{1}{Re^2}\frac{\partial^2\bar{V}}{\partial x^2}. \tag{28b}$$

Thus in the equations for the symmetric part the reduced buoyancy parameter κ appears in the terms of order $Re^{-1/2}$. However, these terms do not influence the equations for leading order terms of the triple deck analysis. For the anti-symmetric parts we obtain

$$\bar{U}\frac{\partial\Delta U}{\partial x} + \Delta U\frac{\partial\bar{U}}{\partial x} + \bar{V}\frac{\partial\Delta U}{\partial Y} + \Delta V\frac{\partial\bar{U}}{\partial Y} =$$
$$-\frac{\partial\Delta P}{\partial x} + \frac{\partial^2\Delta U}{\partial Y^2} + \frac{1}{Re}\frac{\partial^2\Delta U}{\partial x^2}, \tag{29a}$$

$$\frac{1}{Re}\left(\bar{U}\frac{\partial \Delta V}{\partial x} + \Delta U\frac{\partial \bar{V}}{\partial x} + \bar{V}\frac{\partial \Delta V}{\partial Y} + \Delta V\frac{\partial \bar{V}}{\partial Y}\right) =$$

$$-\frac{\partial \Delta P}{\partial Y} + \bar{\theta} + \frac{1}{Re}\frac{\partial^2 \bar{V}}{\partial Y^2} + \frac{1}{Re^2}\frac{\partial^2 \Delta V}{\partial x^2}.$$

(29b)

If the symmetric parts of the flow and pressure field are known the equations for the anti-symmetric part are linear and independent of κ.

In the limit of large Reynolds numbers Re the flow structure near the trailing edge can be described by a triple deck problem, cf. Stewartson (1969); Messiter (1970). The scaling of the different layers is sketched in Figure 13 in Ruban (2010). We define the independent variables in the different layers (lower, main and upper deck) as

$$x_* = Re^{3/8}x, \quad y_* = Re^{3/8}y, \quad Y_* = Re^{1/2}y, \quad Y_* = Re^{5/8}y. \tag{30}$$

Here we summarize the leading order terms of the asymptotic expansion of the symmetric part of the velocity and pressure field in the triple deck region:

$$\bar{u}(x,y) = \begin{cases} 1 + Re^{-1/4}\bar{u}_{*,2}(x_*,y_*) + ..., \\ U_B(Y) + Re^{-1/8}\bar{A}(x_*)U_B'(Y) + ..., \\ Re^{-1/8}\bar{U}_{*,1}(x_*,Y_*) + ..., \end{cases} \tag{31a}$$

$$\bar{v}(x,y) = \begin{cases} Re^{-1/4}\bar{v}_{*,2}(x_*,y_*) + ..., \\ -Re^{-1/4}\bar{A}'(x_*)U_B(Y) + ..., \\ Re^{-3/8}\bar{V}_{*,1}(x_*,Y_*) + ..., \end{cases} \tag{31b}$$

$$\bar{p}(x,y) \sim \begin{cases} Re^{-1/4}\bar{p}_{*,2}(x_*,y_*) + ..., \\ Re^{-1/4}\bar{P}_2(x_*) + ..., \\ Re^{-1/4}\bar{P}_{*,2}(x_*) + ... \quad , \end{cases} \tag{31c}$$

with $\bar{p}_{*,2}(x_*,0) = \bar{P}_2(x_*) = \bar{P}_{*,2}(x_*)$ and $U_B(Y)$ is the Blasius velocity profile in the self-similar boundary-layer at the trailing edge. For further use we define the constant $a_0 = U_B'(0) = 0.332$.

According to Stewartson (1969) the function $\bar{A}$ can be interpreted as the correction of the negative displacement thickness. We recall that the asymptotic behavior of the negative displacement thickness $\bar{A}$ is given by

$$\bar{A}(x_*) \sim A_0\,(x_*)^{1/3} \quad \text{as} \quad x_* \to \infty, \tag{32}$$

with the constant A_0 given in table 2. In analogy to the velocity profile of the symmetric part in the main deck the temperature profile of the symmetric

part is given as

$$\theta \sim \Theta_B(Y) + Re^{-1/8}\bar{A}(x_*)\Theta'_B(Y). \tag{33}$$

In the following we will discuss the interaction problem for the anti-symmetric part of the solution.

3.1 Main deck

We start with the main deck then using the upper deck we derive the interaction law and finally derive the lower deck problem. The anti-symmetric part of the pressure in the main deck can be expanded in the form

$$\Delta p = \Delta P_0 + Re^{-1/8}\Delta P_1 + ... \quad . \tag{34}$$

In contrast to (classical) triple deck problems the pressure is not constant across the main deck. The pressure involved in the interaction mechanism is of order $Re^{-1/8}$, i.e. ΔP_1. The y-momentum equation reduces to

$$\frac{\partial \Delta P_0}{\partial Y} = \bar{\Theta}_0, \quad \frac{\partial \Delta P_1}{\partial Y} = \bar{\Theta}_1, \tag{35}$$

with $\bar{\Theta} = \Theta_B$ and $\bar{\Theta}_1 = \bar{A}\Theta'_B$. Using (33) we obtain

$$\Delta P_0(x_*, Y) = \int_\infty^Y \Theta_B(\tilde{Y}) \ d\tilde{Y} + \Delta p_{*,0}(0,0), \tag{36a}$$

$$\Delta P_1(x_*, Y) = \bar{A}(x_*)\Theta_B(Y) + \Delta P_1(x_*, 0). \tag{36b}$$

The expansions for the velocity components Δu and Δv follow the same lines as Stewartson (1969) and the solution of the equations of the leading order terms can be expressed in terms of an yet undetermined function ΔA of x_*, which can be interpreted as the scaled difference of the negative displacement thicknesses on the upper and lower side of the plate. The leading order terms of the anti-symmetric part of the velocity components are given as

$$\Delta u = \ln Re \frac{c_1}{U'_B(0)}U'_B(Y) + \Delta A(x_*)U'_B(Y) + C_1(Y) + ..., \tag{37a}$$

$$\Delta v = -Re^{-1/8}\Delta A'(x_*)U_B(Y) + ... \quad . \tag{37b}$$

The term of the magnitude $\ln Re$ and the term $C_1(Y)$ are both independent of x_* and arise from matching the main deck solution with the solution of the boundary-layer equations, for the anti-symmetric part of the flow field, cf. (58). The constant c_1 will be determined later in (53). In table 2 all constants, their numerical value, and their definitions are summarized.

3.2   The upper deck

Since the flow in the upper deck is a potential flow with the velocity field

$$\Delta u - i\Delta v = \Delta u_0(0,0) + Re^{-1/8}\left(\Delta u_{*,1}(x_*, y_*) - i\Delta v_{*,1}(x_*, y_*)\right) + ..., \quad (38)$$

where $\Delta u_0(0,0) = \frac{1}{\kappa}u_1(0,0+)$, see (5), and $\Delta u_{*,1}(x_*, 0) = -\Delta p_{*,1}(x_*, 0)$, $\Delta v_{*,1}(x_*, 0) = -\Delta \bar{A}'(x_*)$ holds, the pressure $\Delta p_{*,1}(x_*, 0)$ and the negative displacement thickness $\Delta A'(x_*)$ can be interpreted as the real and imaginary part of a complex analytical function $\Delta\Phi_1$ evaluated on the real axis. We have

$$\Delta\Phi_1(x_*, 0) = -\Delta p_{*,1}(x_*, 0) + i\Delta A'(x_*) =$$

$$\tag{39}$$

$$- \left(\Delta P_1(x_*, 0) - \bar{A}(x_*)\right) + i\Delta A'(x_*).$$

Considering $\Delta P_1(x_*, 0) = 0$ for $x_* > 0$ and using the asymptotic behavior of $\bar{A}$ for $x_* \to \infty$ we conclude that

$$\Delta\Phi_1(z) \sim (a + ib)z^{1/3} \quad \text{for} \quad z \to \infty \tag{40}$$

holds. The constants a and b are determined by using that $\Delta A' \to 0$ for $x^{(3)} \to -\infty$. They turn out to be $a = A_0$ and $b = -\sqrt{3}A_0$. Thus the asymptotic behavior of ΔP_1 and $\Delta A'$ is given by

$$\Delta P_1(x_*, 0) \sim -2A_0|x_*|^{1/3} \quad \text{for} \quad x_* \to -\infty, \tag{41}$$

$$\Delta A'(x_*) \sim -\sqrt{3}A_0|x_*|^{1/3}, \quad \text{for} \quad x_* \to \infty. \tag{42}$$

Note that if $\Delta P_{*,1} - \bar{A}(x_*)$ tends to different constants for $x_* \to \infty$ and $x_* \to -\infty$ the real part of the complex function $\Delta\Phi_1 - (a + ib)z^{1/3}$ would tend to different constant values for $x_* \to -\infty$ and $x_* \to \infty$. Thus the next order term in the expansion of Φ_1 for $z \to \infty$ would be of the form $i\ln z$ contradicting the requirement that $\Delta A'$ vanishes for $x_* \to -\infty$. Thus a possible constant in the expansion of ΔP_1 for $x_* \to -\infty$ must be the same constant as in the expansion of $\Delta P_1 - \bar{A}$ for $x_* \to \infty$. But using the fact that $\Delta P_1(x_*) = 0$ for $x_* > 0$ and equation (4.4a) in Stewartson (1969) we conclude that this constant has to vanish thus showing that $\Delta\Phi_1(z) - (a + ib)z^{1/3} \to 0$ as $z \to \infty$.

Finally the interaction law can be written in the form

$$\Delta A'(x_*) + \sqrt{3}A_0 h(x_*) x_*^{1/3} =$$

$$-\frac{1}{\pi} \int_{-\infty}^{0} \frac{\Delta P_1(\xi, 0) + 2A_0 |\xi|^{1/3}}{x_* - \xi} \, d\xi \tag{43}$$

$$+\frac{1}{\pi} \int_{-\infty}^{\infty} \frac{\bar{A}(\xi) - A_0 h(\xi) |\xi|^{1/3}}{x_* - \xi} \, d\xi,$$

where $h(x)$ denotes the Heaviside function with $h(x) = 1$ for $x > 0$ and $h(x) = 0$ for $x < 0$.

We have written the interaction law in a form such that the singular parts are separated and the integrand in the Hilbert integral decays sufficiently fast to zero for $x_* \to \pm\infty$.

The asymptotic behavior of the vertical velocity component v for $x_* \to \infty$ and $Y \to \pm\infty$ is given by

$$v = \pm\bar{v} + \kappa Re^{-1/4} \Delta v \sim$$

$$\sim - \left(\kappa Re^{-3/8} \Delta A' U_B(Y) \pm Re^{-2/8} \bar{A}' U_B(Y) \right) = \tag{44}$$

$$= \kappa Re^{-3/8} \sqrt{3} A_0 \left(x_* \right)^{1/3} U_B(Y) \pm Re^{-2/8} \frac{1}{3} A_0 x_*^{-2/3} U_B(Y).$$

Rewriting (44) in the outer variables we have

$$v(x, y) \sim \kappa Re^{-2/8} \sqrt{3} A_0 x^{1/3} \pm Re^{-4/8} \frac{1}{3} A_0 x^{-2/3}. \tag{45}$$

Applying the matching principle we conclude for the asymptotic behaviour for of v_1 given in (8)

$$v_1(x, 0) \sim \sqrt{3} A_0 x^{1/3} \quad \text{for} \quad x \to 0+. \tag{46}$$

3.3 The lower deck

The equations for the velocity profile in the lower deck are given by the momentum equation in the x-direction,

$$\bar{U}_{*,1} \frac{\partial \Delta U_{*,0}}{\partial x_*} + \Delta U_{0,*} \frac{\partial \bar{U}_{*,1}}{\partial x_*} + \bar{V}_{*,1} \frac{\partial \Delta U_{0,*}}{\partial Y_*} + \Delta V_{0,*} \frac{\partial \bar{U}_{*,1}}{\partial Y_*} =$$

$$-\frac{\partial \Delta P_{*,1}}{\partial x_*} + \frac{\partial^2 \Delta U_{*,0}}{\partial Y_*^2}, \tag{47}$$

the continuity equation, and the momentum equation in the y-direction which reduces to

$$0 = -\frac{\partial \Delta P_{*,1}}{\partial Y} + \bar{\Theta}_B(0).\tag{48}$$

The boundary conditions are

$$\begin{aligned}\Delta U_{*,0}(x_*,0) = \Delta V_{*,0}(x_*,0) = 0, \quad x_* < 0 \quad \text{at the plate,}\\ \Delta U_{*,0}(x_*,0) = \Delta P_{*,1}(x_*,0) = 0, \quad x_* > 0 \quad \text{in the wake.}\end{aligned}\tag{49}$$

We remark that changes of the temperature profile in the lower deck are too small to influence the leading order terms of the hydrostatic pressure distribution and thus a discussion of the energy equation is not necessary.

Integrating (48) we obtain the pressure difference in the lower deck

$$\Delta P_{*,1}(x_*,Y_+) = \theta_B(0)Y_* + \Delta P_{*,1}(x_*,0),\tag{50}$$

which matches with the pressure difference in the main deck (36). Thus $\Delta P_1(x_*,0) = \Delta P_{*,1}(x_*,0)$ and in the interaction law (43) ΔP_1 can be replaced by $\Delta P_{*,1}$.

It remains to specify the asymptotic behavior of the velocity profile for $x_* \to -\infty$ and $Y_* \to \infty$.

Considering the asymptotic behavior of the pressure $\Delta P_{*,1}$ and of $\bar{U}_{*,1} \sim U_B'(0)Y_*$ for $x_* \to -\infty$ we conclude that the asymptotic behavior of the flow field $\Delta U_{*,0}$, $\Delta V_{*,0}$ in the lower deck is self-similar. Using a scaled stream function E defined by

$$\Delta U_{*,0} \sim E'(\eta), \quad \text{with} \quad \eta = \frac{Y_*}{|x_*|^{1/3}},\tag{51}$$

we obtain the similarity equation for E

$$3E''' - U_B'(0)\left(\eta^2 E'' - \eta E' + E\right) = 2A_0,\tag{52}$$

with the boundary conditions $E(0) = E'(0) = 0$.

The corresponding homogeneous equation has three linearly independent solutions $e_1(\eta) \sim \eta \ln \eta$ for $\eta \to \infty$, $e_2(\eta) = \eta$ and $e_3(\eta)$. The third solution e_3 increases at least exponentially for $\eta \to \infty$. In order to match the velocity profile with the solution of the main deck problem e_3 has to be eliminated. Thus we have

$$E(\eta) = -\frac{2A_0}{U_B'(0)} + c_1 e_1(\eta) + c_2 e_2(\eta) \sim -\frac{2A_0}{U_B'(0)} + c_1 \eta \ln \eta + c_2 \eta, \quad \eta \to \infty.\tag{53}$$

Since there are two boundary conditions at $\eta = 0$ the constants c_1 and c_2 are uniquely defined. Their values can be found in table 2. The corresponding velocity profile is shown in figure 4 labeled with $x_* = -\infty$. The asymptotic behavior of the velocity profile for $x_* \to -\infty$, $Y_* \to \infty$ is given by

$$\Delta u_0(x_*, Y_*) \sim E'(\eta) \sim c_1 \ln Y_* - \frac{c_1}{3} \ln |x_*| + c_1 + c_2. \tag{54}$$

To supplement the lower deck equation (47) with the correct asymptotic boundary condition for $Y_* \to \infty$ we need a condition which is satisfied by the derivatives with respect to Y_* of all linear combinations of the two admissible fundamental solutions 1 and $\ln Y_*$ of the linear ordinary differential equation (52). Such a condition is given by

$$Y_* \frac{\partial^2 \Delta U_{*,0}}{\partial Y_*^2} + \frac{\partial \Delta U_{*,0}}{\partial Y_*} \to 0, \quad \text{for} \quad Y_* \to \infty. \tag{55}$$

The negative displacement thickness ΔA is given by

$$\Delta A(x_*) = \lim_{Y_* \to \infty} \left(\Delta U_{*,0} - Y_* \ln Y_* \frac{\partial \Delta U_{*,0}}{\partial Y_*} \right). \tag{56}$$

The Y_* independent part of the asymptotic behavior of $U_{*,0}$ can be interpreted as the asymptotic behavior of the negative displacement thickness ΔA. Thus we have

$$\Delta A(x_*) \sim (c_1 + c_2) - \frac{c_1}{3} \ln |x_*| \quad \text{as} \quad x_* \to -\infty. \tag{57}$$

Expanding the boundary-layer of the anti-symmetric part of the flow field near the trailing-edge $0 < -x_* \ll 1$ the flow field has a viscous sublayer and an inviscid main part. The solution of the viscous sub-layer is again given by the similarity solution E. Matching the sub-layer with the main part introduces a logarithmic term in the inviscid main part. We have:

$$\Delta U = \begin{cases} E' \left(\frac{Y}{|x|^{1/3}} \right) & \text{for} \quad Y \sim |x|^{1/3}, \\ C_1(Y) - \frac{c_1}{3 U_B'(0)} \ln |x_*| U_B'(Y) + ... & \text{for} \quad Y \gg |x|^{1/3}, \end{cases} \tag{58}$$

with the asymptotic behavior of C_1 given by $C_1 Y \sim c_1 \ln Y$ for $Y \to 0$.

Matching the inviscid main part of the boundary-layer (58) yields the anticipated expansion of the main deck (37a).

In figure 3a the negative displacement thickness ΔA and the interaction pressure $\Delta P_{*,1}(x_*, 0)$ of the anti-symmetric part of the flow field are shown.

The asymptotic behavior for $x_* \to -\infty$ of ΔA and $\Delta P_{*,1}$ is shown in figure 3b on a logarithmic and double logarithmic scale, respectively. Velocity profiles are shown in figure 4.
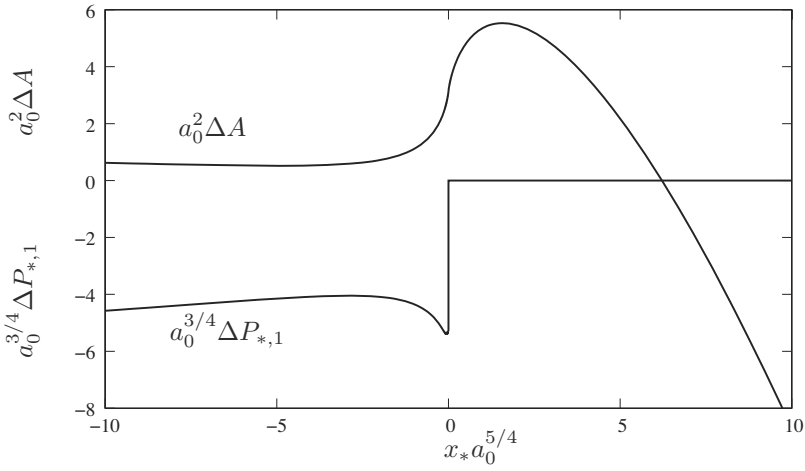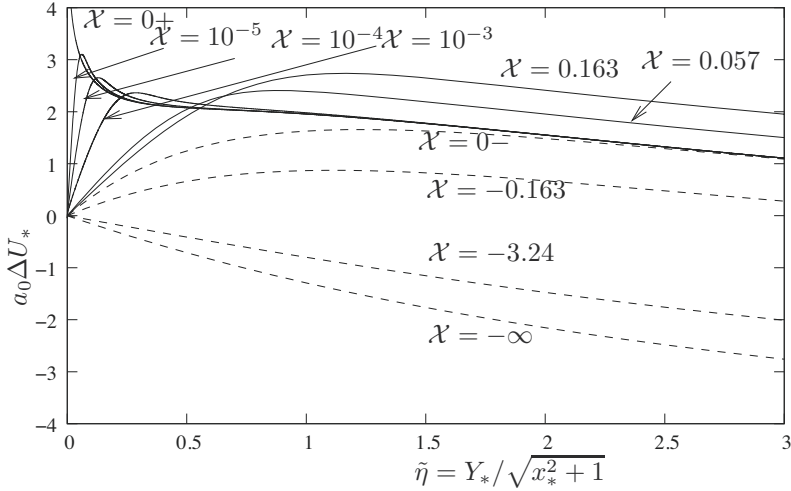
a) Behaviour of ΔA and $\Delta P_{*,1}(x_*, 0)$ near the trailing edge
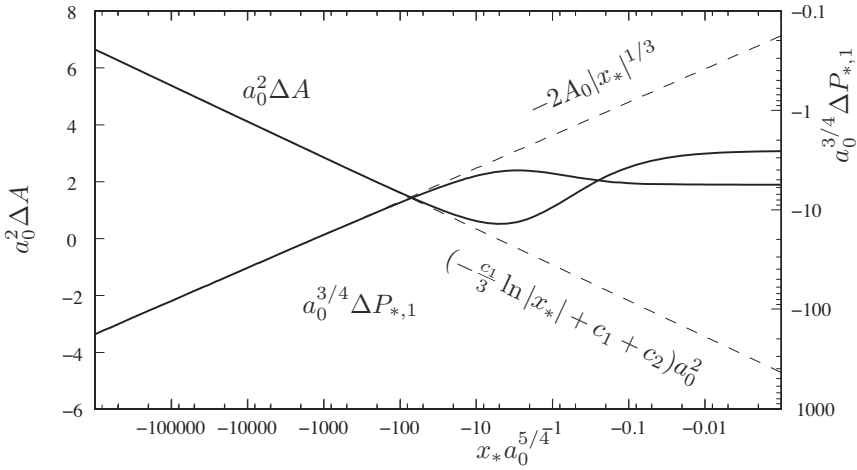
b) Asymptotic behavior of ΔA, and $\Delta P_{*,1}(x_*, 0)$ for $x_* \to -\infty$

Figure 3. Negative displacement thickness ΔA and interaction pressure $\Delta P_{*,1}(x_*, 0)$

Figure 4. Velocity profiles $\Delta U_{*,1}$ at different locations $x_* = a_0^{-5/4} \mathcal{X}$

We remark that $-\Delta A$ can be considered as the inclination of the near wake. Thus at the trailing edge the wake first bends downwards and then turns upwards. For $x_* \to \infty$ we have $-\Delta A' \sim \sqrt{3} A_0 x_*^{1/3}$ which matches with $y'_w = v_1(x,0)$ for $x \to 0$, see eq. (2.11) in Savić and Steinrück (2007).

3.4 The local behavior of the lower deck velocity field near the trailing-edge

It turns out that the interaction pressure $\Delta P_{*,1}$ has a jump discontinuity at the trailing edge $x_* = 0$. As a consequence the derivative of the displacement thickness $\Delta A'$ has a logarithmic singularity at $x_* = 0$. To discuss the behavior of the velocity profile ΔU_* we integrate the momentum equation (47) across the jump discontinuity at x_*. We use the fact that the symmetric part of the flow field $\bar{U}_{*,0}, \bar{V}_{*,0}$ is continuous. Let

$$[\Delta U_*](X_*) = \Delta U_{*,0}(0+, Y_*) - \Delta U_{*,0}(0-, Y_*), \tag{59a}$$

$$[\Delta P_*] = \Delta P_{*,1}(0+) - \Delta P_{*,1}(0-), \tag{59b}$$

$$\hat{V}_*(Y_*) = \lim_{\epsilon \to 0} \int_{-\epsilon}^{\epsilon} \Delta V_{*,0}(x_*, Y_*) \; dx_* \tag{59c}$$

denote the jump in the Δu-component, the jump in the interaction pressure $\Delta P_{*,1}$ and the integral of the ΔV_* component across the jump discontinuity,

respectively. Integrating the momentum equation (47) across the disconti-
nuity at $x_* = 0$ we obtain the ordinary differential equation for $\hat{V}_*$

$$\bar{U}_{*s}\hat{V}'_* - \hat{V}_*\bar{U}'_{*s} = [\Delta P_*], \qquad (60)$$

with the general solution

$$\hat{V}_*(Y_*) = [\Delta P_*] \int_\infty^{Y_*} \frac{\bar{U}_s(Y_*}{(\bar{U}_{*s}(\zeta))^2} \, d\zeta + B\bar{U}_{*s}(Y_*) \qquad (61)$$

where B is a constant and $\bar{U}_{*s}(Y_*) = \bar{U}_{*,1}(0, Y_*)$. The jump in $\Delta U_{*,0}$ is
therefore given by

$$[\Delta U_*](Y_*) = -\hat{V}'_* =$$

$$-[\Delta P_*]\frac{1}{\bar{U}_{*s}(Y_*)} - \left([\Delta P_*]\int_\infty^{Y_*} \frac{d\zeta}{(\bar{U}_{*s}(\zeta))^2} + B\right)\bar{U}'_{*s}(Y_*) \qquad (62)$$

Since the displacement thickness ΔA is continuous we conclude that $[\Delta U_*] \to$
0 as $Y_* \to \infty$ and thus $B = 0$. Considering the behavior of $[\Delta U]$ for $Y_* \to 0$
we obtain

$$[\Delta U] \sim C_{u,log} \ln y^{(5)} + C_{u,0} \qquad (63)$$

with

$$C_{u,log} = [\Delta P_*]\frac{a_2}{a_1^2}, \qquad (64)$$

$$C_{u,0} = [\Delta P_*]\left(\frac{a_2}{a_1^2}\ln a_1 - a_1 \int_\infty^0 \ln U_{*s} \left(\frac{\bar{U}''_{*s}}{(\bar{U}'_{*s})^3}\right)' d\zeta\right), \qquad (65)$$

with $a_1 = \bar{U}'_{*s}(0)$, and $a_2 = \bar{U}''_{*s}(0) = \frac{d\bar{P}_{*2}}{dx_*}(0-)$. Their numerical values can
be found in Sychev et al. (1998) or in Chow and Melnik (1976) and are listed
together with the numerical values of $C_{u,log}$ and $C_{u,0}$ in table 2. In order
to satisfy the boundary condition $\Delta U_{*,0}$ a sub-layer has to be introduced.

3.5   Resolving the pressure discontinuity on main deck scales

In order to resolve the discontinuity of the interaction pressure additional
sub-layers will be introduced.

Due to the discontinuity of the difference pressure $\Delta P_{*,1}$ in the lower deck
at the trailing-edge the pressure difference has a discontinuity in the main
deck as well. In the upper deck the pressure difference $\Delta p_{*,1}$ is singular
at $(0,0)$. Using the calculus of analytic functions of a complex variable

$z_* = x_* + iy_*$ we can infer the behavior of $\Delta p_{*,1}$ close to 0. The velocity field in the upper deck is given locally by

$$\Delta u_{*,1} - i\Delta v_{*,1} \sim \bar{A}(0) - \frac{[\Delta P_*]}{\pi} i \ln z_* =$$

$$\bar{A}(0) + \frac{[\Delta P_*]}{\pi} \left(\arctan \frac{y_*}{x_*} - i \ln \sqrt{x_*^2 + y_*^2} \right).$$

(66)

Thus the pressure and the derivative of the displacement thickness behave locally like

$$\Delta p_{*,1} \sim -\bar{A}(0) - \frac{[\Delta P_*]}{\pi} \arctan \frac{y_*}{x_*}, \quad \Delta A'(x_*) \sim -\frac{[\Delta p]}{\pi} \ln |x_*|. \quad (67)$$

In order to resolve the discontinuity in the main deck we introduce the sub-layer with
$$X = Re^{1/2}x, \quad Y = Re^{1/2}y. \quad (68)$$
The velocity profile has to match with the (x_*, Y)-region (37a),(37b). Thus we use the following expansion of the anti-symmetric part

$$\Delta u \sim \ln Re \frac{c_1}{U_B'(0)} U_B'(Y) + \Delta U_0(0, Y) +$$
$$Re^{-1/8} \ln Re \frac{[\Delta P_*]}{8\pi} X U_B'(Y) + Re^{-1/8} \Delta \tilde{U}_1(X, Y) + \cdots \quad,$$

(69a)

$$\Delta v \sim -Re^{-1/8} \ln Re \frac{[\Delta P_*]}{8\pi} U_B(Y) + Re^{-1/8} \tilde{V}_1(X, Y) + \cdots \quad, \quad (69b)$$

$$\Delta p \sim \Delta P_0(0, Y) + Re^{-1/8} \Delta \tilde{P}_1(X, Y) + \cdots \quad. \quad (69c)$$

The term of order $Re^{-1/8} \ln Re$ in the vertical velocity component Δv arises from matching with the main deck solution and the logarithmic behavior of $\Delta A'$ as $x_* \to 0$. As a consequence a term of the same magnitude must be present in the expansion of the horizontal velocity component Δu. However, in the expansion of the pressure Δp these "logarithmic" terms are missing. The constant c_1 has been introduced in (53).

We obtain the following equations for the leading order terms

$$U_B \frac{\partial \Delta \tilde{U}_1}{\partial X} + \Delta \tilde{V}_1 U_B' = -\frac{\partial \Delta P_1}{\partial X}, \quad (70a)$$

$$U_B \frac{\partial \Delta \tilde{V}_1}{\partial X} = -\frac{\partial \Delta \tilde{P}_1}{\partial Y} + \bar{\Theta}_1, \quad (70b)$$
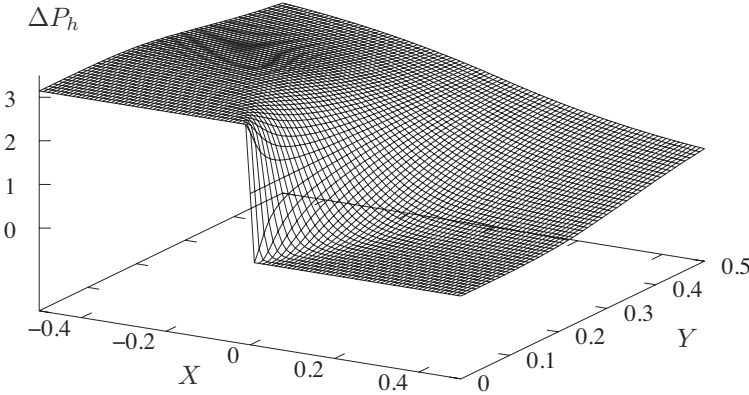
Figure 5. Local behavior of the interaction pressure ΔP_1 near the trailing-edge. The solution ΔP_h of the homogenous problem , cf. (73), is shown

$$\frac{\partial \Delta \tilde{U}_1}{\partial X} + \frac{\partial \Delta \tilde{V}_1}{\partial Y} = 0. \tag{70c}$$

The flow in the (X, Y)-sub-layer is inviscid. But in contrast to the main deck the y-momentum equation is not degenerate. Eliminating $\Delta \tilde{U}_1$ and $\Delta \tilde{V}_1$ an elliptic equation for $\Delta \tilde{P}_1$ can be derived,

$$U_B \left[\frac{\partial^2 \Delta \tilde{P}_1}{\partial X^2} + \frac{\partial^2 \Delta \tilde{P}_1}{\partial Y^2} - \frac{\partial \bar{\Theta}_1}{\partial Y} \right] + 2 U_B' \left[\bar{\Theta}_1 - \frac{\partial \Delta \tilde{P}_1}{\partial Y} \right] = 0. \tag{71}$$

The boundary and matching conditions can be expressed as

$$\Delta \tilde{P}_1 \sim -\frac{|\Delta P_*|}{\pi} \arctan \frac{Y}{X} + \bar{A}(0) \left(\Theta_B(Y) - 1 \right), \tag{72}$$

for $Y = 0$ or $R = \sqrt{X^2 + Y^2} \to \infty$. We note that (72) represents the solution of the Laplace equation. Equation (71) becomes the Laplace equation if U_B' is zero, which is the case for $Y \to \infty$. The matching condition (72) for $R \to \infty$ is obtained from matching $\Delta \tilde{P}_1$ with the upper deck solution (67) and the main deck solution. The boundary condition at $Y = 0$, $Y < 0$ follows from (70a) and $\tilde{V}_1(X, 0) = 0$ for $X < 0$ which in turn is a consequence that ΔA and thus ΔU_0 is continuous at $x_* = 0$.

For the numerical solution we decompose the solution of the linear elliptic partial differential equation (71) into a particular solution and a solution of the homogenous problem:

symbol	numerical value	reference
a_0	0.3321	below (31c)
A_0	$0.8920\,a_0^{-1/3}$	(32)
a_1	$1.343\,a_0$	below (65)
a_2	$-0.301\,a_0^{7/4}$	below (65)
c_1	$-1.644\,a_0^{-1}$	(53)
c_2	$(0.724 - \frac{1.644}{3}\ln a_0)a_0^{-1}$	(53)
$[\Delta P_*]$	$5.27\,a_0^{-3/4}$	(59b)
$C_{\text{u,log}}$	$-0.168[\Delta P_*]\,a_0^{-1/4}$	(64)
$C_{\text{u,0}}$	$(0.042 - 0.168\frac{3}{4}\ln a_0)[\Delta P_*]a_0^{-1/4}$	(65)

Table 2. Constants and their definition

$$\Delta \tilde{P}_1 = -\frac{|\Delta P_*|}{\pi}\Delta P_h(X,Y) + \bar{A}(0)\left(\Theta_B(Y) - 1\right), \tag{73}$$

with $\Delta P_h \sim \arctan Y/X$ for $X^2 + Y^2 \to \infty$ and $\Delta \tilde{P}_h(X,0) = \pi$ for $X < 0$ and $\Delta P_h(X,0) = 0$ for $X > 0$.

The local behavior near the singularity can be discussed by transforming the equation (71) to polar coordinates R, φ. Expanding $\Delta P_h \sim \Delta P_{h,0}(\varphi) + O(R)$ for $R \ll 1$ we obtain

$$\sin\varphi\,\Delta P_{h,0}'' - 2\cos\varphi\Delta P_{h,0} = 0, \quad \Delta P_{h,0}(0) = 0, \quad \Delta P_{h,0}(\pi) = \pi, \tag{74}$$

with the solution

$$\Delta P_{h,0} = \varphi - \frac{1}{2}\sin 2\varphi. \tag{75}$$

A numerical solution for ΔP_h is shown in figure 5. The correct asymptotic behavior for $R \to 0$ and $R \to \infty$ could be verified.

4 Summary and Conclusions

The 2D laminar mixed convection flow past a horizontal plate has been studied. In previous papers (Schneider (2005)) it has been shown that no solution of the outer potential flow problem exists if the oncoming flow is strictly horizontal in an unbounded domain. To circumvent this technical problem two different strategies have been followed. In this paper the oncoming flow was assumed to have a small angle of attack. In Schneider (2005) the horizontal plate has been considered in a horizontal channel.

However in both approaches the wake and the potential flow have to be considered simultaneously. It turns out that if the interaction parameter approaches a critical value a singularity in the wake forms. The nature of this singularity is essentially an inviscid phenomenon. The author believes that also in the case when the plate is placed in a horizontal channel such a singularity can occur, but it has not been investigated up to now.

To resolve the singularity in the flow field at the trailing edge a triple deck problem has been formulated. This problem constitutes a local interaction problem between the a sub-layer of the boundary-layer (lower deck) and the potential flow (upper deck). Here the influence of the hydrostatic pressure on the interaction mechanism has been studied. Surprisingly the interaction pressure at the trailing edge turns out to have a jump discontinuity which can be resolved be introducing additional sub-layers.

Bibliography

R. Chow and E. Melnik. Numerical solutions of triple-deck equations for laminar trailing edge stall. Technical Report RE-526J, Grumman Research Dept, 1976.

P.-Y. Lagree. Thermal mixed convection induced locally by a step change in surface temperature in a Poiseuille flow in the framework of triple deck theory. *Int. J. Heat and Mass Transfer*, 42:2509–2524, 1999.

A. F. Messiter. Boundary layer flow near the trailing edge of flat plate. *SIAM J. Appl. Math*, 18:241–257, 1970.

A. Ruban. Asymptotic theory of separated flows. In H. Steinrück, editor, *Asymptotic Methods in Fluid Mechanics-Recent Advances*, CISM Lecture Notes 523, pages 311–408. Springer, 2010.

Lj. Savić and H. Steinrück. Mixed convection flow past a horizontal plate. *Theor. Appl. Mech.*, 32:1–19, 2005.

Lj. Savić and H. Steinrück. The trailing-edge problem for mixed-convection flow past a horizontal plate. *J. Fluid Mech.*, 588:309–330, 2007.

W. Schneider. Lift, thrust and heat transfer due to mixed convection flow past a horizontal plate. *J. Fluid Mech.*, 529:51–69, 2005.

W. Schneider. *Mathematische Methoden der Strömungslehre*. Vieweg, 1978.

K. Stewartson. On the flow near the trailing edge of a flat plate. *Mathematica*, 16:106–121, 1969.

V. V. Sychev, A. I. Ruban, Vic. V. Sychev, and G. L. Korolev. *Asymptotic theory of separated flows*. Cambridge University Press, 1998.

Asymptotic Theory of Separated Flows

Anatoly I. Ruban

Department of Mathematics, Imperial College London

1 Introduction

Separation is a fluid dynamic phenomenon that influences the behaviour of a wide variety of liquid and gas flows. The difference between an attached flow and its separated counterpart is demonstrated in Figure 1 where the theoretical streamline pattern, given by the classical solution of the inviscid flow theory[1]

$$\varphi + i\psi = V_\infty \left(z + \frac{a^2}{z} \right), \tag{1}$$

is compared with a real flow visualisation for a circular cylinder in a water
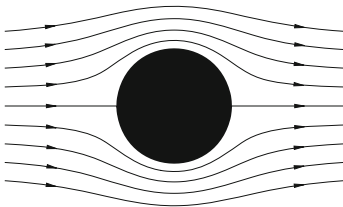
(a) Streamline pattern given by (1)
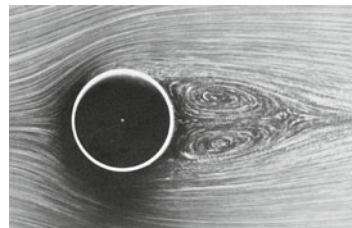
(b) Visualisation of the cylinder flow by Taneda (1956); $Re = 26$

Figure 1. Comparison of the theoretical attached and real separated flows past a circular cylinder.

tank (Taneda, 1956). In the theoretically predicted form of the flow the fluid particles follow closely the cylinder contour from the front stagnation point all the way to the rear stagnation point. Contrary to that in the experimentally observed flow the fluid particles brake away from the cylinder

---

[1]See, for example, Lamb (1932).

surface at a separation point and form a pair of eddies in the wake behind the cylinder.

The irony of the situation is that the theoretical flow in Figure 1(a) has been constructed based on the Euler equations. These are intended for describing the motion of fluids with extremely small viscosity. While the Euler equations admit solutions in the form of attached flows, such flows can not be observed in practice except for some special cases. In fact, experiments clearly indicate that the attached form of fluid motion past rigid bodies is characteristic for relatively small values of the Reynolds number. In particular, the flow past a circular cylinder assumes an attached form only if the Reynolds number $Re = V_\infty a/\nu$, with a being the cylinder radius, is smaller than a critical value of about six. The actual flow shown in Figure 1(b) corresponds to $Re = 26$, and we see that the separation eddies are already well developed. Further increase of the Reynolds number results in an extention of the eddies, and then the flow looses its symmetry and becomes unstable, but it never returns to an attached form (see Figure 2).
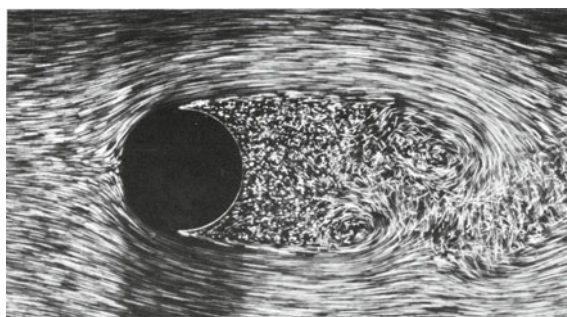
Figure 2. Visualisation of the cylinder flow by Werlé & Gallon (1972); the Reynolds number $Re = 2000$.

Since many "common" gases and liquids, such as air and water, have extremely small viscosity, their flows are characterised by very large values of the Reynolds number. This explains why most liquid and gas flows observed in nature and encountered in engineering applications involve separation. The difference between a separated flow and its theoretical unseparated counterpart (constructed on the basis of inviscid flow analysis) concerns not only the form of trajectories of fluid particles, but also the magnitudes of aerodynamic forces acting on the body. For example, for bluff bodies in an incompressible flow, it is known from experimental observations that the drag force is never zero; furthermore, it does not approach zero as the

Reynolds number becomes large. On the other hand, one of the most famous results of the inviscid flow theory is d'Alembert's paradox which states that a rigid body does not experience any drag in incompressible steady flow. This contradiction is associated with the assumption of an attached form of the flow.

Separation imposes a considerable limitation on the operating characteristics of aircraft wings, helicopter and turbine blades leading to a significant degradation of their performance. It is well known that the separation is normally accompanied by a loss of the lift force, sharp increase of the drag, increase of the heat transfer at the reattachment point, development of flow oscillations, etc.

It is hardly surprising that the problem of flow separation has attracted considerable interest amongst researchers. The first theoretical model of a separated flow was due to Helmholtz (1868) and Kirchhoff (1869) in the framework of the classical theory of inviscid fluid flows. This model was originally applied to the flow past a flat plate perpendicular to the free stream when the separation is known to take place at the plate edges. The Kirchhoff model may be, of course, applied to other body shapes. In particular, Levi-Civita (1907) used this model for the flow past a circular cylinder (see Figure 3). A major conclusion that may be drawn from this theory is that Euler equations allow for a family of solutions where the position of separation point S remains a free parameter.
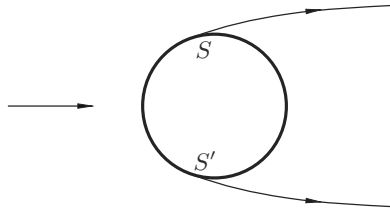
Figure 3. Separated flow past a circular cylinder (Levi-Civita, 1907).

The described non-uniqueness of the solution of the Euler equations poses a theoretician a dilemma, how to find the location of the separation point. Prandtl (1904) was the first to recognise that the resolution to this problem lies with a specific behaviour of the boundary layer. According to Prandtl's theory at large values of the Reynolds number the main part of the flow field may be treated as inviscid. However, for any Reynolds number, no matter how large, there always exists a thin boundary layer developing along the wall where the flow is viscous in nature. The behaviour of the boundary layer depends on the pressure distribution along the wall. If the

pressure gradient is favourable, i.e. the pressure decreases downstream, then the boundary layer remains well attached to the wall. However with adverse pressure gradient, when the pressure starts to rise in the direction of the flow, the boundary layer tends to separate from the body surface. The reason for separation may be explained as follows. Since the velocity in the boundary layer drops towards the wall, the kinetic energy of fluid particles inside the boundary layer appears to be less than that at the outer edge of the boundary layer, in fact the closer a fluid particle is to the wall the smaller appears to be its kinetic energy. This means that while the pressure rise in the outer flow may be quite significant, the fluid particles inside the boundary layer may not be able to get over it. Even a small increase of pressure may cause the fluid particles near the wall to stop and then turn back to form a reverse flow region characteristic of separated flows.

The separation point may be identified as a point of zero skin friction

$$\tau_w = \mu \frac{\partial u}{\partial y}\bigg|_{y=0} = 0. \tag{2}$$

Indeed with τ_w being positive upstream of this point, all the fluid particles in the boundary layer move downstream along the wall (see Figure 4) and the flow appears to be attached to the body surface. However, as soon as the skin friction τ_w turns negative a layer of reversed flow ($u < 0$) emerges near the wall, giving rise to a region of recirculation which, obviously, originates from point S where condition (2) holds.
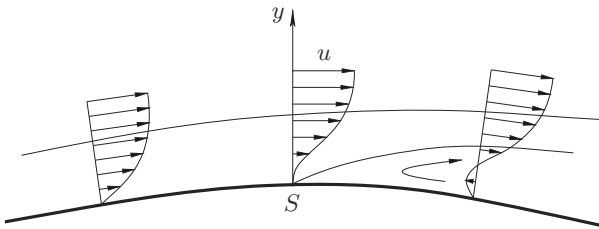
Figure 4. Boundary-layer separation.

It might seem surprising that the clear understanding of the physical processes leading to the separation, could not be converted into a rational mathematical theory for more than half a century. The fact is that the classical boundary-layer theory, which was intended by Prandtl for predicting flow separation, was based on the hierarchical approach when the outer inviscid flow should be calculated first ignoring the existence of the boundary layer, and only after that one can turn to the boundary layer analysis. In

the forties it became obvious that such a strategy leads to a mathematical contradiction associated with the so called Goldstein's singularity. The form of the singularity was first described by Landau & Lifshitz (1944). They demonstrated that the skin friction produced by the boundary layer on the body surface decreases as the separation is approached proportional to the square root $\tau_w \sim \sqrt{s}$ of the distance s from the separation point. Simultaneously the velocity component normal to the body experience unbounded growth being inversely proportional to $\sqrt{s}$. This result was believed to explain why the separation changes the flow field so drastically. If the solution of the boundary-layer equations could be continued smoothly through the separation point then the reversed flow region would be confined within the boundary layer, and its effect on the flow behaviour would be barely noticeable.

Later Goldstein (1948) presented a more rigorous mathematical analysis of the boundary-layer equations in a small vicinity of the zero skin friction point. He not only confirmed the structure of the singularity predicted by Landau & Lifshitz (1944), but also demonstrated (and this result appeared to be of paramount importance for further development of the boundary-layer separation theory) hat the singularity at the separation precludes the solution to be continued beyond the point of zero skin friction, which suggested that the entire approach to the separation problem had to be reexamined.

The Goldstein's theoretical discovery came at the time when an important development was taking place in experimental investigation of separated flows. Most disputable was the effect of upstream influence through the boundary layer in a supersonic flow prior to separation. It might be observed in a number of physical situations, for example, when a shock wave impinges the boundary layer on a rigid body surface. The effect was extensively studied by many experimentalists during the forties and fifties[2], and it may be described using the following simple flow layout.

Let a flat plate be placed in a supersonic flow parallel to the free-stream velocity V_∞ as shown in Figure 5. Let further an oblique shock wave be produced in the flow by an obstacle, say, a wedge, situated above the plate. This shock impinges upon the boundary layer on the plate surface at point A, and the focus of attention of the above mentioned studies was on the behaviour of perturbations induced in the flow through the interaction between the shock wave and boundary layer.

---

[2] A review of these efforts may be found, for example, in Chapman *et al.* (1956). Early theoretical models to explain the phenomenon are reviewed in a resent paper by Lighthill (2000).
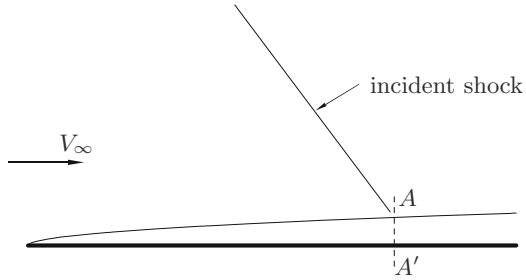
**Figure 5.** Shock wave impinging upon the boundary layer.

If we attempt to describe the flow behaviour based on the classical Prandtl's hierarchical strategy then we have to start with the external invis-cid flow. To the leading order we ignore the existence of the boundary layer and recall that at a supersonic speed the governing Euler equations are hy-perbolic; they do not allow for perturbations to propagate upstream. This suggests that the inviscid flow should remain uniform everywhere in front of the incident shock (see Figure 5). Now turning to the boundary layer on the plate surface we note that with given (constant) pressure, Prandtl's equations governing the flow in the boundary layer are parabolic, and there-fore the boundary layer also is incapable of conducting any perturbations upstream of the cross-section AA'.
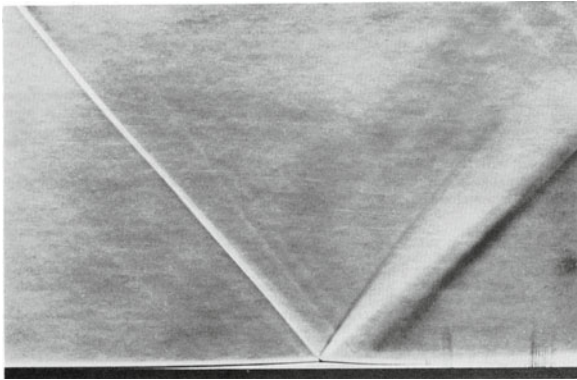
Figure 6. Oblique shock wave interacting boundary layer. Visualisation by Liepmann, Roshko and Dhawan (1952).

These theoretical arguments proved to fail completely in predicting the

real behaviour of the flow. The experiments invariably showed (see, for example, Figure 6) that, unless the incident shock was very weak, the flow separated from the plate surface some distance upstream of the incident shock (see Figure 7). It was also established that the boundary layer was perturbed even upstream of the separation point S, and the distance over which the pressure perturbations were able to propagate upstream of point S through the boundary layer proved to be significantly larger then the boundary-layer thickness. An increase of the pressure in the boundary layer prior to separation and, even more so, the separation of the boundary layer cause the streamlines at the bottom of the inviscid flow region to deviate from the wall giving rise to a secondary shock as shown in Figure 7. Together with the primary shock they form a characteristic shock structure called the λ-structure.
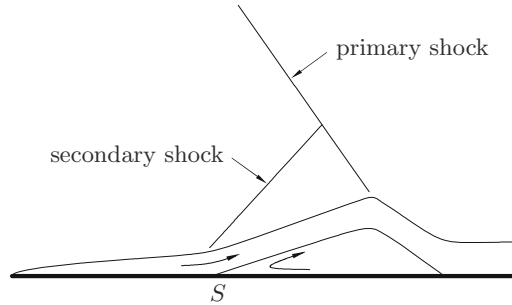

Figure 7. Schematic representation of the separation provoked by impinging shock, and formation of the shock λ-structure.

In order to find an explanation to this unexpected behaviour, the experimental data were carefully examined, and, in particular, it was noticed that the boundary-layer separation process had a universal character being solely determined by the state of the boundary layer immediately prior to the separation. This conclusion was supported by an observation that in a vicinity of the separation point S the flow remained unchanged when instead of the impinging shock the separation was caused, for example, by the forward facing step (see Figure 8) or other obstacle.

It was first suggested by Oswatitsch & Wieghardt (1948) that the observed upstream influence through the boundary layer may be explained by an interaction between the boundary layer and external inviscid part of the flow. The impinging shock (Figure 7) or forward facing step (Figure 8) serve to trigger the interaction, but once started the process proceeds very much independently obeying its own rules. For this reason the interaction of the

boundary layer with supersonic inviscid flow was termed by Chapman *et al.* (1956) the *free-interaction*.
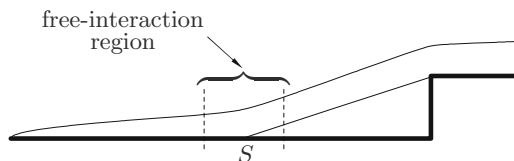
Figure 8. Separation upstream of a forward-facing step.

The phenomenon of free-interaction may be described vaguely in the following way. Let us suppose that for some reason the pressure at the outer edge of the boundary layer starts to rise in the downstream direction. Since the pressure perturbations can freely penetrate into the boundary layer, this would lead to a deceleration of the fluid particles inside the boundary layer and, as a consequence, to a displacement of the streamlines from the wall. The response of the external supersonic flow to the displacement effect of the boundary layer is such that it further increases the pressure, and the chain of events repeats again. We shall see that this process, once initiated, is able of maintaining a monotonic growth of the pressure leading ultimately to the separation of the boundary layer. Asymptotic theory of this phenomenon, which for obvious reasons is called the *self-induced separation*, was developed independently by Neiland (1969) and Stewartson & Williams (1969). We shall now turn to the mathematical description of the theory.

2   Self-Induced Separation

2.1   Formulation of the Problem

The theory that will be discussed here applies to boundary-layer separation in a wide variety of supersonic flow. However, for the purpose of describing the theory it is convenient to choose a particular flow layout, for example, the flow past a flat plate surface; see Figure 9. We shall assume that the plate is aligned with oncoming flow which is supersonic. We shall further assume that the boundary layer on the plate surface separates due to some downstream disturbance. The position of the separation point S depends on the nature of this perturbations, and in this study will be treated as known.

In what follows we shall assume that the gas considered may be treated as perfect. Its motion will be assumed steady and two-dimensional, in which
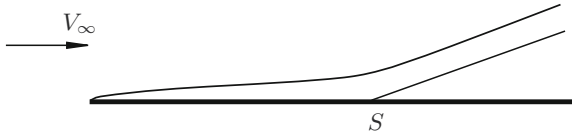
Figure 9. The flow layout.

case the governing Navier-Stokes equations may be written as

$$\hat{\rho}\left(\hat{u}\frac{\partial\hat{u}}{\partial\hat{x}} + \hat{v}\frac{\partial\hat{u}}{\partial\hat{y}}\right) = -\frac{\partial\hat{p}}{\partial\hat{x}} + \frac{\partial}{\partial\hat{x}}\left[\hat{\mu}\left(\frac{4}{3}\frac{\partial\hat{u}}{\partial\hat{x}} - \frac{2}{3}\frac{\partial\hat{v}}{\partial\hat{y}}\right)\right] + \frac{\partial}{\partial\hat{y}}\left[\hat{\mu}\left(\frac{\partial\hat{u}}{\partial\hat{y}} + \frac{\partial\hat{v}}{\partial\hat{x}}\right)\right],$$

$$\hat{\rho}\left(\hat{u}\frac{\partial\hat{v}}{\partial\hat{x}} + \hat{v}\frac{\partial\hat{v}}{\partial\hat{y}}\right) = -\frac{\partial\hat{p}}{\partial\hat{y}} + \frac{\partial}{\partial\hat{y}}\left[\hat{\mu}\left(\frac{4}{3}\frac{\partial\hat{v}}{\partial\hat{y}} - \frac{2}{3}\frac{\partial\hat{u}}{\partial\hat{x}}\right)\right] + \frac{\partial}{\partial\hat{x}}\left[\hat{\mu}\left(\frac{\partial\hat{u}}{\partial\hat{y}} + \frac{\partial\hat{v}}{\partial\hat{x}}\right)\right],$$

$$\hat{\rho}\left(\hat{u}\frac{\partial\hat{h}}{\partial\hat{x}} + \hat{v}\frac{\partial\hat{h}}{\partial\hat{y}}\right) = \hat{u}\frac{\partial\hat{p}}{\partial\hat{x}} + \hat{v}\frac{\partial\hat{p}}{\partial\hat{y}} + \frac{1}{Pr}\left[\frac{\partial}{\partial\hat{x}}\left(\hat{\mu}\frac{\partial\hat{h}}{\partial\hat{x}}\right) + \frac{\partial}{\partial\hat{y}}\left(\hat{\mu}\frac{\partial\hat{h}}{\partial\hat{y}}\right)\right] +$$

$$+ \hat{\mu}\left(\frac{4}{3}\frac{\partial\hat{u}}{\partial\hat{x}} - \frac{2}{3}\frac{\partial\hat{v}}{\partial\hat{y}}\right)\frac{\partial\hat{u}}{\partial\hat{x}} + \hat{\mu}\left(\frac{4}{3}\frac{\partial\hat{v}}{\partial\hat{y}} - \frac{2}{3}\frac{\partial\hat{u}}{\partial\hat{x}}\right)\frac{\partial\hat{v}}{\partial\hat{y}} + \hat{\mu}\left(\frac{\partial\hat{u}}{\partial\hat{y}} + \frac{\partial\hat{v}}{\partial\hat{x}}\right)^2,$$

$$\frac{\partial\hat{\rho}\hat{u}}{\partial\hat{x}} + \frac{\partial\hat{\rho}\hat{v}}{\partial\hat{y}} = 0,$$

$$\hat{h} = \frac{\gamma}{\gamma - 1}\frac{\hat{p}}{\hat{\rho}}$$

We denote the distance from the leading edge to the separation point S by L; the velocity, density, viscosity and pressure in the unperturbed flow upstream of the plate are denoted by V_∞, ρ_∞, μ_∞ and p_∞ respectively. To study the flow we shall use Cartesian coordinate system $\hat{x}O\hat{y}$ with $\hat{x}$ measured parallel to the plate from its leading edge, and $\hat{y}$ in the perpendicular direction. The velocity components in these coordinates are denoted by $\hat{u}$ and $\hat{v}$. Other quantities used in the Navier-Stokes equations are the gas density $\hat{\rho}$, pressure $\hat{p}$, enthalpy $\hat{h}$ and viscosity $\hat{\mu}$. As before, the "hat" denotes dimensional variables. The non-dimensional variables are introduced as

$$\hat{u} = V_\infty u, \qquad \hat{v} = V_\infty v, \qquad \hat{\rho} = \rho_\infty \rho,$$
$$\hat{p} = p_\infty + \rho_\infty V_\infty^2 p, \qquad \hat{h} = V_\infty^2 h, \qquad \hat{\mu} = \mu_\infty \mu,$$
$$\hat{x} = Lx, \qquad \hat{y} = Ly.$$

This allows to convert the Navier-Stokes equations into the non-dimensional form

$$\rho\left(u\frac{\partial u}{\partial x} + v\frac{\partial u}{\partial y}\right) = -\frac{\partial p}{\partial x} + \frac{1}{Re}\left\{\frac{\partial}{\partial x}\left[\mu\left(\frac{4}{3}\frac{\partial u}{\partial x} - \frac{2}{3}\frac{\partial v}{\partial y}\right)\right]+ \right.$$
$$\left. +\frac{\partial}{\partial y}\left[\mu\left(\frac{\partial u}{\partial y} + \frac{\partial v}{\partial x}\right)\right]\right\}, \tag{3a}$$

$$\rho\left(u\frac{\partial v}{\partial x} + v\frac{\partial v}{\partial y}\right) = -\frac{\partial p}{\partial y} + \frac{1}{Re}\left\{\frac{\partial}{\partial y}\left[\mu\left(\frac{4}{3}\frac{\partial v}{\partial y} - \frac{2}{3}\frac{\partial u}{\partial x}\right)\right]+ \right.$$
$$\left. +\frac{\partial}{\partial x}\left[\mu\left(\frac{\partial u}{\partial y} + \frac{\partial v}{\partial x}\right)\right]\right\}, \tag{3b}$$

$$\rho\left(u\frac{\partial h}{\partial x} + v\frac{\partial h}{\partial y}\right) = u\frac{\partial p}{\partial x} + v\frac{\partial p}{\partial y}+$$
$$+\frac{1}{Re}\left\{\frac{1}{Pr}\left[\frac{\partial}{\partial x}\left(\mu\frac{\partial h}{\partial x}\right) + \frac{\partial}{\partial y}\left(\mu\frac{\partial h}{\partial y}\right)\right]+ \right. \tag{3c}$$
$$\left. +\mu\left(\frac{4}{3}\frac{\partial u}{\partial x} - \frac{2}{3}\frac{\partial v}{\partial y}\right)\frac{\partial u}{\partial x} + \mu\left(\frac{4}{3}\frac{\partial v}{\partial y} - \frac{2}{3}\frac{\partial u}{\partial x}\right)\frac{\partial v}{\partial y} + \mu\left(\frac{\partial u}{\partial y} + \frac{\partial v}{\partial x}\right)^2\right\},$$

$$\frac{\partial \rho u}{\partial x} + \frac{\partial \rho v}{\partial y} = 0, \tag{3d}$$

$$h = \frac{1}{(\gamma - 1)M_\infty^2}\frac{1}{\rho} + \frac{\gamma}{\gamma - 1}\frac{p}{\rho}. \tag{3e}$$

Here M_∞ is the free-stream Mach number defined as

$$M_\infty = \frac{V_\infty}{a_\infty}, \qquad a_\infty = \sqrt{\gamma\frac{p_\infty}{\rho_\infty}}.$$

We shall assume that M_∞ is a finite quantity greater than one.

The asymptotic analysis of the Navier-Stokes equations will be conducted assuming that the Reynolds number

$$Re = \frac{\rho_\infty U_\infty L}{\mu_\infty} \to \infty.$$

2.2   The flow upstream of the interaction region

Before analysing the free-interaction region which occupies a small vicinity of the separation point S we need to consider the boundary layer on the plate surface upstream of the interaction, as this boundary layer plays a

role of the background on which the interaction develops. The flow out-side the boundary layer is almost uniform with small perturbations of order $O(Re^{-1/2})$ caused by the presence of the boundary layer.

Asymptotic analysis of the boundary layer is based on the limit proce-dure

$$x = O(1), \quad Y = Re^{1/2}y = O(1), \quad Re \to \infty,$$

and the solution of the Navier-Stokes equations may may be sought in the form of the asymptotic expansions

$$u(x, y; Re) = U_0(x, Y) + \cdots, \quad v(x, y; Re) = Re^{-1/2}V_0(x, Y) + \cdots,$$

$$\rho(x, y; Re) = \rho_0(x, Y) + \cdots, \quad p(x, y; Re) = Re^{-1/2}P_1(x, Y) + \cdots, \quad (4)$$

$$h(x, y; Re) = h_0(x, Y) + \cdots, \quad \mu(x, y; Re) = \mu_0(x, Y) + \cdots.$$

Substitution of (4) into the Navier-Stokes (3) equations leads to the classical boundary-layer equations

$$\rho_0 U_0 \frac{\partial U_0}{\partial x} + \rho_0 V_0 \frac{\partial U_0}{\partial Y} = \frac{\partial}{\partial Y}\left(\mu_0 \frac{\partial U_0}{\partial Y}\right), \tag{5a}$$

$$\rho_0 U_0 \frac{\partial h_0}{\partial x} + \rho_0 V_0 \frac{\partial h_0}{\partial Y} = \frac{1}{Pr}\frac{\partial}{\partial Y}\left(\mu_0 \frac{\partial h_0}{\partial Y}\right) + \mu_0\left(\frac{\partial U_0}{\partial Y}\right)^2, \tag{5b}$$

$$\frac{\partial(\rho_0 U_0)}{\partial x} + \frac{\partial(\rho_0 V_0)}{\partial Y} = 0, \tag{5c}$$

$$h_0 = \frac{1}{(\gamma - 1)M_\infty^2}\frac{1}{\rho_0}. \tag{5d}$$

They should be solved with the free-stream conditions at the leading edge of the flat plate

$$U_0 = 1, \quad h_0 = \frac{1}{(\gamma - 1)M_\infty^2} \quad \text{at} \quad x = 0, \ Y \in [0, \infty) \tag{6}$$

as well as at the outer edge of the boundary layer

$$U_0 = 1, \quad h_0 = \frac{1}{(\gamma - 1)M_\infty^2} \quad \text{at} \quad Y = \infty, \ x \in [0, \infty). \tag{7}$$

On the plate surface the no-slip conditions hold

$$U_0 = V_0 = 0 \quad \text{at} \quad Y = 0, \ x \in [0, 1]. \tag{8}$$

It should be supplemented with a thermal condition. For example, we can assume that the wall temperature is given as a function of x, i.e.

$$h_0 = F(x) \quad \text{at} \quad Y = 0, \ x \in [0, 1] \tag{9a}$$

or the wall is thermally isolated

$$\frac{\partial h_0}{\partial Y} = 0 \quad \text{at} \quad Y = 0, \quad x \in [0, 1]. \tag{9b}$$

Boundary-value problem (5)–(9) admits a self-similar solution for thermally isolated wall (9b) as well as in the case when the wall temperature is known to be constant, i.e. function $F(x)$ in (9a) does not depend on x. However, we do not need to restrict ourselves to these particular flow conditions. If they are not satisfied then the boundary-value problem (5)–(9) may be solved numerically. To proceed further we only need to know that the solution remains smooth when the trailing edge of the plate is approached. Therefore we shall assume that the sought functions U_0, h_0, ρ_0 and μ_0 may be represented in the form of Taylor expansions

$$\left.\begin{aligned}
U_0(x, Y) &= U_{00}(Y) + (-s)U_{01}(Y) + \cdots, \\
h_0(x, Y) &= h_{00}(Y) + (-s)h_{01}(Y) + \cdots, \\
\rho_0(x, Y) &= \rho_{00}(Y) + (-s)\rho_{01}(Y) + \cdots, \\
\mu_0(x, Y) &= \mu_{00}(Y) + (-s)\mu_{01}(Y) + \cdots
\end{aligned}\right\} \quad \text{as} \quad s = x - 1 \to 0^-. \tag{10}$$

The leading order terms in (10) exhibit the following behaviour near the plate surface

$$\left.\begin{aligned}
U_{00}(Y) &= \lambda Y + \cdots, \\
h_{00}(Y) &= h_w + \cdots, \\
\rho_{00}(Y) &= \rho_w + \cdots, \\
\mu_{00}(Y) &= \mu_w + \cdots
\end{aligned}\right\} \quad \text{as} \quad Y \to 0, \tag{11}$$

where λ, h_w, ρ_w, μ_w are positive constants representing the dimensionless skin friction, enthalpy, density and viscosity on the wall surface.

2.3 Inspection analysis of the interaction process

Let us suppose that for some reason a small pressure rise $\Delta p \ll 1$ forms at the outer edge of the boundary layer as shown in Figure 10. Let us further suppose that it acts over a short distance with $\Delta x \ll 1$. It is apparent that this pressure rise will result in a deceleration of fluid particles inside the boundary layer. To estimate the corresponding velocity variation Δu one needs to compare the first convective term on the left hand side of the longitudinal momentum equation (3a) with the pressure gradient

$$\rho u \frac{\partial u}{\partial x} \sim \frac{\partial p}{\partial x}. \tag{12}$$

Indeed, the convective term serves to describe acceleration/deceleration of fluid particles, and since this process is caused by pressure variations, the balance expressed by (12) should hold. Here symbol $\sim$ is used to show that the quantities in (12) are same order of magnitude.

$\Delta p > 0$
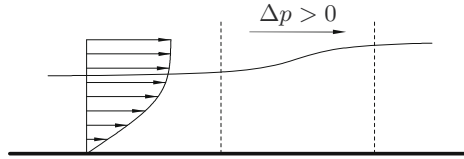
Figure 10. Viscous-inviscid interaction region.

Taking into account that the perturbations are small, and therefore the velocity u and density ρ may be represented by their initial profiles given by the leading order terms in (10), we have

$$\rho_{00} U_{00} \frac{\partial u}{\partial x} \sim \frac{\partial p}{\partial x}.$$

Approximating the derivatives by finite differences, we have

$$\rho_{00} U_{00} \frac{\Delta u}{\Delta x} \sim \frac{\Delta p}{\Delta x},$$

and it follows that

$$\Delta u \sim \frac{\Delta p}{\rho_{00} U_{00}}. \tag{13}$$

Since everywhere in the boundary layer, except near the wall, both ρ_{00} and U_{00} are order one quantities, we can finally write

$$\Delta u \sim \Delta p. \tag{14}$$

Applying the same arguments to the energy equation (3c), we find

$$\Delta h \sim \Delta p,$$

and then it follows from the state equation (3e) that

$$\Delta \rho \sim \Delta p. \tag{15}$$

Let us now we consider a small filament in the boundary layer confined between two neighbouring streamlines with δ being the initial distance between them, as shown in Figure 11. Using the mass conservation law, we can write

$$\rho_{00} U_{00} \delta_i = (\rho_{00} + \Delta \rho)(U_{00} + \Delta u)(\delta_i + \Delta \delta_i).$$

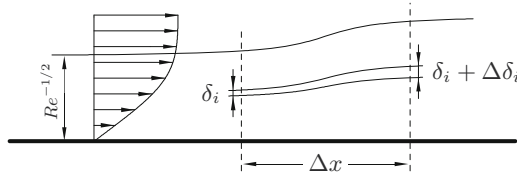Neglecting squares of perturbations in this equation, we can deduce that

$$\frac{\Delta\delta_i}{\delta_i} \sim \frac{\Delta\rho}{\rho_{00}} + \frac{\Delta u}{U_{00}}.$$

Since both ρ_{00} and U_{00} are order one quantities and their variations are given by (14) and (15), we can conclude that the thickness of the filament increases by the value

$$\Delta\delta_i \sim \delta_i \Delta p.$$

The integral effect of the thickening of all the filaments in boundary layer is

$$\Delta\delta = \sum_i \Delta\delta_i \sim \sum_i \left(\delta_i \Delta p\right) \sim \Delta p \sum_i \delta_i \sim Re^{-1/2}\Delta p. \qquad (16)$$

Figure 11. Thickening of a stream filament in the main part of the boundary layer.

The above analysis, obviously, is invalid near the bottom of the boundary layer. Indeed, according to (11) the initial velocity U_{00} tends to zero as $Y \to 0$, and equation (13) predicts unbounded growth of the perturbation velocity. Of course, before it happens non-linear effects take over. In a thin sublayer near the wall, where $\Delta u \sim U_{00}$, equation (13) may be written as

$$\Delta u \sim U_{00} \sim \sqrt{\Delta p}. \qquad (17)$$

Combining (17) with the formula for U_{00} in (11), we can deduce that

$$Y \sim \sqrt{\Delta p},$$

which means that the thickness of the near-wall sublayer

$$y = Re^{-1/2}Y \sim Re^{-1/2}\sqrt{\Delta p}. \qquad (18)$$

To estimate the displacement effect of the sublayer we again use the mass conservation law. Treating the sublayer as one filament (see Figure 12) and

taking into account that along this filament $\Delta u \sim U_{00}$, we have to conclude that the variation of the filament thickness is of the same order as its initial value given by (18), i.e.

$$\Delta\delta \sim Re^{-1/2}\sqrt{\Delta p}. \tag{19}$$
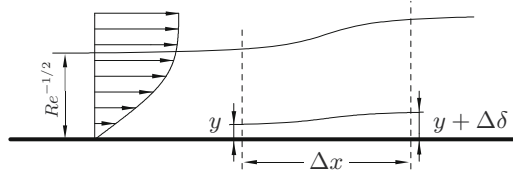
Figure 12. Thickening of the sublayer.

Comparing (19) with (16), we see that for any $\Delta p \ll 1$ the contribution of the sublayer into the displacement effect of the boundary layer is significantly larger than that of the main part of the boundary layer. Hence, the slope angle θ of the streamlines at the outer edge of the boundary layer should be estimated based on the displacement effect of the sublayer (19). We have

$$\theta \sim \frac{\Delta\delta}{\Delta x} \sim \frac{Re^{-1/2}\sqrt{\Delta p}}{\Delta x},$$

Using further the Ackeret formula, we find that the pressure perturbations in the interaction region

$$\Delta p \sim \theta \sim \frac{Re^{-1/2}\sqrt{\Delta p}}{\Delta x}. \tag{20}$$

It remains to recall that the sublayer is adjacent to the wall and therefore should be viscous,

$$\rho u \frac{\partial u}{\partial x} \sim \frac{1}{Re} \frac{\partial}{\partial y}\left(\mu \frac{\partial u}{\partial y}\right). \tag{21}$$

Indeed, if the flow were inviscid, then the Bernoulli equation could be used along each streamline. Near the wall the velocity small, and therefore, we can write this equation in the incompressible form

$$\frac{u^2}{2} + \frac{p}{\rho} = \frac{U_{00}^2}{2}. \tag{22}$$

Here it is taken into account that p denotes the perturbation of the pressure with respect to its value in the oncoming flow; everywhere upstream of the interaction region $p = 0$.

Writing equation (22) in the form

$$\frac{u^2}{2} = \frac{U_{00}^2}{2} - \frac{p}{\rho},\tag{23}$$

we can see that for any increase of pressure, no matter how small, we can always find a streamline close enough to the wall for which the right hand side of (23) appears to be negative. Since this is impossible, we have to conclude that the flow in the sublayer should be viscous.

Taking into account that the density ρ and viscosity μ are order one quantities everywhere in the boundary layer, and representing equation (21) in the finite differences form, we have

$$U_{00}\frac{\Delta u}{\Delta x} \sim \frac{1}{Re}\frac{\Delta u}{(\Delta y)^2}.$$

Since in the sublayer $\Delta y \sim y$, this equation may be written as

$$\frac{U_{00}}{\Delta x} \sim \frac{1}{Re}\frac{1}{y^2}.\tag{24}$$

Let us now summarise the results of the above analysis. Taking into account that in the sublayer the velocity u is same order as initial velocity U_{00} at the bottom of the boundary layer approaching the interaction region, we will write equation (17) as

$$u \sim \sqrt{\Delta p}.\tag{25}$$

Equation (18) for the thickness of the viscous sublayer is written as

$$y \sim Re^{-1/2}\sqrt{\Delta p}.\tag{26}$$

From equation (20), representing the pressure induced in the interaction region, it follows that

$$\sqrt{\Delta p} \sim \frac{Re^{-1/2}}{\Delta x}.\tag{27}$$

In order to close this set of equations we need to add equation (24) which we will now write as

$$\frac{u}{\Delta x} \sim \frac{1}{Re\,y^2}.\tag{28}$$

As a result we have four equations (25) – (28) for four unknowns, the velocity u in the sublayer, characteristic thickness of the sublayer y, induced pressure Δp and longitudinal extent Δx of the interaction region. These equations may be treated as algebraic equations. They are easily solved to give

$$u \sim Re^{-1/8}, \qquad y \sim Re^{-5/8}, \qquad \Delta p \sim Re^{-1/4}, \qquad \Delta x \sim Re^{-3/8}.\tag{29}$$

2.4   Triple-Deck Model

The inspection analysis presented in the previous section serves two purposes. Firstly, it allows to obtain estimates for fluid dynamic quantities in different parts of the flow, which we will use when constructing the corresponding asymptotic expansion of the sought functions. Secondly, it reveals physical nature of the processes involved. In this particular problem it shows that under certain conditions the boundary layer may come into interaction with external inviscid flow; this interaction being termed *viscous-inviscid interaction*. The region of the interaction occupies an $O(Re^{-3/8})$ vicinity of the separation point, and has a three-tiered structure shown in Figure 13. It is composed of the viscous sublayer (shown as region *1*), the main part of the boundary layer (region *2*) and an inviscid potential flow (region *3*) situated outside the boundary layer.
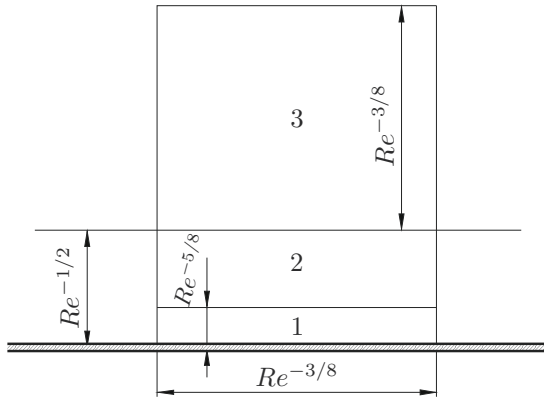
Figure 13. Three-tiered structure of the interaction region.

The characteristic thickness of the viscous sublayer is estimated as being an $O(Re^{-5/8})$ quantity, so that it occupies an $O(Re^{-1/8})$ portion of the boundary layer and is comprised of the stream filaments immediately adjacent to the wall. The flow velocity in this region is $O(Re^{-1/8})$ relative to the free-stream velocity, and due to the slow motion of gas here the flow exhibits high sensitivity to pressure variations. Even a small variation of pressure along the wall may cause significant deceleration/acceleration of fluid particles there. As a result the flow filaments change their thickness leading to a deformation of streamlines. This process is termed the displacement effect of the boundary layer.

The main part of the boundary layer, the middle tier of the interac-

tive structure, represents a continuation of the conventional boundary layer developing along the plate. Its thickness is estimated as $O(Re^{-1/2})$ and the velocity is an order one quantity. The flow in this tier is significantly less sensitive to the pressure variations. It does not produce any noticeable contribution to the displacement effect of the boundary layer, which means that all the streamlines in the middle tier are parallel to each other and carry the deformation produced by the displacement effect of the viscous sublayer.

Finally, the upper tier is situated in the potential flow region outside the boundary layer. It serves to "convert" the perturbations in the form of the streamlines into perturbations of pressure. These are then transmitted through the main part of the boundary layer back to the sublayer, enhancing the process of fluid deceleration. This process is self-sustained, and it drives the boundary layer towards the separation.

We shall start our analysis with the viscous sublayer, region _1_.

Viscous sublayer   Estimates (29) suggest that asymptotic analysis of the Navier-Stokes equations in the viscous sublayer (region _1_) should be based on the limit procedure, where

$$x_* = \frac{x-1}{Re^{-3/8}} = O(1), \quad Y_* = \frac{y}{Re^{-5/8}} = O(1), \quad Re \to \infty. \qquad (30)$$

The solution of the Navier-Stokes equations in this region will be sought in the form of asymptotic expansions

$$\begin{aligned}
u(x,y;Re) &= Re^{-1/8}U^*(x_*,Y_*) + \cdots, \\
v(x,y;Re) &= Re^{-3/8}V^*(x_*,Y_*) + \cdots, \\
p(x,y;Re) &= Re^{-1/4}P^*(x_*,Y_*) + \cdots, \\
h(x,y;Re) &= h^*(x_*,Y_*) + \cdots, \\
\rho(x,y;Re) &= \rho^*(x_*,Y_*) + \cdots, \\
\mu(x,y;Re) &= \mu^*(x_*,Y_*) + \cdots.
\end{aligned} \qquad (31)$$

The form of the asymptotic expansions for u and p directly follows from estimates (29). In order to find an estimate for v we used the continuity equation (3d), viz.

$$\frac{\partial \rho u}{\partial x} \sim \frac{\partial \rho v}{\partial y}.$$

Being written in finite-difference from, it gives

$$\frac{\rho u}{\Delta x} \sim \frac{\rho v}{y} \quad \Longrightarrow \quad v \sim y\frac{u}{\Delta x} \sim Re^{-3/8}.$$

As far as the enthalpy h, density ρ and viscosity μ are concerned, in normal circumstances (when there is no extreme heating or cooling of the wall) they remain order one functions throughout the boundary layer.

Substitution of (31) into the Navier-Stokes equations (3) leads to

$$\rho^* U^* \frac{\partial U^*}{\partial x_*} + \rho^* V^* \frac{\partial U^*}{\partial Y_*} = -\frac{\partial P^*}{\partial x_*} + \frac{\partial}{\partial Y_*}\left(\mu^* \frac{\partial U^*}{\partial Y_*}\right), \tag{32a}$$

$$\frac{\partial P^*}{\partial Y_*} = 0, \tag{32b}$$

$$\rho^* U^* \frac{\partial h^*}{\partial x_*} + \rho^* V^* \frac{\partial h^*}{\partial Y_*} = -\frac{1}{Pr}\frac{\partial}{\partial Y_*}\left(\mu^* \frac{\partial h^*}{\partial Y_*}\right), \tag{32c}$$

$$\frac{\partial \rho^* U^*}{\partial x_*} + \frac{\partial \rho^* V^*}{\partial Y_*} = 0, \tag{32d}$$

$$h^* = \frac{1}{(\gamma-1)M_\infty^2}\frac{1}{\rho^*}. \tag{32e}$$

Since the flow in the viscous sublayer is slow, it should behave as incompressible. To confirm this proposition, we need to consider the energy equation (32c). It is a parabolic equation, and requires an initial condition $(x_* \to -\infty)$, condition on the wall $(Y_* = 0)$ and condition at the outer edge of the sublayer $(Y_* \to \infty)$. We start with the initial condition. It may be formulated by matching with the solution in the boundary layer upstream of the interaction region. This solution may be termed the outer solution for our purposes. According to (4), the outer asymptotic expansion for the enthalpy has the form

$$h(x,y;Re) = h_0(x,Y) + \cdots \tag{33}$$

In order to perform the matching, we have to re-expand (33) in terms of the inner variables (30). We start with the longitudinal coordinate

$$x = 1 + Re^{-3/8}x_*.$$

Since $x - 1$ is small, we can use the Taylor expansion (10) for the enthalpy. Being substituted into (33), it gives

$$h(x,y;Re) = h_{00}(Y) + O(Re^{-3/8}). \tag{34}$$

Now we recall that region 1 is significantly thinner as compared to the boundary layer. Indeed, in the boundary layer

$$y = Re^{-1/2}Y,$$

while in region *1*

$$y = Re^{-5/8}Y_*.$$

Comparing these formulae, we see that

$$Y = Re^{-1/8}Y_*,$$

which means that Y is small, and we can use the asymptotic formula (11) for h_{00} in (33). We have

$$h(x, y; Re) = h_w + \cdots.$$

This is the inner re-expansion of the outer solution. If we compare it with the asymptotic expansion (31) for the enthalpy in region *1*, we can conclude that the sought matching condition may be written as

$$h^* \to h_w \quad \text{as} \quad x_* \to -\infty. \tag{35}$$

On the plate surface we can either prescribe the wall temperature

$$h^* = h_w \quad \text{at} \quad Y_* = 0, \tag{36a}$$

or assume the wall thermally isolated

$$\frac{\partial h^*}{\partial Y_*} = 0 \quad \text{at} \quad Y_* = 0. \tag{36b}$$

Concerning condition (36) it should be noted that even when the wall temperature is not constant, its variation over a short distance occupied by the interaction region is small in normal circumstances, and therefore, should be neglected in the leading order approximation.

It remains to consider the outer edge of the viscous sublayer. At large values of Y_* the energy equation (32c) turns into the inviscid the form

$$U^* \frac{\partial h^*}{\partial x_*} + V^* \frac{\partial h^*}{\partial Y_*} = 0, \tag{37}$$

which shows that the enthalpy h^* does not chance along streamlines. All the streamlines, except in the separation region, originate from an upstream location, where condition (35) holds. Integrating (37) with (35), we arrive at a conclusion that the sought boundary condition may be written as

$$h^* \to h_w \quad \text{as} \quad Y_* \to \infty. \tag{38}$$

The solution of the energy equation (32c), satisfying boundary conditions (35), (36) and (38), is simply

$$h^* = h_w. \tag{39}$$

Thus, we have demonstrated that the enthalpy h^* is constant everywhere inside the viscous sublayer (region *1*). Using now the state equation (32e), we can see that the density ρ^* is also constant, which means that the flow in region *1* may be treated as incompressible. We can further recall that the viscosity μ^* is a function of temperature only, and since h^* is constant, μ^* should also be constant. To be consistent with (11), we write

$$\rho^* = \rho_w, \qquad \mu^* = \mu_w. \tag{40}$$

Now we turn to the momentum (32a) and continuity (32d) equations. Using (39), (40), we can write these equations as

$$\rho_w U^* \frac{\partial U^*}{\partial x_*} + \rho_w V^* \frac{\partial U^*}{\partial Y_*} = -\frac{dP^*}{dx_*} + \mu_w \frac{\partial^2 U^*}{\partial Y_*^2}, \tag{41a}$$

$$\frac{\partial U^*}{\partial x_*} + \frac{\partial V^*}{\partial Y_*} = 0. \tag{41b}$$

According to (32b), the pressure does not change across the viscous sublayer. Function P^* is a function of x_* only, which is why the pressure gradient on the right hand side of (41a) is expressed by an ordinary derivative dP^*/dx_*.

Equations (41) should be solved with the no-slip condition on the plate surface

$$U^* = V^* = 0 \quad \text{at} \quad Y_* = 0. \tag{42}$$

We also need to formulate an initial condition for U^* at $x_* = -\infty$. This is done by matching with the solution in the boundary layer upstream of the interaction region. According to (4), the longitudinal velocity component u is represented in the boundary layer in the form of an asymptotic expansion

$$u(x, y; Re) = U_0(x, Y) + \cdots. \tag{43}$$

To perform the matching, we need to re-expand (43) in terms of the inner variables (30). We have

$$u(x, y; Re) = U_0(1 + Re^{-3/8}x_*, Re^{-1/8}Y_*) + \cdots.$$

Taking into account that the first argument of function U_0 is close to one, and the second is small, we can use the corresponding asymptotic formulae (10), (11), which yields

$$u(x, y; Re) = Re^{-1/8}\lambda Y_* + \cdots. \tag{44}$$

It remains to compare (44) with the asymptotic expansion (31) for u in region *1*, and we will find that the sought initial condition is written as

$$U^* = \lambda Y_* \quad \text{at} \quad x_* = -\infty. \tag{45}$$

Now we shall study asymptotic behaviour of the solution of equations (41) at the outer edge of the viscous sublayer ($Y_* \to \infty$). For this purpose it is convenient to introduce the stream function $\Psi^*(x_*, Y_*)$. Its existence follows from the continuity equation (41b), and we can write

$$U^* = \frac{\partial \Psi^*}{\partial Y_*}, \qquad V^* = -\frac{\partial \Psi^*}{\partial x_*}. \tag{46}$$

Let us try to use for the stream function the following asymptotic expansion

$$\Psi^*(x_*, Y_*) = A_0(x_*)Y_*^\alpha + \cdots \quad \text{as} \quad Y_* \to \infty. \tag{47}$$

Here parameter α and function $A_0(x_*)$ are expected to be found by using the momentum equation (41a).

Substitution of (47) into (46) yields

$$U^* = \alpha A_0(x_*)Y_*^{\alpha-1} + \cdots, \qquad V^* = -A_0'(x_*)Y_*^\alpha + \cdots. \tag{48}$$

Therefore, the convective terms on the left hand side of equation (41a) and the viscous term on the right hand side are written as

$$\rho_w U^* \frac{\partial U^*}{\partial x_*} = \rho_w \alpha A_0 \frac{dA_0}{dx_*} Y_*^{2\alpha-2} + \cdots,$$

$$\rho_w V^* \frac{\partial U^*}{\partial Y_*} = -\rho_w \alpha(\alpha-1)A_0 \frac{dA_0}{dx_*} Y_*^{2\alpha-2} + \cdots,$$

$$\mu_w \frac{\partial^2 U^*}{\partial Y_*^2} = \alpha(\alpha-1)(\alpha-2)A_0 Y_*^{\alpha-3} + \cdots.$$

We see that if we assume, subject to subsequent confirmation, that $\alpha > 1$, then the convective terms will dominate not only over the viscous term, but also over the pressure gradient, which remains finite as $Y_* \to \infty$. We have

$$O(Y_*^{2\alpha-2}): \quad A_0 \frac{dA_0}{dx_*} = 0.$$

The initial condition for this equation may be obtained by substituting the first of formulae (48) into (45). We find

$$A_0(-\infty) = \begin{cases} \lambda/\alpha & \text{if} \quad \alpha = 2, \\ 0 & \text{if} \quad \alpha \neq 2. \end{cases}$$

Hence, a non-trivial solution exists only if $\alpha = 2$, in which case $A_0 = \frac{1}{2}\lambda$, and (47) turns into

$$\Psi^*(x_*, Y_*) = \frac{1}{2}\lambda Y_*^2 + \cdots \quad \text{as} \quad Y_* \to \infty.$$

Now we shall try to find the next order term in this expansion:

$$\Psi^*(x_*, Y_*) = \frac{1}{2}\lambda Y_*^2 + A_1(x_*)Y_*^\alpha + \cdots \quad \text{as} \quad Y_* \to \infty. \tag{49}$$

In order to ensure that the second term in (49) is small as compared with the first one, we have to assume that $\alpha < 2$. Substitution of (49) into (46) yields

$$U^* = \lambda Y_* + \alpha A_1(x_*)Y_*^{\alpha-1} + \cdots , \qquad V^* = -A_1'(x_*)Y_*^\alpha + \cdots .$$

Therefore, the convective terms on the left hand side of equation (41a) and the viscous term on the right hand side are written as

$$\rho_w U^* \frac{\partial U^*}{\partial x_*} = \rho_w \lambda \alpha \frac{dA_1}{dx_*} Y_*^\alpha + \cdots ,$$

$$\rho_w V^* \frac{\partial U^*}{\partial Y_*} = -\rho_w \lambda \frac{dA_1}{dx_*} Y_*^\alpha + \cdots ,$$

$$\mu_w \frac{\partial^2 U^*}{\partial Y_*^2} = \alpha(\alpha-1)(\alpha-2)A_1 Y_*^{\alpha-3} + \cdots .$$

Hence, the convective terms remain dominant provided that $\alpha > 0$, in which case the momentum equation (41a) reduces at

$$O(Y_*^\alpha): \quad (\alpha-1)\frac{dA_1}{dx_*} = 0.$$

Since the initial condition (45) does not contain any terms except the one which matches with the leading order term in (49), we have to conclude that

$$A_1(-\infty) = 0.$$

We see that a non-trivial solution for A_1 exists only if $\alpha = 1$. Function $A_1(x_*)$ remains arbitrary in the framework of the asymptotic analysis of equations (41). We, of course, expect that this function will be found as a part of the solution of the problem as a whole.

Redenoting $A_1(x_*)$ as $A(x_*)$ renders (49) in the form

$$\Psi^* = \frac{1}{2}\lambda Y_*^2 + A(x_*)Y_* + \cdots \quad \text{as} \quad Y_* \to \infty. \tag{50}$$

The physical content of function $A(x_*)$ may be clarified by calculating the
the streamline slope angle

$$\vartheta = \arctan \frac{v}{u}.$$

In the viscous sublayer the velocity components u and v are given by the
asymptotic expansions (31):

$$u = Re^{-1/8}U^*(x_*, Y_*) + \cdots, \qquad v = Re^{-3/8}V^*(x_*, Y_*) + \cdots. \qquad (51)$$

Substitution of (51) into (46) shows that at the outer edge of the viscous
sublayer

$$U^*(x_*, Y_*) = \lambda Y_* + A(x_*) + \cdots, \qquad V^*(x_*, Y_*) = -\frac{dA}{dx_*}Y_* + \cdots, \qquad (52)$$

and we can see that the streamline slope angle ϑ, which is zero on the wall,
reaches at the outer edge of the viscous sublayer the following value

$$\vartheta = \arctan \frac{v}{u} = Re^{-1/4}\frac{V^*}{U^*}\Big|_{Y_*\to\infty} + \cdots = Re^{-1/4}\Big(-\frac{1}{\lambda}\frac{dA}{dx_*}\Big) + \cdots. \qquad (53)$$

In view of this formula, function $A(x_*)$ is called the **displacement func-
tion**.

Main part of the boundary layer   Region *2*, the middle tier of the
triple-deck structure (see Figure 13), is a continuation of the conventional
boundary layer developing on the plate surface before the interaction. Its
thickness is estimated as $y = O(Re^{-1/2})$. The longitudinal extent of region
2 coincides with that of the entire interaction region and is estimated as
$|x - 1| = O(Re^{-3/8})$. Consequently, the asymptotic analysis of the Navier-
Stokes equations (3) in the main part of the boundary layer should be based
on the limit procedure

$$x_* = Re^{3/8}(x - 1) = O(1), \quad Y = Re^{1/2}y = O(1), \quad Re \to \infty. \qquad (54)$$

The form of the asymptotic expansions of the fluid dynamic functions in
region *2* may be predicted by analysing the solution in the overlap region
that lies between regions *1* and *2*. In particular, we found that at the outer
edge of region *1* the velocity components are given by (52). Substituting
(52) into (51), we find that in the overlap region

$$u = Re^{-1/8}\lambda Y_* + Re^{-1/8}A(x_*) + \cdots, \qquad v = Re^{-3/8}\Big(-\frac{dA}{dx_*}Y_*\Big) + \cdots.$$

$$(55)$$

We now express (55) in term of variables (54) of region 2, recalling that $Y = Re^{-1/8}Y_*$. We find that at the bottom of the middle tier (region 2)

$$u = \lambda Y + Re^{-1/8}A(x_*) + \cdots, \qquad v = Re^{-1/4}\left(-\frac{dA}{dx_*}Y\right) + \cdots. \quad (56)$$

This suggests that the solution in region 2 should be written in the form of asymptotic expansions

$$u(x, y; Re) = U_{00}(Y) + Re^{-1/8}\widetilde{U}_1(x_*, Y) + \cdots$$
$$v(x, y, Re) = Re^{-1/4}\widetilde{V}_1(x_*, Y) + \cdots. \quad (57)$$

The leading order term $U_{00}(Y)$ in the expansion for $u(x, y; Re)$ coincides with the velocity profile (10) in the boundary layer immediately before the interaction region. According to (11)

$$U_{00} = \lambda Y + \cdots \quad \text{as} \quad Y \to 0. \quad (58)$$

It further follows from (57) that the perturbation terms $\widetilde{U}_1(x_*, Y)$ and $\widetilde{V}_1(x_*, Y)$ in (57) satisfy the following boundary conditions at the bottom of region 2,

$$\left.\begin{array}{l} \widetilde{U}_1 = A(x_*) + \cdots, \\[2mm] \widetilde{V}_1 = -\dfrac{dA}{dx_*}Y + \cdots. \end{array}\right\} \quad \text{as} \quad Y \to 0. \quad (59)$$

By analogy with the longitudinal velocity component u in (57), we shall seek the enthalpy h, density ρ and viscosity μ in region 2 in the form of asymptotic expansions

$$h(x, y; Re) = h_{00}(Y) + Re^{-1/8}\widetilde{h}_1(x_*, Y) + \cdots,$$
$$\rho(x, y; Re) = \rho_{00}(Y) + Re^{-1/8}\widetilde{\rho}_1(x_*, Y) + \cdots, \quad (60)$$
$$\mu(x, y; Re) = \mu_{00}(Y) + Re^{-1/8}\widetilde{\mu}_1(x_*, Y) + \cdots.$$

Finally, taking into account that in view of (32b) the pressure perturbations in region 2 should be same order as in region 1, we write

$$p(x, y; Re) = Re^{-1/4}\widetilde{P}_1(x_*, Y) + \cdots. \quad (61)$$

Substitution of (57), (60) and (61) into the Navier-Stokes equations (3)

results in

$$U_{00}(Y)\frac{\partial \widetilde{U}_1}{\partial x_*} + \widetilde{V}_1 U'_{00}(Y) = 0, \tag{62a}$$

$$\frac{\partial \widetilde{P}_1}{\partial Y} = 0, \tag{62b}$$

$$U_{00}(Y)\frac{\partial \widetilde{h}_1}{\partial x_*} + \widetilde{V}_1 h'_{00}(Y) = 0, \tag{62c}$$

$$\rho_{00}(Y)\frac{\partial \widetilde{U}_1}{\partial x_*} + U_{00}(Y)\frac{\partial \widetilde{\rho}_1}{\partial x_*} + \rho_{00}(Y)\frac{\partial \widetilde{V}_1}{\partial Y} + \widetilde{V}_1 \rho'_{00}(Y) = 0, \tag{62d}$$

$$h_{00} = \frac{1}{(\gamma-1)M_\infty^2}\frac{1}{\rho_{00}}, \qquad \widetilde{h}_1 = -\frac{1}{(\gamma-1)M_\infty^2}\frac{\widetilde{\rho}_1}{\rho_{00}^2}. \tag{62e}$$

These equations are easily solved using the following elimination process. We first substitute (62e) into the energy equation (62c). This leads to

$$U_{00}(Y)\frac{\partial \widetilde{\rho}_1}{\partial x_*} + \widetilde{V}_1 \rho'_{00}(Y) = 0,$$

showing that the continuity equation (62d) may be written as

$$\frac{\partial \widetilde{U}_1}{\partial x_*} + \frac{\partial \widetilde{V}_1}{\partial Y} = 0. \tag{63}$$

Now, using (63), we can eliminate $\partial \widetilde{U}_1/\partial x_*$ from the longitudinal momentum equation (62a). This results in

$$U_{00}(Y)\frac{\partial \widetilde{V}_1}{\partial Y} - \widetilde{V}_1 U'_{00}(Y) = 0. \tag{64}$$

Dividing both terms in (64) by U_{00}^2, we have

$$\frac{1}{U_{00}(Y)}\frac{\partial \widetilde{V}_1}{\partial Y} - \widetilde{V}_1 \frac{U'_{00}}{U_{00}^2} = 0,$$

or equivalently

$$\frac{\partial}{\partial Y}\left(\frac{\widetilde{V}_1}{U_{00}}\right) = 0.$$

We see that the ratio $\widetilde{V}_1/U_{00}$ is a function of x_* only, say $G(x_*)$, i.e.

$$\frac{\widetilde{V}_1}{U_{00}} = G(x_*).$$

This function may be found by making use of the behaviour of $\widetilde{V}_1$ and U_{00} at the bottom of region 2, as given by (58), (59). We find that

$$G(x_*) = -\frac{1}{\lambda}\frac{dA}{dx_*}.$$

Hence, everywhere across region 2

$$\frac{\widetilde{V}_1}{U_{00}} = -\frac{1}{\lambda}\frac{dA}{dx_*}.$$

Let us now return to the asymptotic expansions (55) of the velocity components, and calculate the streamline slope angle in region 2:

$$\vartheta = \arctan\frac{v}{u} = Re^{-1/4}\frac{\widetilde{V}_1}{U_{00}} + \cdots = Re^{-1/4}\left(-\frac{1}{\lambda}\frac{dA}{dx_*}\right) + \cdots. \qquad (65)$$

We see that ϑ does not depend on Y, i.e. stays unchanged across the main part of the boundary layer. This confirms an important result of the inspection analysis that the displacement effect of the main part of the boundary layer is relatively small, and may be neglected to the leading order. The streamline slope angle (53), produced by the viscous sublayer, is simply transported by the main part of the boundary layer towards the bottom of the the upper tier of the triple-deck structure, shown as region 3 in Figure 13

Interaction law   The flow in region 3 is governed by the linearised equations of inviscid gas motion. The solution of these equation results in the following formula for the pressure at the "bottom" of region 3

$$\hat{p} = p_\infty + \rho_\infty V_\infty^2 \frac{\vartheta}{\sqrt{M_\infty^2 - 1}} \qquad (66)$$

known as the Ackeret formula (see, for example, Siebert (1948)). Since the pressure does not change across regions 2 and 1, we can apply formula (66) directly to the pressure in the viscous sublayer. Converting (66) into non-dimensional form and using (65), we have

$$P^* = -\frac{1}{\lambda\sqrt{M_\infty^2 - 1}}\frac{dA}{dx_*}. \qquad (67)$$

This equation establishes a relationship between the the displacement effect of the boundary layer and the pressure induced in the inviscid from. This is why it is referred to as the ***interaction law.***

Canonical form of the interaction problem   We can now collect to-
gether all the equations governing the interaction process. We fond that
in order to describe the flow in the viscous sublayer we have to solve the
momentum and continuity equations (41)

$$\rho_w U^* \frac{\partial U^*}{\partial x_*} + \rho_w V^* \frac{\partial U^*}{\partial Y_*} = -\frac{dP^*}{dx_*} + \mu_w \frac{\partial^2 U^*}{\partial Y_*^2}, \tag{68}$$

$$\frac{\partial U^*}{\partial x_*} + \frac{\partial V^*}{\partial Y_*} = 0, \tag{69}$$

subject to the no-slip conditions (42)

$$U^* = V^* = 0 \quad \text{at} \quad Y_* = 0, \tag{70}$$

and the initial condition (45)

$$U^* = \lambda Y_* \quad \text{at} \quad x_* = -\infty. \tag{71}$$

Unlike in classical Prandtl's formulation, the pressure gradient in (68) is not
known in advance. Instead the interaction law (67) should be used

$$P^* = -\frac{1}{\lambda\sqrt{M_\infty^2 - 1}} \frac{dA}{dx_*}. \tag{72}$$

It relates the induces pressure P^* to the displacement function $A(x_*)$. This
function may be calculated with the help of the first of equations (52)

$$U^*(x_*, Y_*) = \lambda Y_* + A(x_*) + \cdots . \tag{73}$$

Affine transformations

$$x_* = \frac{\mu_w^{-1/4} \rho_w^{-1/2}}{\lambda^{5/4} \beta^{3/4}} \bar{X}, \qquad Y_* = \frac{\mu_w^{1/4} \rho_w^{-1/2}}{\lambda^{3/4} \beta^{1/4}} \bar{Y}, \qquad U^* = \frac{\mu_w^{1/4} \rho_w^{-1/2}}{\lambda^{-1/4} \beta^{1/4}} \bar{U},$$

$$V^* = \frac{\mu_w^{3/4} \rho_w^{-1/2}}{\lambda^{-3/4} \beta^{-1/4}} \bar{V}, \qquad A = \frac{\mu_w^{1/4} \rho_w^{-1/2}}{\lambda^{-1/4} \beta^{1/4}} \bar{A}, \qquad P^* = \frac{\mu_w^{1/2} \rho_w^{-1/2}}{\lambda^{-1/2} \beta^{1/2}} \bar{P},$$

where $\beta = \sqrt{M_\infty^2 - 1}$, allow to represent the interaction problem (68)–(73)

in the following canonical form.

$$
\left.
\begin{array}{ll}
\bar{U}\dfrac{\partial \bar{U}}{\partial \bar{X}} + \bar{V}\dfrac{\partial \bar{U}}{\partial \bar{Y}} = -\dfrac{d\bar{P}}{d\bar{X}} + \dfrac{\partial^2 \bar{U}}{\partial \bar{Y}^2}, & \\[3mm]
\dfrac{\partial \bar{U}}{\partial \bar{X}} + \dfrac{\partial \bar{V}}{\partial \bar{Y}} = 0, & \\[3mm]
\qquad\qquad \bar{P} = -\dfrac{d\bar{A}}{d\bar{X}}, & \\[3mm]
\bar{U} = \bar{V} = 0 & \text{at} \quad \bar{Y} = 0, \\[2mm]
\bar{U} = \bar{Y} + \cdots & \text{as} \quad \bar{X} \to -\infty, \\[2mm]
\bar{U} = \bar{Y} + \bar{A}(\bar{X}) + \cdots & \text{as} \quad \bar{Y} \to \infty.
\end{array}
\right\}
\tag{74}
$$

Numerical results   Solution of the interaction problem (74) requires spe-
cial numerical techniques. These will not be discussed here; an interested
reader is referred to Chapter 7 of the monograph by Sychev *et al.* (1998).
The calculation results are displayed in Figure 14, where the pressure distri-
bution along the interaction region is shown together with the skin friction.
The latter is defined as

$$
\tau = \left.\frac{\partial \bar{U}}{\partial \bar{Y}}\right|_{\bar{Y}=0}.
$$

(a) Pressure distribution   (b) Skin friction
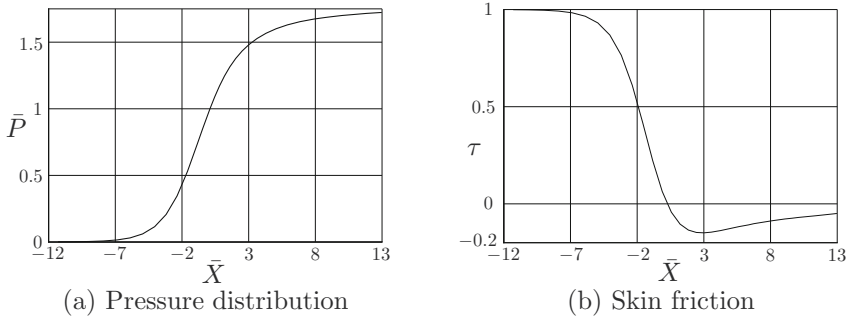
Figure 14. Results of the numerical solution of the interaction problem
(74).

We see that far upstream, where the interaction region matches with
the unperturbed boundary layer, the skin friction $\tau = 1$ and the pressure
perturbation function $\bar{P} = 0$. As the pressure starts to rise in the inter-
action region, it cause the flow in the viscous sublayer to decelerate. This

is revealed by the observed decrease of the skin friction. The skin friction decreases crossing zero at the separation point. It should be noted that the interaction problem (74) is invariant with respect to arbitrary shift in the direction parallel to the body surface,

$$\bar{X} \longrightarrow \bar{X} + C,$$

with C being an arbitrary constant. Keeping this in mind, we have chosen the separation point in Figure 14 to be at $\bar{X} = 0$.

While the pressure continues to grow monotonically, the skin friction reaches a minimum and then starts to rise slowly. While it remains negative, the fluid near the wall is moving in the direction opposite to the rest of the flow. Further downstream $|\tau| \to 0$, which means that the fluid slows down, and the pressure develops a 'plateau' which is clearly seen in Figure 14. At the separation point the pressure was found to be

$$\bar{P}_{separation} = 1.046,$$

and in the plateau region

$$\bar{P}_{plateau} = 1.723 \tag{75}$$

Exercise 1.   Using (75) and the Ackeret formula (66), find the shape of the boundary between the separation region and the main flow above it.

3 Marginal Separation Theory

The Marginal Separation theory was developed independently by Ruban (1981, 1982) and Stewartson *et al.* (1982) who originally applied it to the boundary-layer separation at the leading edge of a thin aerofoil. Later it became clear that the theory describes a variety of subsonic and supersonic flows with a small separation "bubble" forming on a smooth part of the body surface. In this presentation we shall follow the original papers by Ruban (1981, 1982) and Stewartson *et al.* (1982), and use as an example the leading edge separation. It was first observed Jones (1934) in wind tunnel and real flight experiments. Since then many researchers were involved in experimental study of the flow round the leading edge of an aerofoil. A comprehensive account of these efforts may be found, for example, in the review by Tani (1964).
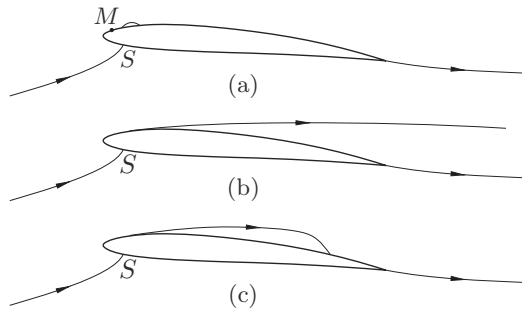
Figure 15. The flow past a thin aerofoil: (a) with a *short* separation bubble; (b) with an extended separation region that forms after the bubble bursting; (c) with a *long* separation bubble.

Experiments show that for thick aerofoils (with thickness to cord ratio larger than 15%) the boundary layer first separates near the trailing edge. For thin aerofoils (with thickness to cord ratio larger than 12%) this is the leading edge separation that causes the stall of the aerodynamic characteristics. For the stall to take place the angle of attack α should exceed a critical value α_c. When α is small, the flow over the aerofoil remains fully attached, and the pressure has its maximum at the front stagnation point S; see Fig. 15(a). As one moves from this point around the aerofoil nose, the pressure first drops dramatically reaching a minimum at some point M on the upper side of the aerofoil, and then starts to recover, so that downstream of point M the boundary layer finds itself under an adverse pressure gradient. Its magnitude increases with increase of the angle of attack, and

the boundary layer separates at $\alpha = \alpha_s$.

When it happens, one can observe the appearance of a closed region of recirculating flow on the upper surface of the aerofoil (Fig. 15a). This region is referred to as a *short bubble.* Its length does not exceed 1% of the aerofoil chord, and therefore, has an extremely weak influence on the flow field and the values of the aerodynamic forces produced by the aerofoil. However, the short separation bubble only exists within an interval $\alpha \in (\alpha_s, \alpha_c)$, and when the angle of attack increases beyond α_c, the bubble suddenly *bursts.* As a result, a new flow regime is formed with an extended separation region which covers the entire upper surface of the aerofoil (Fig. 15b) or, at least, a significant part of it (Fig. 15c). In either case the flow transformation is accompanied by an abrupt decrease in the lift produced by the aerofoil and a significant increase in the drag. This phenomenon is known as the *leading edge stall.* If encountered in a real flight, the consequences are most likely to be catastrophic, which explains why the problem has been receiving undiminishing attention of aeronautic engineers.

We shall now proceed to the theoretical analysis of the described phenomenon.

3.1   Statement of the Problem. Inviscid-Flow Region

Let an aerofoil, placed in a two-dimensional flow of incompressible fluid, be of a relative thickness ε, so that its equation may be written as

$$y' = \begin{cases} \varepsilon Y_+(x') & \text{for the upper surface,} \\ \varepsilon Y_-(x') & \text{for the lower surface.} \end{cases} \tag{76}$$

Here we use Cartesian coordinate system $O'x'y'$ with the origin O' placed at the leading edge aerofoil and the x'-axis directed tangentially to the middle line of the aerofoil at its leading edge (shown as the dashed line in Figure 16). In what follows we shall use dimensionless variables; distances along the x' and y' axes are referred to the aerofoil chord c, the velocity components to the free-stream velocity V_∞, and the increment in pressure (relative to its value at infinity) to ρV_∞^2. In this study the fluid density ρ is assumed constant all over the flow field.

We shall further assume that the nose of the aerofoil is parabolic, in which case the scaling parameter ε in (76) may be chosen such that

$$Y_\pm(x') = \pm\sqrt{2x'} + \cdots \quad \text{as} \quad x' \to 0.$$

With this choice the radius of the curvature of the leading edge appears to be $r = c\varepsilon^2$.
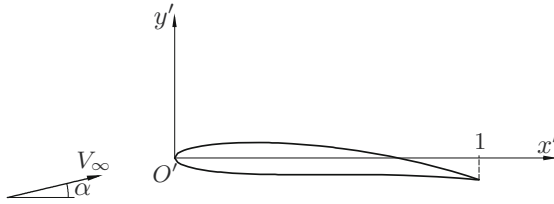
Figure 16. Incompressible flow past a thin aerofoil.

In what follows the flow past the aerofoil will be investigated using the asymptotic analysis of the Navier-Stokes equations with a limit procedure, where the Reynolds number, based on the radius of the leading edge of the profile, tends to infinity, and the thickness of the aerofoil tends to zero, i.e.

$$Re = \frac{V_\infty r}{\nu} \to \infty, \qquad \varepsilon \to 0.$$

Here ν is the kinematic viscosity of the fluid.

Following the routine of the method of matched asymptotic expansions, we have to consider first the main inviscid-flow region whose dimensions are comparable with the aerofoil chord: $x' = O(1)$, $y' = O(1)$. If the angle of attack α is an order ε quantity, that is it can be expressed as

$$\alpha = \varepsilon \alpha_*,$$

with $\alpha_* = O(1)$, then the flow in this region can be described by the classical thin aerofoil theory. The asymptotic expansions for the velocity components (u, c) and pressure p are written as.

$$u = 1 + \varepsilon\, u_1(x, y) + \cdots, \qquad v = \varepsilon\, v_1(x, y) + \cdots, \qquad p = \varepsilon\, p_1(x, y) + \cdots.$$
$$(77)$$

Substituting (77) into the Navier-Stokes equations, and assuming that $\varepsilon \to 0$ and $Re \to \infty$, one can find that the pressure p_1 satisfies the Laplace equation

$$\frac{\partial^2 p_1}{\partial x^2} + \frac{\partial^2 p_1}{\partial y^2} = 0.$$

The solution of this equation, satisfying the impermeability condition of the aerofoil surface and Kutta condition at the trailing edge of the aerofoil, is

written as

$$
p_1(x, 0\pm) = \frac{1}{2\pi} \int\limits_0^1 \frac{Y'_+(\zeta) - Y'_-(\zeta)}{\zeta - x} d\zeta \pm
$$

$$
\pm \sqrt{\frac{1-x}{x}} \left[-\alpha_* + \frac{1}{2\pi} \int\limits_0^1 \sqrt{\frac{\zeta}{1-\zeta}} \frac{Y'_+(\zeta) + Y'_-(\zeta)}{\zeta - x} d\zeta \right].
\tag{78}
$$

Here "plus" corresponds to the upper surface of the aerofoil and "minus" to the lower.

The asymptotic expansion for the pressure in (77) shows that the pressure perturbations in the main inviscid-flow region are too small to the cause the boundary-layer separation. However, the solution in this region develops a singularity near the leading edge. Indeed, it follows from (78) that

$$
p_1(x, 0\pm) = \pm \frac{k}{\sqrt{2x'}},
$$

where

$$
k = \sqrt{2} \left(\alpha_* + \frac{1}{\pi} \int\limits_0^1 \frac{G(x')}{\sqrt{x'(1-x')}} dx' \right), \qquad G = -\frac{1}{2} \left(\frac{dY_+}{dx'} + \frac{dY_-}{dx'} \right). \tag{79}
$$

Consequently, the inviscid flow should be reexamined a region, where

$$
x' = \varepsilon^2 X', \qquad y' = \varepsilon^2 Y',
$$

with X' and Y' being order one quantities. In this new region (in what follows we shall call it region 1) the aerofoil contour is represented by the infinite parabola $Y' = \pm\sqrt{2X'}$; see Figure 17. The tangential component of the velocity vector on the surface of the parabola is given by

$$
U_e = \frac{Y' + k}{\sqrt{Y'^2 + 1}}. \tag{80}
$$

Here Y' is the distance from the point on the surface of the parabola where U_e is calculated to the X'-axis; parameter k measures the degree of non-symmetry of the flow. It is related to the angle of attack and aerofoil shape through equation (79). It is easily seen from (80) that at the stagnation point $Y' = -k$. Differentiating (80) and setting the derivative to zero, one can find that the maximum of the velocity is achieved at the point where $Y' = 1/k$.
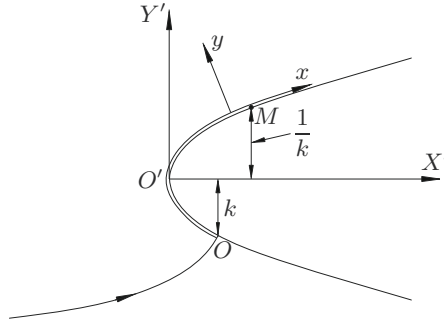
Figure 17. The flow near the leading edge of a thin aerofoil.

3.2   Boundary Layer

When analysing the fluid motion in the boundary layer, that forms on the aerofoil surface near its leading edge, it is convenient to use the "body-fitted" coordinates. These are curvilinear orthogonal coordinate (x, y) with x measured along the the aerofoil surface from the front stagnation point O, as shown in Figure 17, and y in the direction normal to the aerofoil contour. We shall denote the velocity components in these coordinates as V_τ and V_n, respectively, and the stream function as ψ. All the variables are assumed dimensionless. We take the radius $r = \varepsilon^2 c$ of the leading edge of the aerofoil as the unit of length; the velocity components are referred to V_∞, the stream function to rV_∞ and the pressure increment with respect to its value in the free-stream, p_∞ is referred to ρV_∞^2. The Navier-Stokes equations written in these coordinates have the form

$$
\frac{V_\tau}{H_1}\frac{\partial V_\tau}{\partial x} + V_n\frac{\partial V_\tau}{\partial y} + \frac{\kappa V_\tau V_n}{H_1} = -\frac{1}{H_1}\frac{\partial p}{\partial x} + \frac{1}{Re}\left[\frac{1}{H_1}\frac{\partial}{\partial x}\left(\frac{1}{H_1}\frac{\partial V_\tau}{\partial x}\right) + \right.
$$
$$
\left. +\frac{\partial^2 V_\tau}{\partial y^2} + \kappa\frac{\partial}{\partial y}\left(\frac{V_\tau}{H_1}\right) + \frac{\kappa}{H_1^2}\frac{\partial V_n}{\partial x} + \frac{1}{H_1}\frac{\partial}{\partial x}\left(\frac{\kappa V_n}{H_1}\right)\right],
$$
(81a)

$$
\frac{V_\tau}{H_1}\frac{\partial V_n}{\partial x} + V_n\frac{\partial V_n}{\partial y} - \frac{\kappa V_\tau^2}{H_1} = -\frac{\partial p}{\partial y} + \frac{1}{Re}\left[\frac{1}{H_1}\frac{\partial}{\partial x}\left(\frac{1}{H_1}\frac{\partial V_n}{\partial x}\right) + \right.
$$
$$
\left. +\frac{\partial^2 V_n}{\partial y^2} + \kappa\frac{\partial}{\partial y}\left(\frac{V_n}{H_1}\right) - \frac{\kappa}{H_1^2}\frac{\partial V_\tau}{\partial x} - \frac{1}{H_1}\frac{\partial}{\partial x}\left(\frac{\kappa V_\tau}{H_1}\right)\right],
$$
(81b)

$$
\frac{1}{H_1}\frac{\partial V_\tau}{\partial x} + \frac{\partial V_n}{\partial y} + \frac{\kappa V_n}{H_1} = 0.
$$
(81c)

Here κ is the local curvature of the body contour, and H_1 is the Lamé coefficient,

$$H_1 = 1 + \kappa(x)y.$$

The velocity components are related to the stream function through the equations

$$\frac{\partial \psi}{\partial x} = -H_1 V_n, \qquad \frac{\partial \psi}{\partial y} = V_\tau. \tag{82}$$

In the boundary layer the asymptotic expansion of the stream function has the form

$$\psi = Re^{-1/2}\Psi(x, Y) + \cdots, \quad \text{with} \quad y = Re^{-1/2}Y. \tag{83}$$

Substitution of (83) into (82) and then into the Navier-Stokes equations (81), results in the classical boundary-layer equation

$$\frac{\partial \Psi}{\partial Y}\frac{\partial^2 \Psi}{\partial x \partial Y} - \frac{\partial \Psi}{\partial x}\frac{\partial^2 \Psi}{\partial Y^2} = -\frac{dp_e}{dx} + \frac{\partial^3 \Psi}{\partial Y^3}. \tag{84a}$$

It should be solved with the initial condition at the stagnation point O,

$$\Psi = 0 \quad \text{at} \quad x = 0, \tag{84b}$$

no-slip conditions on the aerofoil surface,

$$\Psi = \frac{\partial \Psi}{\partial Y} = 0 \quad \text{at} \quad Y = 0, \tag{84c}$$

and the matching condition with the solution in the inviscid flow region,

$$\frac{\partial \Psi}{\partial Y} = U_e(x) \quad \text{at} \quad Y = \infty. \tag{84d}$$

The pressure gradient dp_e/dx on the right hand side of equation (84a) does not depend on Y, and may be calculated with the help of the Bernoulli equation,

$$p_e + \tfrac{1}{2}U_e^2 = \tfrac{1}{2}. \tag{85}$$

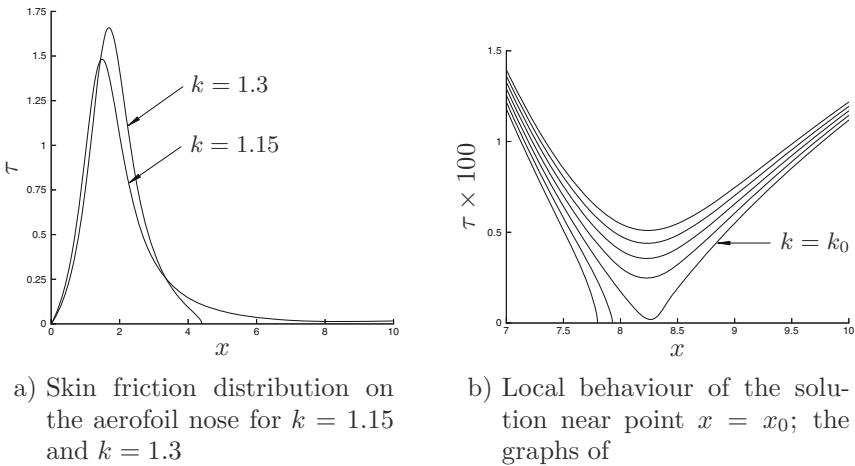Differentiating (85), we have

$$\frac{dp_e}{dx} = -U_e\frac{dU_e}{dx}.$$

Remind that the velocity at the outer edge of the boundary layer, $U_e(x)$, is given by equation (80). It is zero at the front stagnation point O, but

rapidly grows as the fluid flows around the leading edge of the aerofoil. It then reaches a maximum value of $\sqrt{1+k^2}$ at point M on the upper side of the aerofoil, for which $Y' = 1/k$; see Figure 17. Downstream from this point $U_e(x)$ shows monotonic decay, and tends to unity as $x \to \infty$.

The results of numerical solution of problem (84) are shown in Figures 18 in the form of the skin friction distribution along the aerofoil surface. The skin friction is calculated as

$$\tau = \left.\frac{\partial^2 \Psi}{\partial Y^2}\right|_{Y=0}.$$

(86)

It appears that there exists a critical value of parameter $k = k_0 = 1.1575$. If $k > k_0$, then the solution terminates at a finite position where the skin friction turns zero and the Goldstein (1948) singularity develops in the solution. The larger the parameter k, the earlier on the aerofoil surface the singularity is encountered.

a) Skin friction distribution on the aerofoil nose for $k = 1.15$ and $k = 1.3$

b) Local behaviour of the solution near point $x = x_0$; the graphs of

Figure 18. Results of the numerical solution of problem (84).

If, on the other hand, $k < k_0$, then the solution exists for all values of x. Interestingly enough, in this case the skin friction develops a minimum, which tends to zero as $k \to k_0 - 0$. We denote the coordinate of the point where τ first becomes zero by x_0. The calculations show that for the boundary layer on the parabola surface $x_0 = 8.265$.

The solution ahead of the point of zero skin friction   According to the classical viewpoint dating back to the original work of Prandtl (1904),

the position of zero skin friction on the body surface gives the position of flow separation. It is therefore of considerable interest to study the behaviour of the solution of the problem (84) in the vicinity of this point.

We shall denote the point of zero skin friction as x_s. For $k > k_0$ it lies upstream of x_0, and tends to x_0 as $k \to k_0 + 0$. We first consider the region lying before the line $x = x_s$; our task will be to find an asymptotic expansion of the stream function Ψ as $x \to x_s - 0$. At any point (x, Y) in the region upstream of $x = x_s$, the longitudinal velocity component $u = \partial \Psi / \partial Y$ is positive. Consequently, the boundary-layer equation (84a) possesses the standard properties of equations of parabolic type. Its solution $\Psi(x, Y)$ near the line $x = x_s$ depends upon the velocity distribution $U_e(x)$ at the outer edge of the boundary layer throughout the whole range of values of x from the stagnation point O to the point $x = x_s$ of zero skin friction. On the other hand, the asymptotic procedure utilised below is restricted to analysis of a small vicinity of the line $x = x_s$ only, and therefore, does not take into account all the boundary conditions affecting the solution for $\Psi(x, Y)$. This means that the sought asymptotic expansion of $\Psi(x, Y)$ must be based on the eigensolutions of the local problem. The coefficients multiplying the eigenfunctions remain arbitrary from the viewpoint of the local analysis. At the same time, they can be determined uniquely if the solution of the problem (84) is constructed in the entire region $x \in [0, x_s)$.

We start by noticing that the pressure gradient dp_e/dx is a smooth function. Near point $x = x_s$ it may be represented in the form of Taylor expansion

$$\frac{dp_e}{dx} = \lambda_0 + \lambda_1 s + \cdots \quad \text{as} \quad s \to \infty. \tag{87}$$

Here $s = x - x_s$ is the distance from the point $x = x_s$. The leading order term, λ_0 in (87) coincides with the pressure gradient at point $x = x_s$. For all $k \le k_0$, when the zero skin point exists, $\lambda_0 > 0$.

Setting $Y = 0$ in (84a) and using the no-slip conditions (84c), it is easy to find that at any point on the aerofoil surface

$$\frac{\partial^3 \Psi}{\partial Y^3} = \frac{dp_e}{dx}. \tag{88}$$

At the point of zero skin friction, in addition to the no-slip conditions (84a) we also know that

$$\tau(x_s) = \left. \frac{\partial^2 \Psi}{\partial Y^2} \right|_{Y=0} = 0. \tag{89}$$

Substituting (87) into (88), and integrating the resulting equation with (84a) and (89), we find that the leading order term of the asymptotic rep-

resentation of $\Psi(x, Y)$ near the point $x = x_s$ may be written as

$$\Psi = \tfrac{1}{6}\lambda_0 Y^3 + \cdots . \tag{90}$$

We can now determine the thickness of the viscous flow region that forms inside the boundary layer upstream of the point $x = x_s$. In this region the viscous term on the right hand side of equation (84a) should be comparable with either term on the left hand side of (84a). Using, for example, the first of these, we can write

$$\frac{\partial \Psi}{\partial Y}\frac{\partial^2 \Psi}{\partial x \partial Y} \sim \frac{\partial^3 \Psi}{\partial Y^3}. \tag{91}$$

It follows from (90) that the coefficient $\partial \Psi/\partial Y$ in the convective term on the left hand side of (91) may be estimated as an order $O(Y^2)$ quantity, which allows to express (91) in a more simple form,

$$Y^2 \frac{\partial^2 \Psi}{\partial x \partial Y} \sim \frac{\partial^3 \Psi}{\partial Y^3}. \tag{92}$$

Approximating the derivatives in (92) by finite differences, we arrive at a simple algebraic equation

$$Y^2 \frac{\Psi}{(x - x_s)Y} \sim \frac{\Psi}{Y^3}$$

which, being solved for Y, shows that the thickness of the viscous region decreases, as the point $x = x_s$ is approached, according to the law

$$Y = O\big[(-s)^{1/4}\big]. \tag{93}$$

Guided by (90) and (93), we seek the asymptotic expansion of $\Psi(x, Y)$ in the viscous region in the form

$$\Psi(x, Y) = (-s)^{3/4}\tfrac{1}{6}\lambda_0 \eta^3 + (-s)^\alpha f_1(\eta) + (-s)^{2\alpha - 3/4} f_2(\eta) + \cdots \quad \text{as} \quad s \to -0. \tag{94}$$

The first term in (94) is obtained by simply expressing (90) in terms of a new independent variable

$$\eta = \frac{Y}{(-s)^{1/4}}, \tag{95}$$

which, according to (93) remains an order one quantity in the viscous region. The second term represents an eigenfunction with an unknown eigenvalue α. The third term is a forced term, arising in the expansion (94) due to the nonlinearity of the boundary-layer equation (84a).

Substituting (94) together with (95) into (84a), and setting $s \to -0$, we find that function $f_1(\eta)$ satisfies the following ordinary differential equation

$$f_1''' - \frac{1}{8}\lambda_0\eta^3 f_1'' + \frac{1}{2}\lambda_0\left(\alpha + \frac{1}{4}\right)\eta^2 f_1' - \lambda_0\alpha\eta f_1 = 0. \qquad (96)$$

As the region considered adjoins the aerofoil surface, we pose the no-slip conditions

$$f_1(0) = f_1'(0) = 0, \qquad (97)$$

which are deduced by substituting (94), (95) into (84c).

Equation (96) is linear and homogeneous. Three complementary solutions to this equation, $f_{11}(\eta)$, $f_{12}(\eta)$ and $f_{13}(\eta)$, can be chosen such that

$$
\begin{aligned}
f_{11}(0) &= 1, & f_{11}'(0) &= 0, & f_{11}''(0) &= 0, \\
f_{12}(0) &= 0, & f_{12}'(0) &= 1, & f_{12}''(0) &= 0, \\
f_{13}(0) &= 0, & f_{13}'(0) &= 0, & f_{13}''(0) &= 1.
\end{aligned}
\qquad (98)
$$

The first two solutions do not satisfy the boundary conditions (97) and must be rejected. As for the third solution, it can easily be verified by direct substitution into (96) to be simply $f_{13} = \frac{1}{2}\eta^2$. Hence, a non-trivial solution of equation (96) with boundary conditions (97) exists for all α, and may be written in the form

$$f_1(\eta) = \tfrac{1}{2}a_0\eta^2, \qquad (99)$$

where a_0 is an arbitrary constant.

In order to determine the eigenvalue α, it is necessary to consider the third term of the expansion (94). It satisfies the equation

$$f_2''' - \frac{1}{8}\lambda_0\eta^3 f_2'' + \lambda_0\left(\alpha - \frac{1}{4}\right)\eta^2 f_2' - \lambda_0\left(2\alpha - \frac{3}{4}\right)\eta f_2 = \frac{1}{4}(1-2\alpha)a_0^2\eta^2, \quad (100)$$

which also has to be solved with the no-slip conditions

$$f_2(0) = f_2'(0) = 0. \qquad (101)$$

Equation (100) is not homogeneous; in addition to three complementary solutions, $f_{21}(\eta)$, $f_{22}(\eta)$ and $f_{22}(\eta)$, of the homogeneous part of the equation, it requires a particular integral, $f_{2p}(\eta)$. We can choose, for example,

$$f_{2p}(\eta) = \frac{a_0^2}{2\lambda_0}\eta,$$

and then the general solution to (100) is written as

$$f_2(\eta) = C_1 f_{21}(\eta) + C_2 f_{22}(\eta) + C_3 f_{23}(\eta) + \frac{a_0^2}{2\lambda_0}\eta. \qquad (102)$$

Here C_1, C_2 and C_3 are arbitrary constants. Choosing again the complementary solutions according to rule

$$
\begin{aligned}
f_{21}(0) &= 1, & f_{21}'(0) &= 0, & f_{21}''(0) &= 0, \\
f_{22}(0) &= 0, & f_{22}'(0) &= 1, & f_{22}''(0) &= 0, \\
f_{23}(0) &= 0, & f_{23}'(0) &= 0, & f_{23}''(0) &= 1,
\end{aligned}
$$

and applying the no-slip conditions (101), we find

$$C_1 = 0, \qquad C_2 = -\frac{a_0^2}{2\lambda_0}.$$

Taking further into account that $f_{23}(\eta) = \frac{1}{2}\eta^2$, we can express (102) in the form

$$f_2(\eta) = \frac{a_0^2}{2\lambda_0}(\eta - f_{22}) + \frac{1}{2}b_0\eta^2, \qquad (103)$$

with constant $b_0 = C_3$ remaining arbitrary.

Our task now will be to determine the function $f_{22}(\eta)$. It satisfies the homogenous version of equation (100), namely,

$$f_{22}''' = \frac{1}{8}\lambda_0\eta^3 f_{22}'' - \lambda_0\left(\alpha - \frac{1}{4}\right)\eta^2 f_{22}' + \lambda_0\left(2\alpha - \frac{3}{4}\right)\eta f_{22}, \qquad (104)$$

which should be solved with the initial conditions

$$f_{22}(0) = 0, \qquad f_{22}'(0) = 1, \qquad f_{22}''(0) = 0. \qquad (105)$$

If one wants to find $f_{22}(\eta)$ in the form of the power series, then in view of (105) the first term should be written as

$$f_{22}(\eta) = \eta + \cdots . \qquad (106)$$

Using (106) on the right hand side of (104), we find

$$f_{22}''' = \lambda_0\left(\alpha - \frac{1}{2}\right)\eta^2 + \cdots .$$

Integration of this equation with conditions (105) yields the second term in (106),

$$f_{22}(\eta) = \eta + \frac{\lambda_0}{5!}(2\alpha - 1)\eta^5 + \cdots .$$

This procedure can be repeated, leading to a conclusion that the power series for $f_{22}(\eta)$ has the form

$$f_{22}(\eta) = \sum_{n=0}^{\infty} c_n \eta^{4n+1}, \tag{107}$$

where $c_0 = 1$.

A recurrent equation for the coefficients c_n of the series is obtained by substituting $c_n \eta^{4n+1}$ into the right hand side of the equation (104) and $c_{n+1} \eta^{4n+5}$ into its left hand side. We find that

$$c_{n+1} = \frac{\lambda_0}{32} \frac{\left[n - (2\alpha - 1)\right]\left(n - \frac{1}{4}\right)}{\left(n + \frac{3}{4}\right)\left(n + \frac{5}{4}\right)(n+1)} c_n.$$

Using the method of mathematical induction, it may be shown that

$$c_n = -\left(\frac{\lambda_0}{32}\right)^n \frac{(1 - 2\alpha)_n}{(5/4)_n (4n - 1) n!}.$$

Here $(a)_n$ denotes a quantity defined as

$$(a)_n = a(a+1)(a+2)\ldots(a+n-1), \qquad (a)_0 = 1. \tag{108}$$

It may be expressed in terms of the Euler Gamma function[3],

$$(a)_n = \frac{\Gamma(a+n)}{\Gamma(a)}.$$

Therefore,

$$c_n = -\frac{\Gamma(5/4)}{\Gamma(1 - 2\alpha)}\left(\frac{\lambda_0}{32}\right)^n \frac{\Gamma(n + 1 - 2\alpha)}{\Gamma(n + 5/4)(4n - 1) n!}. \tag{109}$$

It remains to substitute (109) back into (107), and we will have

$$f_{22}(\eta) = -\frac{\Gamma(5/4)}{\Gamma(1 - 2\alpha)} \sum_{n=0}^{\infty}\left(\frac{\lambda_0}{32}\right)^n \frac{\Gamma(n + 1 - 2\alpha)}{\Gamma(n + 5/4)(4n - 1) n!} \eta^{4n+1}. \tag{110}$$

Now our task will be to determine the asymptotic behaviour of $f_{22}(\eta)$ as $\eta \to \infty$. For this purpose we shall express $f_{22}(\eta)$ through the Kummer's

---

[3]Here we use a well known property of the Gamma function, $z\Gamma(z) = \Gamma(z + 1)$.

function $M(a, b, z)$, whose properties are well known[4]. Remind that the Kummer's function is a solution of the confluent hypergeometric equation

$$z\frac{d^2w}{dz^2} + (b - z)\frac{dw}{dz} - aw = 0,$$

which remains regular at point $z = 0$. In fact, it may be represented by the Taylor series

$$M(a, b, z) = 1 + \frac{a}{b}z + \frac{(a)_2}{(b)_2 2!}z^2 + \cdots + \frac{(a)_n}{(b)_n n!}z^n + \cdots =$$
$$= \frac{\Gamma(b)}{\Gamma(a)}\sum_{n=0}^{\infty}\frac{\Gamma(a + n)}{\Gamma(b + n)\,n!}z^n \tag{111}$$

convergent at any finite point z in the complex plane.

It may be easily verified that the series (111) for the Kummer function $M(a, b, z)$ may be converted into the series (110) for function $f_{22}(\eta)$ with the help of the following integral transformation,

$$f_{22}(\eta) = \eta - \eta^2\int_0^{\eta}\xi^{-2}\left[M\left(1 - 2\alpha, \frac{5}{4}, \frac{\lambda_0}{32}\xi^4\right) - 1\right]d\xi. \tag{112}$$

In general case the Kummer's function grows exponentially

$$M(a, b, z) = \frac{\Gamma(b)}{\Gamma(a)}e^z z^{a-b} + \cdots \tag{113}$$

as z tends to infinity along a ray that lies in the right half ($\Re z > 0$) of the complex plane z. Through (112) this makes function $f_{22}(\eta)$ also to grow exponentially as $\eta \to \infty$. However, if

$$a = -m, \qquad m = 0,\ 1,\ 2\ldots, \tag{114}$$

then $\Gamma(a) = 0$, and formula (113) cannot be used. In this case $(a)_{m+1}$ and all the subsequent members of the sequence (108) vanish, reducing the Taylor expansion (111) to a polynomial of degree m.

It is important to notice that regardless of the choice of parameter a, the solution (94), (99), (103), (112) for the viscous region does not satisfy the boundary condition (84d) at the outer edge of the boundary layer. Therefore, in addition to viscous region (which is shown as region $2a$ in Figure 19),

---

[4]See, for example, Abramowitz & Stegun (1965).
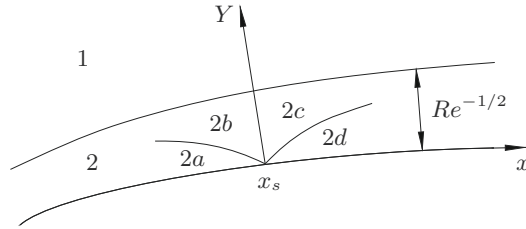
Figure 19. Asymptotic regions' layout near the point of zero skin friction.

it is necessary to consider the main part of the boundary layer (region 2b), where the asymptotic analysis of the boundary-layer equations (84) is based on the limit

$$Y = O(1), \qquad s = x - x_s \to 0 - .$$

Since the boundary layer, we are dealing with, is exposed to a finite pressure gradient, the fluid velocity in region 2b should remain finite. It cannot be matched with the exponentially growing solution in region 2a. Hence, an acceptable solution for region 2a may only be obtained under the condition (114). Setting $a = 1 - 2\alpha$ in (114), leads to a conclusion that the sought eigenvalues are

$$\alpha = \frac{m+1}{2}, \qquad m = 0, \, 1, \, 2 \dots . \tag{115}$$

Goldstein's singularity   Let us now return to the expansion (94). As any other asymptotic expansion, it should obey the rule that each subsequent term in (94) should be smaller than the previous one. This requirement is satisfied if $\alpha > 3/4$. Consequently, the first eigenvalue is

$$\alpha = 1.$$

The coefficient a_0 in the eigenfunction (99) depends on the distribution of the velocity $U_e(x)$ at the outer edge of the boundary layer on the entire interval $x \in [0, x_s]$. We shall see that through special adjustment of $U_e(x)$ the coefficient a_0 may be made zero. However, in general case $a_0 \neq 0$, and the solution (94), (99), (103), (112) in region 2a assumes the form

$$\Psi(x, Y) = (-s)^{3/4} \tfrac{1}{6} \lambda_0 \eta^3 + (-s) f_1(\eta) + (-s)^{5/4} f_2(\eta) + \cdots ,$$
$$f_1(\eta) = \tfrac{1}{2} a_0 \eta^2, \qquad f_2(\eta) = \tfrac{1}{2} b_0 \eta^2 - \frac{a_0^2}{240} \eta^5 . \tag{116}$$

In addition to the terms shown, the expansion (116) contains the sum of an infinite number of successive eigenfunctions, and also includes additional terms produced by the higher order terms in the expansion of the pressure gradient (87). All of these, however, are small as compared to $(-s)^{5/4}f_2(\eta)$ and can be disregarded.

Let us now turn to region 2b, where $Y = O(1)$; see Figure 19. The form of the asymptotic expansion of the stream function $\Psi(x, Y)$ in this region may be determined with the help of the following standard procedure based on the principle of matched asymptotic expansions. We perform the change of variables $\eta = Y/(-s)^{1/4}$ in (116) and, assuming $Y = O(1)$, collect terms of the same order as $s \to 0-$. We find

$$\Psi(x, Y) = \left\{ \frac{1}{6}\lambda_0 Y^3 - \frac{a_0^2}{240}Y^5 + \cdots \right\} + (-s)^{1/2}\left\{ \frac{1}{2}a_0 Y^2 + \cdots \right\} + O\left[(-s)^{3/4}\right].$$

This suggests that the solution in region 2b should be sought in the form

$$\Psi(x, Y) = \Psi_{00}(Y) + (-s)^{1/2}\Psi_{01}(Y) + \cdots \quad \text{as} \quad s \to 0-, \qquad (117)$$

where functions $\Psi_{00}(Y)$ and $\Psi_{01}(Y)$ are such that

$$\left.\begin{aligned} \Psi_{00}(Y) &= \frac{1}{6}\lambda_0 Y^3 - \frac{a_0^2}{240}Y^5 + \cdots, \\ \Psi_{01}(Y) &= \frac{1}{2}a_0 Y^2 + \cdots \end{aligned}\right\} \quad \text{as} \quad Y \to 0. \qquad (118)$$

With (117) the four terms in the boundary-layer equation (84a) are calculated as

$$\frac{\partial \Psi}{\partial Y}\frac{\partial^2 \Psi}{\partial x \partial Y} = -\tfrac{1}{2}(-s)^{-1/2}\Psi'_{00}\Psi'_{01} + \cdots, \qquad \frac{dp_e}{dx} = \lambda_0 + \cdots,$$

$$\frac{\partial \Psi}{\partial x}\frac{\partial^2 \Psi}{\partial Y^2} = -\tfrac{1}{2}(-s)^{-1/2}\Psi_{01}\Psi''_{00} + \cdots, \qquad \frac{\partial^3 \Psi}{\partial Y^3} = \Psi'''_{00} + \cdots.$$

Clearly, the pressure gradient and the viscous term lose their significance as $s \to 0-$, and equation (84a) reduces to

$$\Psi'_{00}\Psi'_{01} - \Psi_{01}\Psi''_{00} = 0.$$

Rearranging this equation as

$$\left(\frac{\Psi_{01}}{\Psi'_{00}}\right)' = 0,$$

and integrating it with the initial conditions (118), we find

$$\Psi_{01} = \frac{a_0}{\lambda_0} \Psi'_{00}(Y). \tag{119}$$

Of course, the velocity profile $\Psi'_{00}(Y)$ at the point of zero skin friction, $x = x_s$, may be only found by calculating the boundary-layer equations (84) from the stagnation point $x = 0$ to the point $x = x_s$.

Substitution of (119) back into (117) renders the solution in region $2b$ in the form

$$\Psi(x,Y) = \Psi_{00}(Y) + (-s)^{1/2} \frac{a_0}{\lambda_0} \Psi'_{00}(Y) + \cdots \quad \text{as} \quad s \to 0-. \tag{120}$$

If we now substitute (84) into (83) and make use of (120), then we will find that the tangential and normal velocity components in region $2b$ are

$$V_\tau = \Psi'_{00}(Y) + \cdots, \qquad V_n = Re^{-1/2}(-s)^{-1/2} \frac{a_0}{2\lambda_0} \Psi'_{00}(Y) + \cdots.$$

We see that V_n develops a singularity on approach to point $x = x_s$. Singular behaviour is exhibited by other fluid functions as well. Let us, for example, calculate the skin friction (86). For this purpose we have to use the solution (116) in region $2a$. We find

$$\tau = (-s)^{1/2} a_0 + O[(-s)^{3/4}] \quad \text{as} \quad s \to 0-.$$

Since the skin friction τ is always positive upstream of the point $x = x_s$ (see Figure 18), we have to conclude that $a_0 > 0$.

The square root form of the singularity at the position of zero skin friction was first predicted by Landau & Lifshitz (1944). Four years later Goldstein (1948) confirmed their conclusions based on a more rigorous analysis of the boundary-layer equations. Goldstein also demonstrated that if the solution develops this form of singularity, then it cannot be continued downstream of the point of zero skin friction.

Indeed, let us assume that the continuation is possible. Then, keeping in mind that the solution of the boundary-layer equation (84a) is sought in the class of continuous functions, we have to assume that the leading order term of the asymptotic expansion of the stream function $\Psi(x,Y)$ in region $2c$ (see Figure 19) is written as

$$\Psi(x,Y) = \Psi_{00}(Y) + \cdots \quad \text{as} \quad s \to 0+, \quad Y = O(1). \tag{121}$$

The velocity profile in the boundary-layer cross-section $x = x_s$ is given by the derivative $\Psi'_{00}(Y)$. According to (118), near the aerofoil surface it

behaves as $\Psi'_{00}(Y) = \frac{1}{2}Y^2$. Therefore, the thickness of the viscous region $2d$ (see Figure 19) may be estimated using again equation (92). We find that $Y \sim s^{1/4}$, which means that the asymptotic analysis of the boundary-layer equation (84a) is based in region $2d$ on the limit

$$s = x - x_s \to 0+, \qquad \xi = \frac{Y}{s^{1/4}} = O(1).$$

We shall seek the stream function in this region in the form of the asymptotic expansion

$$\Psi(x, Y) = s^{3/4}\tfrac{1}{6}\lambda_0\xi^3 + s^{\mu}\hat{f}_1(\xi) + s^{2\mu-3/4}\hat{f}_2(\xi) + \cdots, \qquad (122)$$

with the exponent μ being unknown in advance. The functions $\hat{f}_1(\xi)$ and $\hat{f}_2(\xi)$ are determined in the same way as the functions $f_1(\eta)$ and $f_2(\eta)$ in the solution (94) for region $2a$. We have

$$\hat{f}_1 = \tfrac{1}{2}\hat{a}_0\xi^2, \qquad (123)$$

$$\hat{f}_2 = \frac{\hat{a}_0^2}{2\lambda_0}\xi^2 \int_0^\xi \zeta^{-2}\left[M\left(1 - 2\mu, \frac{5}{4}, -\frac{\lambda_0}{32}\zeta^4\right) - 1\right]d\zeta + \tfrac{1}{2}\hat{b}_0\xi^2, \qquad (124)$$

where $\hat{a}_0$ and $\hat{b}_0$ are arbitrary constants.

It remains to carry out the matching of the solutions in regions $2c$ and $2d$. In order to perform this procedure it is necessary to determine the asymptotic behaviour of the function $\hat{f}_2(\xi)$ at the outer edge of region $2d$. It is known the asymptotic behaviour of the Kummer's function $M(a, b, z)$ depends on a choice of the ray along which z tends to infinity. If the ray lies in the left half-plane ($\Re z < 0$), then

$$M(a, b, z) = \frac{\Gamma(b)}{\Gamma(b - a)}(-z)^{-a}\left[1 + O\left(\frac{1}{z}\right)\right].$$

Using this formula in (124), we find that

$$\hat{f}_2 = \frac{\hat{a}_0^2}{2\lambda_0}\frac{\Gamma(5/4)}{\Gamma(1/4 + 2\mu)}\left(\frac{\lambda_0}{32}\right)^{2\mu-1}\frac{\xi^{8\mu-3}}{8\mu - 5} + \cdots \quad \text{as} \quad \xi \to \infty. \qquad (125)$$

Finally, we substitute (123) and (125) into (122), and recall that $\xi = Y/s^{1/4}$. As a result we find that at the outer edge of region $2d$

$$\Psi = \tfrac{1}{6}\lambda_0 Y^3 + \frac{\hat{a}_0^2}{2\lambda_0}\frac{\Gamma(5/4)}{\Gamma(1/4 + 2\mu)}\left(\frac{\lambda_0}{32}\right)^{2\mu-1}\frac{Y^{8\mu-3}}{8\mu - 5} + \cdots. \qquad (126)$$

On the other hand, the asymptotic representation of the stream function $\Psi(x, Y)$ at the 'bottom' of region $2c$ has the form

$$\Psi = \tfrac{1}{6}\lambda_0 Y^3 - \frac{a_0^2}{240} Y^5 + \cdots . \tag{127}$$

It is obtained by using the first of formulae (118) in the solution (121) in region $2c$.

According to the principle of matched asymptotic expansions, expressions (126) and (127) should coincide with one another. This is only possible if $\mu = 1$ and[5]

$$\hat{a}_0^2 = -a_0^2. \tag{128}$$

While the constant a_0 is found in the process of solving the boundary-layer equation (84a) from the stagnation point $x = 0$ to the point of zero skin friction $x = x_s$, in order to find constant $\hat{a}_0$ one has to use equation (128). As this equation does not allow for a real solution, we can conclude that the solution of the boundary-layer equation (84a) only exists upstream of the line $x = x_s$ and cannot be extended beyond this line.

A Weaker Singularity   Remind that the behaviour of the boundary layer at the leading edge of the aerofoil depends on the parameter k, which is determined by the angle of attack and the profile shape by means of equation (79). If k exceeds the critical value $k_0 = 1.1575$, then the solution terminates at the point of zero skin friction, where the Goldstein singularity is encountered. If, on the other hand, k is smaller than k_0, then the skin friction stays positive and the solution exists for all $x > 0$. In this latter case the skin friction $\tau(x)$ develops a minimum when k becomes close enough to k_0. The value of the minimum decreases with the parameter k approaching k_0, as shown in Figure 18. Finally, when k reaches its critical value k_0, the minimal skin friction becomes zero at point $x_0 = 8.265$.

Let us denote the solution of the boundary-layer problem (84) at $k = k_0$ by $\Psi_0(x, Y)$, and study its behaviour near the point $x = x_0$ separately. We start by noting that the procedure used above for constructing the solution in the vicinity of the point of zero skin friction remains applicable for this particular case. However, one needs to bear in mind that the function $\Psi_0(x, Y)$ may thought of as the limit of the solution of the boundary-layer equation (84a) as $k \to k_0 - 0$. Since for all $k < k_0$ the solution continues through the line $x = x_0$, the same should be true for the limit solution

---

[5]In order to simplify the coefficient in the second term in (126) we used a well known property of the Gamma function, $\Gamma(1 + z) = z\Gamma(z)$.

$\Psi_0(x, Y)$. In view of equation (128), the latter is possible only if the coefficient a_0 in the first eigenfunction in the expansion (116) is zero.

This conjecture is confirmed by the numerical solution of boundary-layer equation (84a). We have seen that for all $k > k_0$, Goldstein's singularity develops in the solution at the point of zero skin friction $x = x_s$. However, as the parameter k decreases, the point of zero friction x_s moves downstream, approaching the point x_0. Simultaneously, the singularity becomes weaker, i.e. the coefficient a_0 decreases. At $k = k_0$ it becomes equal to zero, and the first eigenfunction in (116) disappears.

The second eigenvalue

$$\alpha = \frac{3}{2} \tag{129}$$

corresponds to $m = 2$ in (115). With (129) the solution in region $2a$ (see Figure 19) turns into

$$\Psi_0(x, Y) = (-s)^{3/4} \tfrac{1}{6} \lambda_0 \eta^3 + (-s)^{3/2} f_1(\eta) +$$
$$+ (-s)^{7/4} F_1(\eta) + (-s)^{9/4} f_2(\eta) + \cdots ,$$
$$f_1 = \tfrac{1}{2} a_0 \eta^2, \qquad F_1 = -\tfrac{1}{6} \lambda_1 \eta^3 + \frac{2\lambda_0 \lambda_1}{7!} \eta^7, \tag{130}$$
$$f_2 = \tfrac{1}{2} b_0 \eta^2 - \frac{a_0^2}{5!} \eta^5 + \frac{\lambda_0 a_0^2}{8!} \eta^9.$$

To maintain uniformity in notations we still denote the coefficient in the eigenfunction by a_0 as before; however, it should be kept in mind that now this is the coefficient multiplying the second eigenfunction. The appearance of an additional term $(-s)^{7/4} F_1(\eta)$ in the expansion (130) for $\Psi_0(x, Y)$ is related to the linear term $\lambda_1 s$ in the Taylor expansion of the pressure gradient (87).

The solution in region $2b$ (see Figure 19) is expressed by the asymptotic expansion

$$\Psi_0(x, Y) = \Psi_{00}(Y) + (-s)\Psi_{01}(Y) + \cdots \quad \text{as} \quad s \to 0 - . \tag{131}$$

Substituting (131) into the boundary-layer equation (84a), we find

$$-\Psi'_{00}\Psi'_{01} + \Psi_{01}\Psi''_{00} = -\lambda_0 + \Psi'''_{00},$$

or, equivalently,

$$\left(\frac{\Psi_{01}}{\Psi'_{00}}\right)' = \frac{\lambda_0 - \Psi'''_{00}}{\left(\Psi'_{00}\right)^2}.$$

Integration of this equation yields

$$\Psi_{01}(Y) = \Psi_{00}'(Y)\left[C - \int\limits_0^Y \frac{\Psi_{00}'''(Y') - \lambda_0}{\left[\Psi_{00}'(Y')\right]^2} dY'\right].\tag{132}$$

Matching the solution (131), (132) in region $2b$ with the solution (130) in region $2a$ shows, firstly, that the constant C in (132) is

$$C = \frac{a_0}{\lambda_0},\tag{133}$$

and secondly, that

$$\Psi_{00}(Y) = \tfrac{1}{6}\lambda_0 Y^3 + \frac{2\lambda_0\lambda_1}{7!}Y^7 + \frac{\lambda_0 a_0^2}{8!}Y^9 + \cdots \quad \text{as} \quad Y \to 0.\tag{134}$$

This completes the construction of the solution before the point of zero skin friction, $x = x_0$. It is interesting to notice that substitution of (133) into (132) and then into (131) yields an asymptotic representation of $\Psi_0(x, Y)$,

$$\Psi_0(x, Y) = \Psi_{00}(Y) + s\Psi_{00}'(Y)\left[\int\limits_0^Y \frac{\Psi_{00}'''(Y') - \lambda_0}{\left[\Psi_{00}'(Y')\right]^2} dY' - \frac{a_0}{\lambda_0}\right] + \cdots,\tag{135}$$

which proves to be valid both in region $2b$ and region $2a$; see Exercise 2.

Let us now show that this solution can be continued downstream of point $x = x_0$. We start with region $2c$ (see Figure 19), where $\Psi_0(x, Y)$ is sought in the form

$$\Psi_0(x, Y) = \Psi_{00}(Y) + s\widehat{\Psi}_{01}(Y) + \cdots \quad \text{as} \quad s \to 0+.\tag{136}$$

Function $\widehat{\Psi}_{01}(Y)$ is found through substitution of (136) into the boundary-layer equation (84a), and integrating the resulting equation for $\widehat{\Psi}_{01}(Y)$. We find

$$\widehat{\Psi}_{01}(Y) = \Psi_{00}'(Y)\left[\widehat{C} + \int\limits_0^Y \frac{\Psi_{00}'''(Y') - \lambda_0}{\left[\Psi_{00}'(Y')\right]^2} dY'\right].\tag{137}$$

In region $2d$ the solution is represented by the asymptotic expansion

$$\Psi_0(x, Y) = s^{3/4}\tfrac{1}{6}\lambda_0\xi^3 + s^{3/2}\hat{f}_1(\xi) + s^{7/4}\widehat{F}_1(\xi) + s^{9/4}\hat{f}_2(\xi) + \cdots$$
$$\text{as} \quad s \to 0+,\tag{138a}$$

with $\xi = Y/s^{1/4}$. Substituting (138a) into the boundary-layer equation (84a) and solving the resulting equations for $\hat{f}_1(\xi)$, $\widehat{F}_1(\xi)$ and $\hat{f}_2(\xi)$ with the no-slip conditions on the aerofoil surface (84c), we find

$$\hat{f}_1 = \tfrac{1}{2}\hat{a}_0\xi^2, \qquad \widehat{F}_1 = \tfrac{1}{6}\lambda_1\xi^3 + \frac{2\lambda_0\lambda_1}{7!}\xi^7,$$
$$\hat{f}_2 = \tfrac{1}{2}\hat{b}_0\xi^2 + \frac{\hat{a}_0^2}{5!}\xi^5 + \frac{\lambda_0\hat{a}_0^2}{8!}\xi^9. \tag{138b}$$

It remains to match the expansions (136) and (138). We recall that it is this procedure that was found impossible to perform when an attempt was made to extend the solution with Goldstein's singularity downstream from the point of zero friction. The matching resulted in equation (128), which could not be solved for $\hat{a}_0$ in terms of real numbers. Now instead of (128) we obtain

$$\hat{a}_0^2 = a_0^2. \tag{139}$$

The matching also shows that constant $\widehat{C}$ in (137) is given by

$$\widehat{C} = \frac{\hat{a}_0}{\lambda_0}. \tag{140}$$

Substitution of (140) back into (137) and then into (136) results in the formula

$$\Psi_0(x, Y) = \Psi_{00}(Y) + s\Psi'_{00}(Y)\left[\int_0^Y \frac{\Psi'''_{00}(Y') - \lambda_0}{\left[\Psi'_{00}(Y')\right]^2}dY' + \frac{\hat{a}_0}{\lambda_0}\right] + \cdots, \tag{141}$$

which, similar to (135), may be used not only in the main part of the boundary layer (region 2c) but also in the viscous sublayer (region 2d).

Equation (138) shows that the solution of the boundary-layer problem (84), which is unique before the point of zero friction, can be continued downstream of this point in two ways. The first one is given by

$$\hat{a}_0 = -a_0.$$

In this case the formulae (135) and (141) may be written together

$$\Psi_0(x, Y) = \Psi_{00}(Y) + s\Psi'_{00}(Y)\left[\int_0^Y \frac{\Psi'''_{00}(Y') - \lambda_0}{\left[\Psi'_{00}(Y')\right]^2}dY' - \frac{a_0}{\lambda_0}\right] + O(s^2), \tag{142}$$

showing that the solution is smooth in the vicinity of the point of zero skin friction, $x = x_0$. It follows from (142) that the skin friction changes sign at

this point, namely,

$$\tau = \frac{\partial^2 \Psi_0}{\partial Y^2}\bigg|_{Y=0} = -a_0 s + O(s^2), \tag{143}$$

showing that a region of reverse flow forms downstream of $x = x_0$. Solutions of this kind are typical for the triple-deck theory. In particular, in the first part of this presentation we were dealing with the self-induced separation of the boundary layer in supersonic flow. Figure 14 shows a smooth behaviour of the flow near the separation point.

However, there exists a second branch of the solution with

$$\hat{a}_0 = a_0.$$

In this case, combining (135) and (141) together, we have

$$\Psi_0 = \Psi_{00}(Y) + \Psi'_{00}(Y)\left[\frac{a_0}{\lambda_0}|s| + s\int\limits_0^Y \frac{\Psi'''_{00}(Y') - \lambda_0}{\left[\Psi'_{00}(Y')\right]^2}dY'\right] + O(s^2). \tag{144}$$

This solution has a singularity at $x = x_0$. In particular, let us calculate the angle $\theta = \arctan(V_n/V_\tau)$ made by the streamlines with the aerofoil contour. It follows from (82), (83) and (144) that

$$\theta = Re^{-1/2}\Theta, \tag{145a}$$

where

$$\Theta = -\frac{\partial \Psi_0/\partial x}{\partial \Psi_0/\partial Y} = -\frac{a_0}{\lambda_0}\mathrm{sign}(s) + \int\limits_0^Y \frac{\lambda_0 - \Psi'''_{00}(Y')}{\left[\Psi'_{00}(Y')\right]^2}dY' + O(s). \tag{145b}$$

We can see that Θ has a discontinuity at $x = x_0$.

It further follows from (144) that the skin friction

$$\tau = a_0|s| + O(s^2) \quad \text{as} \quad s \to 0. \tag{146}$$

A characteristic minimum in the distribution of the skin friction (146) shows that it is the singular solution (144) that represents the limiting solution of the boundary-layer equations (84) as $k \to k_0 - 0$.

The formation of the singularity in the boundary layer   Let us now see what happens if the parameter k does not coincide with its critical value

k_0 but the difference $\Delta k = k - k_0$ is small. In this case the velocity at the outer edge of the boundary layer (80) may be represented by the Taylor expansion

$$U_e(x, k) = U_{e,0}(x) + \Delta k U_{e,1}(x) + O[(\Delta k)^2], \qquad (147)$$

where

$$U_{e,0}(x) = U_e(x, k_0), \qquad U_{e,1}(x) = \left.\frac{\partial U_e(x, k)}{\partial k}\right|_{k=k_0}.$$

Using the Bernoulli equation

$$\tfrac{1}{2}U_e^2 + p_e = \tfrac{1}{2},$$

one can then conclude that the pressure in the boundary layer, $p_e(x)$, is also representable by the Taylor expansion

$$p_e(x) = p_0(x) + \Delta k p_1(x) + \cdots. \qquad (148)$$

Here

$$p_0 = \tfrac{1}{2}\left[1 - U_{e,0}^2\right], \qquad p_1 = -U_{e,0}U_{e,1}.$$

Being guided by (147) and (148), we seek a solution of the boundary-layer problem (84) in the form

$$\Psi = \Psi_0(x, Y) + \Delta k \Psi_1(x, Y) + \cdots \quad \text{as} \quad \Delta k \to 0. \qquad (149)$$

The leading order term $\Psi_0(x, Y)$ has been studied in the preceding section. We shall now consider the function $\Psi_1(x, Y)$. Substitution of (149) together with (147) and (148) into (84) yields

$$\frac{\partial \Psi_0}{\partial Y}\frac{\partial^2 \Psi_1}{\partial x \partial Y} + \frac{\partial^2 \Psi_0}{\partial x \partial Y}\frac{\partial \Psi_1}{\partial Y} - \frac{\partial \Psi_0}{\partial x}\frac{\partial^2 \Psi_1}{\partial Y^2} - \frac{\partial^2 \Psi_0}{\partial Y^2}\frac{\partial \Psi_1}{\partial x} = $$
$$-\frac{dp_1}{dx} + \frac{\partial^3 \Psi_1}{\partial Y^3}, \qquad (150a)$$

$$\Psi_1 = 0 \qquad\qquad\qquad\qquad \text{at} \quad x = 0, \qquad (150b)$$

$$\Psi_1 = \frac{\partial \Psi_1}{\partial Y} = 0 \qquad\qquad \text{at} \quad Y = 0, \qquad (150c)$$

$$\frac{\partial \Psi_1}{\partial Y} = U_{e,1}(x) \qquad\qquad \text{at} \quad Y = \infty. \qquad (150d)$$

The solution of (150) near point $x = x_0$ may be constructed in the same way as it was done for the leading order problem. We start with region

2a (see Figure 19), where the asymptotic expansion of function $\Psi_1(x, Y)$ is sought in the form

$$\Psi_1(x, Y) = (-s)^\beta g_1(\eta) + (-s)^{\beta+3/4} g_2(\eta) + \cdots \quad \text{as} \quad s \to 0-, \quad (151)$$

with

$$\eta = \frac{Y}{(-s)^{1/4}} \quad (152)$$

assumed an order one quantity. The leading order term in (151) represents an eigenfunction of the local solution; constant β is the eigenvalue to be determined.

Substitution of (151) together with (130) into (150a) results in the following equation for $g_1(\eta)$:

$$g_1''' - \frac{1}{8}\lambda_0\eta^3 g_1'' + \frac{1}{2}\lambda_0\left(\beta + \frac{1}{4}\right)\eta^2 g_1' - \lambda_0\beta\eta g_1 = 0.$$

For any β, its solution satisfying the no-slip conditions

$$g_1(0) = g_1'(0) = 0,$$

is written as

$$g_1 = \tfrac{1}{2}a_1\eta^2, \quad (153)$$

where a_1 is an arbitrary constant. In order to find the eigenvalue β one needs to consider the second term in (151). Function $g_2(\eta)$ satisfies the equation

$$g_2''' - \frac{1}{8}\lambda_0\eta^3 g_2'' + \frac{1}{2}\lambda_0(\beta+1)\eta^2 g_2' - \lambda_0\left(\beta + \frac{3}{4}\right)\eta g_2 = -\left(\frac{\beta}{2} + \frac{1}{4}\right)a_0 a_1\eta^2. \quad (154)$$

It should be solved with the no-slip conditions on the aerofoil surface

$$g_2(0) = g_2'(0) = 0.$$

The solution to (154) may be constructed in the same way as it was done with equation (100). We find that

$$g_2(\eta) = \frac{a_0 a_1}{\lambda_0}(\eta - g_{22}) + \tfrac{1}{2}b_1\eta^2, \quad (155)$$

where function $g_{22}(\eta)$ allows for the power series representation

$$g_{22}(\eta) = -\sum_{n=0}^{\infty}\left(\frac{\lambda_0}{32}\right)^n \frac{(-\beta - 1/2)_n}{(5/4)_n (4n-1) n!}\eta^{4n+1}, \quad (156)$$

and may be expressed through the Kummer function,

$$g_{22}(\eta) = \eta - \eta^2 \int\limits_0^\eta \xi^{-2} \left[M\left(-\beta - 1/2, \frac{5}{4}, \frac{\lambda_0}{32} \xi^4 \right) - 1 \right] d\xi. \qquad (157)$$

It follows from (157) that $g_{22}(\eta)$ grows exponentially as $\eta \to \infty$ for all values of β except

$$\beta = m - \tfrac{1}{2}, \qquad m = 0,\ 1,\ 2\ldots. \qquad (158)$$

Equation (158) gives the sought sequence of the eigenvalues; the first of these being

$$\beta = -\tfrac{1}{2}. \qquad (159)$$

With (159) all the coefficients in (156), except the first one ($n = 0$), are zeros, and we have

$$g_{22} = \eta. \qquad (160)$$

Using (160) in (155), and substituting (155) together with (159) and (153) into (151), we arrive at a conclusion that the solution of equation (150a) in region $2a$ has the form

$$\Psi_1(x, Y) = (-s)^{-1/2}\tfrac{1}{2}a_1\eta^2 + (-s)^{1/4}\tfrac{1}{2}b_1\eta^2 + \cdots . \qquad (161)$$

In order to predict the form of the solution in region $2b$ (see Figure 19), we rearrange (161) with the help of (152). We have

$$\Psi_1(x, Y) = (-s)^{-1}\tfrac{1}{2}a_1 Y^2 + (-s)^{-1/4}\tfrac{1}{2}b_1 Y^2 + \cdots ,$$

which suggests that in region $2b$, where $Y = O(1)$, the asymptotic expansion of $\Psi_1(x, Y)$ should be written in the form

$$\Psi_1(x, Y) = (-s)^{-1}\Psi_{11}(Y) + O\left[(-s)^{-1/4}\right] \quad \text{as} \quad s \to 0-, \qquad (162)$$

where function $\Psi_{11}(Y)$ is such that

$$\Psi_{11}(Y) = \tfrac{1}{2}a_1 Y^2 + \cdots \quad \text{as} \quad Y \to 0. \qquad (163)$$

Substitution of (163) and (131) into (150a) results in

$$\Psi'_{00}\Psi'_{11} - \Psi''_{00}\Psi_{11} = 0.$$

The solution of this equation, satisfying the boundary condition (163), has the form

$$\Psi_{11} = \frac{a_1}{\lambda_0}\Psi'_{00}(Y). \qquad (164)$$

It remains to substitute (164) back into (162), and we can conclude that in region 2b

$$\Psi_1(x, Y) = (-s)^{-1}\frac{a_1}{\lambda_0}\Psi'_{00}(Y) + O\left[(-s)^{-3/4}\right] \quad \text{as} \quad s \to 0-, \qquad (165)$$

Similar to (135), equation (165) proves to be valid not only in region 2b but also in region 2a; see Exercise 2. This statement is easily verified by substituting (134) into (165) and comparing the resulting expression with (161).

Let us now return to the expansion (149). As any other asymptotic expansion it is expected to have a proper ordering of the terms, namely, each subsequent term should be much smaller than the previous one. The assumption that the expansion (149) satisfies this requirement was used when deriving equation (150a), and became the basis of the entire procedure employed for analysing the behaviour of the function $\Psi_1(x, Y)$. For each point (x, Y) situated upstream of the point $x = x_0$ this assumption is indeed satisfied thanks to the smallness of Δk. However, as $x \to x_0 - 0$ the function $\Psi_1(x, Y)$ increases without bound, leading to violation of the supposed relationship between the terms in (149). Consequently, we have to examine the vicinity of the point $x = x_0$ separately.

In order to find the size of a new region that has to be introduced near $x = x_0$, we notice that the x-dependence of both $\Psi_0(x, Y)$ and $\Psi_1(x, Y)$ is determined by the eigenfunctions in the solutions (130) and (161) for region 2a. Comparing the contribution of the eigenfunctions in the asymptotic expansion (149),

$$(-s)^{3/2}\tfrac{1}{2}a_0\eta^2 \sim \Delta k\,(-s)^{-1/2}a_1\eta^2.$$

we find that the longitudinal extent of the new region is estimated as

$$|x - x_0| \sim \sqrt{\epsilon},$$

where $\epsilon = |\Delta k|$.

The asymptotic structure of this region is shown in Figure 20. It is composed of two layers. The first one (region 3) is a continuation of region 2a into the $O(\sqrt{\epsilon})$ vicinity of the point $x = x_0$. Since $\eta = Y/(-s)^{1/4}$ is an order one quantity in region 2a, the thickness of region 3 may be estimated as

$$Y \sim |x - x_0|^{1/4} \sim \epsilon^{1/8}.$$

We see that in region 3 the asymptotic analysis of the boundary-layer equations (84) is based on the limit

$$x_* = \frac{x - x_0}{\epsilon^{1/2}} = O(1), \qquad Y_* = \frac{Y}{\epsilon^{1/8}} = O(1), \qquad \epsilon \to 0. \qquad (166)$$
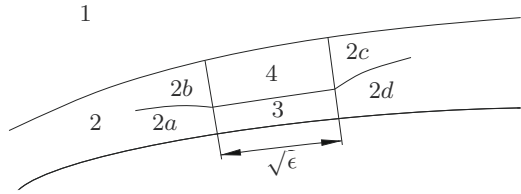
Figure 20. The $O(\sqrt{\epsilon})$ vicinity of the point $x = x_0$.

In order to find the form of the asymptotic expansion of the stream function $\Psi(x, Y)$ in this region, we shall re-expand the solution in region $2a$ in terms of the variables (166). We start by substituting (130) and (161) back into (149),

$$\Psi = (-s)^{3/4}\tfrac{1}{6}\lambda_0\eta^3 + (-s)^{3/2}\tfrac{1}{2}a_0\eta^2 + (-s)^{7/4}\Big(-\tfrac{1}{6}\lambda_1\eta^3 + \frac{2\lambda_0\lambda_1}{7!}\eta^7\Big) +$$

$$+ (-s)^{9/4}\Big(\tfrac{1}{2}b_0\eta^2 - \frac{a_0^2}{5!}\eta^5 + \frac{\lambda_0 a_0^2}{8!}\eta^9\Big) +$$

$$+ \Delta k\Big\{(-s)^{-1/2}\tfrac{1}{2}a_1\eta^2 + (-s)^{1/4}\tfrac{1}{2}b_1\eta^2\Big\} + \cdots. \qquad (167)$$

We then note that

$$(-s) = x_0 - x = \epsilon^{1/2}(-x_*), \qquad \eta = \frac{Y}{(-s)^{1/4}} = \frac{Y_*}{(-x_*)^{1/4}}, \qquad (168)$$

and express Δk in the form

$$\Delta k = \epsilon\,\mathrm{sign}(\Delta k). \qquad (169)$$

These, being substituted into (167), lead to

$$\Psi = \epsilon^{3/8}\frac{1}{6}\lambda_0 Y_*^3 +$$

$$+ \epsilon^{6/8}\Big\{(-x_*)\frac{1}{2}a_0 Y_*^2 + (-x_*)^{-1}\mathrm{sign}(\Delta k)\frac{1}{2}a_1 Y_*^2\Big\} +$$

$$+ \epsilon^{7/8}\Big\{\frac{1}{6}\lambda_1 x_* Y_*^3 + \frac{2\lambda_0\lambda_1}{7!}Y_*^7\Big\} +$$

$$+ \epsilon^{9/8}\Big\{\frac{a_0^2}{5!}x_* Y_*^5 + \frac{\lambda_0 a_0^2}{8!}Y_*^9 + (-x_*)^{7/4}\frac{1}{2}b_0 Y_*^2 + \qquad (170)$$

$$+ (-x_*)^{-1/4}\mathrm{sign}(\Delta k)\frac{1}{2}b_1 Y_*^2\Big\} + \cdots. \qquad (171)$$

This suggests that in region 3 the solution of the boundary layer equations (84) should be sought in the form

$$
\Psi = \epsilon^{3/8} \frac{1}{6} \lambda_0 Y_*^3 + \epsilon^{6/8} \Psi_1^*(x_*, Y_*) +
$$
$$
+ \epsilon^{7/8} \left(\frac{1}{6} \lambda_1 x_* Y_*^3 + \frac{2\lambda_0 \lambda_1}{7!} Y_*^7 \right) + \epsilon^{9/8} \Psi_2^*(x_*, Y_*) + \cdots . \tag{172}
$$

It also follows from (171) that functions $\Psi_1^*(x_*, Y_*)$ and $\Psi_2^*(x_*, Y_*)$ satisfy the following matching conditions with the solution in region 2a,

$$
\Psi_1^* = \frac{1}{2} \Big\{ a_0(-x_*) + \mathrm{sign}(\Delta k) a_1 (-x_*)^{-1} \Big\} Y_*^2 + \cdots \qquad \text{as} \quad x_* \to -\infty \tag{173a}
$$

and

$$
\Psi_2^* = \frac{a_0^2}{5!} x_* Y_*^5 + \frac{\lambda_0 a_0^2}{8!} Y_*^9 +
$$
$$
+ \frac{1}{2} \Big\{ b_0(-x_*)^{7/4} + \mathrm{sign}(\Delta k) b_1 (-x_*)^{-1/4} \Big\} Y_*^2 + \cdots \quad \text{as} \quad x_* \to -\infty. \tag{173b}
$$

We are dealing here with the classical formulation of the boundary-layer equations with the pressure gradient assumed to be known. Differentiating (148) with respect to x, we have

$$
\frac{dp_e}{dx} = \frac{dp_0}{dx} + \Delta k \frac{dp_1}{dx} + \cdots .
$$

In a small vicinity of point $x = x_0$ the first term is given by the Taylor expansion (87), while the second term remain finite. Therefore in region 3 the pressure gradient

$$
\frac{dp_e}{dx} = \lambda_0 + \epsilon^{1/2} \lambda_1 x_* + O(\epsilon). \tag{174}
$$

Substitution of (172) and (174) into (84a) gives in the leading order approximation

$$
\tfrac{1}{2} \lambda_0 Y_*^2 \frac{\partial^2 \Psi_1^*}{\partial x_* \partial Y_*} - \lambda_0 Y_* \frac{\partial \Psi_1^*}{\partial x_*} = \frac{\partial^3 \Psi_1^*}{\partial Y_*^3}. \tag{175}
$$

The solution to this equation should satisfy the no-slip conditions on the aerofoil surface,

$$
\Psi_1^* = \frac{\partial \Psi_1^*}{\partial Y_*} = 0 \quad \text{at} \quad Y_* = 0. \tag{176}
$$

Since equation (175) is linear, and its coefficients do not depend on x_*, the solution to this equation may be constructed using the method of Fourier Transforms. We define the Fourier Transform of function $\Psi_1^*(x_*, Y_*)$ as

$$\breve{\Psi}_1(k, Y_*) = \int_{-\infty}^{\infty} \Psi_1^*(x_*, Y_*) e^{-ikx_*} \, dx_*, \qquad (177)$$

with the inverse transformation being

$$\Psi_1^*(x_*, Y_*) = \frac{1}{2\pi} \int_{-\infty}^{\infty} \breve{\Psi}_1(k, Y_*) e^{ikx_*} \, dk.$$

Here the Fourier variable k is assumed real.

Applying the Fourier transformation to the equation (175) renders it in the form

$$\tfrac{1}{2} ik\lambda_0 Y_*^2 \frac{d\breve{\Psi}_1}{dY_*} - ik\lambda_0 Y_* \breve{\Psi}_1 = \frac{d^3\breve{\Psi}_1}{dY_*^3}, \qquad (178)$$

with the no-slip conditions (176) turning into

$$\breve{\Psi}_1 = \frac{d\breve{\Psi}_1}{dY_*} = 0 \quad \text{at} \quad Y_* = 0. \qquad (179)$$

Since the ordinary differential equation (178) is linear and homogeneous, its general solution may be written as

$$\breve{\Psi}_1 = C_1\psi_{11} + C_2\psi_{12} + C_3\psi_{13}, \qquad (180)$$

where ψ_{11}, ψ_{12} and ψ_{13} are the three complementary solutions of (178). They can be chosen such that

$$\begin{aligned}
\psi_{11}(0) &= 1, & \psi_{11}'(0) &= 0, & \psi_{11}''(0) &= 0, \\
\psi_{12}(0) &= 0, & \psi_{12}'(0) &= 1, & \psi_{12}''(0) &= 0, \\
\psi_{13}(0) &= 0, & \psi_{13}'(0) &= 0, & \psi_{13}''(0) &= 1.
\end{aligned}$$

The first two solutions do not satisfy the conditions (179), and therefore, we have to set $C_1 = C_2 = 0$ in (180). As far as the third solution is concerned, it is written as

$$\psi_{13} = \tfrac{1}{2}Y_*^2,$$

which is easily verified by direct substitution into (178). This reduces (180) to

$$\breve{\Psi}_1 = \tfrac{1}{2}C_3 Y_*^2. \qquad (181)$$

Notice that factor C_3 is an arbitrary function of parameter k. Applying the inverse transform to (181), we can conclude that

$$\Psi_1^*(x_*, Y_*) = \tfrac{1}{2} A_*(x_*) Y_*^2, \tag{182}$$

where $A_*(x_*)$ is an arbitrary function of x_*, except it is known from (173a) that

$$A(x_*) = a_0(-x_*) + \text{sign}(\Delta k) a_1(-x_*)^{-1} + \cdots \quad \text{as} \quad x_* \to -\infty. \tag{183}$$

In order to find $A_*(x_*)$ we need to consider the next term in (172). Function Ψ_2^* satisfies the equation

$$\tfrac{1}{2}\lambda_0 Y_*^2 \frac{\partial^2 \Psi_2^*}{\partial x_* \partial Y_*} - \lambda_0 Y_* \frac{\partial \Psi_2^*}{\partial x_*} = \frac{\partial^3 \Psi_2^*}{\partial Y_*^3} - \tfrac{1}{2} A_* \frac{dA_*}{dx_*} Y_*^2, \tag{184a}$$

and the no-slip conditions

$$\Psi_2^* = \frac{\partial \Psi_2^*}{\partial Y_*} = 0 \quad \text{at} \quad Y_* = 0. \tag{184b}$$

When applying the Fourier Transforms method to (184) one has to keep in mind that the Fourier integral (177) converges only if the function it is applied to tends to zero as $|x_*| \to \infty$. It follows from (173b) that function Ψ_2^* does not satisfy this requirement. Therefore, we introduce a new unknown function Ψ_2 such that

$$\Psi_2^* = \Psi_2 + \frac{\lambda_0 a_0^2}{8!} Y_*^9 + \frac{a_0^2}{5!} x_* Y_*^5 + \tfrac{1}{2} B_*(x_*) Y_*^2 + G_*(x_*) Y_*, \tag{185}$$

where

$$G_*(x_*) = \frac{A_*^2 - a_0^2 x_*^2 - 2a_0 a_1 \text{sign}(\Delta k)}{2\lambda_0}. \tag{186}$$

It follows from (183) that $G_*(x_*) \to 0$ as $x_* \to -\infty$. Notice that the solution of the boundary-value problem (184) is not unique. It can always be supplemented with $\tfrac{1}{2} B_*(x_*) Y_*^2$, where $B_*(x_*)$ is an arbitrary function. It is inserted into (185) to ensure that Ψ_2^* tends to zero as $x_* \to -\infty$. Comparing (185) with (173b), we see that

$$B_*(x_*) = b_0(-x_*)^{7/4} + \text{sign}(\Delta k) b_1(-x_*)^{-1/4} + \cdots \quad \text{as} \quad x_* \to -\infty.$$

The transformation (185) renders the boundary-value problem in the form

$$\tfrac{1}{2}\lambda_0 Y_*^2 \frac{\partial^2 \Psi_2}{\partial x_* \partial Y_*} - \lambda_0 Y_* \frac{\partial \Psi_2}{\partial x_*} = \frac{\partial^3 \Psi_2}{\partial Y_*^3}, \tag{187a}$$

$$\Psi_2 = 0, \quad \frac{\partial \Psi_2}{\partial Y_*} = -G_*(x_*) \quad \text{at} \quad Y_* = 0. \tag{187b}$$

Applying the Fourier transformation to the equation (187a) and boundary conditions (187b) yields

$$\tfrac{1}{2}ik\lambda_0 Y_*^2 \frac{d\breve{\Psi}_2}{dY_*} - ik\lambda_0 Y_* \breve{\Psi}_2 = \frac{d^3\breve{\Psi}_2}{dY_*^3}, \qquad (188a)$$

$$\breve{\Psi}_2 = 0, \quad \frac{d\breve{\Psi}_2}{dY_*} = -\breve{G}(k) \quad \text{at} \quad Y_* = 0. \qquad (188b)$$

Here $\breve{\Psi}_2(k, Y_*)$ and $\breve{G}(k)$ are Fourier Transforms of functions Ψ_2 and G_*, respectively.

The general solution of equation (188a) is written as

$$\breve{\Psi}_2 = C_1\psi_{21} + C_2\psi_{22} + C_3\psi_{23}, \qquad (189)$$

where ψ_{21}, ψ_{22} and ψ_{23} are the three complementary solutions of the equation (188a). We shall choose them using the initial conditions

$$\begin{aligned}
\psi_{21}(0) &= 1, & \psi_{21}'(0) &= 0, & \psi_{21}''(0) &= 0, \\
\psi_{22}(0) &= 0, & \psi_{22}'(0) &= 1, & \psi_{22}''(0) &= 0, \\
\psi_{23}(0) &= 0, & \psi_{23}'(0) &= 0, & \psi_{23}''(0) &= 1.
\end{aligned} \qquad (190)$$

Then it follows from (188b) that

$$C_1 = 0, \qquad C_2 = -\breve{G}(k). \qquad (191)$$

Factor C_3 remains an arbitrary function of k, and the third complementary solution ψ_{23} is easily seen to be

$$\psi_{23} = \tfrac{1}{2}Y_*^2. \qquad (192)$$

Substituting (191) and (192) back into (189), we have

$$\breve{\Psi}_2 = -\breve{G}(k)\psi_{22} + \tfrac{1}{2}C_3(k)Y_*^2. \qquad (193)$$

Our task now will be to determine the function ψ_{22}. The power series presentation of this function may be constructed in the same way as it was done with function $f_{22}(\eta)$ representing the second complementary solution of equation (100). We start with the conditions (190). They show that the first term in the series is

$$\psi_{22} = Y_* + \cdots. \qquad (194)$$

Using (194) on the left hand side of (188a) yields

$$\frac{d^3\psi_{22}}{dY_*^3} = -\tfrac{1}{2}ik\lambda_0 Y_*^2.$$

Integration of this equation gives the second term,

$$\psi_{22} = Y_* - \frac{ik\lambda_0}{120}Y_*^5 + \cdots .$$

This procedure can be repeated as many time as one wishes, leading to a conclusion that the power series of ψ_{22} should be written in the form

$$\psi_{22}(Y_*) = \sum_{n=0}^{\infty} c_n Y_*^{4n+1}. \tag{195}$$

Alternatively we can write

$$\psi_{22}(Y_*) = Y_* + \sum_{n=0}^{\infty} c_{n+1} Y_*^{4n+5}. \tag{196}$$

Using (195) on the left hand side of the equation (188a) and (196) on the right hand side, we find that the coefficients of the series (195) satisfy the following recurrent equation

$$c_{n+1} = \frac{ik\lambda_0}{32} \frac{n - \frac{1}{4}}{\left(n + \frac{3}{4}\right)\left(n + \frac{5}{4}\right)(n+1)} c_n, \tag{197a}$$

which has to be solved starting with

$$c_0 = 1. \tag{197b}$$

By direct substitution one can easily verify that the solution of (197) is

$$c_n = -\left(\frac{ik\lambda_0}{32}\right)^n \frac{\Gamma(5/4)}{\Gamma(n + 5/4)(4n - 1)n!}. \tag{198}$$

Substituting (198) back into (195), we have

$$\psi_{22}(Y_*) = -\Gamma\left(\tfrac{5}{4}\right) \sum_{n=0}^{\infty} \left(\frac{ik\lambda_0}{32}\right)^n \frac{Y_*^{4n+1}}{\Gamma(n + 5/4)(4n - 1)n!}. \tag{199}$$

We shall show now that the function $\psi_{22}(Y_*)$ may be expressed through the Bessel function. It is known (see, for example Abramowitz & Stegun, 1965) that the Bessel function of the first kind and order ν may be represented by the power series

$$J_\nu(z) = \sum_{n=0}^{\infty} \frac{(-1)^n}{\Gamma(n + \nu + 1)n!} \left(\frac{z}{2}\right)^{2n+\nu}, \tag{200}$$

which converges in the entire complex plane z except $z = \infty$. It is also known that in the limit, $|z| \to \infty$,

$$J_\nu(z) = \sqrt{\frac{2}{\pi z}}\left[\cos\left(z - \tfrac{1}{2}\nu\pi - \tfrac{1}{4}\pi\right) + e^{|\Im(z)|}O\left(\frac{1}{z}\right)\right],$$

$$-\pi < \arg z < \pi.$$

(201)

In order to reproduce the Gamma function, $\Gamma(n + 5/4)$, in (199), we choose $\nu = 1/4$, and then, writing the first term in the series (200) separately, we will have

$$J_{1/4}(z) = \frac{1}{\Gamma(5/4)}\left(\frac{z}{2}\right)^{1/4} + \sum_{n=1}^{\infty}\frac{(-1)^n}{\Gamma(n + 5/4)\,n!}\left(\frac{z}{2}\right)^{2n+1/4}. \tag{202}$$

It follows from (202) that

$$\int_0^z \left(\frac{2}{z}\right)^{3/2}\left[\frac{J_{1/4}(z)}{(z/2)^{1/4}} - \frac{1}{\Gamma(5/4)}\right]dz = 4\sum_{n=1}^{\infty}\frac{(-1)^n}{\Gamma(n + 5/4)(4n-1)n!}\left(\frac{z}{2}\right)^{2n-1/2}.$$

Therefore

$$\sum_{n=0}^{\infty}\frac{(-1)^n}{\Gamma(n + 5/4)(4n-1)n!}\left(\frac{z}{2}\right)^{2n+1/2} =$$

$$= \frac{z}{8}\int_0^z \left(\frac{2}{z}\right)^{3/2}\left[\frac{J_{1/4}(z)}{(z/2)^{1/4}} - \frac{1}{\Gamma(5/4)}\right]dz - \frac{1}{\Gamma(5/4)}\left(\frac{z}{2}\right)^{1/2}. \tag{203}$$

We substitute (201) into (203), and restrict our attention to the leading order exponentially growing term. Using the integration by parts with

$$u = \left(\frac{2}{z}\right)^{9/4}, \qquad dv = \cos\left(z - \tfrac{3}{8}\pi\right)dz,$$

$$du = -\frac{9}{8}\left(\frac{2}{z}\right)^{13/4}dz, \qquad v = \sin\left(z - \tfrac{3}{8}\pi\right),$$

we find that

$$\sum_{n=0}^{\infty}\frac{(-1)^n}{\Gamma(n + 5/4)(4n-1)n!}\left(\frac{z}{2}\right)^{2n+1/2} =$$

$$= \frac{1}{4\sqrt{\pi}}\left(\frac{2}{z}\right)^{5/4}\sin\left(z - \tfrac{3}{8}\pi\right) + \cdots \quad \text{as} \quad |z| \to \infty.$$

It remains to set $z = \frac{1}{2}i\Omega^{1/2}Y_*^2$, where $\Omega = \frac{1}{2}ik\lambda_0$, and we will see that function ψ_{22}, given by (199), grows exponentially as $Y_* \to \infty$, namely,

$$\psi_{22}(Y_*) = -\frac{\Gamma(5/4)}{2\sqrt{\pi}e^{i\pi/4}\Omega^{1/4}}\left(\frac{4}{i\Omega^{1/2}Y_*^2}\right)^{5/4}\sin\left(\tfrac{1}{2}i\Omega^{1/2}Y_*^2 - \tfrac{3}{8}\pi\right) + \cdots .$$
(204)

This means that the exponential growth of the solution (193) of the equation (187a) can only be suppressed by setting

$$\check{G}(k) = 0.$$
(205)

Applying the inverse Fourier transformation to (205), we have

$$G_*(x_*) = 0.$$

It remains to recall that the function $G_*(x*)$ is defined by equation (186). We see that

$$A_*^2 - a_0^2 x_*^2 - 2a_0 a_1 \text{sign}(\Delta k) = 0.$$
(206)

The solution of quadratic equation (206), satisfying the condition (183), is written as

$$A_* = a_0\sqrt{x_*^2 + 2\frac{a_1}{a_0}\text{sign}(\Delta k)}.$$
(207)

This completes the flow analysis in region 3. To conclude, we substitute (182) into (172), and neglecting the higher order terms, we have the solution in region 3 in the form

$$\Psi = \epsilon^{3/8}\tfrac{1}{6}\lambda_0 Y_*^3 + \epsilon^{6/8}\tfrac{1}{2}A_*(x_*)Y_*^2 + \cdots ,$$
(208)

with $A_*(x_*)$ being given by (207).

Let us now turn our attention to region 4 (see Figure 20), where the asymptotic analysis of the boundary-layer equation (84a) is based on the limit

$$x_* = \frac{x - x_0}{\epsilon^{1/2}} = O(1), \qquad Y = O(1), \qquad \epsilon \to 0.$$
(209)

We start by re-expanding the solution in region 2b (see Figure 20) in terms of variables (209), namely, we substitute (135), (165) and (169) into (149). Taking into account that $s = x - x_0 = \epsilon^{1/2}x_*$, we will have

$$\Psi = \Psi_{00}(Y)+$$

$$+\epsilon^{1/2}\left\{\Psi_{00}'(Y)\left[x_*\int_0^Y \frac{\Psi_{00}''' - \lambda_0}{\left(\Psi_{00}'\right)^2}dY' + \frac{a_0(-x_*) + a_1\text{sign}(\Delta k)(-x_*)^{-1}}{\lambda_0}\right]\right\}+\cdots .$$

This suggests, firstly, that the asymptotic expansion of the stream function $\Psi(x, Y)$ in region 4 should be sought in the form

$$\Psi(x, Y) = \Psi_{00}(Y) + \epsilon^{1/2}\widetilde{\Psi}_1(x_*, Y) + \cdots . \tag{210}$$

Secondly, we see that the matching condition with the solution in region 2b reads

$$\widetilde{\Psi}_1 = \Psi'_{00}(Y)\left[x_* \int\limits_0^Y \frac{\Psi'''_{00} - \lambda_0}{\left(\Psi'_{00}\right)^2}dY' + \frac{A_*(x_*)}{\lambda_0}\right] + \cdots \quad \text{as} \quad x_* \to -\infty. \tag{211}$$

Here we use the fact that function $A_*(x_*)$ is represented at large negative x_* by (183).

We will also need the matching condition with the solution (208) in region 3. It can be formulated with the help of a usual routine. We start by expressing the solution in region 3 in terms of the variables of region 4. Since the scaled tangential coordinate x_* is common for regions 3 and 4, we just need to recall that the relationship between the normal coordinates is given by (166), i.e.

$$Y_* = \frac{Y}{\epsilon^{1/8}}. \tag{212}$$

Substitution of (212) into (208) yields

$$\Psi = \tfrac{1}{6}\lambda_0 Y^3 + \epsilon^{1/2}A_*(x_*)Y^2 + \cdots . \tag{213}$$

Now we turn our attention to the asymptotic expansion (210) of the stream function in region 4. At the "bottom" of region 4 the leading order term in (210) may be simplified with the help of (134), which turns (210) into

$$\Psi(x, Y) = \tfrac{1}{6}\lambda_0 Y^3 + \epsilon^{1/2}\widetilde{\Psi}_1(x_*, Y) + \cdots . \tag{214}$$

It remains to compare (213) with (214), and we can conclude that the sought matching condition is written as

$$\widetilde{\Psi}_1(x_*, Y) = \tfrac{1}{2}A_*(x_*)Y^2 + \cdots \quad \text{as} \quad Y \to 0. \tag{215}$$

The equation for function $\widetilde{\Psi}_1(x_*, Y)$ is obtained by substituting (210) together with (174) into the boundary-layer equation (84a). We find that

$$\Psi'_{00}\frac{\partial^2\widetilde{\Psi}_1}{\partial x_* \partial Y} - \Psi''_{00}\frac{\partial\widetilde{\Psi}_1}{\partial x_*} = -\lambda_0 + \Psi'''_{00}, \tag{216}$$

or, equivalently,

$$\frac{\partial^2}{\partial x_* \partial Y}\left(\frac{\widetilde{\Psi}_1}{\Psi'_{00}}\right) = \frac{\Psi'''_{00} - \lambda_0}{\left(\Psi'_{00}\right)^2}. \tag{217}$$

It follows from (215) and (134) that

$$\left.\frac{\widetilde{\Psi}_1}{\Psi'_{00}}\right|_{Y=0} = \frac{A_*(x_*)}{\lambda_0}.$$

Therefore, integrating (217) with respect to Y, we have

$$\frac{\partial}{\partial x_*}\left(\frac{\widetilde{\Psi}_1}{\Psi'_{00}}\right) = \int\limits_0^Y \frac{\Psi'''_{00} - \lambda_0}{\left(\Psi'_{00}\right)^2}\,dY + \frac{A'_*(x_*)}{\lambda_0}. \tag{218}$$

It remains to integrate (218) with respect to x_*. When performing the integration, condition (211) has to be used. We find that

$$\widetilde{\Psi}_1(x_*, Y_*) = \Psi'_{00}(Y)\left[x_* \int\limits_0^Y \frac{\Psi'''_{00} - \lambda_0}{\left(\Psi'_{00}\right)^2}\,dY' + \frac{A_*(x_*)}{\lambda_0}\right], \tag{219}$$

where the function $A_*(x_*)$ is given by (207).

Substituting (219) back into (210), we have the solution in region 4 in the form

$$\Psi(x, Y) = \Psi_{00}(Y) + \epsilon^{1/2}\Psi'_{00}(Y)\left[x_* \int\limits_0^Y \frac{\Psi'''_{00} - \lambda_0}{\left(\Psi'_{00}\right)^2}\,dY' + \frac{A_*(x_*)}{\lambda_0}\right] + \cdots. \tag{220}$$

Through making use of (134) one can verify that in region 3, where $Y = \epsilon^{1/2}Y_*$, the expansion (220) reduces to (208). This means that we can use (220) not only in region 4 but also in region 3. Substituting (207) into (220), and returning to the original variable $x = x_0 + \epsilon^{1/2}x_*$, we have

$$\Psi(x, Y) = \Psi_{00} +$$

$$+ \Psi'_{00}\left[\frac{a_0}{\lambda_0}\sqrt{(x - x_0)^2 + 2\frac{a_1}{a_0}\Delta k} + (x - x_0)\int\limits_0^Y \frac{\Psi'''_{00} - \lambda_0}{\left(\Psi'_{00}\right)^2}\,dY'\right] + \cdots. \tag{221}$$

Equation (221) represents an asymptotic solution of the boundary-layer equations (84). It holds in a small vicinity of point $x = x_0$ provided that Δk is small. The domain of existence of the solution is determined by the

sign of the argument of the square root in (221). If $a_1 \Delta k > 0$, then the solution exists for all x. The skin friction

$$\tau = \frac{\partial^2 \Psi}{\partial Y^2}\bigg|_{Y=0} = a_0 \sqrt{(x - x_0)^2 + 2\frac{a_1}{a_0}\Delta k} \tag{222}$$

remains positive everywhere and at the point $x = x_0$ it reaches the minimum, whose value decreases as $\Delta k \to 0$ according to the rule

$$\tau_{\min} = \sqrt{2a_0 a_1 \Delta k}. \tag{223}$$

If, however, $a_1 \Delta k < 0$, then the solution exists only up to the point of zero friction,

$$x_s = x_0 - \sqrt{2\frac{|a_1 \Delta k|}{a_0}};$$

downstream of this point the argument of the square root becomes negative. On approach to the point $x = x_s$ the solution develops Goldstein's singularity. Indeed, it follows from (222) that

$$\tau = \left(8a_0^3 |a_1 \Delta k|\right)^{1/4} \sqrt{x_s - x} + \cdots \quad \text{as} \quad x \to x_s - 0.$$

Notice that the singularity becomes progressively weaker as $\Delta k \to 0$.

According to the numerical calculations (see Figure 18) the first of the situations described is realized for $\Delta k < 0$ and the second for $\Delta k < 0$. This means that the constant a_1 is negative.

Remind that in the case when $\Delta k = 0$, the boundary-layer equations (84) admit two solutions. One of them, given by (142), passes smoothly through the point $x = x_0$, while the second solution, given by (144), develops a singularity at this point. Comparing (142) and (144) with (221), one can see that this is the singular solution (144) that represents the limiting solution of the boundary-layer equations as $k \to k_0 - 0$.

In order to determine the constants a_0 and a_1 we need to compare the analytical solution with the results of the numerical calculations of the boundary-layer equations. Firstly, the skin friction distribution in Figure 18 calculated for $k = k_0$ should exhibit near $x = x_0$ the behaviour predicted by formula (146). Using this fact, we found that the the flow at the leading edge of the aerofoil, $a_0 = 0.0085$. Then constant a_1 was found using formula (223). It appeared that $a_1 = -1.24$.

3.3   Viscous-Inviscid Interaction

Up to this point the analysis of the flow has been carried out in the framework of the classical boundary-layer theory. We started with the inviscid

region where the solution of the Euler equations was constructed using the impermeability conditions on the aerofoil surface, i.e. the existence of the boundary layer was completely ignored. As a result we found the velocity distribution (80) on the aerofoil surface, while the pressure distribution was calculated using the Bernoulli equation. Then, as a second step, the boundary layer was analysed. For this purpose the classical Prandtl's equations (84) were used, with the pressure, p_e, and the velocity at the outer edge of the boundary layer, U_e, assumed uninfluenced by the presence of the boundary layer. This assumption is based on the observation that the boundary layer is only capable of causing an $O(Re^{-1/2})$ displacement of the streamlines from the aerofoil surface. Consequently, as long as the solution in the boundary layer remains regular, its influence on the pressure field remains weak.

The situation changes as the parameter k approaches its critical value k_0, and the singularity forms in the boundary layer. Remind that when $k = k_0$, the streamlines in the boundary layer develop a corner. The deflection angle θ may be calculated using (145). We have

$$\theta = Re^{-1/2}\left(\Theta\Big|_{x=x_0+0} - \Theta\Big|_{x=x_0-0}\right) = -Re^{-1/2}\frac{2a_0}{\lambda_0}. \qquad (224)$$

Then it follows from the small perturbation inviscid flow theory (see Exercise 3) that the pressure induced by the boundary layer

$$p' = Re^{-1/2}\left[\frac{2a_0 U_0^2}{\pi\lambda_0}\ln|x - x_0| + O(1)\right] \quad \text{as} \quad x \to x_0. \qquad (225)$$

Here $U_0 = U_e(x_0)$, and λ_0 is the leading order term in the pressure gradient (87); for an aerofoil with parabolic nose $U_0 = 1.286$ and $\lambda_0 = 0.024$.

We see that the induced pressure gradient exhibits an unbounded growth as the singularity is approached, namely,

$$\frac{dp'}{dx} = Re^{-1/2}\frac{2a_0 U_0^2}{\pi\lambda_0}\frac{1}{x - x_0} + \cdots. \qquad (226)$$

Consequently, one can expect that there exists a small vicinity of the point $x = x_0$, where the pressure perturbations, induced by the displacement effect of the boundary layer, become large enough to start influencing the flow inside the boundary layer in the leading order approximation.

In order to determine the size of this region let us return to the procedure used to analyse the flow in the $O(\sqrt{\epsilon})$ vicinity of the singular point (see Figure 20), and recall that in regions 3 and 4 the dependence of the fluid functions on the longitudinal coordinate x_* is expressed through function

$A_*(x_*)$. The latter is determined by solving equation (184a). As soon as the induced pressure gradient becomes large enough "to find its way" into this equation, the process of viscous-inviscid interaction come into play.

The induced pressure gradient (226) can be compared with any term in equation (184a). Let us consider, for example, the first term on the right hand side of (184a). It is produced by the viscous term $\partial^3\Psi/\partial Y^3$ in equation (84a). In region 3 the stream function is represented by the asymptotic expansion (172). Being differentiated three times with respect to Y, it gives

$$\frac{\partial^3\Psi}{\partial Y^3} = \lambda_0 + \epsilon^{3/8}\frac{\partial^3\Psi_1^*}{\partial Y_*^3} + \epsilon^{1/2}\left(\lambda_1 x_* + \frac{\lambda_0\lambda_1}{12}Y_*^3\right) + \epsilon^{3/4}\frac{\partial^3\Psi_2^*}{\partial Y_*^3} + \cdots.$$

The fourth term in the above expansion is a part of equation (184a). When comparing it with the induced pressure gradient (226),

$$\frac{Re^{-1/2}}{x - x_0} \sim \epsilon^{3/4}, \tag{227}$$

we have to take into account that in the region considered,

$$|x - x_0| \sim \sqrt{\epsilon}. \tag{228}$$

Solving (227) and (228) for ϵ and $|x - x_0|$, we find

$$\epsilon = |\Delta k| \sim Re^{-2/5}, \tag{229}$$

$$|x - x_0| \sim Re^{-1/5}. \tag{230}$$

Therefore, in what follows we shall assume that

$$k = k_0 + Re^{-2/5}k_1, \tag{231}$$

where constant k_1 remains an order one quantity as $Re \to \infty$. Our task will be to study the interaction region which, apparently, has a three-tiered structure. In addition to regions 3 and 4, that lie inside the boundary layer (see Figure 20), we also need to introduce region 5 (see Figure 21). The latter is a part of the potential flow region, and serves to convert the perturbations in the streamline shape into the perturbations of pressure.

Before proceeding further it should be mentioned that the induced pressure gradient is only important in the interaction region. Outside this region the classical boundary-layer theory holds, which means that the solutions for regions 2a and 2b, constructed in the previous section, are still valid.
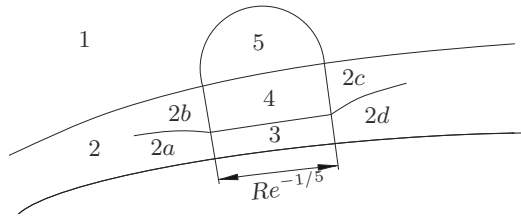
Figure 21. The interaction region.

Upper layer (region 5)   If we return to region 1 (see Figure 17), where X' and Y' are order one quantities, and ignore the existence of the boundary layer, then the solution of the Euler equations in this region would be regular at point $x = x_0$. Keeping in mind that V_n is zero along the aerofoil contour, we can write the Taylor expansions for the velocity components and pressure in a small vicinity of the point $x = x_0$ in the form

$$V_\tau = U_0 + \left\{ a_1(x - x_0) + a_2 y \right\} + \left\{ a_3(x - x_0)^2 + \right.$$
$$\left. + a_4(x - x_0)y + a_5 y^2 \right\} + \cdots ,$$
(232a)

$$V_n = b_2 y + \left\{ b_4(x - x_0)y + b_5 y^2 \right\} + \cdots ,$$
(232b)

$$p = P_{e0} + \left\{ c_1(x - x_0) + c_2 y \right\} + \left\{ c_3(x - x_0)^2 + \right.$$
$$\left. + c_4(x - x_0)y + c_5 y^2 \right\} + \cdots .$$
(232c)

Remind that U_0 denotes the value of the tangential inviscid flow velocity at point $x = x_0$ on the aerofoil surface; P_{e0} is the corresponding value of the pressure. These are related to one another through the Bernoulli equation, $P_{e0} = \frac{1}{2}(1 - U_0^2)$.

Setting $Y = 0$ in (232c), yields the pressure at the outer edge of the boundary layer in the form

$$p_e(x) = p\Big|_{y=0} = P_{e0} + c_1(x - x_0) + c_3(x - x_0)^2 + \cdots .$$
(233)

Comparing (233) with (87), we can see that

$$c_1 = \lambda_0, \qquad c_3 = \tfrac{1}{2}\lambda_1.$$
(234)

Let us now consider the perturbations produced in region 1 due to the presence of the boundary layer. We have already analysed the perturbations of pressure. Now we need to extend the analysis to other fluid dynamic functions as well. We know that at the critical value of the angle

of attack ($k = k_0$) the streamlines in the boundary layer develop a corner with the deflection angle given by (224). Using (224) in (315), we find that perturbations induced by the displacement effect of the boundary layer

$$V'_\tau = -Re^{-1/2}\frac{2a_0U_0}{\pi\lambda_0}\ln\sqrt{(x-x_0)^2+y^2}+\cdots,\tag{235a}$$

$$V'_n = -Re^{-1/2}\frac{2a_0U_0}{\pi\lambda_0}\left[\pi-\arctan\left(\frac{y}{x-x_0}\right)\right]+\cdots,\tag{235b}$$

$$p' = Re^{-1/2}\frac{2a_0U_0^2}{\pi\lambda_0}\ln\sqrt{(x-x_0)^2+y^2}+\cdots.\tag{235c}$$

Let us now turn our attention to region 5; see Figure 21. The longitudinal extent of this region is given by (230). We shall see that the flow in region 5 is described by the Laplace equation (241). The principle of least degeneration requires the lateral size of region 5 to be comparable with its longitudinal size,

$$y \sim |x - x_0| \sim Re^{-1/5}.$$

This means that the asymptotic analysis of the Navier-Stokes equations (81) in region 5 has to be based on the limit procedure

$$x_* = \frac{x-x_0}{Re^{-1/5}} = O(1), \qquad y_* = \frac{y}{Re^{-1/5}} = O(1), \qquad Re \to \infty. \tag{236}$$

In order to predict the form of the asymptotic expansions for the velocity components and pressure in region 5, we shall express (232) and (235) in terms of the new variables (236) and combine these together. Being applied to the tangential velocity component V_τ this procedure yields

$$V_\tau = U_0+Re^{-1/5}\{a_1x_* + a_2y_*\} + Re^{-2/5}\{a_3x_*^2 + a_4x_*y_* + a_5y_*^2\}+$$
$$+ Re^{-1/2}\ln Re\frac{2a_0U_0}{5\pi\lambda_0} - Re^{-1/2}\frac{2a_0U_0}{\pi\lambda}\ln\sqrt{x_*^2+y_*^2}+\cdots.$$

Similarly, for the normal velocity component V_n and pressure p we find

$$V_n = Re^{-1/5}b_2y_* + Re^{-2/5}\{b_4x_*y_* + b_5y_*^2\}-$$
$$- Re^{-1/2}\frac{2a_0U_0}{\pi\lambda_0}\left[\pi - \arctan\left(\frac{y_*}{x_*}\right)\right]+\cdots,$$

$$p = P_{e0}+Re^{-1/5}\{c_1x_* + c_2y_*\} + Re^{-2/5}\{c_3x_*^2 + c_4x_*y_* + c_5y_*^2\}-$$
$$- Re^{-1/2}\ln Re\frac{2a_0U_0^2}{5\pi\lambda_0} + Re^{-1/2}\frac{2a_0U_0^2}{\pi\lambda}\ln\sqrt{x_*^2+y_*^2}+\cdots.$$

This suggests that the solution in region 5 should be sought in the form

$$
\begin{aligned}
V_\tau =& U_0 + Re^{-1/5}\{a_1 x_* + a_2 y_*\} + \\
& + Re^{-2/5}\{a_3 x_*^2 + a_4 x_* y_* + a_5 y_*^2\} + \\
& + Re^{-1/2}\ln Re\,\frac{2a_0 U_0}{5\pi\lambda_0} + Re^{-1/2}u_1^*(x_*, y_*) + \cdots,
\end{aligned}
\tag{237a}
$$

$$
\begin{aligned}
V_n =& Re^{-1/5}b_2 y_* + Re^{-2/5}\{b_4 x_* y_* + b_5 y_*^2\} + \\
& + Re^{-1/2}v_1^*(x_*, y_*) + \cdots,
\end{aligned}
\tag{237b}
$$

$$
\begin{aligned}
p =& P_{e0} + Re^{-1/5}\{c_1 x_* + c_2 y_*\} + \\
& + Re^{-2/5}\{c_3 x_*^2 + c_4 x_* y_* + c_5 y_*^2\} - \\
& - Re^{-1/2}\ln Re\,\frac{2a_0 U_0^2}{5\pi\lambda_0} + Re^{-1/2}p_1^*(x_*, y_*) + \cdots,
\end{aligned}
\tag{237c}
$$

where functions u_1^*, v_1^* and p_1^* satisfy the following matching conditions with the solution in region 1,

$$
\left.
\begin{aligned}
u_1^* &= -\frac{2a_0 U_0}{\pi\lambda_0}\ln\sqrt{x_*^2 + y_*^2} + \cdots, \\
v_1^* &= -\frac{2a_0 U_0}{\pi\lambda_0}\left[\pi - \arctan\left(\frac{y_*}{x_*}\right)\right] + \cdots, \\
p_1^* &= \frac{2a_0 U_0^2}{\pi\lambda_0}\ln\sqrt{x_*^2 + y_*^2} + \cdots
\end{aligned}
\right\}
\quad \text{as} \quad x_*^2 + y_*^2 \to \infty. \tag{238}
$$

The equations for these functions are deduced by substituting (237) into the Navier-Stokes equations (81), and working with the $O(Re^{-3/10})$ terms. We find

$$
U_0\frac{\partial u_1^*}{\partial x_*} = -\frac{\partial p_1^*}{\partial x_*}, \qquad U_0\frac{\partial v_1^*}{\partial x_*} = -\frac{\partial p_1^*}{\partial y_*}, \qquad \frac{\partial u_1^*}{\partial x_*} + \frac{\partial v_1^*}{\partial y_*} = 0. \tag{239}
$$

The set of equations (239) is easily reduced to a single equation for function p_1^*. We start by eliminating u_1^*. This is done by solving the last of equations (239) and substituting the result into the first equation. We have

$$
U_0\frac{\partial v_1^*}{\partial y_*} = \frac{\partial p_1^*}{\partial x_*}, \qquad U_0\frac{\partial v_1^*}{\partial x_*} = -\frac{\partial p_1^*}{\partial y_*}. \tag{240}
$$

Now we eliminate v_1^* by cross-differentiating equations (240). We find that the pressure p_1^* satisfies the Laplace equation

$$
\frac{\partial^2 p_1^*}{\partial x_*^2} + \frac{\partial^2 p_1^*}{\partial y_*^2} = 0. \tag{241}
$$

When solving this equation we will use the method of Fourier Transforms. The later is applicable to functions that tend to zero as $|x_*| \to \infty$. It follows from (238) that p_1^* does not belong to this category. Therefore, we shall differentiate (241) with respect to x_*

$$\frac{\partial^2}{\partial x_*^2}\left(\frac{\partial p_1^*}{\partial x_*}\right) + \frac{\partial^2}{\partial y_*^2}\left(\frac{\partial p_1^*}{\partial x_*}\right) = 0, \tag{242}$$

and treat $\partial p_1^*/\partial x_*$ as the sought function. The "far-field" boundary condition for this function is written as

$$\frac{\partial p_1^*}{\partial x_*} = \frac{2a_0 U_0^2}{\pi \lambda_0}\frac{x_*}{x_*^2 + y_*^2} \to 0 \quad \text{as} \quad x_*^2 + y_*^2 \to \infty. \tag{243}$$

The equation (242) also requires a boundary condition at $y_* = 0$. It will be formulated in the course of the flow analysis in regions 3 and 4; see Figure 21.

Viscous syblayer (region 3)   When analysing the interactive flow regimes with the parameter k in the range (229), we can write the independent variables (166) in region 3 as

$$x_* = \frac{x - x_0}{Re^{-1/5}}, \qquad Y_* = \frac{y}{Re^{-11/20}}. \tag{244}$$

Remind that (x, y) are curvilinear orthogonal coordinates introduced as shown in Figure (17).

In order to predict the form of the asymptotic expansion of the stream function in region 3 we shall again recast the solution in region 2a in terms of variables (244). Recall that when the flow was analysed in the frame of classical boundary-layer theory (see Section ?), this procedure led to the equation (171). Now instead of (168) and (169) we have to use

$$(-s) = Re^{-1/5}(-x_*), \qquad \eta = \frac{Y_*}{(-x_*)^{1/4}}, \qquad \Delta k = k - k_0 = Re^{-2/5}k_1,$$

which, being substituted into (167), yield

$$\psi = Re^{-1/2}\Psi = Re^{-13/20}\frac{1}{6}\lambda_0 Y_*^3 +$$

$$+ Re^{-16/20}\left\{(-x_*)\frac{1}{2}a_0 Y_*^2 + (-x_*)^{-1}\frac{1}{2}k_1 a_1 Y_*^2\right\}+$$

$$+ Re^{-17/20}\left\{\frac{1}{6}\lambda_1 x_* Y_*^3 + \frac{2\lambda_0\lambda_1}{7!}Y_*^7\right\}+$$

$$+ Re^{-19/20}\left\{\frac{a_0^2}{5!}x_* Y_*^5 + \frac{\lambda_0 a_0^2}{8!}Y_*^9 + (-x_*)^{7/4}\frac{1}{2}b_0 Y_*^2 +\right.$$

$$\left.(-x_*)^{-1/4}\frac{1}{2}k_1 b_1 Y_*^2\right\} + \cdots .$$

This suggests that the asymptotic expansion of the stream function ψ in region 3 should be sought in the form

$$\psi = Re^{-13/20}\frac{1}{6}\lambda_0 Y_*^3 + Re^{-16/20}\Psi_1^*(x_*, Y_*) +$$

$$+ Re^{-17/20}\left(\frac{1}{6}\lambda_1 x_* Y_*^3 + \frac{2\lambda_0\lambda_1}{7!}Y_*^7\right) + Re^{-19/20}\Psi_2^*(x_*, Y_*) + \cdots ,$$

$$(245)$$

where functions $\Psi_1^*(x_*, Y_*)$ and $\Psi_2^*(x_*, Y_*)$ are such that

$$\Psi_1^* = \frac{1}{2}\left\{a_0(-x_*) + k_1 a_1(-x_*)^{-1}\right\}Y_*^2 + \cdots \qquad \text{as} \quad x_* \to -\infty \quad (246a)$$

and

$$\Psi_2^* = \frac{a_0^2}{5!}x_* Y_*^5 + \frac{\lambda_0 a_0^2}{8!}Y_*^9 +$$

$$+ \frac{1}{2}\left\{b_0(-x_*)^{7/4} + k_1 b_1(-x_*)^{-1/4}\right\}Y_*^2 + \cdots \quad \text{as} \quad x_* \to -\infty. \quad (246b)$$

We shall represent the pressure in region 3 by the asymptotic expansion

$$p = P_{e0} + Re^{-1/5}\lambda_0 x_* + Re^{-2/5}\frac{1}{2}\lambda_1 x_*^2 -$$

$$- Re^{-1/2}\ln Re\frac{2a_0 U_0^2}{5\pi\lambda_0} + Re^{-1/2}P^*(x_*, Y_*) + \cdots ,$$

$$(247)$$

the form of which is obtained by setting $y_* = 0$ in (237c) and using (234).

We are now ready to formulate the equations of fluid motion in region 3. We start by substituting (245), (244) into (82). This leads to the following

expressions of the velocity components in region 3,

$$
\begin{aligned}
V_\tau =& Re^{-2/20}\frac{1}{2}\lambda_0 Y_*^2 + Re^{-5/20}\frac{\partial\Psi_1^*}{\partial Y_*} + \\
& + Re^{-6/20}\left(\frac{1}{2}\lambda_1 x_* Y_*^2 + \frac{2\lambda_0\lambda_1}{6!}Y_*^6\right) + Re^{-8/20}\frac{\partial\Psi_2^*}{\partial Y_*} + \cdots,
\end{aligned}
\tag{248a}
$$

$$
V_n = -Re^{-12/20}\frac{\partial\Psi_1^*}{\partial x_*} - Re^{-13/20}\frac{1}{6}\lambda_1 Y_*^3 - Re^{-15/20}\frac{\partial\Psi_2^*}{\partial x_*} + \cdots.
\tag{248b}
$$

We then substitute (248) together with (247) into the Navier-Stokes equations (81). We find from the x-momentum equation (81a) that the equation (175) for Ψ_1^* retains its form

$$
\tfrac{1}{2}\lambda_0 Y_*^2 \frac{\partial^2\Psi_1^*}{\partial x_*\partial Y_*} - \lambda_0 Y_* \frac{\partial\Psi_1^*}{\partial x_*} = \frac{\partial^3\Psi_1^*}{\partial Y_*^3}.
$$

Its solution , satisfying the no-slip conditions

$$
\Psi_1^* = \frac{\partial\Psi_1^*}{\partial Y_*} = 0 \quad \text{at} \quad Y_* = 0,
$$

is written as

$$
\Psi_1^* = \tfrac{1}{2}A_*(x_*)Y_*^2.
\tag{249}
$$

At this stage, the function $A_*(x_*)$ remains arbitrary; we can only claim that in view of (246a),

$$
A_*(x_*) = a_0(-x_*) + k_1 a_1(-x_*)^{-1} + \cdots \quad \text{as} \quad x_* \to -\infty.
\tag{250}
$$

The equation (184a) for function Ψ_2^* now acquires an additional term, the induced pressure gradient,

$$
\tfrac{1}{2}\lambda_0 Y_*^2 \frac{\partial^2\Psi_2^*}{\partial x_*\partial Y_*} - \lambda_0 Y_* \frac{\partial\Psi_2^*}{\partial x_*} = \frac{\partial^3\Psi_2^*}{\partial Y_*^3} - \tfrac{1}{2}A_*\frac{dA_*}{dx_*}Y_*^2 - \frac{\partial P^*}{\partial x_*}.
\tag{251}
$$

Substitution of (247), (248) into the y-momentum equation (81b) shows that P^* does not change across region 3, namely,

$$
\frac{\partial P^*}{\partial Y_*} = 0.
\tag{252}
$$

Main part of the boundary layer (region 4) When the parameter k belongs to the range (229), the asymptotic expansion (210) of the stream function in region 4 is written as

$$\psi = Re^{-1/2}\Psi_{00}(Y) + Re^{-7/10}\widetilde{\Psi}_1(x_*, Y) + \cdots .\qquad(253)$$

Here

$$x_* = \frac{x - x_0}{Re^{-1/5}}, \qquad Y = \frac{y}{Re^{-1/2}}.$$

By analogy with (247) we shall seek the asymptotic expansion for the pressure in region 4 in the form

$$p = P_{e0} + Re^{-1/5}\lambda_0 x_* + Re^{-2/5}\tfrac{1}{2}\lambda_1 x_*^2 -$$
$$- Re^{-1/2}\ln Re\frac{2a_0 U_0^2}{5\pi\lambda_0} + Re^{-1/2}\widetilde{P}(x_*, Y) + \cdots .$$
$$(254)$$

Substitution of (253) into (82), yields

$$V_\tau = \Psi'_{00}(Y) + Re^{-1/5}\frac{\partial\widetilde{\Psi}_1}{\partial Y} + \cdots , \qquad V_n = -Re^{-1/2}\frac{\partial\widetilde{\Psi}_1}{\partial x_*} + \cdots . \quad(255)$$

We then substitute (255) and (254) into the x-momentum equation (81a). We find that the equation (216) retains its form[6]. Since the boundary conditions (211) and (215) also remain unchanged, we can use for $\widetilde{\Psi}_1$ the solution given by (219),

$$\widetilde{\Psi}_1(x_*, Y_*) = \Psi'_{00}(Y)\left[x_* \int_0^Y \frac{\Psi'''_{00} - \lambda_0}{\left(\Psi'_{00}\right)^2}dY' + \frac{A_*(x_*)}{\lambda_0}\right].\qquad(256)$$

It follows from (255) and (256) that the angle made by the streamlines with the aerofoil contour is calculated as

$$\vartheta = \frac{V_n}{V_\tau} = Re^{-1/2}\left[\int_0^Y \frac{\lambda_0 - \Psi'''_{00}}{\left(\Psi'_{00}\right)^2}dY' - \frac{1}{\lambda_0}\frac{dA_*}{dx_*}\right] + \cdots .$$

It obviously changes with Y, but the curvature of the streamlines

$$\frac{\partial\vartheta}{\partial x} = -Re^{-3/10}\frac{1}{\lambda_0}\frac{d^2 A_*}{dx_*^2} + \cdots \qquad(257)$$

---

[6]The induced pressure gradient $\partial P^*/\partial x_*$ is simply too weak to affect the flow in region 4.

stays constant across region 4.

To complete the flow analysis in region 4 we substitute (255) and (254) into the y-momentum equation (81b). Restricting our attention to the leading order terms, we find

$$\frac{\partial \widetilde{P}}{\partial Y} = \kappa(x_0) \big[\Psi'_{00}(Y) \big]^2.$$

Here $\kappa(x_0)$ is the curvature of the aerofoil contour at point $x = x_0$. We see that while the pressure $\widetilde{P}$ changes with Y, the pressure gradient $\partial \widetilde{P} / \partial x_*$ remains constant across region 4:

$$\frac{\partial}{\partial Y} \left(\frac{\partial \widetilde{P}}{\partial x_*} \right) = 0.$$

The Interaction Problem In order to describe the flow behaviour in the interaction region, one needs to solve equation (251) in region 3,

$$\tfrac{1}{2}\lambda_0 Y_*^2 \frac{\partial^2 \Psi_2^*}{\partial x_* \partial Y_*} - \lambda_0 Y_* \frac{\partial \Psi_2^*}{\partial x_*} = \frac{\partial^3 \Psi_2^*}{\partial Y_*^3} - \tfrac{1}{2} A_* \frac{dA_*}{dx_*} Y_*^2 - \frac{\partial P^*}{\partial x_*}, \qquad (258)$$

subject to the no-slip conditions on the aerofoil surface

$$\Psi_2^* = \frac{\partial \Psi_2^*}{\partial Y_*} = 0 \quad \text{at} \quad Y_* = 0, \qquad (259)$$

and the matching condition (246b) with the solution in region $2a$,

$$\Psi_2^* = \frac{a_0^2}{5!} x_* Y_*^5 + \frac{\lambda_0 a_0^2}{8!} Y_*^9 + $$
$$+ \frac{1}{2} \Big\{ b_0(-x_*)^{7/4} + k_1 b_1 (-x_*)^{-1/4} \Big\} Y_*^2 + \cdots \quad \text{as} \quad x_* \to -\infty. \qquad (260)$$

As the pressure gradient $\partial P^* / \partial x_*$ in (258) is not known, we also need to solve equation (242) in region 5,

$$\frac{\partial^2}{\partial x_*^2} \left(\frac{\partial p_1^*}{\partial x_*} \right) + \frac{\partial^2}{\partial y_*^2} \left(\frac{\partial p_1^*}{\partial x_*} \right) = 0. \qquad (261)$$

The solution has to satisfy the attenuation condition (243) in the "far-field",

$$\frac{\partial p_1^*}{\partial x_*} \to 0 \quad \text{as} \quad x_*^2 + y_*^2 \to \infty, \qquad (262)$$

and a matching condition with the solution in region 4, which will now be deduced.

We know that the curvature of the streamlines in region 4 is given by (257),

$$\frac{\partial \vartheta}{\partial x} = -Re^{-3/10}\frac{1}{\lambda_0}\frac{d^2 A_*}{dx_*^2} + \cdots \tag{263}$$

It follows from (237a), (237b) that at the "bottom" of region 5 the angle made by the streamlines with the aerofoil surface is calculated as

$$\vartheta = \left.\frac{V_n}{V_\tau}\right|_{y_*=0} = Re^{-1/2}\frac{v_1^*(x_*,0)}{U_0} + \cdots . \tag{264}$$

Differentiation of (264) with respect to x results in

$$\frac{\partial \vartheta}{\partial x} = Re^{-3/10}\frac{1}{U_0}\left.\frac{\partial v_1^*}{\partial x_*}\right|_{y_*=0} + \cdots . \tag{265}$$

Comparing (265) with (263), we can conclude that the sought matching condition is written as

$$\left.\frac{\partial v_1^*}{\partial x_*}\right|_{y_*=0} = -\frac{U_0}{\lambda_0}\frac{d^2 A_*}{dx_*^2}.$$

It remains to reformulate this condition for the pressure gradient. For this purpose the second equation in (240) is used. Differentiating the equation with respect to x_* and setting $y_* = 0$ we find

$$\frac{\partial}{\partial y_*}\left(\frac{\partial p_1^*}{\partial x_*}\right) = \frac{U_0^2}{\lambda_0}\frac{d^3 A_*}{dx_*^3} \quad \text{at} \quad y_* = 0. \tag{266}$$

This completes the formulation of the viscous-inviscid interaction problem. In order to describe the flow in the interaction region, we need to solve simultaneously equation (258) subject to the boundary conditions (259), (260) and equation (261) subject to the boundary conditions (262), (266).

Before solving the interaction problem, we shall express it in canonic form. In the viscous sublayer (region 3) we introduce a new unknown function Ψ_2 such that

$$\Psi_2^* = \Psi_2 + \frac{\lambda_0 a_0^2}{8!}Y_*^9 + \frac{a_0^2}{5!}x_* Y_*^5 + \tfrac{1}{2}B_*(x_*)Y_*^2 + G_*(x_*)Y_*,$$

with

$$G_*(x_*) = \frac{A_*^2 - a_0^2 x_*^2 - 2k_1 a_0 a_1}{2\lambda_0},$$

and perform the affine transformations

$$\Psi_2 = \frac{a_0^{11/10} U_0^{9/5}}{\lambda_0^{17/10}} \bar{\Psi}, \qquad A_* = \frac{a_0^{3/5} U_0^{4/5}}{\lambda_0^{1/5}} A, \qquad \frac{\partial P^*}{\partial x_*} = \frac{a_0^{7/5} U_0^{6/5}}{\lambda_0^{4/5}} R(X),$$

$$G_* = \frac{a_0^{6/5} U_0^{8/5}}{\lambda_0^{7/5}} G(X), \qquad x_* = \frac{U_0^{4/5}}{a_0^{2/5} \lambda_0^{1/5}} X, \qquad Y_* = \frac{U_0^{1/5}}{a_0^{1/10} \lambda_0^{3/10}} \bar{Y}.$$

As a result the equation (258) and boundary conditions (259), (260) assume the form

$$\tfrac{1}{2}\bar{Y}^2 \frac{\partial^2 \bar{\Psi}}{\partial X \partial Y} - \bar{Y}\frac{\partial \bar{\Psi}}{\partial X} = \frac{\partial^3 \bar{\Psi}}{\partial \bar{Y}^3} - R(X), \tag{267a}$$

$$\bar{\Psi} = 0, \quad \frac{\partial \bar{\Psi}}{\partial \bar{Y}} = -G(X) \quad \text{at} \quad \bar{Y} = 0, \tag{267b}$$

$$\bar{\Psi} \to 0 \quad \text{as} \quad X \to -\infty. \tag{267c}$$

Here

$$G(X) = \tfrac{1}{2}\big(A^2 - X^2 + 2a\big), \tag{268}$$

with parameter a defined as

$$a = k_1 \frac{(-a_1)\lambda_0^{2/5}}{a_0^{1/5} U_0^{8/5}}. \tag{269}$$

In the new variables the condition (250) is written as

$$A(X) = (-X) - a(-X)^{-1} + \cdots \quad \text{as} \quad X \to -\infty, \tag{270}$$

which means that $G(X)$ tends to zero as $X \to -\infty$.

In the upper tier (region 5) the affine transformations are written as

$$\frac{\partial p_1^*}{\partial x_*} = \frac{a_0^{7/5} U_0^{6/5}}{\lambda_0^{4/5}} r(X, \bar{y}), \qquad x_* = \frac{U_0^{4/5}}{a_0^{2/5} \lambda_0^{1/5}} X, \qquad y_* = \frac{U_0^{4/5}}{a_0^{2/5} \lambda_0^{1/5}} \bar{y}.$$

They render the equation (261) and boundary conditions (262), (266) in the form

$$\frac{\partial^2 r}{\partial X^2} + \frac{\partial^2 r}{\partial \bar{y}^2} = 0, \tag{271a}$$

$$r \to 0 \quad \text{as} \quad X^2 + \bar{y}^2 \to \infty, \tag{271b}$$

$$\left.\frac{\partial r}{\partial \bar{y}}\right|_{\bar{y}=0} = \frac{dQ}{dX}, \tag{271c}$$

where $Q(X)$ denotes the second derivative of function $A(X)$,

$$Q(X) = A''(X).$$

Finally, taking into account that the pressure gradient does not change across the middle tier (region 4), we can write

$$r\Big|_{\bar{y}=0} = R(X). \tag{272}$$

Notice that being written in the new variables, the equations (267), (271) describing the flow in the interaction region, involve a single controlling parameter (269), which measures the deviation of the angle of attack from its critical value; as $a_1 < 0$, the parameter a increases with k_1, and hence, with the angle of attack.

We shall now try to solve the equations of viscous-inviscid interaction with the help of Fourier Transforms. We start with the inviscid flow in region 5. It is easily seen that the Fourier transformation renders (271) in the form

$$\frac{d^2 \breve{r}}{d\bar{y}^2} - k^2 \breve{r} = 0, \tag{273a}$$

$$\breve{r} = 0 \quad \text{at} \quad \bar{y} = \infty, \tag{273b}$$

$$\frac{d\breve{r}}{d\bar{y}} = ik\breve{Q} \quad \text{at} \quad \bar{y} = 0. \tag{273c}$$

Here $\breve{r}(k, \bar{y})$ stands for the Fourier Transform of the function $r(X, \bar{y})$ defined as

$$\breve{r}(k, \bar{y}) = \int\limits_{-\infty}^{\infty} r(X, \bar{y}) e^{-ikX} dX,$$

and $\breve{Q}(k)$ denotes the Fourier Transform of the function $Q(X)$.

The general solution of the equation (273a) has the form

$$\breve{r} = C_1 e^{k\bar{y}} + C_2 e^{-k\bar{y}}. \tag{274}$$

In order to satisfy the boundary condition (273b) one has to set $C_1 = 0$ for all $k > 0$, and $C_2 = 0$ for all $k < 0$. Therefore, we shall write (274) in the form

$$\breve{r} = C e^{-|k|\bar{y}}. \tag{275}$$

Substitution of (275) into (273c) yields

$$C = -\frac{ik}{|k|} \breve{Q}. \tag{276}$$

It remains to substitute (276) back into (275), and we will have the solution of the problem (273) in the form

$$\check{r} = -\frac{ik}{|k|}\check{Q}e^{-|k|\bar{y}}. \tag{277}$$

Let us now consider the flow in the viscous sublayer (region 3). The Fourier transformation converts the problem (267) for this region into

$$\tfrac{1}{2}ik\bar{Y}^2\frac{d\check{\Psi}}{d\bar{Y}} - ik\bar{Y}\check{\Psi} = \frac{d^3\check{\Psi}}{d\bar{Y}^3} - \check{R}, \tag{278a}$$

$$\check{\Psi} = 0, \quad \frac{d\check{\Psi}}{d\bar{Y}} = -\check{G}(k) \quad \text{at} \quad \bar{Y} = 0. \tag{278b}$$

Here $\check{\Psi}(k,\bar{Y})$, $\check{G}(k)$ and $\check{R}(k)$ are the Fourier Transforms of functions $\bar{\Psi}$, $G(X)$ and $R(X)$, respectively.

Unlike (188a) the equation (278a) is not homogeneous. Therefore, its general solution is written as

$$\check{\Psi} = C_1\psi_{21} + C_2\psi_{22} + C_3\psi_{23} + \psi_{2p}, \tag{279}$$

where ψ_{2p} is a particular solution of the equation (278a) and ψ_{21}, ψ_{22} and ψ_{23} are the complementary solutions of the homogeneous part of (278a). These may be chosen such that

$$
\begin{aligned}
\psi_{21}(0) &= 1, & \psi_{21}'(0) &= 0, & \psi_{21}''(0) &= 0, \\
\psi_{22}(0) &= 0, & \psi_{22}'(0) &= 1, & \psi_{22}''(0) &= 0, \\
\psi_{23}(0) &= 0, & \psi_{23}'(0) &= 0, & \psi_{23}''(0) &= 1, \\
\psi_{2p}(0) &= 0, & \psi_{2p}'(0) &= 0, & \psi_{2p}''(0) &= 0.
\end{aligned}
\tag{280}
$$

It then follows from the boundary conditions (278b) that $C_1 = 0$, and $C_2 = -\check{G}(k)$. Factor C_3 remains arbitrary, and the third complementary solution is easily seen to be $\psi_{23} = \tfrac{1}{2}\bar{Y}^2$. Taking these into account, we can write (279) as

$$\check{\Psi} = -\check{G}(k)\psi_{22} + \tfrac{1}{2}C_3(k)\bar{Y}^2 + \psi_{2p}. \tag{281}$$

The behaviour of the function $\psi_{22}(\bar{Y})$ has been already studied in detail. In particular, we found that its asymptotic behaviour at the outer edge of region 3 is given by (204), namely,

$$\psi_{22}(\bar{Y}) = -\frac{\Gamma(5/4)}{2\sqrt{\pi}e^{i\frac{\pi}{4}}\Omega^{1/4}}\left(\frac{4}{i\Omega^{1/2}\bar{Y}^2}\right)^{5/4}\sin\left(\tfrac{1}{2}i\Omega^{1/2}\bar{Y}^2 - \tfrac{3}{8}\pi\right) + \cdots \tag{282}$$

$$\text{as} \quad \bar{Y} \to \infty,$$

with $\Omega = \frac{1}{2}ik$.

Now our task will be to study the particular solution $\psi_{2p}(\bar{Y})$. Function $\psi_{2p}(\bar{Y})$ satisfies the equation (278a). If we set $\bar{Y} = 0$ in this equation, we will find that

$$\frac{d^3\psi_{2p}}{d\bar{Y}^3} = \breve{R}. \tag{283}$$

Integration of (283) with the boundary conditions (280) yields

$$\psi_{2p}(\bar{Y}) = \frac{1}{6}\breve{R}\bar{Y}^3. \tag{284}$$

We then use (284) to calculate the left hand side in (278a), and perform the integration again. We find

$$\psi_{2p}(\bar{Y}) = \frac{1}{6}\breve{R}\bar{Y}^3 + \frac{2}{7!}ik\breve{R}\bar{Y}^7.$$

The above procedure may be repeated as many times as one wishes, leading to a conclusion that the power series of function ψ_{2p} should be sought in the form

$$\psi_{2p}(\bar{Y}) = \frac{1}{6}\breve{R}\bar{Y}^3 + \sum_{n=0}^{\infty} c_{n+1}\bar{Y}^{7+4n}. \tag{285}$$

Alternatively, we can write (285) as

$$\psi_{2p}(\bar{Y}) = \sum_{n=0}^{\infty} c_n\bar{Y}^{3+4n}. \tag{286}$$

Using (286) on the left hand side of the equation (278a), and (285) on the right hand side, results in the following recurrent equation for the coefficients c_n,

$$c_{n+1} = \frac{ik}{32}\frac{n + \frac{1}{4}}{\left(n + \frac{7}{4}\right)\left(n + \frac{5}{4}\right)\left(n + \frac{3}{2}\right)}c_n,$$

which has to be solved starting with $c_0 = \frac{1}{6}\breve{R}$. The solution is written as

$$c_n = \frac{\breve{R}}{6}\left(\frac{ik}{32}\right)^n \frac{\Gamma(3/2)\Gamma(7/4)}{\Gamma(n + 3/2)\Gamma(n + 7/4)(4n + 1)}. \tag{287}$$

It remains to substitute (287) back into (286), and we will have[7]

$$\psi_{2p}(\bar{Y}) = \frac{\sqrt{\pi}}{16}\breve{R}\Gamma\left(\frac{3}{4}\right)\sum_{n=0}^{\infty}\left(\frac{ik}{32}\right)^n \frac{\bar{Y}^{4n+3}}{\Gamma(n + 3/2)\Gamma(n + 7/4)(4n + 1)}. \tag{288}$$

---

[7]Here it is taken into account that
$$\Gamma(3/2) = \frac{1}{2}\sqrt{\pi} \quad \text{and} \quad \Gamma(7/4) = \frac{3}{4}\Gamma(3/4).$$

We shall now show that the function $\psi_{2p}(\bar{Y})$ may be expressed in terms of the Struve function $H_\nu(z)$. It is known that the Struve function may be represented by the power series

$$H_\nu(z) = \sum_{n=0}^{\infty} \frac{(-1)^n}{\Gamma(n + 3/2)\Gamma(n + \nu + 3/2)} \left(\frac{z}{2}\right)^{2n+\nu+1}, \qquad (289)$$

which converges for all finite values of z. It is also known that

$$H_\nu(z) = \sqrt{\frac{2}{\pi z}} \sin\left(z - \tfrac{1}{2}\nu\pi - \tfrac{1}{4}\pi\right) + \cdots \quad \text{as} \quad |z| \to \infty, \quad (|\arg z| < \pi). \tag{290}$$

We choose the order of the Struve function to be $\nu = \frac{1}{4}$, and then it easily follows from (289) that

$$\sum_{n=0}^{\infty} \frac{(-1)^n}{\Gamma(n + 3/2)\Gamma(n + 7/4)(4n + 1)} \left(\frac{z}{2}\right)^{2n+3/2} = \frac{z}{8} \int_0^z \left(\frac{2}{z}\right)^{7/4} H_{1/4}(z)dz. \tag{291}$$

Substituting (290) into the integral in (291) and performing the integration by parts with

$$u = \left(\frac{2}{z}\right)^{9/4}, \qquad dv = \sin\left(z - \tfrac{3}{8}\pi\right) dz,$$

$$du = -\frac{9}{8}\left(\frac{2}{z}\right)^{13/4} dz, \qquad v = -\cos\left(z - \tfrac{3}{8}\pi\right),$$

we find that

$$\sum_{n=0}^{\infty} \frac{(-1)^n}{\Gamma(n + 3/2)\Gamma(n + 7/4)(4n + 1)} \left(\frac{z}{2}\right)^{2n+3/2} =$$

$$= -\frac{1}{4\sqrt{\pi}}\left(\frac{2}{z}\right)^{5/4} \cos\left(z - \tfrac{3}{8}\pi\right) + \cdots \quad \text{as} \quad |z| \to \infty. \tag{292}$$

If we now set

$$\Omega = \tfrac{1}{2}ik, \qquad z = \tfrac{1}{2}i\Omega^{1/2}\bar{Y}^2, \tag{293}$$

then the equation (292) will turn into

$$\sum_{n=0}^{\infty} \left(\frac{ik}{32}\right)^n \frac{\bar{Y}^{4n+3}}{\Gamma(n + 3/2)\Gamma(n + 7/4)(4n + 1)} =$$

$$= -\frac{2}{\sqrt{\pi}e^{i\frac{3}{4}\pi}\Omega^{3/4}} \left(\frac{4}{i\Omega^{1/2}\bar{Y}^2}\right)^{5/4} \cos\left(\tfrac{1}{2}i\Omega^{1/2}\bar{Y}^2 - \tfrac{3}{8}\pi\right) + \cdots. \tag{294}$$

It remains to substitute (294) into (288), and we can conclude that

$$\psi_{2p}(\bar{Y}) = -\frac{\check{R}\,\Gamma(3/4)}{8e^{i\frac{3}{4}\pi}\Omega^{3/4}}\left(\frac{4}{i\Omega^{1/2}\bar{Y}^2}\right)^{5/4}\cos\left(\tfrac{1}{2}i\Omega^{1/2}\bar{Y}^2 - \tfrac{3}{8}\pi\right) + \cdots \quad (295)$$

as $\bar{Y} \to \infty$. To progress further we need to define more precisely the way an analytic branch of the square root of $\frac{1}{2}ik$ is introduced in (293). For our purposes it is convenient to make a branch cut in the complex plane k along positive imaginary semi-axis, as shown in Figure 22(a). Expressing k in the form $k = re^{i\vartheta}$, we find that for k lying on the real axis, equations (293) give

$$z = \begin{cases} \frac{1}{2}\sqrt{\frac{k}{2}}e^{i\frac{3}{4}\pi}\bar{Y}^2 & \text{if } k > 0, \\ \frac{1}{2}\sqrt{\frac{(-k)}{2}}e^{i\frac{1}{4}\pi}\bar{Y}^2 & \text{if } k < 0. \end{cases}$$

This means that as $\bar{Y}$ tends to infinity the corresponding point in the complex z-plane runs to infinity along one of the rays shown in Figure 22(b); which one depends on the sign of k. On both rays $\Re\{iz\} < 0$. Consequently,
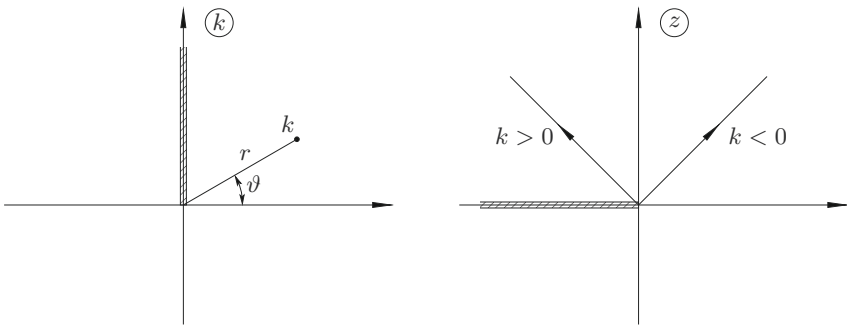
a) Complex plane of the Fourier   b) Complex plane z
   variable k.

Figure 22. Graphical illustration of equations (293).

$$\left.\begin{array}{l} \sin\left(z - \tfrac{3}{8}\pi\right) = \dfrac{e^{i\left(z-\frac{3}{8}\pi\right)} - e^{-i\left(z-\frac{3}{8}\pi\right)}}{2i} = -\dfrac{1}{2i}e^{-i\left(z-\frac{3}{8}\pi\right)} + \cdots, \\[4mm] \cos\left(z - \tfrac{3}{8}\pi\right) = \dfrac{e^{i\left(z-\frac{3}{8}\pi\right)} + e^{-i\left(z-\frac{3}{8}\pi\right)}}{2} = \dfrac{1}{2}e^{-i\left(z-\frac{3}{8}\pi\right)} + \cdots \end{array}\right\} \quad (296)$$

as $\bar{Y} \to \infty$.

Substituting (296) into (295) and (282), and then into (281), we find that at the outer edge of region 3 (see Figure 21),

$$\breve{\Psi} = -\frac{1}{4e^{i\frac{3}{4}\pi}\Omega^{1/4}}\left[\frac{\Gamma(5/4)}{\sqrt{\pi}}\breve{G}(k)+\frac{\Gamma(3/4)}{4\Omega^{1/2}}\breve{R}(k)\right]\left(\frac{4}{i\Omega^{1/2}\bar{Y}^2}\right)^{5/4}e^{-i\left(z-\frac{3}{8}\pi\right)}+\cdots.$$

In order to ensure that the solution in region 3 can be matched with the solution in region 4, we have to suppress the exponential growth of the function $\breve{\Psi}$, which is done by setting

$$\frac{\Gamma(5/4)}{\sqrt{\pi}}\breve{G}(k) + \frac{\Gamma(3/4)}{4\Omega^{1/2}}\breve{R}(k) = 0. \tag{297}$$

The above equation relates (in the Fourier space) the pressure gradient in region 3 with the function $A(X)$. The second relationship between these functions is given by the solution (277) in region 5. The solutions in regions 3 and 5 are linked to one another through the equation (272). Writing this equation in terms of the Fourier Transforms, and using (277), we find that

$$\breve{R}(k) = \breve{r}\Big|_{\bar{y}=0} = -\frac{ik}{|k|}\breve{Q}(k). \tag{298}$$

The Fourier Transform of the pressure gradient, $\breve{R}(k)$, may be easily eliminated from (298) and (297), leading to

$$\breve{G}(k) = \frac{\sqrt{\pi}}{2}\Lambda\frac{(ik)^{1/2}}{|k|}\breve{Q}(k). \tag{299}$$

Here Λ is a constant given by

$$\Lambda = \frac{\Gamma(3/4)}{\sqrt{2}\Gamma(5/4)}.$$

We shall now try to express (299) in physical variables. Applying the inverse Fourier transformation to the equation (299), renders it in the form[8]

$$\tfrac{1}{2}\left(A^2 - X^2 + 2a\right) = \frac{\sqrt{\pi}}{2}\Lambda\frac{1}{2\pi}\int\limits_{-\infty}^{\infty}\frac{(ik)^{1/2}}{|k|}\breve{Q}(k)e^{ikX}dk. \tag{300}$$

Here $\breve{Q}(k)$ is the Fourier Transform of A'':

$$\breve{Q}(k) = \int\limits_{-\infty}^{\infty}A''(\xi)e^{-ik\xi}d\xi. \tag{301}$$

---

[8]Recall that $\breve{G}(k)$ is the Fourier Transform of the function $G(X) = \tfrac{1}{2}\left(A^2 - X^2 + 2a\right)$.

If we substitute (301) into the integral on the right hand side of (300) and change the order of integration, we will find that

$$A^2 - X^2 + 2a = \frac{\Lambda}{2\sqrt{\pi}} \int\limits_{-\infty}^{\infty} A''(\xi)I(X,\xi)d\xi, \tag{302}$$

where

$$I(X,\xi) = \int\limits_{-\infty}^{\infty} \frac{(ik)^{1/2}}{|k|} e^{ik(X-\xi)} dk. \tag{303}$$

It may be shown (see Exercise 4) that

$$I(X,\xi) = \begin{cases} 0 & \text{if} \quad \xi < X, \\ 2\sqrt{\frac{\pi}{\xi-X}}, & \text{if} \quad \xi > X. \end{cases} \tag{304}$$

Substitution of (304) into (302) results in the following integro-differential equation for function $A(X)$,

$$A^2 - X^2 + 2a = \Lambda \int\limits_{X}^{\infty} \frac{A''(\xi)}{\sqrt{\xi - X}} d\xi. \tag{305}$$

This equation does not allow for further simplification, and should be solved numerically. When performing the calculations one needs to use appropriate boundary conditions. The first of these is given by (270),

$$A(X) = (-X) - a(-X)^{-1} + \cdots \quad \text{as} \quad X \to -\infty, \tag{306}$$

and represents the condition of matching with the solution in the boundary layer upstream of the interaction region. It should be noted, however, that this condition alone does not make the solution of (305) unique. In addition to solutions with short separation bubbles, we are interested in, it also allows for the solutions with semi-infinite separation regions. Indeed, if, to make it simple, we choose $a = 0$, then the equation (305) with the boundary condition (306) will admit the solution $A = -X$. The latter matches with the smooth branch (143) of the solution to the boundary-layer equation outside the interaction region. In order to ensure the matching with the singular branch (146), we shall require

$$A(X) = X + \cdots \quad \text{as} \quad X \to \infty. \tag{307}$$

For more detailed analysis of the asymptotic behaviour of $A(X)$ at large values of $|X|$ see Exercise 5.

The results of the calculations are presented in Figures (23)–(26). Figure (23) shows how function $A(X)$ changes as the parameter a is gradually increased. It should be noted that the function $A(X)$ plays a dual role in the Marginal Separation theory. Firstly, through equation (257), it defines the shape of the streamlines in region 4, and therefore, similar to the corresponding function in the conventional triple-deck theory, it may be termed the displacement function. However, in the Marginal Separation theory it also appears to be proportional to the shear stress on the aerofoil surface. Indeed, according to (245), (249) and (244) the two-term asymptotic expansion of the stream function in the region 3 is written as

$$\psi = Re^{-13/20}\tfrac{1}{6}\lambda_0 Y_*^3 + Re^{-16/20}\tfrac{1}{2}A_*(x_*)Y_*^2 + \cdots , \qquad y = Re^{-11/20}Y_*.$$

Consequently, the dimensionless skin friction

$$\tau = \frac{1}{\sqrt{Re}}\frac{\partial^2\psi}{\partial y^2}\bigg|_{y=0} = Re^{-1/5}A_*(x_*) = Re^{-1/5}\frac{a_0^{3/5}U_0^{4/5}}{\lambda_0^{1/5}}A(X).$$
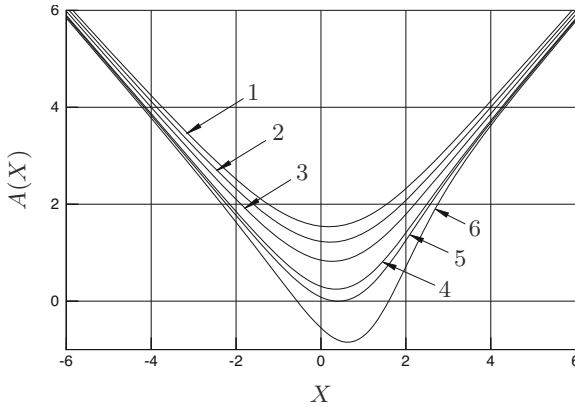
Figure 23. Solutions of the equation (305) on the upper branch of the fundamental curve: 1) $a = -0.5$; 2) $a = 0.0$; 3) $a = 0.5$; 4) $a = 1.0$; 5) $a = a_s = 1.139$; 6) $a = a_c = 1.330$.

Graph 2 in Figure 23 is plotted for $a = 0$, which corresponds to the critical value of the angle of attack, as estimated based on the classical boundary-layer theory. When the viscous-inviscid interaction is ignored, the Prandtl equations yield a singular solution with the skin friction given by (146). We see that the interaction acts to smooth out the singularity. The

minimal skin friction is lifted, and the skin friction appears to be positive for all values of $X \in (-\infty, \infty)$. For graph 5 the parameter a has been adjusted in such a way that the minimal skin friction returns back to zero to capture the incipience of the separation. We found that this happens at point $X = 0.406$ when the parameter a reaches the value $a_s = 1.139$. Finally, graph 6 is plotted for the critical value of the parameter $a_c = 1.330$. It shows a region of negative A between $X = -0.566$ and $X = 1.605$, occupied by the separation bubble. Interestingly enough, the solution does not exist beyond $a = a_c$.

This important result is illustrated by Figure 23, where the so called *fundamental curve* is displayed. This curve shows the entire set of admissible solutions of the Marginal Separation theory. It is constructed in the following way. Given a, the solution of the boundary value problem (305), (306), (307) yields the distribution of the shear stress $A(X)$ along the aerofoil surface. Each such solution is represented by a point on the fundamental curve, which is obtained by taking the value of $A(X)$ at $X = 0$, and plotting $A(0)$ against the parameter a. The numbered circles on the fundamental curve
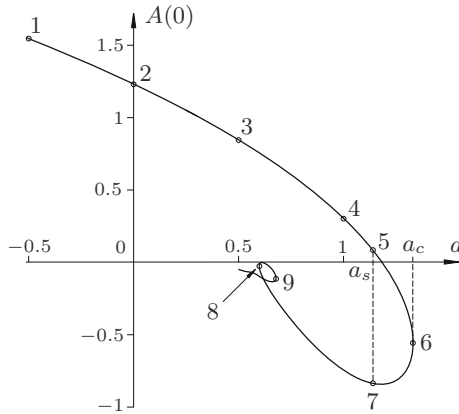
Figure 24. The fundamental curve.

represent the corresponding graphs of Figure 23. Notice that for $a = a_s$ (graph 5) the minimal skin friction is zero, but $A(0)$ is still positive. This explains why the corresponding point on the fundamental curve is situated above the abscissa.

When the parameter a reaches its critical value a_c the fundamental curve turns back to form the second branch of the solutions. In figure 25 we compare the solutions on the upper and lower branches for $a = a_s$. The first of these represents the flow with the separation region just about to appear;
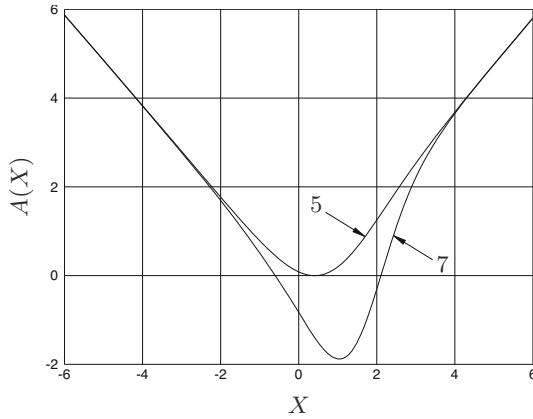
**Figure 25.** Comparison of the solutions on the upper and lower branches for $a = a_s = 1.139$.

in the second the separation region is already well developed. In fact, the length of the separation region grows monotonically as an "observer" follows the fundamental curve from the point 5 towards the critical point 6 and then all the way along the lower branch. This trend is demonstrated by Figure 26, where in addition to the solution at point 7 the solutions at points 8 and 9, that lie on a small loop on the lower branch, are shown.

Despite the parameter a is still rather large on the loop, the solution already shows an asymptotic behaviour characteristic of small a. When $a = 0$ the equation (305) admits two solutions

$$A = -X \quad \text{and} \quad A = X. \tag{308}$$

Neither of these satisfy both boundary conditions (306), (307), but they are clearly visible in Figure 26 as two major fragments of the curves 8 and 9, being connected to one another through a sharp jump in a region that becomes progressively shorter and moves to the right as $a \to 0-$.

Summarising the results of the above analysis, we can conclude that according to the Marginal Separation theory the flow near the leading edge of a thin aerofoil exhibits a *hysteresis* behaviour. It should be noted that hysteresis is routinely observed in experiments with aerofoils. These are normally conducted in such a way that the angle of attack is at first increased slowly enough to keep the flow quasi-steady, and then, after achieving the *aerofoil stall*, it is gradually decreased. What one usually observes is that the angle of attack at which the separation region forms on the upper surface of the aerofoil does not coincide with the angle of attack at which the flow
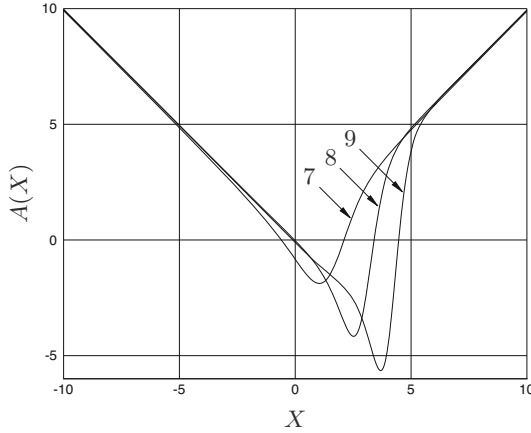
Figure 26. Solutions on the lower branch of the fundamental curve: 7) $a = a_s = 1.139$; 8) $a = 0.600$; 9) $a = 0.680$.

returns back to attached form. As a result the graph of the lift force versus the angle of attack assumes the shape of a hysteresis curve. Within the hysteresis loop, for each value of the angle of attack two flow states become possible. The choice between them depends on the flow history of the development of the flow.

Still experimental observations of the short separation bubbles show that these are formed in a smooth manner without abrupt change of the flow field, which is only possible if the solution remains on the upper branch of the fundamental curve when the parameter a passes through a_s. Of course, the flow cannot continue to change smoothly when the parameter a passes through the critical value a_c. The non-existence of the solution to (305), (306), (307) for $a > a_c$ suggests that the flow has to undergo a sudden change, known from experiment as the "bubble bursting".

In order to calculate the values of the angle of attack at the incipience of the short separation bubble and at the bubble bursting, we need to return to the equation (79). Combining it with (231) and (269), we find that the scaled angle of attack $\alpha_* = \alpha/\varepsilon$ is given by

$$\alpha_* = \frac{1}{\sqrt{2}}\left[k_0 + Re^{-2/5}\frac{a_0^{1/5}U_0^{8/5}}{(-a_1)\lambda_0^{2/5}}\, a \right] - \frac{1}{\pi}\int\limits_0^1 \frac{G(x')}{\sqrt{x'(1-x')}}\, dx'. \qquad (309)$$

Remind that constants k_0, U_0, λ_0, a_0 and a_1 are found by solving the Prandtl's equations of the classical boundary-layer theory. For an aerofoil

with parabolic nose

$$k_0 = 1.1575, \quad U_0 = 1.286, \quad \lambda_0 = 0.024, \quad a_0 = 0.0085, \quad a_1 = -1.24. \tag{310}$$

Using (310) in the equation (309), renders it in the form

$$\alpha_* = 0.8185 + 1.4610 \cdot Re^{-2/5} a - \frac{1}{\pi} \int_0^1 \frac{G(x')}{\sqrt{x'(1-x')}} \, dx'.$$

If we assume, to make it even more simple, that the aerofoil is symmetric $(G \equiv 0)$, then we will have

$$\alpha_* = 0.8185 + 1.4610 \cdot Re^{-2/5} a + \cdots \quad \text{as} \quad Re \to \infty. \tag{311}$$

Setting $a = a_s = 1.139$ in (311) gives the angle of attack at moment of the formation of the short separation bubble

$$\alpha_s = \varepsilon \left(0.8185 + 1.6641 \cdot Re^{-2/5} + \cdots \right). \tag{312}$$

If, instead, we choose $a = a_c = 1.33$, then we will find that the bubble bursting has to be expected at the angle of attack

$$\alpha_c = \varepsilon \left(0.8185 + 1.9431 \cdot Re^{-2/5} + \cdots \right). \tag{313}$$

When applying these results to real flows one needs to keep in mind that the Marginal Separation theory relies on the assumption of laminar flow. This assumption is well justified for attached flows near the leading edge of a thin aerofoil. The reason is that the characteristic length scale here is not the aerofoil cord, c, but a much smaller quantity, the radius of the aerofoil nose, $r = c\varepsilon^2$. Under conditions typical of aerodynamic applications, the Reynolds number $Re = V_\infty r/\nu$, calculated based on r, is not large enough for the attached boundary layer to become turbulent. In fact, the flow is observed to remain laminar even after the formation of the short separation bubble. However, before the bubble bursting, the flow in the bubble changes its character and becomes partly turbulent. The separated flows are known to be less stable and can undergo a rather rapid laminar-turbulent transition. In the leading edge bubble the flow is observed to separate laminar, becomes turbulent before the reattachement. The transition has a significant effect on the behaviour of the separation bubble. For example, when the turbulence is enhanced by introducing an additional acoustic noise in the wind tunnel test section, it always delays the bubble bursting. This explains why the formula (312) proves to be fairly accurate (see Hsiao & Pauley, 1994), while the formula (313) might underestimate the critical angle of attack α_c.

Exercise 2. Simplify (135) with the help of the asymptotic expansion (134), and confirm that the resulting expression reproduces the solution (130) in region 2a.

Exercise 3. Consider two-dimensional steady incompressible inviscid fluid flow near a corner point O on a rigid body surface as shown in Figure 27. Assuming the wall deflection angle θ small, represent the solution of the
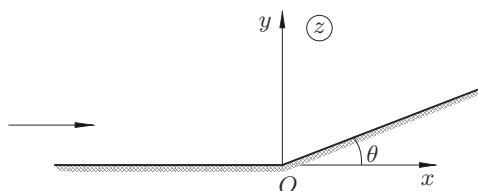
Figure 27. Flow past a corner point of a rigid body surface.

Euler equations in the form of asymptotic expansions

$$u = U_0 + \theta u_1(x, y) + \cdots, \quad v = \theta v_1(x, y) + \cdots, \quad p = \theta p_1(x, y) + \cdots.$$

Here u, v and p are the non-dimensional velocity components and pressure; U_0 denotes the value of the tangential velocity u that would be observed in the flow if the angle θ was zero.

Prove that $f(z) = p_1 + iU_0 v_1$ is an analytic function of the complex variable $z = x + iy$, and try to find the solution for $f(z)$ near the corner in the form

$$p_1 + iU_0 v_1 = (C_r + iC_i)\ln z + (D_r + iD_i) + \cdots \quad \text{as} \quad z \to 0. \quad (314)$$

Set $z = re^{i\vartheta}$ in (314), and using the impermeability condition on the body surface upstream and downstream of the corner point O,

$$\frac{v}{u} = \tan\theta \approx \theta \quad \text{at} \quad y = 0, \ x > 0,$$

$$\frac{v}{u} = 0 \qquad\qquad \text{at} \quad y = 0, \ x < 0,$$

show that

$$C_r = -\frac{U_0^2}{\pi}, \qquad C_i = 0, \qquad D_i = U_0^2.$$

Hence, deduce that in a small vicinity of the corner point

$$
\left.
\begin{aligned}
p &= -\theta \frac{U_0^2}{\pi} \ln r + \cdots, \\
u &= \theta \frac{U_0}{\pi} \ln r + \cdots, \\
v &= \theta U_0 \left(1 - \frac{\vartheta}{\pi}\right) + \cdots
\end{aligned}
\right\} \quad \text{as} \quad r \to 0.
\tag{315}
$$

Exercise 4.   Split the integral (303) into two

$$
I(X,\xi) = \int_{-\infty}^{0} \frac{(ik)^{1/2}}{-k} e^{ik(X-\xi)} dk + \int_{0}^{\infty} \frac{(ik)^{1/2}}{k} e^{ik(X-\xi)} dk,
\tag{316}
$$

and assume, first, that $\xi < X$. In this case, when calculating the first integral, I_1 ,in (316) change the contour of integration from the negative real semi-axis (contour C_1 in Figure 28a) to the positive imaginary semi-axis, C_1'. Observe that, according to Jordan's lemma, the integral along the
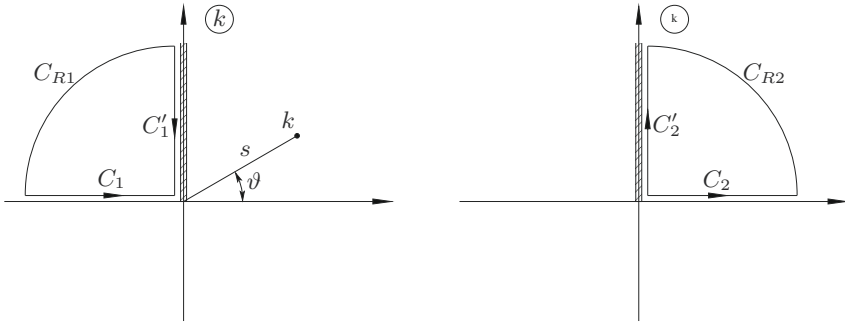
a) Contour change for the first   b) Contour change for the second
   integral in (316).   integral in (316).

Figure 28. Calculation of the integrals in (316) for $\xi < X$.

quarter-circle, C_{R1}, tends to zero as its radius R tends to infinity. Introduce a new integration variable s, such that $k = is$, with s being the distance

from a point on C_1' to the coordinate origin, and confirm that the adopted rule of calculating $(ik)^{1/2}$ gives on C_1',

$$(ik)^{1/2} = -is^{1/2}.$$

Hence, show that

$$I_1 = -i \int_0^\infty \frac{e^{-(X-\xi)s}}{\sqrt{s}} ds.$$

When calculating the second integral, I_2, in (316), change the contour of integration as shown in Figure 28(b). Show that
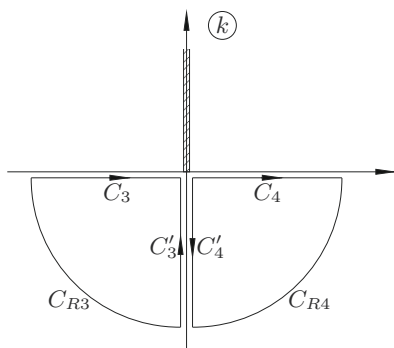
$$I_2 = i \int_0^\infty \frac{e^{-(X-\xi)s}}{\sqrt{s}} ds,$$

and conclude that

$$I(X,\xi) = I_1 + I_2 = 0 \quad \text{for} \quad \xi < X.$$

For the case when $\xi > X$, change the contour of integration for the two integrals in (316) as indicated in Figure 29, and show that

$$I_1 = I_2 = \frac{\sqrt{\pi}}{\sqrt{\xi - X}}.$$

Figure 29. Calculation of the integrals in (316) for $\xi > X$.

Exercise 5. Notice that the right hand side of the equation (305) tends to zero as $X \to \infty$. This means that the first two terms of the asymptotic expansion of $A(X)$ at large positive values of X may be written as

$$A(X) = X - \frac{a}{X} + \cdots \quad \text{as} \quad X \to \infty. \tag{317}$$

Differentiate (317) twice, and substitute the result into the integral on the right hand side of (305). Perform the integration using the following chain of substitutions: $\xi = Xs$, then $s = t^2 + 1$ and, finally, $t = \tan\theta$. Conclude that

$$A^2 - X^2 + 2a = -\tfrac{3}{4}a\Lambda\pi X^{-5/2} + \cdots \quad \text{as} \quad X \to \infty. \tag{318}$$

Now, assume that $X \to -\infty$, and split the integral on the right hand side of (305) as

$$\int\limits_{X}^{\infty} \frac{A''(\xi)}{\sqrt{\xi - X}}d\xi = \int\limits_{X}^{-\Delta} \frac{A''(\xi)}{\sqrt{\xi - X}}d\xi + \int\limits_{-\Delta}^{\Delta} \frac{A''(\xi)}{\sqrt{\xi - X}}d\xi + \int\limits_{\Delta}^{\infty} \frac{A''(\xi)}{\sqrt{\xi - X}}d\xi, \tag{319}$$

where parameter Δ is such that

$$\Delta \ll (-X), \quad \text{but} \quad \Delta \gg (-X)^{1/3}. \tag{320}$$

Consider, first, the middle integral. Notice that thanks to the first inequality in (320) it may be approximated as

$$I_2 \approx \int\limits_{-\Delta}^{\Delta} \frac{A''(\xi)}{\sqrt{-X}}d\xi = \frac{1}{\sqrt{-X}} \int\limits_{-\Delta}^{\Delta} A''(\xi)d\xi = \frac{1}{\sqrt{-X}}\Big[A'(\Delta) - A'(-\Delta)\Big].$$

Keeping in mind that Δ is large, calculate $A'(\Delta)$ and $A'(-\Delta)$ using (317) and (306), respectively. Conclude that

$$I_2 = \frac{2}{\sqrt{-X}} + \cdots. \tag{321}$$

When evaluating the first integral in (319), calculate $A''(\xi)$ with the help of (306). Then use the fact that $(-\xi) \le \Delta$ everywhere in the integration interval, and show that

$$|I_1| \le \frac{2a}{\Delta^3} \int\limits_{X}^{-\Delta} \frac{d\xi}{\sqrt{\xi - X}} = \frac{4a}{\Delta^3}\sqrt{(-X) - \Delta}.$$

Finally, consider the third integral,

$$I_3 = \int\limits_{\Delta}^{\infty} \frac{A''(\xi)}{\sqrt{\xi - X}} d\xi. \tag{322}$$

Use the asymptotic expansion (317) to calculate $A''(\xi)$ in (322), and introduce a new integration variable t through the substitution $\xi = (-X)(t^2 - 1)$. This leads to

$$I_3 = -\frac{4a}{(-X)^{5/2}} \int\limits_{\sqrt{1 + \frac{\Delta}{(-X)}}}^{\infty} \frac{dt}{(t-1)^3(t+1)^3}.$$

Notice that $t + 1 > 2$ everywhere in the integration interval. Hence, deduce that

$$|I_3| \leq \frac{4a}{(-X)^{5/2}} \frac{1}{8} \int\limits_{\sqrt{1 + \frac{\Delta}{(-X)}}}^{\infty} \frac{dt}{(t-1)^3} \approx \frac{a}{4(-X)^{1/2}} \frac{1}{\Delta^2}.$$

Confirm that under the conditions (320), integrals I_1 and I_3 are much smaller than I_2. Substitute (321) into (319), and conclude that

$$A^2 - X^2 + 2a = \frac{2\Lambda}{\sqrt{-X}} + \cdots \quad \text{as} \quad X \to -\infty.$$

Exercise 6.   Show that the equation (305) may be inverted to take the form

$$A'(X) = 1 - \frac{1}{\pi\Lambda} \int\limits_{X}^{\infty} \frac{A^2(\xi) - \xi^2 + 2a}{\sqrt{\xi - X}} d\xi.$$

For this purpose introduce a new function $S(X)$ such that $S = G'(X)$, and deduce from the equation (299) that

$$\breve{Q} = \frac{2}{\sqrt{\pi}\Lambda} \frac{|k|}{(ik)^{3/2}} \breve{S}. \tag{323}$$

Apply the inverse Fourier transformation to (323), and using the technique described in Exercise 4, show that

$$A''(X) = -\frac{1}{2\pi\Lambda} \int\limits_{X}^{\infty} \frac{S(\xi)}{\sqrt{\xi - X}} d\xi. \tag{324}$$

Now, consider the integral

$$F(X) = \int\limits_{X}^{\infty} \frac{G(\xi)}{\sqrt{\xi - X}} d\xi, \tag{325}$$

Recall that the function $G(X)$ was introduced through the equation (268), and it follows from (318) that $G(X) = O(X^{-5/2})$ as $X \to \infty$. Keeping this in mind, apply the integration by parts to (325), and show that

$$F(X) = -2 \int\limits_{X}^{\infty} \sqrt{\xi - X} S(\xi) d\xi. \tag{326}$$

Then differentiate (326) with respect to X, and deduce that

$$F'(X) = \int\limits_{X}^{\infty} \frac{S(\xi)}{\sqrt{\xi - X}} d\xi. \tag{327}$$

Finally, substitute (327) into (324) and integrate the resulting equation using the fact that, according to (317), $A' = 1$ at $X = \infty$.

Bibliography

Abramowitz, M. & Stegun, I. A. 1965 *Handbook of Mathematical Functions*, 3rd edn. Dover Publications.

Chapman, D. R., Kuehn, D. M. & Larson, H. K. 1956 Investigation of separated flows in supersonic and subsonic streams with emphasis on the effect of transition *NACA Rep.* 1356.

Goldstein, S. 1948 On laminar boundary-layer flow near a position of separation. *Q. J. Mech. Appl. Math.* **1** (1), 43–69.

Helmholtz, H. 1868 Über diskontinuirliche Flüssigkeitsbewegungen. *Monatsbericht Akad. Wiss. Berlin* pp. 215–228.

Hsiao, C. T. & Pauley, L. L. 1994 Comparison of the triple-deck theory, interactive boundary layer method, and Navier-Stokes computations for marginal separation. *Trans. ASME J. Fluids Eng.* **116**, 22–28.

Jones, B. M. 1934 Stalling. *J. Roy. Aero. Soc.* **38**, 753–770.

Kirchhoff, G. 1869 Zur Theorie Freier Flüssigkeitsstrahlen. *J. für die Reine und Angew. Math.* **70** (4), 289–298.

Lamb, H. 1932 *Hydrodynamics*, 6th edn. Cambridge University Press.

Landau, L. D. & Lifshitz, E. M. 1944 *Mechanics of Continuous Media*. Gostekhizdat, Moscow.

Levi-Civita, T. 1907 Scie e leggi di resistenza. *Rendconte de Circolo Matematico di Palermo* **X**XIII, 1–37.

Lighthill, J. 2000 Upstream influence in boundary layers 45 years ago. *Phil. Trans. R. Soc. London,* **A 3**58 (1777), 3047–3061.

Neiland, V. Y. 1969 Theory of laminar boundary layer separation in supersonic flow. *Izv. Akad. Nauk SSSR, Mech. Zhidk. Gaza* (4), 53–57.

Oswatitsch, K. & Wieghardt, K. 1948 Theoretical analysis of stationary potential flows and boundary layers at high speed *NACA Tech. Memo.* 1189.

Ruban, A. I. 1981 A singular solution of the boundary-layer equations which can be extended continuously through the point of zero skin friction. *Izv. Akad. Nauk SSSR, Mech. Zhid. Gaza* (6), 42–52.

Ruban, A. I. 1982 Asymptotic theory of short separation bubbles at the leading edge of a thin airfoil. *Izv. Akad. Nauk SSSR, Mech. Zhid. Gaza* (1), 42–52.

Siebert, H. M. 1948 *High-Speed Aerodynamics*. Prentice Hall, New York.

Stewartson, K., Smith, F. T. & Kaups, K. 1982 Marginal separation. *Stud. Appl. Math.* **67** (1), 45–61.

Stewartson, K. & Williams, P. G. 1969 Self-induced separation. *Proc. Roy. Soc. London* **A** 312, 181–206.

Sychev, V. V., Ruban, A. I., Sychev, Vic. V. & Korolev, G. L. 1998 *Asymptotic Theory of Separated Flows*. Cambridge University Press.

Taneda, S. 1956 Experimental investigation of the wakes behind cylinders and plates at low reynolds numbers. *J. Phys. Soc. Jpn.* **1**1, 302–307.

Tani, I. 1964 Low-speed flows involving bubble separations. *Progr. Aeronaut. Sci.* **5**, 70–103.

Werlé, H. & Gallon, M. 1972 Controle d'ecoulements par jet transversal. aéronaut. astronaut. *Aéronaut. Astronaut.* **3**4, 21–33.

Weakly 3D effects upstream a surface mounted obstacle in transonic flows

A. Kluwick[*] and M. Kornfeld[*]

[*] Institute of Fluid Mechanics and Heat Transfer, Vienna University of Technology, Vienna, Austria

Abstract Steady transonic flows through channels so narrow that the classical boundary layer approach fails are considered. The resulting viscous inviscid interaction problem for weakly three dimensional laminar flows is formulated for perfect gases under the requirement that the channel is sufficiently narrow so that the flow outside the viscous wall layers becomes two-dimensional in the leading order approximation. The behavior of the flow upstream of a surface mounted three-dimensional obstacle will be demonstrated.

1 Problem formulation

The viscous inviscid interactions of steady weakly three-dimensional transonic flows in narrow channels are considered which are triggered, for example, by a shallow deformation of the channel walls. Using asymptotic analysis for large Reynolds number $Re = \tilde{u}_r \tilde{L}/\tilde{\nu} \gg 1$ Kluwick and Gittler, assuming two dimensional steady flows of a perfect gas, showed that a consistent interaction theory can be formulated in which the flow inside the inviscid core region is almost one-dimensional, A. Kluwick [2001]. The former theory can be extended to the weakly three dimensional case if the heights $\tilde{H}$ and $\tilde{h}$ of the channel and the surface mounted obstacle are of orders $\epsilon^3 \tilde{L}$ and $\epsilon^7 \tilde{L}$ and if the length Δ_X and width Δ_Z of the obstacle are of orders $\epsilon^3 \tilde{L}$ and $\epsilon^2 \tilde{L}$ with $\epsilon = Re^{-1/12} \ll 1$. Here $\tilde{u}_r$, $\tilde{L}$ and $\tilde{\nu}$ denote the flow velocity in the core region just upstream of the local interaction region, a characteristic length associated with the unperturbed boundary layer adjacent to the channel wall and a reference value of the kinematic viscosity. As in A. Kluwick [2001] the field quantities inside the inviscid core region do not depend on the distance measured perpendicular to the channel wall in leading order resulting, however, in a two-dimensional rather than one-dimensional flow behavior.

The interaction region exhibits a triple deck structure, where as in the classical triple deck theory, e.g. see Stewartson [1974], the role of the main deck

is to transfer the displacement effects excerted by the lower deck unchanged
to the upper deck and to transfer the resulting pressure disturbances again
unchanged back to the lower deck. Here, the fluid motion is governed by
a weakly three dimensional and incompressible form of the boundary layer
equations

$$\frac{\partial U}{\partial X} + \frac{\partial V}{\partial Y} = 0,$$

$$U\frac{\partial U}{\partial X} + V\frac{\partial U}{\partial Y} = -\frac{\partial P}{\partial X} + \frac{\partial^2 U}{\partial Y^2}, \tag{1}$$

$$U\frac{\partial W}{\partial X} + V\frac{\partial W}{\partial Y} = -\frac{\partial P}{\partial Z} + \frac{\partial^2 W}{\partial Y^2},$$

where (X, Y, Z), (U, V, W) and P denote Cartesian coordinates parallel and
perpendicular to the channel wall and the lateral direction, the correspond-
ing velocity components and the pressure. All quantities are suitable scaled.
The boundary conditions include the no slip condition on the channel walls,
the requirement that the unperturbed velocity profile is recovered in the
limit $X \to -\infty$ and a matching condition between the lower and main deck
for large Y

$$Y = S(X, Z) : U = V = W = 0, \quad X \to -\infty : U = Y,$$

$$Y \to \infty : U = Y + A(X, Z), \quad W = -\frac{1}{Y}\int_{-\infty}^{X}\frac{\partial P}{\partial Z}d\zeta = 0, \tag{2}$$

where $A(X, Z)$ denotes the perturbation of the displacement thickness caused
by the interaction process. The flow in the upper deck is a quasi planar flow
weakly perturbed by the boundary layer displacement. As a result, pres-
sure disturbances resulting from the boundary layer displacement can be
calculated from elementary properties of the massflux velocity relationship
and the well known leading order approximation between the pressure and
velocity disturbances.
Taylor series expansions for $|M_\infty - 1| \ll 1$ up to second order and substi-
tution of the scaled quantities used in equation (1) and (2) then yields

$$P^2 + 2sign(K)P - \Lambda\left(A(X, Z) + \frac{1}{f}\int_{-\infty}^{X}\frac{\partial w_{u1}}{\partial Z}d\bar{X}\right) = 0, \quad \frac{\partial w_{u1}}{\partial X} = -\frac{|K|}{2\Gamma}\frac{\partial P}{\partial Z}, \tag{3}$$

where Λ represents a transonic similarity parameter, Γ denotes the funda-
mental derivative of gasdynamics, e.g. see Kluwick [1993], w_{u1} the lateral
velocity component in the upper deck, f a scaling parameter and K is
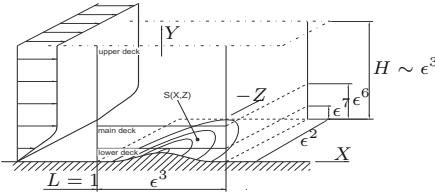
Figure 1. Triple deck structure of interaction region; $\epsilon := Re^{-1/12}$.
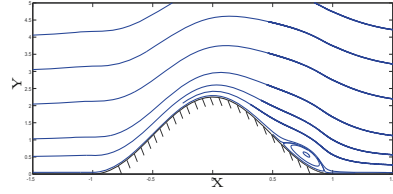
**Figure 2.** Stream lines and separation bubble through the centerline of the hump

proportional to the difference between the Mach number M_∞ in the unperturbed core region and its critical value $M = 1$. For $K \to \pm\infty$ one recovers the cases of purely sub- and supersonic flow, respectively.

2 Results

For the numerical solution of the boundary layer equations (1) to (3) a pseudo spectral method is used. Figure 3 shows the streamlines (dashed lines) as well as the separation stream line (solid line) in a cross section through the center line of the surface mounted hump ($Z = 0$) with $S(X, Z) = h \cdot cos^2(\frac{\pi}{2}\sqrt{X^2 + Z^2})$ and a height $h = 2.25$ for $\Lambda = 2.5, K = 1$ (subsonic flow). The analytical separation angle ϑ (dashed dotted line), obtained by Oswatitsch [1980], at the lee side of the hump matches the angle of the separation streamline at the wall quite well.

For a constriction with $h = 1$ (to avoid the above mentioned effect of flow separation) the pressure perturbation increases with decreasing absolute values $|K|$ under both, sub- and supersonic flow conditions, see Figure 4. In the subsonic case, if $|K|$ is small enough, i.e. the flow is close enough to the point of transition $P = -1$, the flow exhibits a local supersonic region in the upper deck. There is no corresponding local subsonic region in the core region, i.e a pressure perturbation greater than $P = 1$, under supersonic flow conditions for this surface perturbation.

Another remarkable effect is the phenomenon of upstream influence. For supersonic flow conditions a first mathematical explanation of this effect was given by Lighthill [1953]. For the two-dimensional subsonic case A. Kluwick [to appear 2010] showed, that there is strictly no upstream influence. In contrast to these results one finds an upstream influence in the three-
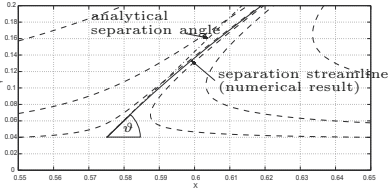
Figure 3. Stream lines near the separation point and separation angle.
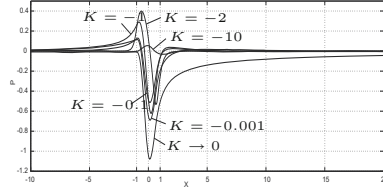
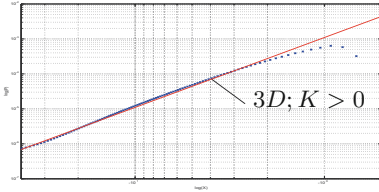**Figure 4.** Pressure perturbation at $Z = 0$ for the supersonic case.

also under subsonic flow conditions. A deeper insight into the effect of upstream influence is gained through studying the linearized problem in spectral space. The pressure perturbation in spectral space is found to be

$$P^{**} = \frac{sign(K)\frac{\Lambda}{2}k^2}{-k^2 - sign(K)\frac{1}{|K|}l^2 + sign(K)\frac{\Lambda}{2}\gamma^{-4/3}(ik)^{7/3}} S^{**} \tag{4}$$

with $\gamma^{-4/3} = -\frac{1}{3Ai'(0)}$, where $Ai'(0)$ denotes the first derivative of the Airy function and k, l the spectral variables corresponding to the physical variables X and Z, respectively. Investigation of the poles of the pressure perturbation (4) shows that there is at least one pole causing an upstream influence even in the 3D subsonic case. Consequently, the upstream behavior for $-X \gg 1$ and $Z = 0$ is found to be $P \sim -\frac{1}{X} e^{8\frac{\gamma^4}{\Lambda^3}X}$ for the supersonic case $K < 0$ and $P \sim \frac{1}{X^2}$ for the subsonic case $K > 0$. In the supersonic case the pressure decays algebraic-exponentially with the same exponent as in the two-dimensional case, which is not surprising since a weakly three-dimensional problem is studied and solutions deviating only slightly from strictly two-dimensional solutions are expected. In the subsonic case an algebraic decay, which is typical for the decay of perturbations under subsonic conditions, is found.

Both analytical results match the numerical results, found upstream of a perturbation caused by a surface mounted hump, cf. Figure 6 and Figure 5, quite well. Following the idea of Lighthill to formulate a free interaction theory under supersonic conditions we are looking for solutions of the form

$$U \sim Y + \frac{1}{X}e^{8\frac{\gamma^4}{\Lambda^3}X}cos(\beta(X)Z)\tilde{U}(Y), \quad V \sim -\frac{1}{X}e^{8\frac{\gamma^4}{\Lambda^3}X}cos(\beta(X)Z)\tilde{V}(Y),$$

$$P \sim -\frac{1}{X}e^{8\frac{\gamma^4}{\Lambda^3}X}cos(\beta(X)Z), \quad A \sim +\frac{1}{X}e^{8\frac{\gamma^4}{\Lambda^3}X}cos(\beta(X)Z)\tilde{U}(\infty), \tag{5}$$

Figure 5. Decay of the effect of the upstream influence for $K > 0$
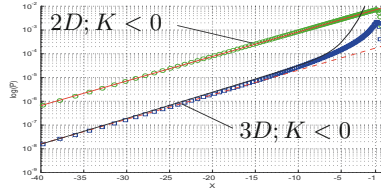
Figure 6. Decay of the effect of the upstream influence for $K < 0$

suggested by the previous results. Evaluating the governing equations with the given ansatz one finally obtains

$$\beta(X) \sim \frac{1}{\sqrt{3}} \sqrt{8 \frac{\gamma^4 |K|}{\Lambda^3 |X|}}. \tag{6}$$

Consequently, the three-dimensional structure of the perturbations is getting weaker as $-X$ increases, which is confirmed by numerical results. In the limiting case $|K| \to 0$ a two-dimensional behavior with no upstream influence is obtained.

With the above discussed results of the effect of upstream influence there arises the question if there exists a weakly three-dimensional regularized shock profile similar to the two-dimensional case, e.g. a regularized shock with a curved shock front. Since the weakly three-dimensional problem covers the two-dimensional shock solution each additional weakly three-dimensional solution would cause a non-uniqueness. In this case the aspects of the stability of the solutions as well as the transition between these solutions are of interest.

Bibliography

G. Meyer A. Kluwick. Shock regularisation in dense gases by viscous inviscid preparation. *J. Fluid Mech.*, 664:473–507, 2010.

Ph. Gittler A. Kluwick. Transonic laminar interacting boundary layers in narrow channels. *ZAMM*, 81:473–474, 2001.

A. Kluwick. Transonic nozzle flow of dense gases. *J. Fluid Mech.*, 247: 661–699, 1993.

M.J. Lighthill. On boundary layers and upstream influence. *Proc. Roy. Soc. A, 217*, pages 344–356, 1953.

K. Oswatitsch. *Contributions to the Development of Gasdynamics*. Vieweg, 1980.

K. Stewartson. Multistructured boundary layers on flat plates and related bodies. *Adv. Appl. Mech.*, 14:145–239, 1974.

Self-Similar Blow-up Structures in Unsteady Marginally Separated Flows

Mario Aigner[*] and Stefan Braun

Institute of Fluid Mechanics and Heat Transfer, Vienna University of Technology

Abstract In the present study we consider unsteady three-dimensional marginally separated boundary layer flows in the limit of high Reynolds numbers. Special emphasis is placed on solutions which blow up within finite time. In analogy to strictly two-dimensional flows the blow-up profile is self-similar and numerical results strongly suggest its uniqueness. Furthermore, the leading order blow-up structure is generic in the sense that it determines the terminal form of both local and global three-dimensional flows.

1 Fundamental Equations

For a comprehensive description of the underlying theory based on matched asymptotic expansions the reader is referred to Ruban (2010) of this monograph and to Sychev et al. (1998) for the case of steady planar flows. Extensions of the theory to incorporate transient and three-dimensional effects can be found in Smith (1982), Ruban (1983), Duck (1990) and Braun & Kluwick (2004), respectively. Our main concern is the investigation of the Cauchy problem associated with the evolution of the displacement function or equivalently the local wall shear stress $A = A(x,t)$ and $A = A(x,z,t)$ governed by the fundamental equations

$$A^2 - x^2 + \Gamma = \lambda \mathbf{J}^*[\partial_x^2 A] - \gamma \mathbf{I}[\partial_t A] + g(x,t) \quad \text{for} \quad x \in \mathbb{R}, \ t \geq 0, \qquad (1)$$

for a strictly planar and

$$A^2 - x^2 + \Gamma = -\frac{\lambda}{2\pi} \mathbf{J}\mathbf{K}[\Delta A] - \gamma \mathbf{I}[\partial_t A] + g(x,z,t) \quad \text{for} \ (x,z) \in \mathbb{R}^2, \ t \geq 0, \ (2)$$

for a local three-dimensionally perturbed two-dimensional boundary layer flow. Here Δ denotes the Laplace operator in spatial coordinates and x, z, t, Γ, λ, γ denote non-dimensionalised, suitably scaled coordinates in

---

stream- and spanwise direction, the time, a control parameter and positive constants. The functions g in (1) and (2), which remain bounded $\forall t \geq 0$, account for flow control devices which provide physically meaningful initial conditions for A at $t = 0$, see Braun & Kluwick (2004). Also, we have formally introduced the following integral operators

$$\mathbf{J}^*[f](x, \cdot) = \int\limits_x^\infty \frac{1}{(\xi - x)^{1/2}} f(\xi, \cdot) d\xi,$$

$$\mathbf{J}[f](x, \cdot) = \int\limits_{-\infty}^x \frac{1}{(x - \xi)^{1/2}} f(\xi, \cdot) d\xi, \quad \mathbf{I}[f](x, \cdot) = \int\limits_{-\infty}^x \frac{1}{(x - \xi)^{1/4}} f(\xi, \cdot) d\xi,$$

$$\mathbf{K}[f](x, z) = \iint\limits_{\mathbb{R}^2} \frac{x - \xi}{((x - \xi)^2 + (z - \eta)^2)^{3/2}} f(\xi, \eta) d\xi d\eta,$$

$$\text{(3)}$$

sometimes referred to as *fractional derivatives*, *Weyl operators* or *Riesz potentials*.

Remark 1.1. If we consider problem (1) in the stationary case (i.e. $\partial_t A \equiv 0$ and $g \equiv 0$) the resulting equation coincides exactly with the fundamental problem derived in Ruban (2010) of this monograph (cf. equation (305) therein, where $x = X$, $\Gamma = 2a$ and $\lambda = \Lambda$).

It is well known (see Smith (1982) and Duck (1990)) that solutions to equations (1) and (2) may blow up at a finite time $t = t_s > 0$. In this short treatise we focus on the terminal structure of these solutions as $t \to t_s$ (see section 2).

Remark 1.2. Matching to the classical boundary layer flow requires the far-field behaviour for equations (1) and (2) to be

$$A(x, \cdot) \sim |x| \text{ as } x \to \pm\infty \quad \text{and} \quad A(x, z, \cdot) \sim |x| \text{ as } x \to \pm\infty \qquad \text{(4)}$$

whereas $A(x, z, \cdot)$ stays at least bounded as $z \to \pm\infty$.

Remark 1.3. Duck (1990) considered a fully three-dimensional incompressible marginally separated boundary layer flow in a line of symmetry which led to a different z-dependent left hand side than in (2). As in the usual approach use was made of the interaction law, which relates the pressure P to the displacement function A via $P = \mathbf{K}[\partial_x A]$. In this case the fundamental equation reads (omitting positive coefficients)

$$A^2 + \gamma(z, t) - \mu^2(\beta x^2 + z^2) = \mathbf{J}[\partial_x P + \int\limits_{-\infty}^x \partial_z^2 P d\xi] - \mathbf{I}[\partial_t A] \qquad \text{(5)}$$

for $(x, z) \in \mathbb{R}^2$, $t \geq 0$ and with the far-field behaviour $A(x, z, \cdot) \sim \mu(\beta x^2 + z^2)^{1/2}$ as $x^2 + z^2 \to \infty$. Here μ is a lengthscale parameter and β takes into account the aspect ratio of the elliptic domain. The function γ is analogous to the control parameter Γ in equation (2) and remains bounded $\forall t \geq 0$.

Remark 1.4. Substituting the interaction law into the fundamental equation (5) and integrating by parts shows the right-hand side operators in (2) and (5) to be equivalent. We thus obtain that the only difference in the fundamental equations between a locally and globally three-dimensional flow studied by Duck (1990) lies in the z-dependent left-hand side and the far-field behaviour.

2   Finite Time Blow-up and its Self-Similarity

Under certain conditions there is strong numerical evidence – as demonstrated in Smith (1982) and Duck (1990), for a more recent investigation see also Scheichl et al. (2008) – that solutions to equations (1), (2) and (5) only exist within a finite time interval $0 \leqslant t < t_s$. As the blow-up time is approached, the displacement function A becomes unbounded at a single point x_s and (x_s, z_s) (in case of three-dimensional flow), respectively. An order of magnitude estimate, performed in Smith (1982) and Duck (1990), suggests the appropriate similarity variables as $t \to t_s$

$$\tau = |t_s - t|, \quad \bar{x} = x - x_s = \tau^{4/9}\hat{x}, \quad \bar{z} = z - z_s = \tau^{4/9}\hat{z},$$

$$A(x, z, t) = \tau^{-2/3}\hat{A}(\hat{x}, \hat{z}) + \mathrm{o}(\tau^{-2/3}). \tag{6}$$

Substitution of (6) into (1) and taking the formal limit $\tau \to 0$ yields

$$\hat{A}^2 = \lambda\mathbf{J}^*[\hat{A}''] - \tfrac{2}{3}\gamma\mathbf{I}[\hat{A} + \tfrac{2}{3}\hat{x}\hat{A}'] \quad \hat{x} \in \mathbb{R}, \tag{7}$$

for the planar flow case, where $(\cdot)'$ denotes the derivative with respect to $\hat{x}$ and $\hat{A}(\hat{x}) \sim c_{\pm}|\hat{x}|^{-3/2}$ as $\hat{x} \to \pm\infty$, $c_{\pm} = const. \in \mathbb{R}$, arising from matching with the outer region where A remains an O(1) quantity. A detailed investigation of the far-field behaviour is presented in Scheichl et al. (2008).

Most interestingly, the scalings (6) lead to the same terminal structure for both fundamental equations, (2) and (5), initially describing different (local and global) three-dimensional marginally separated flows. Their common blow-up profile $\hat{A}(\hat{x}, \hat{z})$ then is governed by

$$\hat{A}^2 = -\tfrac{\lambda}{2\pi}\mathbf{JK}[\Delta\hat{A}] - \tfrac{2}{3}\gamma\mathbf{I}[\hat{A} + \tfrac{2}{3}(\hat{x}\partial_{\hat{x}} + \hat{z}\partial_{\hat{z}})\hat{A}] \quad (\hat{x}, \hat{z}) \in \mathbb{R}^2. \tag{8}$$

Remark 2.1. As indicated above, the singular behaviour of A as $t \to t_s$ is restricted to a single point (x_s, z_s) and hence everywhere else A remains

bounded. Thus, by matching $\hat{A}$ with A at $|(\bar{x}, \bar{z})| = O(1)$, and using polar coordinates $(\hat{x}, \hat{z}) \mapsto (\hat{r}, \hat{\phi})$ the far-field condition for (8)

$$\hat{A} = \hat{A}(\hat{r}, \hat{\phi}) \sim c(\hat{\phi})\,\hat{r}^{-3/2} \quad \text{as} \quad \hat{r} \to \infty \tag{9}$$

can be deduced, where $c = c(\hat{\phi})$ is assumed to be smooth in some sense. This is in agreement with the far-field behaviour given in Duck (1990), such that equations (2) and (5) evolve into the same blow-up structure.

Remark 2.2. Let $\hat{A} = \hat{A}(\hat{x})$ be independent of $\hat{z}$, then equations (1) and (2) are equivalent (with the same far-field condition). In other words, the fundamental equation for a planar flow can be considered as a special case of the locally three-dimensional problem. This also holds for the blow-up profile (cf. equations (7) and (8)).

Remark 2.3. It should be mentioned, that because of (9) $\hat{A}$ can not be expected to be in $L^1(\mathbb{R}^2)$ but in $L^2(\mathbb{R}^2)$ and hence the Fourier-Transform of $\hat{A}$ does not exist in the *usual* sense.

Remark 2.4. A solution of (8) exhibits several symmetry and invariance properties: the change of variables $z \to -(z - z_0)$ (reflection and translation invariance), $t - t_s \to -(t - t_s - t_0)$ (translation and time-reversal invariance) leaves the equation unchanged, where z_0 and t_0 can be chosen arbitrarily.

3   Numerical Solution

A first attempt to gain insight into the behaviour of equations (1) and (7) can be found in Smith (1982), which has been extended by Scheichl et al. (2008) to a more detailed survey. Therein a finite differencing scheme to solve equations (1) and (7) is presented. Performed numerical experiments give strong evidence for the existence and uniqueness of a non-trivial solution of (7).

To solve the singular, nonlinear, homogeneous, partial integro-differential equation (8) numerically we follow the approach of Scheichl et al. (2008) for a discretization of the singular integrals appearing in (3). A nontrivial solution is sought in the form $\hat{A}(\hat{x}, \hat{z}) = \hat{A}(\hat{x}^*, \hat{z}^*)\phi(\hat{x}, \hat{z})$, where $A(\hat{x}^*, \hat{z}^*) \neq 0$ for a fixed $(\hat{x}^*, \hat{z}^*)$ (and since we want $\hat{A}$ to be smooth in some sense, this is true for a whole neighbourhood). Thus $\phi \not\equiv 0$ with $\phi(\hat{x}^*, \hat{z}^*) = 1$.

Another key for a stable scheme is to find an appropriate, bijective map $\psi : \mathcal{C} \to \mathbb{R}^2$, where $\mathcal{C} \subset \mathbb{R}^2$ is compact, such that one can impose boundary conditions $\hat{A}(\psi(\mathbf{u})) = 0$ for $\mathbf{u} \in \partial\mathcal{C}$. The applied methods lead to an inhomogeneous system (in the sense, that the null vector is not a possible

solution) for the (discretized) unknown ϕ, which is solved using a Newton algorithm. The results are depicted in Figures 1 and 2 (calculated on a $50{\times}40$ $\hat{x}$-$\hat{z}$ grid). Most interestingly, the behaviour of $\hat{A}$ at the line of
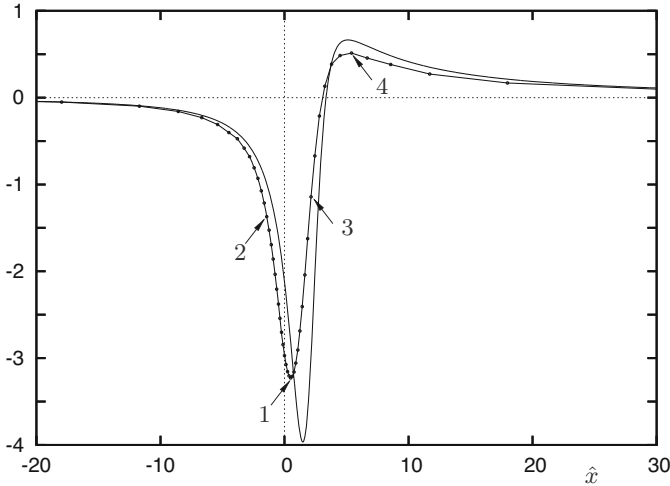

Figure 1. The solution $\hat{A} = \hat{A}(\hat{x}, 0)$ of (8) (with dots) in comparison to that of (7) $\hat{A} = \hat{A}(\hat{x})$ (solid line), Scheichl et al. (2008).

symmetry $\hat{z} = 0$ is similar to the solution $\hat{A}(\hat{x})$ obtained in Scheichl et al. (2008) (due to the Fredholm operator **K** this can not be seen directly from equation (8)). From Figure 2 one would claim the z-behaviour to be similar to a function $g = g(\hat{z})$ with algebraic decay and in further consequence that the solution can be written as $\hat{A}(\hat{x}, \hat{z}) = \hat{A}(\hat{x}, 0)g(\hat{z})$. Again this is not possible, since **K** and the $\hat{z}$-derivative in the argument of **I** do not allow the equation to be separated into a pure $\hat{x}$ and $\hat{z}$ dependent part.

Remark 3.1. The convergence of the used Newton method depends quite sensitively on the map ψ, due to which the $\hat{x}$-$\hat{z}$ grid on the whole $\mathbb{R}^2$ is non-equidistant. As a consequence, increasing the grid points does not directly imply a more accurate solution. One additionally has to use an accordingly modified ψ.

Despite all the faced difficulties, the numerical solution still provides a good first insight into equation (8) and gives further ideas for some analytical investigation.
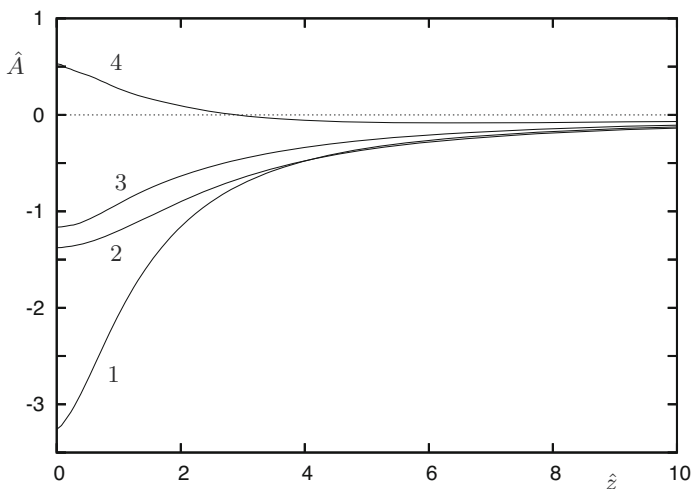
Figure 2. The solution $\hat{A} = \hat{A}(\hat{x}_i, \hat{z})$ of (8) for $i = 1, \ldots, 4$ as indicated in Fig. 1.

Bibliography

Braun, S., Kluwick, A. *Unsteady three-dimensional marginal separation caused by surface-mounted obstacles and/or local suction*, J. Fluid Mech. **514**, 121-152, 2004.

Duck, P.W. *Unsteady three-dimensional marginal separation, including breakdown*, J. Fluid Mech. **220**, 85-98, 1990.

Ruban, A.I. *Stability of preseparation boundary layer on the leading edge of a thin airfoil*, Izv. Akad. Nauk SSSR: Mekh. Zhidk. Gaza **6**, 55-63, (Engl. transl. *Fluid Dyn.* **17**, 835-843), 1983.

Ruban, A.I. *Asymptotic Theory of Separated Flows* in Steinrück, ed. *Asymptotic Methods in Fluid Mechanics: Survey and Recent Advances*, CISM Courses and Lectures Vol. 523, Springer, 311–408, 2010.

Scheichl, S., Braun, S., Kluwick, A. *On a similarity solution in the theory of unsteady marginal separation*, Acta Mech. **201**, 153-170, 2008.

Smith, F.T. *Concerning dynamic stall*, Aeron. Quart. **33**, 331-352, 1982.

Sychev, V.V., Ruban, A.I., Sychev, Vik.V., Korolev, G.L. *Asymptotic Theory of Separated Flows*, Cambridge University Press, Cambridge, 1998.